HANDBOOK ON
MECHANICAL PROPERTIES OF ROCKS

VOLUME IV

R. D. LAMA · V. S. VUTUKURI

SERIES ON ROCK AND SOIL MECHANICS

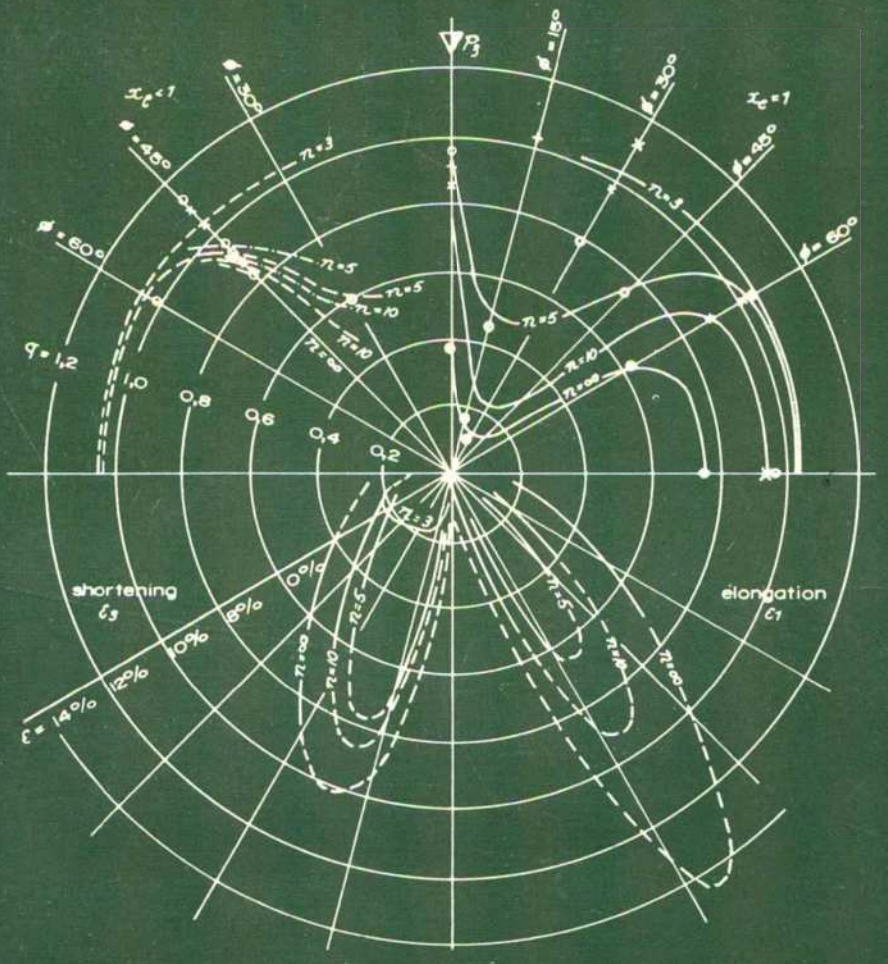

TRANS TECH PUBLICATIONS

Handbook on Mechanical Properties of Rocks

Other volumes in the
Series on Rock and Soil Mechanics

W. Dreyer:
The Science of Rock Mechanics
Part I Strength Properties of Rocks
1972

T. H. Hanna:
Foundation Instrumentation
1973

C. E. Gregory:
Explosives for North American Engineers
1973

M. & A. Reimbert:
Retaining Walls Vol. I
– Anchorages and Sheet Piling –
1974

Vutukuri, Lama, Saluja:
Handbook on Mechanical Properties
of Rocks Vol. I
1974

M. & A. Reimbert:
Retaining Walls Vol. II
– Study of Passive Resistance in Foundation Structures –
1976

H. R. Hardy, Jr. & F. W. Leighton:
First Conference on Acoustic Emission/Microseismic Activity
in Geologic Structures and Materials
1977

L. L. Karafiath & E. A. Nowatzki:
Soil Mechanics for Off-Road Vehicle Engineering
1978

Baguelin, Jézéquel, Shields:
The Pressuremeter and Foundation
Engineering
1978

R. D. Lama & V. S. Vutukuri:
Handbook on Mechanical Properties
of Rocks Vol. II + III
1978

Editor-in-Chief
Professor Dr. H. Wöhlbier

Series on Rock and Soil Mechanics
Vol. 3 (1978) No. 3

HANDBOOK ON MECHANICAL PROPERTIES OF ROCKS

– Testing Techniques and Results –

Volume IV

by

R. D. Lama

CSIRO
Division of Applied Geomechanics
Australia

V. S. Vutukuri

Department of Mining Engineering
Broken Hill Division
University of New South Wales
Australia

First Printing
1978

TRANS TECH PUBLICATIONS

Distributed by
TRANS TECH S. A.
CH-4711 Aedermannsdorf, Switzerland

International Standard Book Number

ISBN O-87849-023-X

Printed in Germany
by Druckerei E. Jungfer, Herzberg

FOREWORD

The subject of rock mechanics has gained increasing acceptance as a necessary input in the design of mining and civil engineering works. In addition of these traditional fields of application, changing political and economic conditions have resulted in the need to store oil and other materials underground, to dispose of nuclear waste materials and to develop underground factories and carparks in order to preserve the surface environment.

These ever growing demands have created an urgent need for the development of a variety of design methods and practical solutions in rock mechanics and these needs have generated a demand for information on all aspects of the behaviour of rock and rock masses. This information is currently scattered throughout the scientific and technical literature and the design engineer or research worker is faced with the formidable task of locating such information before embarking upon a specific study.

The authors of the four volumes of the "Handbook on Mechanical Properties of Rocks" have done a commendable service in bringing together a significant proportion of the available information on rock and rock mass behaviour. This compilation of data is all the more useful because the authors have not attempted to impose too many of their own interpretations upon the information but have presented data accompanied by a range of possible theoretical explanations. This approach makes these volumes useful as a starting point for the research worker or for the design engineer who does not wish to rely on the few standard text book solutions which are available.

This volume, containing discussions on the mechanical behaviour of jointed rock and the classification of rock, touches on the very heart of practical rock mechanics which is more concerned with the response of the rock mass than with the behaviour of laboratory specimens. Because of the practical difficulty and enormous expense of full scale in situ tests on rock mass behaviour, the understanding of this subject has been built up from model studies on equivalent materials and from theoretical models of the interaction of the elements which form the rock mass. The major studies which have contributed to this field of knowledge have been summarised in this volume and it is hoped that this summary will encourage others to carry out further work to enhance our understanding of this important subject.

February 1978

DR. EVERT HOEK
Principal, Golder Associates Ltd.
(Formerly Professor of Rock Mechanics,
Imperial College, London).

CONTENTS

Volume IV

Tables of Contents

CHAPTER 10

Mechanical Behaviour of Jointed Rock

10.1. Introduction

The rock in its most general form is an anisotropic, discontinuous mass containing cracks, fissures, joints, faults and bedding planes with varying degrees of cohesion along these discontinuities. The accepted mathematical models for the analysis of stresses, strains and stability of rock structures which have been so frequently applied in the last half century in civil engineering and mine design have always been associated with a parameter of doubt in the minds of practical engineers. In the last 15 years, greater effort has been concentrated on testing rock masses in situ and this has brought out very clearly the enormous variations that exist in the mechanical behaviour of the rock from place to place. A practical design engineer is convinced that a continuum model approach to the problems of rock design cannot be accepted and that any acceptable solution must take into account not only the anisotropy of the rock mass but also the discontinuities which play a far more important role in the stability of a rock-structure. As such, the fundamental concepts of rock mechanics design can be summarised as follows:

1. For most of the rock engineering problems, the engineering properties of a rock mass depend far more on the system of geological separations within the rock mass than on the strength of the rock material itself.
2. The strength of a rock mass is in fact its residual strength which, together with its anisotropy, is governed by the interlocking bonds of the unit "elements" forming the rock mass.
3. The deformability of a rock mass and its anisotropy results predominantly from the displacements of the unit elements composing the structure of the rock mass.

The first problem, therefore, in the study of the properties of a rock mass is the determination of the character of the discontinuities. Recently some works on this subject have been published and it is noted that the joint surfaces may be very smooth like slickensides to quite rough like the ones obtained in tensile fractures (MULLER, 1963; WAGNER, 1964; WOHNLICH, 1968; FECKER, 1970; BOCK, 1971). Based upon the study of the discontinuities, there exists an opinion that a rock mass may be represented by some sort of a clastic model.

The principal feature of a unit clastic model is that it is anisotropic and has a limited number of clearly defined axes of symmetry. A three-dimensional rock mass may be represented by a randon distribution of individual units, the unit being anisotropic both with respect to the physical properties and shape. The shape and size of the unit is determined by the parameters of the rock system which the model is supposed to represent.

A number of shapes of the elemental units have been proposed and used in clastic mechanics approach by different workers in solving different problems (LITWINISZYN, 1964; TROLLOPE, 1968). In the field of rock mechanics, some of the most common units and their shapes (in two dimensions) have been circular, square, rectangular, parallelogram and hexagonal (Fig. 10-1). From the theoretical standpoint, it is evident that the shape of the unit will restrict the physical nature of the forces generated between the units and hence influence the mechanical behaviour of the system. No comparative study has been made as yet of the systems with different elemental shapes to bring out the differences. But in the last 10 years or so, emphasis has been placed on studying the factors which influence the behaviour of a simplified model of a jointed rock mass consisting of sliding plates or blocks. A number of theoretical and model studies have been carried out which have yielded interesting results. Some of these studies have been very imaginative but still not very realistic due to the absence of any reliable data on the nature, distribution, method of classification and the properties of the joints which exist in rocks. Nevertheless, the results of these studies permit one to conclude that the mechanical behaviour of the jointed rock system is dependent upon the following factors:

1. The mechanical behaviour of the individual elements constituting the system. This has been dealt in detail in Chapters 2 to 5 (Vol. I), in Chapters 6 and 7 (Vol. II) and in Chapter 9 (Vol. III).
2. The sliding characteristics of joints.
3. The configuration of the system.
4. The operating stress field.

The influence of these factors and methods used for determining the frictional properties of joints along with the factors influencing frictional behaviour are discussed. The influence of joints on the uniaxial compressive strength, tensile strength, shear strength and the behaviour under multiaxial stress field is given.

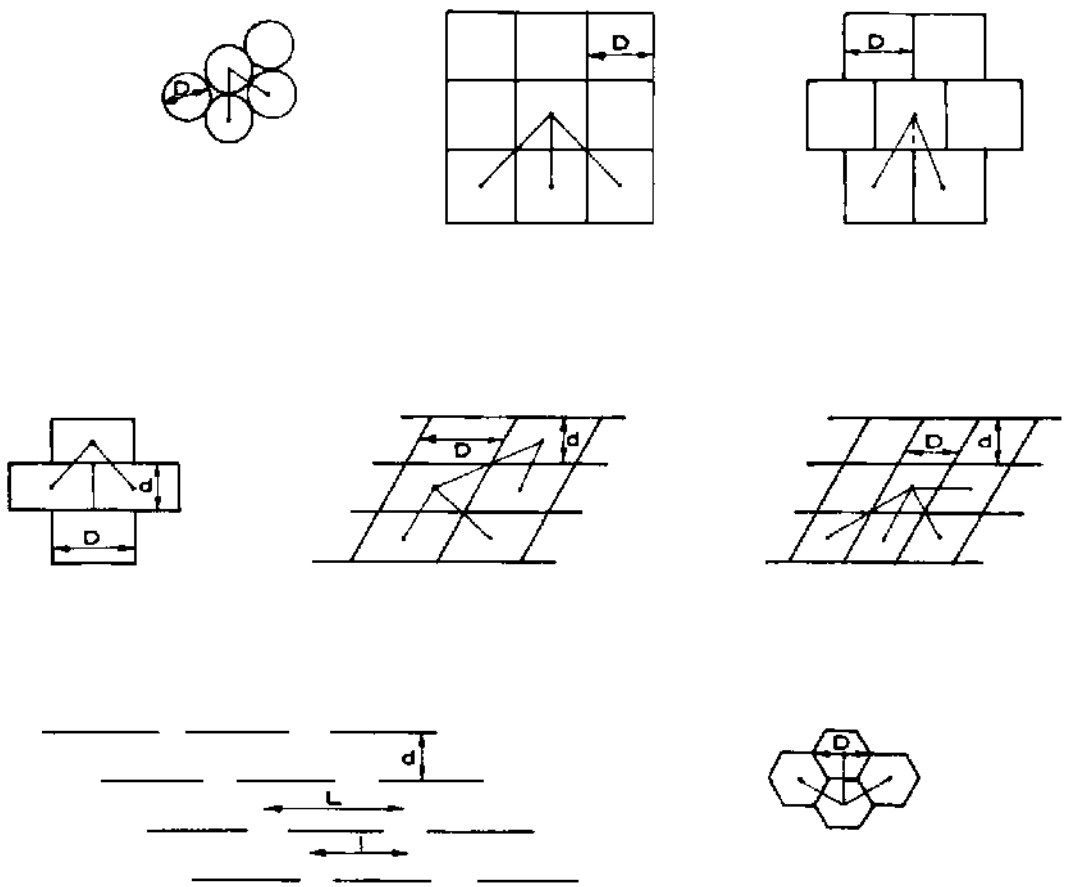

Fig. 10-1. Some typical types of systones in elastic mechanics applied to rock mechanics. The term "systone" is defined as a systematically arranged group of units. It is, however, not essential that the unit in each group be of identical size.

10.2. Theory of Sliding Along a Joint

When a rock element slides over another rock element, an important phenomenon that is brought into play is that of friction. The amount of work done on the phenomenon of friction in rocks has been rather limited and one is bound to look into the various views prevailing in the field of metal friction and wear. These views can be divided into four groups (LAMA, 1972).

The first group developed at the end of the seventeenth century and the beginning of the eighteenth century when the mechanics of rigid bodies were being developed. This view is based solely on geometric considerations and explains friction in terms of the lifting of microasperities over each other (KRAGELSKII, 1965).

With the developments in the concept of the molecular nature of solids, a second view developed which explains friction as a result of overcoming the forces of molecular attraction between the two solids (BOWDEN and TABOR, 1967).

The third group visualises friction arising from the deformation of certain amount of material which is penetrated on one solid by the asperity of the other solid. As movement takes place a wave of deformation moves ahead and the resistance to motion is introduced by the displacement of the material surrounding the asperity.

The fourth group considers a composite theory, which also includes COULOMB's theory, representing friction as resulting from interlocking of the surface roughnesses and the lifting of the microasperities over each other.

The mechanism of friction in brittle materials such as rocks is bound to be slightly different. The concept of molecular attraction and plastic deformation at low stress levels is likely to be absent. On the other hand, it may be expected that due to the development of tensile stresses in the wedge type asperities, they may fail. BYERLEE (1966), basing his interpretation on the theory of linear elasticity, considers that tips of asperities which are subjected to a normal force and lateral (shear) force, crush to a certain extent under the action of the normal force and, on application of the shear force, induced tensile stresses locally exceed the tensile strength. If all possible shapes of asperities are equally probable, the applied shear stress, τ and the normal stress, σ_n can be related to each other as follows (EINSTEIN, BRUHN and HIRSCHFELD, 1970):

$$\frac{\tau}{\sigma_n} = c_1 + \frac{\sigma_t}{\sigma_c} + c_2 \tag{10.1}$$

where c_1, c_2 = constants independent of the material and

$\frac{\sigma_t}{\sigma_c}$ = ratio of tensile to compressive strength, e.g. $\simeq 0.1$ for rock

and the value of $\frac{\tau}{\sigma_n}$ according to the above formula works out to be 0.1 to 0.15 depending upon the shape of the asperity which is much lower than experimental values. BYERLEE's theory does not take into consideration the influence of interlocking of asperities.

The influence of various factors on friction and the values obtained for different rocks by different investigators under varied conditions are discussed later. Here, it may only be mentioned that the coefficient values are quite different from those predicted above which indicates that there is definitely some other phenomenon contributing to the high values of the coefficients.

NEWLAND and ALLELY (1957) were probably the first to indicate that shear is not an intrinsic property but depends upon the average angle of deviation of particle displacements from the direction of the applied stress. PATTON (1966a, b) studied the influence of asperities and the phenomenon of inter-

locking on the failure envelopes. He tested kaoline and plaster mixes with different angles of inclination of asperities ($i = 25$, 35 , 45) and different numbers of asperities. He found that the failure envelope of the specimens with $i = 25$ can be represented by a straight line (A), (Fig. 10-2), but for specimens with $i = 35$ and $i = 45$, each envelope has to be represented by two straight lines (B and C). The line (D) represents the residual strength of all the

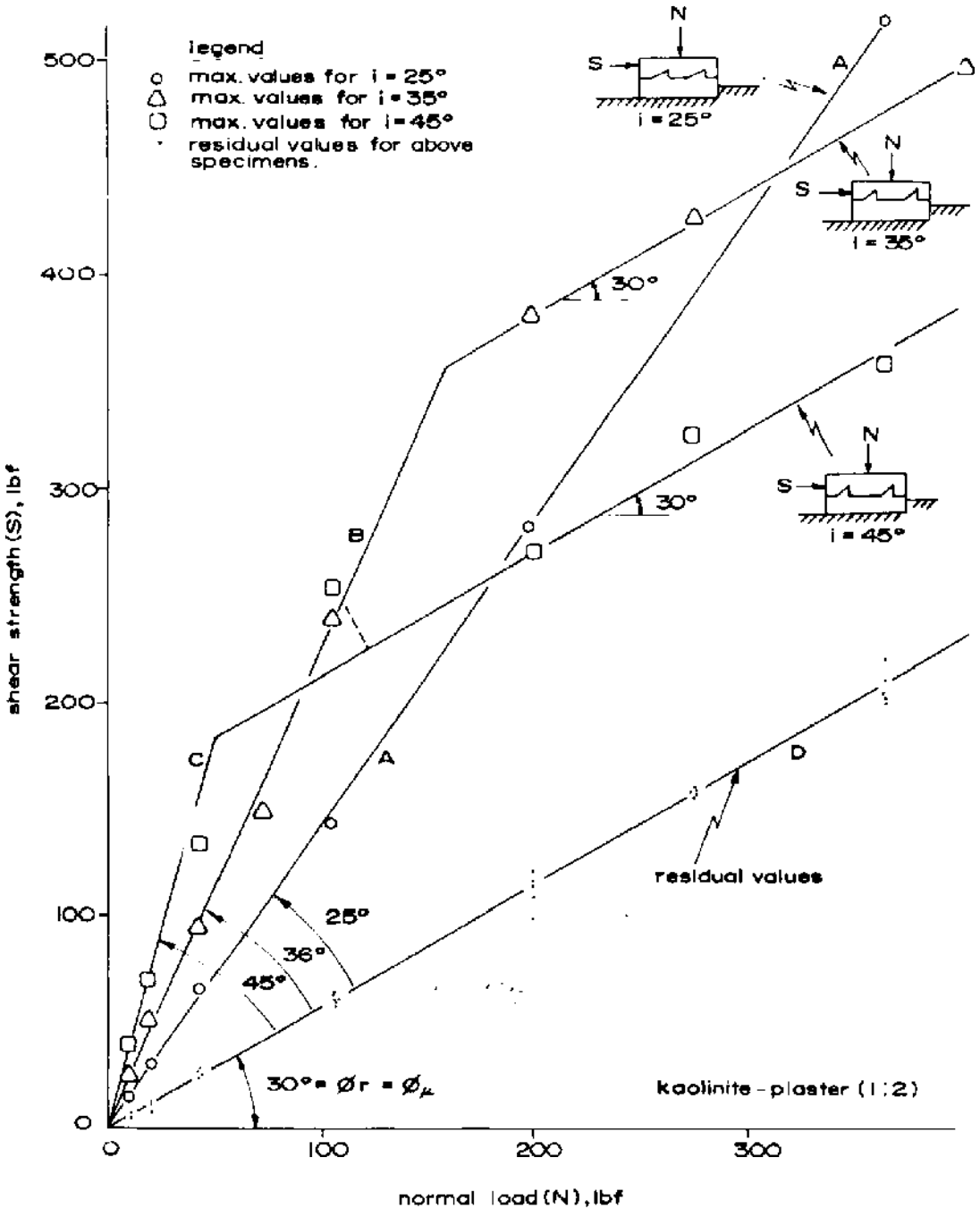

Fig. 10-2. Failure envelopes for specimens with different inclinations of teeth (after PATTON, 1966a).

three series and its value is ± 1 of the sliding friction of the flat surfaces ($\phi_\mu = 31°$ for stronger plaster, kaoline-plaster 1:2; or 27–1/2° for weaker plaster, kaoline-plaster 1:1) depending upon the mix. The inclinations of the upper or the secondary portions of the lines (B and C) are very close to ϕ_r and primary portions (lower) are within one degree of $(\phi_\mu + i)$. The abrupt changes in the slope of the lines (B and C) are related to the change in the mode of failure. Below these change points, the maximum shear strengths are related to the frictional resistance along the inclined surface while above, the transition slope is unrelated to the increased surface resistance due to the inclination of the teeth or the asperity. In the case (C), the transition occurs at lower normal load and in (A) it does not occur because the value of the normal load used is not high enough to reach the transition in the mode of failure.

The influence of increasing the number of asperities is shown in Fig. 10-3. Here also the steep portion of the curve is inclined at an angle of $(\phi_\mu + i)$. The effect of doubling the number of asperities from two to four (specimens identical in other respects) is to move the abrupt change in slope of the failure envelope to a higher normal load and to move the secondary portion of the failure envelope about twice as far above the residual envelope as the failure envelope for the two teeth. This also holds good for specimens prepared with higher strength materials. For stronger specimens, the change in mode takes place at higher normal loads and thus increasing the strength of the specimen is like increasing the number of teeth. Fig. 10-4 represents the results of investigations on two series of specimens with identical surface configuration but different internal strengths (A- for stronger specimens, B- for weaker specimens). In practice such a double line relationship has not been obtained in tests conducted on rock joints which PATTON (1966b) himself states because of superposition of various modes and a more complicated nature of failure of asperities.

EINSTEIN, BRUHN and HIRSCHFELD (1970) explained the influence of asperities and the phenomenon of interlocking in rock friction. According to them the two surfaces will normally be not in plane contact but will interlock where certain portions are in tip to tip contact, but major portions will be staggered (Fig. 10-5). This interlocking influences the relationship between the shear force and the normal force. At small to medium values of the normal force, the asperities slide over each other and the shear resistance can be represented by the equation

$$S = N \tan (\phi_\mu + i) \tag{10.2}$$

where S = shear force
N = normal force
ϕ_μ = angle of frictional sliding resistance along a plane surface and
i = inclination of the asperity with the horizontal along the axis of movement.

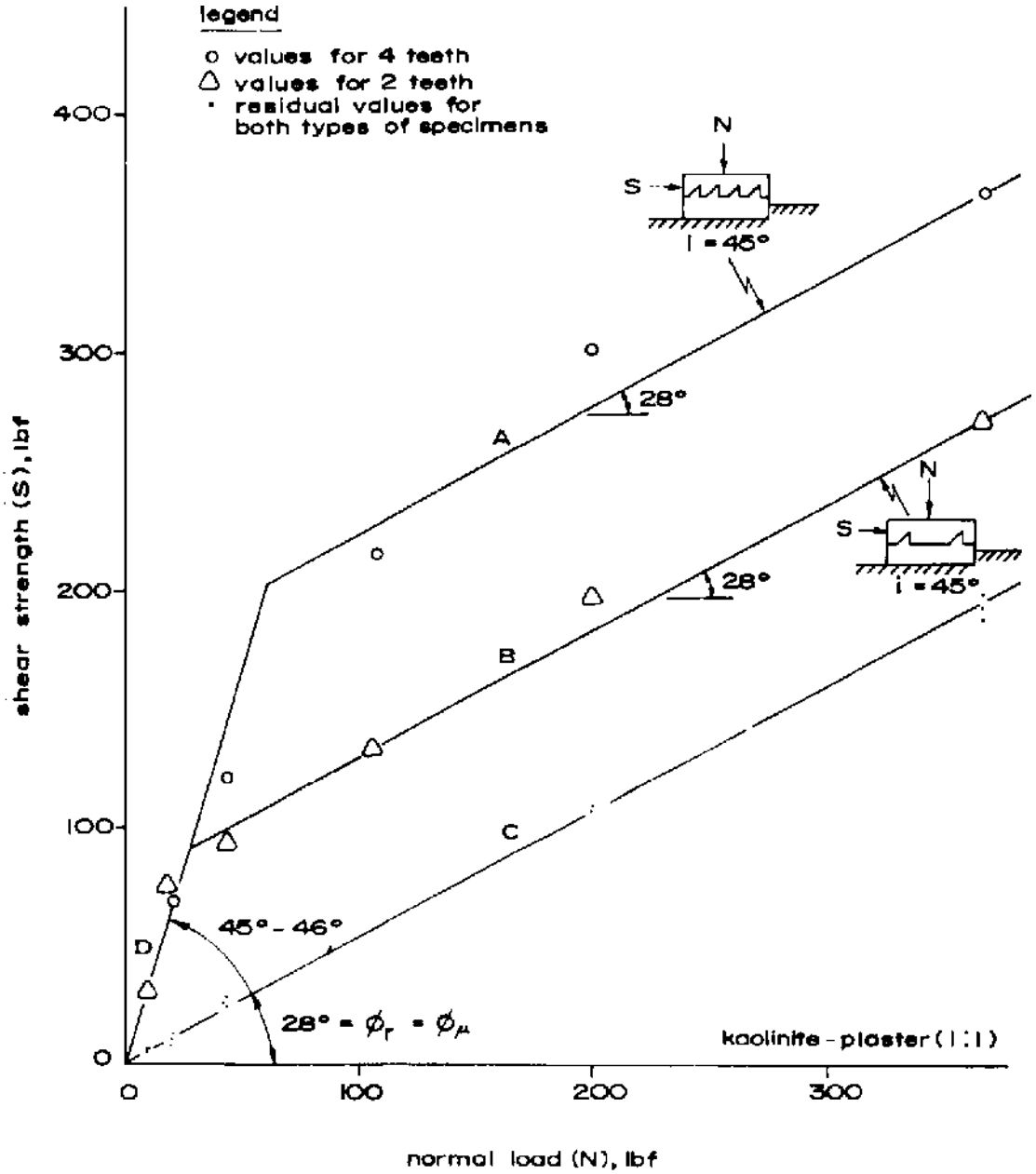

Fig. 10-3. Failure envelopes for specimens for different number of teeth (after PATTON, 1966a).

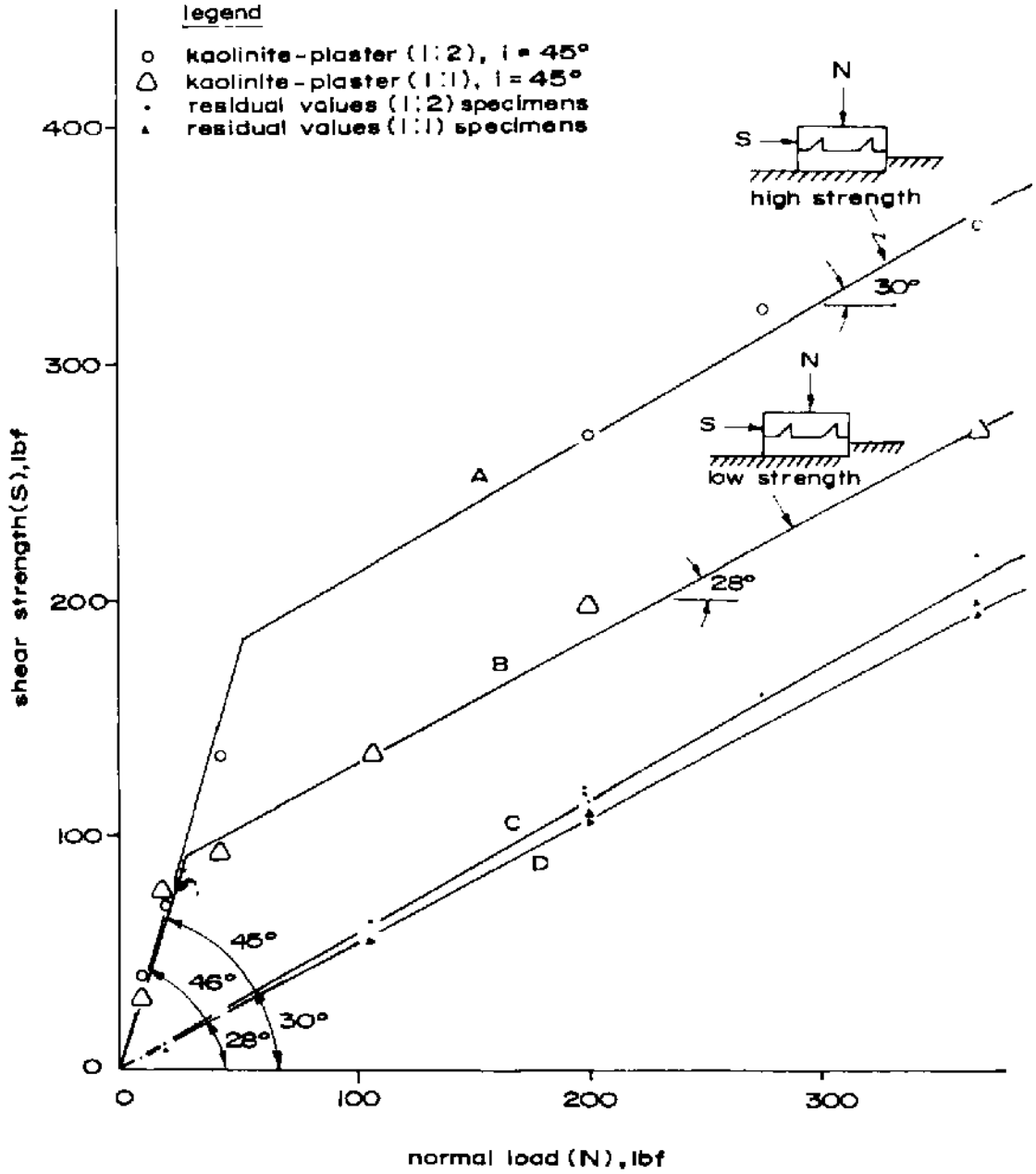

Fig. 10-4. Failure envelopes of specimens with different internal strengths (after PATTON, 1966a).

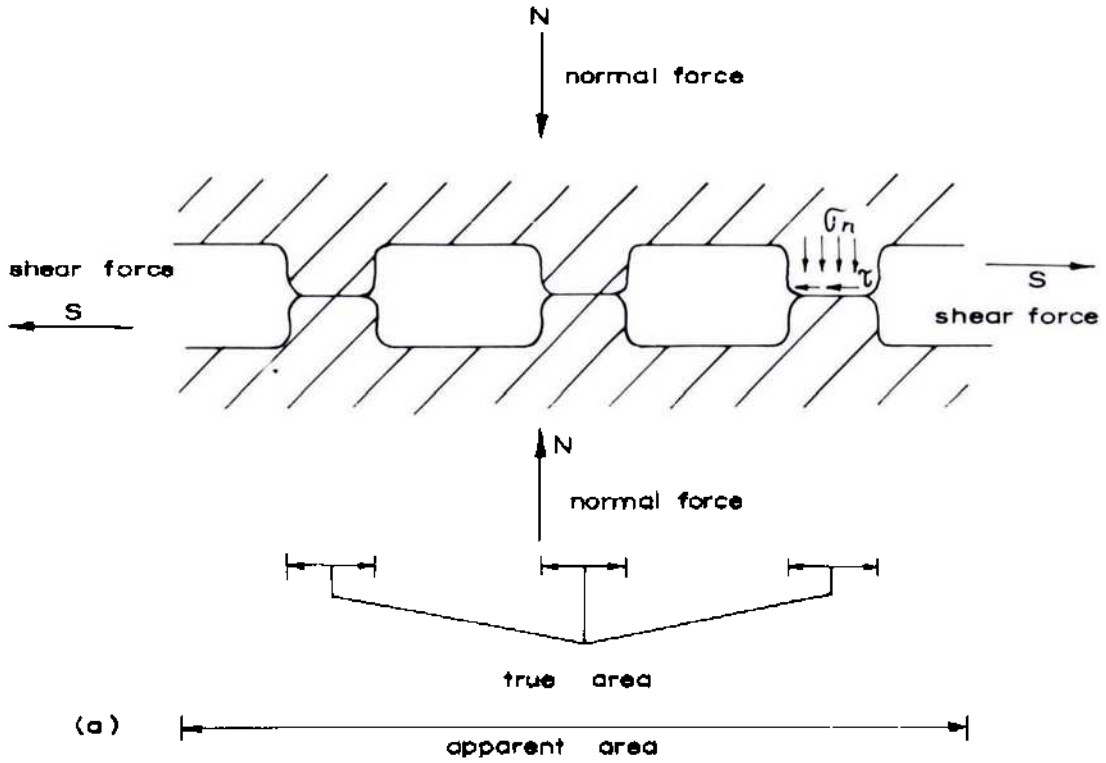

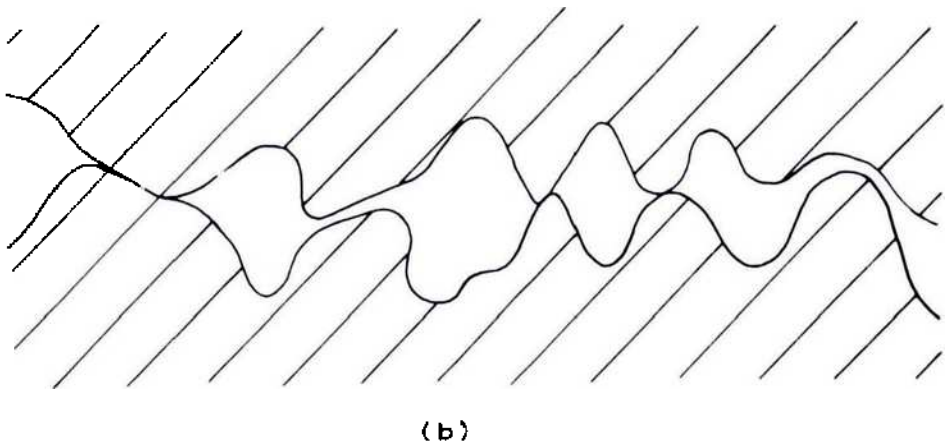

Fig. 10-5. (a) Contact of asperities
(b) Interlocking of asperities
(after EINSTEIN, BRUHN and HIRSCHFELD, 1970).

After a pair of interlocked asperities have ridden over up to a certain level, the stresses in the asperity will reach the strength of the asperity and the asperity will shear off at this level. This stage can be represented by equation

$$S = K + N\tan\phi \tag{10.3}$$

where ϕ_r = angle of residual shearing resistance of the material and
K = constant, equal to the ordinate of the intersection with the shear force axis of the straight line that can be used to approximate the S- N curve at relatively high normal force (Fig. 10-6).

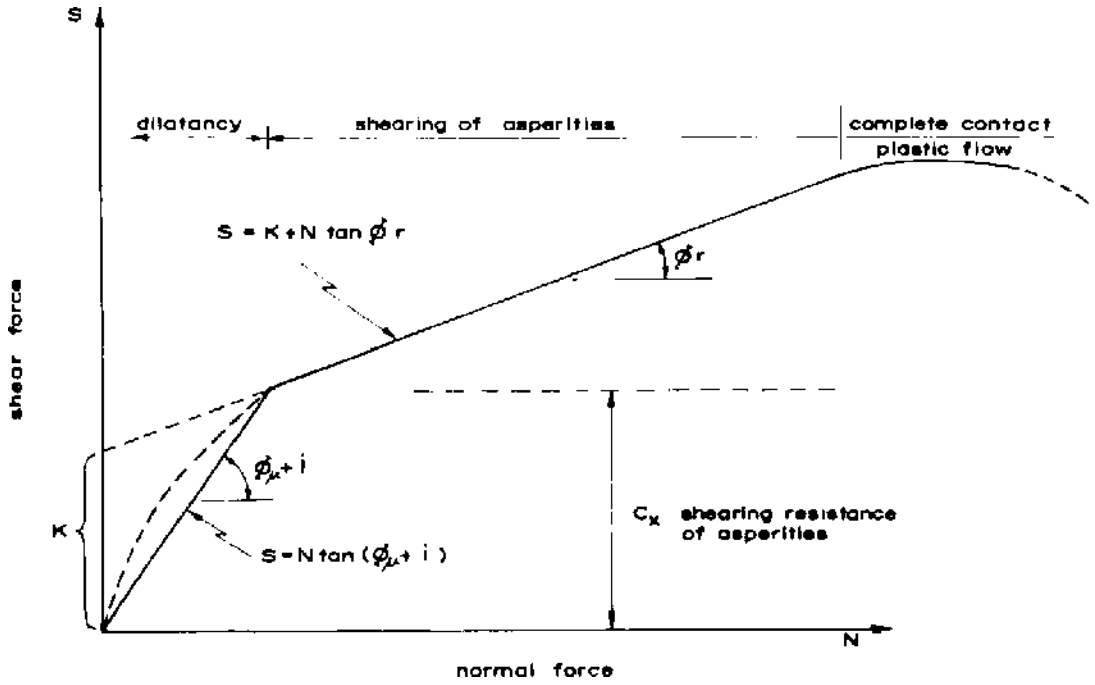

Fig. 10-6. Dilatancy of specimen and shearing of asperities in a typical MOHR's envelope.

The riding over of the asperities gives rise to changes in the value of deformation at right angles to the direction of application of shear force which has been termed "dilatancy". A schematic representation of dilatancy and the shear force versus displacement curves are given in Fig. 10-7.

Equations 10.2 and 10.3 are valid only when shearing takes place along a surface conforming with the geometry of the asperities and with full degree of interlocking. These assumptions are rarely true. In practice the distribution of interlocking at different points of contact is different and this influences the friction effect. CORTHOUTS (1966) simulated the process of dilatancy and shearing of asperities in a finite element programme using two asperities which are at 45° inclined to the horizontal and also symmetrical. The stresses caused by a combination of transverse and normal external loading were computed to determine

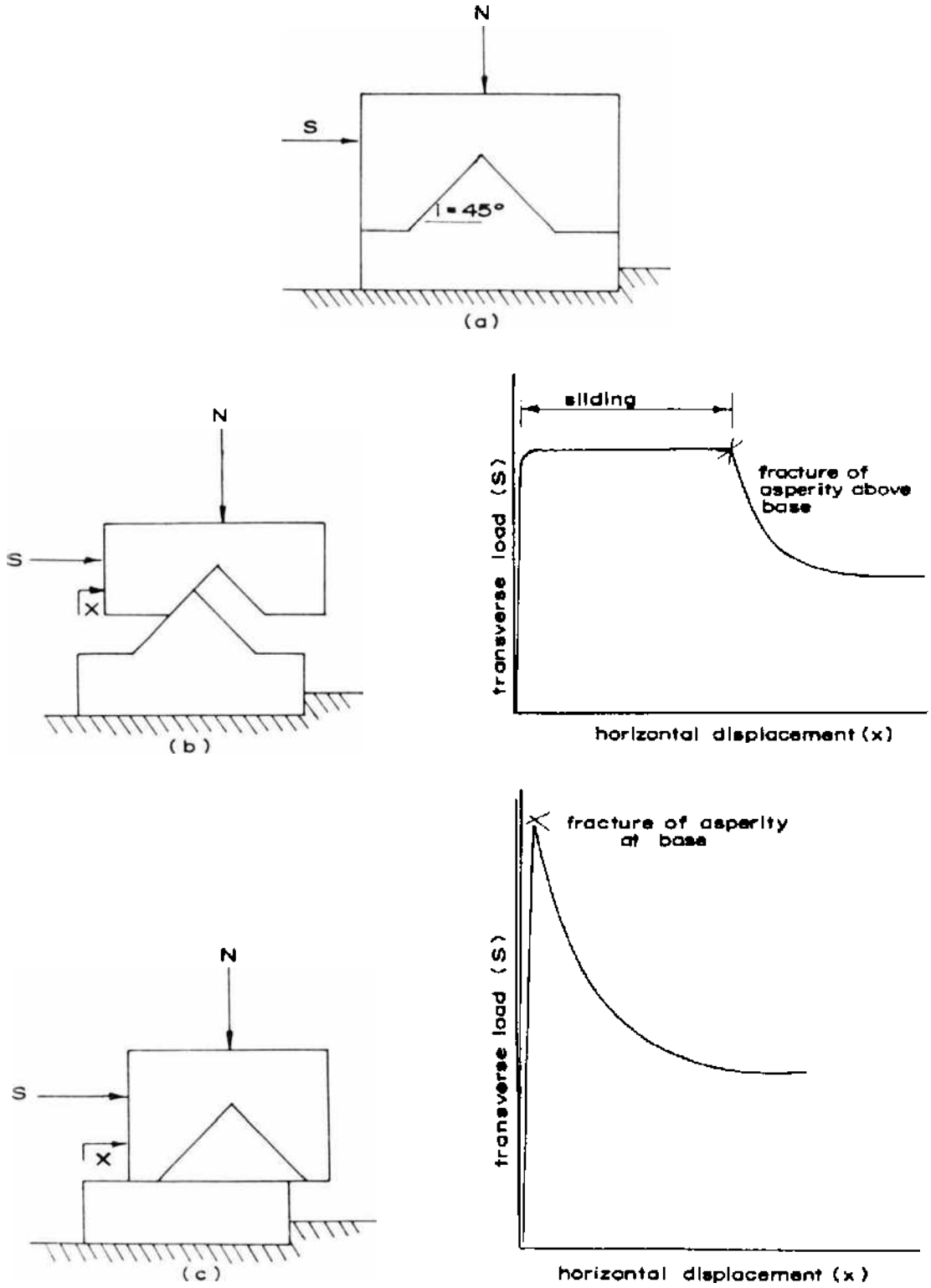

Fig. 10-7. The mechanism of dilatancy and shearing of the asperity with the corresponding load - displacement curves.
(a) Initial state (before displacement)
(b) Displacement with dilatancy and shear at a later stage
(c) Shearing without dilatancy
(after EINSTEIN, BRUHN and HIRSCHFELD, 1970).

if in any element along the line B – C – D (Fig. 10-8) the tensile stresses are greater than the tensile strength. The transverse and normal loads are changed till the tensile stress is greater than the tensile strength when the shearing off of the asperity takes place and then the external loading conditions are terminated. If no failure occurs due to tensile stresses, the computer programme checks if the average shear stress along the line B–C (Fig. 10-8a) is greater than that allowed by the relationship

$$\tau_1 = \sigma_n \tan \phi_\mu \tag{10.4}$$

where τ_1 = shear strength of the material and
σ_n = normal stress.

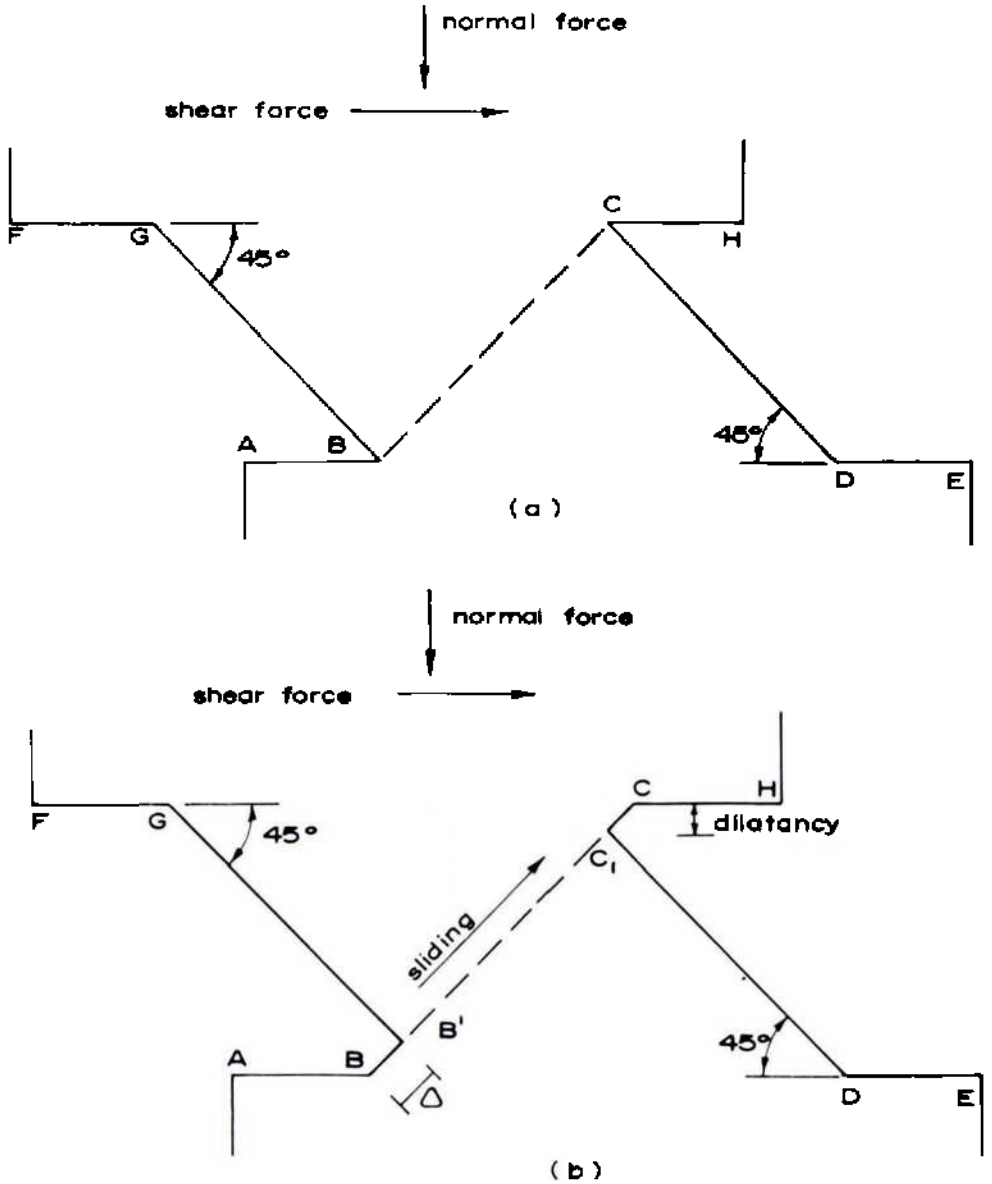

Fig. 10-8. Analytical model used by CORTHOUTS (1966) for finite element analysis. The model consists of two asperities subjected to normal and shear forces.
(a) Initial situation (b) First step after sliding.

If the average mobilised shear stress τ is greater than $\sigma_n \tan\phi_\mu$ i.e. if sliding and dilatancy occur, a small displacement Δ along B–C is introduced and the computing cycle is repeated to check if the shear failure occurs in the asperity or if further dilatancy will take place. Taking $\phi_\mu = 11.3$ CORTHOUTS obtained the bilinear MOHR's envelope as shown in Fig. 10-9. According to the static relationship of Eq. 10.2, the slope of the two linear portions of the envelope should be $(\phi_\mu + i)$ and (ϕ_μ) or 56.3° and 11.3°. The corresponding values for the envelopes determined using the finite element method were 71.5 and 15.6 showing thereby large discrepancies.

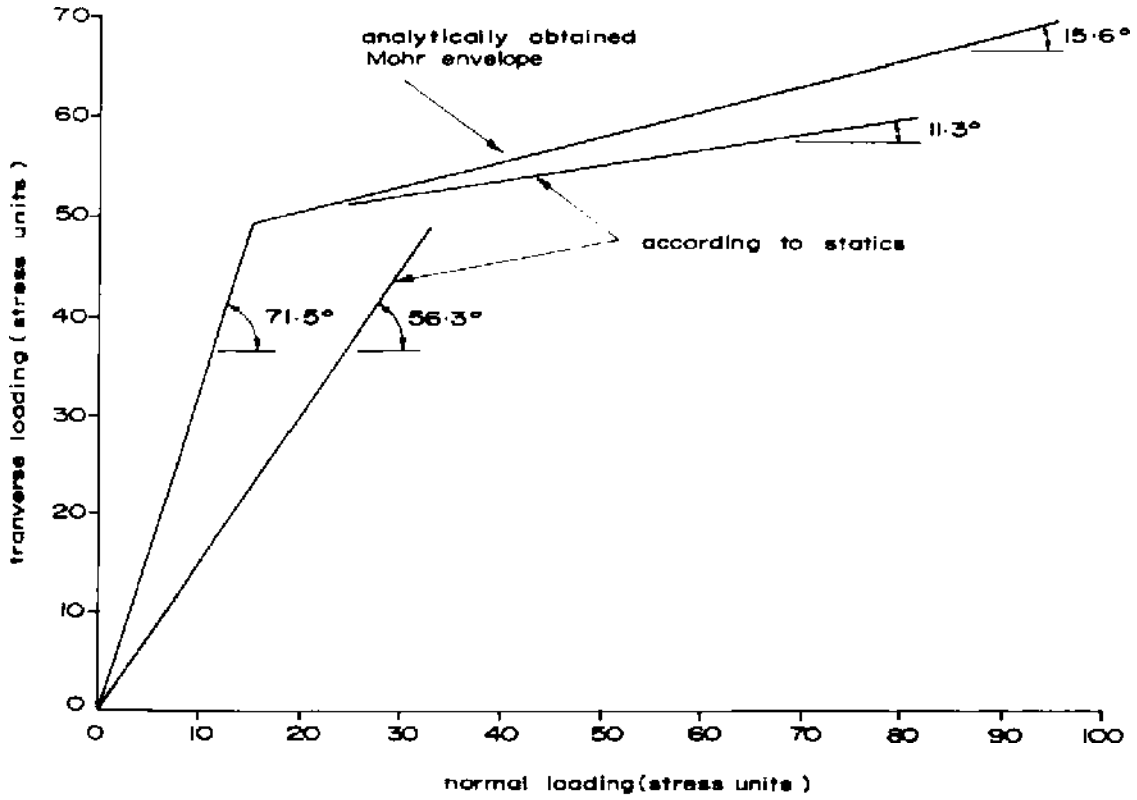

Fig. 10-9. Comparison between the MOHR's envelopes for two asperities obtained by CORTHOUTS (1966) for the case shown in Fig. 10-8 ($\Phi_\mu = 11.3$, $\sigma_1 = 3090$ lbf/in^2).

According to LADANYI and ARCHAMBAULT (1969), the fact that the experimental envelopes deviate from the bilinear model and lie considerably lower is due, firstly, to the sensible loss of interlock before failure as a result of small displacement which is essential to mobilise the sliding friction and, secondly, the non-uniform stress distribution on the surface of the asperities which partially break the asperities before the maximum strength is reached. As such more detailed analysis of the shear test is required.

ROWE, BARDEN and LEE (1964) considered the direct shear test in detail. According to them, the shear force S may be divided into 3 components

$$S = S_1 + S_2 + S_3 \tag{10.5}$$

where S_1 = shear force component due to external work done in dilating against the external normal force N

S_2 = shear force component due to additional internal work done in friction due to dilatancy and

S_3 = shear force component due to work done in internal friction if the specimen did not change in volume in shear.

With reference to Fig. 10-10, it can be seen that

$$S_1 dx = N dy; \qquad S_1 = N \frac{dy}{dx} \tag{10.6}$$

or

$$S_1 = N \tan i$$
$$= N\dot{V}$$

where $\dot{V}$ = rate of dilation at failure, i.e. $\frac{dy}{dx}$.

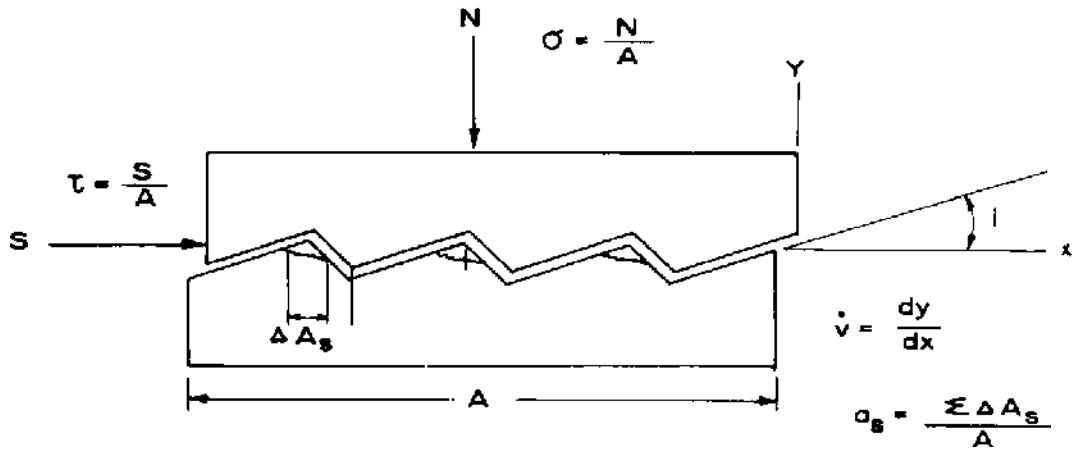

Fig. 10-10. Definition of the dilation rate $\dot{V}$ and the shear area ratio of a_s.

Since $(S_2 \cos i)$ is the shear stress parallel to the plane of sliding and $(S \sin i)$ is the total force normal to the plane arising simply because of the dilation when $i \neq 0$

$$S_2 \cos i = S \sin i \tan \phi_\mu \tag{107}$$

$$S_2 = S \tan i \tan \phi_\mu$$
$$= S\dot{V} \tan \phi_\mu \tag{108}$$

As it shall be shown later that the value of μ is not constant and depends upon the roughness of the surface, asperity orientation, etc., Equation 10.8 can better be written down as

$$S_2 = S\dot{V}\tan\phi_f$$

where ϕ_f denotes the statistical average value of the friction angle when sliding occurs along the irregularities of different orientations.

ROWE, BARDEN and LEE (1964) gave the value of $\phi_f = \phi_\mu$ for highly packed sand, but for loose media its value may be $\phi_f = \phi_\mu + 50\%$.

When there is no dilation, i.e. an ideally flat surface

$$S_3 = N\tan\phi_\mu \tag{10.9}$$

Thus, from Eqs. 10.6, 10.8 and 10.9

$$S = N\tan i + S\tan i\tan\phi_\mu + N\tan\phi_\mu$$

or

$$\frac{S}{N} = \tan i + \frac{S}{N}\tan i\tan\phi_\mu + \tan\phi_\mu$$

$$= \tan(\phi_\mu + i) \tag{10.10}$$

Thus the equation obtained by substituting the values of S_1, S_2, S_3 in Eq. 10.5 is the same as Eq. 10.2.

LADANYI and ARCHAMBAULT (1969) carried the argument further by stating that by shearing along an irregular rock surface there is the fourth component which occurs as a result of the shearing of the teeth and the value of this component (S_4) may be determined by assuming that all the teeth are sheared off at the base. The shear force, S_4 then may be equal to

$$S_4 = AK + N\tan\phi_0 \tag{10.11}$$

where A = total projected area of the teeth at the plane of shear and
K and ϕ_0 = the COULOMB shear parameters related to the strength of the rock substance.

In reality, in shearing along an irregular surface the two modes of failure occur simultaneously, i.e. sliding and shearing. If the asperities are sheared off only over a portion of the projected area given by, A_s, i.e. $\Sigma A A_s$ and sliding occurs over the area $(A - A_s)$, then the total shear force can be written by,

$$S = (S_1 + S_2 + S_3)(1 - a_s) + S_4 a_s \tag{10.12}$$

where $a_s = A_s/A$ and is called the shear area ratio.

Substituting the values of S_1, S_2, S_3, S_4 in Eq. 10.12, and dividing by the area A, the following expression is obtained for the conventional shear strength τ:

$$\tau = \frac{S}{A} = \frac{\sigma_n(1-a_s)(\dot{V}+\tan\phi_\mu)+(\sigma_n\tan\phi_0+K)a_s}{1-(1-a_s)\dot{V}\tan\phi_\mu} \qquad (10.13)$$

When $\dot{V}=0$.

$$\tau = \sigma_n(1-a_s)\tan\phi_\mu + a_s(\sigma_n\tan\phi_0+K) \qquad (10.14)$$

which gives the shear strength of a partially cemented flat shear plane or a discontinuous joint surface.

For engineering practice the use of these equations requires the knowledge of the parameters a_s, ϕ_0, ϕ_μ, K, and V. The value of ϕ_μ can be obtained by performing tests at low normal pressure for flat surfaces such that $a_s \simeq 0$ and the value can be calculated from the relationship

$$\tan\phi_\mu = \frac{(\tau/\sigma_n)-\dot{V}}{1+\dot{V}(\tau/\sigma_n)} \qquad (10.15)$$

which has been obtained from Eq. 10.13 by putting $a_s = 0$.

To overcome the difficulty of determining the value of K and ϕ_0 (or ϕ_r) and keeping in view that MOHR's envelope will not consist of two straight lines but of an initially curved shape (shown dotted in Fig. 10-6) as a result of different heights and inclinations of a multiple of asperities which get sheared off at different stages, a modification of the above is necessary. The initial stage of the MOHR's envelope is also associated with large dilatancy in the direction normal to the plane of sliding. If the dilatancy is restricted at this stage (as may happen in nature), this will tend to magnify the influence of interlocking and the MOHR's evelope assumes a straight line curve. As such, LADANYI and ARCHAMBAULT (1969) used the parabolic law proposed by FAIRHURST (1964) instead of the original straight line concept. According to FAIRHURST (1964)

$$\tau = \sigma_c\left(\frac{m-1}{n}\right)\left(1+n\frac{\sigma_n}{\sigma_c}\right)^{1/2}$$

where $n = \dfrac{\sigma_c}{-\sigma_t}$

σ_c = uniaxial compressive strength of solid rock
σ_t = uniaxial tensile strength of solid rock and
$m = (n+1)^2$.

Equation 10.13 then becomes

$$\tau = \frac{\sigma_n(1-a_s)(\dot{V}+\tan\phi_\mu)+a_s\sigma_c\left(\frac{m-1}{n}\right)\left(1+n\frac{\sigma_n}{\sigma_c}\right)^{1/2}}{1-(1-a_s)\dot{V}\tan\phi_\mu} \qquad (10.16)$$

The above discussion is valid as long as the cracks are tightly closed and interlocking is complete. In case the interlocking is not complete and cracks get partially opened up, which invariably happens before any failure takes place (MULLER and HOFMANN, 1970), the actual contact area will decrease and the degree of interlocking will cease to be unity. If the degree of interlocking be given by η, the true shear and normal stresses will increase and can be given by

$$\tau' = \tau/\eta$$
$$\sigma' = (\sigma_n/\eta)$$
$$\eta = \left(1-\frac{\Delta X}{\Delta L}\right)$$

where ΔX = open projected length (Fig. 10-11 a) and
ΔL = total projected length of asperity.

The total area to be sheared off will decrease by a multiple of η, and hence Eq. 10-13 will become

$$\tau = \frac{\sigma_n(1-a_s)(\dot{V}+\tan\phi_\mu)+a_s(\sigma_n\tan\phi_0+K\eta)}{1-(1-a_s)\dot{V}\tan\phi_\mu} \qquad (10.17)$$

and Eq. 10.16 will become

$$\tau = \frac{\sigma_n(1-a_s)(\dot{V}+\tan\phi_\mu)+a_s\eta\sigma_c\left(\frac{m-1}{n}\right)\left(1+\frac{\eta\sigma_n}{\eta\sigma_c}\right)^{1/2}}{1-(1-a_s)\dot{V}\tan\phi_\mu} \qquad (10.18)$$

This decrease in interlocking exerts a marked influence on the shear strength manifested by the rock mass. Graphically, these are represented in Fig. 10-11. LADANYI and ARCHAMBAULT (1972) found quite good correlation between this equation and the shear strength of models composed of small elements in a biaxial shear test.

The values of a_s, $\dot{V}$ and η in Eq. 10.18 require to be determined for a given rock surface and as yet no correlation has been obtained between these para-

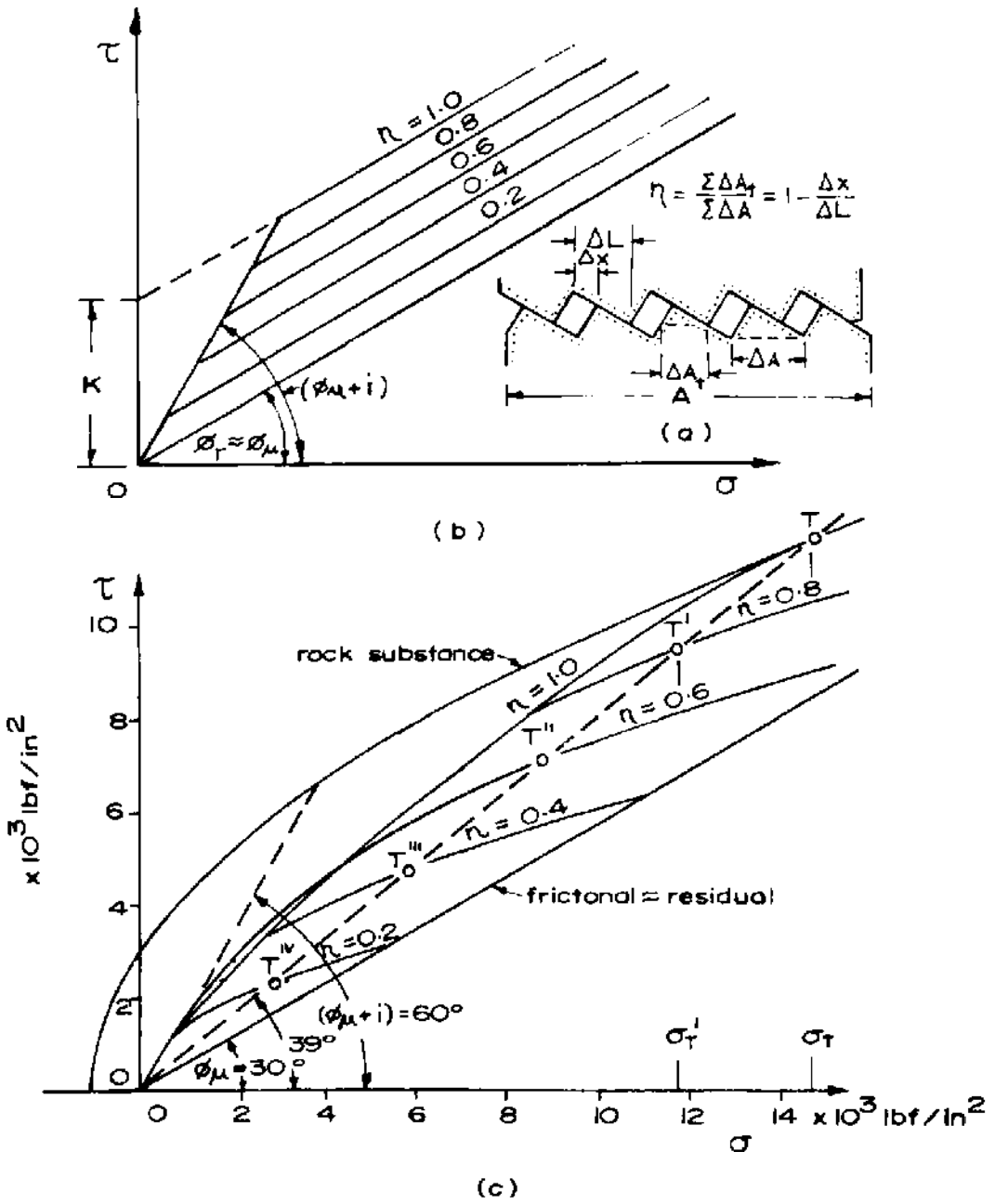

Fig. 10-11. Influence of decreasing degree of interlocking of asperities on the shear strength along irregular rock surfaces.
(a) Definition of the degree of interlocking
(b) Results according to bilinear model
(c) Results according to Equation 10.18.
(after LADANYI and ARCHAMBAULT, 1969).

meters and normal stress and rock surface type. Under the assumption that no shearing of the asperity takes place then $a_s = A_s/A \to o$, $(A_s \to 0)$ and $\dot{V} \to \tan i$. This will happen at an extremely small normal stress. At extremely high normal stresses when the asperities are completely sheared off $A_s \to 1$

and $\dot{V} \to 0$. At intermediate values of normal stress, the values of a_s and $\dot{V}$ will vary from 0 to 1 with a_s increasing from 0 to 1 with increase in stress and $\dot{V}$ decreasing from 1 to 0. Approximate values of the two can be obtained from the following relationships under the limits $0 < \sigma_n < \sigma_T$:

$$a_s \simeq 1 - \left(1 - \frac{\sigma_n}{\sigma_T}\right)^{k_1} \tag{10.19}$$

$$\text{and} \quad \dot{V} \simeq \left(1 - \frac{\sigma_n}{\sigma_T}\right) \tan i \tag{10.20}$$

where σ_T = transition normal stress at which $a_s = 1$ and $\dot{V} = 0$

k_1 = constant $\simeq \frac{3}{2}$ and

k_2 = constant $\simeq 4$.

The value of σ_T could be taken as the point where the normal stress is so high that the pre-existing joint has no influence on the specimen strength and this represents the intersection of the MOHR envelope for the joint with the MOHR envelope for the rock substance (Fig. 10-11; point T on the envelope) which corresponds to the line with an inclination of 39° and passing through the origin (MOGI, 1966) separating the region of ductile and brittle failures. The inclination is only an average value of different rock types and varies from rock to rock, for example, granites have higher value and limestones lower (MOGI, 1972). BYERLEE (1968a) also expressed that the inclination does not seem to be independent of the rock type.

10.3. Influence of the Configuration of the System with Respect to the Stress Field

The influence of the configuration of the joint system with respect to the stress field is a complex problem and studies have been made only in a limited number of simple cases. Most of the theoretical studies conducted so far relate to the following aspects:

1. Single joint orientation.
2. Double or multiple joint orientation.

10.3.1. Single Joint Orientation

The influence of a single joint orientation has been explained by considering a two dimensional theory, assuming that the simple criterion of slip along a plane as given by Eq. 10-3 applies. In a biaxial plane stress case, it can be easily proved that (Fig. 10-12)

$$\sigma_n = {}^1/_2(\sigma_1+\sigma_2)+{}^1/_2(\sigma_1-\sigma_2)\cos 2\alpha \tag{10.21}$$

and $$\tau = -{}^1/_2(\sigma_1-\sigma_2)\sin 2\alpha \tag{10.22}$$

where σ_1 and σ_2 = principal stresses

α = the angle which the normal to the plane of weakness makes with the major principal stress σ_1 and

σ_n and τ = normal and shear stresses on the plane of weakness.

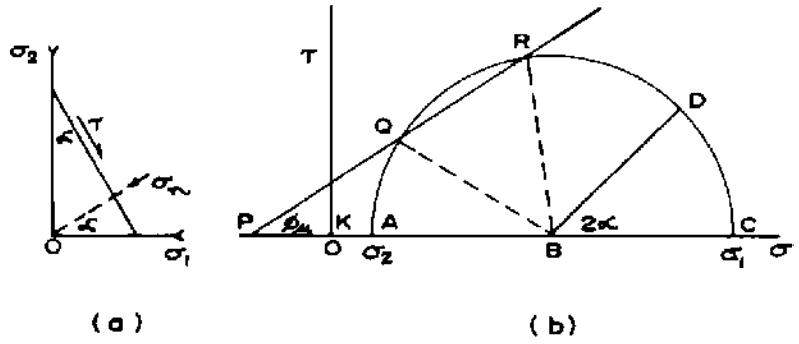

Fig. 10-12. Sliding on a plane of weakness: two-dimensional theory.

Putting

$$\sigma_m = {}^1/_2(\sigma_1+\sigma_2)$$
$$\tau_m = {}^1/_2(\sigma_1-\sigma_2)$$

into Eqs. 10.21 and 10.22

$$\sigma_n = \sigma_m+\tau_m\cos 2\alpha \tag{10.23}$$
$$\tau = -\tau_m\sin 2\alpha \tag{10.24}$$

Putting $\tan\phi_\mu = \mu$ and using Eqs. 10.23 and 10.24, the Eq. 10.3 can be rewritten in the form (JAEGER and COOK, 1969a)

$$\tau_m[\sin 2\alpha-\tan\phi_\mu\cos 2\alpha] = K+\sigma_m\tan\phi_\mu \tag{10.25}$$

or $$\tau_m = (\sigma_m+K\cot\phi_\mu)\tan\delta \tag{10.26}$$

where $$\tan\delta = \sin\phi_\mu\,\mathrm{cosec}\,(2\alpha-\phi_\mu) \tag{10.27}$$

Alternatively, the criterion of slip can be written down

$$\sigma_1-\sigma_2 = \frac{2K+2\mu\sigma_2}{(1-\mu\cot\alpha)\sin 2\alpha} \tag{10.28}$$

and if $n = \dfrac{\sigma_2}{\sigma_1}$, then

$$\sigma_1 = \frac{2K\cot\phi_\mu}{(1-n)\sin(2\alpha-\phi_\mu)\operatorname{cosec}\phi_\mu-(1+n)} \tag{10.29}$$

The Eqs. 10.25, 10.26, 10.28, and 10.29 are the different ways which represent the same criterion. It is seen from the Eq. 10.28 that the stress difference necessary to cause failure varies with α and as $\alpha \to \frac{\pi}{2}$, i.e. the plane moves towards the direction of σ_1, $\sigma_1-\sigma_2 \to \infty$. Also, when the $\alpha \to \tan^{-1}\mu = \phi_\mu$, the value of $\sigma_1-\sigma_2 \to \infty$. This means that failure is possible only when $\phi_\mu < \alpha < \frac{\pi}{2}$, and the minimum value of $(\sigma_1-\sigma_2)$ can be given by

$$(\sigma_1-\sigma_2) = 2(K+\mu\sigma_2)\left[(\mu^2+1)^{1/2}+\mu\right] \tag{10.30}$$

The variation of σ_1 with α for the case $\mu = 0.5$ is shown in Fig. 10-13 for various values of σ_2. This situation is also made clear from MOHR diagram (Fig. 10-12b). The criterion for failure is represented by the line $P-Q-R$

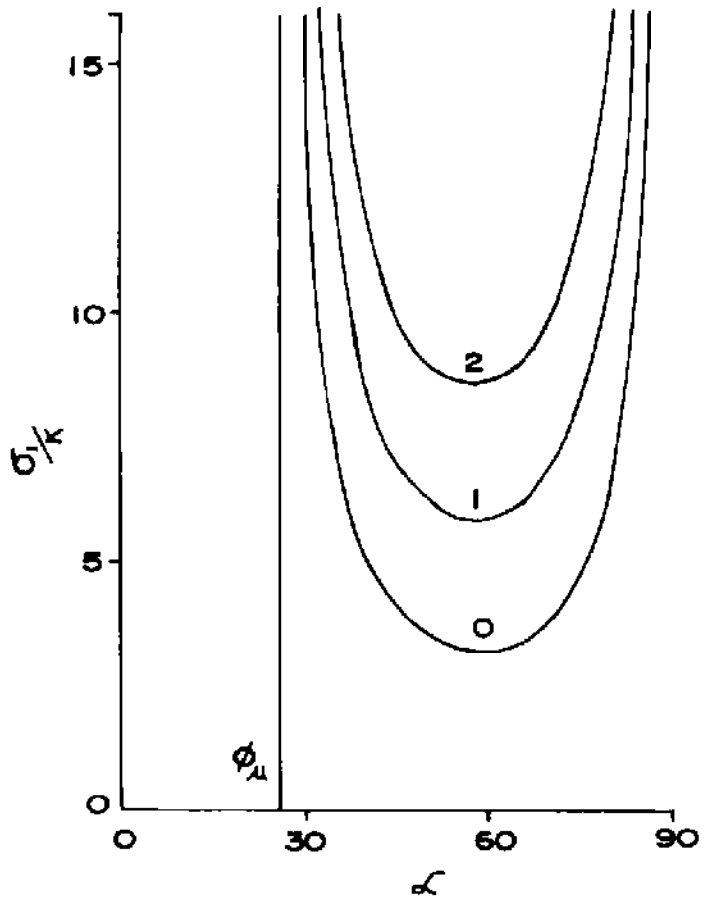

Fig. 10-13. The variation of σ_1 with α for sliding on a plane of weakness with $\mu = 0.5$. Numbers on the curves are the values of σ_2/K (after JAEGER and COOK, 1969a).

inclined at an angle ϕ_μ to the $0-\sigma$ axis and making an intercept $OP = -K \cot \phi_\mu$ on this axis. If σ_1 and σ_2 are the principal stresses, the normal and shear stresses across the plane whose normal is inclined at α to the σ_1 direction are represented by the point D on the MOHR circle on AC as diameter. If D lies in either of the arcs $A-Q$ or $R-C$, these stresses will not be sufficient to cause slip but if it lies in the arc $Q-R$, then stresses will be sufficient to cause slip.

The above theory is applicable for (*i*) the sliding across open joints in which case K will be the shear strength of the joint and μ the coefficient of friction of the joint; (*ii*) the sliding along filled joints where K will be the shear strength of the filling material and μ coefficient of internal friction of the filling material; (*iii*) the anisotropic material with parallel planes of weakness which behave in the same way as materials with planes of weaknesses.

There is, however, a possibility that failure may take place through the material in a plane which intersects the plane of weakness. If the inherent shear strength of the material is S_0 and the coefficient of internal friction (COULOMB criterion concept) μ_0, and assuming that there is a plane of weakness whose normal is inclined at an angle of α with the greatest principal stress σ_1 such that $S_0 > K$ and $\mu_0 > \mu$, the situation can be represented by Fig. 10-14a.

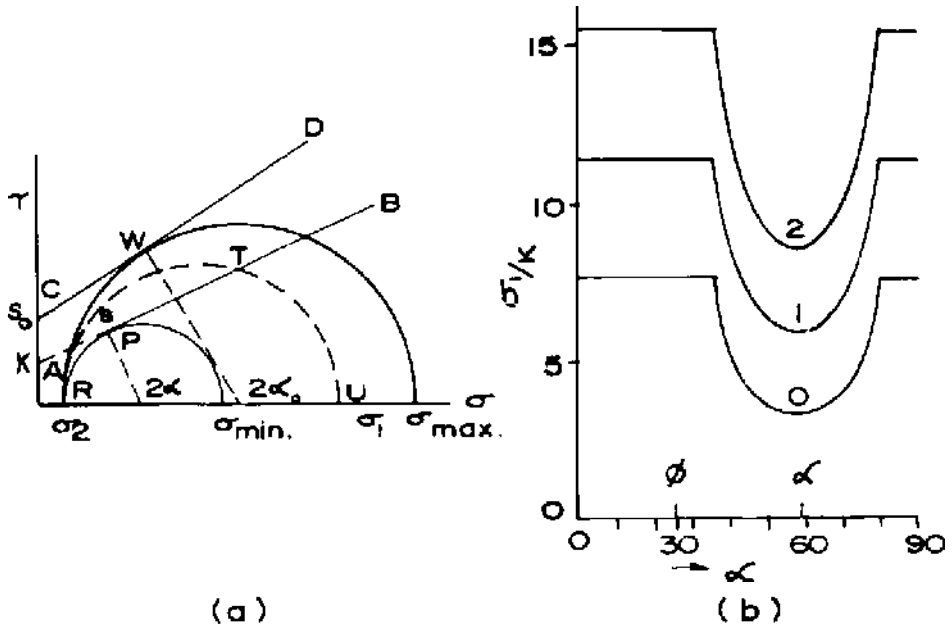

Fig. 10-14. (a) Fracture in and across parallel planes of weakness in a material
(b) Variation of σ_1 with α for the case $\mu = 0.5$, $\mu_0 = 0.7$, $S_0 = 2K$
Numbers on the curves refer to the ratio σ_2/K
(after JAEGER and COOK, 1969a).

As already shown, failure is possible when $\phi_\mu < \alpha < \frac{\pi}{2}$, and the criterion of slip between these limits can be represented by Eq. 10.28 which can be rewritten as follows:

$$\sigma_1 = \sigma_2 + \frac{2K + 2\mu\sigma_2}{(1 - \mu\cot\alpha)(\sin 2\alpha)} \tag{10.31}$$

For a given value of σ_2, the minimum value of σ_1 (σ_{min}) occurs when

$$\tan 2\alpha = -\frac{1}{\mu}$$

$$\sigma_{min} = \sigma_2 + 2(K + \mu\sigma_2)[(\mu^2 + 1)^{1/2} + \mu)] \tag{10.32}$$

If the value of σ_2 is constant, and σ_1 is increased, to the point when $\sigma_1 = \sigma_{min}$, failure will occur on the plane represented by the line $A - B$ (Fig. 10-14a), i.e. along the plane of weakness α, but if it is possible to increase the stress conditions such that $\sigma_1 = \sigma_{max}$, then failure is possible along the plane represented by the line $C - D$ (Fig. 10-14a), i.e. along the plane of weakness α_0. Since the line $C - D$ represents the MOHR envelope for the solid material, the maximum value of σ_1 can then be represented by

$$\sigma_{max} = \sigma_2 + 2(S_0 + \mu_0\sigma_2)[(\mu_0^2 + 1)^{1/2} + \mu_0] \tag{10.33}$$

Thus minimum and maximum values of σ_1 are represented by Eqs. 10.32 and 10.33 when the angle of possible failure varies from α to α_0. The variation of σ_1 with α for a particular case is shown in Fig. 10.14b. The influence of the stress value σ_2 is simply to raise the curves up. It shall be of interest to state that the experimental results obtained by a number of investigators are more or less in accordance with the above (HOEK, 1964; JAEGER and ROSENGREN, 1969; EINSTEIN, BRUHN and HIRSCHFELD, 1970; HORINO and ELLICKSON, 1970).

Another very simple way of representation which is quite useful from practical engineering point of view is by making use of the σ_1/σ_2 ratio. Thus in MOHR circle representation when the normal stresses and shear stresses can be represented by Eqs. 10.21 and 10.22 and the equilibrium criterion by Eq. 10.3; by putting Eqs. 10.21 and 10.22 into Eq. 10.3 and rearranging it, the equilibrium condition can be put as

$$\sigma_1 = \frac{\sigma_2[\sin(2\alpha - \phi_\mu) + \sin\phi_\mu] + 2K\cos\phi_\mu}{\sin(2\alpha - \phi_\mu) - \sin\phi_\mu} \tag{10.34}$$

or when $K = 0$

$$\frac{\sigma_1}{\sigma_2} = \frac{\sin(2\alpha - \phi_\mu) + \sin\phi_\mu}{\sin(2\alpha - \phi_\mu) - \sin\phi_\mu} \tag{10.35}$$

The results of Eq. 10.35 when plotted in polar co-ordinates for different values of σ_1/σ_2 and ϕ_μ and α, are shown in Fig. 10-17 (consider the parabolas for each joint set separately). This indicates that decreasing the value of ϕ_μ is to make the region of slippage wider and hence increasing the chance of slippage.

10.3.2. Double or Multiple Joint Orientation

The case of a multiple joint orientation can be studied by considering a three dimensional case. The three dimensional case can be represented quite easily by MOHR's representation. Fig. 10-12b can be slightly modified by shifting the line of origin from 0 to the point P which means that the different stresses σ_1 and σ_2 have been increased by the amount $OP = \dfrac{K}{\mu}$. Similarly, if there be any pore pressure to be taken into account, this can easily be done by making use of the "effective stress concept" which replaces σ_1, σ_2 and σ_3 by $\sigma_1 - p$, $\sigma_2 - p$, $\sigma_3 - p$. Thus for a general case, MOHR envelope can be represented by replacing the values of σ_1, σ_2, σ_3, by the effective stress values as follows:

$$\begin{aligned} \sigma_1' &= \sigma_1 - p + (K/\mu) \\ \sigma_2' &= \sigma_2 - p + (K/\mu) \\ \sigma_3' &= \sigma_3 - p + (K/\mu) \end{aligned} \tag{10.36}$$

and COULOMB's criterion is reduced to

$$\tau = \mu\sigma \tag{10.37}$$

Two extreme cases can be considered; first when $\sigma_1' > \sigma_2' = \sigma_3'$, and second $\sigma_1' = \sigma_2' > \sigma_3'$. In the first case there is symmetry about the σ_1' axis and in the second case there is symmetry about the σ_3' axis. These cases can be represented by Fig. 10-15a, assuming that σ_1' is the greatest principal stress and σ_3' is the least principal stress, the value of σ_2' lies between the two extremes. The line $0 - C$ represents the failure criterion. The sliding can take place only when the normals to the joints correspond to the points on the arc M and N and make an angle α_1 and α_2 with the σ_1' direction. This result can also be represented in Fig. 10-15b which shows the direction of the principal stress in an octant of a unit sphere. Under the conditions of $\sigma_1 > \sigma_2 = \sigma_3$, possible slip planes are those whose normals make angles α_1 and α_2 with σ_1' and lie in the zone $ABCD$ symmetrical about σ_1' axis. Under the conditions $\sigma_1' = \sigma_2' > \sigma_3'$, possible slip planes are those whose normals make angles of $90 - \alpha_1$ and $90 - \alpha_2$ with σ_3' and lie in the zone $ADEF$ symmetrical about the σ_3' axis.

This makes very clear the influence of the intermediate stress as it varies between the two extremes (intermediate principal stress σ_2' changes from

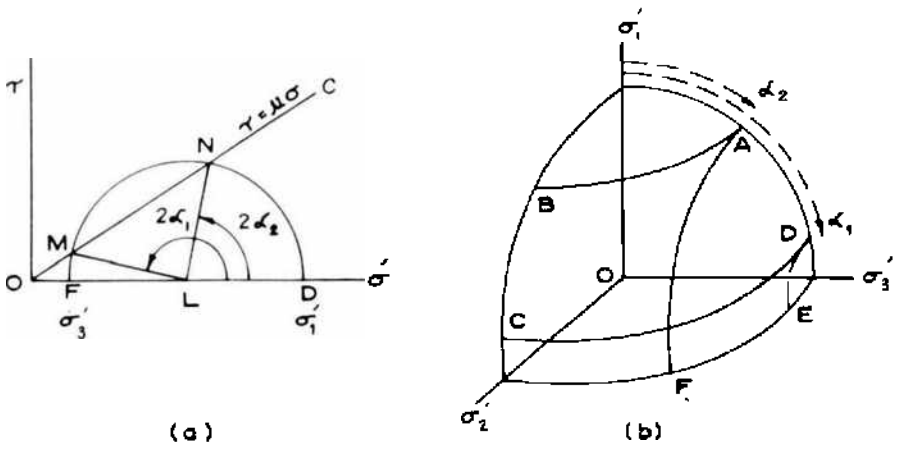

Fig. 10-15. (a) MOHR's diagram for the cases $\sigma_2' = \sigma_3'$ or $\sigma_2' = \sigma_1'$
(b) An octant of a sphere showing the region ABCD in which sliding is possible if $\sigma_2' = \sigma_3'$ and the region ADEF in which sliding is possible when $\sigma_1' = \sigma_2'$
(after JAEGER and COOK, 1969a).

$\sigma_2' = \sigma_3'$ to $\sigma_2' = \sigma_1'$) on the solid angle within which angle normal to the plane of weakness must lie for possible slip to occur. For different combinations of the principal stresses, and different values of μ, different patterns of equal area projection nets are shown in Fig. 10-16 (for details see Appendix V).

The influence of two (or even more) joints occurring together can be clearly shown using the interpretation given in Fig. 10-17. In this it is possible to superimpose two joints or joint groups. Fig. 10-17 shows two joint systems k_1 and k_2 placed at an angle of 90° to each other for different values ϕ_μ (joint k_1, $\phi_\mu = 40°$ and 25°) plotted in polar coordinate system. Depending upon the angle of orientation of these joints with respect to the principal stress conditions the possibilities of sliding can be marked.

KUZNECOV (1970) utilised the above graphical technique for 3 types of joints and gave examples to calculate the possible direction of failure and movement for a given stress field and the technique is now widely used in the design of rock slopes (HOEK and BRAY, 1974).

There are certain limitations of the theory outlined above. The theory assumes that criterion along a joint slippage can be represented by the simple equation given in Eq. 10.3. As already indicated, this is not quite true and this is bound to have some effects on the results so represented. It is also assumed that stress distribution in rock mass as a result of the jointed nature of the system is uniform in the system and remains unchanged even when the system is deformed. This is far from true. There is a third condition which assumes that failure takes place as a shear failure along a plane. Certain experimental observations have shown that the failure of a jointed mass is also associated with rotation and bending of the individual blocks resulting in the developing of tensile cracks. This theory does not take into account this phenomenon.

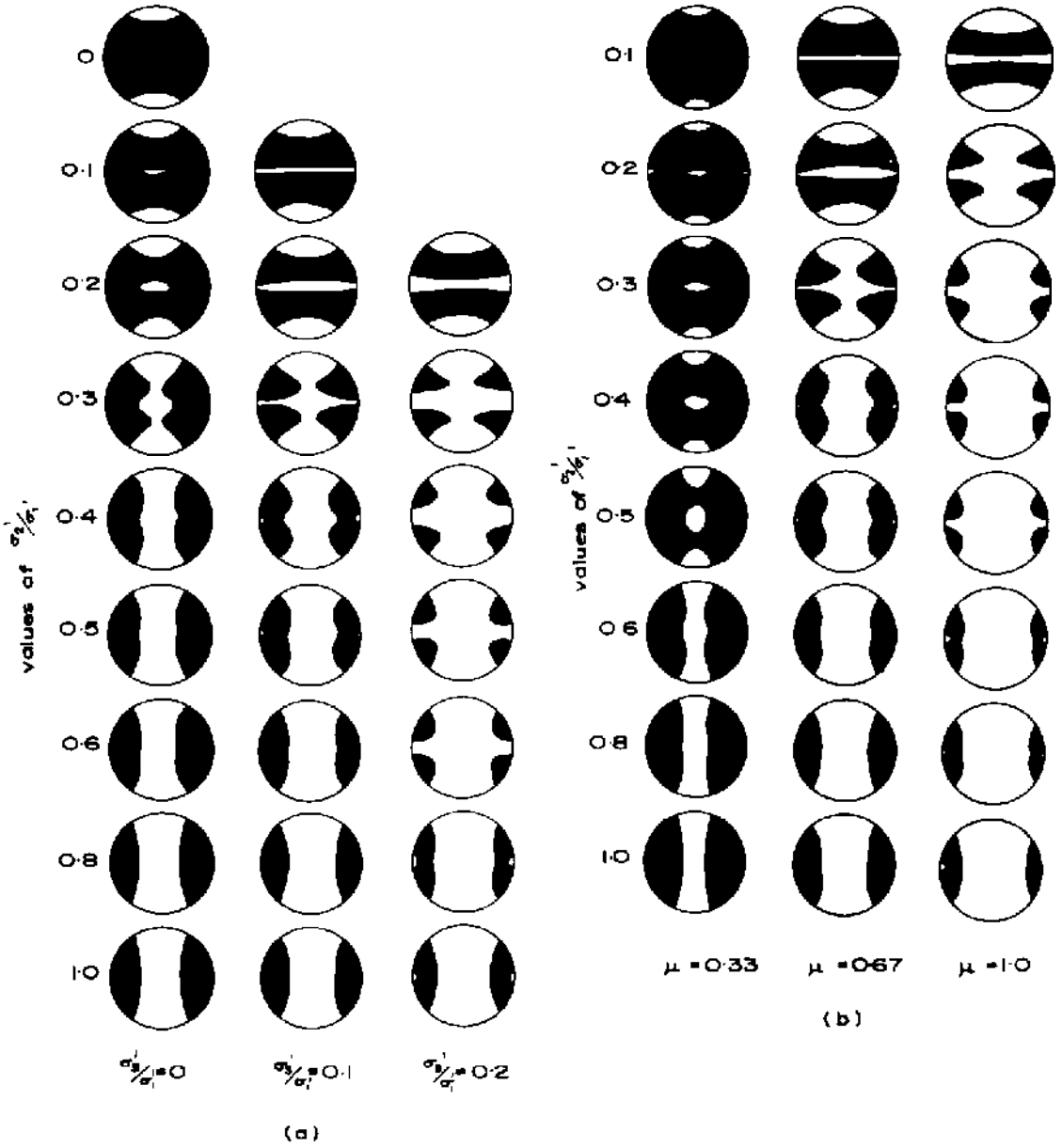

Fig. 10-16. Equal area projections showing the areas (shaded) where slip is possible
(a) for $\mu = \frac{2}{3}$ and various values of $\frac{\sigma_2'}{\sigma_1'}$ and $\frac{\sigma_3'}{\sigma_1'}$
(b) for $\frac{\sigma_3'}{\sigma_1'} = 0.1$ and various values of $\frac{\sigma_2'}{\sigma_1'}$ and μ
(after JAEGER and ROSENGREN, 1969).

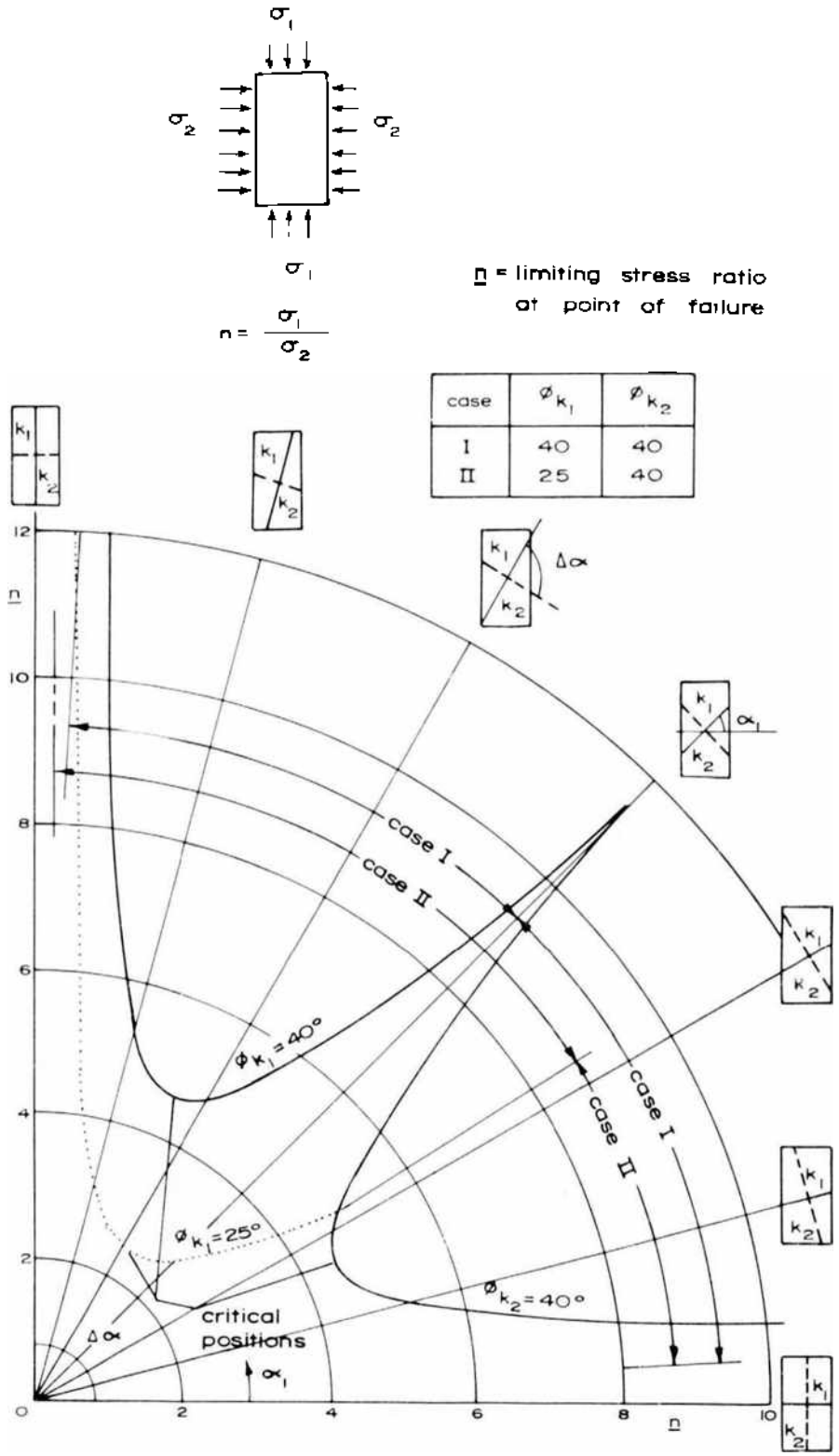

Fig. 10-17. Superimposition of the curves of limiting stress ratios for two orthogonal joints k_1 and k_2 for different values of the friction angles ($\phi_{k1} = 40°$, 25° and $\Phi_{k2} = 40°$)
Case I refers to $\chi_c = 1$
Case II refers to $\chi_c = 0.5$ where χ_c = degree of continuity of the joint
(after JOHN, 1969)

10.4. Behaviour During Sliding Along Joints

10.4.1. Investigations on Friction along Joints

A number of techniques have been used by various investigators for studying friction along rock joints. These techniques may be grouped into the following classes (Fig. 10-18):

1. Slider sliding over another surface
2. Conventional shear box test
3. Double shear test
4. Triaxial test
5. Rotation of cylinders
6. In situ shear tests

Principles underlying the above methods are given below. For more details of some of these tests refer to Chapters 4.5 (Vol. I) and 8 (Vol. III).

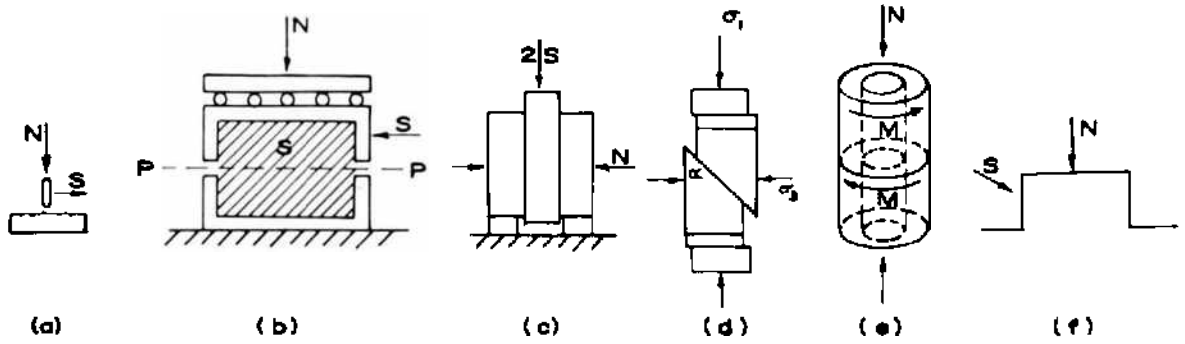

Fig. 10-18. Systems of measuring friction properties along joints
(a) Slider sliding on another surface
(b) Conventional shear box test arrangement
(c) Double shear test arrangement
(d) Triaxial test arrangement
(e) Rotation of cylinders
(f) In situ shear test.

1. Slider sliding over another surface

It is perhaps the oldest method of investigating friction and was used for determining the sliding characteristics of minerals and rocks by HORN and DEERE (1962), BYERLEE (1967a) and JAEGER and COOK (1969b). There are two variations of the method. In the first case a small slider is made to slide on a large surface in which case the normal load applied cannot be too large. In this system (Fig. 10-18a), while the larger surface is always fresh, it is the same surface of the slider which is in contact. The method is more suitable for wear

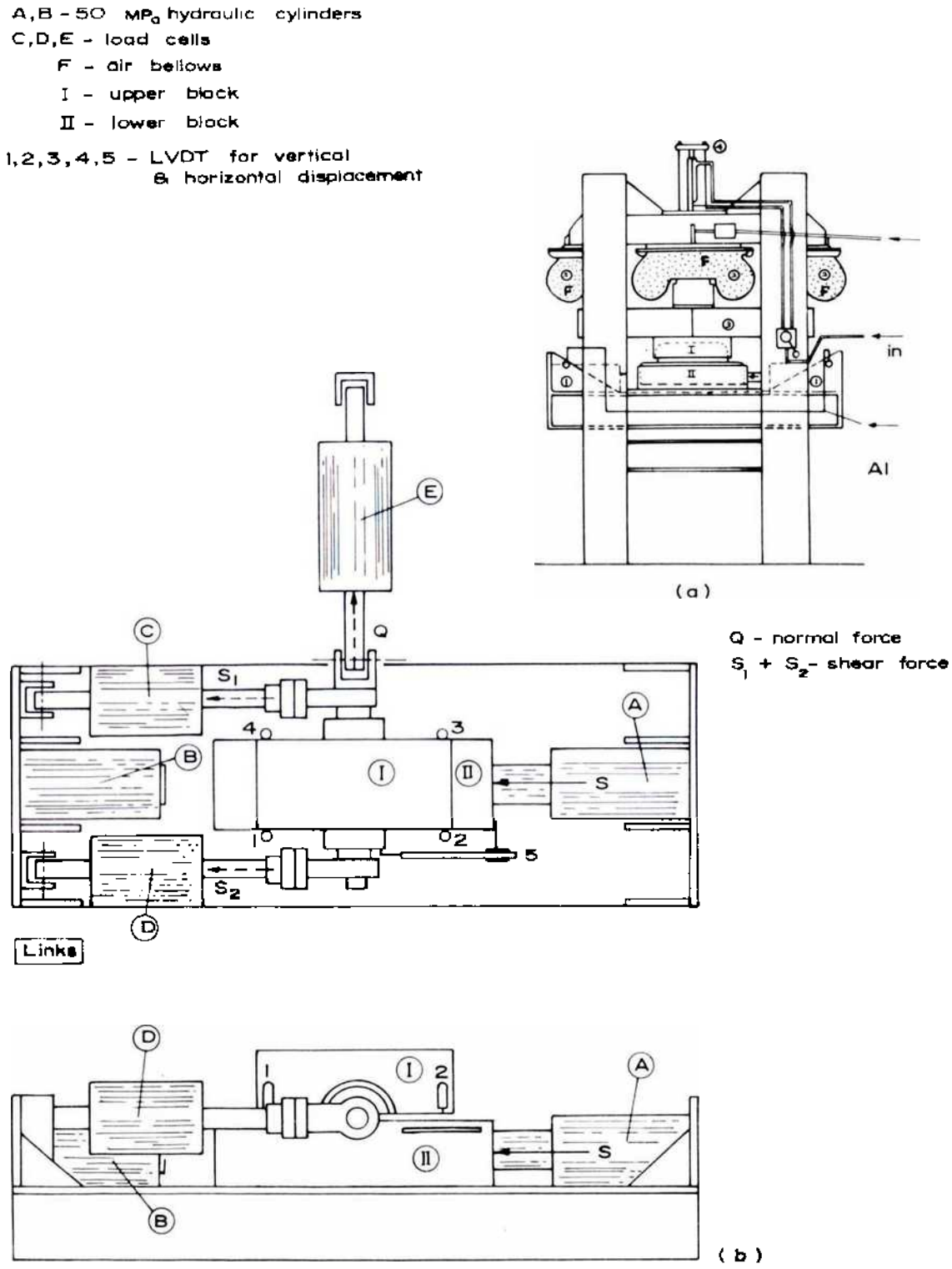

Fig. 10-19. Large friction machine
(a) Overall view of machine
(b) Location of cylinders, load cells and L.V.D.T.s
(after RENGERS, 1971)

than for friction studies except perhaps when the residual friction values are needed. The method, however, does not represent conditions that occur in nature.

A modification of the technique was used by RENGERS (1971) where the size of the two sliding blocks is not the same and the size of the surfaces is large. The important problem posed by such an arrangement is that it is difficult to ensure uniformity of normal load over the whole of the surface at different stages of movement of blocks. RENGERS solved this difficulty by building a special loading machine where the normal force is applied by air-pressure-rubber bellows (Fig. 10-19). The horizontal load (shear force) is applied through a set of two cylinders and the shear force is measured by a load cell. The machine has a friction plane of 600 cm^2 (93 in^2) and a normal stress 50 MPa (7252 lbf/in^2) with maximum relative movement of the specimens 200 mm (7.9 in). This design has the following advantages:

1. Regulation of normal pressure without loss of force
2. Uniform normal load similar to dead weight load
3. Uniform normal load independent of the position of the slider
4. Possibility of following any loading path (dependency between normal force and dilatancy) by programming air pressure in the bellows.

More recently, a number of servo-controlled shear machines have been designed and put into operation using this method in the USA (U.S.B.M. Spokane Mining Research Centre), West Germany (Institute of Soil Mechanics and Rock Mechanics at University of Karlsruhe) and CSIRO Australia (Division of Applied Geomechanics at Syndal, Vic.).

The method has certain advantages over other methods. It permits ease of determination of dilatation and a relatively greater amount of movement between the surfaces. The value of the normal force can be easily selected at will and the sliding surfaces are available for inspection at any stage of the test.

2. Conventional shear box test

Conventional shear box was used by a number of investigators (YEVDOKIMOV and SAPEGIN, 1967; KRSMANOVIC, 1967; HOEK and PENTZ, 1969; LAMA, 1974b). The system has all the advantages of the first method while permitting determination of the initial peak shear strength. The method consists of setting the rock specimens, prismatic or cylindrical or of irregular shape, with the joint plane at the mid-half of the shear box. A simple arrangement used by LOCHER (1968) is shown in Fig. 10-20. The rock specimen is cast in mortar with the joint plane accurately located at the predetermined position in the mould. Two hydraulic jacks exert the normal force (N) and the shear force (S) and the

test equipment is capable of giving a movement of 1 cm (0.394 in). Since the transmission of the normal force is through proving rings, the system suffers from the disadvantage that any dilatation or contraction (-ve dilatation) changes the value of the normal force. If the normal and the shear forces can simultaneously be recorded, the arrangement gives an easy way of directly determining the normal – shear force envelope.

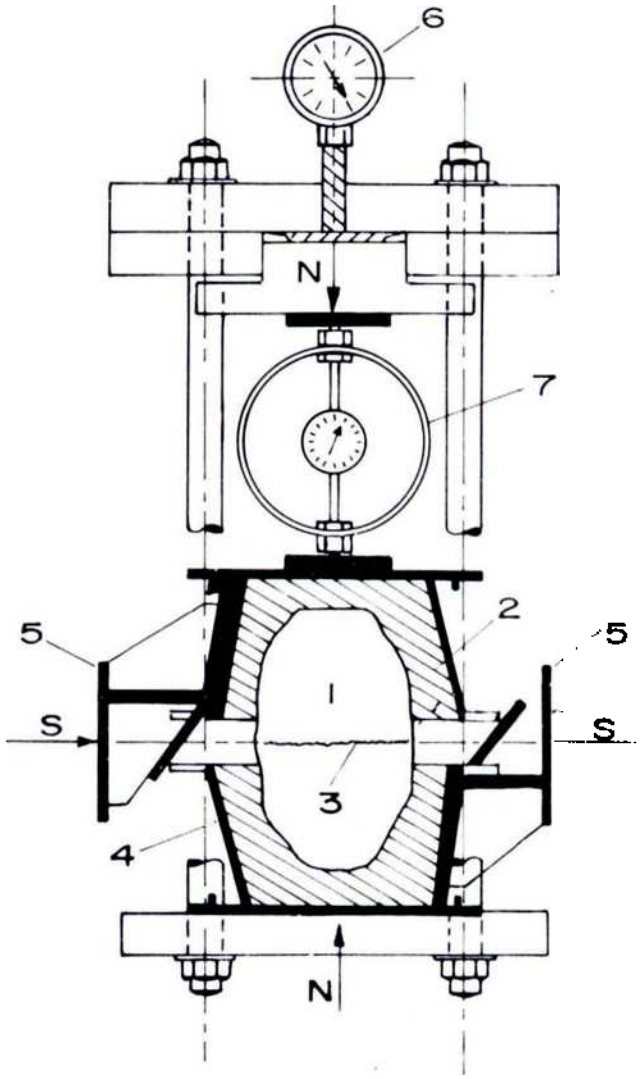

Fig. 10-20. Schematic layout of shear testing apparatus:
1. Sample
2. Mortar
3. Discontinuity to be tested
4. Double steel form
5. Exchangeable shoes transmitting force S
6. Manometer for high loads and control of force N
7. Proving ring for force N (proving ring for force S not shown)
(after LOCHER, 1968).

KRSMANOVIC (1967) performed large size laboratory shear tests to determine the joint properties. The arrangement used by him is given in Fig. 10-21. The normal force is applied through two hydraulic cylinders of 0.25 MN (25 ton) each and the shear force by four cylinders (two on each side) of 0.25 MN (25 ton) each. The setting of the apparatus is such that the applied shear force makes an angle of 4 with the shear surface so that shear strength even at small normal loads can be determined with minimum of disturbance. The shear box can accommodate specimens of 40 cm × 40 cm × 20 cm (15.7 in × × 15.7 in × 7.9 in) with the shearing area of about 1600 cm^2 (248 in^2). It simulates the conditions of direct shear to be obtained at normal stresses up to 3.92 MPa (568 lbf/in^2) and shear stress of 7.84 MPa (1136 lbf/in^2), intensities which are normally met in the design of large civil engineering foundation structures.

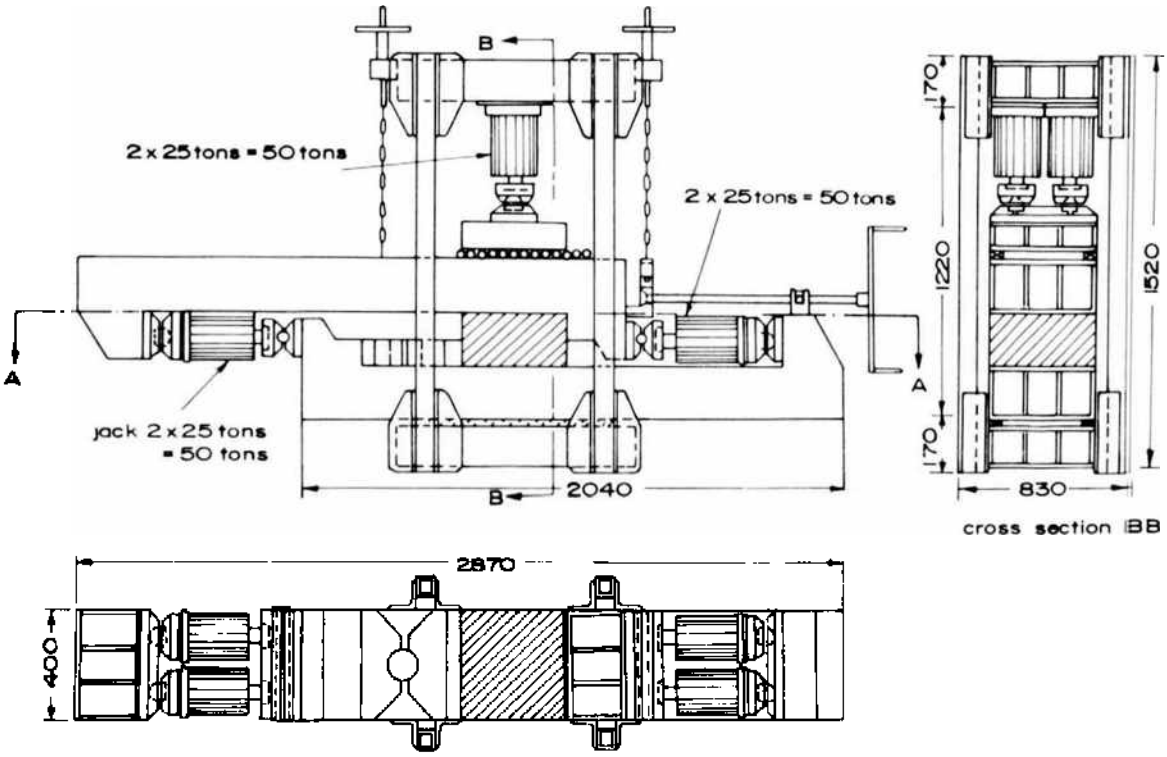

Fig. 10 21. Schematic diagram of the 0.5/1.0 MN (50/100 tons) capacity shearing apparatus
(after KRSMANOVIC, 1967).

When vertical load is applied through hydraulic cylinders, the measurement of dilatation is not possible. The change in pressures in the cylinders applying vertical load may be monitored using pressure transducers. The system has also the disadvantage that vertical constraint of the specimens is uncertain unless it is monitored and that correction for the friction in the bearings must be made.

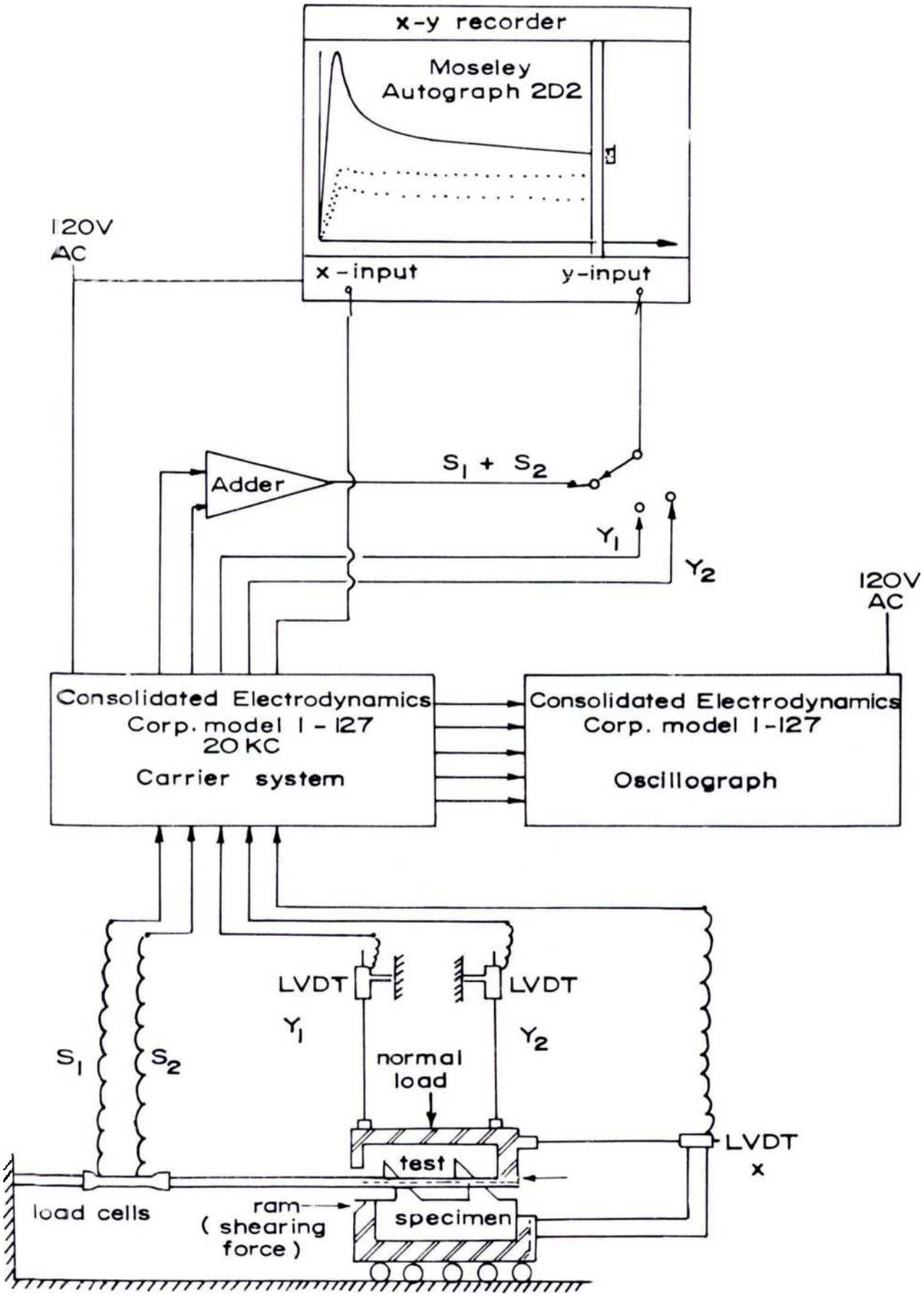

Fig. 10-22. Schematic diagram of the testing and recording equipment (after PATTON, 1966a).

PATTON (1966a) used a direct shear machine with the modification that normal force remains stationary and the bearing friction was greatly eliminated by making the lower block move on the roller bearings—the upper block remaining in a stationary position (Fig. 10-22). The shear force is measured by two load cells attached to the tension tie bar. The vertical and the horizontal displacements are measured by using LVDT-s. The method has the advantage that dilatation can be measured for any value of normal force. A similar arrangement was also used by COULSON (1970).

3. Double shear test

A modification of the single shear test is the double shear test (see also section 4.4.3) where the shear load is applied through a testing machine or a jack and the normal load by a horizontal jack. The principle of the test is shown in Fig. 10-18c and was used by a number of investigators (HOSKINS, JAEGER and ROSENGREN, 1968; ROSENGREN, 1968; JAEGER and ROSENGREN, 1969; DIETERICH, 1972). HOSKINS, JAEGER and ROSENGREN (1968) used 30.5 cm (12 in) square blocks sliding between two other blocks supported at the base while the displacement of the central block was measured by an LVDT and the lateral load was applied through a flat jack.

The method is particularly useful for the determination of friction along the contact surfaces of a rock or frictional force along a surface which has been artificially prepared but the method is not useful when shear along a discontinuous (unseparated) joint is to be studied.

4. Triaxial test

Triaxial apparatus has been most extensively used and was perhaps the first method of studying the behaviour of any discontinuity. The method was perhaps first used by the U.S. Bureau of Reclamation (1954) for testing the bond strength between mortar and aggregate and then by JAEGER (1959) for the study of the sliding of a variety of artificially prepared joint surfaces in rocks.

The method consists in using a cylindrical specimen (for details of equipment see Chapter 5) with the joint plane suitably oriented at an angle γ to the axis of the specimen and subjecting it to a given value of lateral and axial pressures in a triaxial cell. The normal and shear stresses can be calculated by the relationship (Fig. 10-18d)

$$\sigma_n = \sigma_3 + (\sigma_1 - \sigma_3)\sin^2\gamma \tag{10.38}$$

$$\tau = (\sigma_1 - \sigma_3)\sin\gamma\cos\gamma \tag{10.39}$$

where σ_1 = axial stress
σ_3 = lateral stress and
γ = angle of inclination of the discontinuity with the principal stress σ_1.

This method was also used for the study of the residual sliding characteristics of fractured surfaces by LANE and HECK (1964), MURRELL (1965), HOBBS (1966, 1970), BYERLEE and BRACE (1968), BYERLEE (1975) and many others because of its simplicity in obtaining a fracture surface under different stress conditions.

The method suffers from certain drawbacks. Firstly, the method does not allow independent variation of the shear force and the normal force since these are related to each other by the relationships Eqs. 10.38 and 10.39. Secondly the method is not suitable for study under low normal stresses since the normal stress σ_n is 2 3 times the shear stress. It is suggested that this method be used only for normal stresses $\sigma_n > 1$ MPa (10 bars) (145 lbf/in^2) (JAEGER, 1971). The method is quite handy for testing joints at high normal pressures and was used by BRACE and BYERLEE (1966a, b), BYERLEE (1966, 1967a, b) and HANDIN (1972a, b) used it to study friction along existing joints and faults in deep regions of the earth's crust for problems concerning extension of faults and earthquakes etc. Thirdly, there are certain other difficulties due to the geometry of the testing apparatus. HOSKINS et al (1968) discussed the geometry effect in detail. Most of the investigators in the triaxial apparatus use either no spherical seat or only one spherical seat (at the top). As displacement proceeds, the stress system changes so that the results are accurate only for the initiation of sliding. In the case of no spherical seat (Fig. 10-23), there are certain lateral stresses introduced depending upon the lateral stiffness of the machine. In the case of a

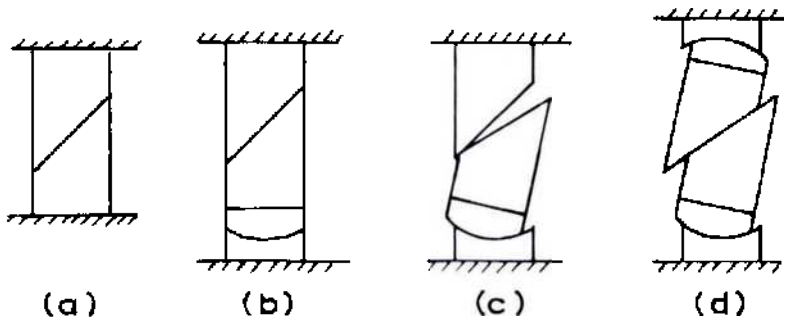

Fig. 10-23. Experimental arrangements for determining frictional properties along joints in triaxial apparatus and the influence of geometry
(a) No spherical seat
(b) Single spherical seat – at the start of the movement along the joint
(c) Single spherical seat after the progress of the movement
(d) Double spherical seat after the movement
(after HOSKINS et al, 1968).

single spherical seat there is rotation of the part of the specimen in contact with the spherical seat while the other part does not change its position. The use of two spherical seats (Fig. 10-23d) allows contact to be retained over the whole of the surfaces, but the area of contact changes and frictional and lateral forces are introduced at the seats. The best method seems to be to use a pair of hardened steel washers with 'molybond' between the ends of the specimen and the platens (Fig. 10-18d) where the situation can be really described as 'running in' and behaviour can be studied in the range after the failure has been initiated. However, an appropriate correction in the value of the normal force needs to be applied as the area of contact decreases with advancement of movement along the plane. Also, there could be problems associated with the tendency of spherical seats to lock under high normal stresses.

5. Rotation of cylinders

The method consists of pressing together two hollow cylinders (Fig. 10-18e) under axial load N and a torque M is applied so as to rotate them along their axis. The two cylinders slide over each other at the surfaces of their contact. This type of apparatus was built by N.G.W. COOK at the Mining Research Laboratory, Johannesburg, South Africa. The system has the advantage that a large amount of sliding can be obtained without disturbing the geometry of the system. Also it allows the study of the influence of water on friction by introducing it in the inside of the hollow cylinders. The method is applicable both to artificially made as well as natural joints when cores can be obtained with the joint plane at right angle to the core axis. However, the measurement of dilatation is difficult.

The method has been used by a number of investigators (KUTTER, 1974; CHRISTENSEN et al, 1974, also see Chapter 8). Laboratory studies on Westerly granite in torsion (CHRISTENSEN et al, 1974) gave friction values which agree with those obtained by BYERLEE (1968) in triaxial cell.

Torsional shear strength drops with increase in axial stress on specimens as it exceeds a certain limiting value and this aspect should be borne in mind while evaluating results by this method. This results in lower cohesion values than obtained from conventional tests (DURAND and COMES, 1974).

6. Testing of joints in situ

The determination of joint properties in large scale in situ tests is being increasingly adapted in civil engineering works in site investigation and in many cases this represents the most important mechanical property in determining the foundation conditions of structures and slope stability analysis. In the last 10 years, a number of tests have been conducted in many countries to determine

the influence of joints (LINK, 1967). The method in principle is very simple (Fig. 10-18f). A block containing the joint to be investigated (or for determining the shear strength of the rock mass in general) is prepared and is subjected to the normal and shear loads. A simple shear arrangement is given in Fig. 10-24 which is extensively used by LNEC, Lisbon and consists of making a block of 70 cm × 70 cm (27.6 in × 27.6 in) (in certain cases blocks of areas of several square metres (yards) have been used). More details have been given in Chapter 8. The block is surrounded by a reinforced concrete or steel frame and the normal and the shear loads are applied through cylinders. Very often the shear force is applied at an angle θ and in such a case, the normal and the shear stresses can be given by the relationships (Fig. 10-24)

$$\sigma_n = \frac{S \sin\theta}{A} + \frac{N}{A} \tag{10.40}$$

$$\tau = \frac{S \cos\theta}{A} \tag{10.41}$$

where S = inclined shear force
N = normal force
A = area of cross-section of the specimen at the base and
θ = inclination of the shear force with the base.

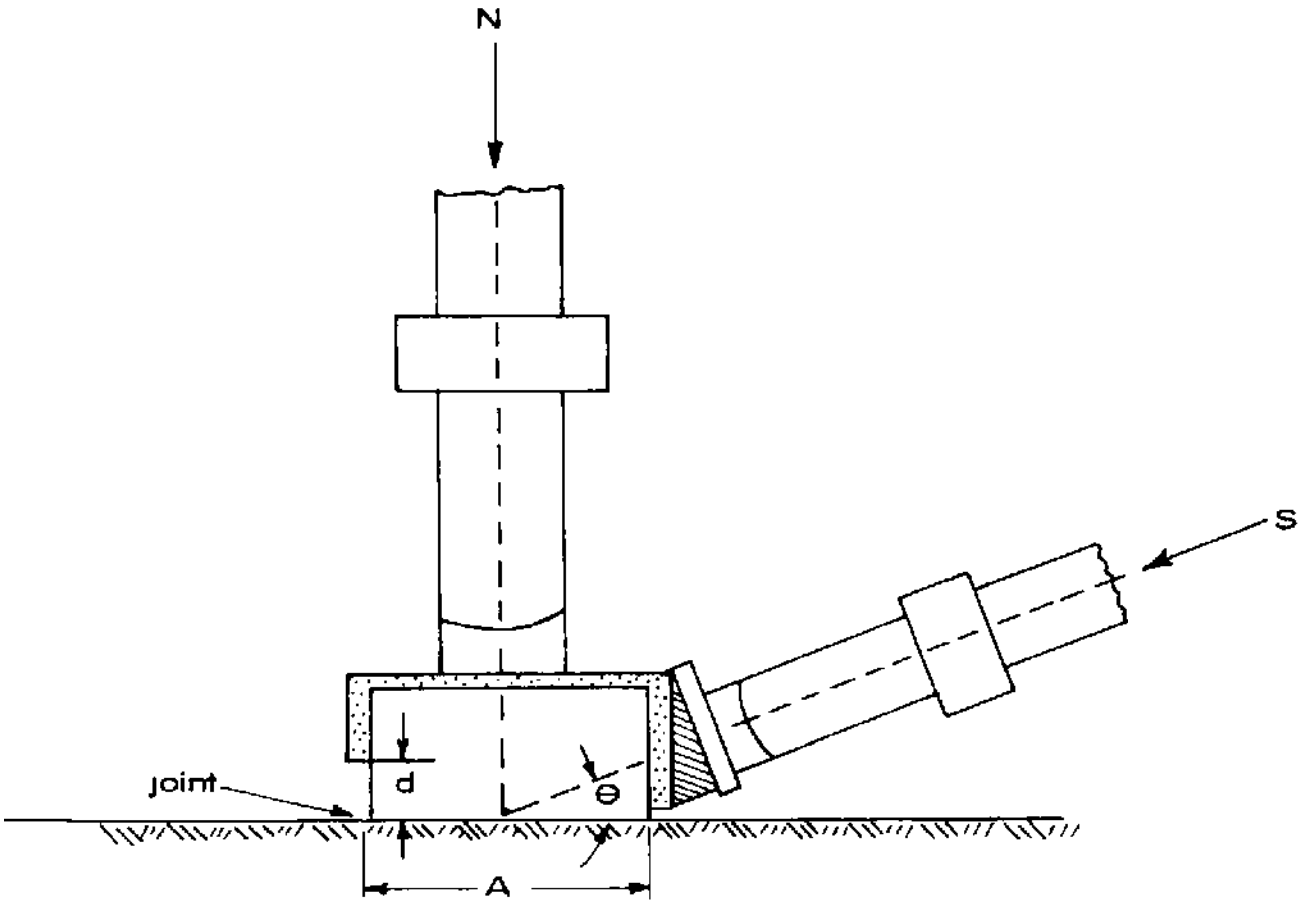

Fig. 10-24. In situ testing of a joint plane.

The value of θ may vary from test to test, but in case it is in the range from 30 to 40 , it is very usual to make $N = 0$ and thus only one hydraulic jack is necessary. When two jacks are applied, the geometry of the test should be such that the axes of the jacks pass through the centre of the base of the specimen.

The purpose of application of the shear force at an angle is (1) to limit the amount of excavation required for placing of the jack and (2) to avoid development of tensile stresses due to bending. Ruiz et al (1968) conducted model tests for $\theta = 20$ and the results of their investigations are given in Figs. 10-25

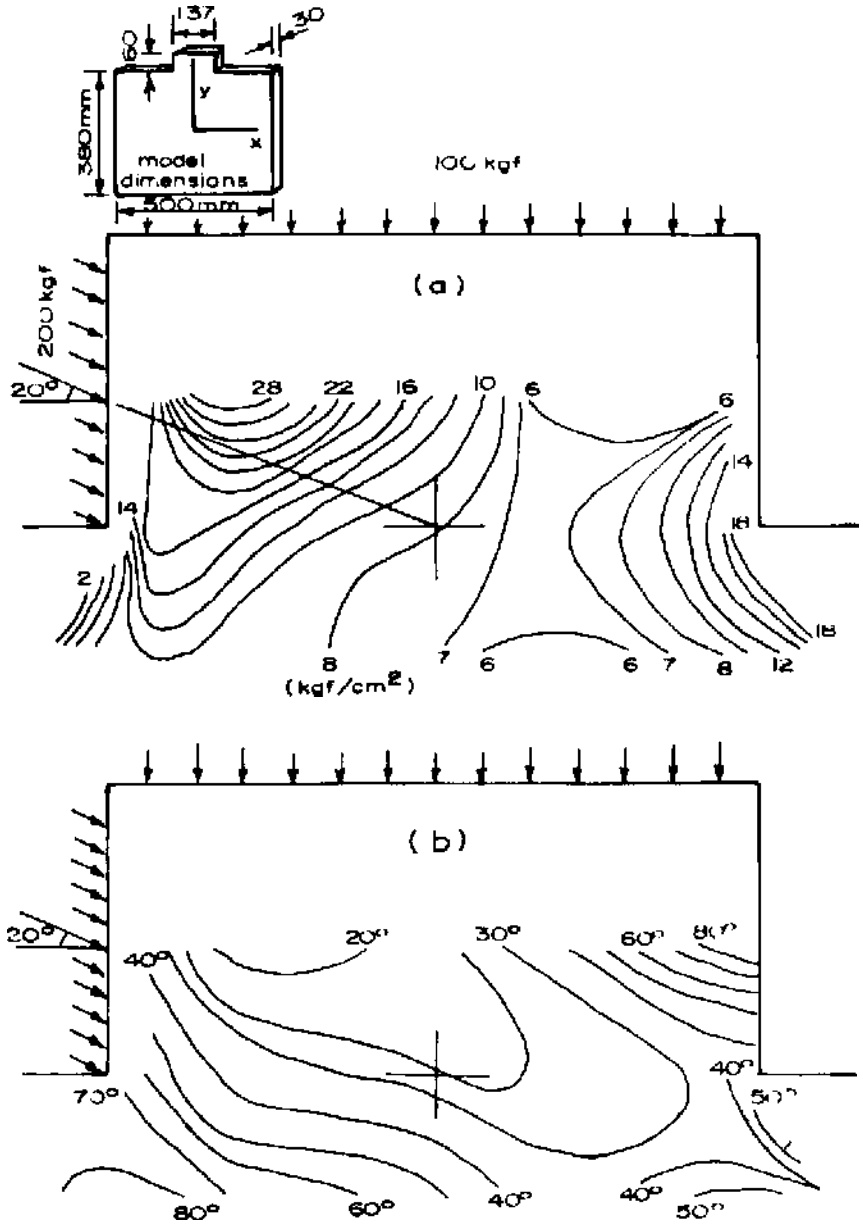

Fig. 10-25. Isoclinics and loci of points of equal σ_1 (compression) (after Ruiz et al, 1968).

and 10-26. These clearly indicate the existence of non-uniform stress distribution at the base of the block and also the existence of tensile stresses. This, very often, leads to failure occurring in the plane of the base of the block but running in the block or below in the rock.

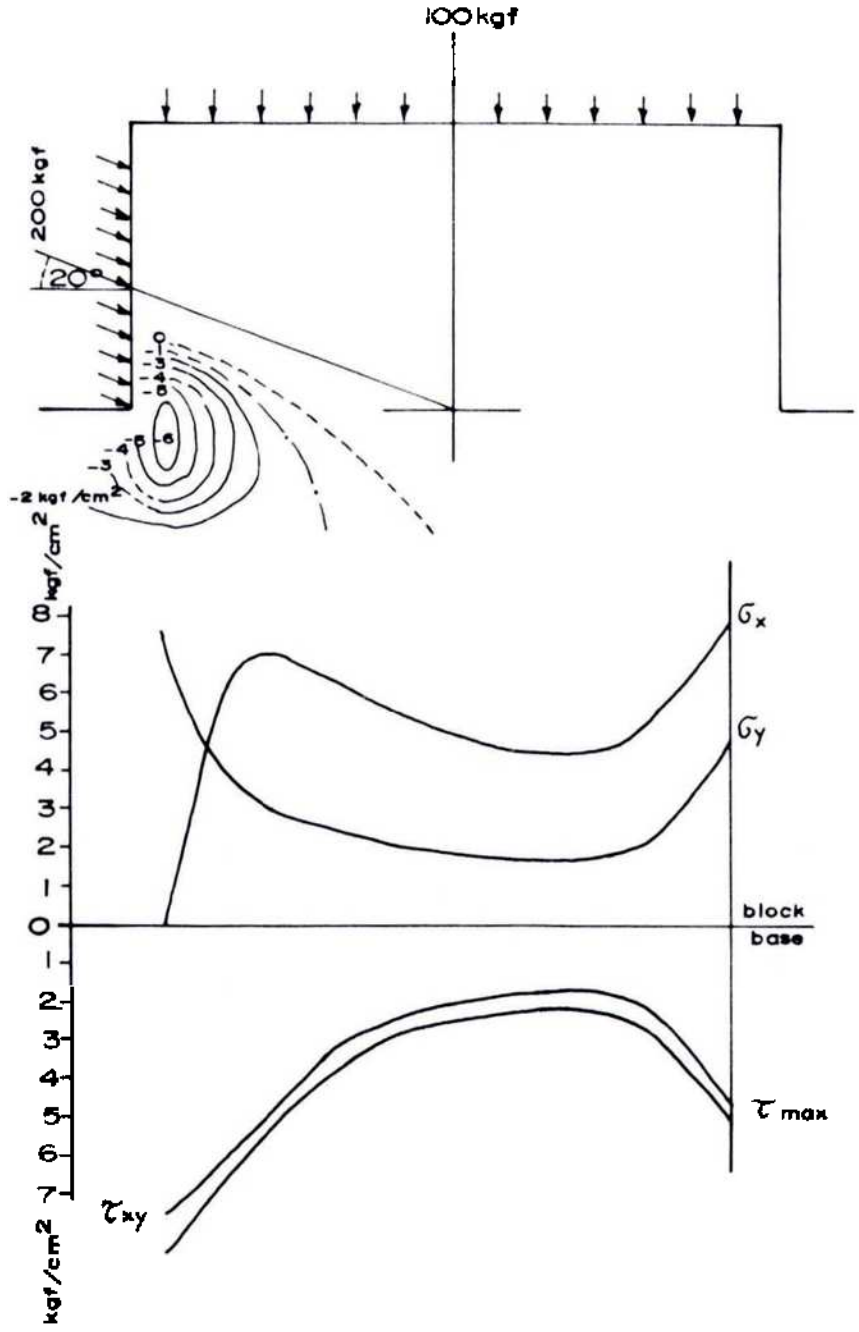

Fig. 10 26. Zone of tensile stresses. Shear and normal stresses at the base of the block (after RUIZ et al, 1968).

To avoid development of tensile stresses, ROCHA (1964) suggested that the value of d (Fig. 10-24) plays an important role. According to him the value of d should be so chosen that

$$S = \frac{AN}{3d} \tag{10.42}$$

in which case the tension due to bending will equal compression. If the value of S is above this limit, tensile stresses may occur and it is advisable to check the occurrence of tensile cracks in the test. The usual value of d may be taken as $\frac{A}{4} \rightarrow \frac{A}{8}$, depending upon the angle of friction of the rock, provided N is not very small.

There is another factor which is very important and influences the results greatly. There may be concentration of the shear stresses which are higher the lower the value of d. (It is in general noted that the shear strength decreases with increase in the value of d.) To avoid this, the shear force frame should be as rigid as possible. The best arrangement naturally would be to apply the shear force with the plane to be investigated placed in the centre of the specimen. But this arrangement is more costly both in terms of equipment and conduct of tests.

Types of surfaces investigated

A number of different types of surfaces have been studied from the point of friction properties. These are given below:

Laboratory shear surfaces produced in direct shear or triaxial tests (JAEGER, 1959; MAURER, 1966; HOBBS, 1970; DONATH, FRUTH and OLSSON, 1972). These surfaces are normally quite irregular and contain a considerable amount of detrital material depending upon the test conditions producing the shear surface and the rock type while having the advantage of producing a surface under known stress conditions.

Laboratory extension surfaces produced by tensile test (BYERLEE, 1967b; BARTON, 1971a, b; RENGERS, 1971; SCHNEIDER, 1972; LAMA, 1975a). The surfaces are very rough and highly interlocked.

Cut and polished surfaces. They are easily prepared by cutting the specimens and then polishing them if so desired. Such surfaces have been studied by the majority of investigators. These are characterised by flatness but still complete contact (100% contact area) may not be attained particularly on larger specimens.

Artificially combined surfaces produced from cast models with different shapes of the asperities. They have been studied to simulate different types of roughnesses and to throw light on the mechanism of friction (PATTON, 1966a, b; LAJTAI, 1969a, b; LADANYI and ARCHAMBAULT, 1972). The behaviour obtained is naturally dependent upon the shape of the surface and the model material.

Natural joints of different types, filled and unfilled, as obtained from cores. These have been studied by a number of investigators. Tests have also been conducted in situ. These give a direct insight into the property of the joint but results obtained are difficult to correlate in the absence of any data about the joint surface. Since a large number of factors influence the behaviour of the joint, the results may be highly scattered even when the rock type and the place of sampling is the same. On the other hand, they are costly but have direct application in the design under the conditions.

Loading sequence in testing of joint properties

In the conduct of the test, two variations are possible.

1. The samples may be tested at a fixed value of σ_n giving a shear stress versus displacement ($\tau - \Delta s$) curve. From this curve the values of τ_t, τ_r as well as the values of shear strength at any specified displacement Δs can be read off. The tests may be conducted at different values of σ_n for different specimens and the $\tau - \Delta s$ curves for different values of σ_n may be drawn (KRSMANOVIC and LANGOF, 1964; KRSMANOVIC, 1967). A typical curve obtained in such a test along with an idealised curve is given in Fig. 10-27. The peak and residual shear stresses (or any other value of shear stress for a given displacement) are plotted against the normal stress to obtain the MOHR envelope for the joint.

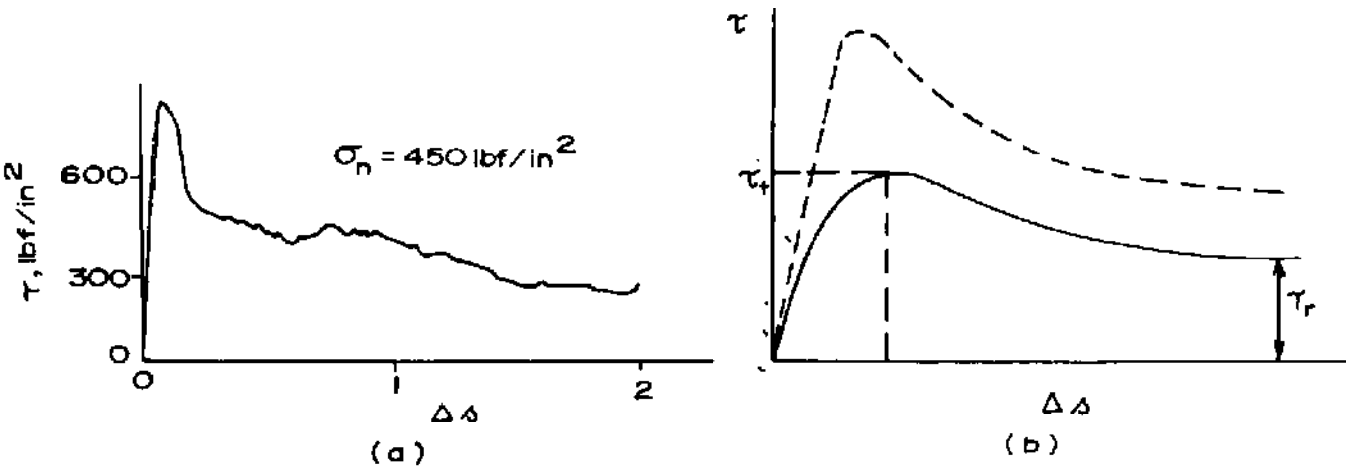

Fig. 10-27. (a) Typical curve of shear stress against displacement for a natural joint, (b) Idealised curve (after JAEGER, 1971).

The test suffers from the disadvantage that specimens from the same joint vary considerably and hence a wide scatter in results may be expected even for the same joint. Besides, a number of tests have to be performed on different specimens to determine the shear envelope for the joint.

2. In the second case, the sample can be tested where the value of the normal stress σ_n can be varied once the peak for a particular value of σ_n is passed and the conditions have been stabilised. The normal stress can be changed in steps by certain specific amounts (either increased or decreased). It may, however, be kept in view that the results obtained in the two cases may be different since the properties of the sliding surface at any time are dependent upon the normal stress to which it has been subjected. Besides, the properties change with sliding.

This method of loading, however, has the advantage that a plot of the $\tau - \sigma_n$ can be made from a single specimen. This sequence was adopted by LANE and HECK (1964), MURRELL (1965), RUIZ et al (1968), JAEGER (1959), JAEGER and ROSENGREN (1969), HOBBS (1970), DONATH, FRUTH and OLSSON, 1972 and LAMA (1975b). A typical test curve obtained by this method is given in Fig. 10-28.

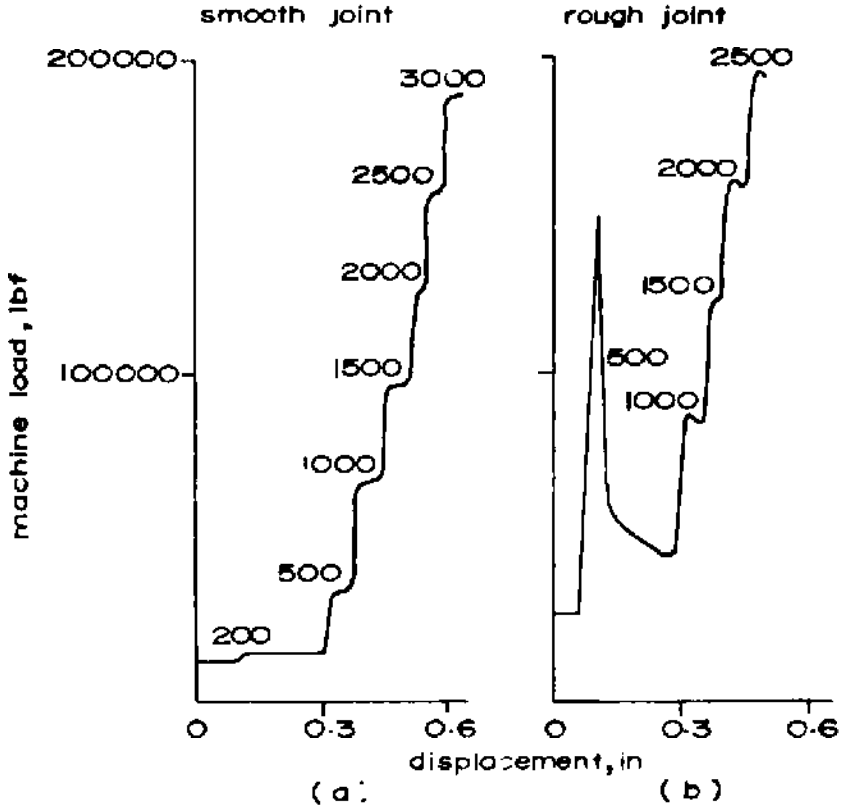

Fig. 10-28. Load-displacement curves for graphite coated joints in six-inch core tested triaxially.
Numbers on curves are confining pressures in lbf/in^2
(after JAEGER, 1971).

Recording the roughness of joint surfaces

RENGERS (1971) developed a very useful method of measuring and recording the surface roughness of joints, though most of the investigators confine themselves only to the measurement of roughness by using a profilograph or stereomicroscopy, depending upon the size of the surface.

RENGERS (1970, 1971) used a stereo depth measuring microscope (Fig. 10-29). A rock sample or its negative (silicone rubber cast) is moved parallel to the reference plane with the help of a suitable micrometer or screw arrangement while a floating mark in the optical system of the stereo depth measuring microscope is moved up and down to keep it on the surface. The horizontal and the vertical movements of the floating mark are recorded on an *X*-*Y* recorder with appropriate enlargement (5X 20X). The method gives an accuracy of profiling better than 0.1 mm (0.004 in) for 10X.

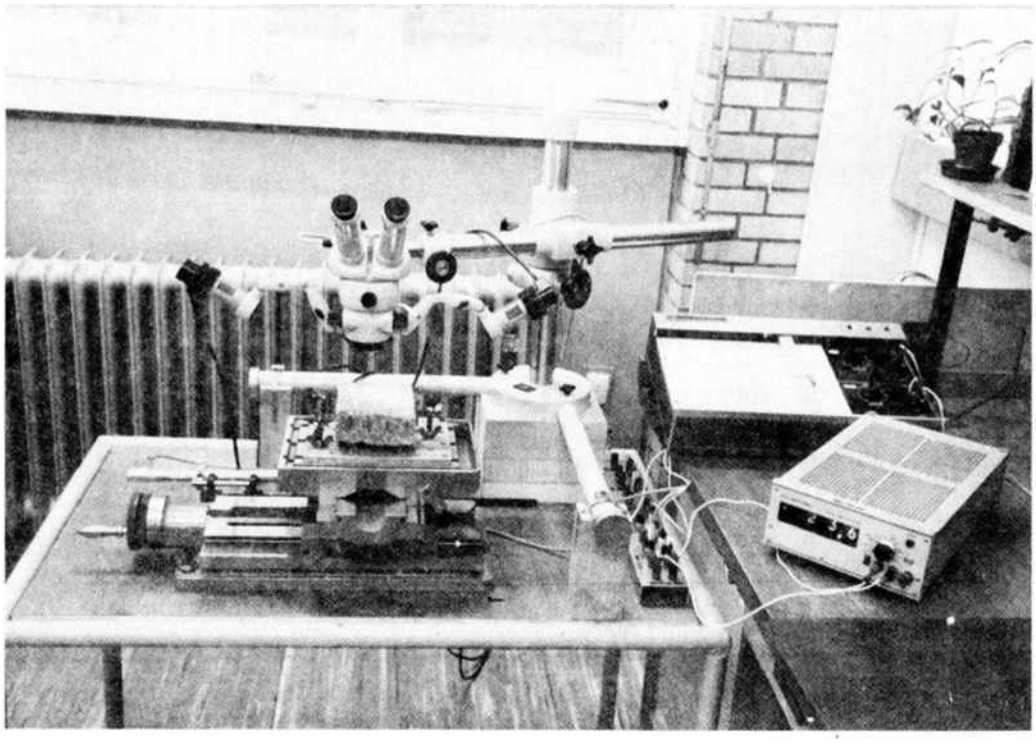

Fig. 10-29. Stereo depth measurement microscope (after RENGERS, 1971).

For larger size specimens, a profilograph was developed by FECKER and RENGERS (1971) (Fig. 10-30). This profilograph is suitable for surfaces 20- 200 cm (8- 80 in) long. The guide arm of the profilograph is mounted on the surface parallel to the direction along which the profile is required to be

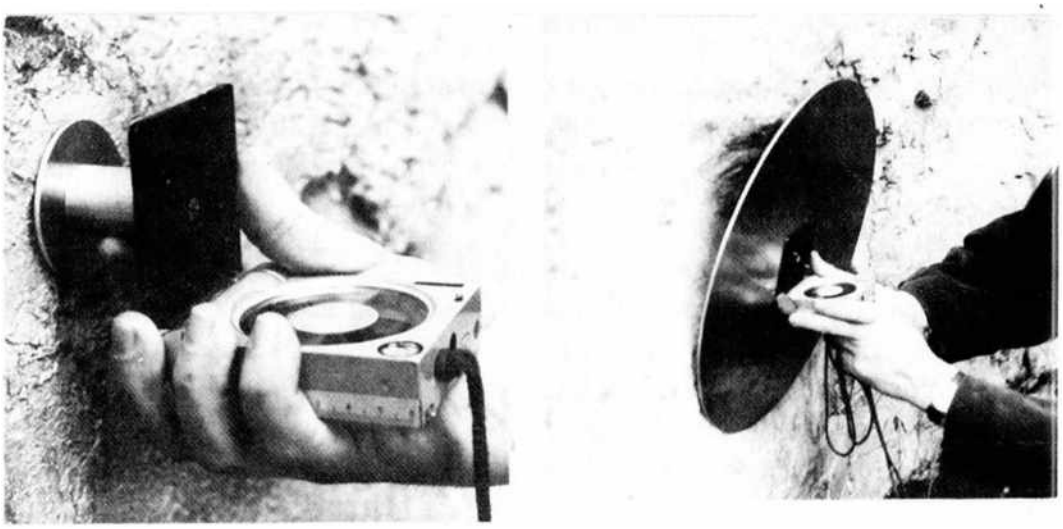

Fig. 10-30. Profilograph
(after FECKER and RENGERS, 1971).

traced. The vertical displacement with respect to the reference plane (in this case guide rod) is recorded on the rotating drum on a scale 1:1 with the horizontal scale reduced by 1/5.

Both these methods are quite time consuming and are rather unsuitable for measurements on larger surface exposures. Larger surfaces in situ can better be recorded by terrestrial photogrammetry.

Another very simple and useful method was developed by FECKER (1970), FECKER and RENGERS (1971), which makes use of the normal geological compass for the measurement of the roughness of the surface. The compass is placed randomly on the exposed joint surface at certain selected points (Fig. 10-31) and the angle of dip is read out. Since the scatter of the compass measurements laid randomly on the joint surface is determined by the rough-

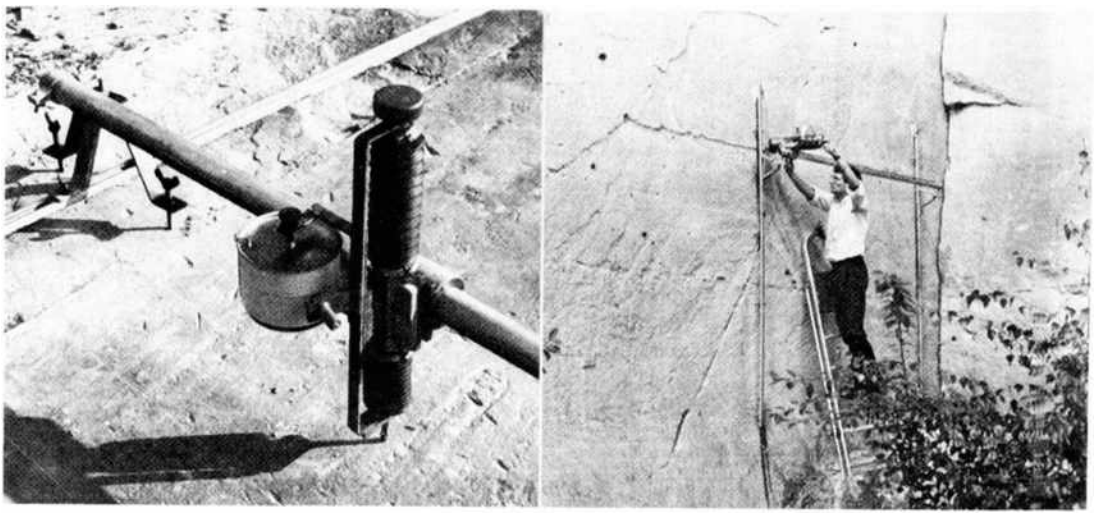

Fig. 10-31. Profiling of joint surface with the help of a geological compass
(after FECKER and RENGERS, 1971).

ness of the surface as well as by the size of the base plate, different sizes of the base plate of the compass are required and measurements are repeated at the selected points by using different base plates. The results of these measurements are then plotted on a polar equal-area net on which the orientation of the reference plane along which profile is required to be determined is also marked. The poles then are rotated so that the reference plane is in horizontal position. The scatter of the compass measurements depends upon the size of the base plate and increases as the size of the base plate decreases. The poles with the largest distance from the centre represent the largest angle between the reference plane and the roughness tangent measured by the compass. These poles with the largest distance are connected, forming contours of maximum scatter (Fig. 10-32) from which the values of the tangent can be read in any direction. The comparison of the results obtained by the compass method and profilograph method is given in Fig. 10-32.

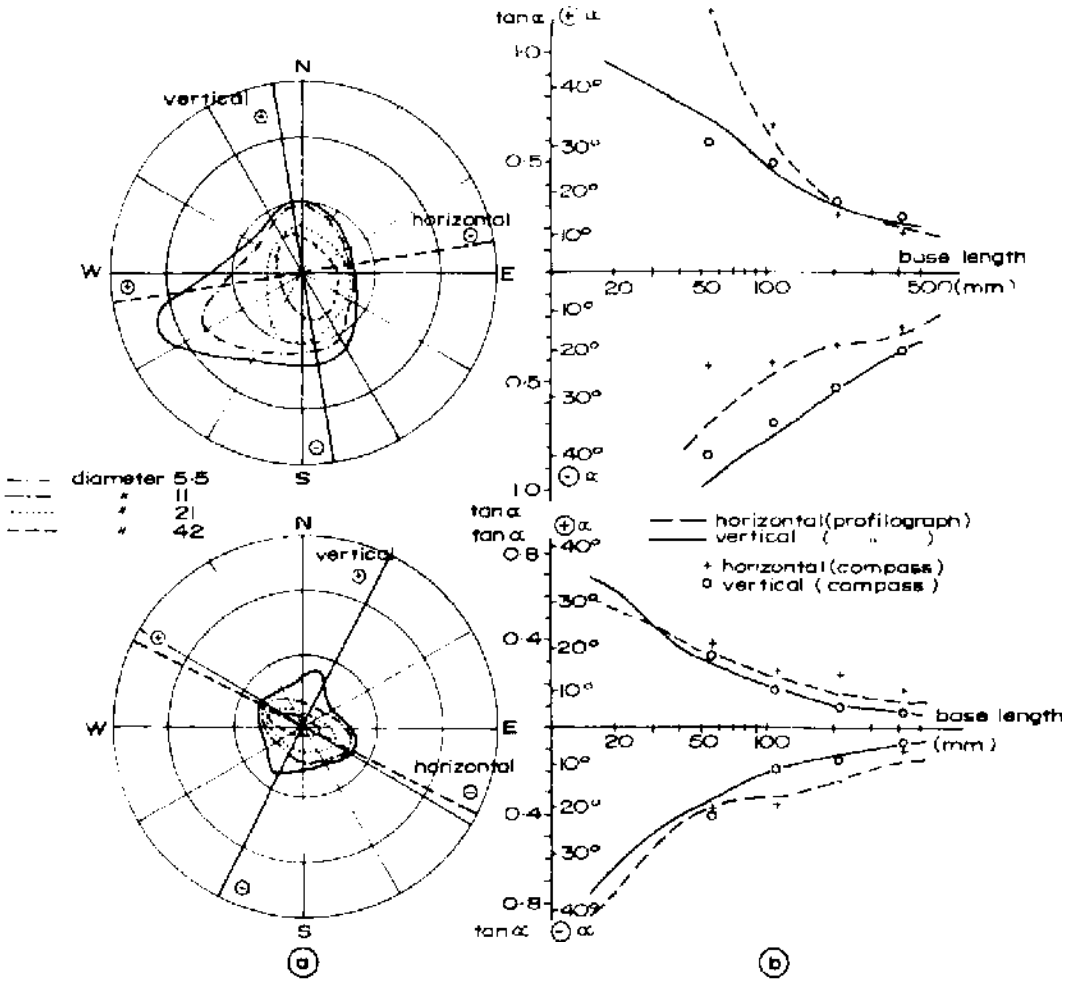

Fig. 10-32. (a) Curves of the maximum scattering from different base plates of the compass (b) Comparison from compass measurements and profilograph measurements by the curve of the "extreme values of α"
(after FECKER and RENGERS, 1971).

GOODMAN, HEUZE and OHNISHI (1972) determined the influence of the length of the observation base (in other words the size of the base plate or distance between two measuring points by profilograph method) with the average slope angle for surfaces of different roughnesses (sawed, sawed and sandblasted, split) in specimens of size 12.07 cm × 12.07 cm (4.75 in × 4.75 in). They found that when the observation length was increased from 12.7 mm (0.5 in) to a few centimetres (inches) there is a sharp decrease in slope angle.

Description of the surface roughness of joints

Because of the non-repetitive stochastic nature of the asperities of the joint surfaces, their description in terms of any trigonometric function as usually done in the case of metal surfaces is not possible. Simply profiling the surface and determining the tangent value at the various points do not give very useful results particularly when certain comparative data are required.

One of the simplest methods is to describe the average height of the asperity, but the values so obtained are not very useful. RENGERS (1971) adopted the trigonometric function (tangent values) as used in the description of the metal surfaces in a very special way. An asperity is described by the angle between the horizontal base plane of the asperity and the tangent to its surface at the base (KRAGELSKII, 1965). The method consists of choosing a reference plane parallel to the largest observable extension of the separation plane (when roughness measurements on different scales are made, the reference planes are taken parallel). On the profile obtained, measuring points are laid with a mutual distance L measured parallel to the reference plane (Fig. 10-33). The distance L is usually taken as 1 mm (0.04 in) which depending upon the method of profilographing or the recording scale may correspond to 0.1 – 20 mm (0.004 – 0.8 in) (for stereomicroscope scale 10 : 1 ; 0.1 mm (0.004 in) ; profilograph

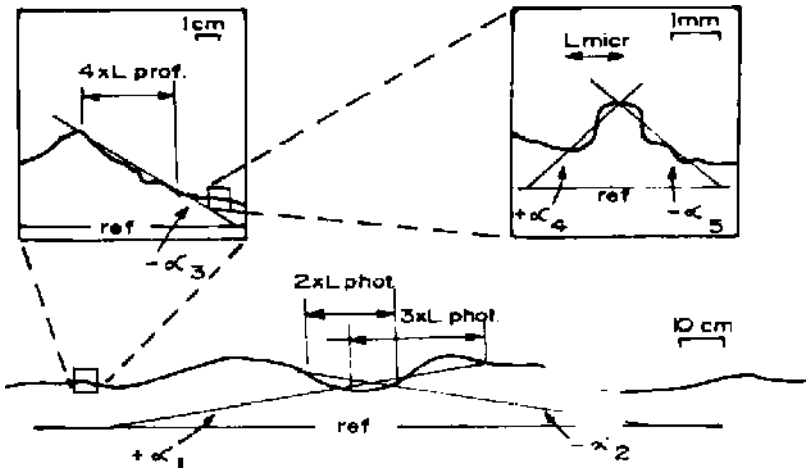

Fig. 10-33. Representation of surface roughness (after RENGERS, 1971).

scale 1:10; 10 mm (0.4 in); photogrammetric scale 1:20; 20 mm (0.8 in)). For every point on the profile, connecting lines are drawn to other points at distances multiples of the step size (L, $2L \ldots nL$). The step sizes are so chosen that $nL = \frac{1}{\text{profile scale}}$ $(= n\bar{L})$ equalises one of the 36 "real step sizes". The "real step sizes" used by RENGERS were 0.01, 0.015, 0.02, 0.03, 0.04, 0.06, 0.08, 0.10, 0.15, 0.20, 0.30 ... till 1000 cm (0.0004 in till 32.81 ft). The connecting lines make positive and negative angles, α (Fig. 10-33) with the reference line. The tangent values of these angles obtained from different step sizes are plotted against step size (Fig. 10-34). A computer programme can be used for cal-

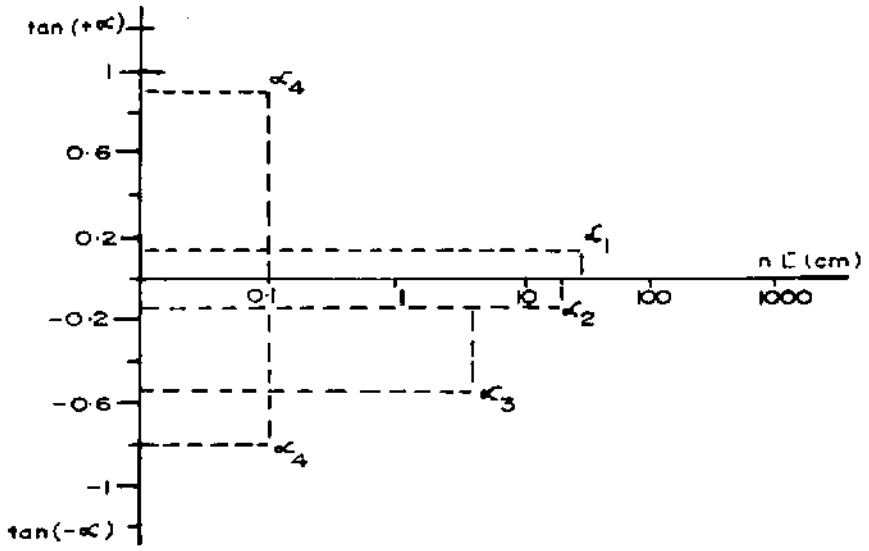

Fig. 10-34. Graphical representation of the angles of α of Fig. 10-33 (after RENGERS, 1971).

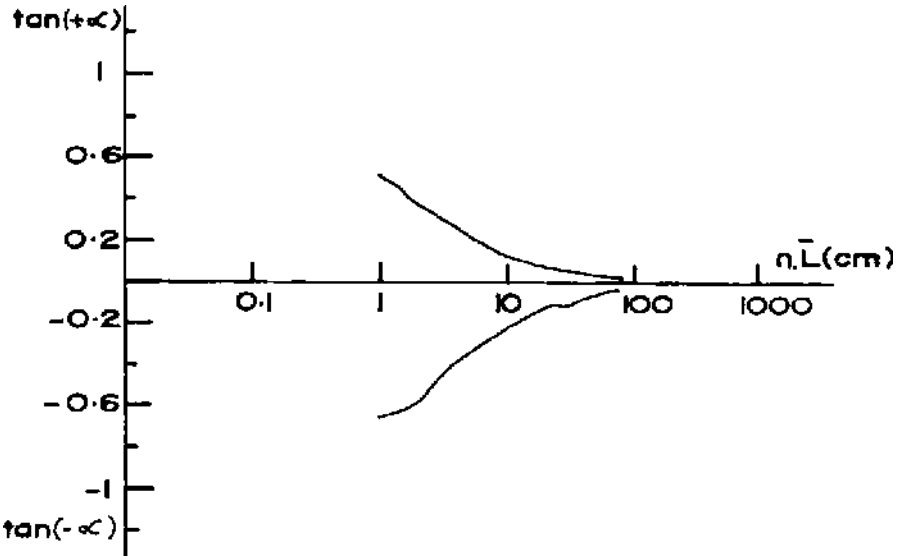

Fig. 10-35. Maximum values of tan α for the respective real step sizes $n.\bar{L}$ for a separation plane in granite. Based on 45000 values of tan α. Recorded with the profilograph (after RENGERS, 1971).

culating and plotting these values which, depending upon the number of profile lines and the length of a profile line, may run to several thousands or hundred thousands. (RENGERS had the total number of tangent α values for 10 parallel profiles exceeding 45,000). Fig. 10-35 represents the plot of the values of tan α for different step sizes.

This technique of representation of surface roughness has several advantages over the usual method of describing the average height of the asperity. If the roughness pattern shows different characteristics for positive and negative angles of α, it is an indication that relative movement along the profile in the two directions will have different frictional properties. The method also gives a quick idea of the possible amount of dilatation during movement if all the asperities are overridden and there is no shearing off since the dilatation Δh for any

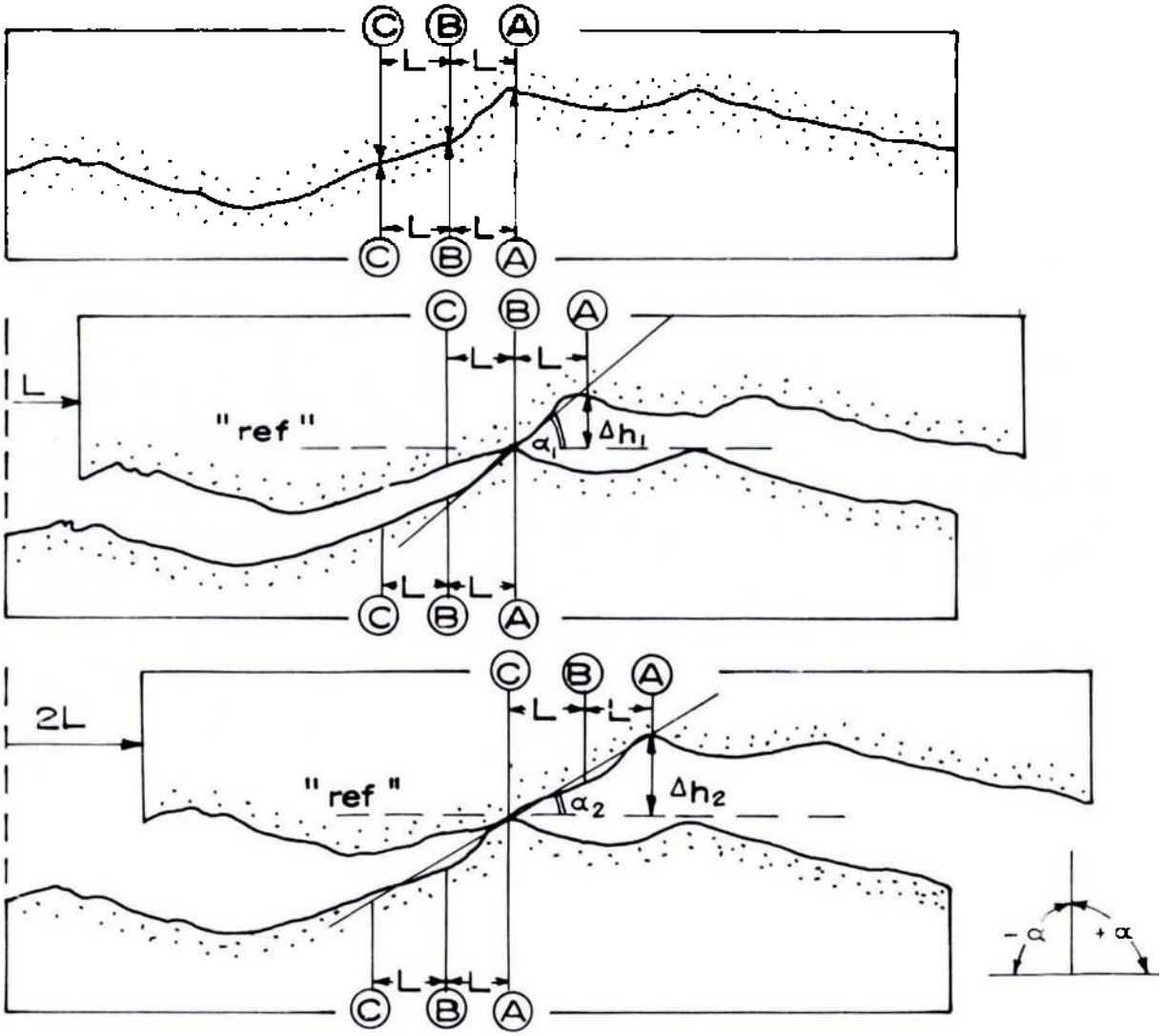

Fig. 10-36. Relationship between surface geometry and dilatation during shear displacement
(after FECKER and RENGERS, 1971).

displacement nL is dependent upon tan α (Fig. 10-36) and can be given by the relationship

$$\Delta h_n = nL \tan \alpha_n \tag{10.43}$$

where Δh_n = dilatation
nL = displacement (n steps of length L) and
α_n = maximum angle between the reference plane and the profile for the base length nL.

Fig. 10-37 represents dilatation and relative movement for free dilatation (zero normal pressure) calculated for the surface roughness of Fig. 10-35 using the above relationship.

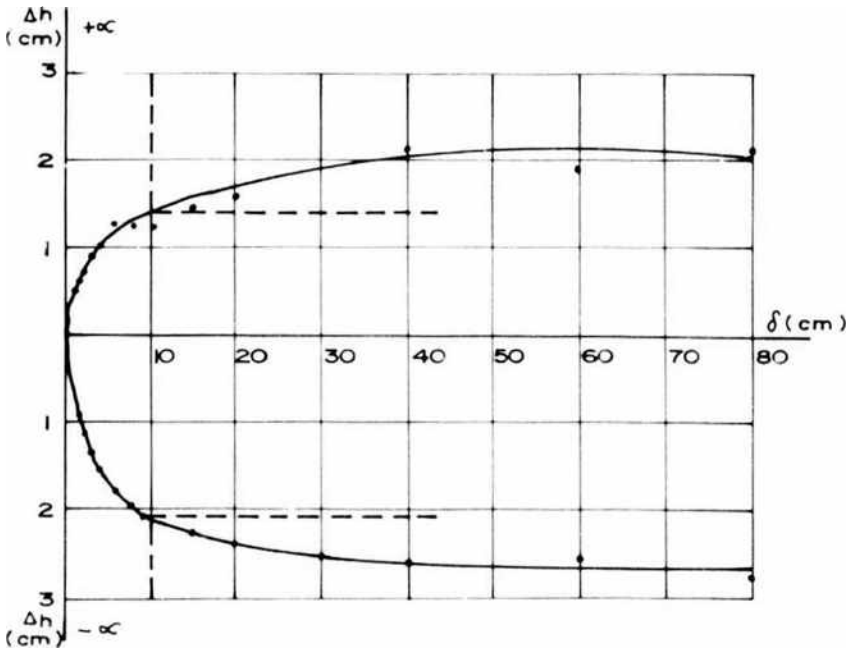

Fig. 10-37. Relationship between dilatation and relative movement with free dilatation possibilities for the plane with the surface roughness described in Fig. 10-35 (after RENGERS, 1970).

In another method of representing surface roughness, the variation in the surface profile from the mean or centre line is determined. The results are then reported in terms of the arithmetic average roughness defined as

$$Y = \left[\frac{1}{l}\int_{n=0}^{n=l} |y| dx\right] \tag{10.44}$$

where Y = arithmetic average deviation from the centre line
y = ordinate of the curve of the profile measured
l = length over which the average is measured.

Sometimes, instead of the arithmetic average, root mean square average may be used, when

$$Y_{rms} = \left[\frac{1}{l} \int_{n=0}^{n=l} (y^2) dx \right] \tag{10.45}$$

Roughness measuring instruments calibrated for root mean square average read approximately 11% higher on a given surface than those calibrated for average roughness.

Mutual area of contact of surfaces along joints

As a consequence of the roughness of the surfaces, the contact area between the two surfaces along the joint is always discrete, i.e. it occurs at individual points. These points in contact are deformed on application of normal load. This decreases the distance of separation between the two surfaces and hence increases the number of discrete contact points. Depending upon the angle of inclination of the asperities (shape), the distribution of the asperity height, and mechanical properties of the material, some of the asperities shall be deformed elastically, plastically or crushed on the application of load and hence the area of contact will change non-linearly with increase in load.

The mutual area of contact at any stage can be divided into 3 classes (Fig. 10-38):

1. The apparent (geometrical) contact area A_a which is the geometrical locus of all possible real contact areas outlined by the dimensions of the contacting solids and is independent of the load.

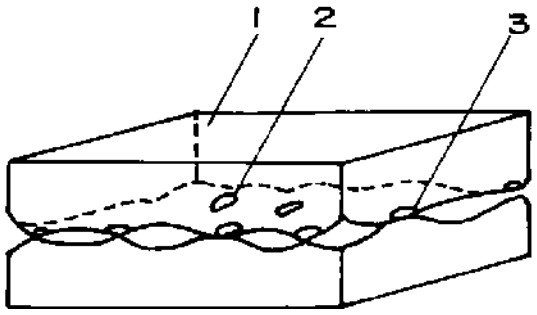

Fig. 10-38. Schematic diagram of two rough surfaces in contact:
1. apparent area
2. contour area
3. real area.

2. The contour area A_c which is the area constituted by the deformation of the surface undulations. The real contact areas are situated within the contour area; the latter depends upon the geometrical outline of the surface and the load.

3. The real (physical) area of contact A_r is the sum of all the small areas over which the two surfaces touch. This real area is a function of the geometrical contour of the individual irregularities and the load on each. The most important characteristic of the real area is the contact density which is given by the number of spots per unit area.

It is usually convenient to express the areas in dimensionless quantities:

$$\eta_1 = \frac{A_r}{A_c}$$
$$\eta_2 = \frac{A_c}{A_a} \tag{10.46}$$
$$\eta_3 = \frac{A_r}{A_a} = \eta_1 \times \eta_2$$

No work has been done on the area of contact between joint surfaces in rocks. In the field of metal friction, where the surfaces in contact are mechanically prepared by some form of repetitive processes (cutting, milling, polishing) a number of models have been developed to calculate the area theoretically. Some special cases are as follows (KRAGELSKII, 1965):

(a) Elastic contact between two rough surfaces:
   (*i*) Models involving hemispherical asperities in contact with a rigid plane.
   (*ii*) Models involving an assembly of rods.
(b) Elastic-plastic contact between a rough surface and a rigid plane without work hardening.

None of these theoretical models can be applied for rocks for in these idealisations, the amplitude and shape are repetitive in terms of their frequency which is not so true in case of joints except in special cases such as planes of discontinuities with ripple marks. The exact distribution and shape of asperities on rock surfaces have not been studied so far and it is not possible to predict which of the models will fit best.

No work has so far been done on the measurement of the surface of contact along joints. To a limited extent, methods used in metal friction studies may be applied for determining the real area of contact of rock surfaces. The methods used in metal friction can be divided into the following groups:
1. When both the bodies in contact are opaque.
2. When both the bodies in contact are translucent.

1. (a) Electrical resistance method:

BOWDEN and TABOR (1939) made use of the changes in electrical resistance for the measurement of actual area of contact between a moving and a stationary surface. The method is not free from error, because the magnitude of resistance is not only dependent upon the total area of contact but also on the diameter of the individual regions within the area. HOLM (1946) gave a detailed analysis of the method. The total resistance of a rough surface is given by:

$$R_2 = \frac{1}{4R\lambda} + \frac{1}{4n_a\lambda\rho_1} \tag{10.47}$$

where R_2 = total resistance of a rough surface
λ = conductivity
R = contour radius
n_a = number of individual contact spots and
ρ_1 = radius of each of these regions.

The difficulty experienced with rock is that the values of R, n_a and ρ_1 are not easy to determine.

1. (b) Adhesion method:

In this method a layer of radioactive isotope or a luminous phosphor is applied to one of the surfaces which on slight rubbing is transferred to the other surface. The intensity of the radiations per unit area is then measured. The method is quite simple but the major disadvantage is the difficulty of controlling the thickness of the applied layer of the material containing the radioactive isotope or the phosphor since the intensity of radiations is dependent upon its thickness.

Another approach to the adhesion method is by using a paint containing small quantities of a fluorescent material and photographing it which permits high contrast pictures of paint thickness of $0.01-0.1\ \mu$ ($3.9\times10^{-7}-3.9\times10^{-6}$ in) i.e. 10–100 times smaller than usual paint films. Both the layer of the paint transferred to the second surface and that remaining on the first can be determined. As an alternative, a paint of silver can be applied by electrodeposition. The points which are obtained by transfer of silver to the second member can then be examined in polarised light. A more rough technique is to use the paint to cover the surface which gives contrast pictures when rubbed off or transferred to the second surface. These contrast spots can then be metered to determine the contact area.

2. Light deflection method:

The method requires the making of transparent moulds of the two surfaces whose contact areas are required to be determined. The principle underlying the method is that when a light beam passes from a medium of high density to a medium of low density, it is deflected from its original direction. When the two surfaces are put together and a parallel beam of light is directed through one of them (Fig. 10-39), the light passes undeflected at the regions of contact while at other points it is scattered. The regions of contrast can directly be observed or photographed. The method is suitable for the study of rough surfaces but not for very smooth surfaces because light can be transmitted through very small air gaps and this results in a slight overestimation of the area of contact. This error may sometimes be 30–40 % for smooth surfaces.

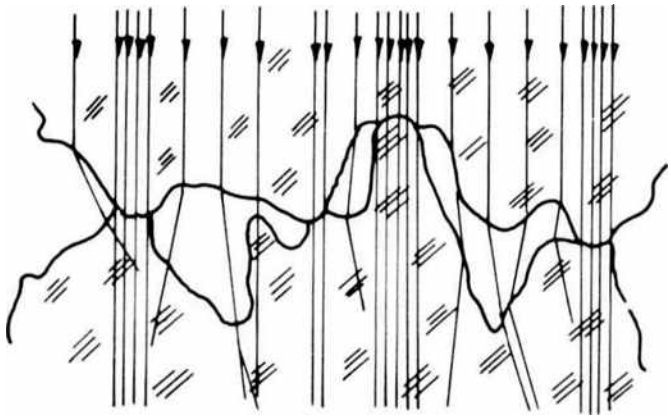

Fig. 10-39. Path of a light beam in two transparent surfaces in contact.

10.4.2. Factors Influencing Frictional Resistance of Rock Surfaces

Various factors that influence friction between the joint surfaces are:
1. Roughness of the surface
2. Displacement history
3. Normal load
4. Water
5. Filling material.

Their influence in detail is discussed below.

1. Roughness

Surface roughness is perhaps the most important factor influencing friction between joint surfaces. TSCHEBOTARIOFF and WELCH (1948) performed friction tests between quartz blocks sliding over quartz particles which were first polished and then roughened. They found that while the frictional coefficient for polished mineral particles under dessicator ($CaCl_2$) conditions was 0.106, its value rose to 0.370 for roughened particles.

RIPLEY and LEE (1961) tested specimens of sandstone, siltstone and shale. The frictional values so measured were corrected for dilatation (sliding up) and found that coefficient values so obtained were higher for rough surfaces than for ground surfaces (Table 1).

TABLE 1

Sliding resistance friction angles obtained from plane and rough surfaces

(after RIPLEY and LEE, 1961)

	Plane surfaces (Series B) 2.3 in (58 mm) square		Natural rough surfaces (Series A) 6 in (150 mm) diameter			
			Corrected		Measured	
	Ground smooth	Sand-blast	lower	peak	lower	peak
Sandstone	25°	29°	27°	36°	40°	54°
Siltstone	25°	31°	32°	34°	43°	47°
				31*		45*
			21°	24°	26°	34°
Shale	26°	27°	24°	35°	26°	35°
			25°	39°	31°	39°

* Test not carried beyond peak value.

The results of EINSTEIN et al (1969) are contrary to the conclusions of RIPLEY and LEE. EINSTEIN et al compared the MOHR's envelope for sliding along a pre-existing joint with the MOHR's envelope for "residual sliding" (sliding along a failure surface formed after fracturing which is without doubt rougher) for gypsum plaster as a model material. They reported that both the envelopes have the same inclination with the difference that the apparent intercept on the τ axis is greater for rougher surfaces.

HORN and DEERE (1962) found that etching of the polished quartz in a strong solution of ammonium bifluoride and water for 30 minutes slightly lowered

the friction value (Fig. 10-40) under oven-dried air-equilibrated conditions, and a substantial increase in the friction value under saturated conditions. Surfaces ground rough with No. 240 carborundum grit showed higher coefficients (Fig. 10-41) under both test conditions.

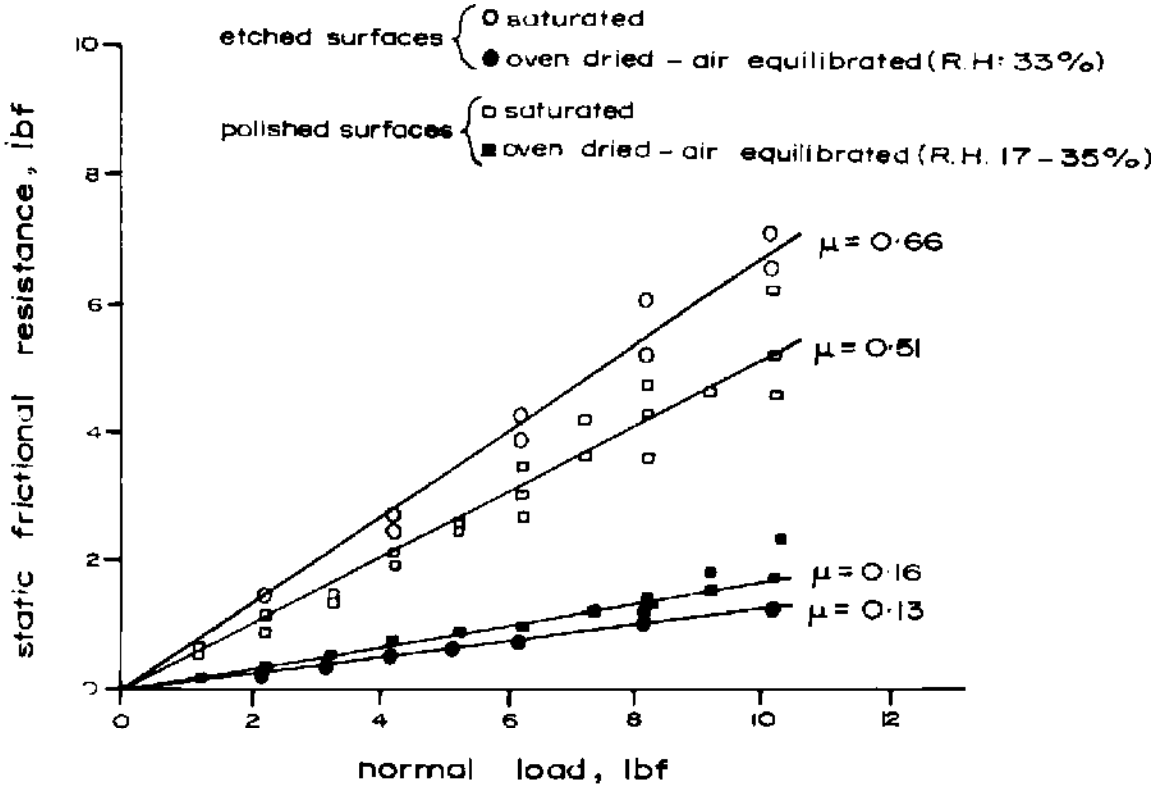

Fig. 10-40. The effect of etching on the static frictional characteristics of polished surfaces of milky quartz (Wisconsin) (after HORN and DEERE, 1962).

RAE (1963) measured coefficient of friction values between limestone slider and sandstone friction wheel and found that after a certain amount of wear, the coefficient of friction fell considerably (from 0.45 to 0.3).

BYERLEE (1967b) conducted tests on polished surfaces and reported that the coefficient of friction of finely ground surfaces is lower than that for coarsely ground surfaces. A considerable scatter in results obtained by him makes this conclusion doubtful. According to him, both for the ground surfaces and the mated surfaces (surfaces obtained by Brazilian test), the relationships between the shear stress τ and normal stress σ_n can be represented by

$$\begin{aligned} \tau &= 0.5 + 0.6\sigma_n \text{ (maximum friction on ground surfaces)} \\ \tau &= 0.5 + 0.6\sigma_n \text{ (initial friction on mated surfaces)} \end{aligned} \tag{10.48}$$

which indicate that the coefficient values are the same.

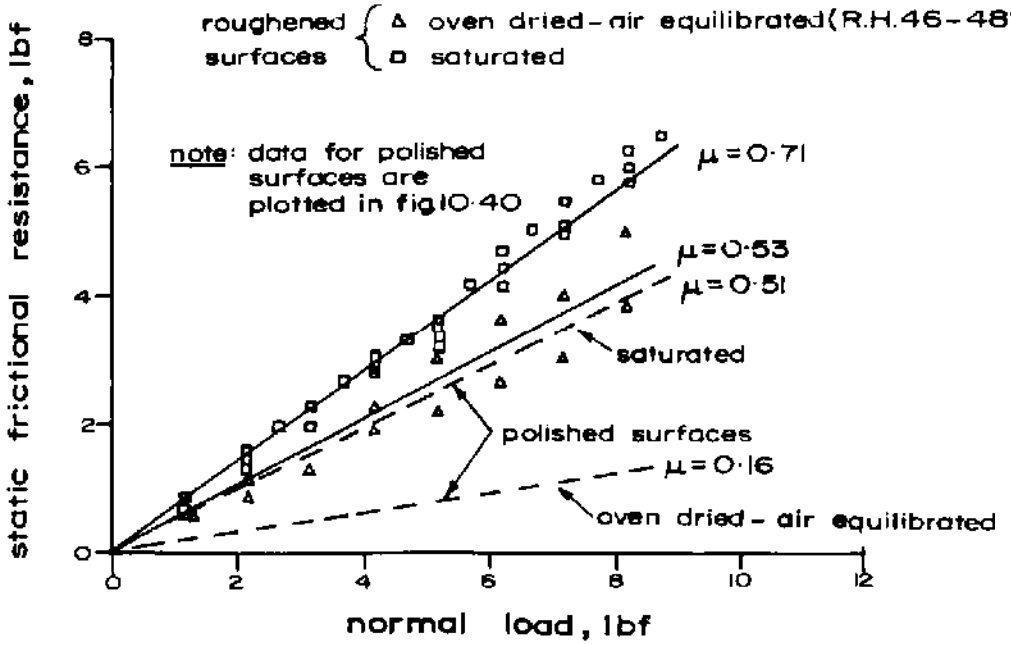

Fig. 10-41. The effect of surface roughness on the frictional characteristics of milky quartz (Wisconsin) (after HORN and DEERE, 1962).

HOSKINS, JAEGER and ROSENGREN (1968) suggested that the tangential stress between sliding surfaces is dependent upon the surface roughness. They found that the coefficient of friction for rough surfaces of trachyte was 0.68 and for polished surfaces (surface roughness 762 889 μ cm (300 350 μ in)) 0.58.

Studies conducted by COULSON (1970) indicate that surface roughness effectively increases initial friction for all rock types tested by him (basalt, granite, sandstone, gneiss, dolomite, limestone, siltstone, shale). The smooth surface polished with # 600 grit has the lowest coefficient of friction while # 80 grit polished and sandblasted surfaces have successively higher values. The difference at normal pressure of 0.07 MPa (10 lbf/in^2) is on the average 0.2 (for # 600 grit polished surface $\mu = 0.5$; for # 80 grit polished surface $\mu = 0.7$) and decreases to 0.1 at normal pressure of 6.89 MPa (1000 lbf/in^2). The effect of surface roughness on the residual coefficient of friction is a function of the normal force N. For normal pressure less than 0.69 MPa (100 lbf/in^2) surface damage is slight and roughness affects the residual coefficient of friction in the same manner as it affects the initial value of coefficient of friction. At normal pressure greater than 6.89 MPa (1000 lbf/in^2), surface damage tends to neutralise the effect of surface roughness and residual coefficients of friction are approximately equal for the different surfaces (# 80 grit polished, # 80 grit polished, sand blasted, # 600 grit polished).

CHAPPELL (1975) tested 6 in (15.2 cm) cores in a conventional shear box and found that for smooth graphite coated joints, $\mu = 0.29$ and for rough graphite

coated joints, $\mu = 0.42$. For similar smooth and rough joints tested by JAEGER (1971) in a triaxial machine, the values are 0.15 and 0.31 while on 2 in (5.04 cm) cores ROSENGREN (1968), in triaxial tests, found values of 0.2 and 0.44 respectively. The test technique did influence the results, but in all cases, the rough surfaces gave higher values.

Work conducted at the Centre for Tectonophysics, Texas A & M University (HANDIN, 1972b) has shown very interesting results. The experiments were conducted in a triaxial cell using cylindrical specimens which had been cut at a certain angle (29 37) to the specimen axis. Tests on Tennessee sandstone with the cut prepared with different roughnesses (saw cut—average roughness 1651 μ cm (650 μ in), # 80 grit wheel polished —average roughness 1219 μ cm (480 μ in), light # 600 grit lapping—average roughness 1016 μ cm (400 μ in), extensive # 600 grit lapping— average roughness 813 μ cm (320 μ in)) were carried out. The results showed that both smoother and rougher surfaces were stronger and that stress drops (stick-slips) are generally greater than for the 1016 μ cm (400 μ in) surface (Fig. 10-42). The values of the coefficient of friction showed these are higher both for highly smooth and rough surfaces (Fig. 10-43).

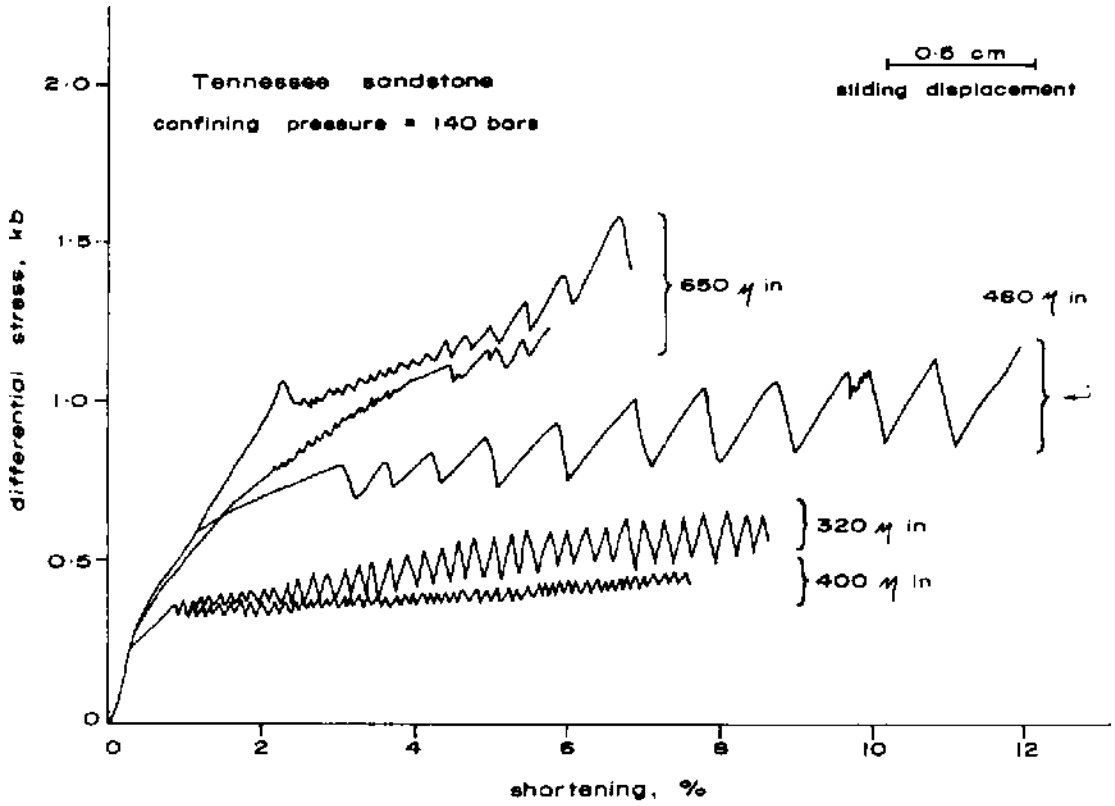

Fig. 10-42. Differential stress versus shortening curves for Tennessee sandstone obtained for various surface roughnesses. All tests were done at a confining pressure of 140 bars, room temperature and a constant rate of shortening of 10^{-4}/s (after HANDIN, 1972b).

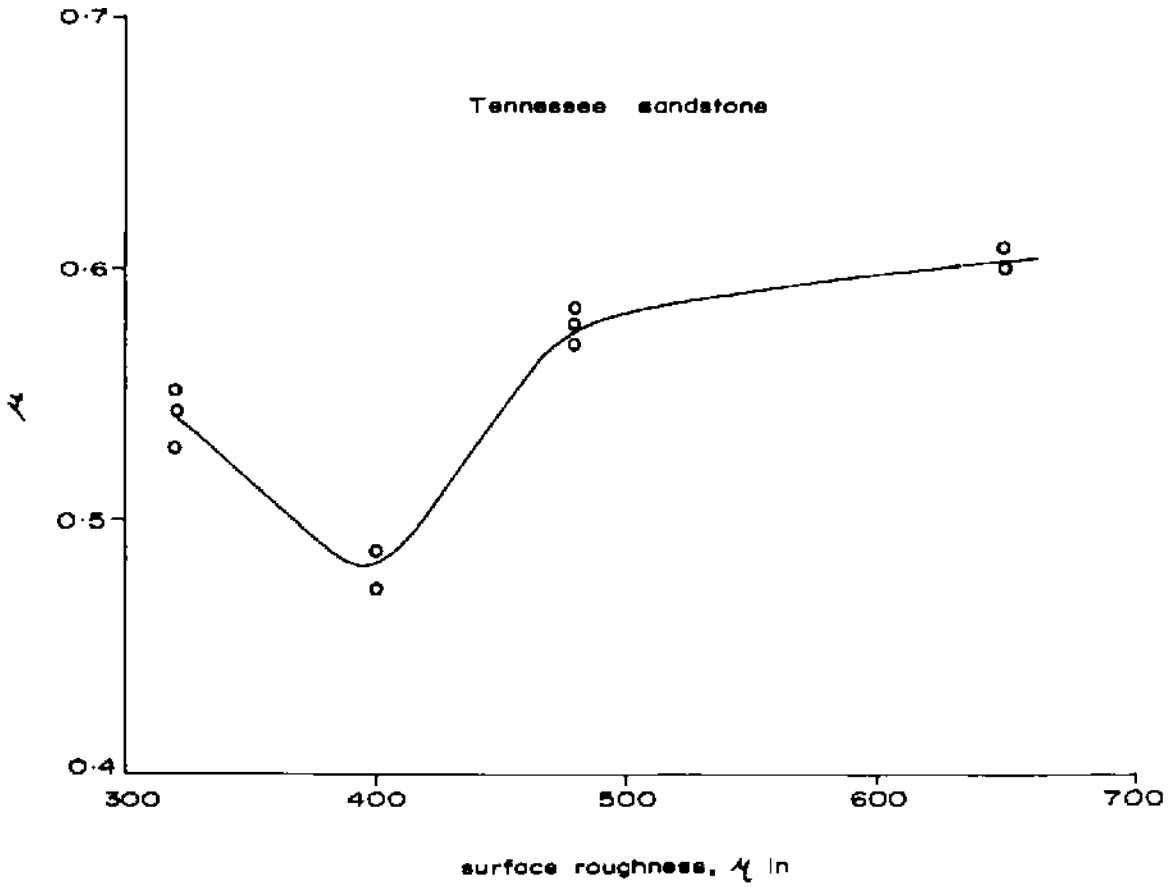

Fig. 10-43. Coefficient of friction, μ, versus surface roughness in microinches. Values were calculated at the ultimate strength for each experiment. All experiments were conducted at 140 bars confining pressure, room temperature and a constant rate of shortening of 10^{-4}/s (after HANDIN, 1972b).

It is suspected that both dilation and relative rotation of the block influence the values of friction obtained and if these influences can be accounted for, the final friction value will be independent of the nature of the surface. Dilation correction can be easily incorporated using the concept given in Eq. 10.10 but the rotational correction is not easy to apply. At high normal loads, the possibility of rotation is decreased and the μ approaches the value of smooth joints. That is why HANDIN (1972b) observed high values for both highly smooth and rough joints. At higher pressures, the frictional value will tend to equal that of a smooth surface as indicated in Fig. 10-44.

2. Displacement history

It is a common observation in many in situ and laboratory shear tests that the shear force increases with displacement until it reaches a maximum value and then drops to a certain residual value.

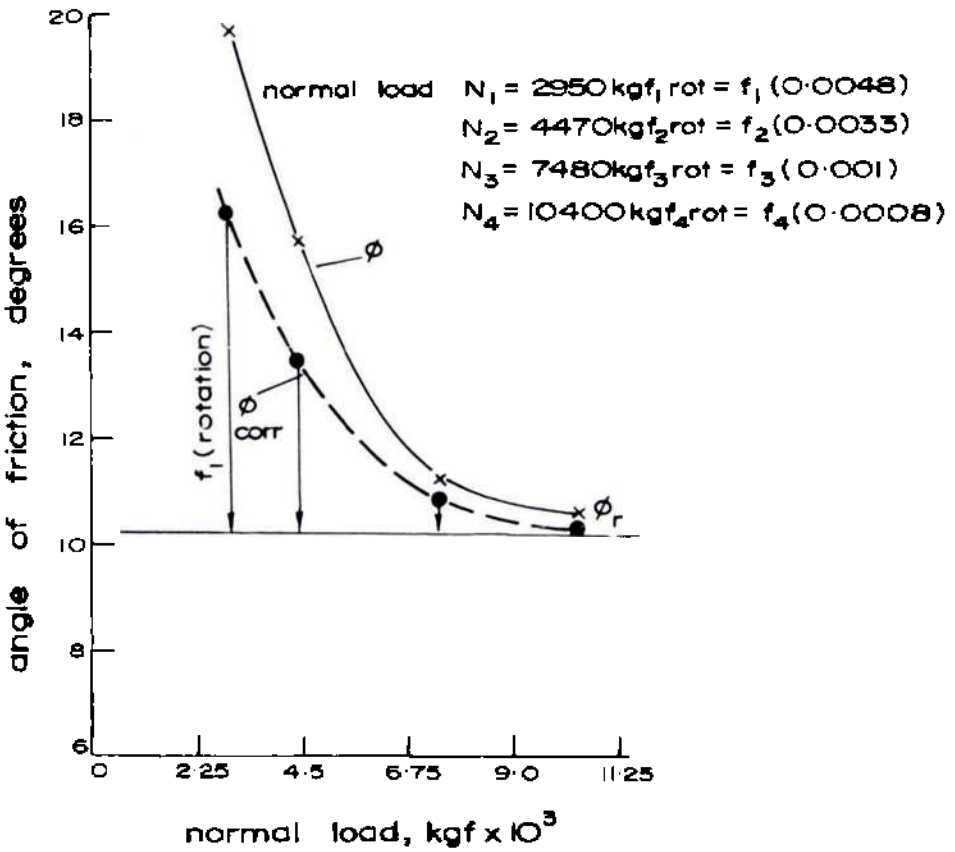

Fig. 10-44. The effect of rotation on the correction for the apparent angle of friction to give the angle of friction for a smooth joint. Values in brackets give rotation angle (radians) (after CHAPPELL, 1975).

BYERLEE (1966) conducted tests on Westerly granite specimens of 3 to 8 cm (1.2 to 3.1 in) long, 1.58 cm (0.62 in) diameter with sliding surface 45 to the axis of the specimens and found that for ground specimens frictional force increased with displacement until a maximum was reached after approximately 0.1 cm (0.04 in) of sliding and then decreased to a constant value after about 0.5 cm (0.22 in) of relative displacement between the two surfaces. The difference in the maximum and residual values of frictional force was only about 7%.

BARTON (1971a, b) conducted a series of tests on rough tension joints in a weak model material and reported that peak strength reached after tangential displacements of approximately 1% of the length of the joint and that the drop of the peak strength towards residual strength occurred at a displacement of approximately 10% of the length of the joint.

HOSKINS, JAEGER and ROSENGREN (1968), testing friction properties of laboratory prepared surfaces in a double shear apparatus, showed that at different normal loads, the frictional force for rough surfaces first increases rapidly with displacement and subsequently at a steadily decreasing rate. The shear force

varies with the amount of displacement that the two surfaces have undergone and is dependent upon the ultimate characteristic of the surface and perhaps the normal stress.

MATHEWS (1970) conducted tests on graphite coated joint surfaces and the results obtained by him are shown in Fig. 10-45. It shows the contour lines for the graphite coated joint while Fig. 10-45b shows the variations in the shear force and dilatation. Fig. 10-45c shows the position of the two surfaces after 2.54 cm (1 in) of sliding. It is clear that increase in the shear force is not associated with dilatation and its maximum value is attained at a displacement of less than 0.25 cm (0.1 in) while maximum value of dilatation is reached at a displacement of about 1.73 cm (0.68 in). The contact of the surfaces is only at a very small number of points where intense shearing and removal of material occurs and this sheared material ultimately fills the hollows.

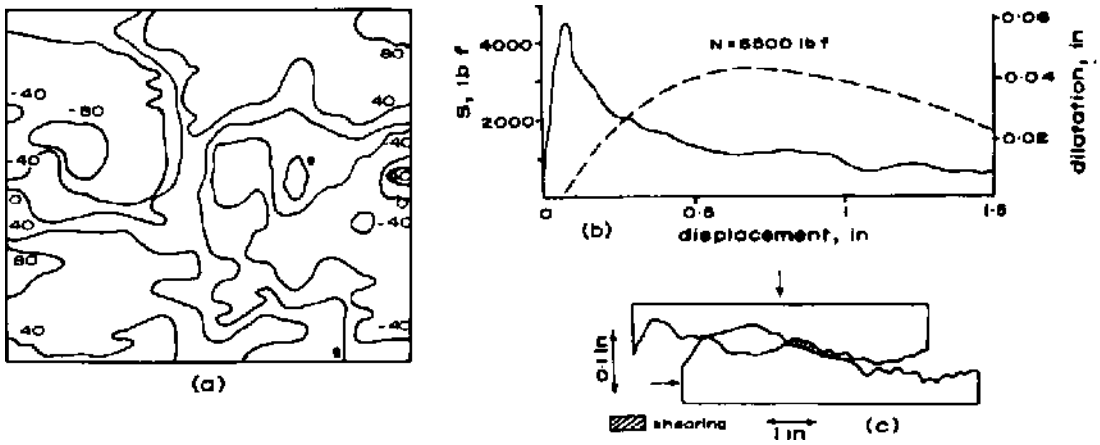

Fig. 10-45. (a) Contour lines (units of 0.001 in) for a graphite coated joint surface of area 5 in by 6 in
(b) Shear force and dilatation for the joint in a shear box with normal load of 6500 lbf.
(c) Relative positions of a cross-section of the surface after 1 in of sliding (after MATHEWS, 1970).

Repetitive experiments were carried out by JAEGER (1971) on a pair of mated surfaces of Bowral trachyte in the double shear test apparatus (Fig. 10-18c). The surfaces were prepared by Brazilian test and had irregularities of 0.25 cm (0.1 in) with grain size of 0.076 cm (0.03 in). The first cycle of loading was at a normal load of 1350 lbf (6005 N) (Fig. 10-46). (Numbers in the figure refer to the cycle.) After about 1.016 cm (0.4 in) of displacement, surfaces were taken apart, the debris was brushed aside and remated and retested to obtain the second cycle. The curve 7 shows the seventh cycle with normal loads of 9119 N. 12055 N and 15391 N (2050 lbf, 2710 lbf and 3460 lbf). The 15th run showed that all traces of initial peak had disappeared and the surfaces had been ground down to moderately rounded asperities occupying almost 80% of the total area

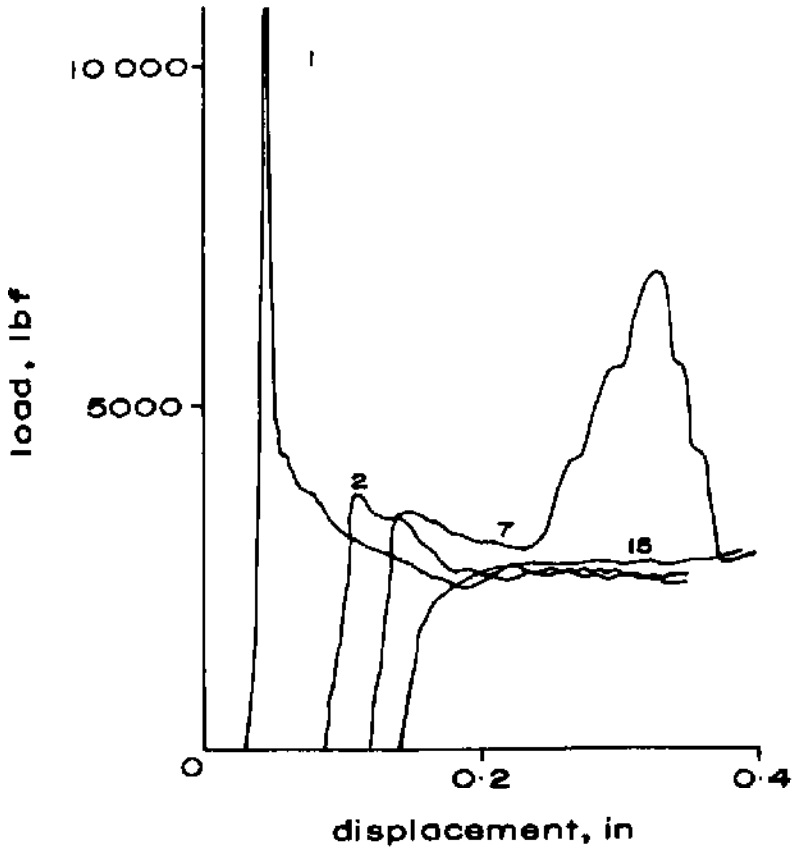

Fig. 10-46. Variation of frictional force with displacement for a surface of tensile fracture in Bowral trachyte; area 5.2 in^2; normal load 1350 lbf. (after JAEGER, 1971).

with hollows of original surfaces in between them. The shape of the shear load displacement curve changed with each cycle and in the 15th cycle the peak had disappeared with the residual (also maximum) shear force reaching at about 0.25 cm (0.1 in) of displacement.

Different behaviour is obtained when a rough surface slides over a smooth surface. JAEGER (1971) conducted tests on the sliding of a block of Bowral trachyte with ground plane-parallel surfaces placed between a pair of rough surfaces obtained by extension fractures. The results obtained are shown in Fig. 10-47. The curves 1, 6, 18 represent the first, sixth and eighteenth cycle each for the displacement amplitude of 1.27 cm (0.5 in). The shear force first increases with displacement and then is maintained. The maximum value of the shear force at the first cycle is lower than in the later cycles. With displacement, the regions of tension cracks are always in contact with the opposite surface and the areas of these contacts grow steadily. Similar results were obtained by JAEGER and COOK (1969b) for sliding of gravel on plane surfaces.

Even with completely ground surfaces, it has been found that there is a considerable variation in the shear force with displacement and the constant value of the tangential force is approached rather slowly.

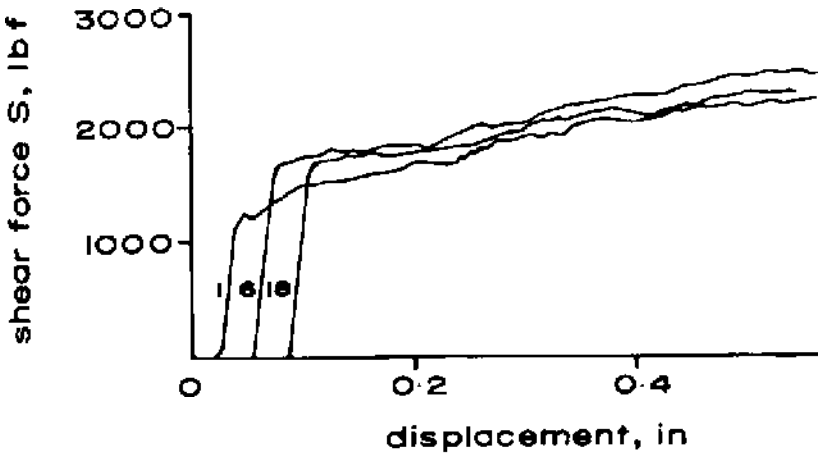

Fig. 10-47. Variation of frictional force with displacement for sliding of surfaces of extension fractures on a flat surface (after JAEGER, 1971).

With natural joints which are rather discontinuous, the shear force usually rises to a peak value with small displacement and then falls sharply. This peak is followed by considerable fluctuations before the residual value is reached (KRSMANOVIC, 1967).

According to PATTON (1966a), the effective width of the asperity (i.e. length along the base of the asperity) plays an important role in the shear force displacement behaviour of a joint. Fig. 10-48 represents the shear strength

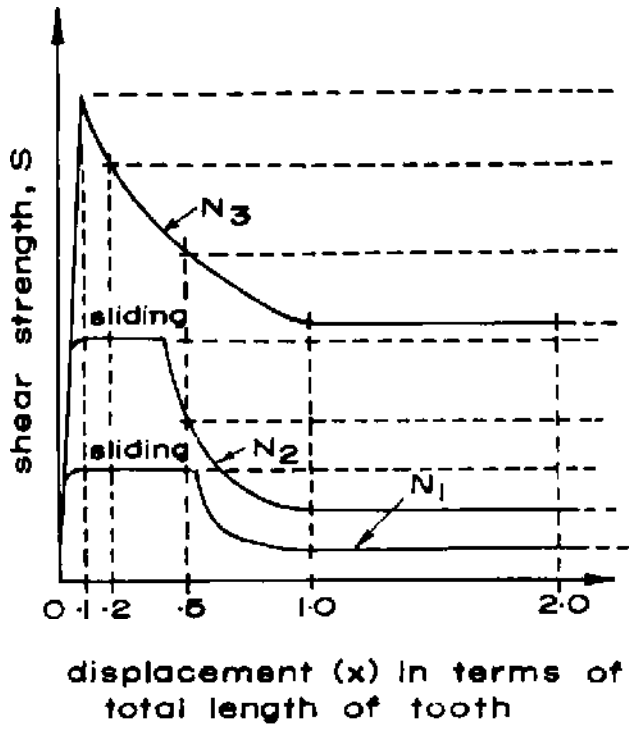

Fig. 10-48. Shear strength displacement curve (after PATTON, 1966a).

curve for 3 specimens with different values of normal loads $N_3 > N_2 > N_1$. The peak values obtained are dependent upon the position of shearing of the asperities. When the specimen is sheared off along the base of the asperity (N_3) the highest value is obtained at a small displacement (0.1 x asperity base) followed by the residual shear strength. When the shearing takes place after a certain amount of displacement along the asperity (N_2 and N_1), the highest value of shear strength obtained is lower. Residual values are obtained when the displacement reaches a value of 1.0 x asperity base.

COULSON's (1970) results on lapped sandstone surfaces show that the displacement required to reach residual shear strength is dependent upon rock type, surface roughness, moisture and the type of surface damage manifested during shearing. When polishing and profuse gouging occur, the shear strength increases with further displacement. The development of indurated crust and low gouging is associated with decreasing shear strength with displacement. The increase in pressure results in decreasing the displacement required for residual shear strength of joints.

DRENNON and HANDY (1972) found that for tests on clean blocks of limestone at normal stress of 0.98 MPa (142 lbf/in^2) (10 kgf/cm^2) and under, the coefficient of friction tended to remain stable or slowly rose, but for tests with debris introduced in between the blocks, the initial static coefficient of friction ranged from 0.406 to 0.551 and climbed rapidly to values much above those reached on tests with clean blocks, reaching in one case a value of 1.002 (Fig. 10-49).

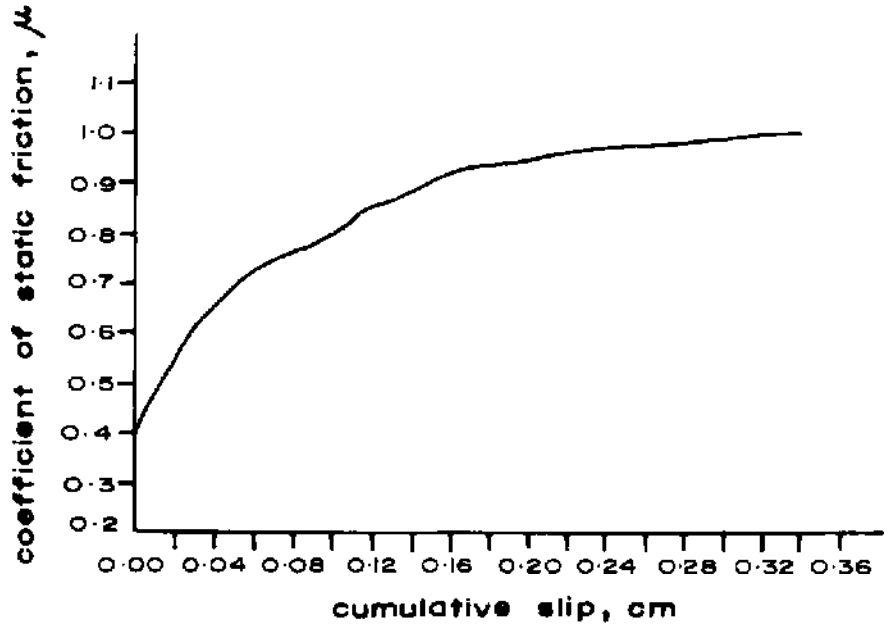

Fig. 10-49. Increase of coefficient of static friction with slip.
Test 99C, 10 kgf/cm^2, at 125 C, debris test
(after DRENNON and HANDY, 1972).

JAEGER and ROSENGREN (1969) divided the displacement behaviour of the joints according to the nature of the joint (Table 2). The corresponding characteristic curves are given in Fig. 10-50.

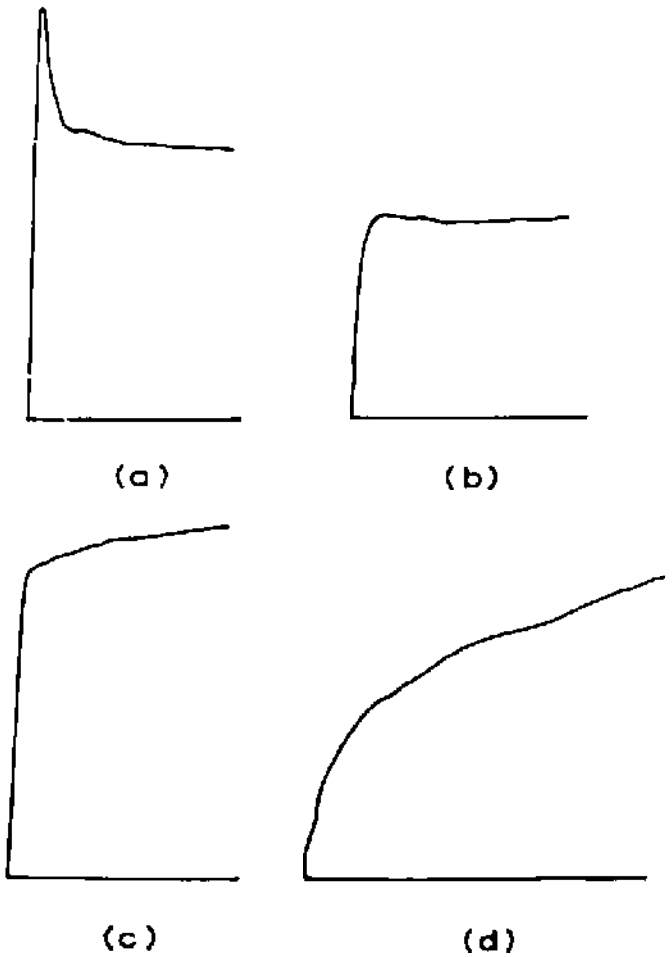

Fig. 10-50. Types of load – displacement curves for natural joints.
For description see Table 2
(after JAEGER and ROSENGREN, 1969).

Very conclusive evidence of the shape of the curve as a function of the surface geometry is given by SCHNEIDER (1972) and LAMA (1975b). Using 3 different geometries obtained in tension tests (granite, sandstone and limestone) and producing replicas using plaster of Paris as the model material, SCHNEIDER (1972) conducted tests at different normal pressures. The results are summarised in Fig. 10-51. The properties of the model material remaining constant, the shear stress-displacement curve is different for different surfaces. The granite surface is much rougher while the limestone surface is rather smooth. The first gives a peak shear strength followed by a drop in its value while the second gives almost no drop in shear strength with displacement. The curve for sandstone which has medium surface roughness has shear characteristics somewhat in between. Similarly, dilation is higher for rougher joints and smaller for smoother joints.

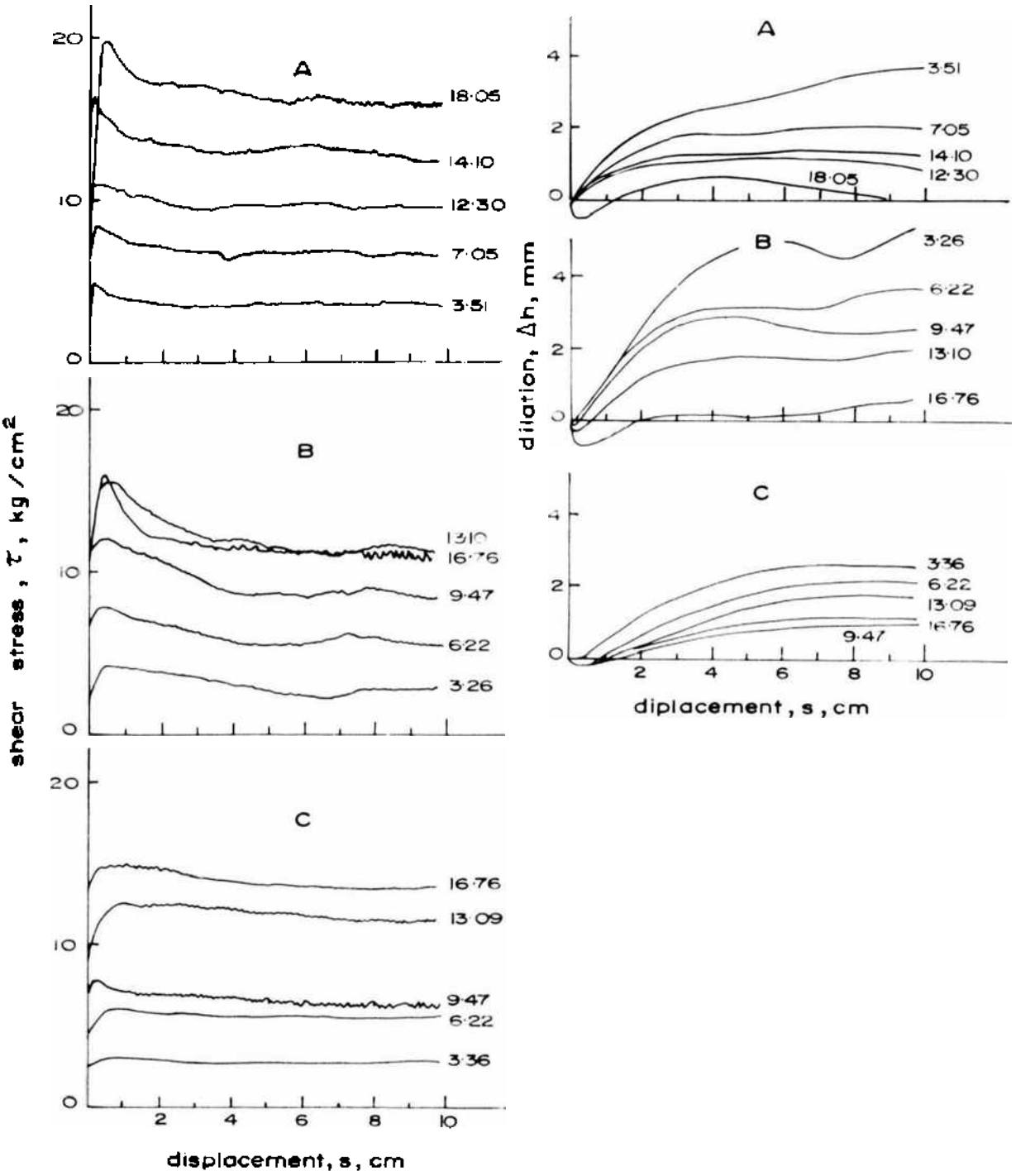

Fig. 10-51. Shear stress – displacement and dilation-displacement curves for the different roughnesses using gypsum as a model material
A – granite; B – sandstone; C – limestone
(after SCHNEIDER, 1972).

TABLE 2

Load-displacement curve characteristics

(after JAEGER and ROSENGREN, 1969)

Type of behaviour	Characteristic joints
A. No slip until peak load then gradual drop off to residual value Fig. 10-50(a)	Joints with large interlocking asperities; bedding planes with cross ripples; faults with cross slickensides or grooves.
B. Well defined initial slip which continues at constant load Fig. 10-50(b)	Joints with hard, fairly smooth surfaces; also Narrandera quartzite.
C. Well defined initial slip which ontinues with rising load Fig. 10-50(c)	Relatively rough, chlorite or graphite coated surfaces; very smooth hard surfaces.
D. Continuous curvature of load displacement curve Fig. 10-50(d)	Faults with smooth or polished chloritic surfaces.

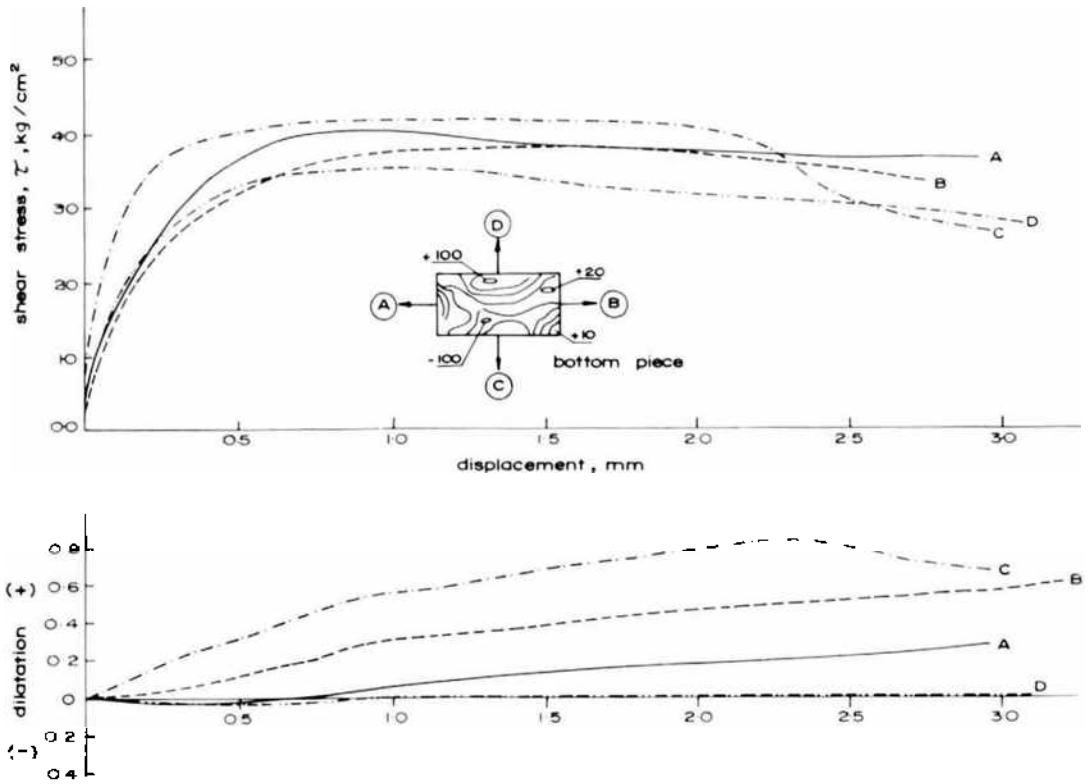

Fig. 10-52. Influence of direction of displacement on the shear behaviour of model joints of marble surface obtained in a Brazilian test (model material gypsum).
σ_n = 0.289 MPa; Displacement rate = 0.12 mm min.
(after LAMA, 1975b).

Roughness produced in different directions is not the same depending upon grain orientation and fracture anisotropy. This affects the surface geometry and the shear-displacement curve. The results obtained by LAMA (1975b) where the tests were conducted using the same geometry and same model material but the shear direction was changed are shown in Fig. 10-52. The phenomenon is not simple but is influenced by the material property and interaction between the material property and the surface geometry (LAMA, 1975b). This view has also been expressed by DONATH, FRUTH and OLSSON (1972).

3. Normal stress

The value of the coefficient of friction μ does not remain constant with change in the value of the normal stress. The residual frictional force from which the coefficient of friction is calculated is not only due to pure sliding of the two blocks but is also influenced by the crushing of the broken asperities, and rolling and induration into the enclosing surfaces. The possibility of crushing of these pieces increases with increase in the value of the normal force and hence at higher values of normal force, the movement shall be more and more governed by turning of the crushed pieces and less and less due to shearing of the asperities. As such, the value of the frictional coefficient calculated is likely to be smaller with higher value of normal force.

HANDIN and STEARNS (1964) found that the coefficient of friction at a higher normal stress is lower than at lower values of normal stress for dolomite, limestone and sandstone. They suggested that the existence of lower friction coefficients at higher normal stresses was because the surfaces became smoother. RALEIGH and PATERSON (1965) also found that the coefficient of friction of peridotite sliding on shear surfaces decreased with confining pressure.

JAEGER and COOK (1969b) reported that for spherical trachyte contacts sliding on trachyte with varying areas of contact at higher normal loads the value of $\mu = 0.32$ and at lower normal loads $\mu = 0.48$. COULSON (1970) found that the result of increasing normal pressure from 0.069 to 6.89 MPa (10 to 1000 lbf/in^2) is to reduce the initial coefficient of friction for all surface roughnesses from 5 to 20%. In the case of rocks with low porosity and low strength an increase in the coefficient of friction with an increase in normal pressure was observed. He explained this as being due to deep penetration of the asperities into the opposing surface upon application of normal pressure. This asperity penetration and surface interaction increases with increase in normal pressure.

MAURER (1966) conducted several tests on sandstone, limestone, marble, shale, dolomite, granite and basalt at various normal pressures and found that the coefficient of friction when determined from residual shear resistance is dependent upon normal stress and decreases as contact pressure increases. According

to him, the friction coefficient can be related to the normal pressure by the equation

$$\tan \phi_r = a(\sigma_n)^k \tag{10.49}$$

The values of a and k are given in Table 3.

TABLE 3

The values of a and k in Eq. 10.49

(after MAURER, 1966)

Rock type	a	k
Beckmantown dolomite	36.0	0.60
Berea sandstone	6.4	0.80
Carthage marble	29.0	0.63
Chico limestone	22.0	0.65
Georgia granite	46.0	0.55
Indiana limestone	60.0	0.46
Knippa basalt	48.5	0.56
Rush Springs sandstone	14.0	0.71
Seminole shale	3.7	0.73

The coefficients of friction for stronger rocks are nearly equal decreasing from 1.8 to 0.8 as the normal pressure is increased from 13.79 MPa (2000 lbf/in^2) to the uniaxial compressive strength of the rock. The coefficients of friction for weaker rocks are also much the same as for stronger rocks and the friction angle is independent of the strength of the rock.

HOBBS (1970) conducted tests on broken cylindrical specimens of coal measure rocks in a triaxial cell with a single spherical seat (top). The specimens were first subjected to a given confining pressure 20.7 MPa (3000 lbf/in^2) and then axially loaded to failure. The pressure was then raised by increments and the axial load to cause slip at each increment was determined. He found that shear and normal stresses to cause movement of the broken cylinders can be represented by the relationship

$$\tau = k(\sigma_n)^a \tag{10.50}$$

where k and a are constants.

The values of k and a found by him are given in Table 4.

TABLE 4

The values of k and a in Eq. 10-50 (after Hobbs, 1970)

Rock type	k	a
Ormonde siltstone	1.58	0.756
Bilsthorpe silty mudstone	1.53	0.736
Hucknall shale	1.46	0.784
Bilsthorpe mudstone	1.15	0.817

The values of k and a are dependent upon the confining pressure at which the specimens were broken previous to the test. The value of k decreases while that of a increases with increase in the initial confining pressure values. This is possibly due to the initial movement which takes place—the magnitude of which is high for low confining pressures.

Byerlee's (1966) tests on Westerly granite showed that for sliding along a surface when shear stress is plotted against normal stress a straight line is obtained with a positive intercept on the shear axis showing shear strength at zero normal stress. He found no discontinuity in the experimental data indicating thereby no change in the physical process involved during sliding which would otherwise be expected if the failure process changed from brittle to ductile under high normal pressures. The coefficient of friction, he argued, is due to the interlocking of the asperities which have a finite strength at zero normal load across the sliding plane. He represented the coefficient of friction by the relationship

$$\mu_n = A + \frac{\tau_i}{\sigma_n} \tag{10.51}$$

where μ_n = coefficient of friction at normal stress σ_n
A = rate of change in the strength of the material with increase in normal stress
τ_i = shear strength of the material at zero normal stress and
σ_n = normal stress.

Further tests conducted by Byerlee (1968a, 1975) showed that the influence of normal stress could be represented either by two straight lines or a parabola. For example, for Weber sandstone (a grey to dark red coloured sandstone containing calcite as a binding material with limonite and hematite), the shear strength of joints could be represented by

$$S = 0.85N \qquad \text{for } 0 < N < 2\,kb$$

and

$$S = 0.5 + 0.6N \qquad \text{for } N > 2kb.$$

At lower values a power law of the form given in Eq. 10.50 best describes the shear and normal stress behaviour.

DRENNON and HANDY (1972) determined the coefficient of friction of limestone in both smooth slip and in the load and unload modes of stick slip. They found that during initial loading static coefficient of friction of fresh blocks ranged from 0.198 to 0.533, being low at low normal stresses and high at high normal stresses. They also observed that at low normal stresses, the value of static coefficient of friction varied considerably depending upon the past frictional history of the specimen.

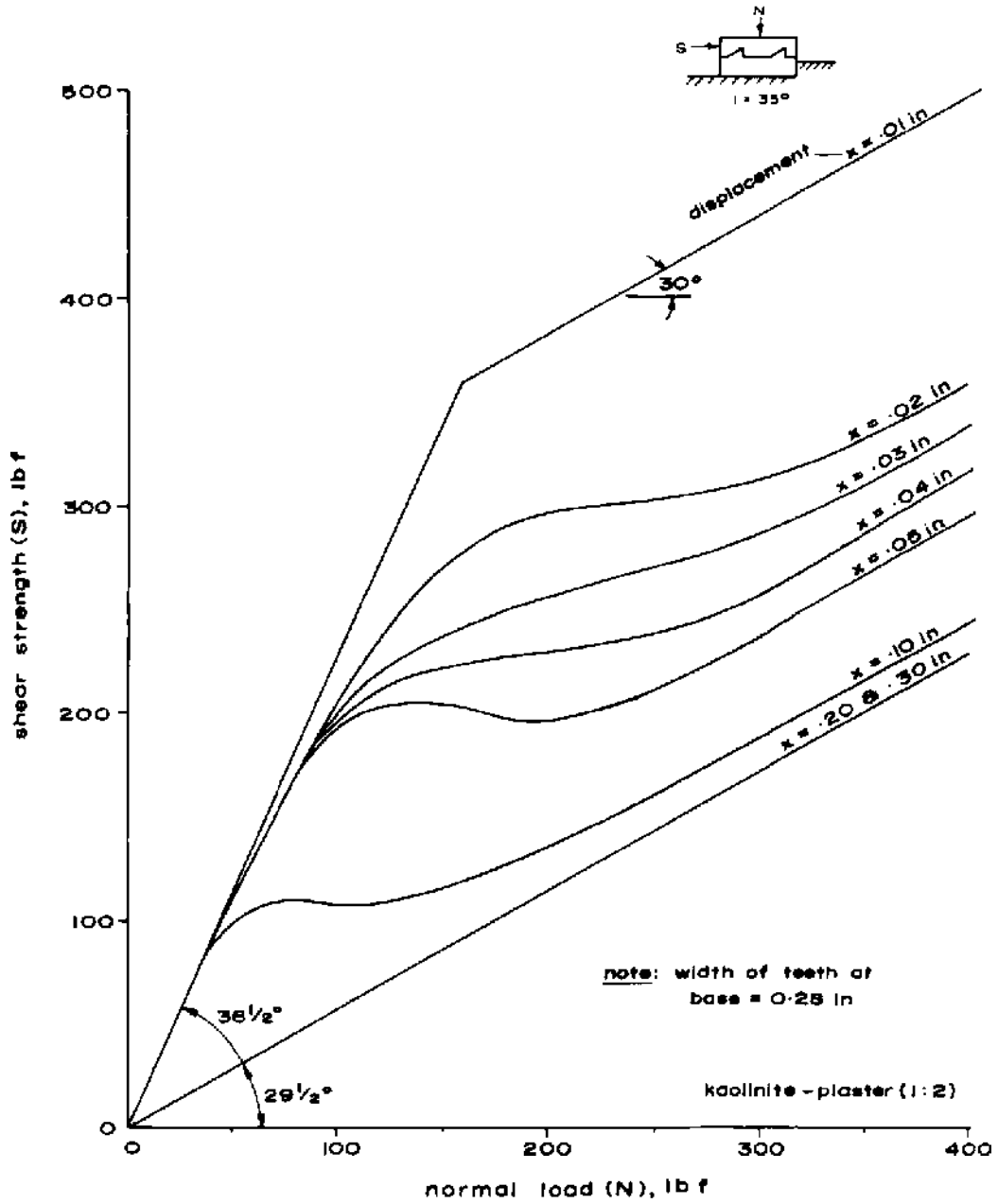

Fig. 10-53. Shear strength – displacement envelopes (after PATTON, 1966a).

PATTON's (1966a) results on the influence of normal load on the shear strength displacement diagram are given in Fig. 10-53. The curves are obtained by calculating the shear resistance after equal intervals of horizontal displacement and joining the points representing equivalent displacements. It is seen that at high normal loads a large reduction in strength occurs with small displacements. At lower normal loads, displacement can be much greater before a serious loss in strength occurs.

Besides normal stress, normal stiffness of the test system influences the results. High normal load stiffness tends to limit dilation of the joint and may increase shear strength depending upon the relative normal stiffness and the tensile strength of the material (assuming that failure in shear is due to tensile failure of the asperities). Tests on granite and sandstone using double shear (Chapter 4, Section 4.4.3.) and at various normal stiffnesses (k = 0.02 MN/m – 200 MN/m) have shown that peak shear strength at lower normal stress is not significantly different for different normal stiffnesses but at higher normal stresses, the results obtained with high stiffness testing system may be almost 20% higher (OBERT, BRADY and SCHMECHEL, 1976).

4. Water

TSCHEBOTARIOFF and WELCH (1948) found that an appreciable difference existed in the frictional values between dry and moist conditions and that the slightest humidity in the surroundings rapidly affected the friction results. The coefficient of friction values obtained by them for different minerals are given in Table 5. There is an increase in the value of the coefficient of friction only for quartz and calcite. They explained this difference as being presumably due to absorbed layer of water on the surface of these minerals.

HORN and DEERE (1962) found that frictional coefficients of oven dried surfaces and those of oven dried air equilibrated surfaces did not differ much for the massive structured minerals but a distinct difference existed for the layer lattice minerals (Table 6). They also found that the relative humidity of the surrounding air influenced the coefficient of friction values and its influence depended upon the structure of the mineral. Results obtained on quartz (massive structure) showed that the coefficient of friction is fairly constant at low relative humidities and does not change appreciably until a 'threshold' relative humidity (about 40%) is reached after which it increases rapidly until the saturated coefficient is reached at a relative humidity of 100% (Fig. 10-54). In case of muscovite (layered-lattice structure), the coefficient of friction is particularly sensitive to variations in relative humidity below 40% while above 40%, it decreases in almost a linear fashion till at about saturation point when it drops suddenly. The results at saturated air equilibrated surfaces are much the same as those for the saturated surface with a minimum of 1.59 mm (1/16 in) of layer of distilled water.

TABLE 5

Average values of friction coefficients obtained under dry and moist conditions

(after TSCHEBOTARIOFF and WELCH, 1948)

Mineral	Dry[a]	Moist	Submerged
Quartz on quartz	0.106	0.455	0.455
Calcite on calcite	0.107	0.268	0.263
Pyrophyllite on pyrophyllite	0.163	0.120	0.122
Pagodite on pagodite	0.198	0.166	0.165
Quartz on calcite	0.098	0.266	0.333
Quartz on pyrophyllite	0.152	0.194	0.180
Quartz on pagodite	0.179	0.162	0.168
Calcite on pagodite	0.168	0.157	0.152
Calcite on pyrophyllite	0.233	0.127	0.134
Pyrophyllite on pagodite	0.179	0.113	0.113

[a] Dried in $CaCl_2$ desiccator and then quickly tested.

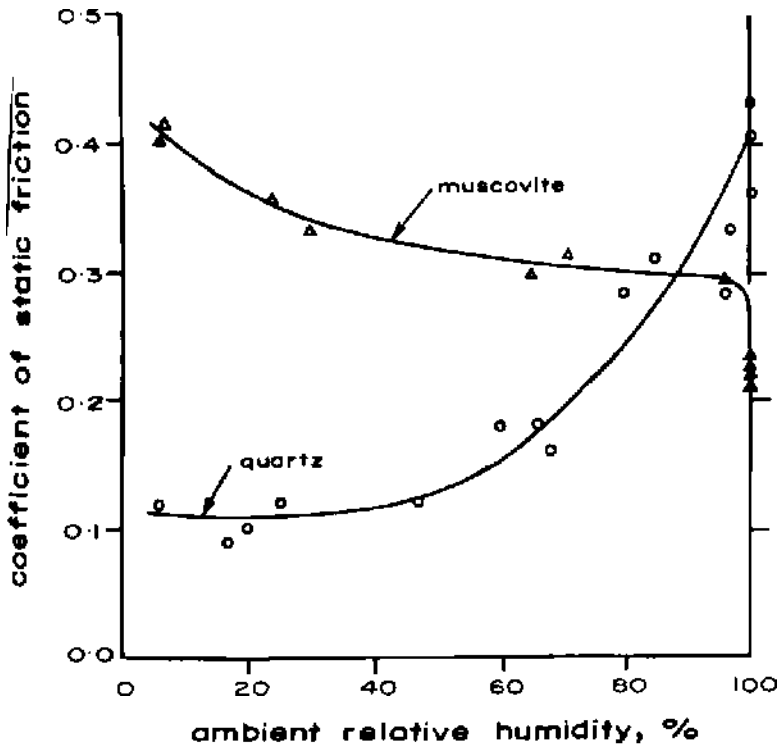

Fig. 10-54. Relationships between the coefficient of static friction and the ambient relative humidity for muscovite (Brazil) and clear quartz (N. Carolina) (after HORN and DEERE, 1962).

The influence of moisture on the coefficient of friction depends upon the crystal structure of the mineral. Water acts as an anti-lubricant in case of massive (three dimensional) crystal structures (quartz, microcline feldspar, calcite) while it serves as a lubricant in case of layered-lattice (two dimensional) minerals (muscovite, biotite, phlogopite, chlorite etc.). The ratio of the coefficient of static friction for saturated and oven-dried surfaces of massive structure minerals varies from 3 to 7 and for the layered-lattice minerals from 0.4 to 0.6 (Table 6).

This differential behaviour of water was explained by HARDY and HARDY (1919) as being the action of water which reduces the mobility of the adsorbed film composed of highly oriented molecules. The force field associated with the polar molecules disrupts the orientation of the adsorbed layer increasing friction. This phenomenon was demonstrated by MENTER (1950) who showed by electron diffraction studies the influence of disorientation of the molecules of a boundary lubricant on increase in the frictional resistance.

BROMWELL (1966) showed that the coefficient of friction of dry chemically clean polished quartz is 0.9 and that this remains unchanged when wetted. This indicates that water is basically neutral to quartz and that its antilubricating influence is due to its reaction with the lubricant boundary layer. LAMBE and WHITMAN (1969) have given a further discussion on the antilubricating influence of water.

A completely different viewpoint was put forward by BYERLEE (1966). According to him, the influence of the fluid is to increase attractive force between the surfaces due to the surface tension effect. It is possible that for polished surfaces, this plays a certain role.

HORN and DEERE (1962) investigated the influence of non-polar and polar fluids. They reported that the influence of high polarity fluids (water, ethylene glycol, amylamine) on frictional coefficient was much more than the non-polar fluids (carbon tetrachloride, decahydronaphthalene). They explainded that the influence of these fluids on the layer-lattice minerals is governed by two parameters: (*i*) scratching of the surface during rubbing. (*ii*) cohesive force that exists between fresh cleavage faces of layer-lattice minerals. But the phenomenon is not clear as yet.

The above results are based upon tests on minerals sliding one over the other under extremely small normal loads or under free sliding conditions. The results of experiments conducted by JAEGER (1959) on soaked specimens of sandstone and granitic gneiss showed a rather slight decrease in the coefficient of sliding friction. No pore pressure measurements were taken and hence it is not clear if change in the pore pressure did not influence the results. It is well known that in case of undrained-wet specimens the effective stress theory is applicable. Pore pressure greatly influences the sliding force due to decreased effective

TABLE 6

Frictional coefficients for three conditions of surface moisture

(after HORN and DEERE, 1962)

	Mineral	Origin	Oven-dried		Oven-dried/air-equilibrated		Saturated		$\frac{\mu_s^s}{\mu_d^s}$	$\frac{\mu_s^k}{\mu_d^k}$
			Static μ_d^s	Kinetic μ_d^k	Static μ_m^s	Kinetic μ_m^k	Static μ_s^s	Kinetic μ_s^k		
Massive-structured minerals	Clear quartz	N.Carolina	0.11	0.10	0.11	0.10	0.42	0.23*	3.82	2.30
	Milky quartz	Wisconsin	0.14	0.14	0.16	0.16	0.51	0.27*	3.64	1.91
	Rose quartz	Unknown	0.13	0.11	0.13	0.11	0.45	0.26*	3.45	2.36
	Microcline feldspar	Unknown-A	0.11	0.11	0.13	0.11	0.76	0.76	6.90	6.90
	Microcline feldspar	Unknown-B	0.12	0.12	0.12	0.12	0.77	0.77	6.42	6.42
	Calcite (Scratching)	N. Jersey			0.21	0.21	0.60	0.60	–	
	Calcite (N.S.)	N. Jersey	---	--	0.12	0.12		--	---	
	Calcite (N.S.)	Kansas	0.14	0.14	0.14	0.14	0.68	0.68	4.85	4.85
Layer-lattice minerals	Muscovite	Penna.	0.43	0.43	0.30	0.30	0.23	0.23	0.54	0.54
	Muscovite	Brazil	0.41	0.41	0.32	0.32	0.22	0.22	0.54	0.54
	Muscovite	Unknown	0.45	0.45	0.36	0.36	0.26	0.26	0.58	0.58
	Phlogopite	Madagascar	0.31	0.31	0.25	0.25	0.15	0.15	0.48	0.48
	Phlogopite	Canada	0.29	0.30	0.22	0.22	0.16	0.16	0.55	0.53
	Biotite	Canada	0.31	0.31	0.26	0.26	0.13	0.13	0.42	0.42
	Chlorite	Vermont	0.53	0.53	0.35	0.35	0.22	0.22	0.42	0.42
	Serpentine	Vermont	0.62	0.62	0.50	0.47	0.29	0.26	0.47	0.42
	Serpentine	Unknown	0.76	0.76	0.65	0.65	0.48	0.48	0.63	0.63
	Steatite	N.Carolina	0.38	0.38	0.26	0.26	0.23	0.19	0.61	0.50
	Talc	Vermont	0.36	0.36	0.24	0.24	0.16	0.16	0.45	0.45

Notes 1. The above coefficients are for very smooth surfaces.
2. These coefficients are based on a rate of sliding of 0.7 in/min.
3. The coefficients refer to the friction developed between surfaces of the same mineral, e.g., quartz on quartz.
4. Relative humidity during oven-dried/air-equilibrated tests ranged between 17% and 35%.
5. The normal load ranged between 0.65 lbf and 10.2 lbf.
* Denotes approximate coefficient of kinetic friction; based on average of maximum and minimum values of frictional resistance during stick-slip movement.

TABLE 7 ▶

Effect of water on the coefficient of friction of rock joints

(after BARTON, 1973a)

Rock type	Description of discontinuity	Dry Φ^0	Dry μ	Wet Φ^0	Wet μ	Reference
Quartzite	artificial, planar, polished (σ_n: 30–400 kgf/cm^2)					JAEGER and ROSENGREN (1969)
Shales, siltstones and slates	minor faults; smooth, polished or slickensided, graphite coated		no change in general			ROSENGREN (1968)
Shales, siltstones and slates	extension fractures; coated with limonite, pyrite, quartz					ROSENGREN (1968)
			reduction			
Granite, gneiss, sandstone	shear fractures from failure of intact specimens (σ_n: 100–2,500 kgf/cm^2)		0.71 0.52		0.61 0.47	JAEGER (1959)
		Φ_r		Φ_r		
Sandstones, carbonates	artificial, rough sawn, equivalent to residual	25–33	34–39	24–32	33–36	PATTON (1966a)
Shales, siltstones and slates	minor fault, smooth, polished, chlorite coated		0.49		0.40	ROSENGREN (1968)
Dolerite	joint	52		37		DUNCAN (1969)
Granite	artificial surface	38		31		
Gneiss	natural schistose plane, "keyed"	49		44		
Phyllite	schistose plane	40		32		
Shale	joint	37		27		
Quartzite	joint	44		34–37		DUNCAN and SHEERMAN-CHASE (1965–66)
Marble	joint	49		42		
			increase			
Sandstone	artificial, planar, polished (equivalent to slickenside)	Φ_r		Φ_r		
		27–32		30–38		PATTON (1966a)
Gabbro	joint	47		48		
Oolitic limestone	joint	44		48		DUNCAN
Chalk (2 of 3 types)	joint	40		41		(1969)
Quartzite	artificial, planar, polished	23		30		DUNCAN and
Basalt	artificial, planar, polished	33		35		SHEERMAN-CHASE (1965–66)
Schistose gneiss, granite, sandstone	artificial, planar, polished with increasing polish during shear			—		COULSON (1970)

value of the normal force and this phenomenon is amply demonstrated by MORGENSTERN (1970). BYERLEE's (1967b) tests showed that the pore pressure strongly influences the coefficient values so calculated and should be taken into account to avoid anomalous results. It is seen that law of effective stress holds good for joint surfaces (BYERLEE, 1975) and even very high pressures may develop when joints slide past each other (GOODMAN, HEUZE and OHNISHI, 1972).

Table 7 gives the results obtained by a number of workers on the frictional coefficient of rocks when wet or dry. Tests conducted by JAEGER (1959) and JAEGER and ROSENGREN (1969) were at high normal pressures but the other tests are at relatively low normal pressures. The polished surfaces in general are not affected by the presence of water while rough surfaces show a slight decrease. JAEGER (1959) suggested the ease of development of slickenside in wet joints causing reduction in shear strength of rough joints is due to adverse effect of moisture on the tensile strength of the rock material. Certain other factors such as displacement rate and temperature have been investigated by some workers. HANDIN (1972a, b) and DIETERICH (1972) reported results on the time-dependent behaviour of joints. In general, the coefficients of friction of joints were found to remain constant or to increase with loading duration depending on the roughness of the joint surfaces and on the amount of accumulated gouge. Stress drops during unstable sliding on effectively smooth joint surfaces or on unfilled joints became greater as well. Thus, for the type of joints which were studied by them, it appears that the long-term ultimate strength of joints might actually exceed the short-term strength.

WAWERSIK and BROWN (1973) also made a few measurements on granite specimens containing artificially created tension joints. These measurements suggest that creep on rough, unfilled joints is negligibly small. The coefficient of friction on such joints was found to increase with the time that the joint surfaces were subjected to constant normal and shear stresses. These observations corroborate results of HANDIN (1972a, b) and DIETERICH (1972).

DONATH, FRUTH and OLSSON (1972) have examined the influence of strain rate on the coefficient of friction of sandstone, limestone and slate. The effect seems to be very unsystematic. Similar results were obtained by LAMA (1975a) on a number of rocks including granite, sandstone, limestone, marble using saw cut, polished, tensile fracture surfaces at displacement rates from 0.67 to 0.0001 mm/s. The effect of displacement rate seems to be overridden by the difference in the surfaces obtained and material property changes in each test specimen. When the same surface is reproduced using a controlled model material, the influence of the displacement rate becomes more discernible. The results obtained by LAMA (1975a) are shown in Figs. 10-55 to 10-58. It looks that at lower normal stresses there is some form of dynamic friction effect and the coefficient

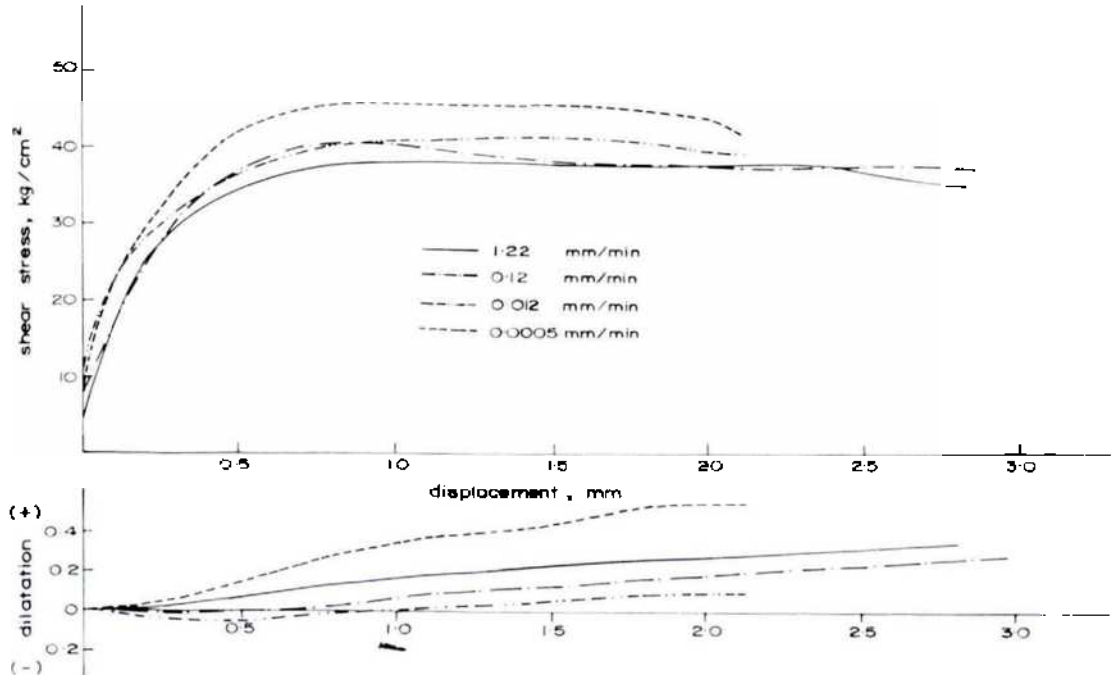

Fig. 10-55. Shear and dilatation behaviour of model joints of marble surface obtained in Brazilian test (model material — gypsum) at $\sigma_n = 0.289$ MPa and at different displacement rates (after LAMA, 1975a).

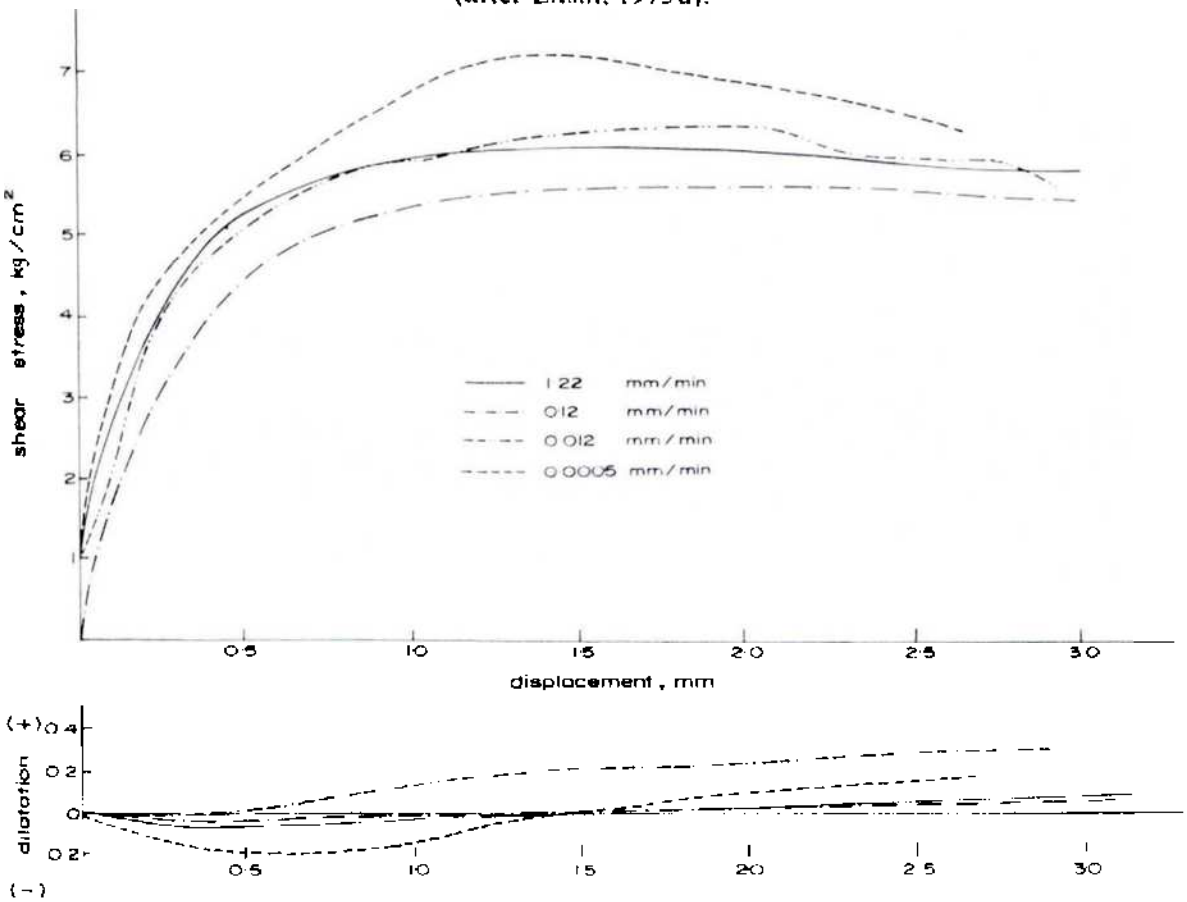

Fig. 10-56. Shear and dilatation behaviour of model joints of marble surface obtained in Brazilian test (model material — gypsum) at $\sigma_n = 0.539$ MPa and at different displacement rates (after LAMA, 1975a).

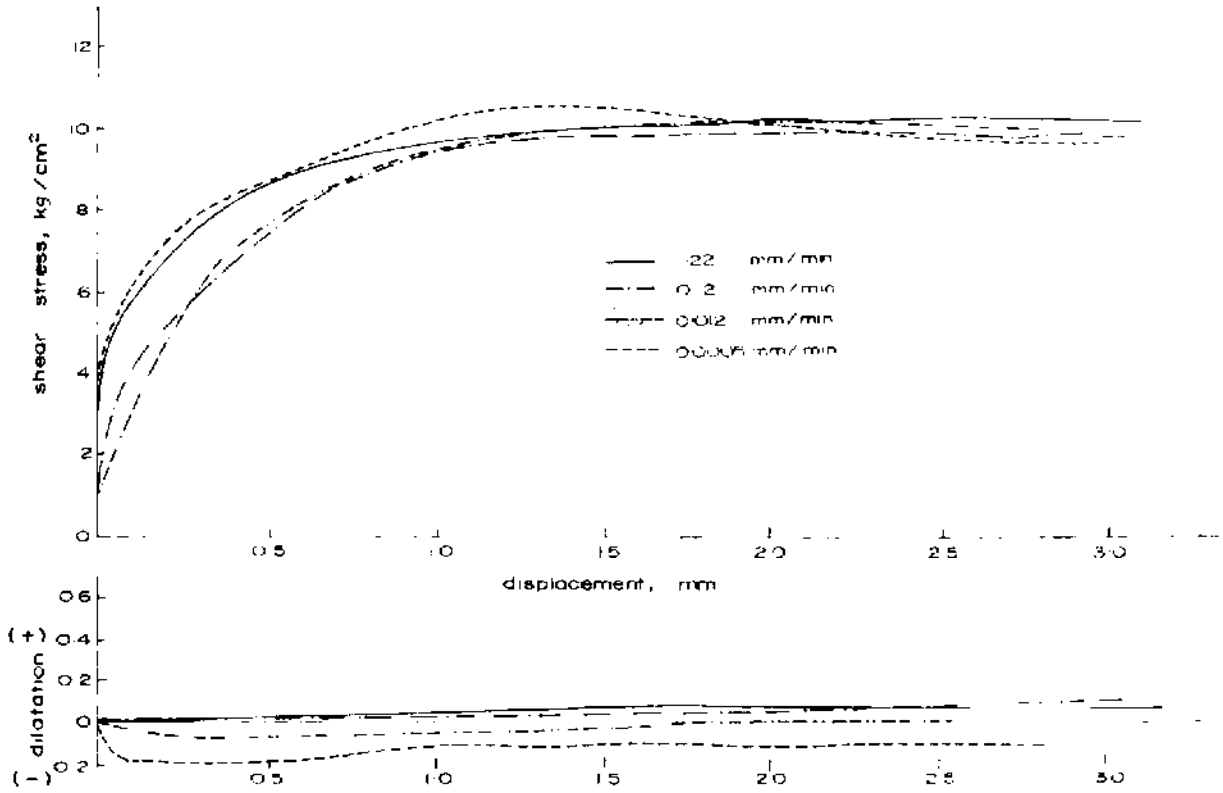

Fig. 10-57. Shear and dilatation behaviour of model joints of marble surface obtained in Brazilian test (model material - gypsum) at $\sigma_n = 1.008$ MPa and at different displacement rates (after LAMA, 1975a).

TABLE 8

Coefficient of friction of granite (tension joints) at $\sigma_n = 9.30$ kgf/cm² (0.97 MPa) (13.5 lbf/in²)

(after LAMA, 1975b)

Displacement rate	ϕ
40 mm/min.	32.1
1.22 mm/min.	32.1
0.18 mm/min.	33.1
0.024 mm/min.	35.3

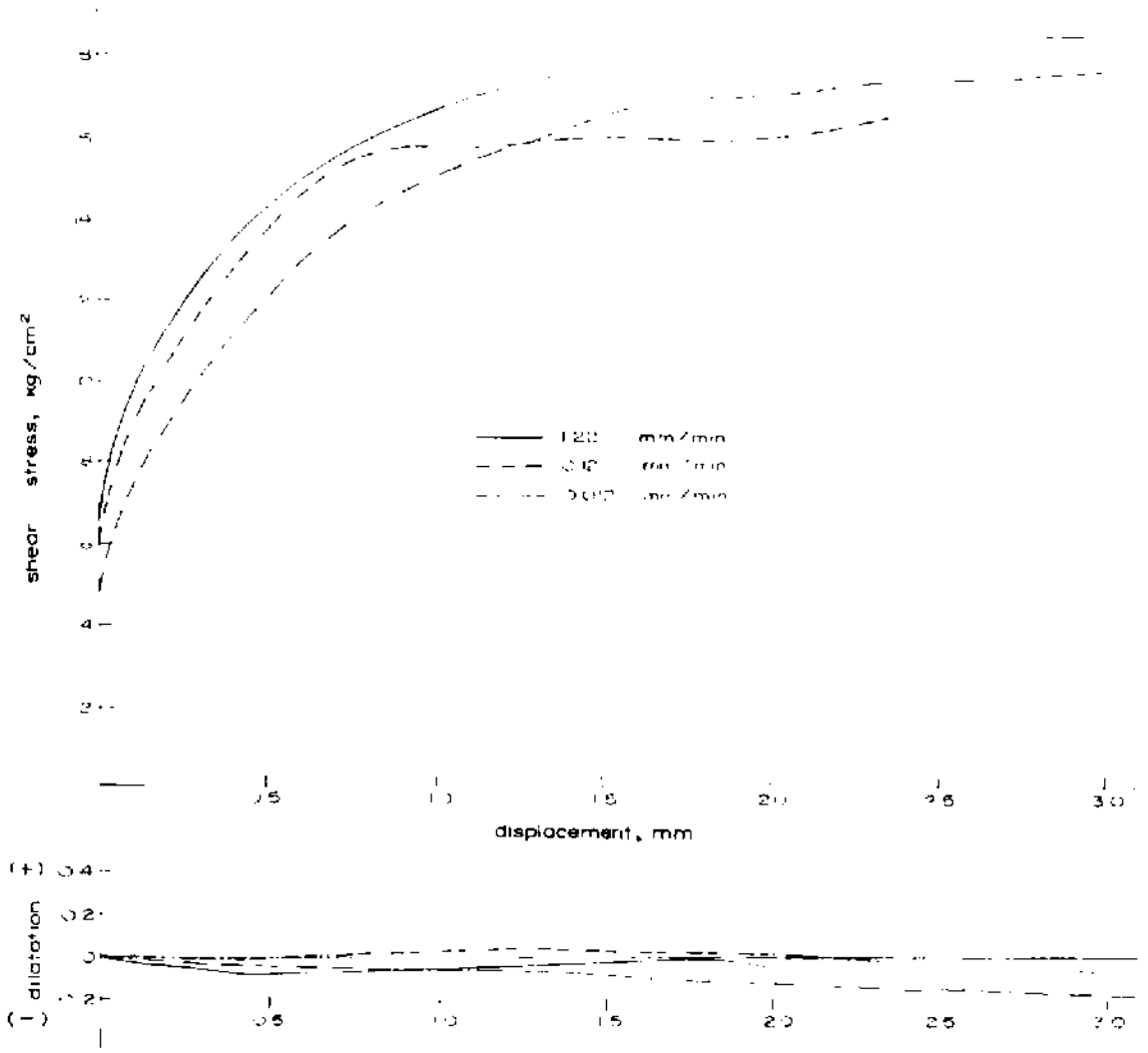

Fig. 10-58. Shear and dilatation behaviour of model joints of marble surface obtained in Brazilian test (model material—gypsum) at $\sigma_n = 2.005$ MPa and at different displacement rates
(after LAMA, 1975a).

of friction has a slightly smaller value at high displacement rates. At higher normal stresses, the material property plays a more important role and the coefficient of friction increases and has a higher value at high displacement rates. The curve at 1.22 mm/min displacement rate tends to rise with increasing normal stress. Values obtained for granite are given in Table 8.

The influence of temperature has been found to increase the coefficient of friction of sandstone and decrease that of limestone whilst slate surface was unaffected by it (Fig. 10-59).

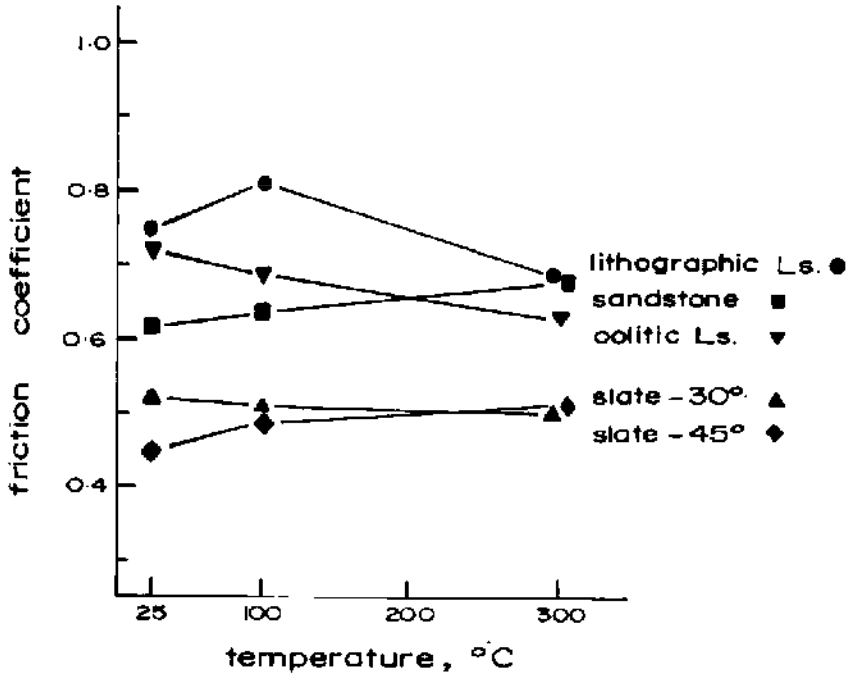

Fig. 10-59. Friction coefficient (μ) versus temperature.

5. Filling material

The filling material in joints may consist of the sediments due to the hydrothermal deposition similar in strength to the enclosing rock or may be partially loose to completely loose cohesionless soil (clay, sand, coarse fragmentary material, etc.) deposited into open joints or formed in-place due to the weathering of the joint surface. Accordingly, the filling material may be divided into the following four types:

1. Loose material from tectonically crushed zones.
2. Products of decomposition and weathering of joint walls.
3. Deposition by ground water flow containing products of leaching of calcareous rocks.
4. Filling material brought from the surface.

The mechanical behaviour of the joint filled with any material is dependent upon the type of the filling material, the thickness of the filling material and the height of the asperities.

GOODMAN, HEUZE and OHNISHI (1972) examined the influence of the thickness of the filling material (in this case kaoline clay) in granite and sandstone joints. The results are shown in Fig. 10-60. The $\tau - \sigma_n$ curve for the filling material alone is shown dotted. The numbers on the points refer to the ratio (R/t_i) of filling material thickness (R) and mean asperity height (t_i). Tests showed that for very small thicknesses of the filling materials, there is augmentation of the strength as a virtue of the geometry of the rough walls of the joint. As the thickness

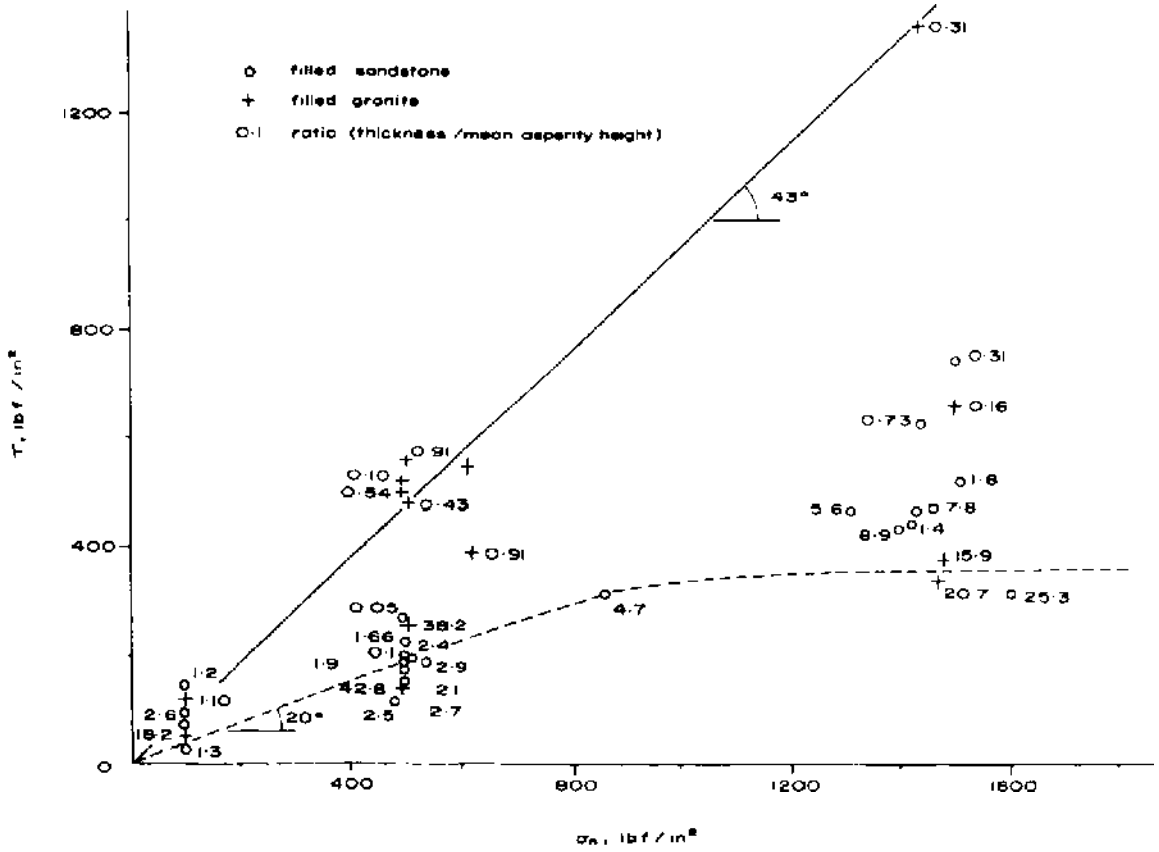

Fig. 10-60. Strength data for clay filled joints (after GOODMAN, HEUZE and OHNISHI, 1972).

increased, clay filling reduces the strength and at $R/t_i = 3$, the strength is reduced to that of the filling material. For idealised saw tooth geometry, GOODMAN (1969) found the (R/t_i) ratio to be about 1.5.

BARTON (1973a, b) has examined the question in detail and related the mean thickness of the filling (f) and the mean roughness amplitude (a) (given by the distance between the two parallel lines which run as tangents to the uneven profile of the rock joint) and the displacement (d) required for the rock to rock contact of the joint walls. The results obtained by him are given in Table 9.

TULINOV and MOLOKOV (1971) tested a number of joints with different filling materials and under variable conditions of moisture. According to them a thin sand layer as a filler between the hard rocks (sandstone, limestone) does not have any significant influence but in case of relatively weak rocks (clay and marl) its influence is rather to increase the angle of friction. The shear plane in a thick layer of sand is limited in the sandbed itself. In the case of clay fillers also, the shear plane is limited along the weakest contact and traverses through clay. The influence of the clay bands is very much affected by the presence of humidity. The drop in shear strength is observed with increase in humidity

TABLE 9

Relationship between joint filling, roughness amplitude at zero dilation to obtain displacement of joint wall contact

(after BARTON, 1973a)

f/a	d/a
> 1.00	∞
0.75	2.34
0.50	1.32
0.25	0.43
0	0

even under conditions such that the clay band is not squeezed out. With further increase in humidity to a stage that clay becomes plastic and starts getting extruded out, the joint slowly closes and as the two surfaces of the rock come in contact, the shear strength values change. This critical change starts at 25% moisture content of clay and at 52% moisture content the clay band is completely

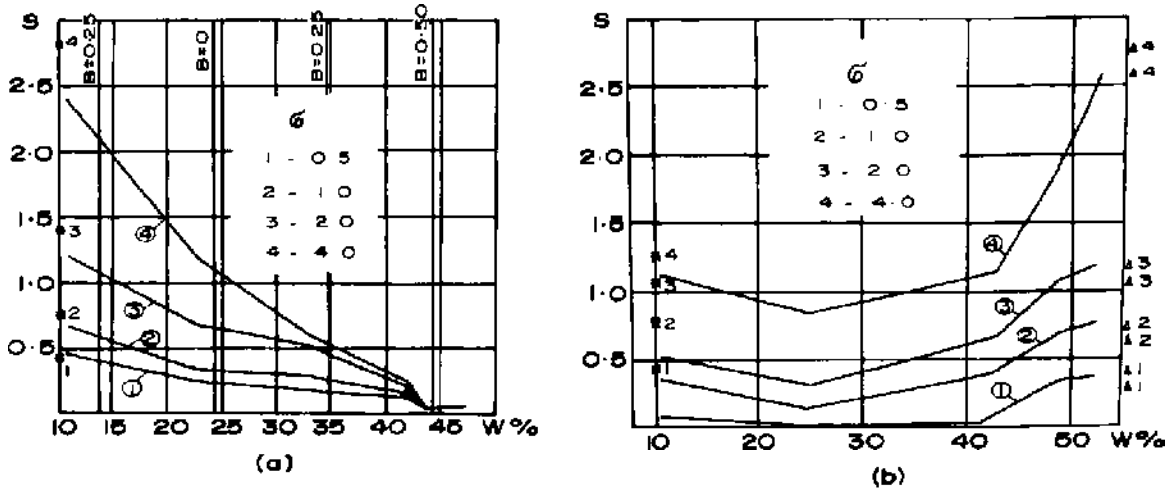

Fig. 10-61. (a) The relation of the shear strength to the humidity of the clay interbed (R = 5 mm) between the sandstone plates.
S the shear resistance of sandstone plates on sandstone
B consistency index
R thickness of filling material.
(b) Relation of the shear strength to humidity of ground clay slate (R = 6 mm) between the plates of limestone and sandstone at possible soil extrusion.
S shear strength of undisturbed clay slate between the plates of limestone and sandstone.
Shear strength of limestone plates on sandstone:
△: on dry surface (W = 1.7%);
▲: on moistened surface
W – percentage of water
(after TULINOV and MOLOKOV, 1971).

extruded out (this experiment was conducted with 6 mm (0.24 in) clay band between limestone and sandstone plates) and the original value of the shear strength of the joint is achieved (Fig. 10-61). In the case of coarse fragmentary filling material, the shear plane is also located within the thick layer of filling material independent of the smoothness or roughness of the joint. The coefficient of friction increases with increase in the fragment size from 2 mm to 20–30 mm (0.079 in to 0.787–1.181 in) and further increase in fragment size does not exert any influence on the friction coefficient (Fig. 10-62). Curve 1 refers to the case of a compacted filling material and curve 2 refers to the case of a loose filling material. The coefficient of friction in the former case is about 20 to 25% higher than the latter case.

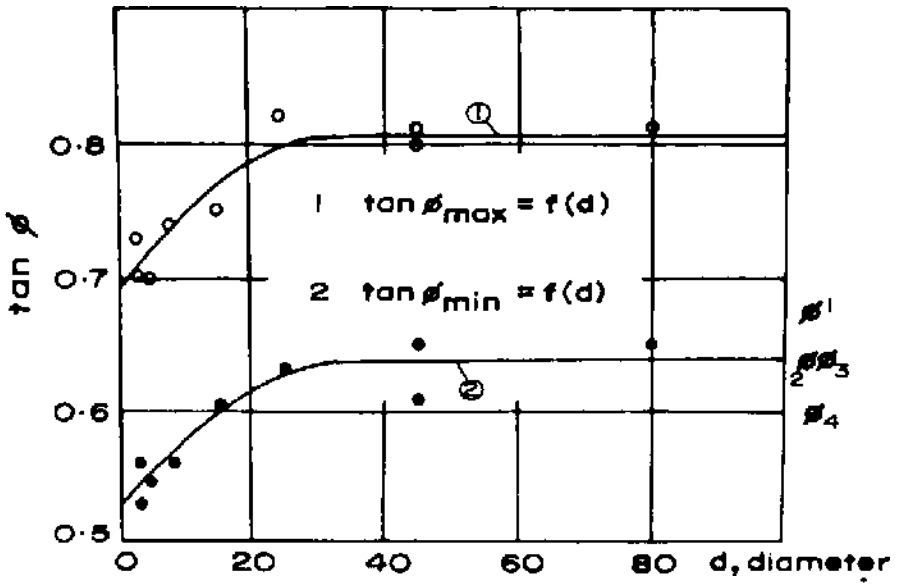

Fig. 10-62. Coefficient of internal friction – fragments diameter relation
Φ – lump test results
1 – sandstone on sandstone
2 – limestone on sandstone
3 limestone on sandstone with fine-grained sand between them
4 limestone on sandstone on moistened surface
(after TULINOV and MOLOKOV, 1971).

When crushed stone with clay is present as a filling material, the shear resistance is mainly determined by the humidity of the clay component. With hard dry clay, the crushed stone has almost no influence and the coefficient of friction is that of clay. At semihard semiplastic consistency, the shear strength goes up with increase in fragment content percentage from 20–30% up to 90%. At fully plastic consistency, the fragmentary material affects very much the shear resistance only at fragment content percentage from 60–75% upwards. The range of values of residual angle of friction for a variety of clays and clay mixtures is given in Fig. 10-63. The influence of grain size on the

residual friction angles determined assuming thickness of the joint fillings is large enough not to be influenced by the joint wall asperities is given in Table 10. Some highly plastic clays may have friction angle of 5 to 12°.

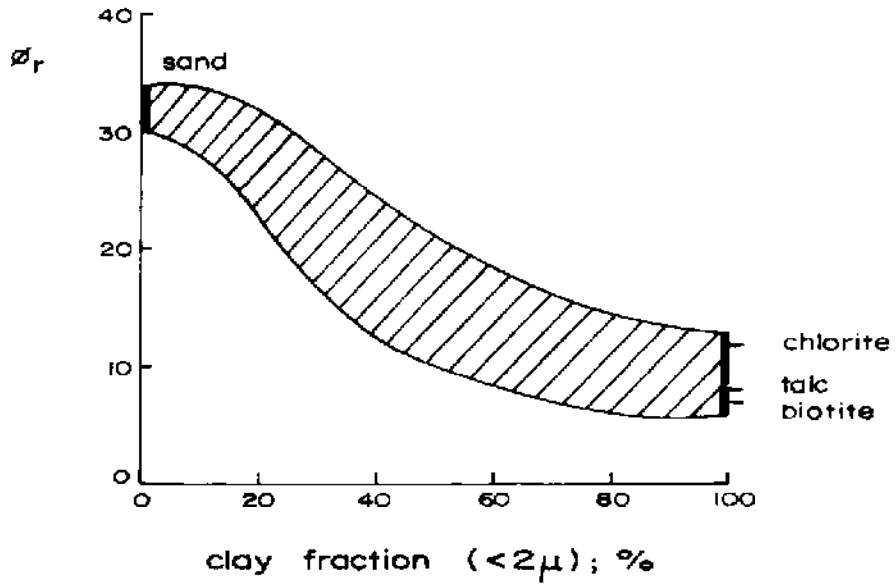

Fig. 10-63. Dependence of residual shear strength on clay fraction (after SKEMPTON, 1964).

TABLE 10

Friction angle, Φ_r, for silts, sands and gravel

(after TERZAGHI and PECK, 1967)

Material	Φ_r	
	Loose	Dense
Sand, round grains, uniform	27.5	34
Sand, angular grains, well graded	33	45
Sand gravel	35	50
Silt sandy	27 to 33	30 to 34
Inorganic silt	27 to 30	30 to 35

The influence of rate of shearing or time has not been determined on filled rock joints. But tests conducted on certain marine clays (SKEMPTON and HUTCHINSON, 1969; BJERRUM, 1973) show that the long term strength may be taken 10 to 15% lower and that in overconsolidated clays reduction in strength be taken as 0.5 to 2% per log cycle of time.

HANDIN (1972a, b) investigated the influence of the gouge composition on the strength of a joint in Tennessee sandstone specimens. The experiments were conducted with grain size of the gouge between 120 and 250 μ (4.7×10^{-3} and 9.8×10^{-3} in) diameter with the gouge layer thickness of 0.15 cm (0.059 in) at a confining pressure of 100 MPa (14,500 lbf/in^2) (1 kb) and a constant rate of shortening of 10^{-4}/s with different gouge materials (Fig. 10-64). He found that specimens with limestone sand are stronger than quartz sand and is of the opinion that the important parameter playing the role is the relative ductility of the gouge.

The influence of grout fillings very commonly adopted in foundation work to reduce permeability is important. Grouting may increase or decrease the strength

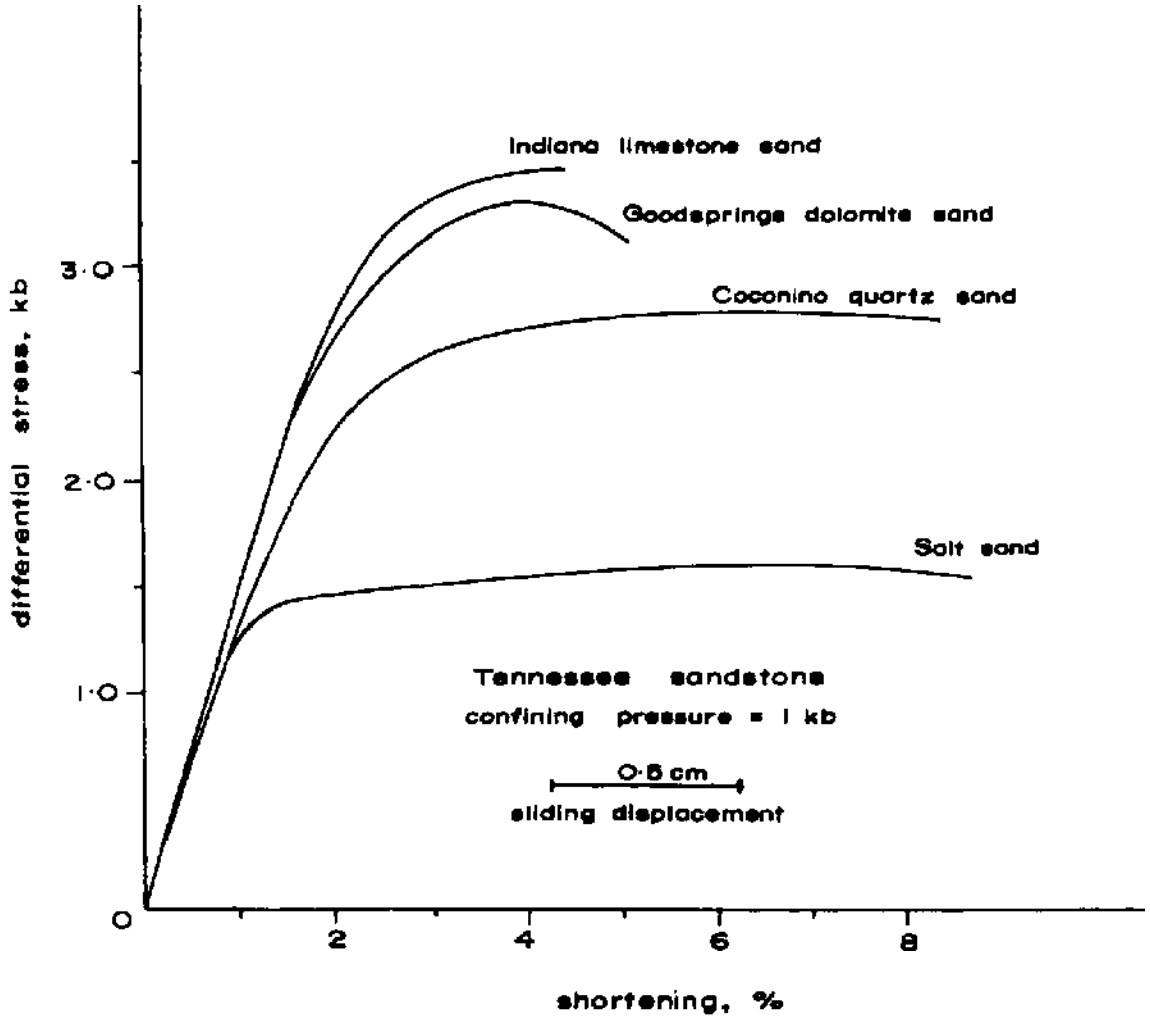

Fig. 10-64. Differential stress versus shortening curves for Tennessee sandstone with various compositions of gouge. Each gouge zone was 0.15 cm thick. The specimens were deformed at 1 kb, room temperature and a constant rate of shortening of 10^{-4}/s. (after HANDIN, 1972b).

of the joints depending upon the joint roughness. COULSON (1970) examined artificial tension joints in coarse and fine grained granite with grout fillings of 0.8 to 6.4 mm and his results are given in Fig. 10-65.

These tests clearly show a detrimental influence in peak and ultimate strengths at higher values of normal stress. At lower values (< 4 kgf/cm^2) the peak strength of grouted joints is higher than natural joints. Results of BORROSO

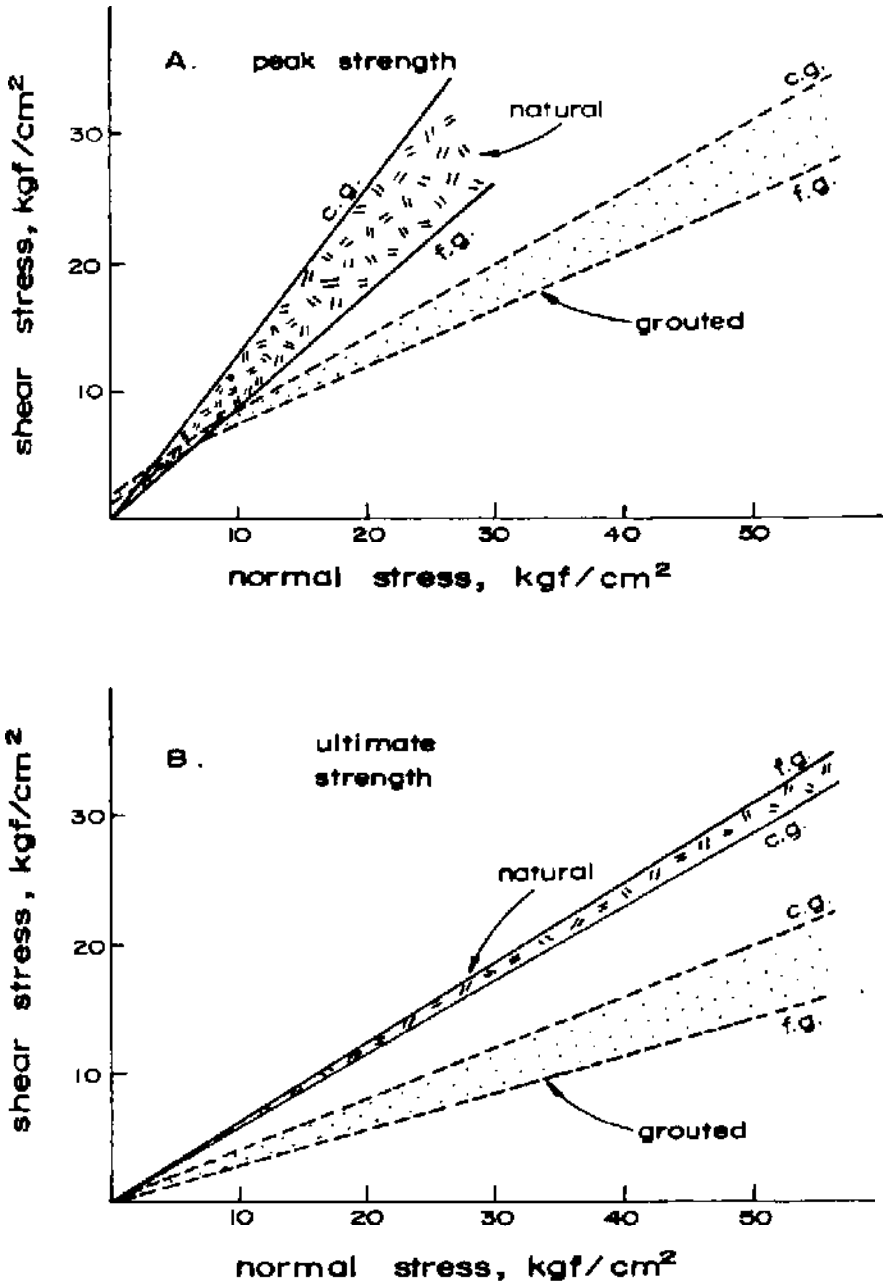

Fig. 10-65. Comparison of peak and ultimate strengths for natural and grouted joint surfaces for coarse-grained (c. g.) and fine-grained (f. g.) granite (after COULSON, 1970).

(1970) on planar surfaces have shown that there is an improvement in the friction angle from 25 to 30 after grouting while in the case of shales, there was no improvement. It is important to note that the relative strengths of grout and rock are important which determine the positive or negative influence of grouting. Depending upon water/cement ratio and grout strength, the improvement shall be expected only in the case of very weak rocks which work on the principle of the weakest link in the rock-grout-rock shear zone. If the shear strength of the grout is higher than rock, the rock will control the shear strength and vice-versa.

10.4.3. Dilatation of Joints

Two ways of representation of dilatation (or dilation) have been frequently used by investigators. The most commonly used method of representation is the vertical displacement against the horizontal displacement. The amount of vertical displacement at any moment is dependent upon the relative position of the different asperities of the sliding surface (Fig. 10-36).

In the second method of representation, the relationship between the vertical displacement with respect to the horizontal displacement (dv/dh) (where dv = = vertical displacement perpendicular to the direction of shear force, dh = = horizontal displacement in the direction of application of shear force) against a certain dimensionless ratio such as (τ/σ_n) or $\left(\frac{\sigma_n}{\sigma_c}\right)$ are plotted. This method gives a more useful result where the maximum angle of dilation at any stage of displacement or under given conditions of τ, σ_n, etc. can be read out.

BARTON (1971a) conducted a series of model tests on tension joints using a model material and found that there exists a linear variation of peak dilation angle α_n and the peak stress ratio $\tan^{-1}\left(\frac{\tau}{\sigma_n}\right)$ (Fig. 10-66) which can be represented by the relationship

$$\frac{\tau}{\sigma_n} = \tan (1.78\,\alpha_n + 32.88^\circ) \tag{10.52}$$

BARTON also tested model joints at various normal stresses depending upon the relative compressive strength of the material. He found that the dilation angle decreased with increase in the ratio of $\frac{\text{normal stress}}{\text{compressive strength}}$ (Fig. 10-67a).

If the data in the Fig. 10-67a is represented on a logarithmic scale, the relationship is linear and can be represented by (Fig. 10-67b).

$$\log_{10}\left(\frac{\sigma_n}{\sigma_c}\right) = -0.1056\alpha_n + 0.1184 \tag{10.53}$$

or

$$\log_{10}\left(\frac{\sigma_n}{\sigma_c}\right) = -0.100\,\alpha_n \tag{10.54}$$

or

$$\alpha_n = 10\,\log_{10}\left(\frac{\sigma_c}{\sigma_n}\right) \tag{10.55}$$

The results of the equation (10.55) are given in Table 11.

Peak dilation angles measured during the shear test by some investigators are given in Table 12.

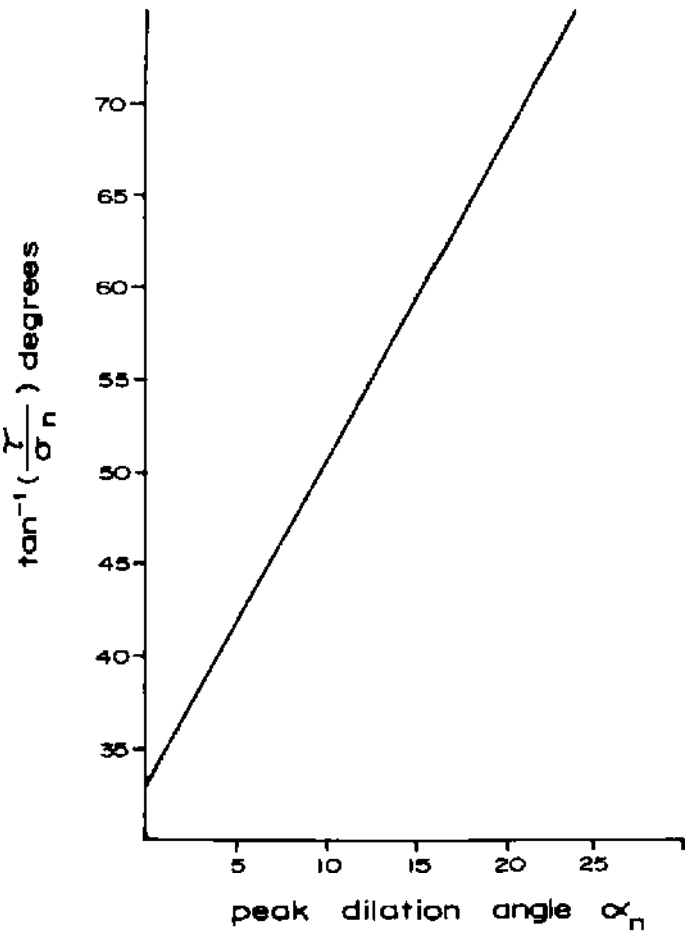

Fig. 10-66. Linear variation of peak dilation angle with peak stress ratio (after BARTON, 1971b).

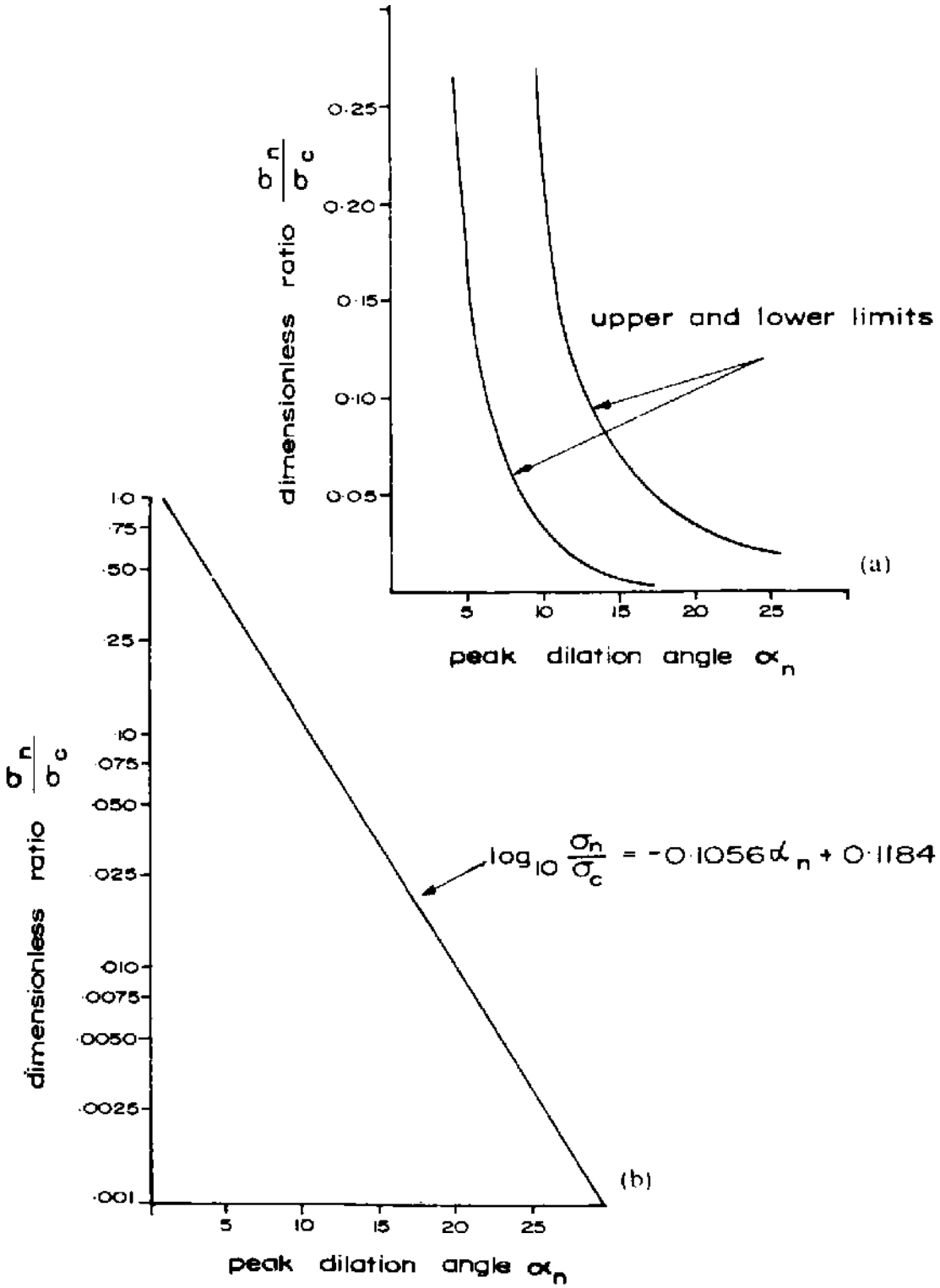

Fig. 10-67. (a) Variation of peak dilation angle with ratio of normal stress to compressive strength.

(b) Linear variation of peak dilation angle with logarithmic ratio of normal stress to compressive strength (after BARTON, 1971 b).

TABLE 11
Results of Eq. 10.55
(after BARTON, 1971b)

σ_c/σ_n	χ_n, degrees
1.0	0
10	10
100	20
1000	30

10.4.4. Scale Effect in Joints

As already demonstrated, the properties of rock specimens are dependent upon the dimensions of the specimens and it is obviously necessary to investigate the behaviour of the joint properties with respect to the area of cross-section of the joint.

In the discussion on the measurement of the roughness of the joint surface, it has been pointed out that the angle of the asperity α, which represents roughness of the surface is dependent upon the base so chosen. As such, the value of the inclination of the asperity (i) shall be dependent upon the scale at which these have been measured and represented. Since the shear strength of the joint surface is dependent upon the angle (i), it is probable that the joint properties determined from small laboratory specimens of 5.1 to 15.2 cm (2 to 6 in) size and even from smaller in situ tests 0.91 to 3.05 m (3 to 10 ft) will not represent the true values since these small specimens could only represent the second and third order surface roughnesses. This is likely to be more true for the rough tension joints and some faults than for smooth joints. Also, the inclination values of the first and second order discontinuities are quite different and difficult to take into account in field analysis of slopes. An example of the different values so obtained is given in Fig. 10-68.

BARTON (1971b) conducted a series of tests on 4 different model materials representing the same prototype at different scale ratios. He, however, found no significant size relationship for rough tension joints. According to him small steep asperities seem to control the peak strength to a greater degree than the large amplitude low-inclination asperities of the first order. These become important only at considerably higher normal stresses at displacements greater than those required to develop peak strength.

TABLE 12

Peak dilation angles measured during shear tests

(after BARTON, 1973a)

Rock type (σ_c, kgf/cm^2)	Description of joints	No. of tests	Mean σ_n (kgf/cm^2)	Mean τ (kgf/cm^2)	Mean χ_n^0	Reference
Coarse-grained Grand Coulee granite (1675)	natural, undulating iron staining, calcite and epidote present in various combinations	8	1.12	1.84	24.0	COULSON (1970)
		1	7.05	7.19	15.0	
		2	21.1	25.9	13.0	
Fine-grained Grand Coulee granite (1985)	natural, undulating smooth: calcite and zeolite present	4	1.08	1.03	7.6	COULSON (1970)
		2	7.15	5.59	6.2	
Hackensack siltstone (1252)	natural, undulating; most surfaces covered with thin layer of calcite	2	1.06	1.01	8.5	COULSON (1970)
		3	1.03	2.60	30.1	
		4	3.48	6.27	21.5	
		4	7.08	12.7	24.5	
		4	20.9	31.8	20.4	
		2	35.0	47.9	16.6	
		3	56.2	58.8	6.6	
Sandstone (1240)	natural, undulating open joints	3	1 to 2.5 (approx.)		18 (approx.)	RIPLEY and LEE (1961)
Siltstone (575)	natural, undulating open joints	5	1 to 10 (approx.)		13.5 (approx.)	RIPLEY and LEE (1961)
Blackstone granite (2040)	rough, undulating, artificial extension fractures	2	12.5	25.8	23.4	
		2	14.3	37.2	19.2	
		1	17.5	52.9	20.2	
Granite (1504)	rough, undulating, artificial extension fractures	1	1.5	4.5	24.0	RENGERS (1971)
		2	3.5	9.2	18.7	
		1	6.5	18.5	22.0	
		2	14.0	21.0	19.0	

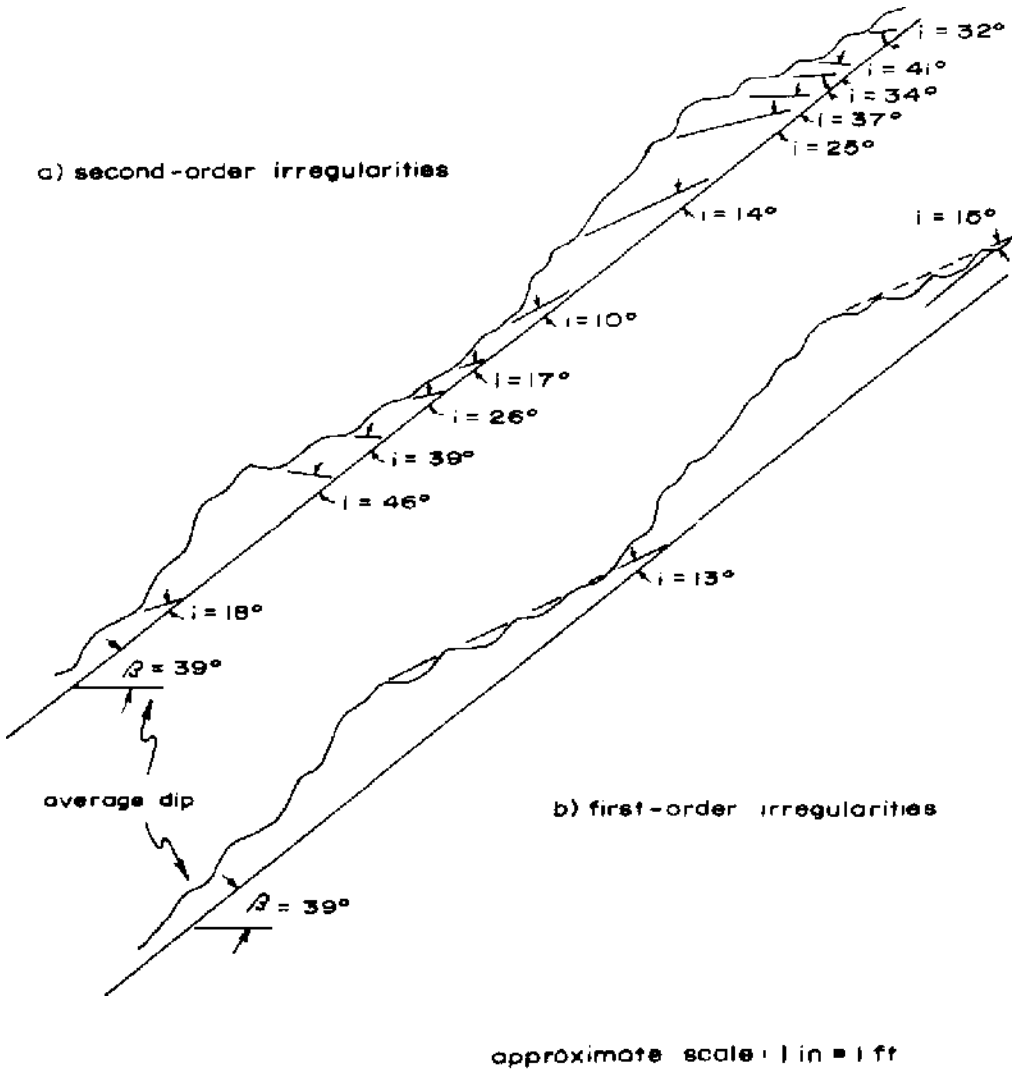

Fig. 10-68. An example of a discontinuity illustrating first - and second order irregularities
(after PATTON, 1966a).

SERAFIM and GUERREIRO (1968) analysed in situ shear tests on different areas of cross-section of the specimens [5 m^2 (53.8 ft^2), 16 m^2 (172.2 ft^2) and 30 m^2 (322.9 ft^2)]. The 16 m^2 (172.2 ft^2) tests were performed by JIMENEZ SALAS and URIEL (1964) in Spain and 30 m^2 (322.9 ft^2) by RUIZ and DE CAMARGO (1966) in Brazil. More detailed discussion of size effects and test techniques of in situ shear is given in Chapter 8, section 8.10. It is suggested that for the strength of masses that have joints separated by large distances, an area of the order of tens of square metres (yards) is probably the maximum that can be used. When studying the strength along faults, joints or planes of stratification, probably an area of some tenths of a square metre ($\sim$ 5 ft^2) is adequate.

As for the displacement, the results of laboratory and field investigations show that maximum resistance is developed within about 0.25 to 38 mm (0.01 to 1.5 in) of the displacement. In the laboratory tests on specimens of size 15 to 30 cm (6 to 12 in) the peak resistance is reached in a fraction of a centimetre (GOODMAN, 1969). In large laboratory tests on specimens 40 cm × 40 cm (15.7 in × 15.7 in) (KRSMANOVIC and LANGOF, 1964), results show that the maximum shear strength is developed at 0.05 to 0.20 mm (0.002 to 0.008 in). In some of the in situ shear tests, the maximum resistance is developed at a displacement of 1.5 to 5.0 cm (0.6 to 2.0 in) depending upon the joint surface.

In the model tests conducted by BARTON (1971a), the displacement at maximum resistance is scale dependent and he gives the value as approximately 1% of the length of the joint. The applicability of these model test results has been questioned by several investigators though it looks as though that these results are not very much off the mark when one takes the extreme values obtained in large in situ tests.

10.4.5. Physical Process of Sliding between Joint Surfaces

Almost all workers investigating the process of friction and sliding of rock surfaces reported the presence of the following features.

1. Rock flour loose or compacted
2. Gouge and gouge zones
3. Polished areas
4. Indurated crusts.

BYERLEE (1966) examined the physical process of sliding between two blocks in detail from the point of view of the mechanism associated with brittle materials. He found that in the case of polished granite specimens sliding over each other, the damage to the surface within the first 0.1 mm (0.004 in) displacement was confined to the isolated regions. When the displacement corresponding to the maximum or peak value of friction was reached, there was minor damage to the whole of the specimen surface with the presence of a fine layer of crushed material. Beyond this maximum, the layer of comminuted material on the surface increased in thickness and the friction coefficient measured in this region was that required to shear through the layer of loose particles on a substratum of solid material. This comminuted material consisted of finely crushed grains of rock having optical continuity and sharp angular edges. The thickness of the layer of ground material was much less than that of the height of the asperities on the surface. BYERLEE concluded that the interlocking of irregularities must be sheared-off as a result of the development of high tensile stresses. If the contact area is small, the force required to shear the

asperities is small and vice-versa. The physical process involved in the sliding when the contact between the surfaces is confined to isolated regions is no different from the physical process when the contact is made over the whole of the surface.

PATTON (1966a) when examining the influence of the number of teeth considered that when two surfaces have asperities sheared off, the shearing force acts primarily on the external teeth and these are sheared off before the full length of the central teeth can be utilised. The phenomenon of frictional sliding is then of progressive failure of the asperities with displacement and not the failure of all the interlocking asperities at one time.

HOSKINS, JAEGER and ROSENGREN (1968) found a great deal of surface damage and slickenside with rough surfaces, but for smooth surfaces on which stick-slip oscillations have taken place there was very little evidence of surface damage. The measured surface roughness did not increase and there was little evidence of detrital material or fracturing of crystals.

JAEGER (1971) concluded that with sliding of rough surfaces which are at first in intimate contact (completely interlocked), the contact is lost except in a few regions where intense shearing and removal of material take place. This sheared material fills the hollows giving the end result a surface of gouge material. In cases, where the rough surface slides over a relatively flat surface, the highest spots of the rough surface are worn down and may also score the originally flat surface. In such cases, the same regions of the rough surface are always in contact with the opposite and the result is a gradual increase in the contact area with progress in displacement. At places of contact where profuse gouge material is formed the rubbing blocks may fail by indirect tension caused by local stress at contacts.

COULSON (1970) examined the phenomenon of surface damage in quite detail. He classified the types of damage or wear of the sliding surface into 3 main categories (Fig. 10-69) namely, polishing, induration, and rock flour and gouge. COULSON found that gouging and generation of rock flour is chiefly associated with rougher and sandblasted surfaces.

Under a microscope, it was observed that the gouge material and rock flour consists of small discrete angular particles which could be separated from their neighbours with absence of any fusion in between them, indicating the absence of any plastic deformation. (COULSON's tests were conducted at and the rocks tested by him were limestones, sandstone and granite.) The compacted gouge flour in the gouge trough gives the appearance of a typical slickenside (Fig. 10-70) and chatter marks similar to those associated with rock being abraded at the base of moving glaciers. At the bottom of the gouge

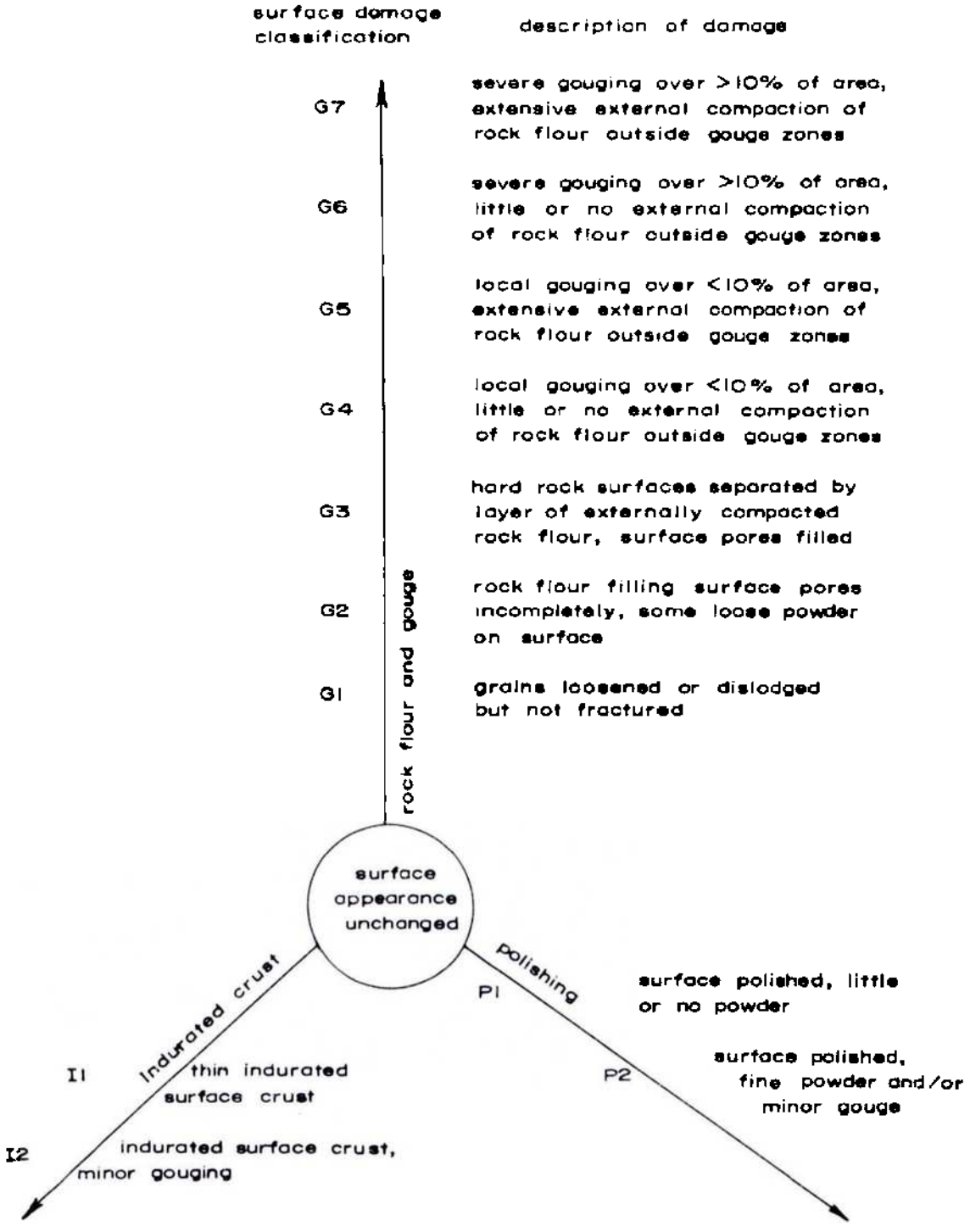

Fig. 10-69. Surface damage classification system (after COULSON, 1970).

material appear step like features opposing the direction of shear (contrary to that of the structural geology concept) with dip of 17-1/2 and an average dip of 20 . These step like features are similar to the "RIEDEL shears" observed by many investigators (first reported by CLOOS (1928) and RIEDEL (1929)), the

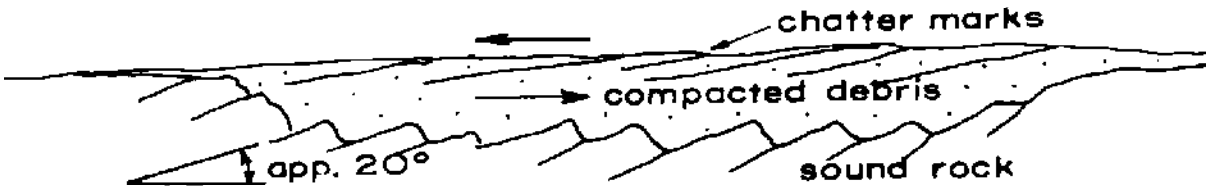

Fig. 10-70. Schematic cross-section of gouge zone developed on a Solenhofen limestone surface sheared dry under a normal pressure of 1177 lbf/in^2 (after COULSON, 1970).

difference being that in the CLOOS-RIEDEL experiments the "RIEDEL shears" form first followed by shears parallel to the direction of slip which coalesce to form the principal slip surface. The RIEDEL shear formed in the process of shearing is a secondary feature, the prepared surface of sliding being the primary feature.

Because of the orientation of the RIEDEL shears, slip along them is hindered, the fragments get detached and reduced to rock flour accompanied by an increase in volume. Under high pressures, the compaction of this gouge, so formed, takes place and this may locally behave as a compact mass giving rise to new RIEDEL shears and the process repeats itself.

According to COULSON, this type of phenomenon is only associated with the surface damage classification G_4, G_5, G_6, G_7 and P_2 and occurs only at high normal pressures. RIEDEL shear and deep gouge develop only after enough debris has been generated to completely fill the pores and the partings between the two sliding surfaces. Similar observations were made by EINSTEIN et al (1969) in their studies on jointed specimens who found that the steep sides formed are opposed to the direction of sliding (Fig. 10-71). According to them, these steps are a part of secondary conjugate shear planes along which displacement occurs after the primary shear surface has been created. This phenomenon occurs only at confining pressures up to 6.895 MPa (1000 lbf/in^2) and is absent at higher confining pressures.

HANDIN (1972b) investigated the gouge development under different experimental conditions. In his tests precut specimens were subjected to axial and varying confining pressures and strain rates. He found that the gouge development changes systematically, that is, the abundance of thick, clumped gouge increases while undisturbed original surface and "welded gouge" decreases with increase in the angle which the precut makes with the axial load. This change, he suggested, may be related to the change in the normal pressure across the sliding plane which increases with increase in the angle of precut. He also found that gouge abundance increases with increasing confining pressure while the rate of strain (range 10 s to 10^{-4}/s) has no perceptible influence (Fig. 10-72).

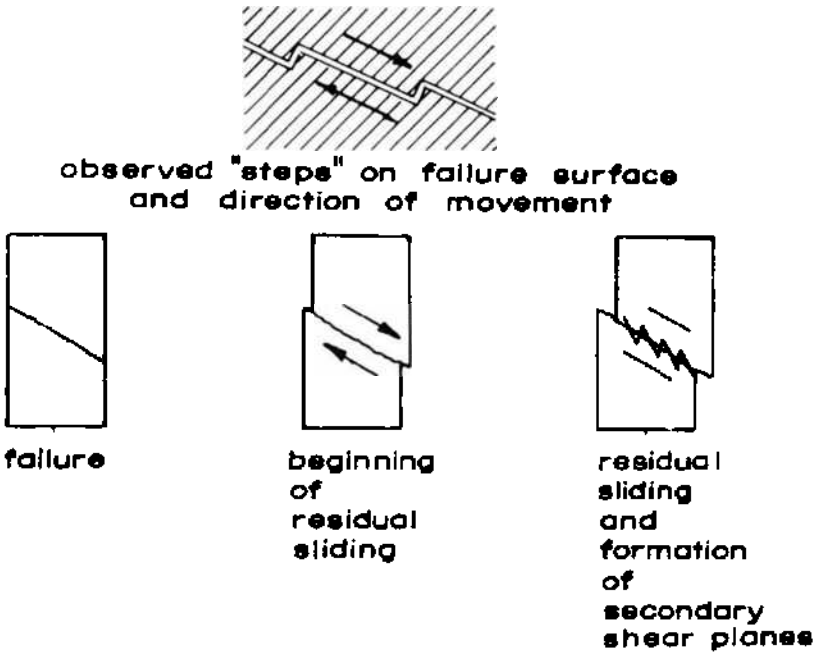

Fig. 10-71. Failure surface development (after EINSTEIN et al, 1969).

HANDIN also made a detailed analysis of the "welded gouge" so produced. This welded gouge is an indurated material that can be easily flaked from the sliding surface and can withstand small loads without breaking up and supports brittle fracture. Under high magnifications this is shown to be composed of randomly oriented, poorly-sorted, fine fragments of quartz that are imbedded in and indurated by an isotropic matrix. The isotropic matrix has a refractive index of 1.516 ± 0.002 which is close to that of glass produced by a grinding wheel when purposely jammed into the specimen. X-ray and scanning electron microscope studies carried out on the welded gouge led to the conclusion that this welding of the gouge probably involves fusion of silica and impurities to produce a glassy matrix which implies very high temperatures obtained locally during frictional sliding. These hot spots may be extremely small and attain temperatures of 1500 C (2732 F) and are short lived. This suggests that at the asperities, some gliding flow may accompany cataclasis during frictional sliding.

The phenomenon of polishing in sliding is associated only with lapped surface (# 600 grit) and is basically an abrasion process where the mineral hardness plays an important role. COULSON found no polishing in calcite rocks such as Bedford limestone, Solenhofen limestone (MOH's hardness = 3) while quartz rich rocks (MOH's hardness = 7) did polish. BOWDEN and TABOR (1967) are of the opinion that the chief mechanism involved in the polishing of metallic surfaces is surface flow produced by frictional heating. If this mechanism is

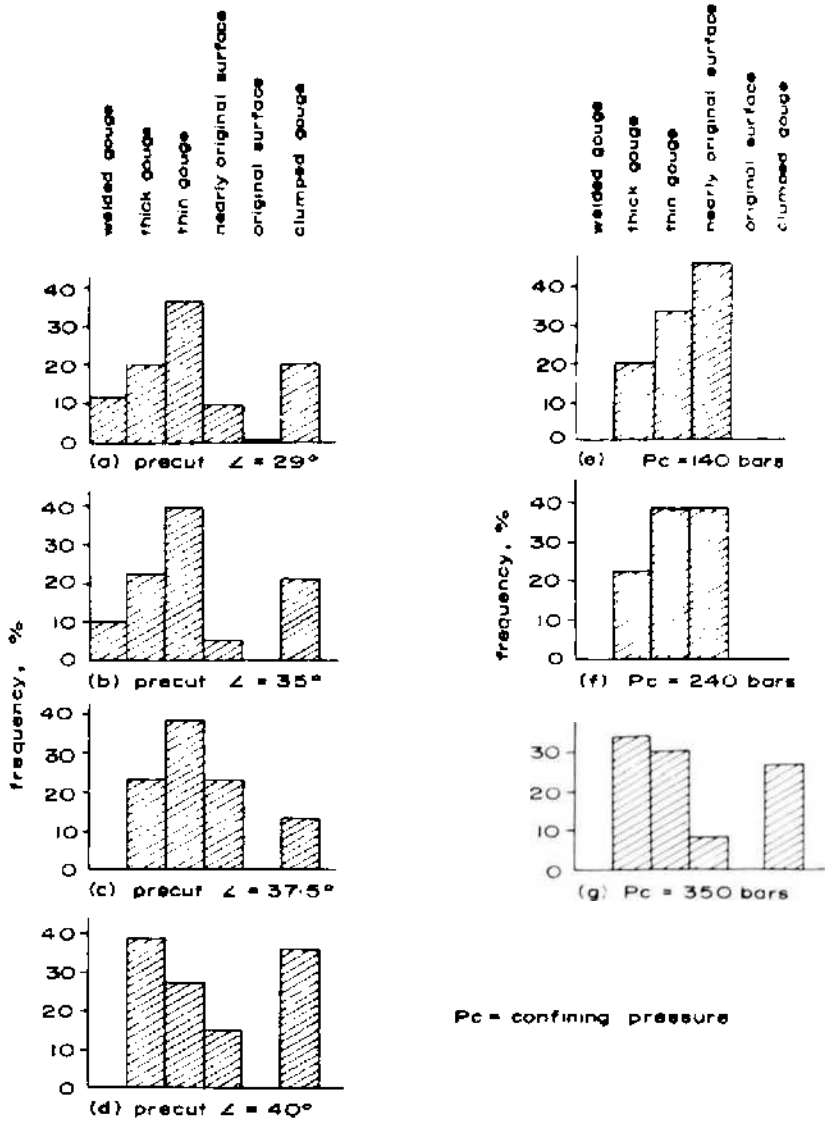

Fig. 10-72. Histograms showing gouge development in frictional gliding experiments. Tennessee sandstone. Frequency in the occurrence of gouge types are based on point counting methods; total counts are 423, 358, 290, 240, 330, 300, and 282 in histograms a-g, respectively. (a-d) Histograms show gouge changes for increase in angle of precut in tests run at 140 bars confining pressure, 24 C, 10 $^{-4}$/s. Initial surfaces were prepared with grinder only. (e-g) Histograms show gouge changes for increasing confining pressure at fixed precut angle of 35 . Initial surface prepared with grinder plus polishing with 600 grit abrasive (after HANDIN, 1972b).

important for rocks also, then one could expect that limestone with its melting point of 800 C (1472 F) should polish more easily than quartz which melts at about 1500 C (2732 F).

The phenomenon of induration of the surface is associated with an extensive amount of "cut and fill" in the original rock surface. The indurated rock

surface is flat except for striations parallel to the direction of shear and occurs only in the case of wet surfaces (COULSON, 1970). This is due to a decrease in bond strength. COULSON observed this only in case of calcite rocks (Bedford limestone and Oneota dolomite).

10.4.6. Phenomenon of Stick-slip

The phenomenon of stick-slip is quite well known in metal friction. The stick-slips are relaxation oscillations which occur when the coefficient of dynamic friction is less than the coefficient of static friction.

It has been observed by several investigators that when a rock surface slides over another surface, the movement between the surfaces takes place in a jerky manner with a sudden drop in the value of the shearing force. BRIDGMAN (1936) was perhaps the first to report this phenomenon while shearing brittle materials at normal stresses. JAEGER (1959) in his tests on flat surfaces at confining pressures of 20 MPa (200 bars) (2900 lbf/in^2) (flatness within 0.05 mm (0.00197 in)) observed that after a short initial period of sliding, during which possibly an intimate contact is established, subsequent movement takes place by a violent stick-slip process of large amplitude (Fig. 10-73). In this test (Fig. 10-73), after two such slips had taken place at B, the confining pressure was raised to 40 MPa (400 bars) (5800 lbf/in^2) (C) and then to 60 MPa (600 bars) (8700 lbf/in^2) (DE), 80 MPa (800 bars) (11800 lbf/in^2) (FG) and 100 MPa (1000 bars) (14500 lbf/in^2) (HK). It is seen that stick-slips occurred at all these pressures and the loads at which they occurred were surprisingly reproducible. BYERLEE (1966) in his tests on Westerly granite, found that at the end of the slip movement, the shear force in most cases dropped to about 2/3 of

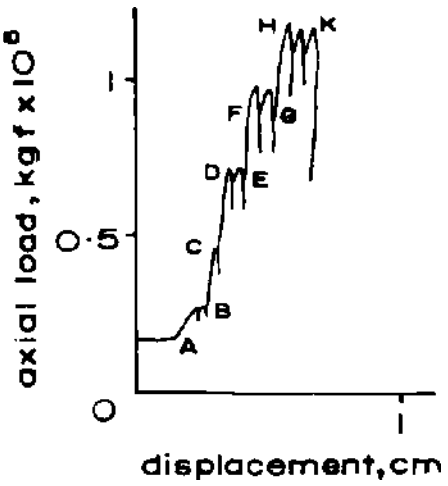

Fig. 10-73. Load-displacement curve for sliding over bare surfaces at $\alpha = 25$ (α = angle of inclination of precut with the axial force).

the shear stress required to initiate movement. Similar results have been reported by CHRISTENSEN et al (1974) on ground surfaces of Westerly granite using torsional shear test.

HOSKINS, JAEGER and ROSENGREN (1968) tested blocks of Red granite having lapped surfaces with roughness of $0.889 \pm 0.127\,\mu$m ($35 \pm 5\,\mu$in) in the equipment (Fig. 10-18c) and reported that after an initial rise in load, a sudden slip occurred and stick-slip proceeded regularly with increasing amplitude (Fig. 10-74). Fig. 10-74a is taken from the machine recorder and on an enlarged scale it is shown in Fig. 10-74b. The portion of the oscillations below the dotted line PQ are caused by motion of the testing machine pendulum and the actual amplitude of the oscillations is the distance between the upper portion and the line PQ. If the highest and lowest values of the τ are calculated and the $\tau - \sigma_n$ curves are plotted, straight lines are obtained (Fig. 10-75) with different values of the intercepts on the τ axis giving different cohesive strengths (c) and different friction values (μ). These values so calculated for different rocks are given in Table 13.

TABLE 13

Coefficient of friction and cohesion for rock surfaces exhibiting stick-slip behaviour

(after HOSKINS, JAEGER and ROSENGREN, 1968)

Rock	Surface roughness μin (μcm)		μ	μ^*	μ'	c	c^*	$(F - F^*)/X$ lbf/in (N/m)
Red granite	35 ± 5	(89 ± 13)	0.53	0.31	0.42	40	40	5.1×10^6 (894×10^6)
Red granite	80 ± 20	(203 ± 51)	0.53	0.48	0.50	50	50	4.7×10^6 (823×10^6)
Gabbro	35 ± 5	(89 ± 13)	0.32	0.25	0.28	35	30	3.4×10^6 (596×10^6)
Gabbro	50	(127)	0.18	0.15	0.16	40	30	2.9×10^6 (508×10^6)
Trachyte	30	(76)	0.63	0.54	0.58	60	70	5.0×10^6 (876×10^6)
Carrara marble	55	(140)	0.41	0.39	0.40	120	110	

μ = coefficient of friction before slip (Fig. 10-75)
μ^* = coefficient of friction after slip
μ' = average value of coefficient of friction equal to coefficient of dynamic friction
c = intercept on τ axis before-slip curve
c^* = intercept on τ axis after-slip curve
$\frac{F - F^*}{X}$ = stiffness of the machine
F = load before slip
F* = load after slip
X = displacement during slip

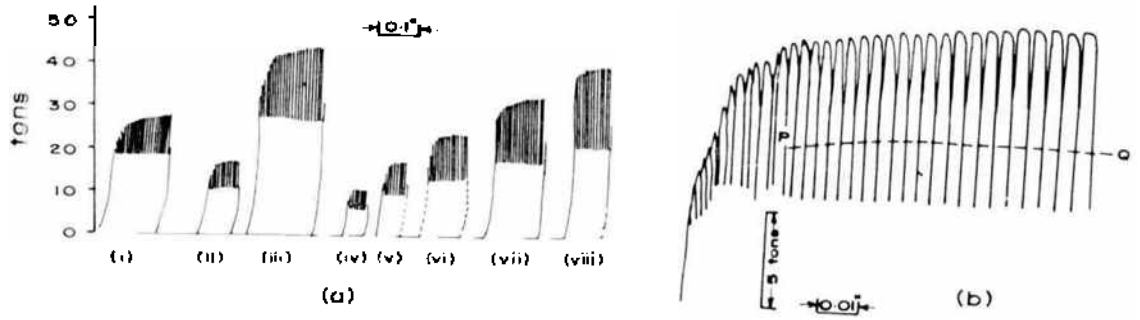

Fig. 10-74. (a) Testing machine recorder load-displacement curves for smooth Red granite with surface roughness $35 \pm 5 \mu$in. Flat jack pressures (i) 500 lbf/in^2; (ii) 250; (iii) 750; (iv) 125; (v) 250; (vi) 375; (vii) 500; (viii) 625. (b) The oscillations of Fig. 10-74 (a) (i) on a magnified scale (after HOSKINS, JAEGER and ROSENGREN, 1968).

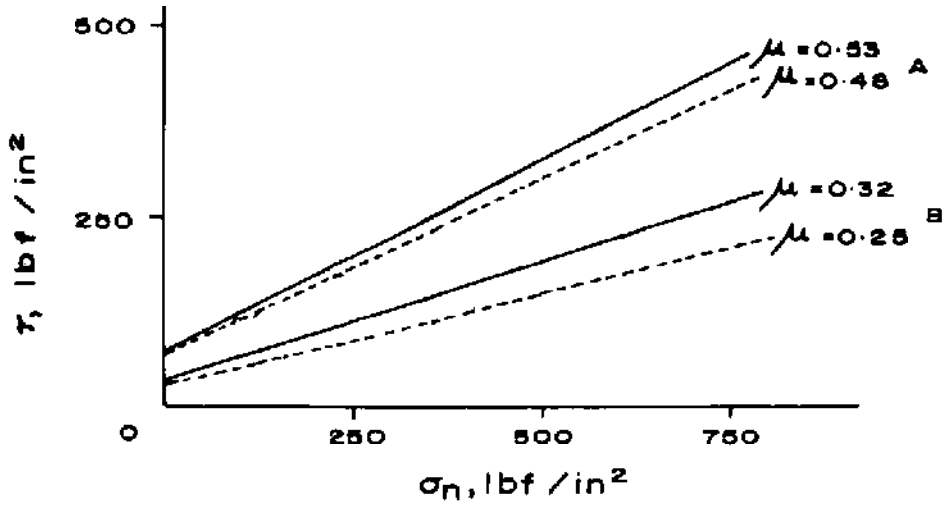

Fig. 10-75. Typical shear stress-normal stress relations for surfaces which show stick-slip. A. Red granite 35 μin; B. Gabbro 35 μin (after HOSKINS, JAEGER, and ROSENGREN, 1968).

The phenomenon of stick-slip is not very clear as yet. HOSKINS, JAEGER and ROSENGREN (1968) observed that these were associated only with surfaces of high finish and that this behaviour can be inhibited by reworking of the surfaces. They found that when the surface of Red granite was reworked from 0.889 $\pm$ 0.127 μm (35 $\pm$ 5 μin) to 4.562 $\pm$ 0.508 μm (180 $\pm$ 20 μin), the stick-slip oscillations disappeared. JAEGER (1959) also observed these oscillations with ground surfaces but there are indications that similar oscillations existed in his tests on plaster filled joints at large displacements. JAEGER and ROSENGREN (1969) reported that oscillations occur only when the surface roughness is less than 0.00254 mm (0.0001 in) and that these oscillations are sometimes irregular. BRACE and BYERLEE (1966a, b) and BYERLEE (1967a) stated that

these oscillations are more pronounced with rough than with smooth surfaces. It looks as if for each type of rock, certain conditions have to be met in order for stick-slip to take place. Work conducted at the Centre for Tectonophysics, Texas A & M University (HANDIN, 1972a, b) indicates that for stick-slip to occur the rock should not be of carbonate composition nor contain alteration products that will be highly ductile under the experimental conditions. LOGAN et al (1973) are of the opinion that the porosity of the rock should be low. Relatively moderate confining pressures, low temperatures and medium to slow rates of strain enhance slip. In triaxial tests, slip is enhanced when the sliding surface makes an angle of 30 to 40 to the load axis. HANDIN (1972a, b) is of the opinion that the sliding surface should be flat, planar, free from large interlocking asperities and no gouge should be present.

The mechanism of stick-slip may be divided into two distinct classes. Firstly, the individual movements which may be associated with the shearing of the asperities and which, due to the stiffness of the loading system, result in a sudden drop of the shear force. Such movements are likely to be associated with rough surfaces. Secondly, there are the relaxation oscillations which are due to the difference in the dynamic and static coefficients of friction of the rock surfaces.

The first type of movement is an accidental phenomenon and is non-repetitive. With movement of blocks the surfaces become smoother, the area of contact increases and so does the adhesion between the blocks. As sliding takes place, some grains are fractured while others are broken at the grain boundaries and plucked out and some may even undergo ductile behaviour. But a majority of the grains are elastically strained (Fig. 10-76a). More and more of these grains are elastically strained as the displacement continues until a critical number of grains reach a threshold value of elastic strain and their failure occurs (Fig. 10-76b). At this stage the resistance to sliding is lowered, rapid displacement takes place and stress drops giving stick-slip. The cycle repeats itself, but because of the planar nature and uniform roughness of the surface, the critical stress is reached on a reproducible and cyclic basis.

The above explanation assumes that after a certain (but perhaps quite large) displacement or repeated displacements when the two surfaces become truly parallel, then the stick-slip phenomenon should disappear.

It is at this stage that the second factor comes to play a dominant role. When the surfaces are truly flat, their cohesion is very high and they behave similar to metals. That is why oscillations have been observed either in rough surfaces or in case of extremely smooth surfaces.

HOSKINS, JAEGER and ROSENGREN (1968) analysed these oscillations in terms of a model of mass M pressed against a surface by a force W and moved along

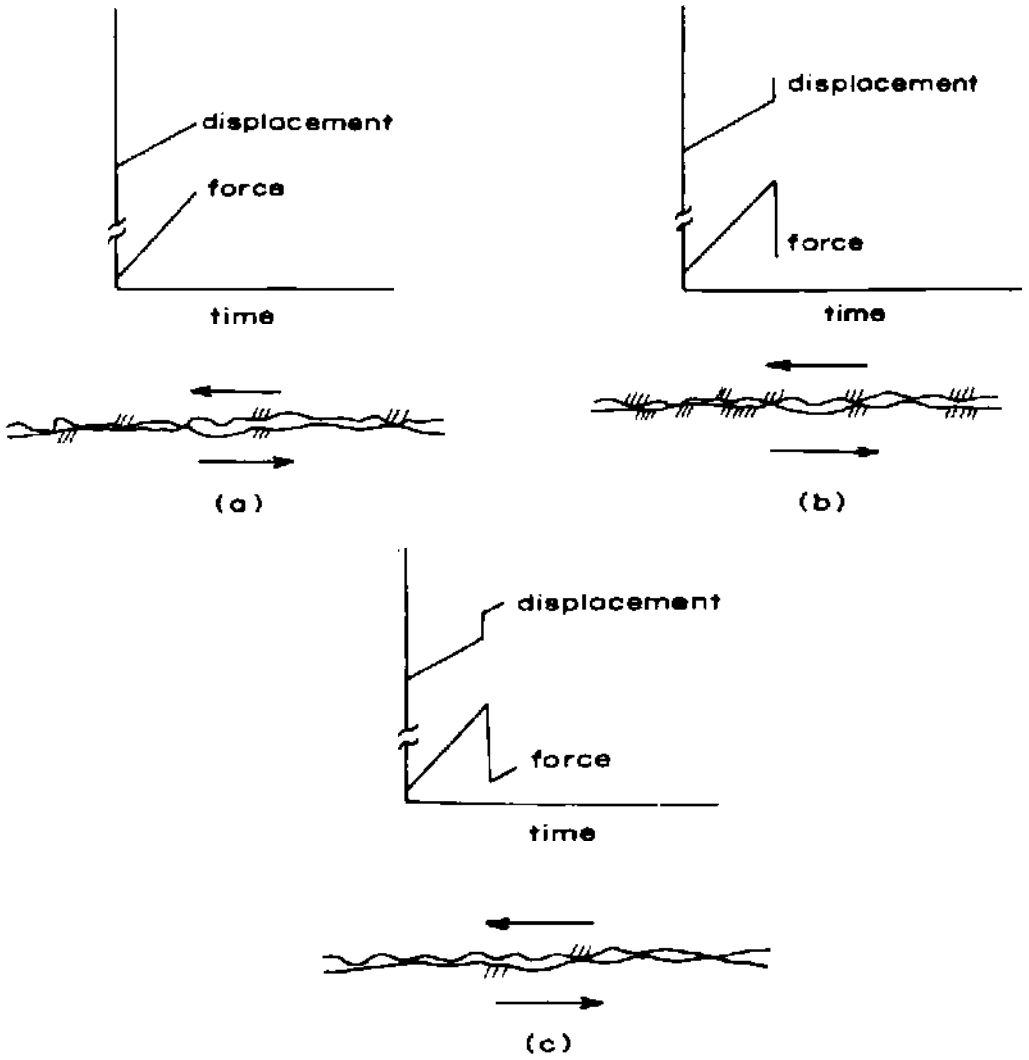

Fig. 10-76. Schematic diagrams of concept of surface deformation during stick-slip. Shaded areas indicate elastic straining of rock at sliding surface (after HANDIN, 1972b).

the surface by a spring OM of stiffness λ whose one end O is moved with a constant speed V (Fig. 10-77a). The mass will remain at rest relative to the plane until the force F exerted by the spring reaches the value given by the equation

$$F = \mu W \tag{10.56}$$

At this time it will slip and its motion will be resisted by the force of dynamic friction $\mu' W$. During slipping, if V is small, its displacement X relative to the plane is approximately given by

$$X = (\mu - \mu')\, W[1 - \cos nt]/\lambda \tag{10.57}$$

where $n = (\lambda/M)^{1/2}$.

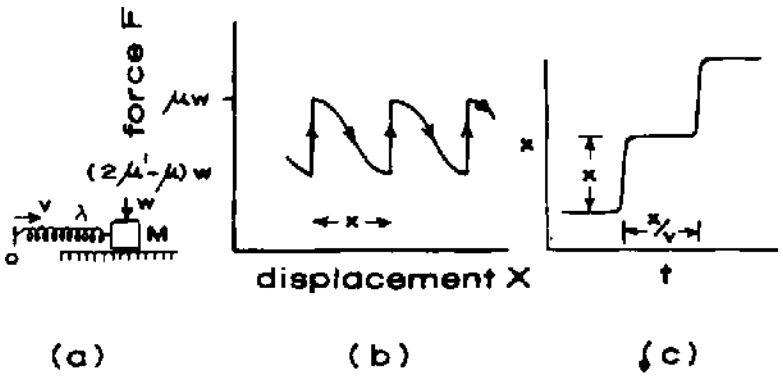

Fig. 10-77. (a) Simple model for stick-slip oscillations
(b) Force-displacement curve
(c) Displacement-time curve
(after HOSKINS, JAEGER and ROSENGREN, 1968).

The mass comes to rest again at time $t = \pi/n$, approximately, and the spring begins to compress again. The displacement X at each slip is given by

$$X = 2(\mu - \mu') \frac{W}{\lambda} \tag{10.58}$$

The force F^* exerted by the spring when motion has just ceased is given by

$$F^* = (2\mu' - \mu) W \tag{10.59}$$

It follows from Eqs. (10.56), (10.58) and (10.59) that

$$X = \frac{(F - F^*)}{\lambda} \tag{10.60}$$

and the period of oscillations is

$$\frac{2(\mu - \mu')}{\lambda V} W \tag{10.61}$$

The force-displacement curve is given in Fig. 10-77b and the displacement-time curve in Fig. 10-77c.

It shall be seen that the actual curves so obtained have a close resemblance to the theoretical curve (Fig. 10-78). The oscillations take the form σAC in which σA represents the small displacement when the load is building up, AC represents the slipping phase and BC is the effect of machine pendulum.

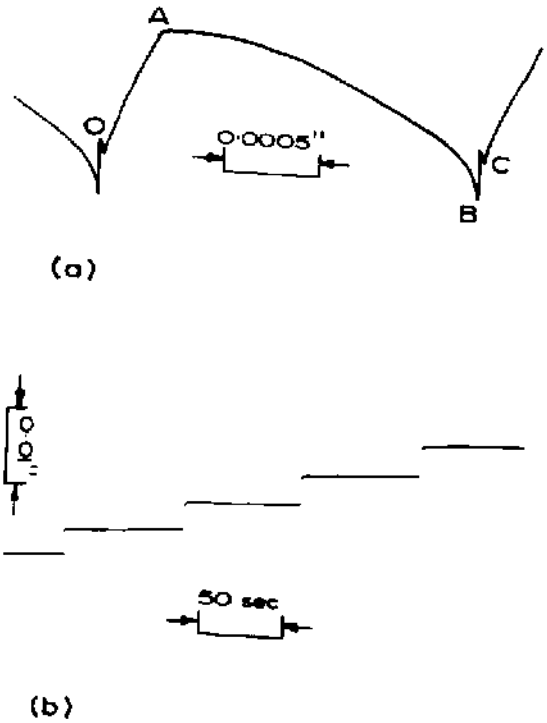

Fig. 10-78. (a) One cycle of the oscillation of Fig. 10.74b on an enlarged scale. (b) The same showing displacement against time (after HOSKINS, JAEGER and ROSENGREN, 1968).

High speed records have shown that slippage takes place in a time less than 2 ms corresponding to $n > 1500$/s.

It shall be seen from Fig. 10-74b that the displacement X at each slip increases with the amplitude of the oscillation and the mean value of $\left(\frac{F-F^*}{X}\right)$ should represent the stiffness of the machine (Table 13). The values are in the range of 625.6 to 876.0 $\times 10^6$ N/m (3 to 5 $\times 10^6$ lbf/in) which are in good agreement.

From Eqs. 10.56 and 10.59 the coefficient of dynamic friction μ' is the arithmetic mean of μ and μ^* (Table 13).

HANDIN (1972b) conducted tests at strain rates (axial shortening of precut cylinders in a triaxial apparatus) varying from 10^{-7} to 10^{-3}/s. At a confining pressure of 14 MPa (140 kgf/cm^2) (2030 lbf/in^2) and rate of strain of 10^{-4}/s the stress drops at stick-slip were approximately 1 to 2 MPa (10 to 20 bars) (145–290 lbf/in^2) and when the strain rate was decreased to 10^{-7}/s, the stress drop increased to 10 MPa (100 bars) (1450 lbf/in^2) (Fig. 10-79). At a strain rate of 10^{-3}, there was almost a complete suppression of the stick-slip. Similar results were reported by DIETERICH (1970) and SCHOLZ, MOLNAR and JOHNSON (1972). The value of the strain rate at which stick-slip will disappear depends upon the method of preparation of the specimen, rock type, confining pressure and a host of other features.

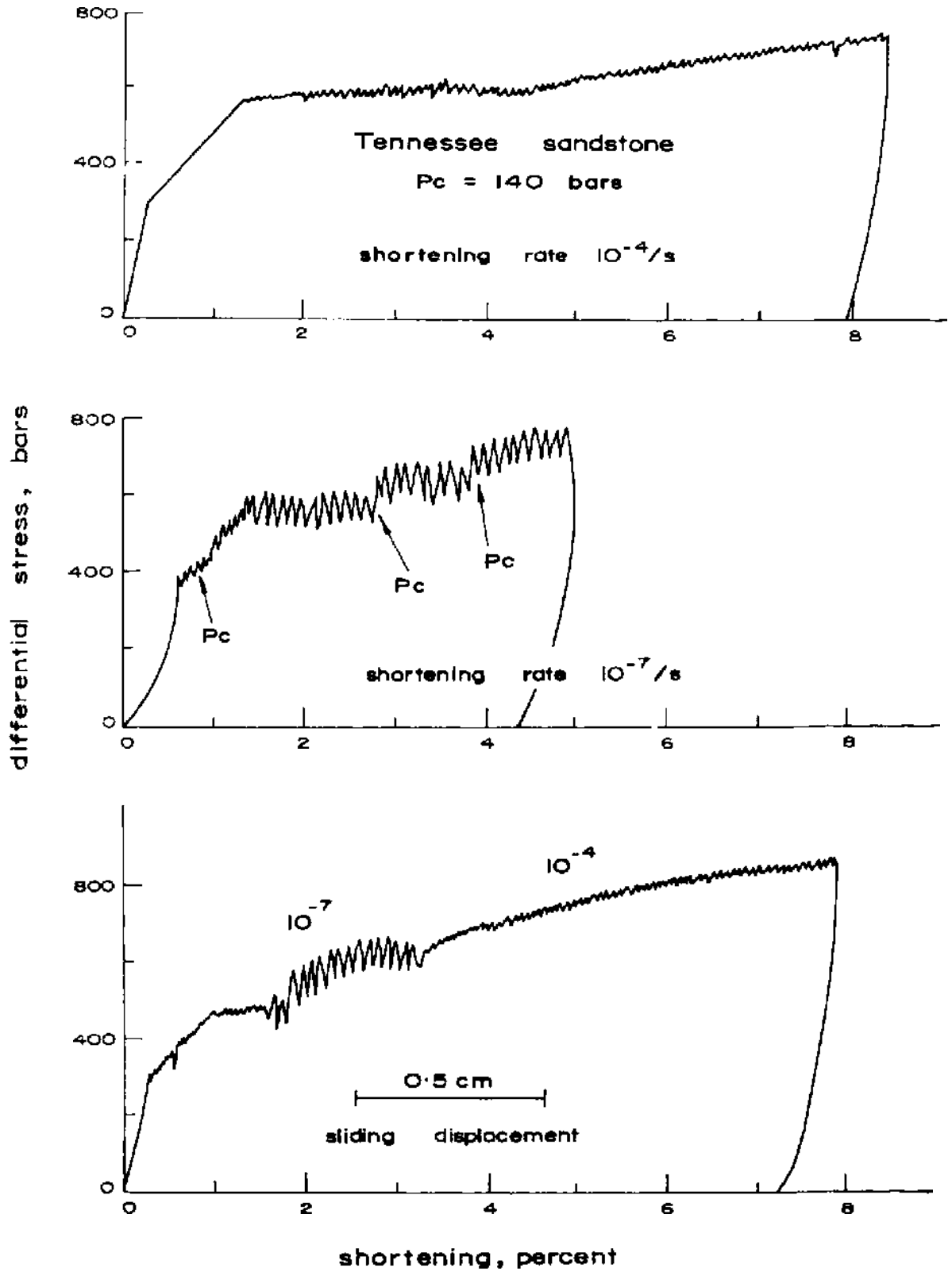

Fig. 10-79. Differential stress versus shortening for Tennessee sandstone deformed at a constant rate of shortening of 10^{-4}/s and 10^{-7}/s. Tests were done at 140 bars confining pressure (P_c) and room temperature.
Specimens contained a saw cut at 35° to the load axis
(after HANDIN, 1972b).

Tests were conducted by BYERLEE and BRACE (1968) on the influence of various factors such as rock type, pressure, strain rate and stiffness of the system on the phenomenon of stick-slip. They found that certain rock types (granite, gabbro, granodiorite, dunite, etc.) give rise to stick-slip and the stick-slip amplitude increases with increase in pressure (Fig. 10-80). At low pressures the

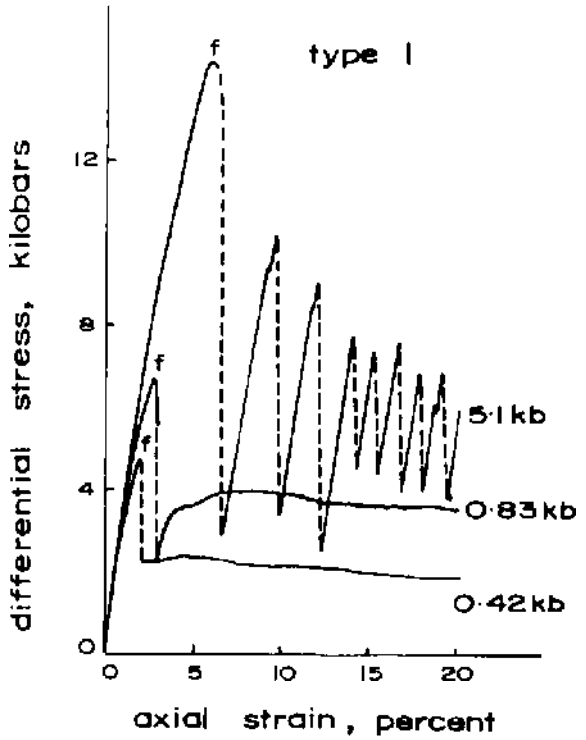

Fig. 10-80. Differential stress versus axial strain for San Marcos gabbro. The value at the end of each curve gives the confining pressure in kilobars (after BYERLEE and BRACE, 1968).

rocks give stable sliding and only at intermediate and high pressures do these give stick-slip. In other rocks (e. g. Solenhofen limestone, marble, granite, rhyolite tuff, Spruce Pine dunite, etc.) no stick-slip occurs even at pressures up to 500 MPa (5 kb) (72,500 lbf/in^2) (Fig. 10-81). They concluded that stick-slip is controlled by mineral type and porosity. Stick-slip does not occur with high porosity rocks like tuff and is also absent in rocks containing calcite, serpentine, etc. The increase of 3% of serpentine in two dunites tested by them completely changed the frictional characteristics. The presence of large amounts of minerals such as mica and chalcocite has little influence and as such they concluded that the role of alteration is not certain. They also found that the stiffness of the system has influence on the phenomenon of stick-slip and that very elastic systems shall give rise to a greater drop in the stick-slip (RABINOWICZ, 1965). The maximum stiffness of the system used by BYERLEE and BRACE (1968) was however of the order of 19,618 $\times$ 10^4 N/m (20 $\times$ 10^4 kgf/cm) (111.9 $\times$ 10^4 lbf/in)

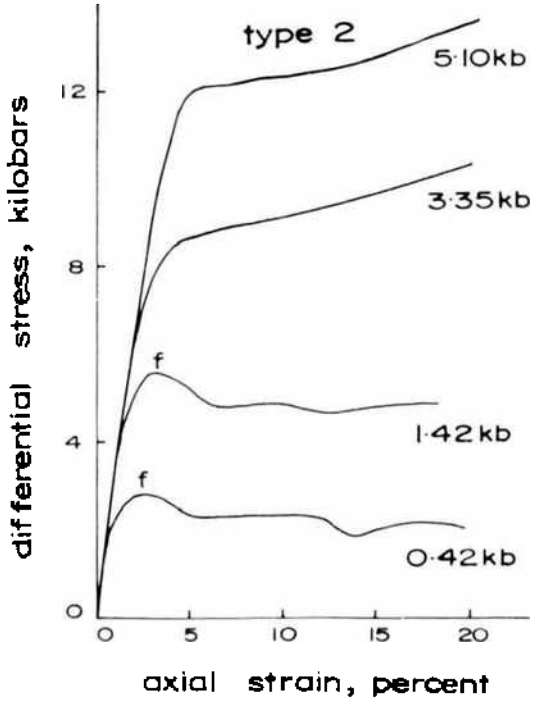

Fig. 10-81. Differential stress versus axial strain for Spruce Pine dunite. The value at the end of each curve gives the confining pressure in kilobars (after BYERLEE and BRACE, 1968).

which was of the order of the specimen stiffness and the lower range was of the order of 1961.8×10^4 N/m (2×10^4 kgf/cm) (11.19×10^4 lbf/in).

Tests conducted by LAMA (1975a) on models of marble surface obtained in a Brazilian test using plaster-water mixture as a model material showed distinct stick-slip phenomenon on these highly rough surfaces as well as on polished surfaces. The amplitude of stick-slip is related to the normal stress and the shear displacement rate. Fig. 10-82 shows parts of the shear-displacement curves at a total displacement of 2 mm at different shear displacement rates and normal stresses for the same joint surface reproduced every time using silicone rubber mould. The amplitude decreases with increase in shear displacement rate and increases with normal stress. The stick-slip amplitude seems to be dependent upon the machine stiffness and decreases with increase in the shear stiffness of the machine.

COULSON (1970) tested specimens in the stiffness range from 350.4×10^4 to 6657.6×10^4 N/m (2×10^4 to 38×10^4 lbf/in) (i.e. stiffness systems much lower than those used by BYERLEE and BRACE, 1968) and found decreased stiffness increased the severity of the stick-slip. The stiffness of the faults in the earth's crust is of about 4 to 5 order of magnitude smaller than the laboratory testing machines (WALSH, 1971) and hence stick-slips occurring in nature shall be much more severe.

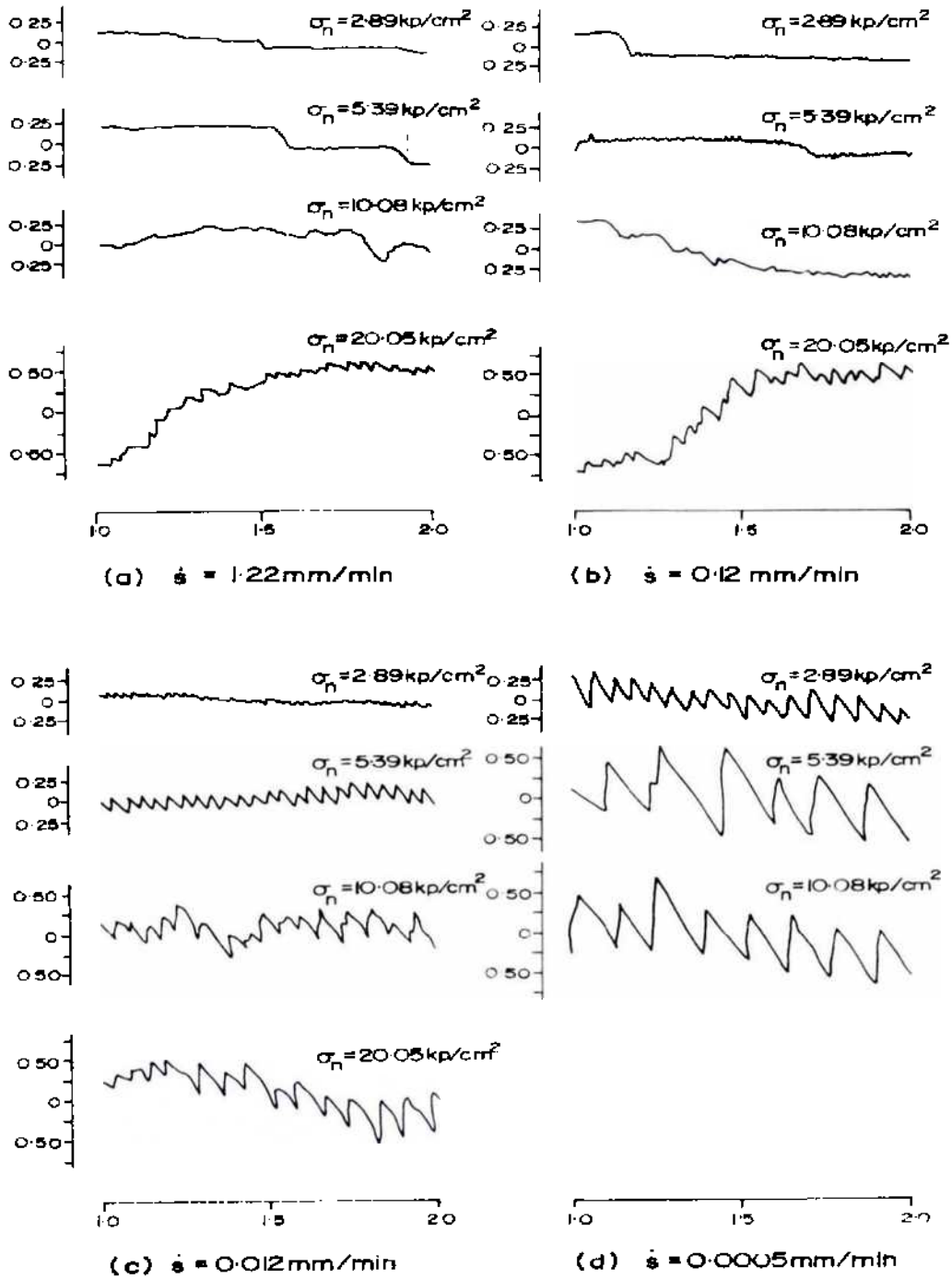

Fig. 10-82. Stick-slip as a function of displacement rate and normal stress in the displacement ranges 1 to 2 mm (after LAMA, 1975a).

The equipment used by HOSKINS, JAEGER and ROSENGREN (1968) had stiffnesses of 625.6 to 876.0 × 10^6 N/m (3 to 5 × 10^6 lbf/in) and even with this high stiffnesses they observed stick-slip in trachyte, granite and gabbro.

The presence of water and pore pressure will reduce the effective stress and hence cause reduction in the stress drop. BRACE and MARTIN (1968) found that violent stress drop disappears under high pore-pressures at low strain rates. COULSON (1970) also found that stick-slip is more common for dry specimens than for wet surfaces.

The influence of temperature (30 to 200 C) (86 to 392 F) on stick-slip at normal pressures of 0.073 to 1.958 MPa (0.75 to 20 kgf/cm^2) (10.65 to 284 lbf/in^2) was studied by DRENNON and HANDY (1972). They found that an increase in temperature of the rock undergoing stick-slip caused an increase in stick-time, a corresponding increase in the length of the individual slips and an increase in the amount of relaxation of the shearing load upon slip. On decrease in temperature, the amount of stick-slip and load relaxation decreased (though non-linearly) until smooth slip finally occurred. The temperature at which stick-slip disappears depends upon the normal load.

The gouge present in the fault plane influences the stick-slip behaviour. Saw cut granite specimens tested at confining pressures of 0.75 kb – 6.72 kb (10,900 lbf/in^2 – 92,100 lbf/in^2) with gouge thickness of 0.25 mm – 4.0 mm (0.01 in – 1.6 in) showed that stick-slip was absent at low confining pressures (0.75 kb) and appears at higher pressures only. The pressure at which this transition takes place increases with increase in gouge thickness (BYERLEE and SUMMERS, 1976). This influence of gouge probably explains why certain investigators observed stick-slip with clean surfaces only (ENGELDER, 1973). The interaction with the normal pressure is important. The gouge material which is more or less granular undergoes compaction at higher pressures and then dilates under shear (BYERLEE, 1968b). If the transition from high pressure compaction to dilatation at comparatively high pressure leads to weakening of the material, then it is possible that this mechanical instability caused is responsible for stick-slip.

It is also anticipated that stick-slip in rough joints is associated with the fracture of the asperities. The influence of time for which as asperity indents into the opposite surface under both normal and shear loads will naturally show some creep depending upon the stress and the creep properties of the rock. Its penetration increases the contact area and hence requires higher shear force for sliding. This suggests that dynamic and static frictional values should be velocity dependent and obey some form of logarithmic creep law. This is likely to happen only if the asperities remain undamaged under these high stresses. Tests conducted using diamond asperities on different rock surfaces tend to support it (SCHOLZ and ENGELDER, 1976).

Shear stiffness of the system and the brittle fracture are important contributing factors which should not be ignored.

10.5. Fracture of Jointed Rock in Uniaxial Compression

BORETTI-ONYSZKIEWICZ (1966) studied the effect of direction of loading in relation to bedding planes on the compressive strength of sandstones in both air-dry and water saturation conditions. When the specimens were tested by loading along the bedding planes, the strength was considerably less than when loaded at right angles to the bedding planes (Table 8, Vol. I).

GOLDSTEIN et al (1966) tested composite specimens of different sizes made from cubes of plaster of Paris and sand mixtures of different strengths (elemental cubes were of 2 cm × 2 cm × 2 cm (0.79 in × 0.79 in × 0.79 in)). They designated the ratio of the length of the model (L) to the length of the element (l) as the "block index (L/l) (joint spacing) and the results obtained by them are given in Fig. 10-83. According to them, these results can be represented by the relationship

$$\frac{\sigma_{c_m}}{\sigma_{c_e}} = a + b\left(\frac{l}{L}\right)^{\beta} \tag{10.62}$$

where σ_{c_m} = compressive strength of the model (composite block)
σ_{c_e} = compressive strength of the element constituting the block
l = length of each element
L = length of the model and
a, b, β = constants, where $\beta < 1$ and $b = (1-a)$ (Fig. 10-84).

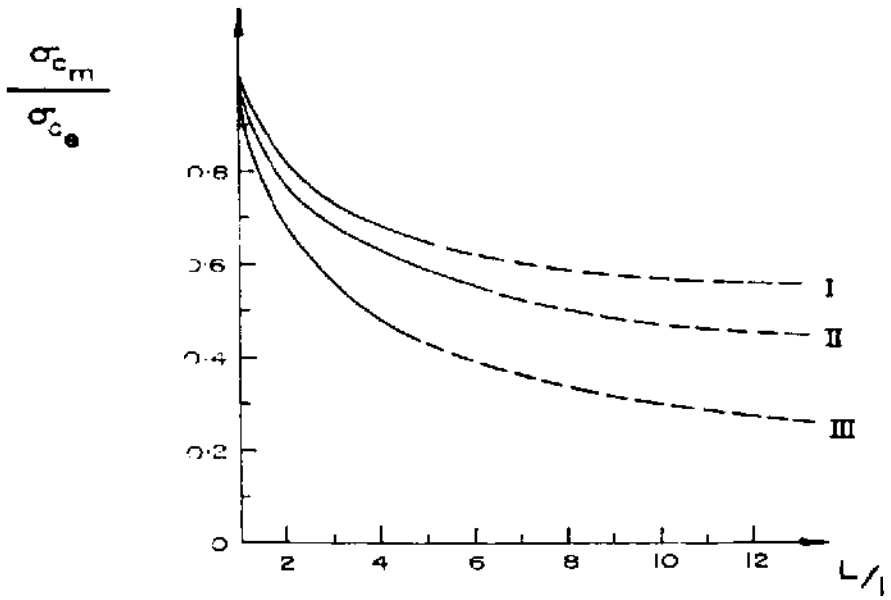

Fig. 10-83. The relative strength of the composite specimens
I σ_{c_e} = 10 kgf/cm²
II σ_{c_e} = 20 kgf/cm²
III σ_{c_e} = 30 kgf/cm²
(after GOLDSTEIN et al, 1966).

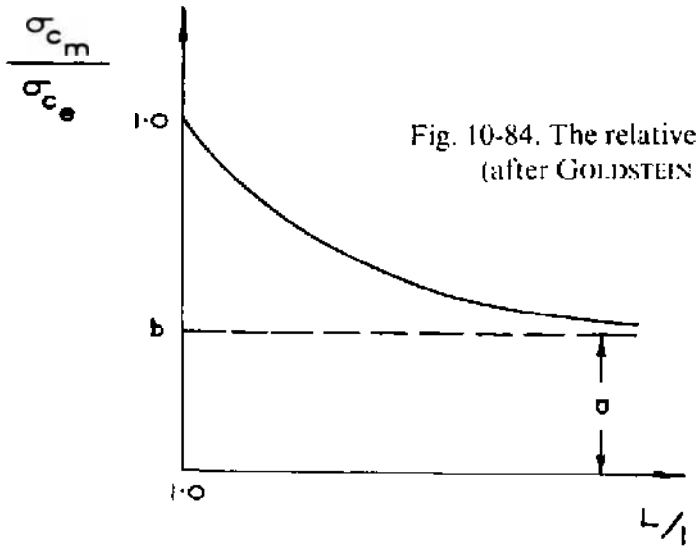

Fig. 10-84. The relative strength of mass (after GOLDSTEIN et al. 1966).

It shall be seen from Fig. 10-83 that the influence of increase in the value of (L/l) is greater for models with higher elemental strength (σ_{c_e}) than for models with lower elemental strength. After a certain number of elements, the strength almost becomes constant but the number of these elements was not determined by GOLDSTEIN et al. They, however, measured the ultrasonic longitudinal wave velocity and found a similar asymptotic relationship between $\frac{V_{l_m}}{V_{l_e}}$ and (L/l) (where V_{l_m}-ultrasonic longitudinal wave velocity in the model and V_{l_e}-ultrasonic longitudinal wave velocity in the element), and found that this ratio $\frac{V_{l_m}}{V_{l_e}}$ becomes almost asymptotic at $(L/l) = 15$, which perhaps suggests that this value could be taken for the strength relationship (Eq. 10.62). Very similar results have been obtained by CVETKOVIĆ (1974).

HAYASHI (1966) conducted tests on the uniaxial strength of jointed specimens prepared out of plaster of Paris (compressive strength 3.652 MPa (37.3 kgf/cm^2) (529.7 lbf/in^2), tensile strength 0.832 MPa (8.5 kgf/cm^2) (120.7 lbf/in^2) (direct pull test)). The joints were produced by inserting a wax paper during casting. He found that the uniaxial compressive strength decreased with the increase in the number of joints even if the total area of the intermittent joints was equal (Fig. 10-85). According to him, the relationship can be expressed in the form of an equation

$$\frac{\sigma_{c_n}}{\sigma_{c_1}} = 1 - v\sqrt{2\log n} + v\left(\frac{\log(\log n) + \log 4\pi}{2\sqrt{2\log n}}\right) \qquad (10.63)$$

where σ_{c_n} = uniaxial compressive strength of a specimen with n number of joints

σ_{c_1} = uniaxial compressive strength of a specimen with one joint and

v = coefficient of variation.

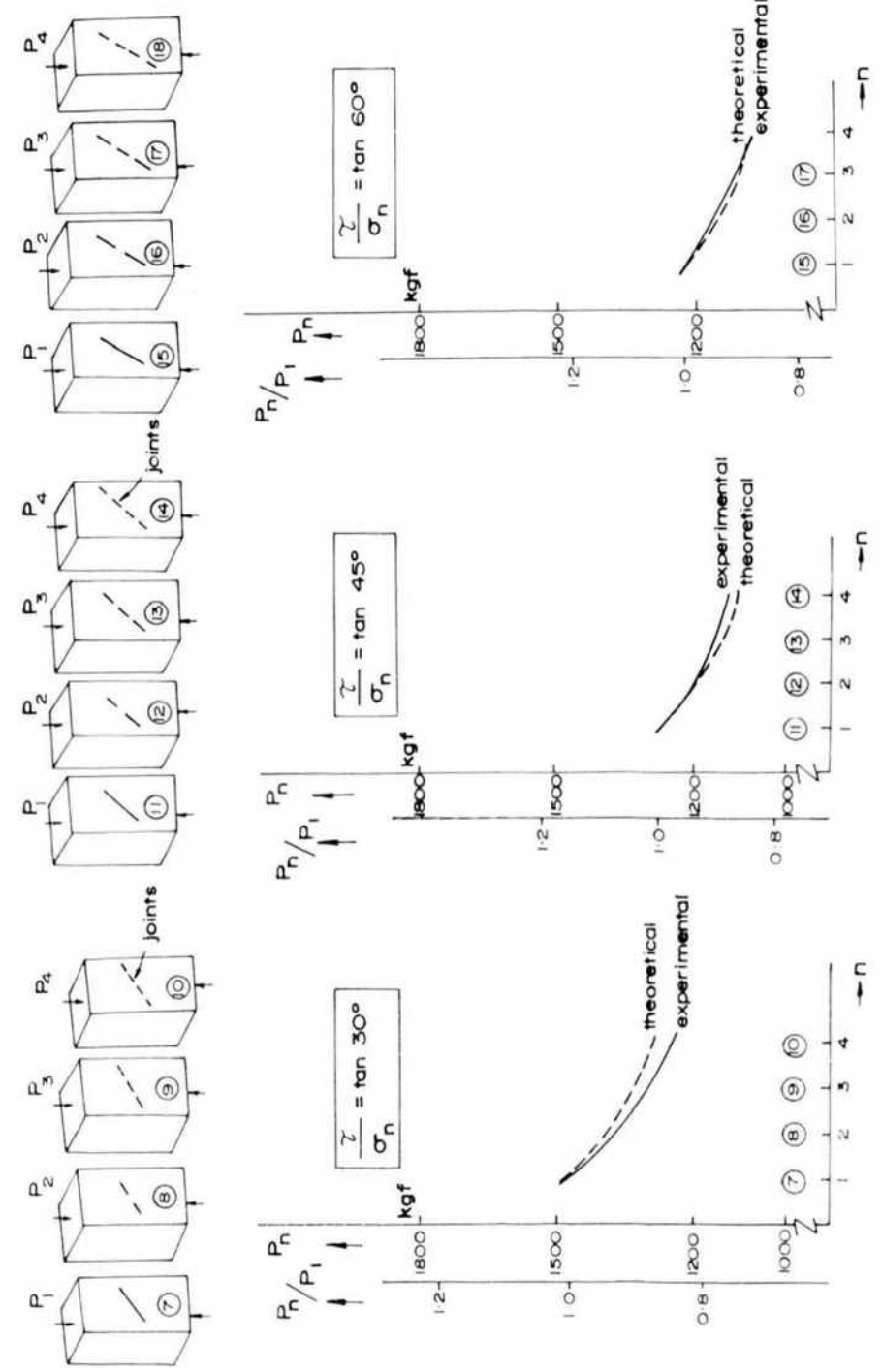

Fig. 10-85. Compressive load P_n decreases depending on the intermittent frequency of joints n regardless of whether the total area of joints is equal (after HAYASHI, 1966).

Fig. 10-86 illustrates the effect of parallel rows of joints. Strength decreases with the number of rows even if the volume of the specimen is equal and the above relationship holds good. HAYASHI also tested specimens with varying joint inclinations with respect to the application of force and found that the specimen having a joint with an inclination of 30 had the lowest strength.

LAJTAI (1967) conducted tests to determine the influence of discontinuities on the uniaxial compressive strength using plaster of Paris as a model material. The discontinuities were in the form of interlocking teeth inclined at various angles (30 to 50) to the direction of loading with varying widths of the teeth. He found a linear relationship between the uniaxial compressive strength and the angle of inclination (in degrees) in the range 30 to 54 with the minimum value at 30 . The compressive strength of the narrow teeth (6.4 mm) (1/4 in) specimens was lower than that of wide teeth (25.4 mm) (1 in) specimens (Fig. 10-87). The influence of the tooth width on the compressive strength for specimens having inclinations 45 ± 2 and 33 ± 3 is shown in Fig. 10-88. (The height of the teeth in all the cases was kept constant). It is seen that the compressive strength increases greatly with teeth size till a certain value of the teeth size (12.7 mm – 1/2 in for 45 ± 2 and 19.5 mm – 3/4 in for 33 ± 3) at which it attains a constant value. This sudden change in the strength curve was explained by LAJTAI due to the change in the failure mechanism as the size of the teeth increases. The large tooth width results in the shear failure while in the case of small tooth widths, the failure is tensile caused due to bending.

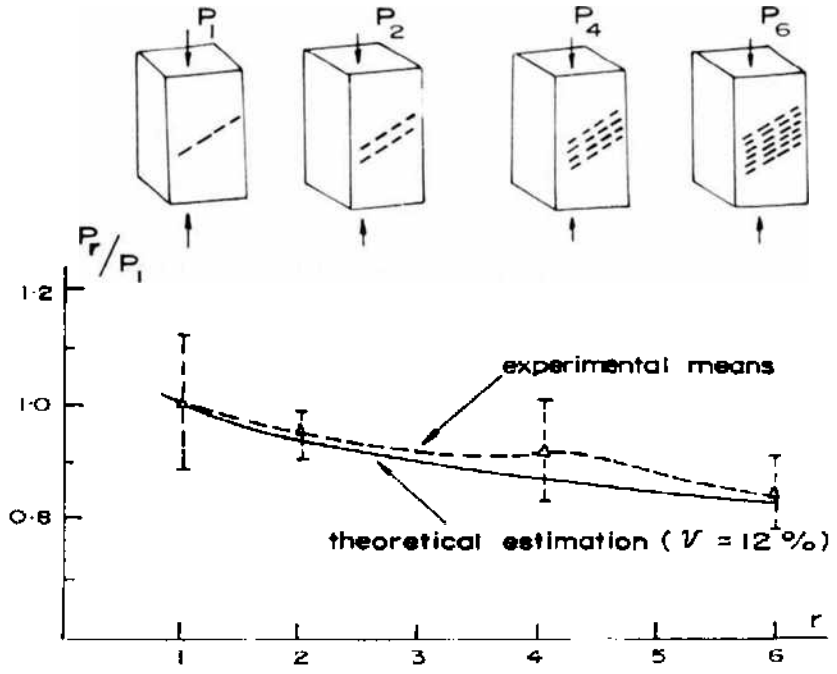

Fig. 10-86. Compressive load P_r decreases depending on the number of parallel rows of joints r (after HAYASHI, 1966).

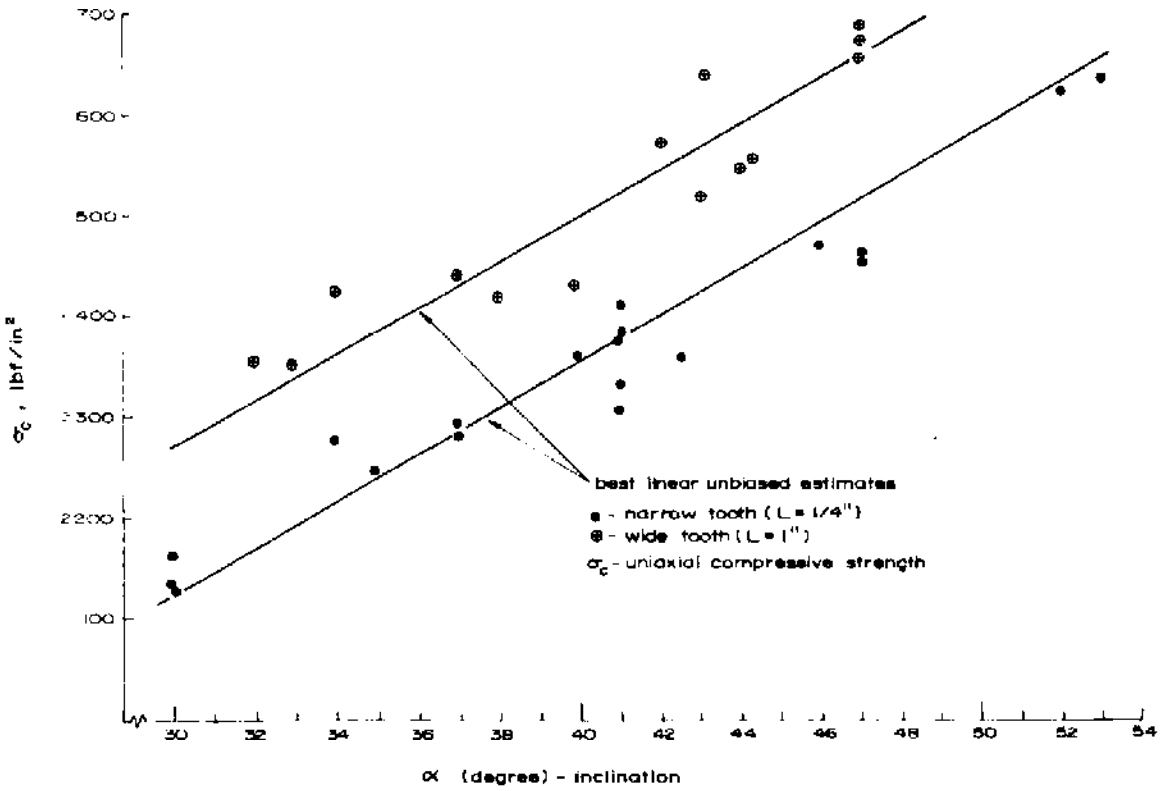

Fig. 10-87. The relationship between uniaxial compressive strength (σ_c) and discontinuity inclination (α) (after LAJTAI, 1967).

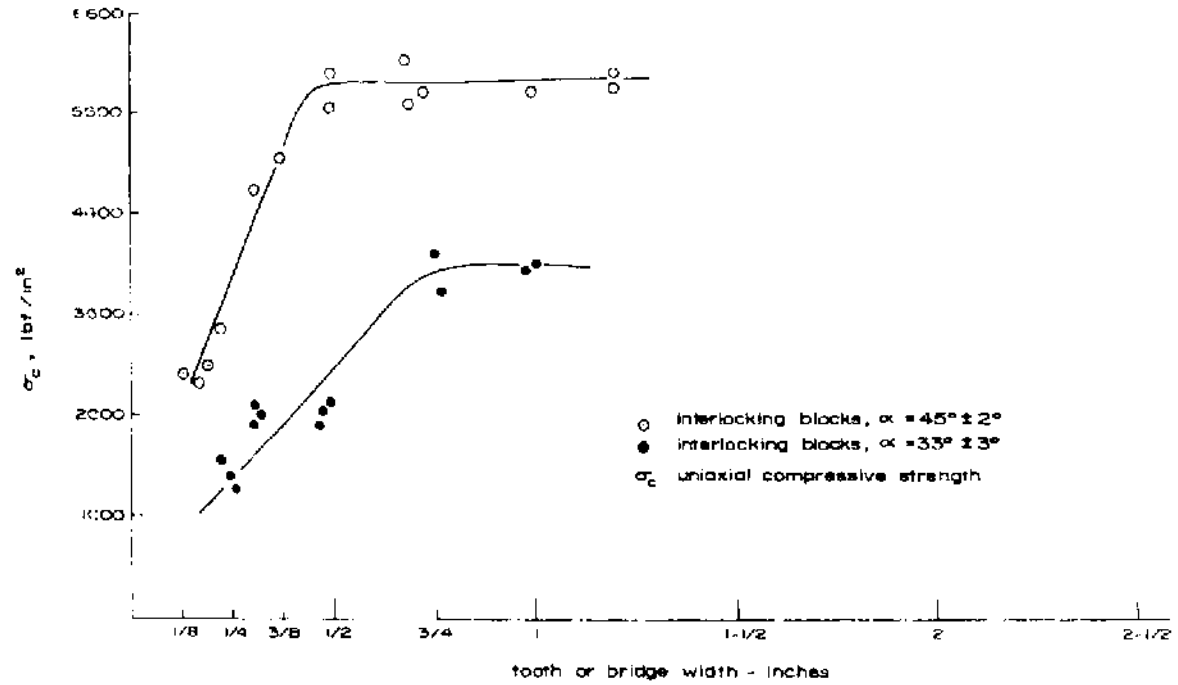

Fig. 10-88. The dependence of uniaxial compressive strength (σ_c) on tooth or bridge width (after LAJTAI, 1967).

HORINO (1968) determined the effect of the angle and spacing of noncohesive planes of weakness on the compressive strength of limestone, sandstone and granite cores. The angle of the planes of weakness, measured from the horizontal, varied from 0 to 57 in approximately 15 increments. When two planes of weakness were incorporated, the thickness-to-diameter ratio of the wafer was 1/4, 1/2 and 1.

His results indicate that the strength decreases rapidly as the angle of the plane of weakness increases from 30 to 57 . For a given angle, the strength varies with the fracture spacing. The strength first decreases as the spacing decreases to a certain minimum and then strength increases as the spacing decreases. For limestone, the results are given in Figs. 10-89 and 10-90.

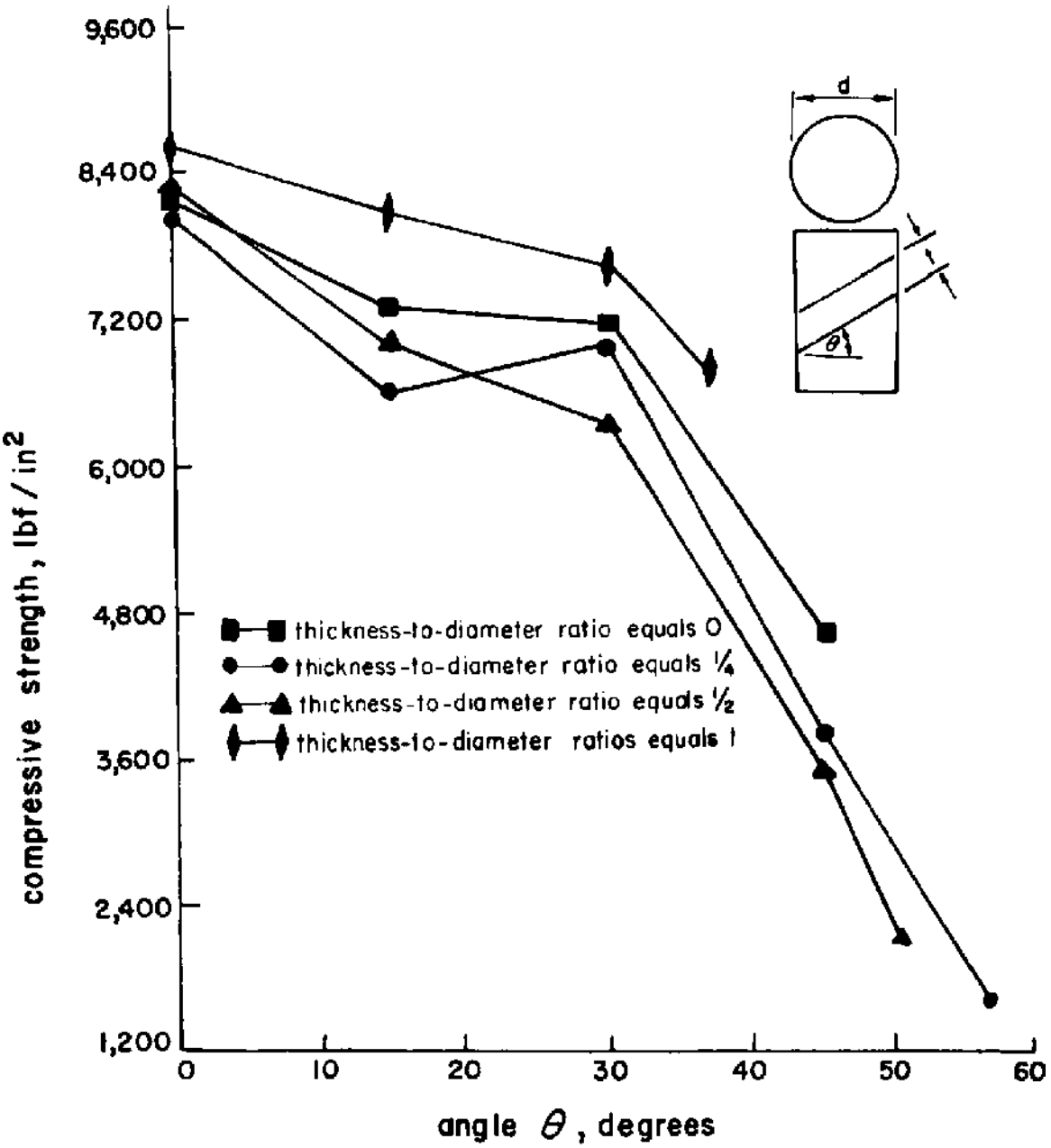

Fig. 10-89. Compressive strength versus inclination of fractures for limestone (after HORINO, 1968).

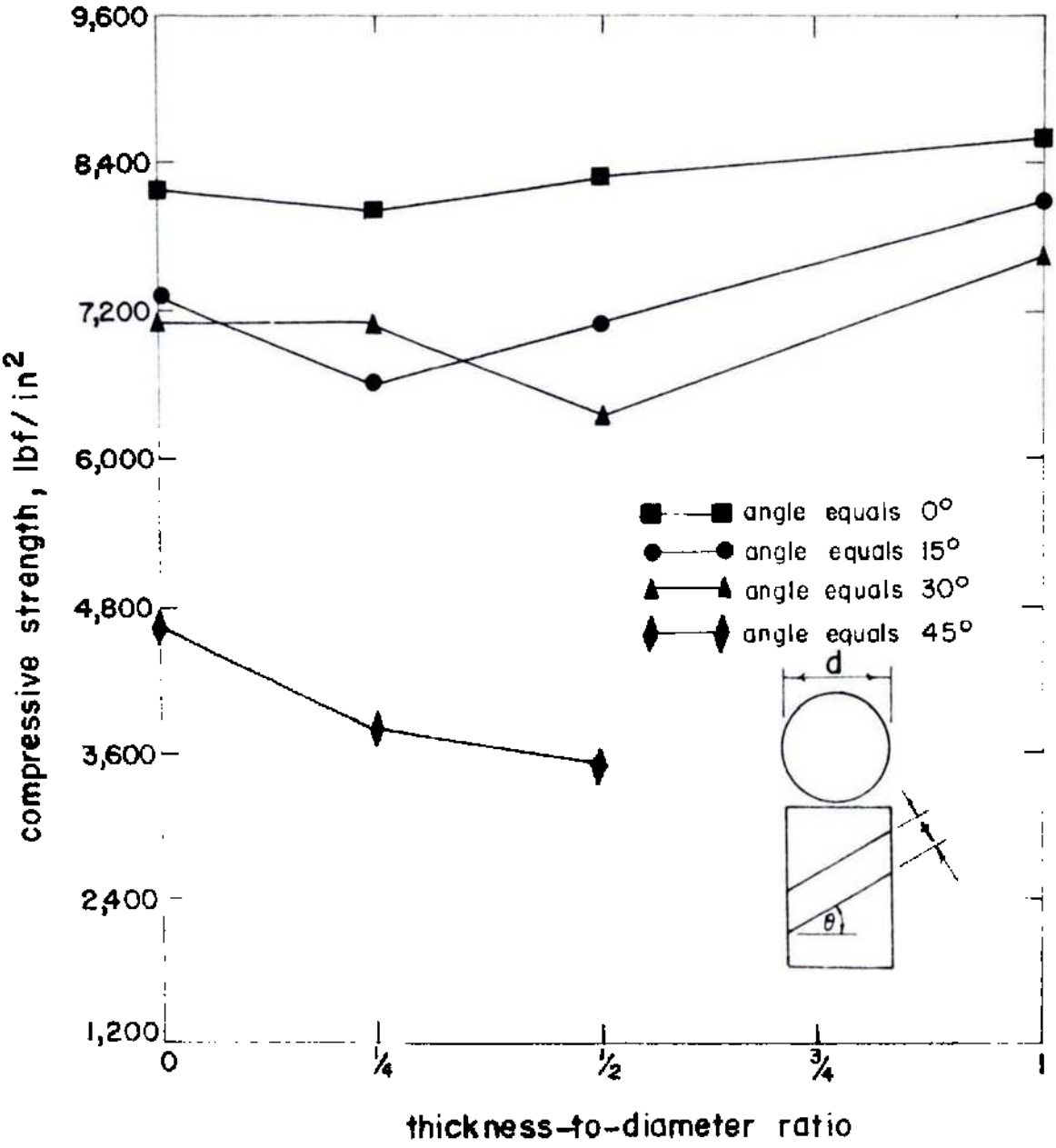

Fig. 10-90. Compressive strength versus thickness-to-diameter ratio for limestone (after HORINO, 1968).

The effect of the number of horizontal planes of weakness, with a spacing of 1/4 and 1/2 of the diameter, upon the compressive strength was also investigated. These results indicate that as the number of planes of weakness increases the compressive strength decreases. The following explanation was given for this decrease in strength:

Due to the end frictional restraint between the steel platens and a specimen, a short specimen with a $\frac{h}{d}$ ratio of 1 or less is usually stronger than a specimen

with a $\frac{h}{d}$ ratio of 2. In the presence of a plane of weakness in the specimen, the strain gradient between the steel specimen interface and the plane of weakness (specimen-specimen interface) becomes larger as these discontinuities get closer to each other. As the number of planes of weakness for a given specimen increases, the distance between the platen and the planes of weakness becomes smaller, increasing the possibility of a small tensile fracture initiating at the specimen-specimen interface nearest to the steel-specimen interface due to the strain gradient. Also there may be reduction in the coefficient of friction because of the absorption of impurities and water vapour or the formation of oxides on the sliding surfaces. The greater number of surfaces allows for a greater amount of absorption and less restraint at each interface.

BAMFORD (1969) reported the effect of bedding planes on the compressive strength and mode of failure of Silurian siltstone. His results on compressive strength versus bedding dip are given in Fig. 10-91. For dips of bedding planes greater than 50°, the failure was by shear along these planes. For dips 32 to 45°

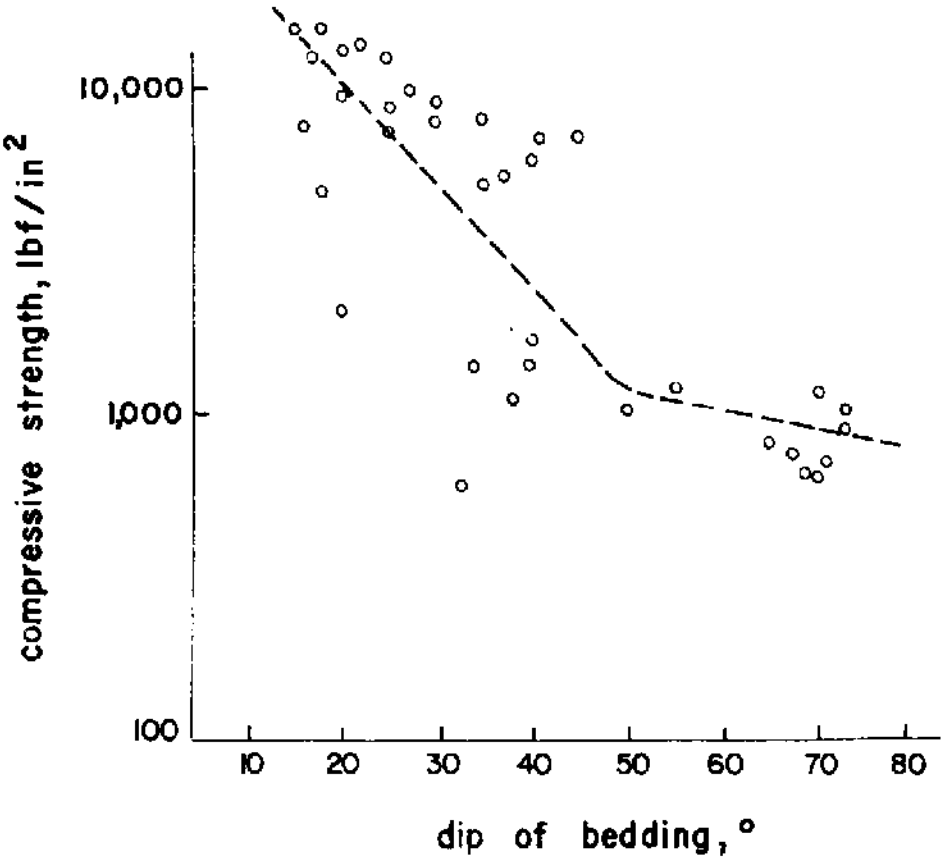

Fig. 10-91. Compressive strength of Silurian siltstone core specimens ($h/d = 1$) versus bedding dip (after BAMFORD, 1969).

a combination of shear failure along bedding and axial cleavage fracturing took place. For dips flatter than 32 . only axial cleavage fracturing took place. (Axial cleavage fracturing implies tensile failure.)

AKAI, YAMAMOTO and ARIOKA (1970) investigated the change in the compressive strength due to the inclination of lamination. They performed tests on two kinds of schists using cylindrical specimens. The influence of the inclination of lamination on compressive strength is maximum for $\alpha = 30°$ (α = angle between maximum principal stress and plane of lamination), the decrease in strength being 75 to 90 % of that for $\alpha = 90°$ (Fig. 10-92).

LAJTAI (1970) also reported the influence of joint planes on compressive strength from model tests. Comparison of stress levels at first fracturing and maximum strength in uniaxial compression is given in Fig. 10-93.

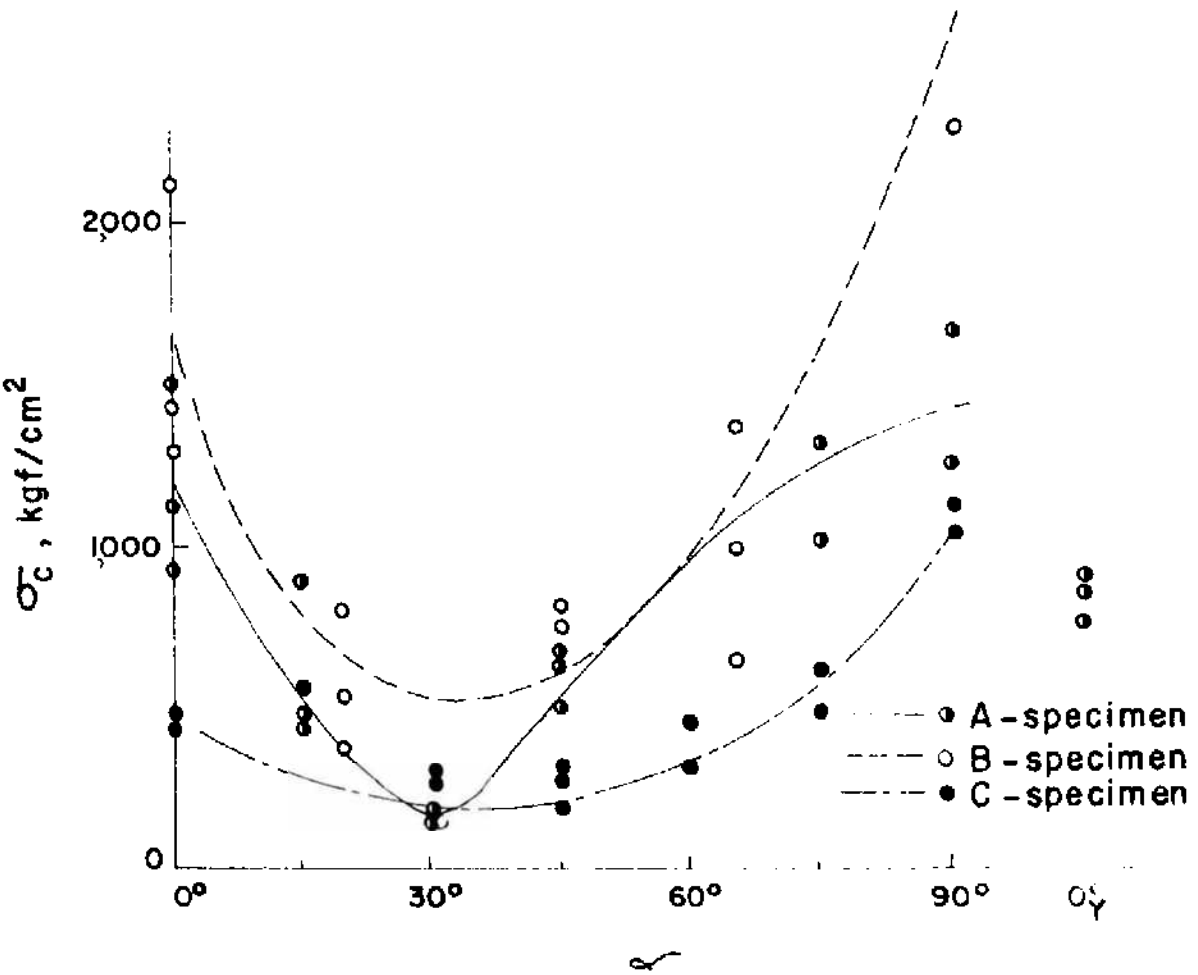

Fig. 10-92. Correlation between the inclination angle of jointed plane and the compressive strength of schists (after AKAI, YAMAMOTO and ARIOKA, 1970).

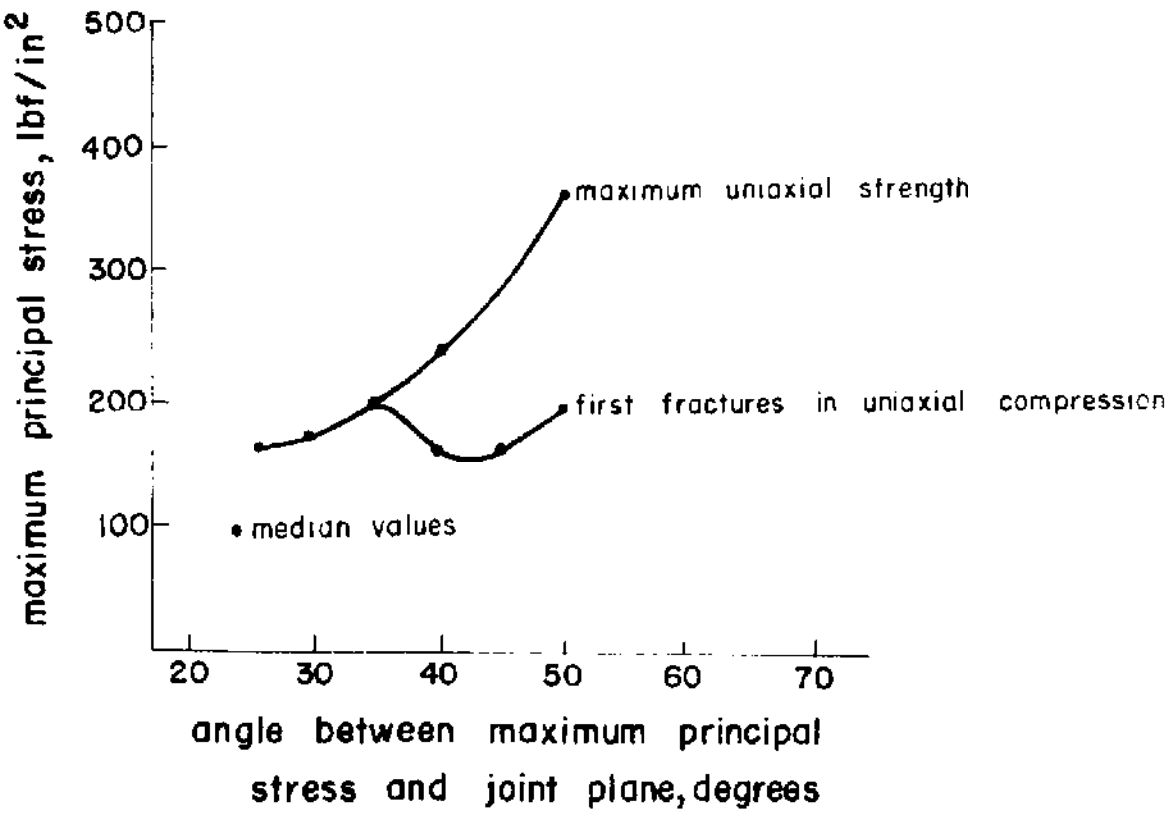

Fig. 10-93. Comparison of stress levels at first fracturing and maximum strength in uniaxial compression (after LAJTAI, 1970).

WALKER (1971) conducted some tests on slabs of plaster placed parallel to each other under uniaxial compression and found that strength decreases with increase in the number of slabs. He obtained similar asymptotic curves as GOLDSTEIN et al (1966), but in his case compressive strength became constant and reached a value of about 50% when the number of slabs placed to each other serving as columns reached 5 (the overall size of the test block in each case remaining the same). When the slabs are placed one above the other, the strength reduced slowly and with the number of joints equal to 5, its value was about 40% of the strength of an unjointed block (Fig. 10-94). Modulus (the stress-strain curves were obtained by mounting gauges on the specimens) versus jointing number is shown in Fig. 10-95.

Extensive tests have been conducted by LAMA (1974a) on the effect of density of both horizontal, vertical and orthogonal joints on compressive strength and deformation modulus using model materials of different strengths. The different model arrangements are shown in Fig. 10-96. The influence of the number of horizontal and vertical joints on both the deformation modulus and strength is shown in Figs. 10-97 and 10-98. The drop in both the deformation

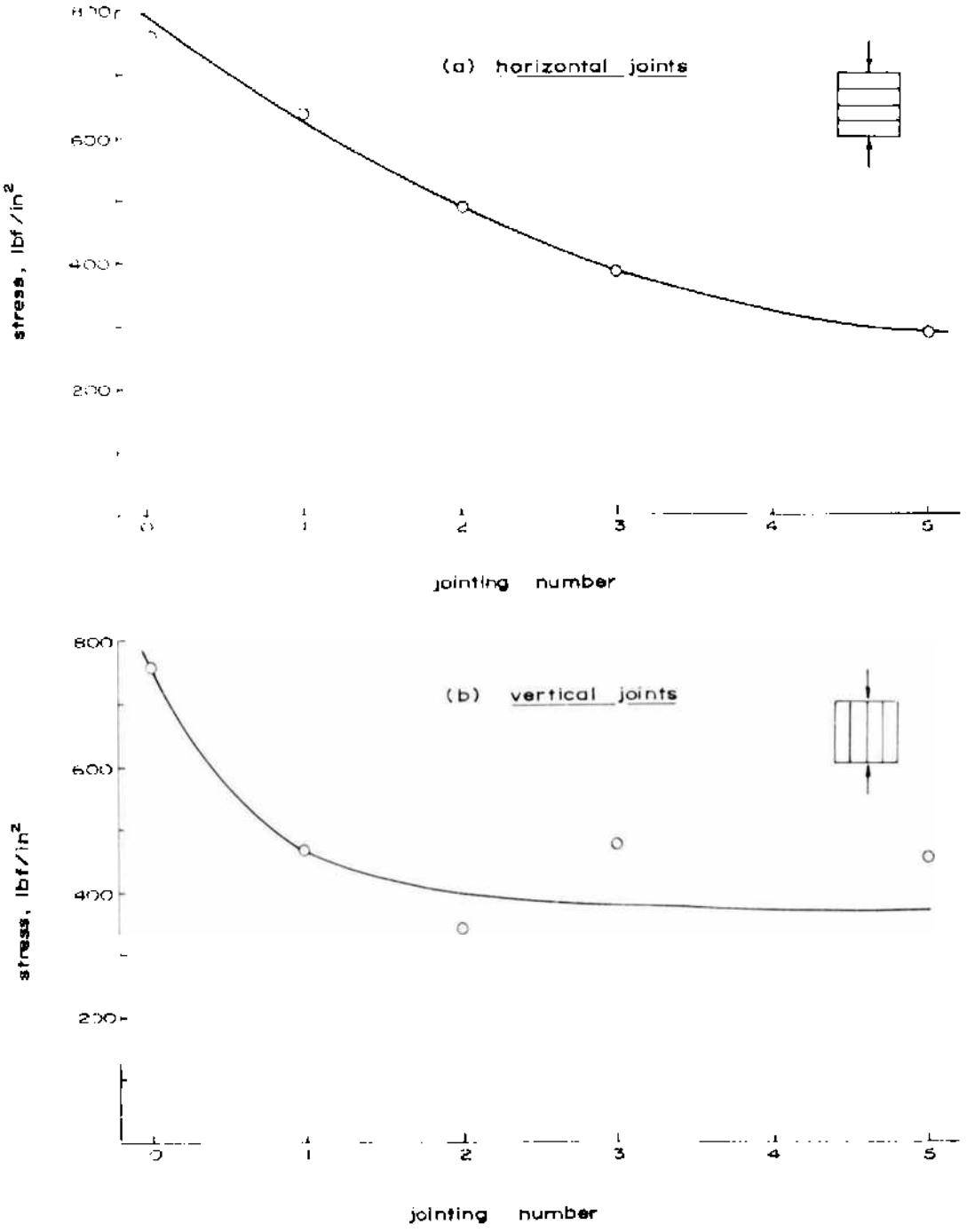

Fig. 10-94. Uniaxial compressive strength versus jointing number (after WALKER, 1971).

modulus and strength is small after the number of joints exceed 6 and is in accordance with the result obtained by GOLDSTEIN et al (1966) and WALKER (1971). On percentage basis, the decrease in the strength of rock with horizontal or vertical joints is about 30%, but the modulus values for horizontal joints fall to almost 30 to 40% and vertical joints 60 to 70%. The modulus values

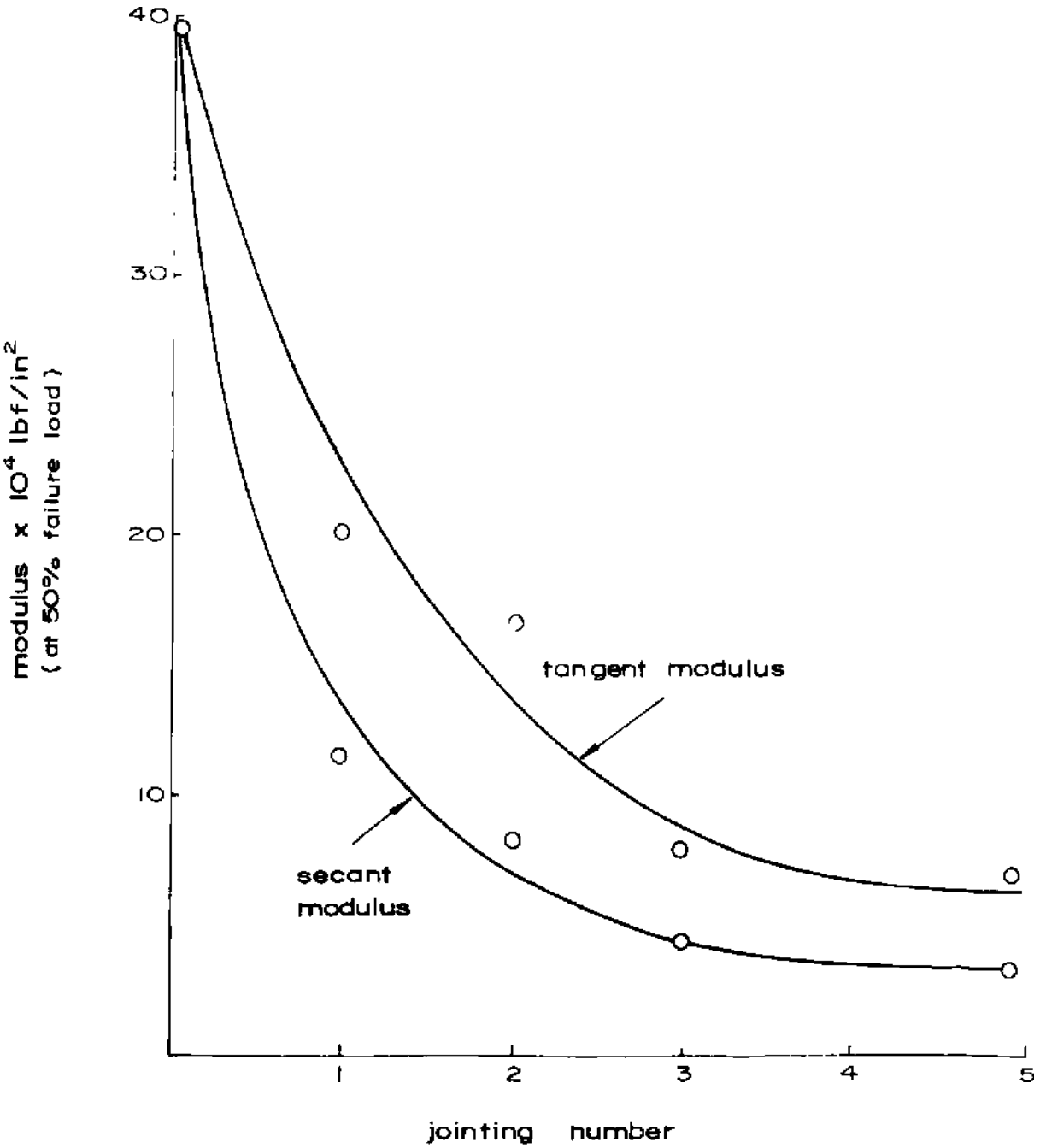

Fig. 10-95. Modulus versus jointing number (after WALKER, 1971).

are higher for the vertical joints and scatter of the results is also higher. The failure of models with horizontal joints takes place with the development of cracks at the middle, at the joint planes, and spreads upwards and downwards while in models with vertical joints, the columns fail independently. It looks that mechanics of deformation of the specimens with two different joint systems is different. In the case of horizontal joints, the stiffness of the joints plays a

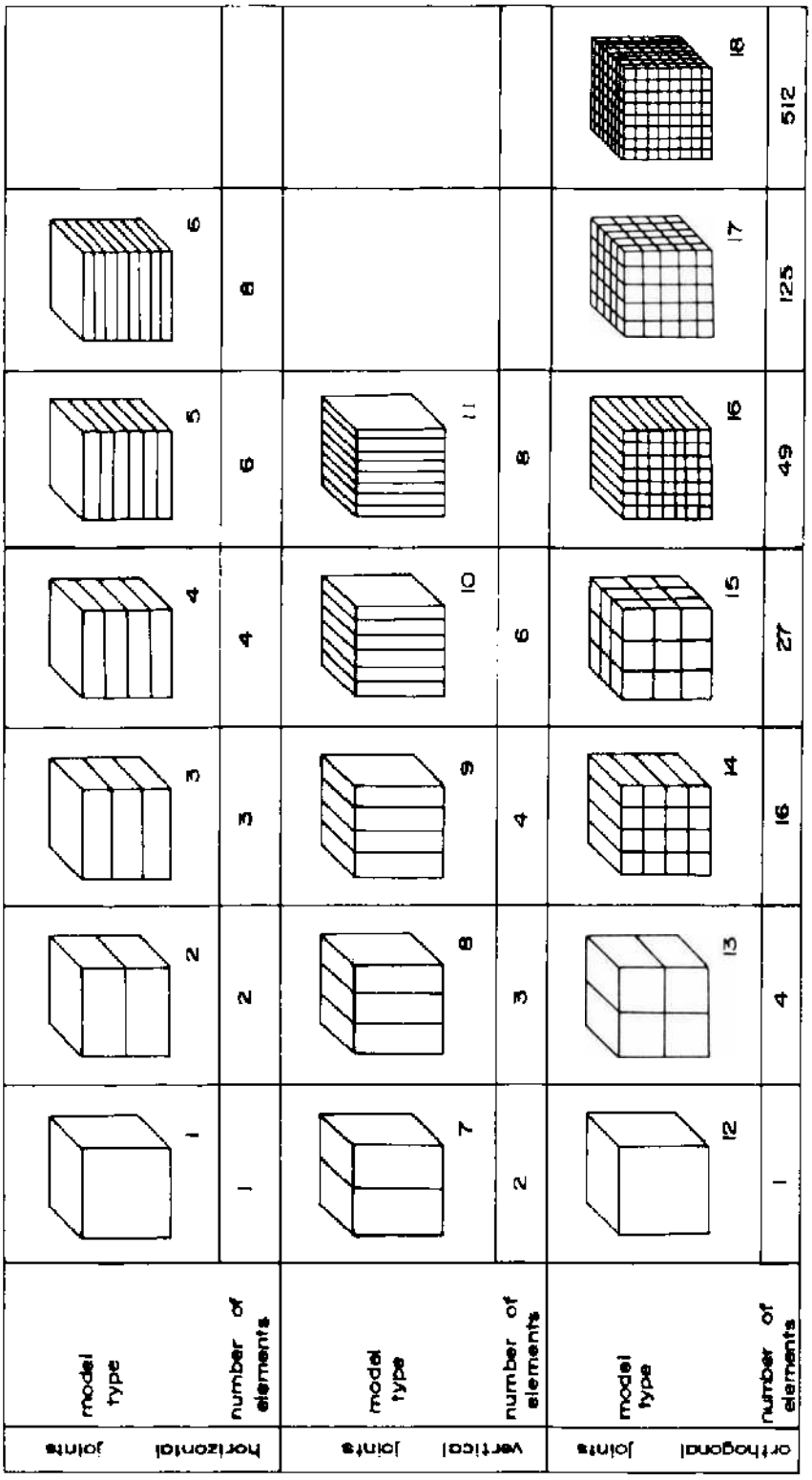

Fig. 10-96. Different types of composite – models used in tests (after LAMA, 1974a).

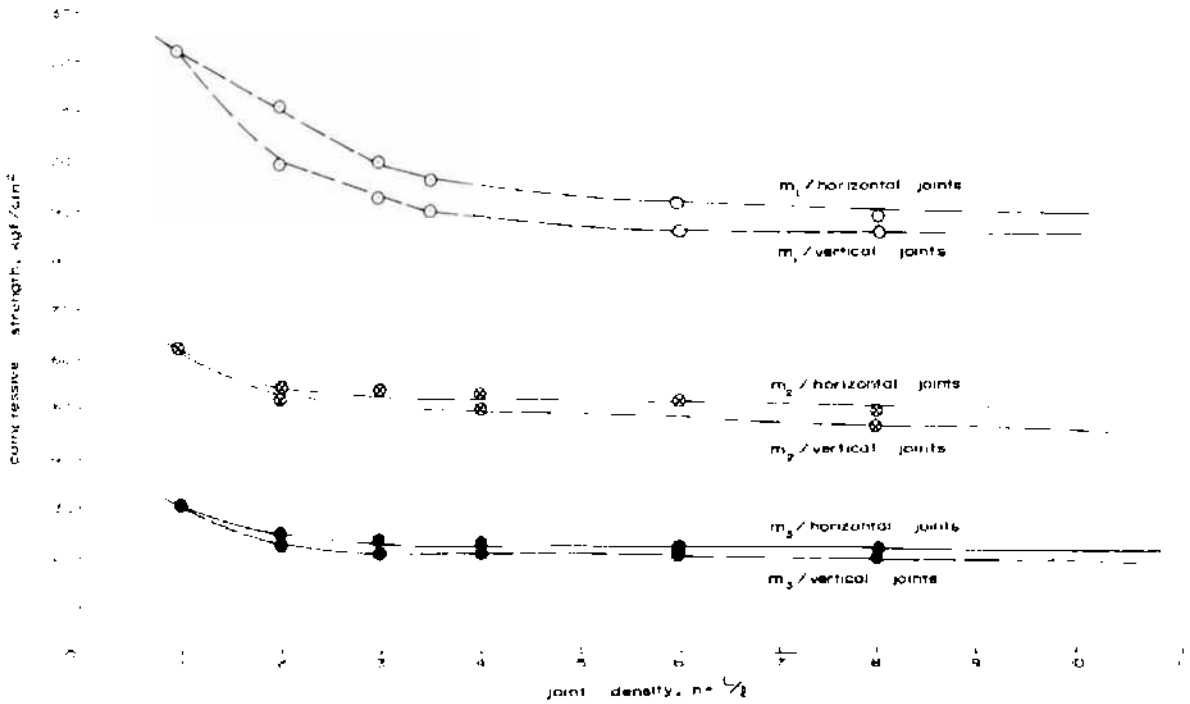

Fig. 10-97. Influence of horizontal and vertical joints on compressive strength of a model (after LAMA, 1974a).

role, while in the case of vertical joints it is the decrease of lateral constraint that slightly decreases the modulus value. As the columns become slender, the outer columns bend outwards at the mid-height shedding off some of their load resulting in slightly over loading of the central columns and hence decreasing the strength of the model. This seems to be the reason why the strength of the specimens with vertical joints is slightly lower than with horizontal joints.

When models with horizontal joints were cyclically loaded, the deformation modulus in the second cycle was almost equal to that of the specimen with vertical joints. This is because of the closure of the joints and evening-out of the asperities.

The cubes of different size were assembled to model orthogonal joints and the results obtained are represented in Figs. 10-99 and 10-100. It is seen that the strength as well as the deformation modulus drop as the number of elements (n) (joint density $n = \frac{L}{l}$) increases. Both the modulus and the strength achieve more or less a constant value when the number of elements contained in the model reaches about 150. The relationship between strength and joint density and modulus of deformation and joint density for cubic elements (orthogonal joints placed at equal intervals in all the three directions) can be represented by

$$\sigma_c \text{ or } E_d = K + \left(\frac{L}{l}\right)^{\beta} \tag{10.64}$$

where σ_c = compressive strength
E_d = deformation modulus
K = strength (or deformation) of the model containing more than 150 joints (real strength or deformation of the system)
β = constant
L = length of the model and
l = length of the element.

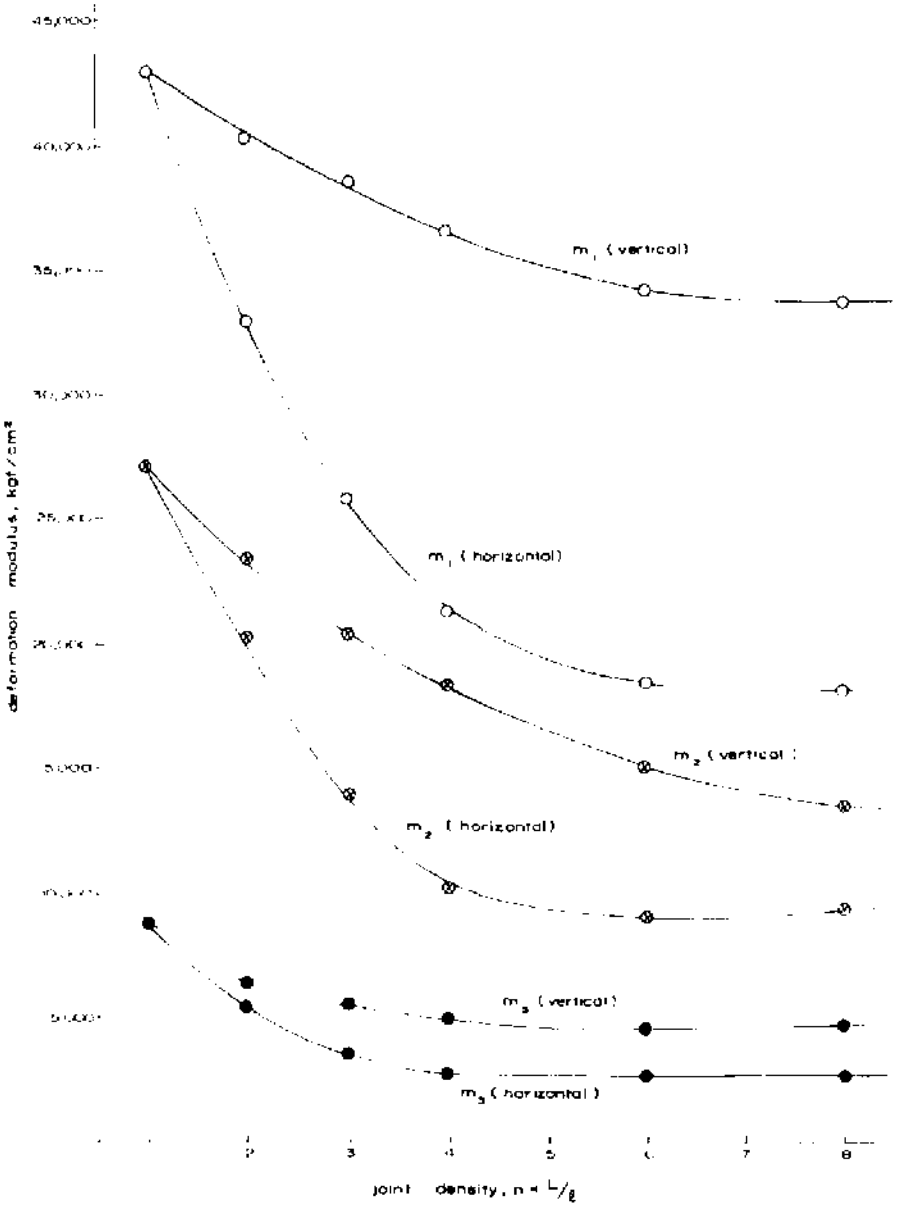

Fig. 10-98. Influence of horizontal and vertical joints on deformation modulus of a model (after LAMA, 1974a).

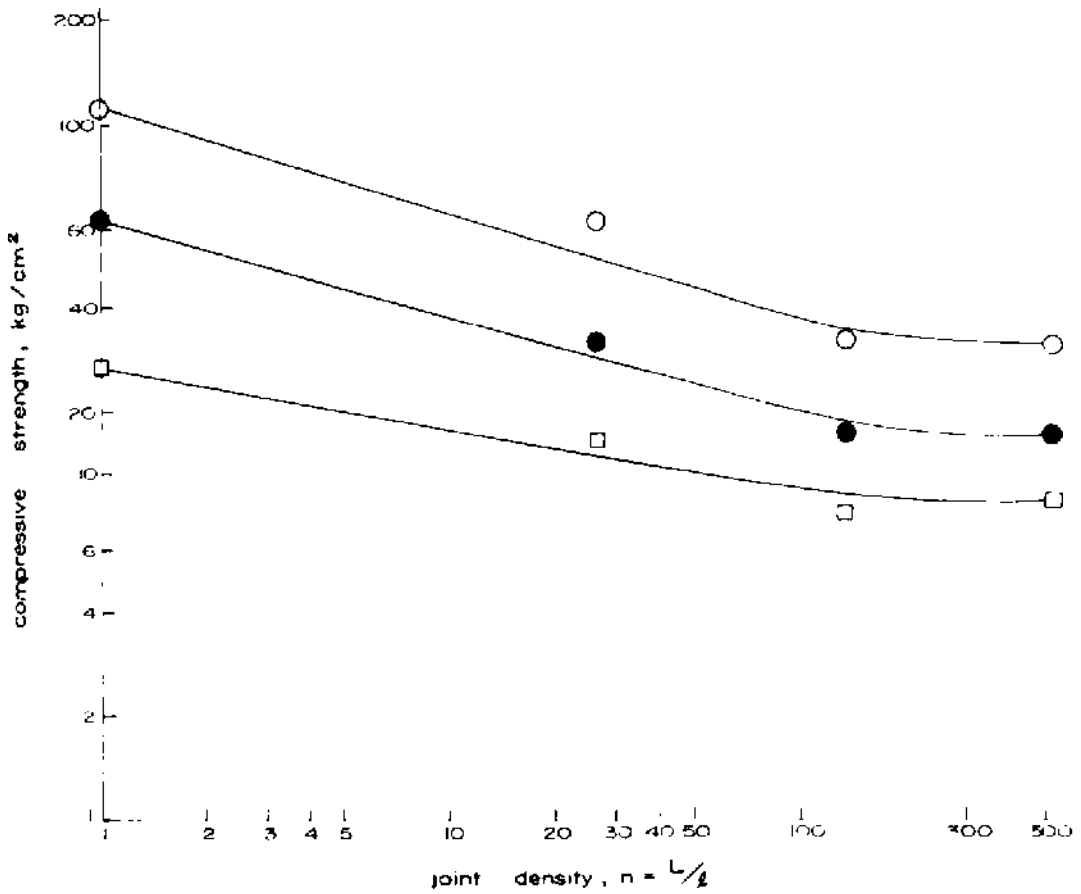

Fig. 10-99. Influence of joint density on compressive strength of a model (cubic elements) (after LAMA, 1974a).

For the case of compressive strength, the value of β is higher for stronger rocks and comparatively lower for weaker rocks. For the different materials investigated, β varied from 0.30 for the material m_1; 0.27 for material m_2; to 0.18 for the material m_3.

For the case of deformation modulus, the values of β varied between 0.57 for the material m_1; 1.0 for material m_2 and 0.72 for the material m_3. Very similar results have been obtained by GONANO (1974) using orthogonal blocks though in his tests the model had 36 blocks of rectangular shape (Model type 14; Fig. 10-96). The influence of the decrease in strength is due to two main factors:

(1) The assembling of a model using small blocks results in certain misfittings giving stress gradients. The strength improves if the matching is improved (GONANO, 1974; DEMIRIS, 1974; LAMA and GONANO, 1976) (Fig. 10-101).

(2) The law of probability of failure of any single unit in a composite block and here the weakest link theory or the WEIBULL (1939) distribution function

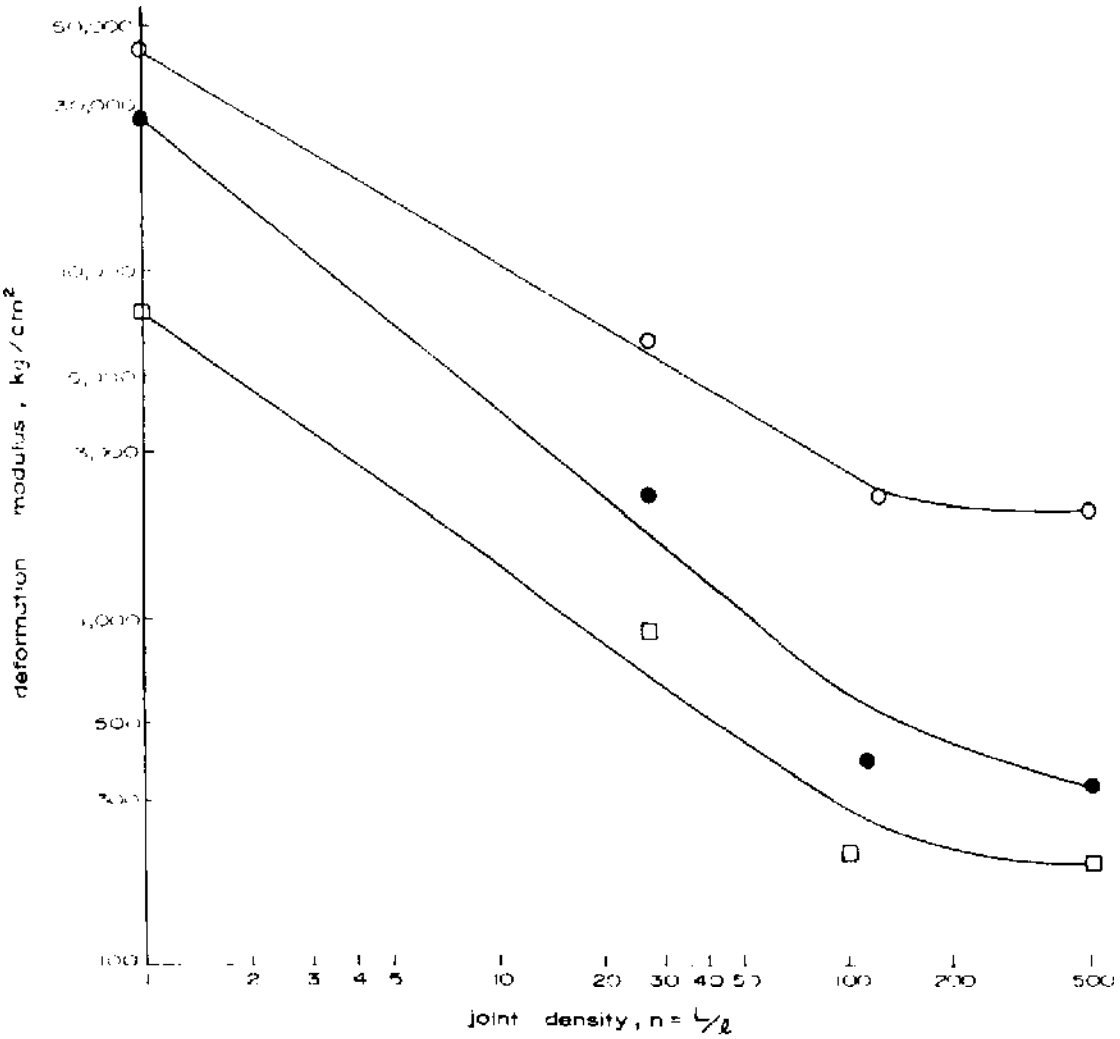

Fig. 10-100. Influence of joint density on deformation modulus of a model (cubic elements) (after LAMA, 1974a).

has been applied by many investigators to predict the volume effect in compression (EVANS and POMEROY, 1958; LUNDBORG, 1972). There seems to be however certain limitations in the application of this theory to a block jointed models which have a constant (more or less) type of flaw. The WEIBULL's theory fails if this is applied to a set of observations made on models with different element-shapes plotted together (Figs. 10-102 and 10-103). The curves are very confusing as if they consist of two separate parts. It is because the shape of the elements plays an important role. It is well known that the strength of rectangular elements is about 10 to 15% higher than cubic elements. Taking this aspect into account, the compressive strength-n curve is drawn by the dotted lines (Fig. 10-102). The influence of shapes is more marked for higher strength material than for lower strength material. It looks, therefore, that some different mechanism of failure starts to play which is a function of the element shape.

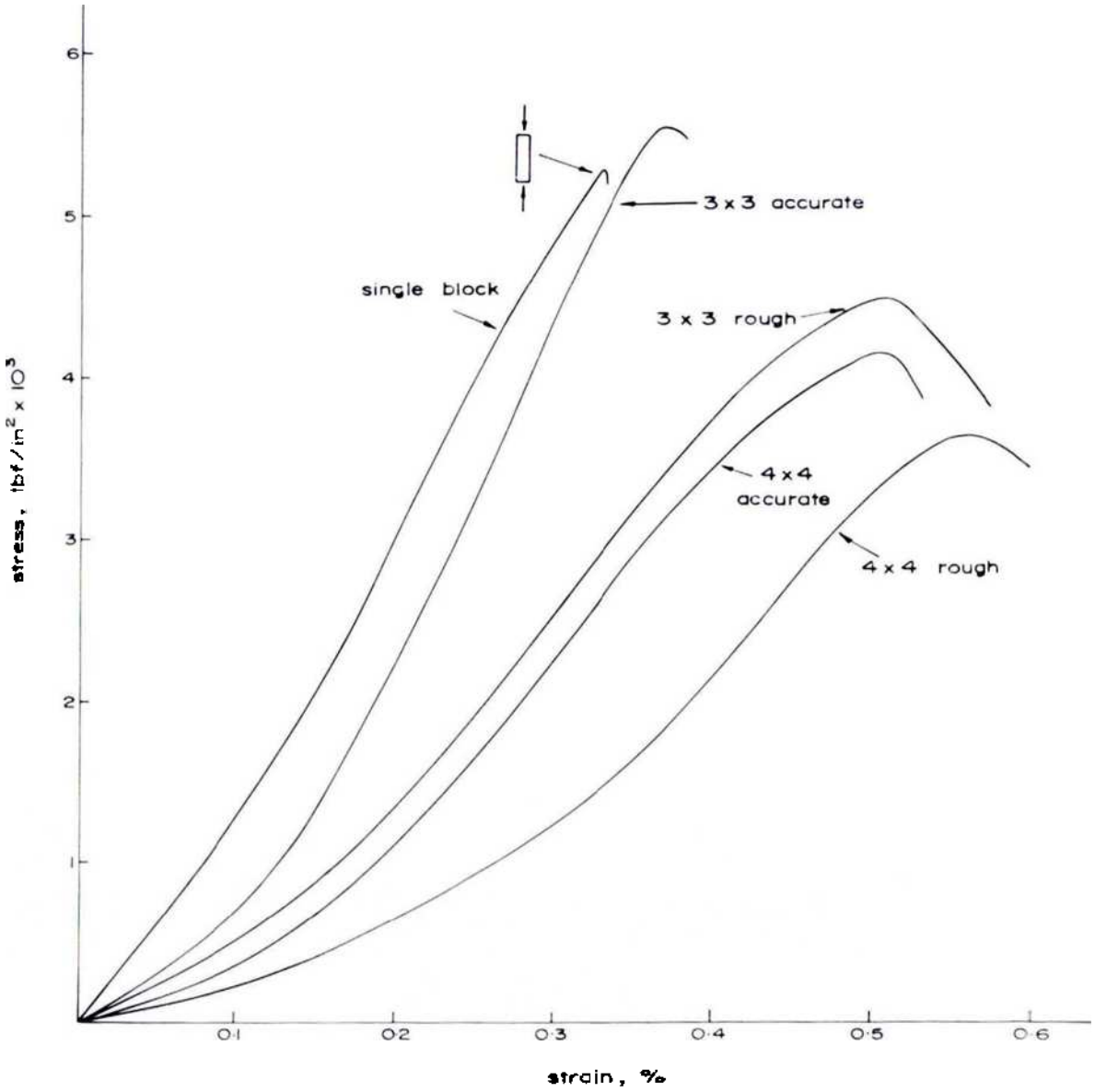

Fig. 10-101. Stress-strain curves for block-jointed accurately matched and roughly matched models.
(after LAMA and GONANO, 1976)

The mode of failure in composite models is not sudden as is usually observed in specimens with a single element. In the model consisting of a number of elements the mode of failure is a "progressive failure". The failure starts with one or two elements and proceeds with more and more number of elements failing with increase in deformation (Figs. 10-104 and 10-105). Even at very large deformation, exceeding 30 %, there are always some blocks to be found which are still intact (Fig. 10-106). This figure is more clearly visible in the post-failure curve obtained on models of elements of size 1 cm × 1.6 cm × 1.6 cm in a limited number of tests (Fig. 10-107). The post-failure curves are flatter for models containing a large number of elements.

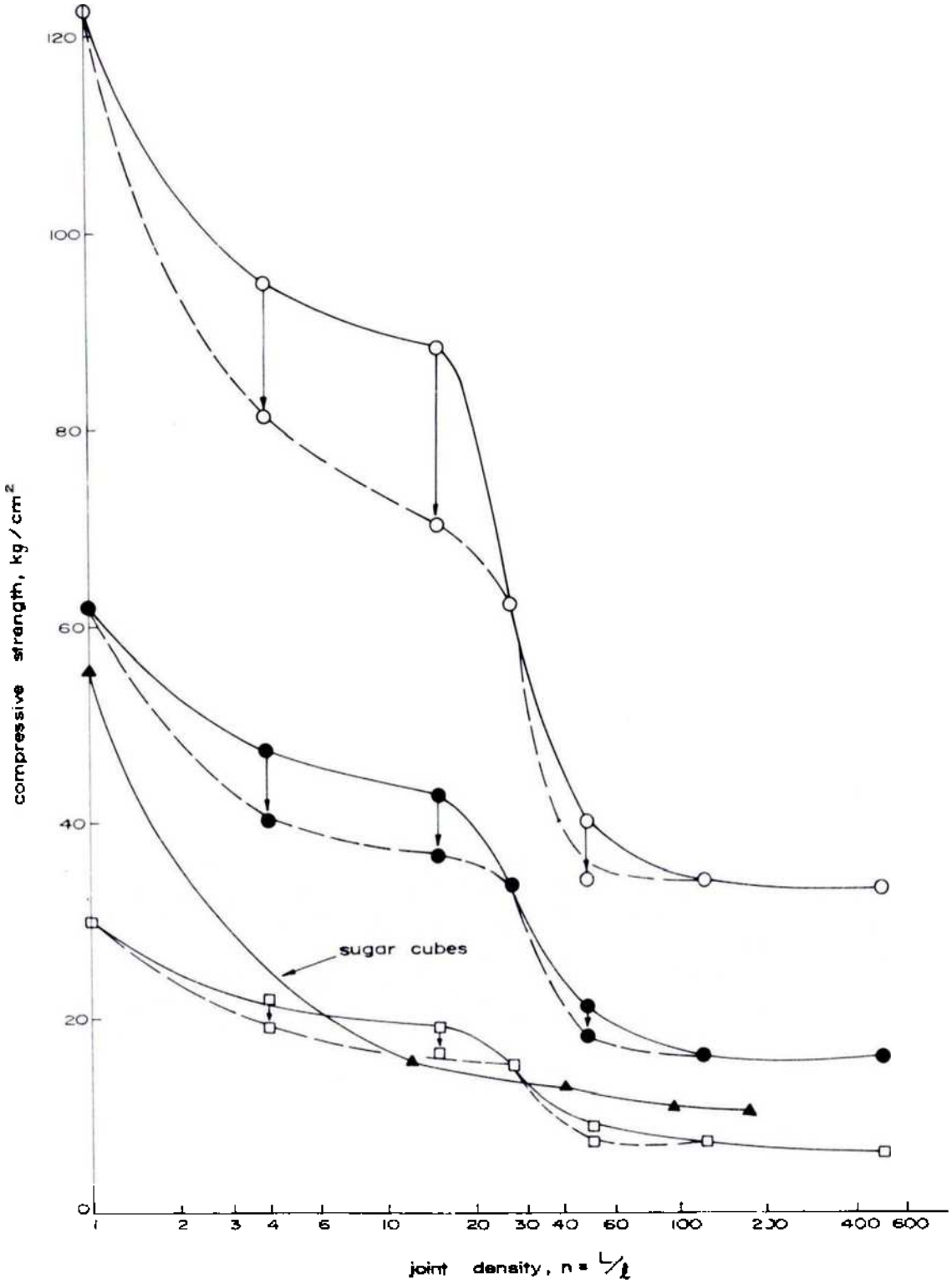

Fig. 10-102. Decrease of strength as a function of joint density in a composite model consisting of elements of different shapes (after LAMA, 1974a).

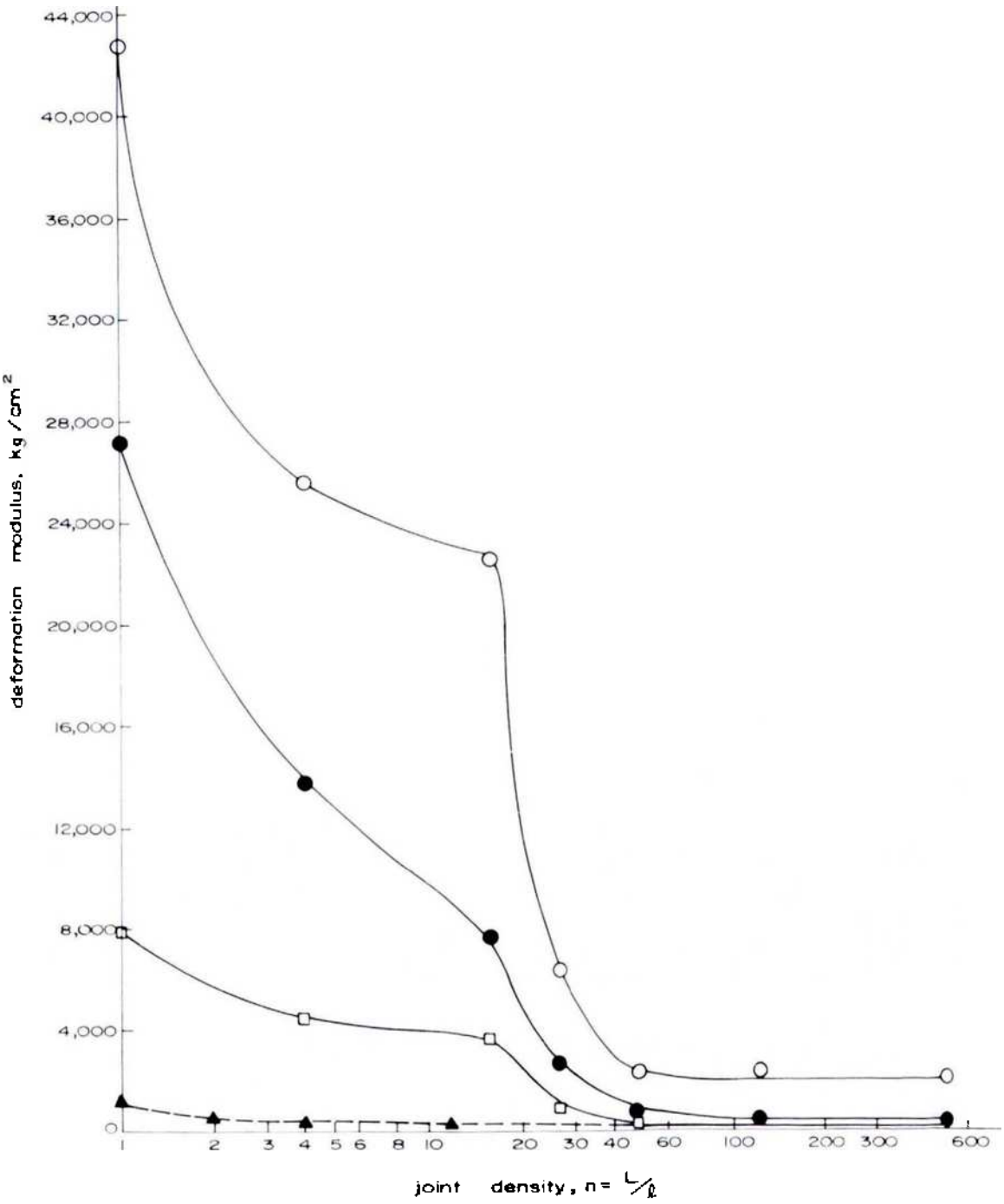

Fig. 10-103. Decrease in deformation modulus as a function of joint density in a composite model consisting of elements of different shapes (after LAMA, 1974a).

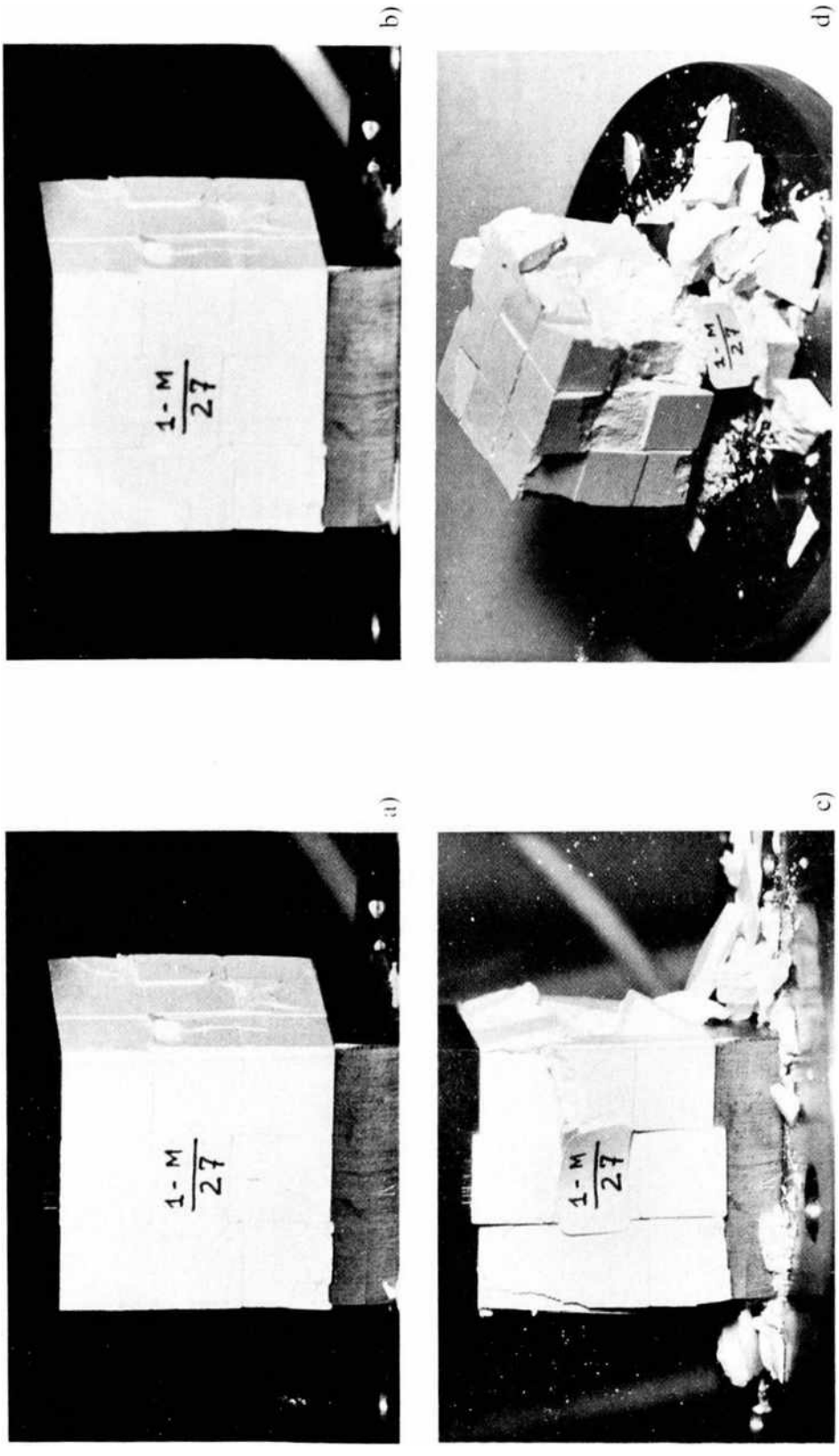

Fig. 10-104. (a- d) Gradual failure of a jointed model ($n = 27$) at different stages after the peak strength (post peak range) (after LAMA, 1974a).

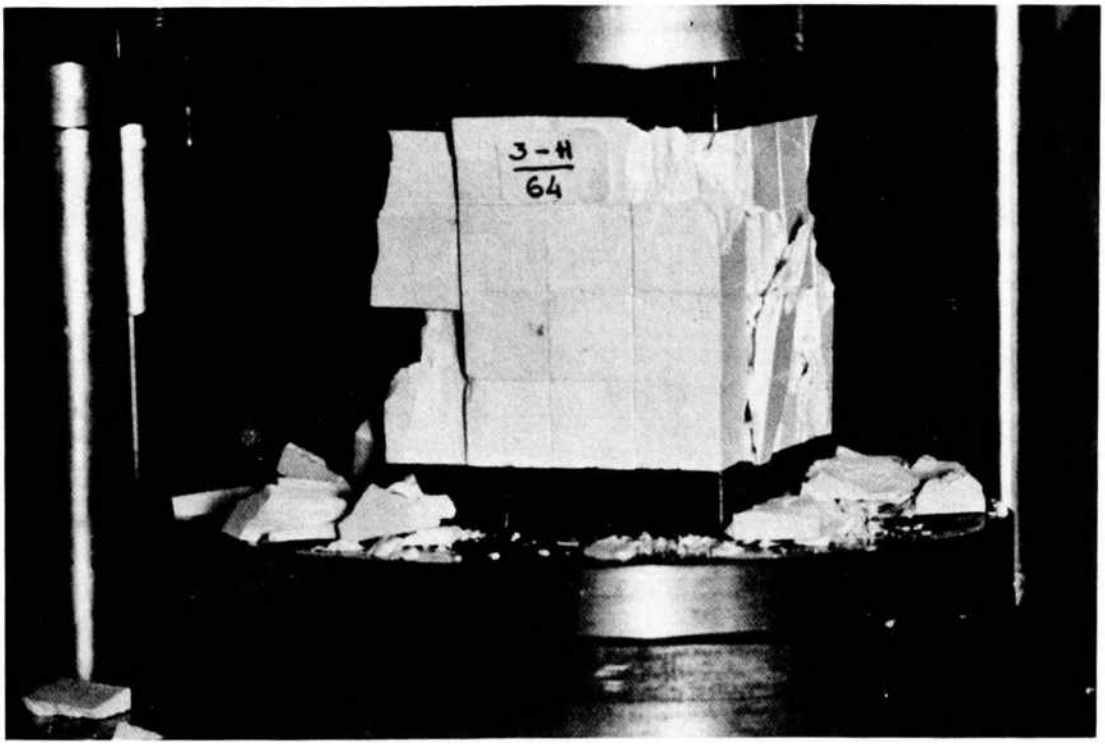

Fig. 10-105. Failure of a jointed model ($n = 64$) at residual strength (strain $> 8\,\%$) (after LAMA, 1974a).

Fig. 10-106. Jointed model ($n = 125$) at 30 % of strain showing presence of some blocks still intact (unfractured) (after LAMA, 1974a).

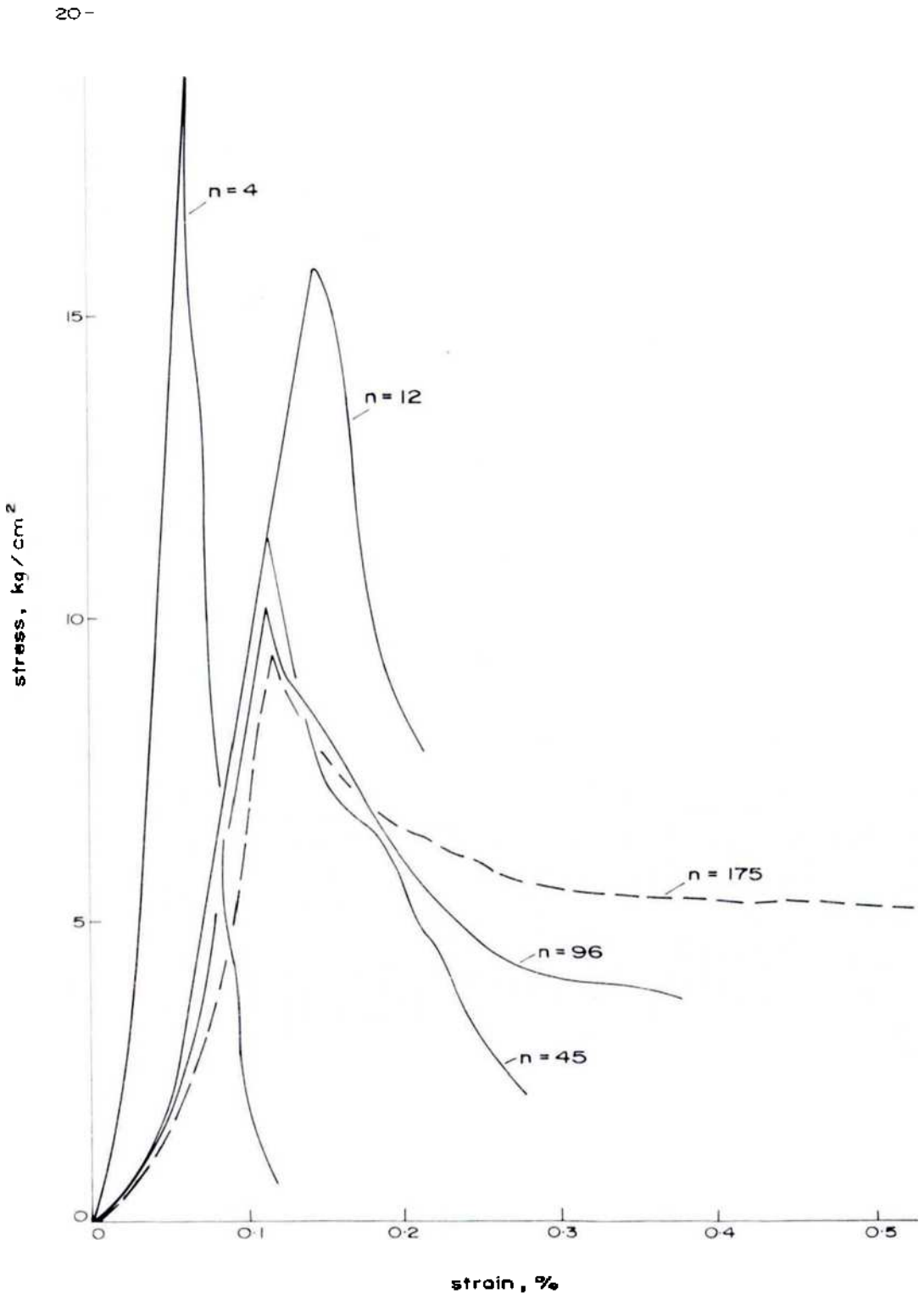

Fig. 10-107. Stress-strain behaviour of composite models with different joint density, n (after LAMA, 1974a).

The strength and deformation modulus are very much dependent upon the angle of orientation of joints. Tests were conducted by LAMA (1975a) on models with inclination of joint angle with respect to the model axis $\phi = 15$, 30 , 45 and 60 using two sets of joints and for joint continuity $\chi = 2/3$ and 1/3. These values were compared with $\chi = 0$. Both the strength and deformation modulus values are given in Figs. 10-108 and 10-109. The fracture stress at failure drops to almost 10% at 30 which is almost equal to the friction angle of the rock. The value of the deformation modulus is also lowest for this value of the ϕ angle. The values increase as the angle is increased but fall again at 60 , because of the 2nd joint set now playing a dominant role.

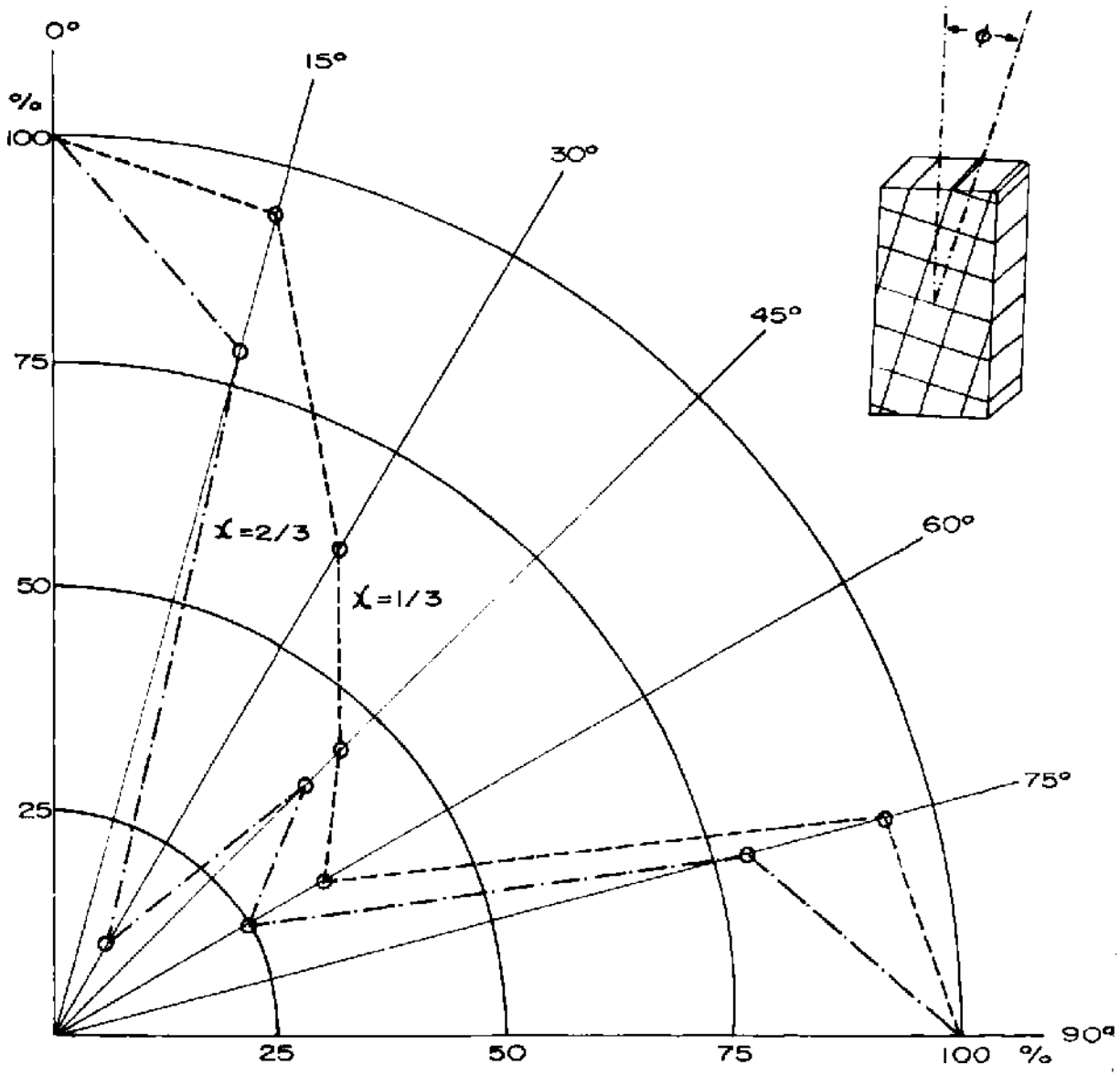

Fig. 10-108. Influence of orientation of joint angle (Φ) on the composite model compressive strength (mean) (Model material gypsum: element size 12 mm × 12 mm × 36 mm) (after LAMA, 1975a).

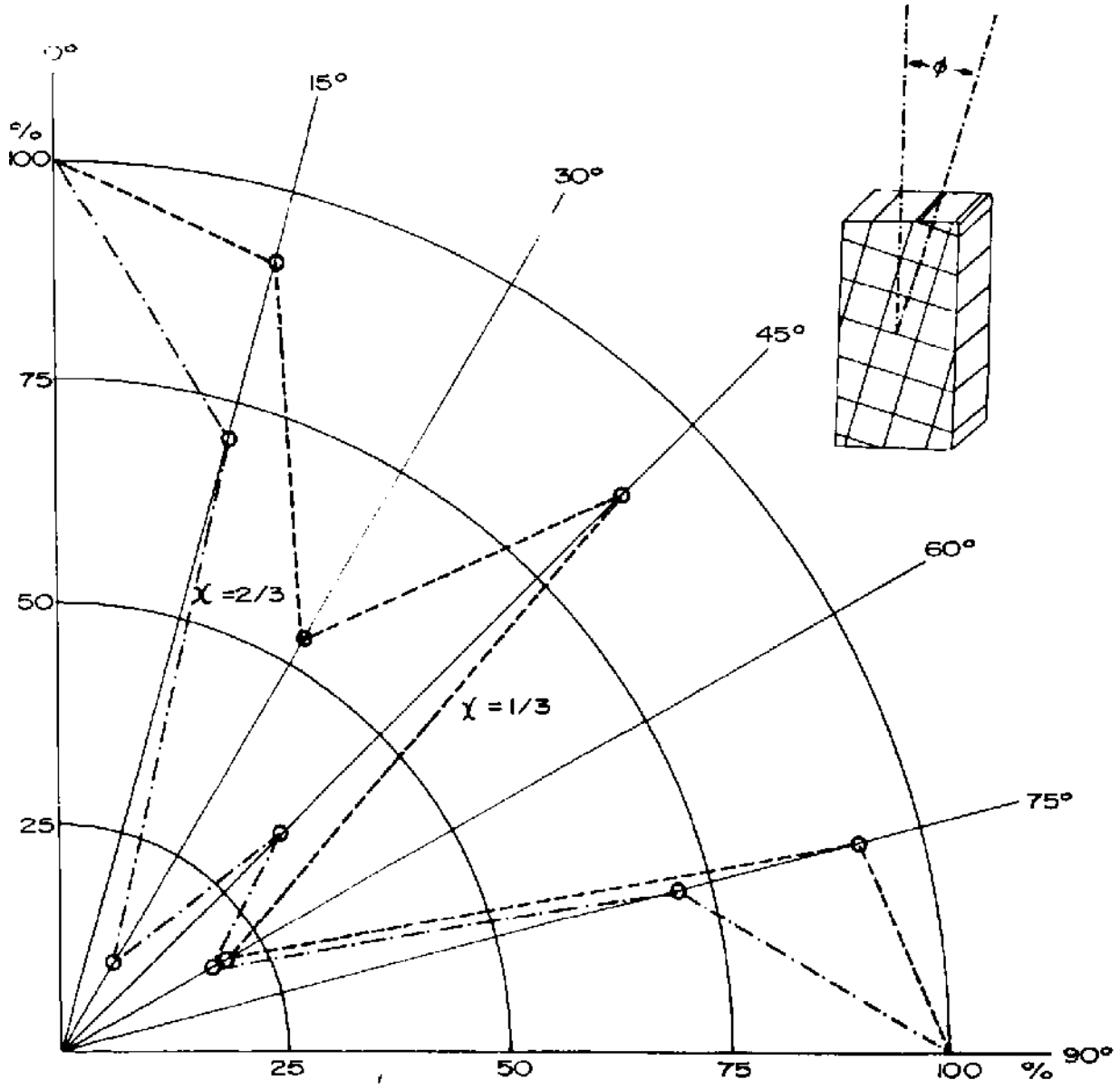

Fig. 10-109. Influence of orientation of joint angle (Φ) on the composite model tangent modulus at 50% compressive strength (mean) (Model material – gypsum; element size 12 mm × 12 mm × 36 mm)
(after LAMA, 1975a).

An increase in the value of χ greatly decreases both the strength as well as deformation modulus. Both these agree to some extent to the general shape of the curve obtained applying the simple COULOMB-MOHR concept of failure.

Figs. 10-110 to 10-113 give the post-failure curves obtained for the different angles of orientation and joint continuities. As long as the orientation of the angles ϕ were not critical, the curves for $\chi = 0$, 1/3 or 2/3 lie close to each other (Fig. 10-110) but separate out very rapidly for ϕ angle reaching 30° (Fig. 10-111);

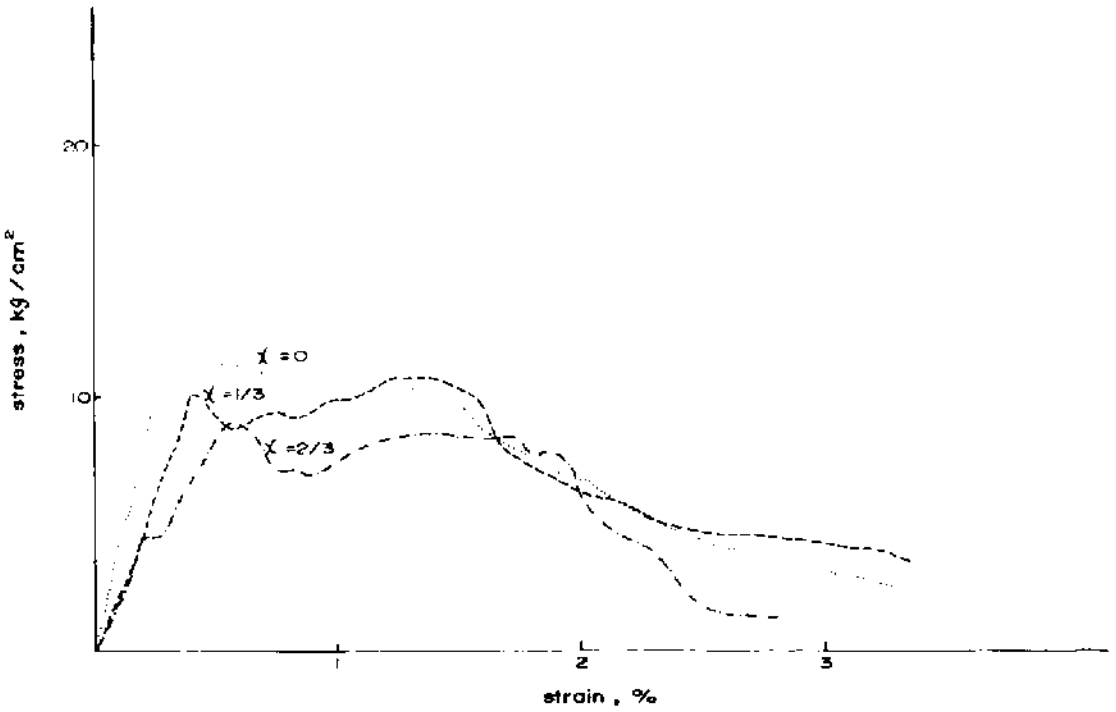

Fig. 10-110. Stress-strain curves for joint inclination angle $\Phi = 15^\circ$, with different values of χ (after LAMA, 1975a).

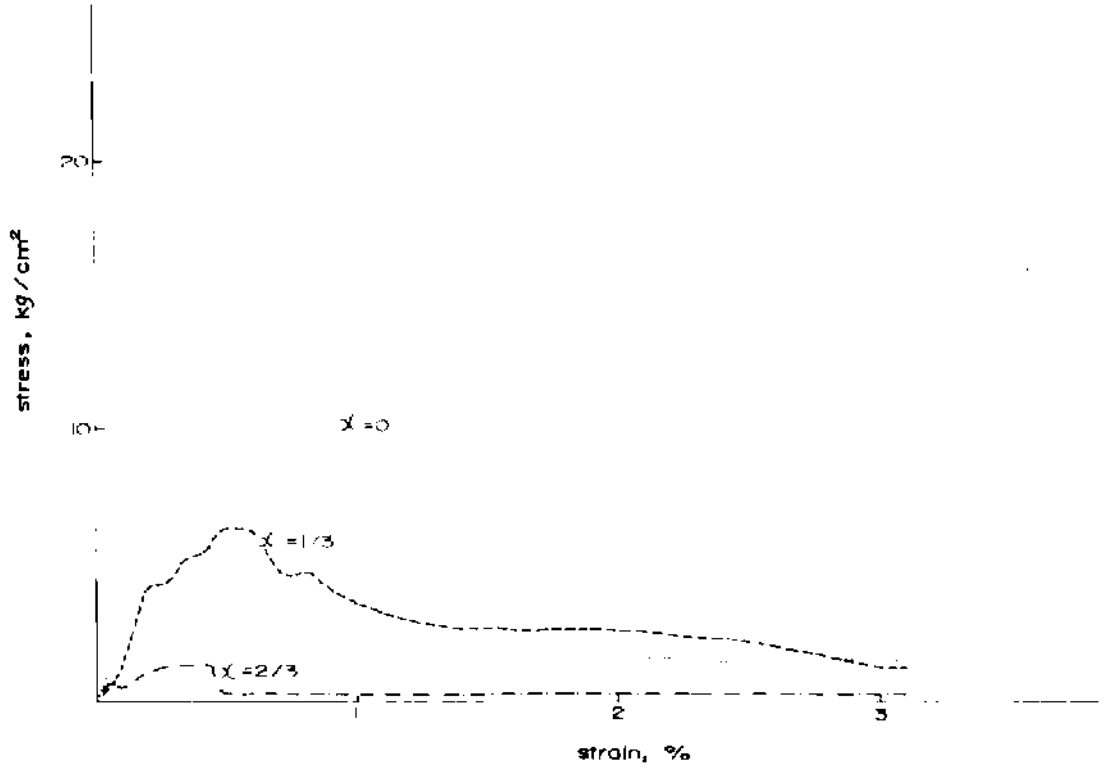

Fig. 10-111. Stress-strain curves for joint inclination angle $\Phi = 30^\circ$, with different values of χ (after LAMA, 1975a).

Fig. 10-112. Stress-strain curves for joint inclination angle $\Phi = 45$, with different values of χ (after LAMA, 1975a).

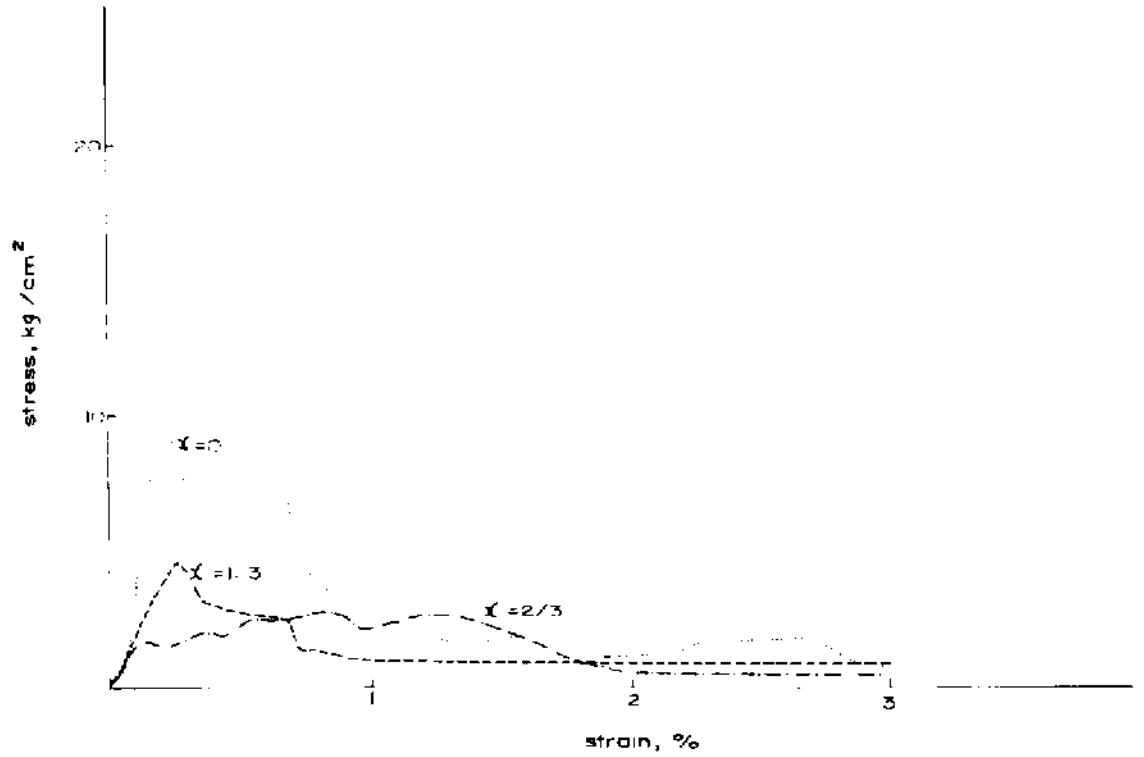

Fig. 10-113. Stress-strain curves for joint inclination angle $\Phi = 60$, with different values of χ (after LAMA, 1975a).

trying to close up again for $\phi = 45^\circ$ (Fig. 10-112) and down again for 60° (Fig. 10-113). The strain at which the load drops to ultimate value is lower for higher value of χ and is dependent upon ϕ. The results are given in Table 14.

TABLE 14

Influence of joint continuity and joint inclination on strain values at ultimate strength

(after LAMA, 1975a)

Joint continuity	Joint inclination			
	Strain at ultimate strength, %			
	15	30	45	60
$\chi = 0$	3.5	2.1	2.8	1.4
$\chi = 1/3$	3.5	1.0	0.8	0.65
$\chi = 2/3$	2.6	0.55	0.25	0.65

Fig. 10-114. Fracture of a jointed model with joint inclinations $\kappa_1 = 15^\circ$, $\kappa_2 = 75^\circ$, $\chi = 1/3$, showing failure along κ_1 joint (after LAMA, 1975a).

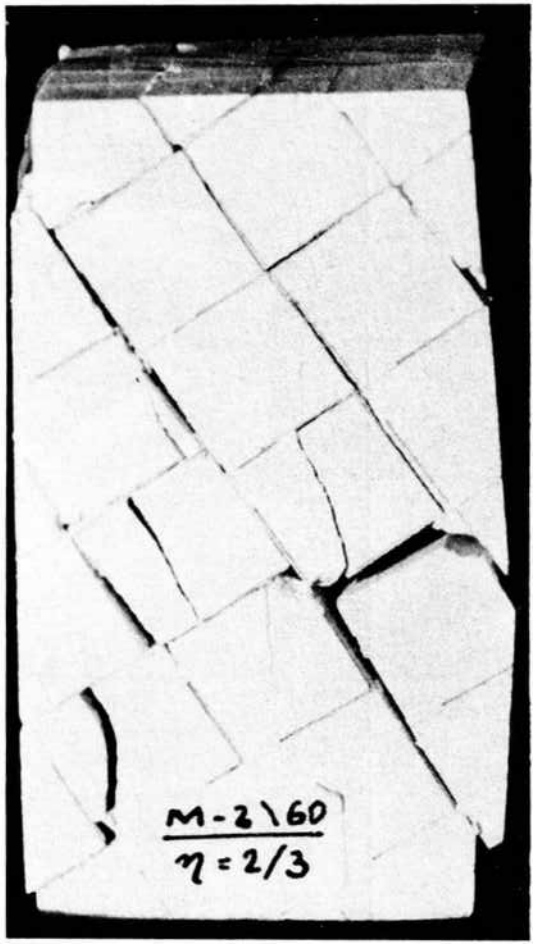

Fig. 10-115. Fracture of a jointed model with joint inclinations $\kappa_1 = 60$, $\kappa_2 = 30$, $\chi = 2/3$, with failure along κ_2 joint and with development of secondary fracures originating from joint interfaces (after LAMA, 1975a).

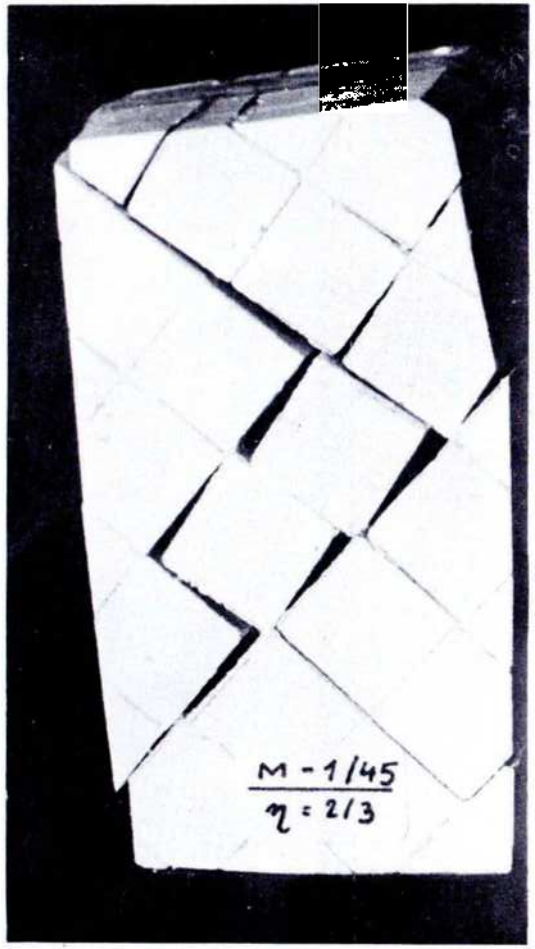

Fig. 10-116. Fracture of a jointed model with joint inclinations $\kappa_1 = 45°$, $\kappa_2 = 45°$, $\chi = 2/3$, with failure by shear along both the joints with dilation due to rotation of blocks (after LAMA, 1975a).

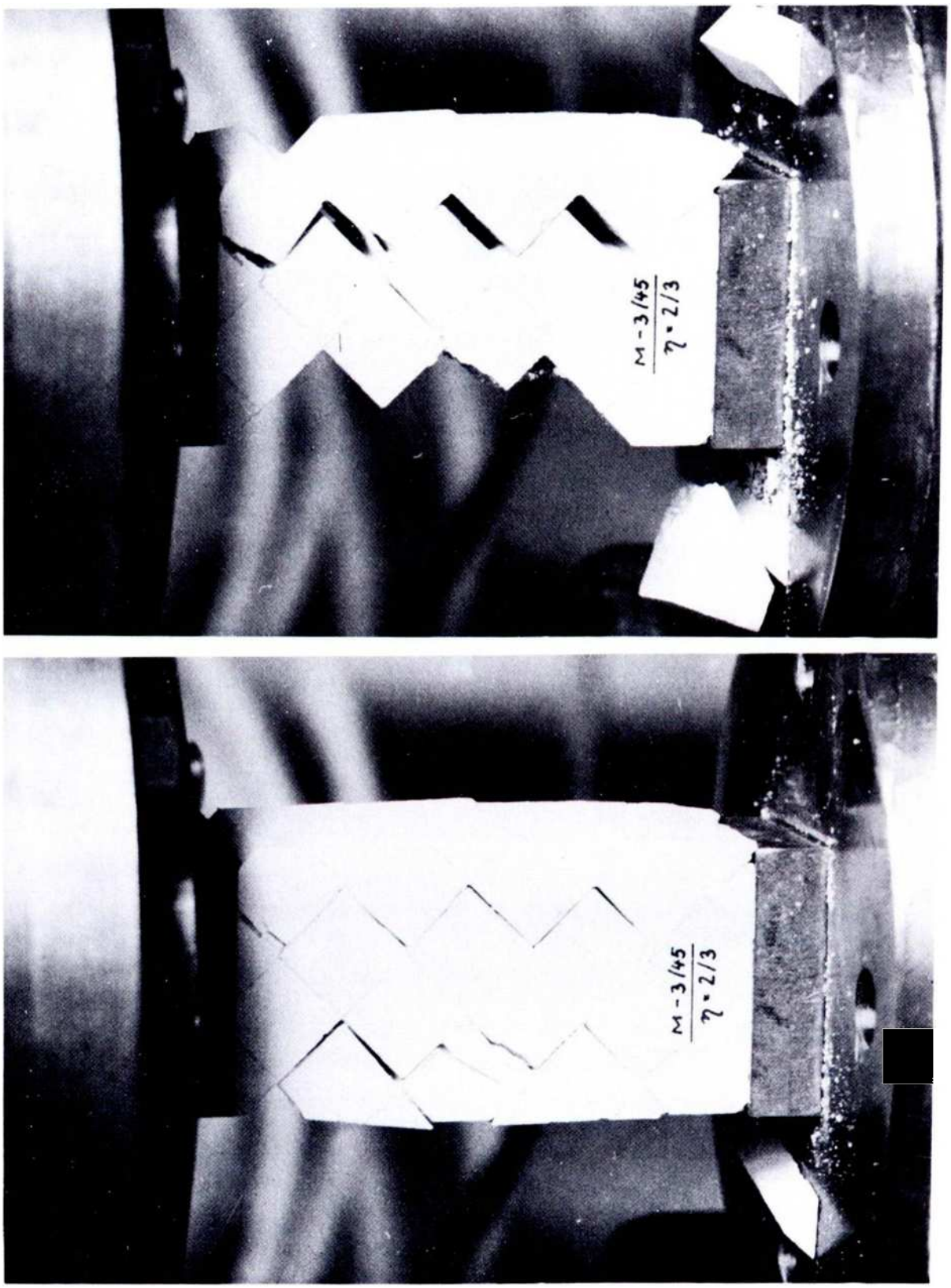

Fig. 10-117. Failure of a jointed model showing stages of dilation of the model and gradual collapse (after LAMA, 1975a).

The mode of failure of oriented orthogonal jointed models is dependent upon joint orientation (Figs. 10-114 and 10-115). Failure occurs with the extension of joint in its plane for lower values of ϕ and for values increasing to 45 and more, the failure occurs with development of crack at the end of the joint but following through the material. In any case the joints play an important role. The dilation occurs along the joints at stages and the rocks fall apart along these surfaces as shown in Figs. 10-116 and 10-117.

10.6. Fracture of Jointed Rock in Tension

YOUASH (1966) conducted direct tension tests on a shale, a gneiss and two sandstones. Cores 5.4 cm by 10 cm (2 1/8 in by 4 1/4 in) were prepared with the layers dipping at 0 , 15 , 30 , 45 , 60 , 75 and 90 to the short cylinder axis. Rupture strength increases as the dip increases from 0 to 60 , for which failure occurs along layering. For 75 and 90 cores, failure occurs across layering and with a sharp increase in rupture strength. Rupture strength in tension versus inclination of layering for one sandstone is given in Fig. 10-118.

DAYRE (1970) studied the influence of the lineation and the cleavage on the maximum bending moment during failure of slaty shales. His results are given in Fig. 10-119.

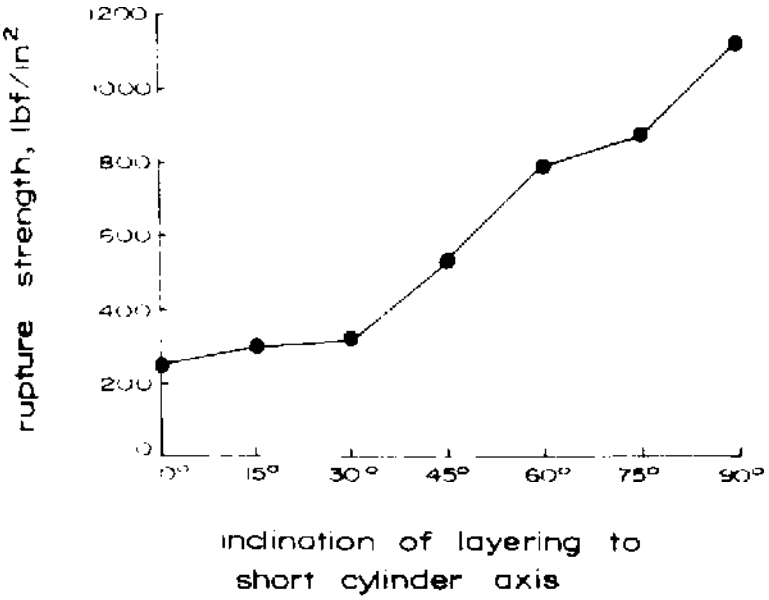

Fig. 10-118. Rupture strength in tension versus inclination of layering for sandstone of Lyons Formation (after YOUASH, 1966).

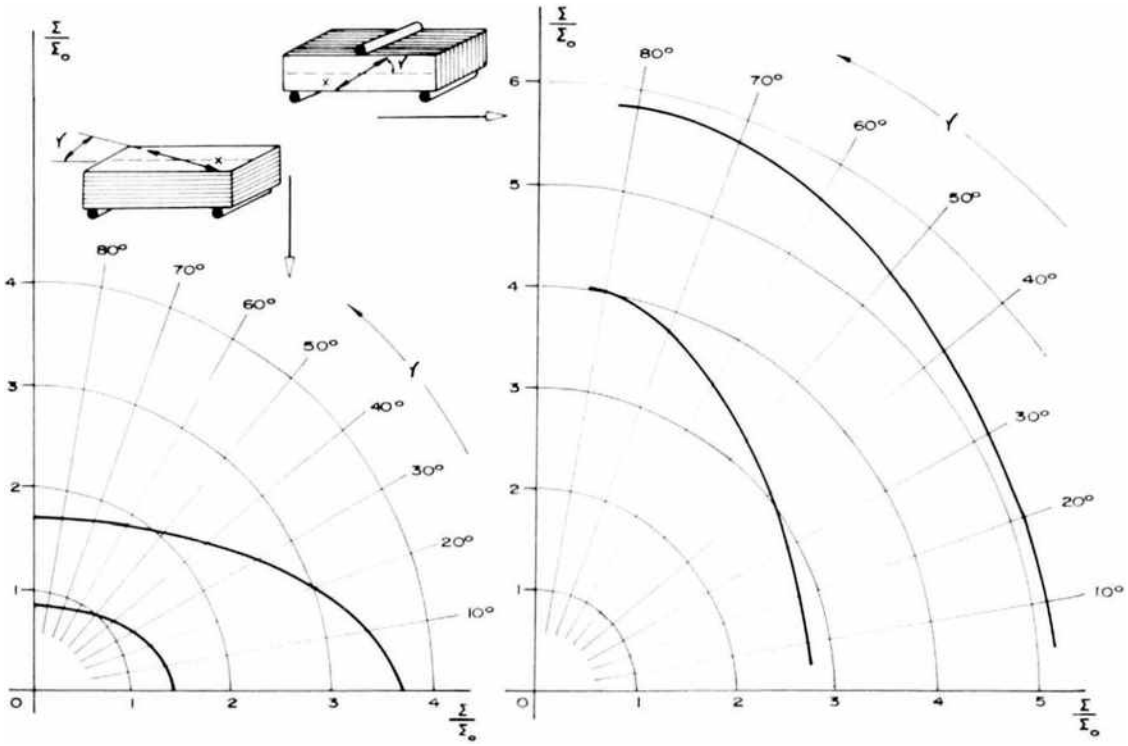

Fig. 10-119. Bending: Anisotropy of the maximum bending moment during failure. $\Sigma = \frac{M}{I}$ where M is the maximum bending moment at failure; I is the moment of inertia of the bar. Σ_0 = the value of $\frac{M}{I}$ obtained in the case of loading along oz with $\gamma = 90$ (after DAYRE, 1970).

TABLE 15

Comparison of total defects in six angular intervals with tensile strength in Barre granite

(after WILLARD and MCWILLIAMS, 1969)

Angular interval	Defects	Tensile strength MPa	(lbf/in^2)	Line-load angle
0 ±15	213	15.5	(2244)	0
30 ±15	160	14.8	(2145)	30
60 ±15	105	9.5	(1385)	60
90 ±15	76	10.7	(1553)	90
120 ±15	77	11.7	(1695)	120
150 ±15	172	13.7	(1981)	150

WILLARD and MCWILLIAMS (1969) developed microstructural techniques to investigate relations between rock fabric and mechanical properties. In Table 15 defect frequency orientation totals are compared with the tensile strength of Barre granite from Brazilian tests. The tensile strength was calculated from each of these line-load angles. The frequency of defects tends to be inversely proportional to strength, suggesting that the direction of weakest tensile strength is approximately normal to the direction of most defects.

BERENBAUM and BRODIE (1959) prepared and tested coal specimens for tensile strength by Brazilian test at various orientations of the planes of weakness. The four types of discs used are illustrated in Fig. 10-120 and are referred to as discs of type (a), (b), (c) and (d) respectively. Their results are given in Fig. 10-121. On each set of discs, measurements were made at five different angles to the planes perpendicular to the faces of the set; these angles were 0°, 25°, 45°, 65°, and 90°. The discs used had a mean thickness of 0.79 cm (0.31 in). The mean diameter was 2.54 cm (1.00 in). Broadly speaking, the strength is greatest at 0° to the bedding planes and lowest at 90° but whereas in Barnsley Hard coal the tensile strength decreases monotonically as the angle with the bedding plane increases, in Cwmtillery coal the lowest value is

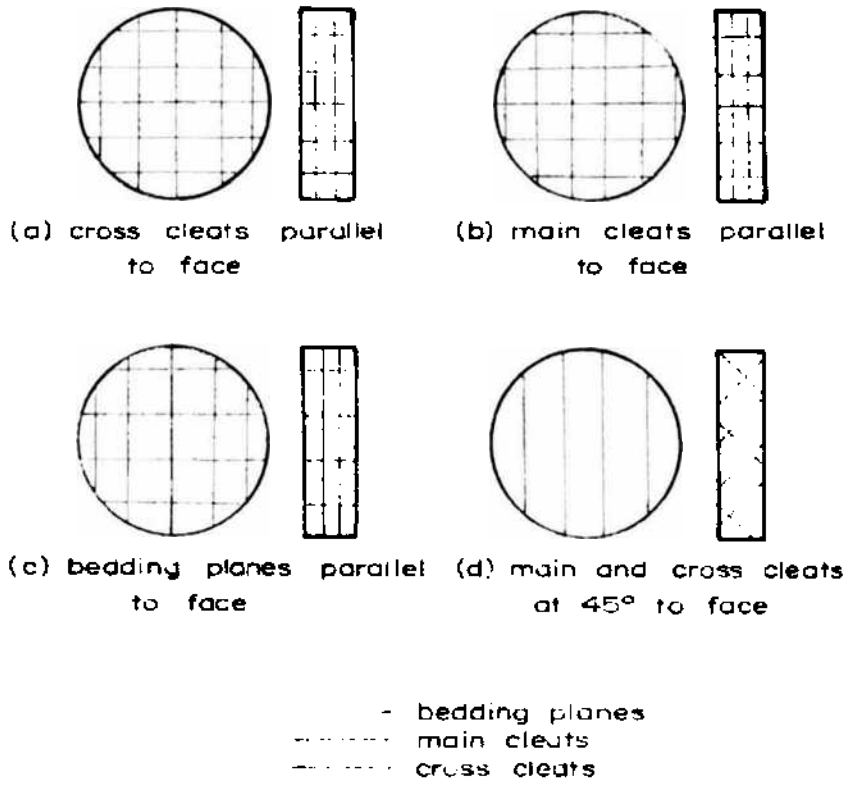

Fig. 10-120. Disc specimens for test on coal (after BERENBAUM and BRODIE, 1959).

found at angles with the bedding plane varying about 55 to 75° (depending on the cleat orientation) and there is evidence that the greatest strength may be found at angles up to 25° with the bedding plane (again depending on cleat orientation).

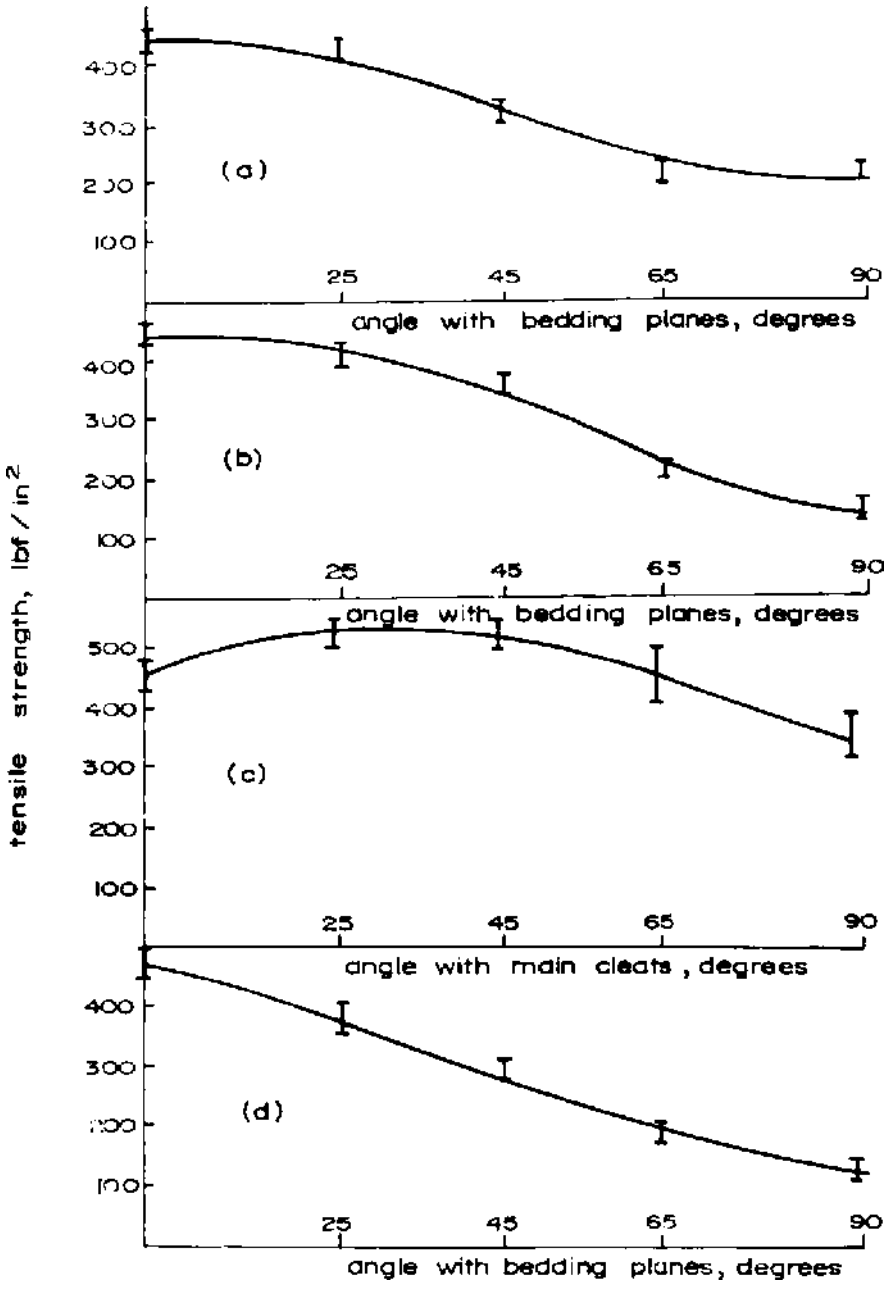

Fig. 10-121a. Tensile strength results for Barnsley Hard coal (after BERENBAUM and BRODIE, 1959).

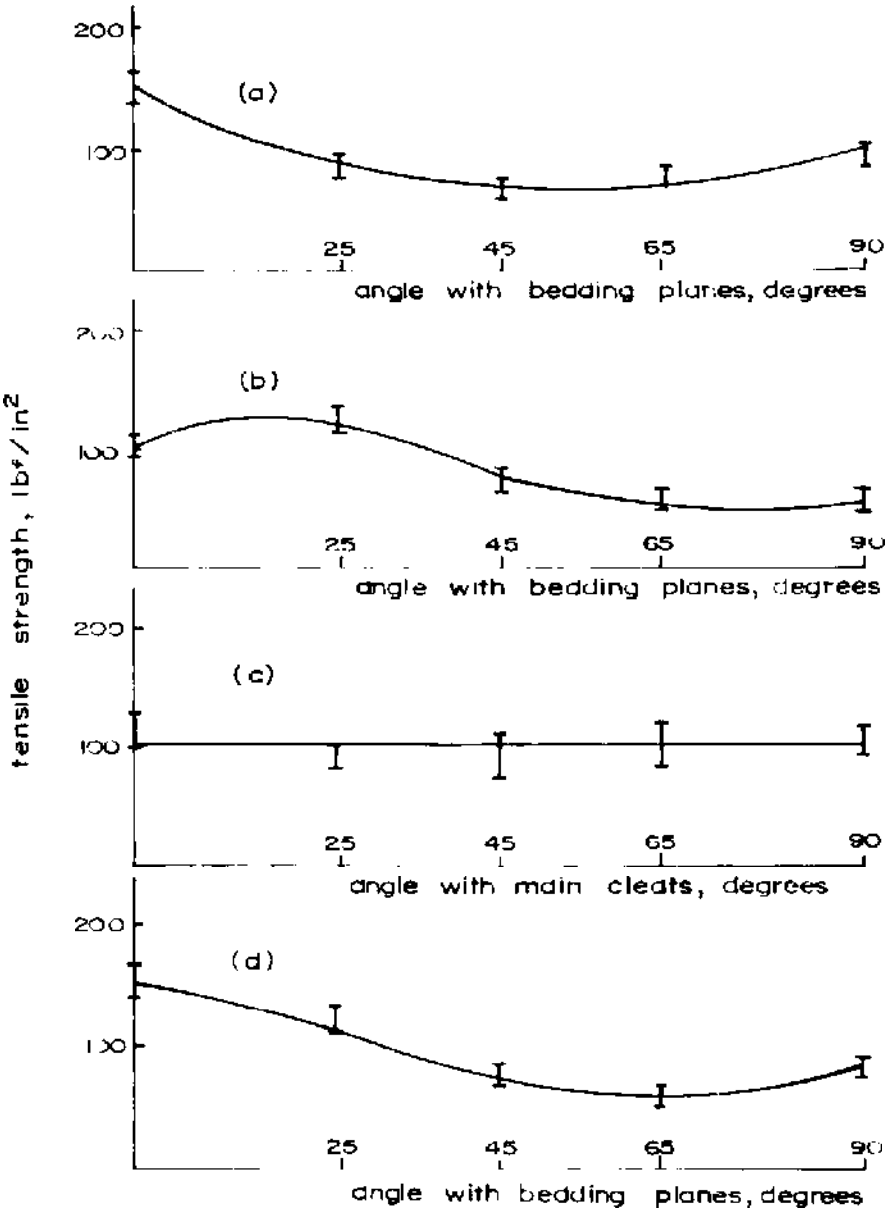

Fig. 10-121b. Tensile strength results for Cwmtillery coal (after BERENBAUM and BRODIE, 1959).

DUBE and SINGH (1969) compressed specimens to failure (Brazilian test) along lines which were inclined at different angles to the bedding planes. The results indicate that the strength of the specimens is greatest when the applied load acts 80 to the bedding planes and it decreases as the angle of inclination increases (Fig. 10-122). It is lowest when the direction of the bedding plane is parallel to the direction of the applied load. The ratio between the lowest and the highest strength was 0.66 and 0.76 for the 30 mm (1.2 in) and 54 mm (2.1 in) diameter discs respectively.

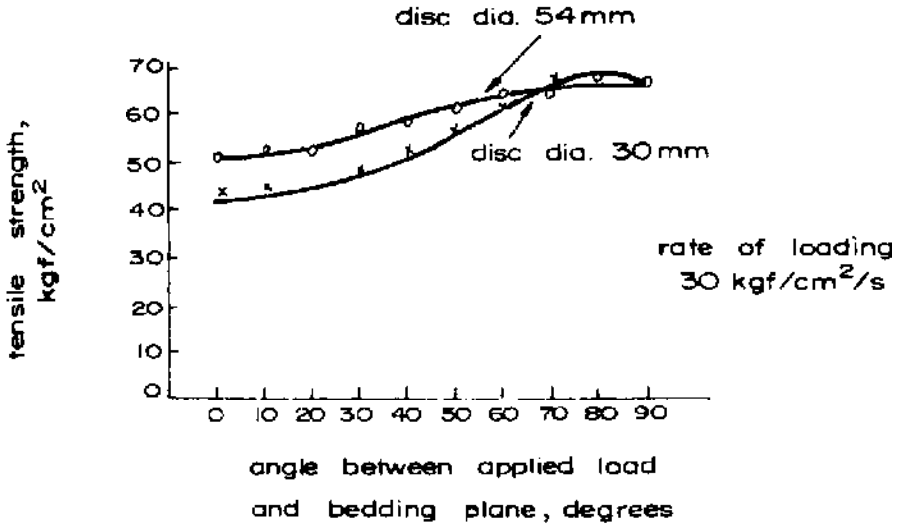

Fig. 10-122. Effect of direction of loading (with respect to bedding plane) on tensile strength of sandstone (after DUBE and SINGH, 1969).

Using the ring test, HOBBS (1964) evaluated the effect of orientation of the bedding planes on the tensile strength of rocks. He used discs of 2.54 cm (1 in) external diameter, 0.64 cm (0.25 in) thick with a 0.32 cm (0.125 in) diameter hole. The results are given in Table 16. It is seen that tensile strength is greatest when the tensile stress generated is at 0° to the lamination (laminations at right angle to the loaded axis). However, there are two exceptions. The Kirkby siltstone shows minimum tensile strength at 75° to the laminations and maximum at 30° to the laminations. Cefn Coed sandstone shows little variation in tensile strength with lamination orientation. The majority of the discs failed along the loaded diameter irrespective of the orientation of the laminations. Subsidiary cracks tending to follow the plane of the laminations also occurred. Certain specimens loaded at 60° to the laminations sheared along one or more planes parallel to the direction of laminations.

BARRON (1971) has evaluated the effect of orientation of the bedding planes on the tensile strength of siltstone using the ring test. All specimens failed directly across the loading diameter. The results are very similar to those of HOBBS.

BERENBAUM and BRODIE (1959) studied the variation of the tensile strength of Barnsley Hard coal at various angles with the bedding planes by two methods, namely, indentation method (compression of square plate along a diameter) and Brazilian test method (Table 17). They are in good agreement.

Similar results have been obtained in direct pull out tests on cylindrical specimens of serpentineous schist (Val Malenco, Italy) and gneiss (Entracque, Val Gesso, Italy) (Fig. 10-123). The maximum value of tensile strength and the

TABLE 16

The dependence of tensile strength on lamination orientation

(after HOBBS, 1964)

Rock	Tensile strength, MPa (lbf/in^2)							
	Laminations perpendicular to disc face							Laminations parallel to disc face
	0° to laminations	15°	30°	45°	60°	75°	90°	
Kirkby siltstone	23.9 ± 2.1 (3470 ± 300) [4]	28.1 ± 2.1 (4070 ± 300) [4]	30.2 ± 1.7 (4380 ± 240) [4]	22.6 ± 1.4 (3280 ± 210) [4]	23.5 ± 2.2 (3410 ± 320) [4]	9.7 ± 1.3 (1410 ± 190) [4]	15.2 ± 2.7 (2210 ± 390) [4]	
Donisthorpe siltstone	27.3 ± 0.8 (3960 ± 120) [23]	26.3 ± 0.7 (3810 ± 100) [23]	24.7 ± 0.9 (3580 ± 130) [22]	24.6 ± 0.8 (3570 ± 110) [19]	21.9 ± 0.8 (3170 ± 120) [21]	16.8 ± 1.2 (2440 ± 180) [20]	15.9 ± 1.6 (2310 ± 230) [23]	34.1 ± 1.7 (4940 ± 240) [11]
Cefn Coed sandstone	68.7 ± 4.1 (9960 ± 590) [4]	–	67.6 ± 4.0 (9810 ± 580) [4]	—	58.1 ± 4.6 (8430 ± 660) [4]		68.8 ± 2.4 (9980 ± 350) [4]	
Chiselet sandstone	53.6 ± 3.0 (7770 ± 430) [5]	50.3 ± 5.0 (7290 ± 720) [4]	40.5 ± 3.1 (5880 ± 450) [4]	51.3 ± 3.0 (7440 ± 430) [4]	47.6 ± 3.3 (6910 ± 480) [4]	39.6 ± 2.1 (5750 ± 310) [4]	47.0 ± 6.6 (6810 ± 950) [4]	
Ormonde siltstone 1	36.1 ± 0.7 (5230 ± 100) [11]	33.8 ± 0.6 (4900 ± 80) [11]	31.9 ± 0.5 (4620 ± 70) [11]	30.8 ± 1.0 (4470 ± 140) [11]	23.3 ± 1.7 (3380 ± 240) [9]	23.0 ± 2.0 (3330 ± 290) [9]	22.4 ± 1.4 (3250 ± 200) [11]	
Ormonde siltstone 2	27.4 ± 1.0 (3970 ± 150) [4]		23.9 ± 1.5 (3470 ± 220) [4]		15.9 ± 1.0 (2310 ± 140) [4]		7.9 ± 0.5 (1150 ± 70) [4]	30.1 ± 1.0 (4370 ± 140) [12]
Ellington mudstone 1	11.8 ± 1.5 (1710 ± 220) [4]		9.8 ± 1.2 (1420 ± 180) [2]		8.3 ± 1.4 (1210 ± 210) [3]		3.8 ± 1.4 (550 ± 210) [4]	

Note: Numbers in [] refer to the numbers of specimens tested.

TABLE 17

Variation of the tensile strength of Barnsley Hard coal with orientation to the bedding planes

(All specimens cut from the same block)

(after BERENBAUM and BRODIE, 1959)

Method	Tensile strength, MPa (lbf/in^2)				
	Angle between tensile stresses and bedding planes				
	0	25	45	65	90
Indentation (0.95 cm (3/8 in) indenter) 15 specimens at each angle	2.8 ± 0.19 (408 ± 27)	2.3 ± 0.28 (329 ± 41)	1.7 ± 0.10 (242 ± 14)	1.6 ± 0.10 (226 ± 14)	1.3 ± 0.12 (191 ± 18)
Brazilian 20 specimens at each angle	2.8 ± 0.19 (408 ± 27)	2.9 ± 0.27 (415 ± 39)	1.9 ± 0.22 (279 ± 32)	1.6 ± 0.10 (226 ± 14)	1.2 ± 0.10 (168 ± 14)

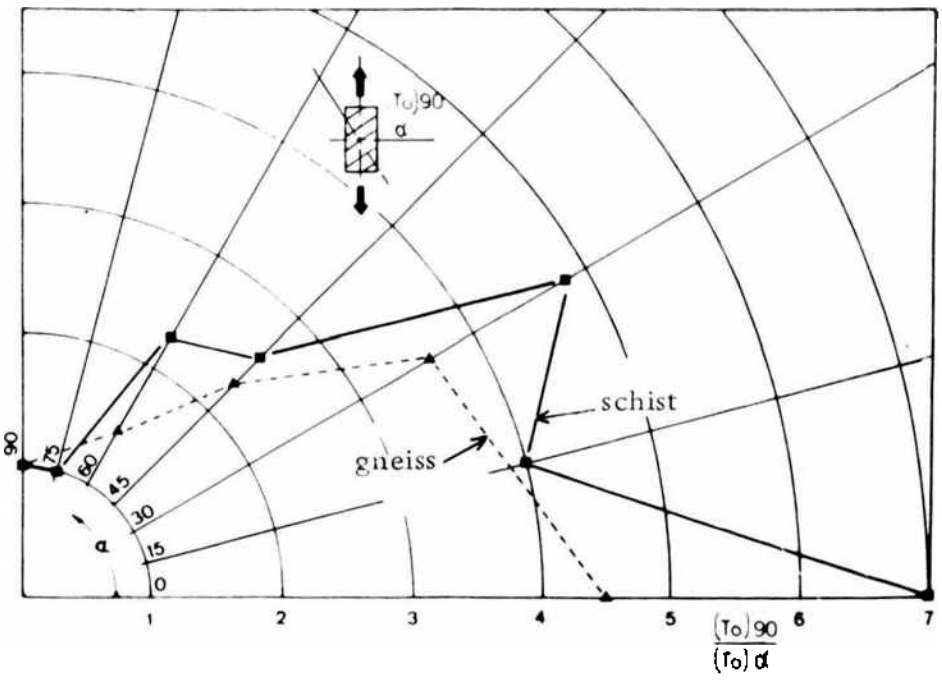

Fig. 10-123a. Ratio of the tensile strengths $\frac{(T_o)_{90}}{(T_o)_\alpha}$ versus α

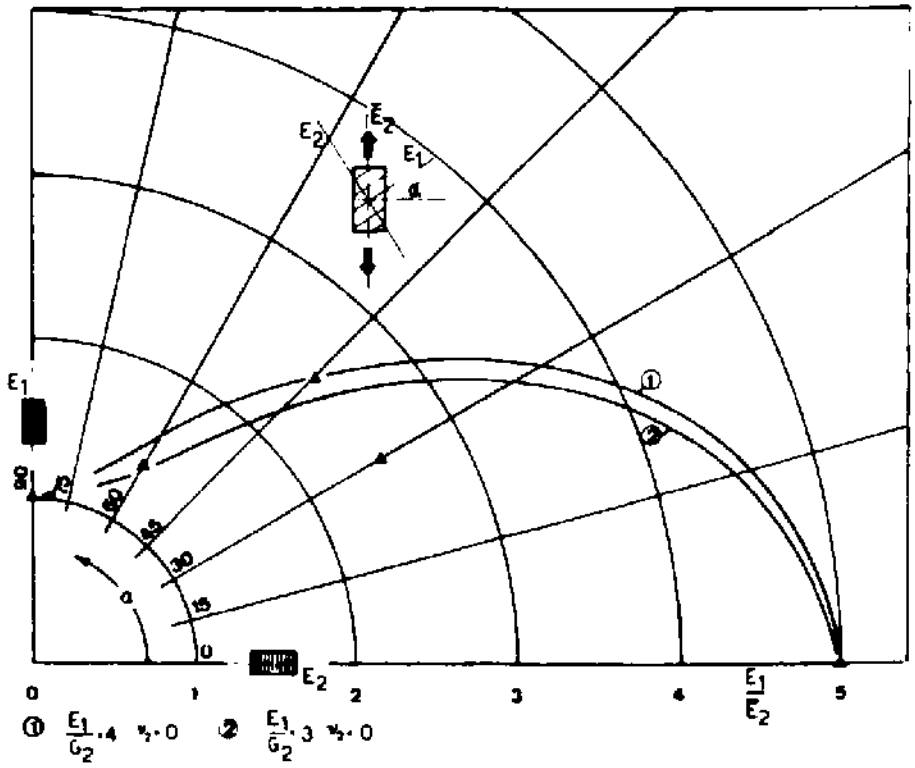

Fig. 10-123b. Ratio of the elastic moduli $\left(\frac{E_1}{E_2} \right)$ for gneiss versus α

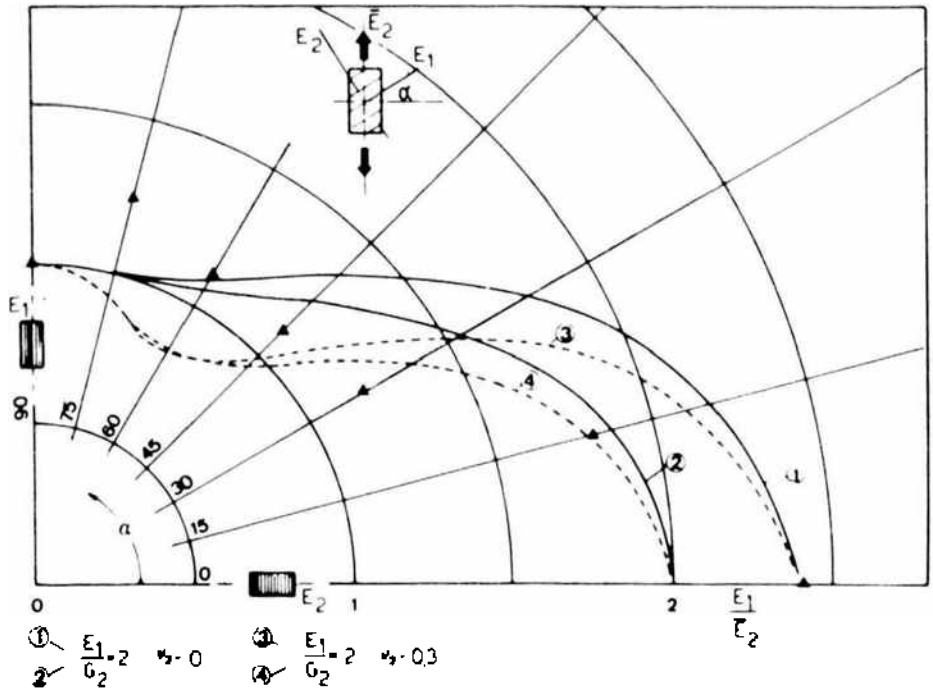

Fig. 10-123c. Ratio of the elastic moduli $\left(\frac{E_1}{E_2} \right)$ for serpentinous schist versus α (after BARLA & GOFFI, 1974).

elastic modulus occurs when the tensile load is applied parallel to the plane of laminations. The minimum values for these rocks are obtained when the load is applied perpendicular to the same plane. The anisotropies of deformability and strength seem to coincide with the gneiss but this does not hold for the serpentineous schist. The change in elastic modulus with orientation does not seem to agree with the tensorial transformations for elastic constants which hold true for a transversely isotropic medium.

10.7. Fracture of Jointed Rock in Direct Shear

KRSMANOVIC and LANGOF (1964) conducted tests on stratified and jointed limestone in a direct shear machine and their results are given in Fig. 10-124. There are three typical $\tau - \Delta s$ lines (obtained at approximately the same values of normal stress σ).

The first type occurs in the solid rock where there is cohesion (the line for the first Series "A"). Its characteristics are very high shear resistance with slight deformations necessary to develop maximum shear resistance: Δs approximately 0.1 to 0.5 mm (0.004 to 0.02 in). The high value of the relation τ_i/τ_r is also noted, which in the cases tested was always greater than 2.0.

The second typical $\tau - \Delta s$ diagram, is observed for stratification surfaces of different degrees of roughness (lines for the Series B1 to B3) and fissures of great roughness (lines of Series D2 and D3). Their characteristics are (1) the deformations necessary to develop shear resistance are considerably greater (2 to 5 mm) (0.08 to 0.2 in) and (2) the value of the relation τ_i/τ_r ranges between 1.0 and 2.0.

Third $\tau - \Delta s$ line is characterised by slight or great deformations necessary for activation of shear resistance, but in this case the relation τ_i/τ_r is approximately equal to 1.0 (Series C2 and D3).

LAJTAI (1969a, b) tested several plane, open and closed, joints with rock bridges and identified 3 modes of failure:
1. Failure in tension at low normal stresses.
2. Failure in shear at intermediate normal stresses.
3. Ultimate failure—failure of crushed material at high normal stresses.

According to him, the total shear strength of a plane of weakness consisting of discontinuities separated by solid bridges can be considered as a sum of cohesional strength (fundamental shear strength (τ_0), internal friction in the solid bridges (ϕ_i), and friction angle along the open joints (ϕ_μ). Accordingly, it is possible that along a plane of weakness frictional resistance is not fully mobilised before first fracturing as the deformation may be quite large and

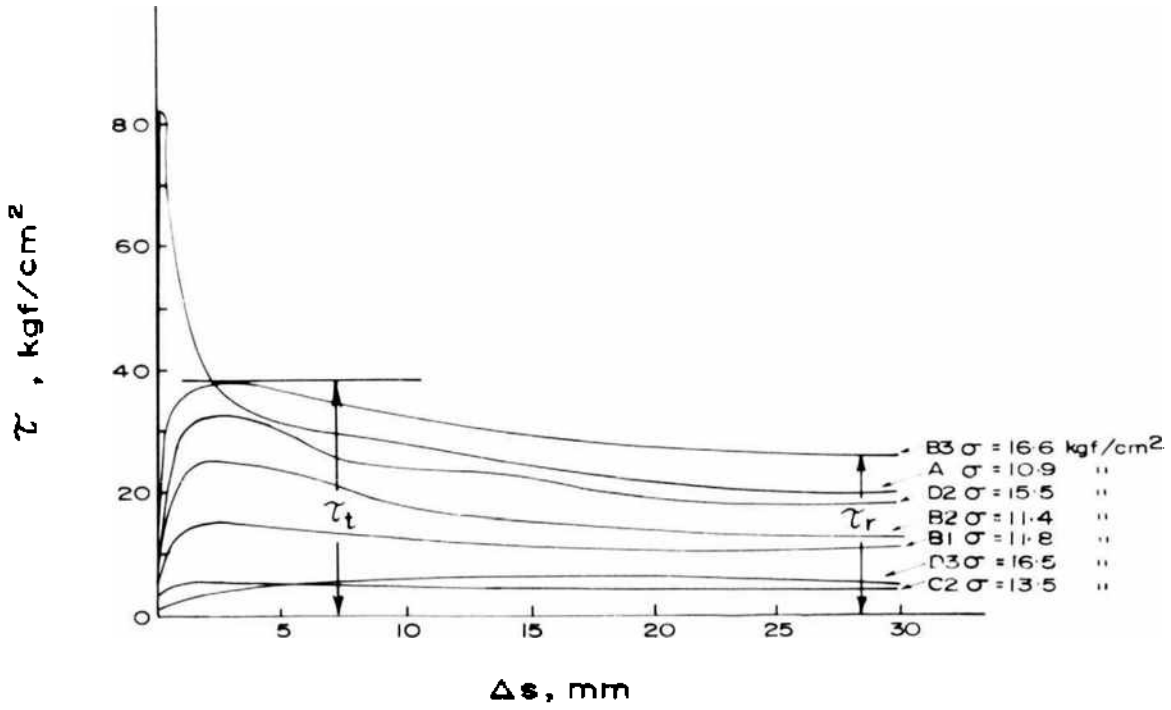

series A – intact limestone
series B – stratification surfaces (bedding joints)
1 – thin calcareous foliated layer;
2 – rough stratification surface;
3 – very rough stratification surface;
series C2 – thin, 2 – 5 cm (0·8 – 2 in) plastic sedimentation layers
series D2 – clean, very rough fissures
D3 – rough fissures with detrital material

Fig. 10-124. Diagrams $\tau - \Delta s$ for typical specimens of various series (after KRSMANOVIC and LANGOF, 1964).

the "bridges" may not take this without failure. (This concept has been supported by in situ shear tests on large samples where it was found that the displacement at the point nearer to the application of shear load is greater than the displacement at other points away from the shear loading surface and this is also the region of first fracture.) As such, he introduced the term called

the "mobilisation factor" (C) in his analysis. According to him, the minimum resistance of a joint (when no friction is mobilised) is a function of the tensile strength of the rock bridge and is given by the form

$$\tau_{t(\min)} = (1-k)A\left(\sigma_t(\sigma_t - \frac{\bar{\sigma}_n}{1-k})\right)^{1/2}$$

or

$$\tau_{t(\min)} = A\left(\bar{\sigma}_t(\bar{\sigma}_t - \bar{\sigma}_n)\right)^{1/2} \tag{10.65}$$

and maximum resistance (with mobilisation of frictional resistance)

$$\tau_{t(\max)} = A - \sigma_t(1-k)A + C_1 k A \bar{\sigma}_n \tan\phi \tag{10.66}$$

where $\tau_{t(\min)}$ and $\tau_{t(\max)}$ = minimum and maximum shear resistances

k = degree of jointing or degree of separation
σ_t = uniaxial tensile strength of the material
$\bar{\sigma}_t$ = average uniaxial tensile strength
$(\bar{\sigma}_t = (1-k)\sigma_t)$
$\bar{\sigma}_n$ = average normal stress
C_1 = mobilisation factor for joint friction, assuming values $0 \leq C_1 \leq 1$
A = total shear surface and
ϕ = angle of joint friction.

The Eq. 10.65 is valid for both tension and compression zone while Eq. 10.66 is valid only for $\bar{\sigma}_n > 0$. When the value of $\bar{\sigma}_n$ is increased approximately above 2/3rd of compressive strength, the shear resistance is reduced to the ultimate value, i.e.,

$$\tau_{t(ult)} = A\bar{\sigma}_n\mu_0 \tag{10.67}$$

where μ_0 = coefficient of internal friction of the granular material. LAJTAI found good agreement between laboratory results and this equation.

Tests have been conducted by HAYASHI (1966) on regularly jointed models of plaster having compressive strength of 3.652 MPa (37.3 kgf/cm^2) (530 lbf/in^2), tensile strength (direct tensile test) of 0.832 MPa (8.5 kgf/cm^2) (120.7 lbf/in^2), shear strength of 1.076 MPa (11.0 kgf/cm^2) (156.2 lbf/in^2), and bending strength of 1.292 MPa (13.2 kgf/cm^2) (187.4 lbf/in^2), YOUNG's modulus of 2693 MPa (27,500 kgf/cm^2) (390,500 lbf/in^2) and POISSON's ratio of 0.19. The coefficient of friction was simulated using wax paper or by filing of plaster strips giving values of 0.45 and 1.05 respectively. Some 450 tests on layered, crossed, intermittent and parallel joints were conducted. The results of these investigations are given below.

1. The shear load T at failure of a specimen with transversal joints decreased with an increase in the number of joints, n (even if the specimens had equal volume) and can be represented by an equation similar to Eq. 10.63 (Fig. 10-125).

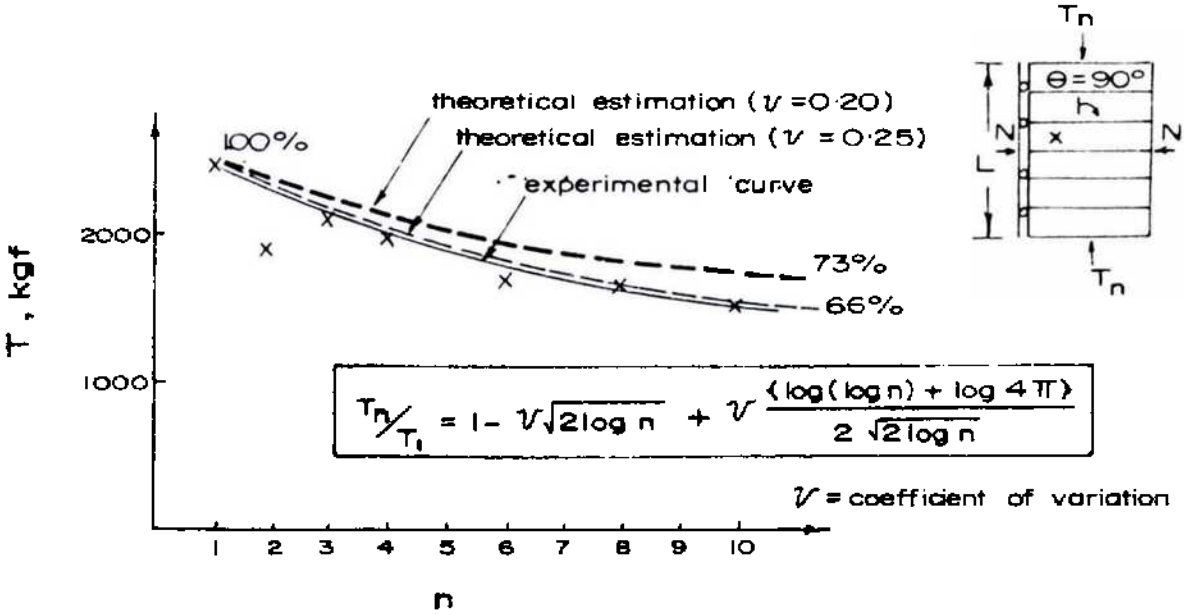

Fig. 10-125. Shear load T_n decreases depending on the number of jointed bodies n in equal shearing length $L(\theta = 90^\circ$, confining condition of lateral dilatancy in direction x) (after HAYASHI, 1966).

2. The shear load at failure of a continuously jointed (layered) material under one sided constraint showed that specimens with positive joint system were weaker than those with negative joint system (Fig. 10-126). The load at failure increased with increase in the constraining force N (Fig. 10-127) and if no dilatancy was allowed, the value of constraining force required was extremely high (Fig. 10-128). The interesting point in these investigations is that the constraining force N required for the negative joint system is far higher than for the positive joint system.

Cohesion c and coefficient of friction μ are given in Figs. 10-129 and 10-130.

For the case of shear on a single joint, there is evidence to suggest that there is a significant scale effect in cohesion, but apparently little similar effect in internal friction. A simple explanation of this is that the frictional coefficient along the joint is not dependent on the area of contact, and the failure can be resisted by the higher strength parts of the joint.

On the other hand, for the case of shear on a large number of parallel joints, as in the shear deformation of a blocky mass, there is a freedom of choice in

defining the failure surface, and greater deformation takes place along lower strength joints. Thus the greater the number of joints, the higher the probability of defining a series of failure surfaces in lower strength components, and greater the magnitude of scale effect.

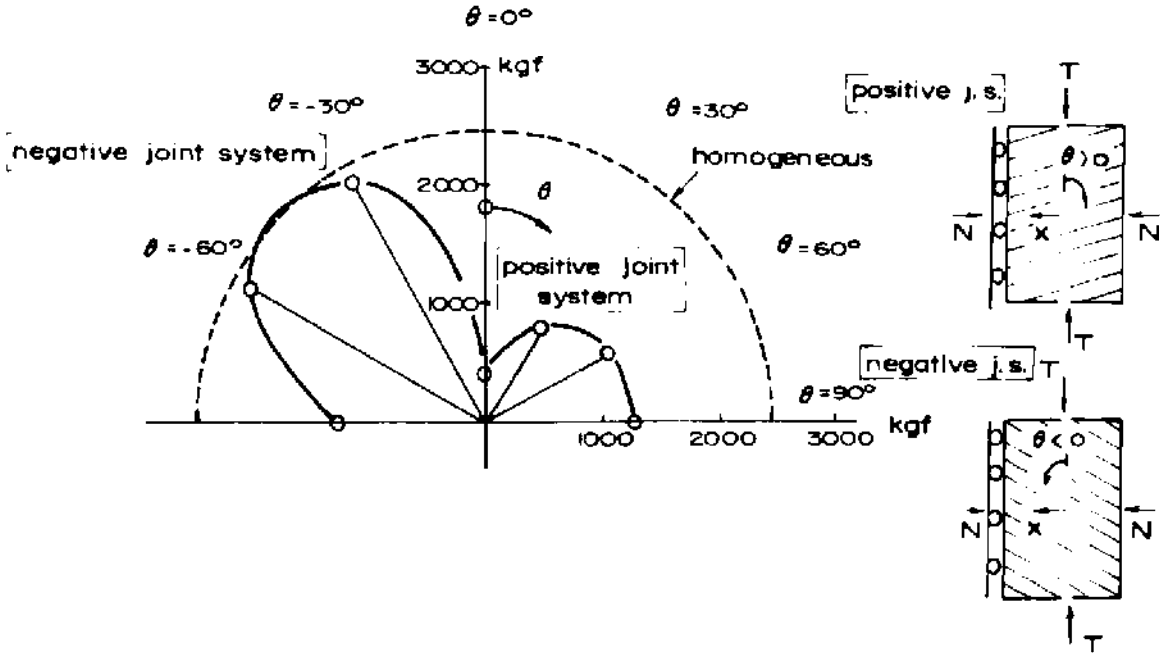

Fig. 10-126. Anisotropy of shear load at failure T in confining the lateral dilatancy in direction x (after HAYASHI, 1966).

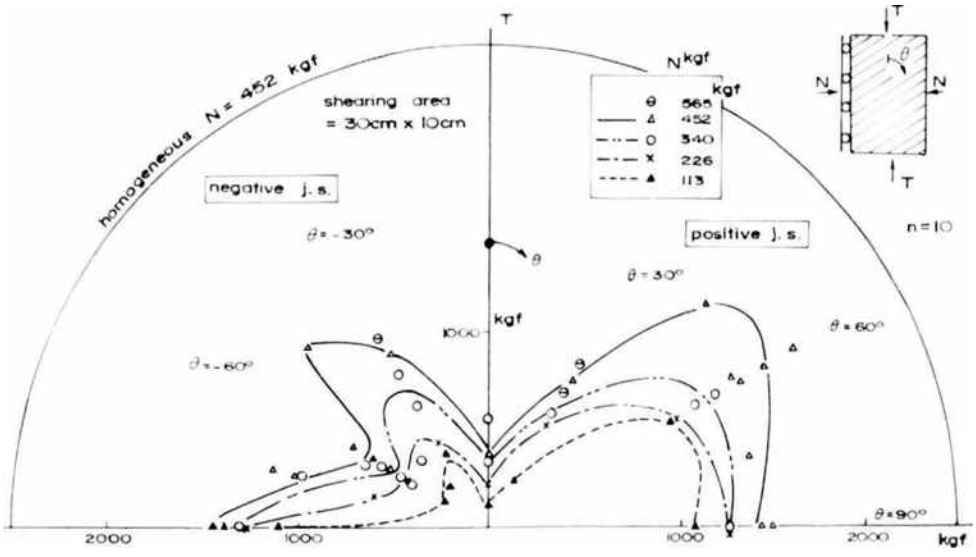

Fig. 10-127. Anisotropy of shear load at failure T under normal force N (after HAYASHI, 1966).

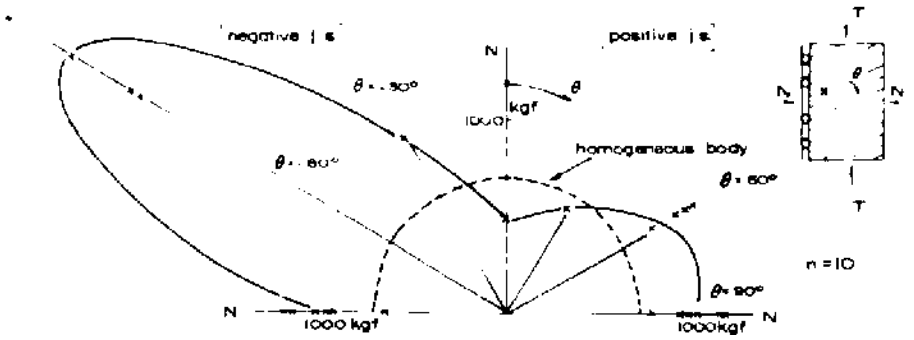

Fig. 10-128. Anisotropy of restraint force N which was needed to confine the lateral dilatancy in direction x
(after HAYASHI, 1966).

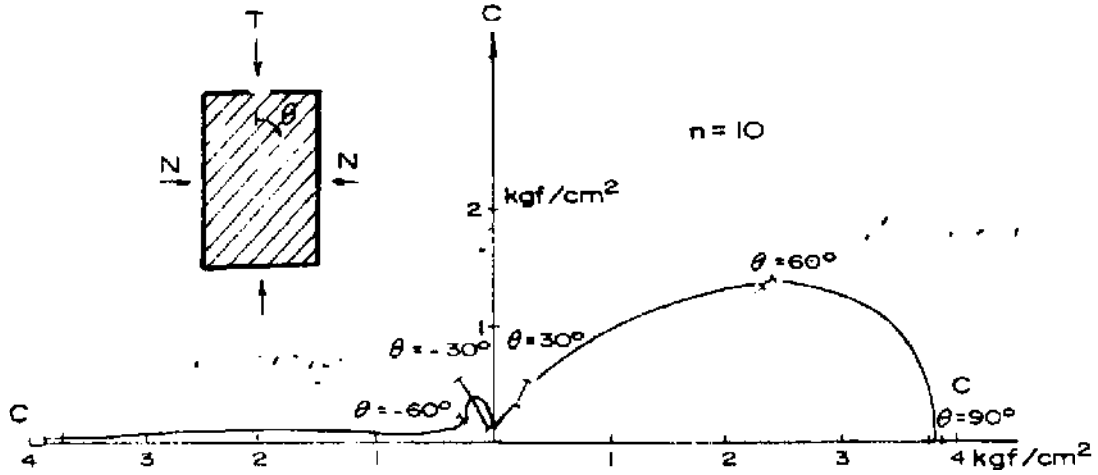

Fig. 10-129. Anisotropy of apparent cohesion (cohesion of material itself $c = 11$ kgf/cm^2)
(after HAYASHI, 1966).

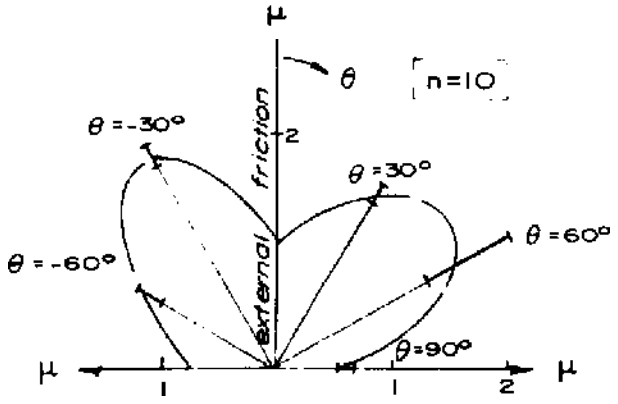

Fig. 10-130. Polar plot of apparent internal friction factor μ (external friction of joint plane: 1.0)
(after HAYASHI, 1966).

3. The pitch of the cross-joints (c) does not have any influence on the shear strength for the inclination of the bedding $\theta = 90$. For $\theta = 60$, the influence is more for the negative joint system than for the positive joint system (Fig. 10-131).

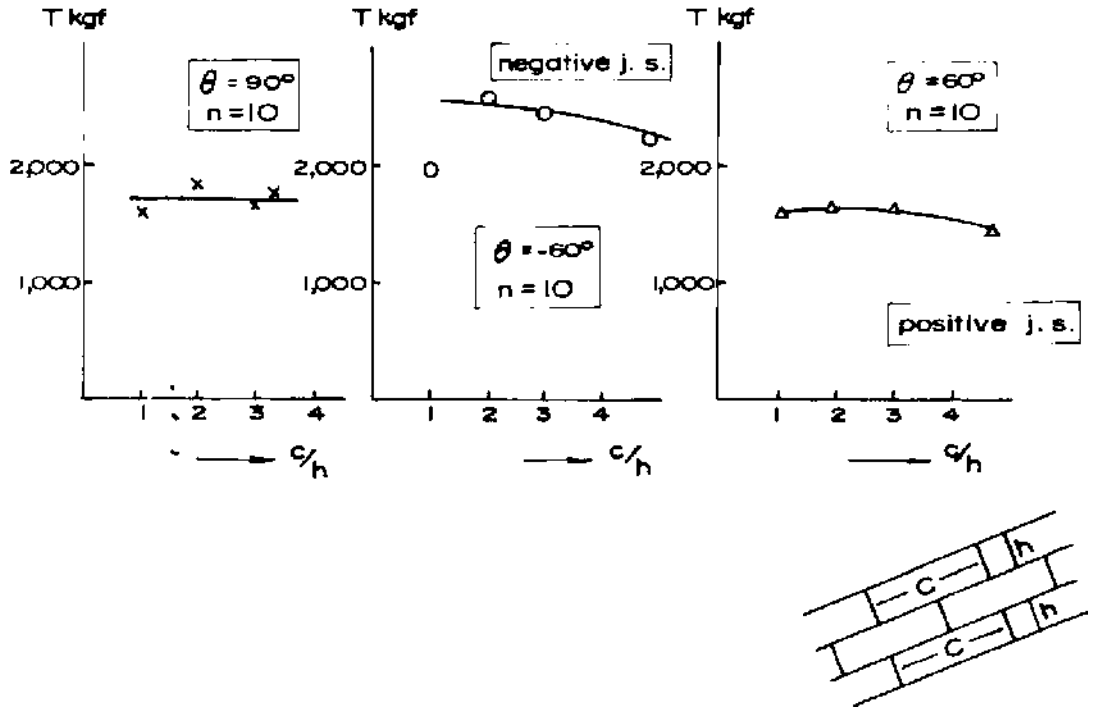

Fig. 10-131. Shear load at failure T is almost independent of pitch C of cross-joints. (In confining condition of lateral dilatancy δx) (after HAYASHI, 1966).

HAYASHI (1966) found that depending upon the direction of inclination of the joints and the restraint ($-ve$ or $+ve$ joint inclination—Fig. 10-127), there is possibility of joint opening or joint closing due to tensile or compressive stresses developed in the jointed system which gives rise to internal buckling resulting in tensile stresses.

Similar tests were performed by KAWAMOTO (1970) on jointed and layered plaster-sand models. The intermittent parallel joints were prepared by inserting a number of small steel sheets of 0.1 mm (0.004 in) in thickness (Fig. 10-132). The types of joint systems tested by him are shown in Table 18. Fig. 10-133 shows the results obtained by him representing the relationships between the directions of joints and the shearing load at failure at the normal load of 490.6 N (50 kgf) (110.25 lbf) for the 3 types of joint system both for the appearance of crack and at failure. The pattern of the results is similar to that obtained by HAYASHI (1966) with the difference that the maximum shear

strength obtained by KAWAMOTO is at an angle $\theta = -22^1/_2$ while by HAYASHI it is at an angle of about 45 . It looks like the confining of lateral dilatancy influences the results. KAWAMOTO's results further show that the shear strength at the appearance of the crack (Fig. 10-133a) is not much affected by the joint direction and that the influence of degree of separation of the joint planes and relative density of the joints on the ultimate shear strength is greater for the negative joint system than for the positive joint system.

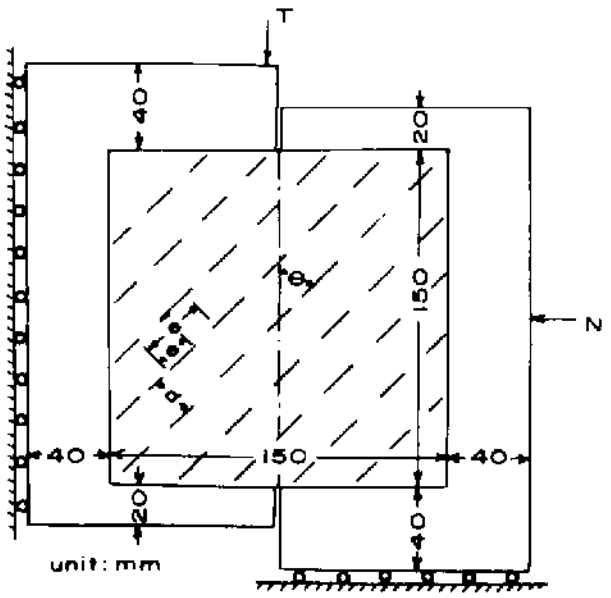

Fig. 10-132. Scheme of direct single shear test by shearing box and factors of jointed medium (after KAWAMOTO, 1970).

TABLE 18

Types of joint system in jointed models (c.f. Fig. 10-132)

(after KAWAMOTO, 1970)

Type	e mm (in)	$\bar{e}$ mm (in)	d mm (in)	Degree of separation of joint planes $k = e/\bar{e}$	Relative density of joints $w = \bar{e}/d$
A	10 (0.39)	20 (0.79)	10 (0.39)	0.5	1.0
B	10 (0.39)	20 (0.79)	20 (0.79)	0.5	0.5
C	5 (0.20)	10 (0.39)	10 (0.39)	0.5	0.5

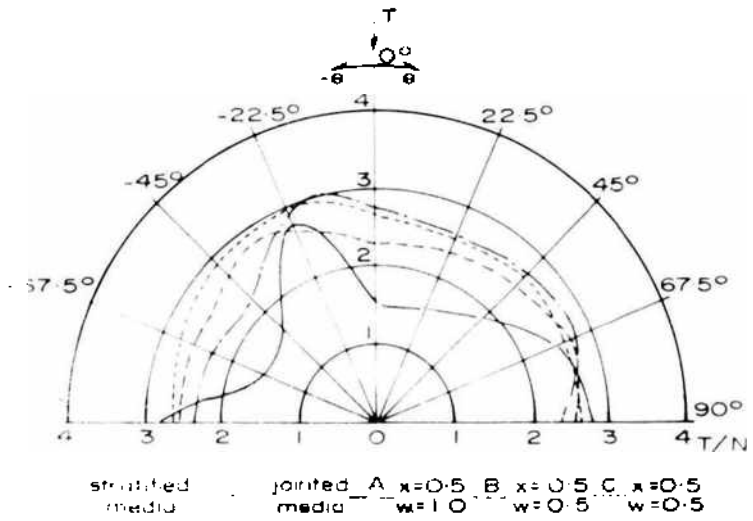

(a)

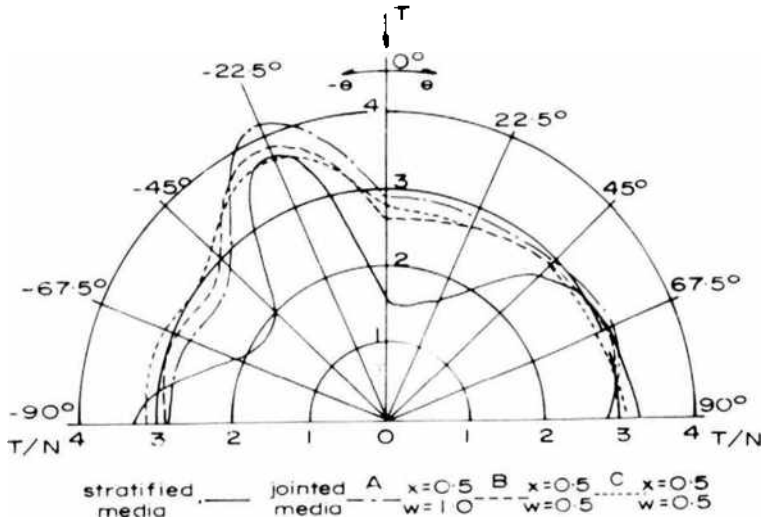

(b)

Fig. 10-133. Shear load at failure of jointed and layered media under direct shear using shearing box; (a) at appearance of crack; (b) at failure (Macroscopic shear strength) (after KAWAMOTO, 1970).

The typical failure patterns are given in Fig. 10-134 for various joint systems. The fracturing can be described as rupture involving joints (sliding or shearing rupture), rupture through solid (cleavage and shearing rupture) and combined rupture.

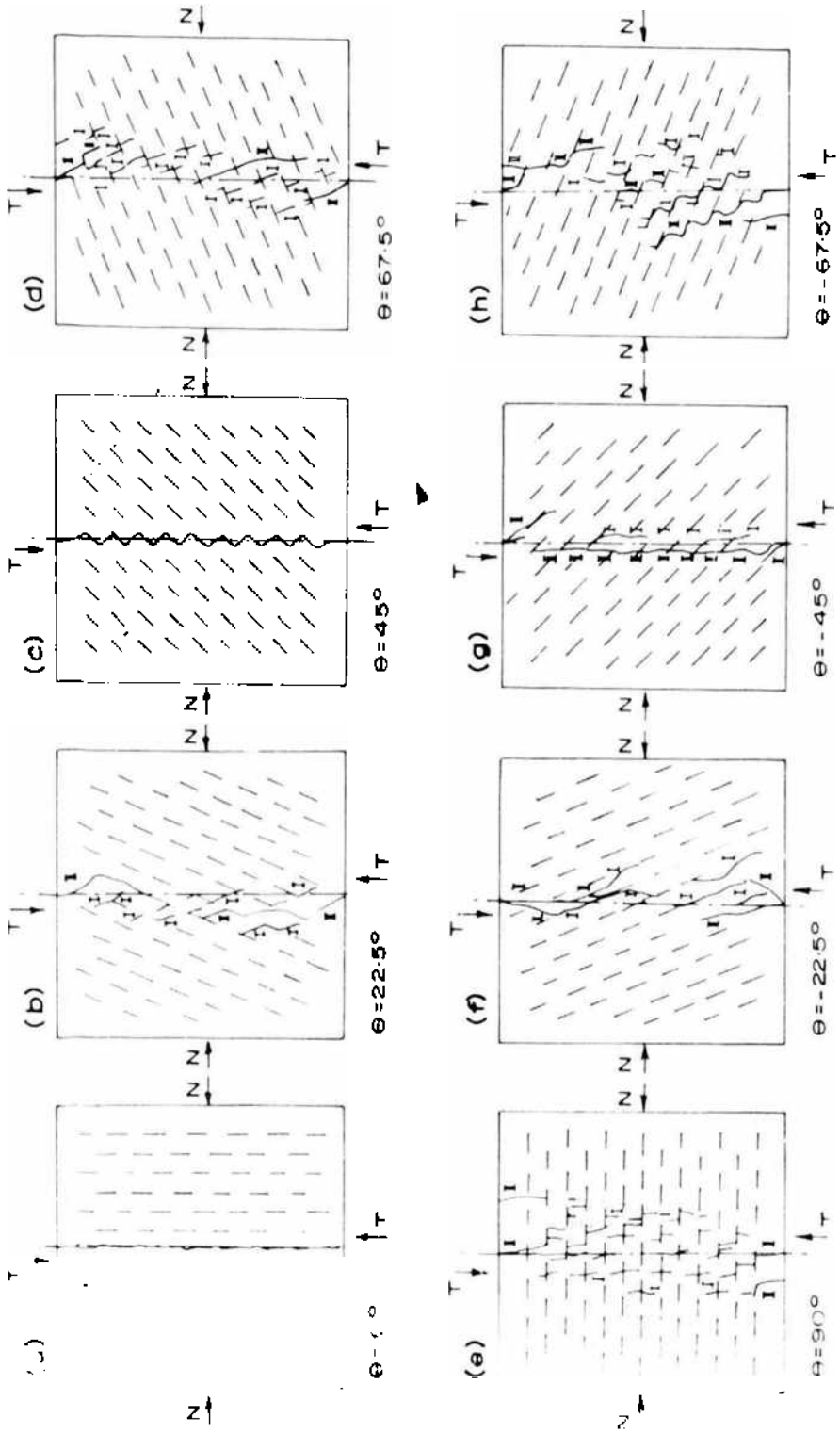

Fig. 10-134. Failure patterns of jointed media by direct shear test using shearing box (after KAWAMOTO, 1970).

The failure by pure shearing rupture may be caused only when $\theta = 0$. In the cases of the positive joint system, the proportion of the shearing rupture out of the combined rupture is comparatively large for $\theta < 22.5°$, but it decreases rapidly as θ increases, since the appearance of cracks due to the increase of tensile stress around the joints, the concentration of tensile stress at the tips of cracks and the partial bending after the appearance of crack becomes significant for progressive failure.

In the cases of the negative joint system, the occurrence of cracks around the joints may be the main cause of failure and the location and orientation of joints and the progressive state of connection of cracks give considerable variation to the width of the fractured zone along the fictitious shear plane.

UFF and NASH (1967) measured the shear strength of a shale along the bedding planes in various directions from dip to strike using a shear box. Parallel to these planes the strength parameters c and ϕ were found to vary with the orientation relative to the dip. Fig. 10-135 shows a complete set of results for the specimens at 20° to the dip, with envelopes of peak and residual shear strength. In Figs. 10-136 and 10-137, the shear strength parameters are plotted against the direction of shearing. These graphs suggest that the maximum peak values of friction and cohesion in the bedding plane occur in the directions of strike and dip respectively, with the minimum values at right angles. The values of 'residual' friction and cohesion appear to be constant within the order of scatter of peak values. In Fig. 10-138, the actual variations of peak shear strength for different values of normal pressure are illustrated.

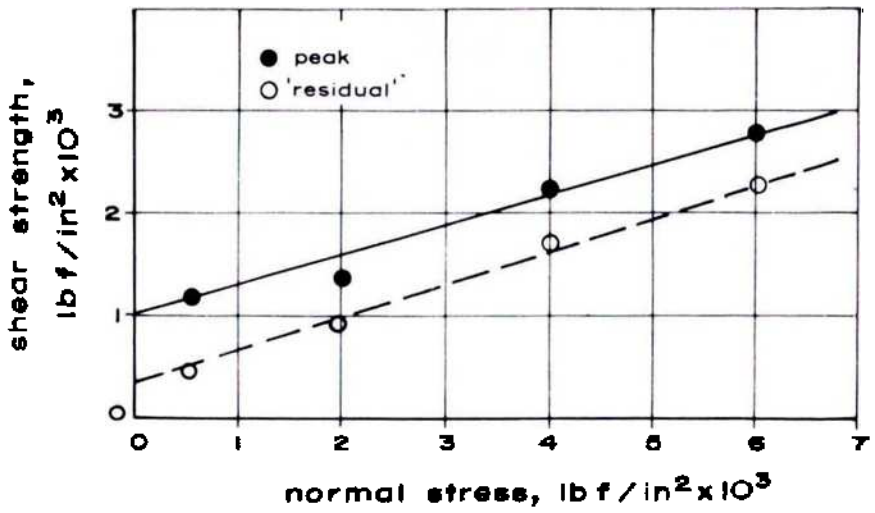

Fig. 10-135. Strength envelope of shale tested at 20° to dip (after UFF and NASH, 1967).

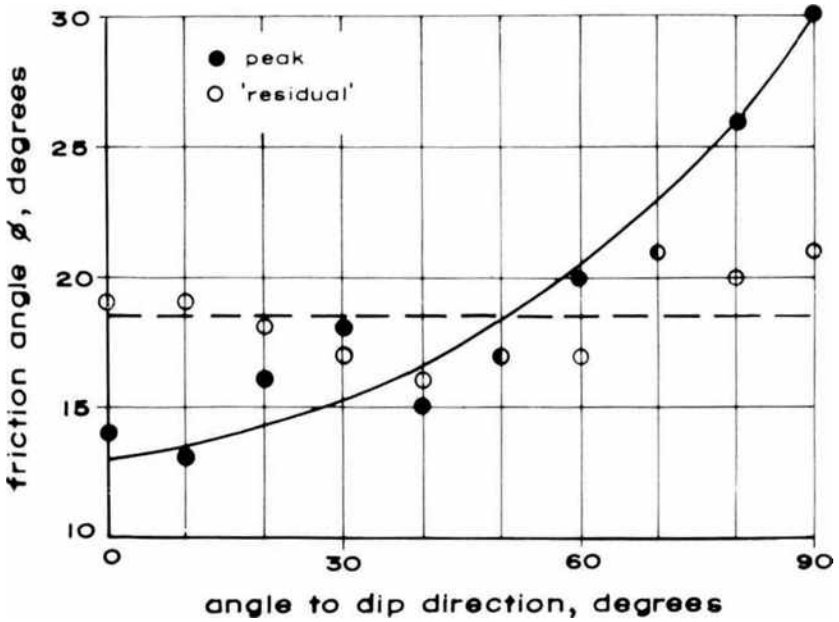

Fig. 10-136. Relationship between Φ and angle to dip (after UFF and NASH, 1967).

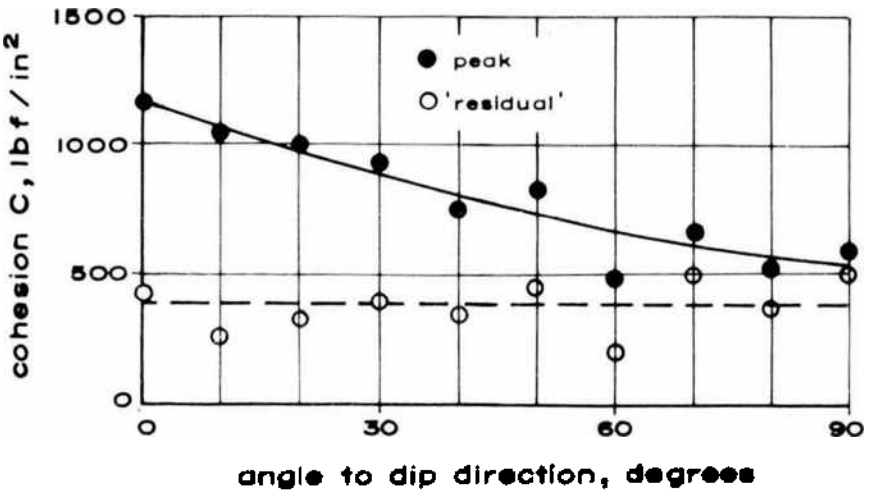

Fig. 10-137. Relationship between c and angle to dip (after UFF and NASH, 1967).

WALKER (1971) conducted direct shear tests on models consisting of cubic blocks oriented at different angles to the direction of normal and shear stresses. He observed sliding along joints, rotation of blocks and failure through the blocks depending upon the direction of orientation of blocks with respect to the applied stress field. When the normal stress existing on the imposed shear plane is high with low value of the normal stress on the orthogonal joint plane

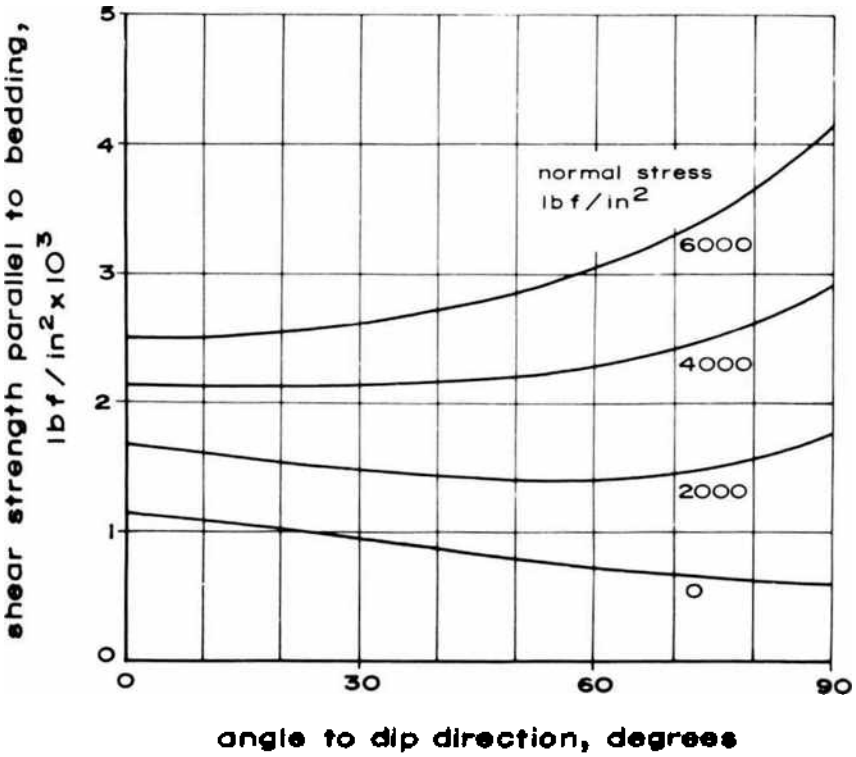

Fig. 10-138. Relationship between shear strength and angle to dip for various normal pressures (after UFF and NASH, 1967).

(Fig. 10-139), then instead of slippage occurring along the expected plane, the unit blocks rotate and in fact slip occurs on the orthogonal joint plane where resistance to sliding is much lower. In such a case, a set of unit blocks rotate around their axes resulting in high dilation, crushing and giving wider shear zone.

A similar type of failure was reported by LADANYI and ARCHAUMBAULT (1972) who termed it as "kink band". They found that when such a failure occurs, the strength of the jointed mass is much lower than that predicted by the MOHR-COULOMB's concept.

The shear strength at different values of normal stress plotted on polar co-ordinates is given in Fig. 10-140. β is the angle which a joint set makes with the direction of application of shear force. The lowest shear strength was naturally for $\beta = 0$ and the highest for $\beta = 67^1/_2$ which is in accordance with the results of KAWAMOTO (1970). WALKER also determined the load displacement curves and found that yield point was quite well defined when models failed through plaster blocks and was less and less defined as the mode of failure moved towards slippage along the joints (Fig. 10-141). He found that when failure was along a single sliding plane, there was no dilatation while failure along a number of

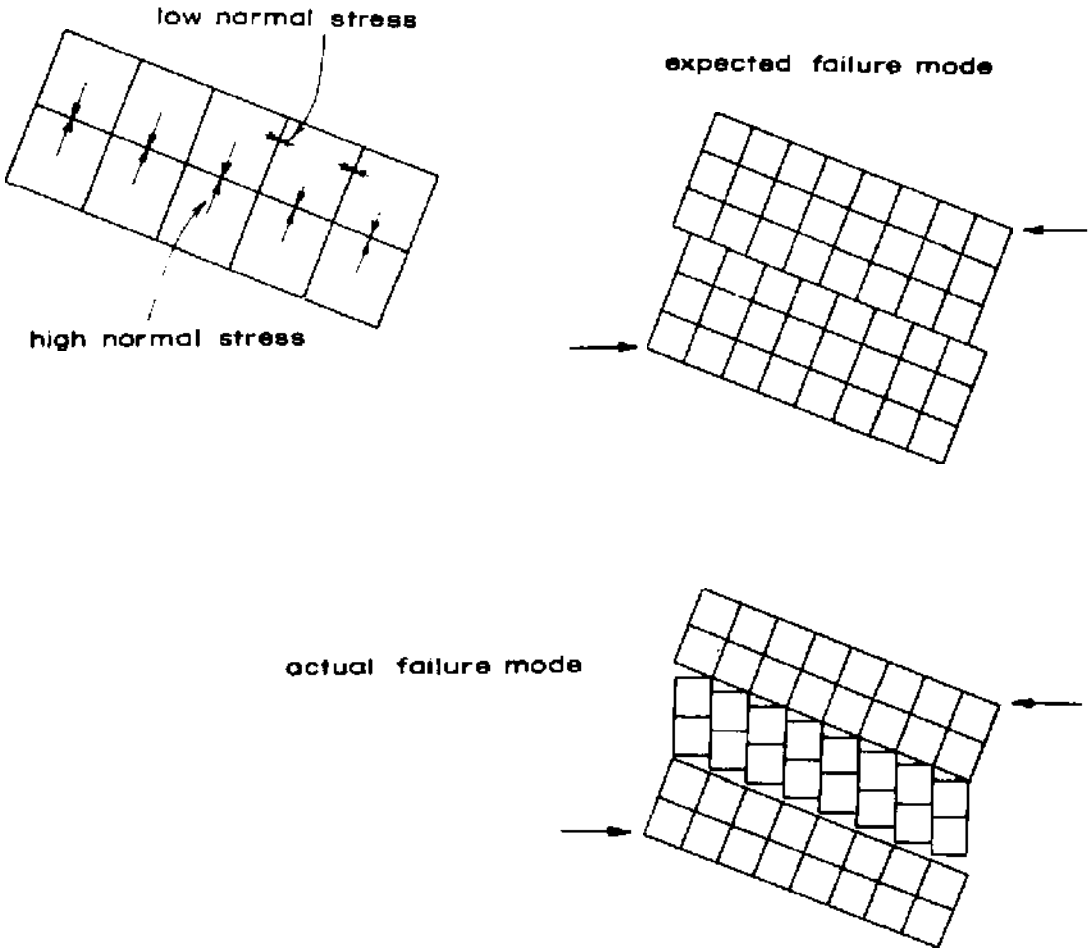

Fig. 10-139. Rotationary failure mode (after WALKER, 1971).

sliding planes and through plaster resulted in volumetric changes. The highest change in volume was at $\beta = 22^{\circ}$ and this was associated with rotation of blocks. The increase in volume increased with increase in normal stress at $\beta = 22^{\circ}$ and 45° and was also associated with higher displacement as a cause of failure (Fig. 10-142). Fig. 10-142b shows the dilatancy at a displacement of 10.16 mm (0.4 in) at which all models failed – and it clearly shows that at higher normal stresses compression of models started after failure had occurred.

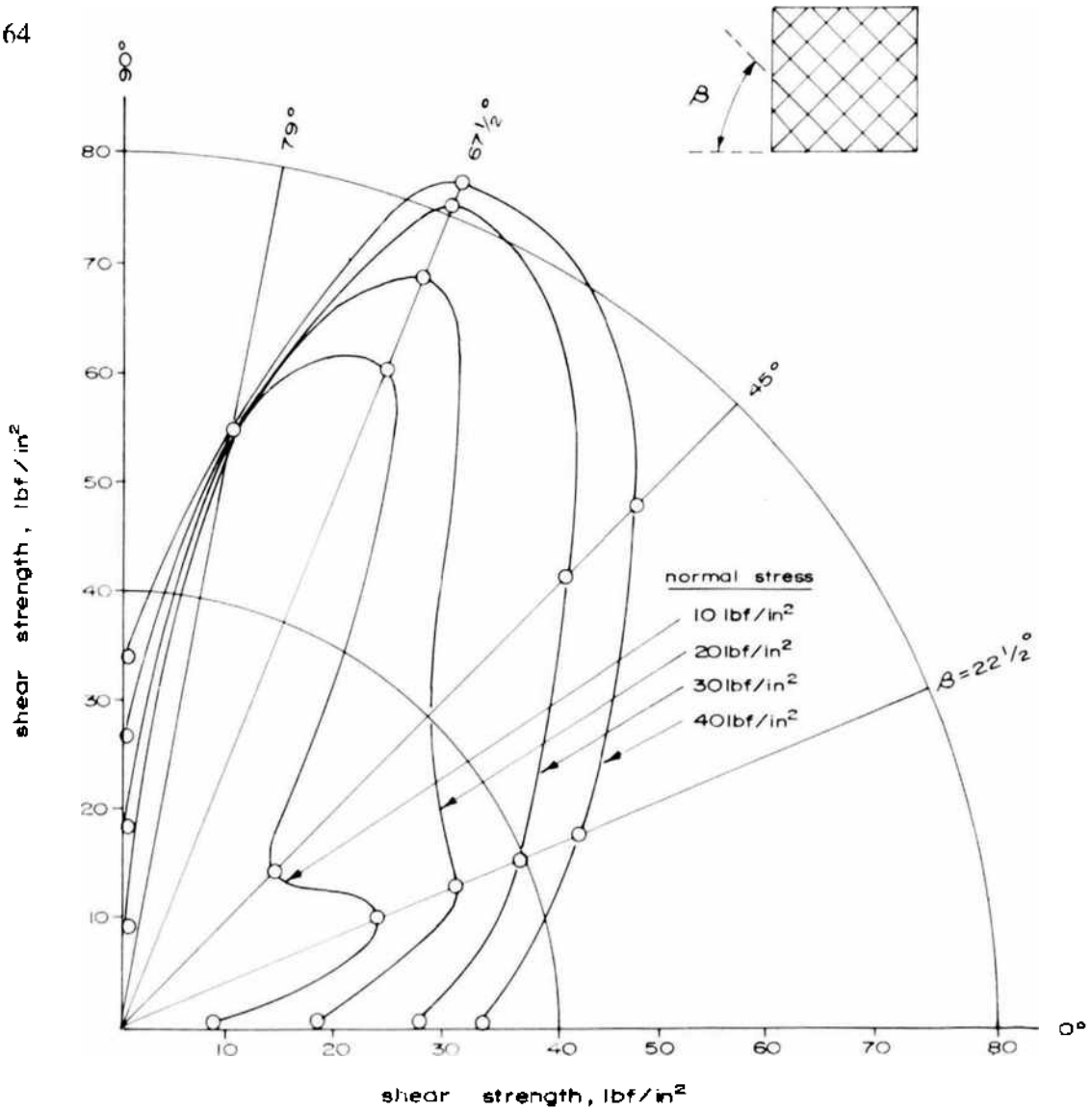

Fig. 10-140. Polar distribution of shear strength at different normal stresses (after WALKER, 1971).

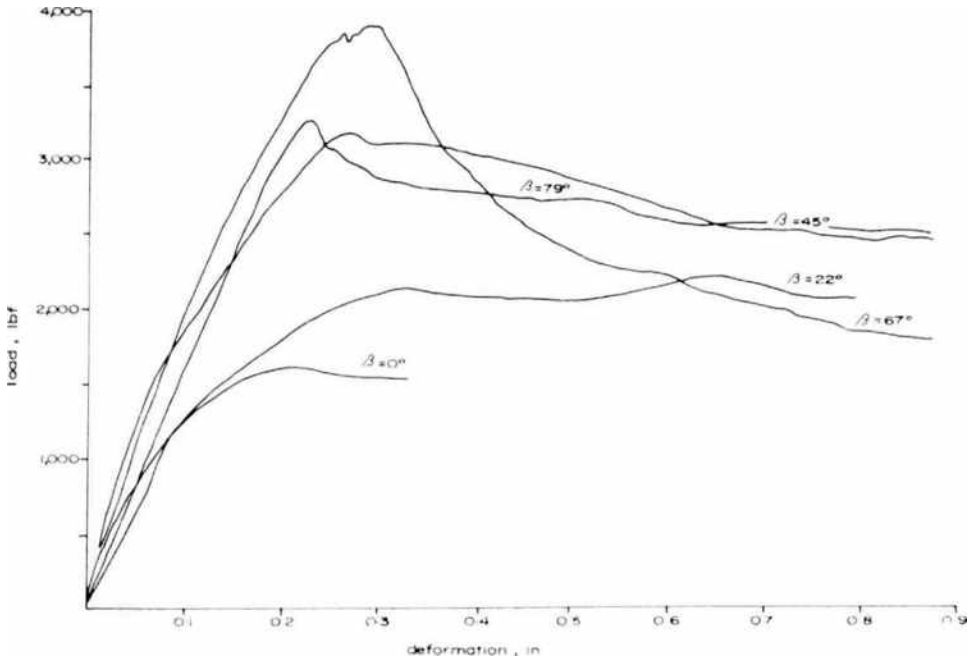

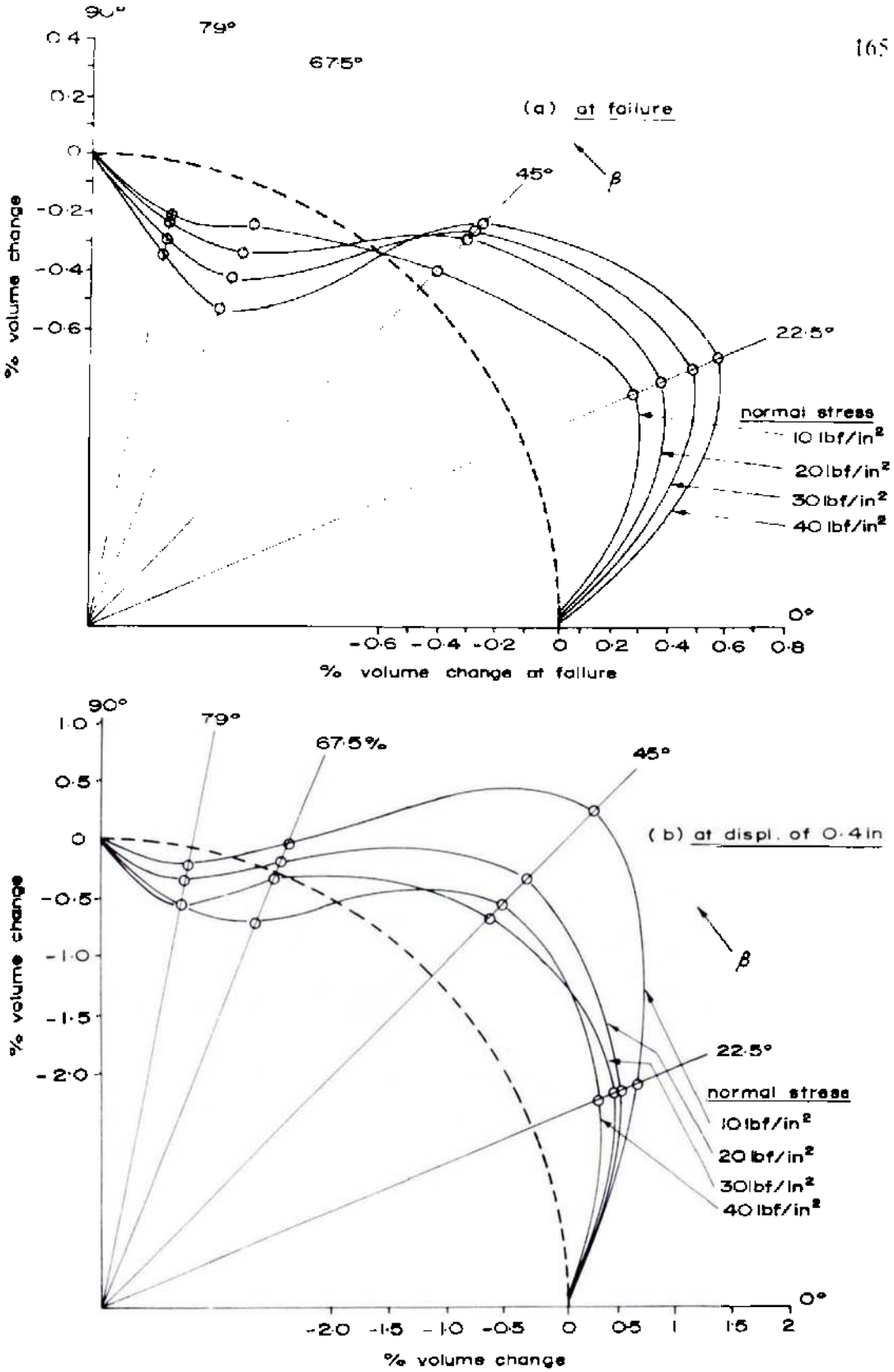

Fig. 10-142. Volumetric changes in shear as a function of β (after WALKER, 1971).

◀ Fig. 10-141. Load-displacement curves for different values of β at normal pressure of 40 lbf/in^2 (after WALKER, 1971).

10.8. Fracture of Jointed Rock in Multiaxial Compression

Quite a number of investigations have been done in the last few years under biaxial and triaxial loading conditions to determine the behaviour of jointed rocks. All these studies have been made on model materials because they are easier to cast in any desired shape and the testing can be done in lower capacity equipment since the strength of the model materials can be changed as desired. The results of these investigations are given below.

10.8.1. Biaxial Conditions

MÜLLER and PACHER (1965) carried out tests on models of size 70 cm × 70 cm × 30 cm (27.6 in × 27.6 in × 11.8 in) with one set of joints loaded biaxially by a pair of hydraulic jacks. The angle ϕ between the plane of the joint set and the direction of the greatest principal stress was varied from 0 to 60 in steps of 0 , 15 , 30 , 45 , 60 . Tests were also conducted with discontinuous joints of different "degree of separation" $\chi_e = 0,\ 1/3,\ 2/3,\ 1$ at different ratios of the principal stresses $p_3/p_1 = n = 3,\ 5,\ 10,\ \infty$. The results obtained by them are given in Fig. 10-143. The upper half of the curve refers to the strength for different values of n and $\chi_e = 1$ (first quadrant) and $\chi_e < 1$ (second quadrant). The lower half refers to the deformation measured in the centre of the test body. It is clear that the angle ϕ, as in the case of uniaxial shear strength, has a great influence on the strength of the jointed mass. The strength falls very rapidly as ϕ increases from 0 and reaches a minimum at $\phi = 30$. For $\phi > 60$ the presence of these joints has almost no influence and the strength is that of the unjointed mass. At $\phi = 30$, ($\chi_e = 1$, $n = \infty$) the strength of the jointed mass almost falls to 10 to 20% of the unjointed mass. For $n = 3$, the strength remains almost constant equal to that of the unjointed mass.

It is also seen that the degree of jointing (χ_e) has an important influence on the failure strength and that its influence is a function of the angle ϕ and n.

According to them, the experimental results can be represented by the "method of resistance quotient" (JOHN, 1962). The comparison of the theoretical and experimental results is given in Fig. 10-144. The difference between the theoretical and experimental results lies merely in the fact that the maxima for the theoretically calculated results lies at $\phi = 28$ while for the actual tests it lies between 22 and 30 . They also compared the results obtained by DONATH (1963) which are represented in Fig. 10.144c which support the calculation technique of "method of resistance quotient".

Results obtained by MULLER and PACHER (1965) show that for a single set of joints, the mode of failure under biaxial conditions is dependent upon $n = (p_3/p_1)$, i.e. the ratio between the principal stresses, and the orientation

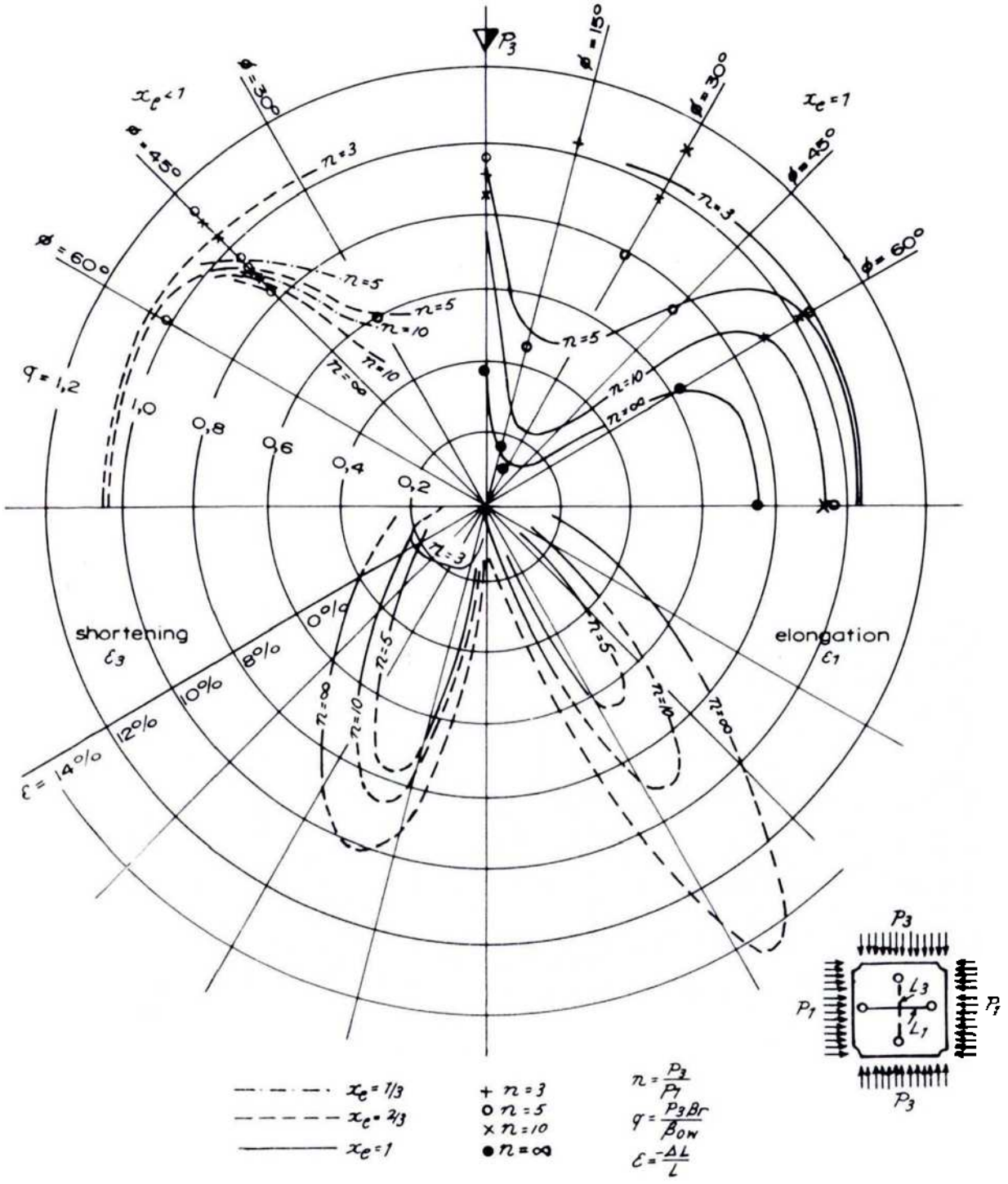

Fig. 10-143. Test results; reduction of strength (above) and deformation in the direction of principal stresses (below) versus angle Φ (after MÜLLER and PACHER, 1965).

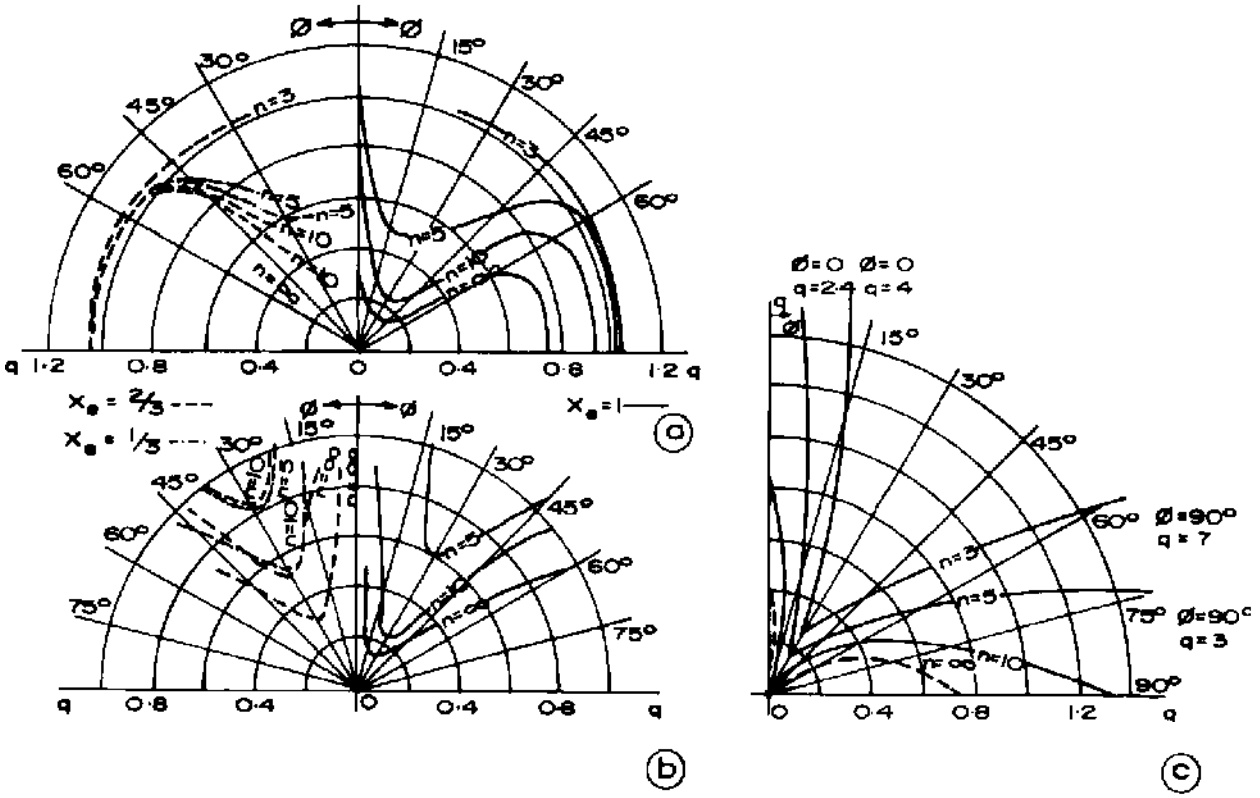

Fig. 10-144. Comparison of the test results (a) with the results of analysis by the method of resistance quotient, according to MÜLLER and PACHER (b) and with the results of the tests on slates according to DONATH (c) Suppositions for calculation to (b): $\rho = 35$; $c_0 = 0{,}4; 0{,}9; 1{,}5; 2{,}1$; belonging to $\chi_c = 1; 2/3; 1/3; 0$; $n = p_3/p_1$; $q = p_3\ Br/\beta DW$; $p_3\ Br$ = principal load p_3 at failure, βDW = uniaxial compression strength, tested on cubes, and compression strength resp., normal to the planes of schistosity (DONATH), tested on cylindrical prisms under confining pressure; recalculated for cubes (after MÜLLER and PACHER, 1965).

of the joints ϕ with respect to the maximum stress direction. For lower values of n and ϕ, failure occurs involving joints alone and is associated with slip. For higher values of n, the failure changes from that taking place partially through the material and partially through the joints to that which fully takes place through the material (Fig. 10-145).

JOHN (1969) carried out biaxial tests on jointed models with both continuous and intermittent joint sets. The test bodies were prepared out of prisms 40 mm × 40 mm × 120 mm (1.53 in × 1.53 in × 4.60 in) and the size of the test bodies was 80 cm × 40 cm (31.5 in × 15.7 in). He found that failure occurs due to slippage along the joint sets having a lower angle of friction which may be considered as the "critical sliding plane" and accordingly, the critical load stress conditions for the various joint groups can be superimposed in the form

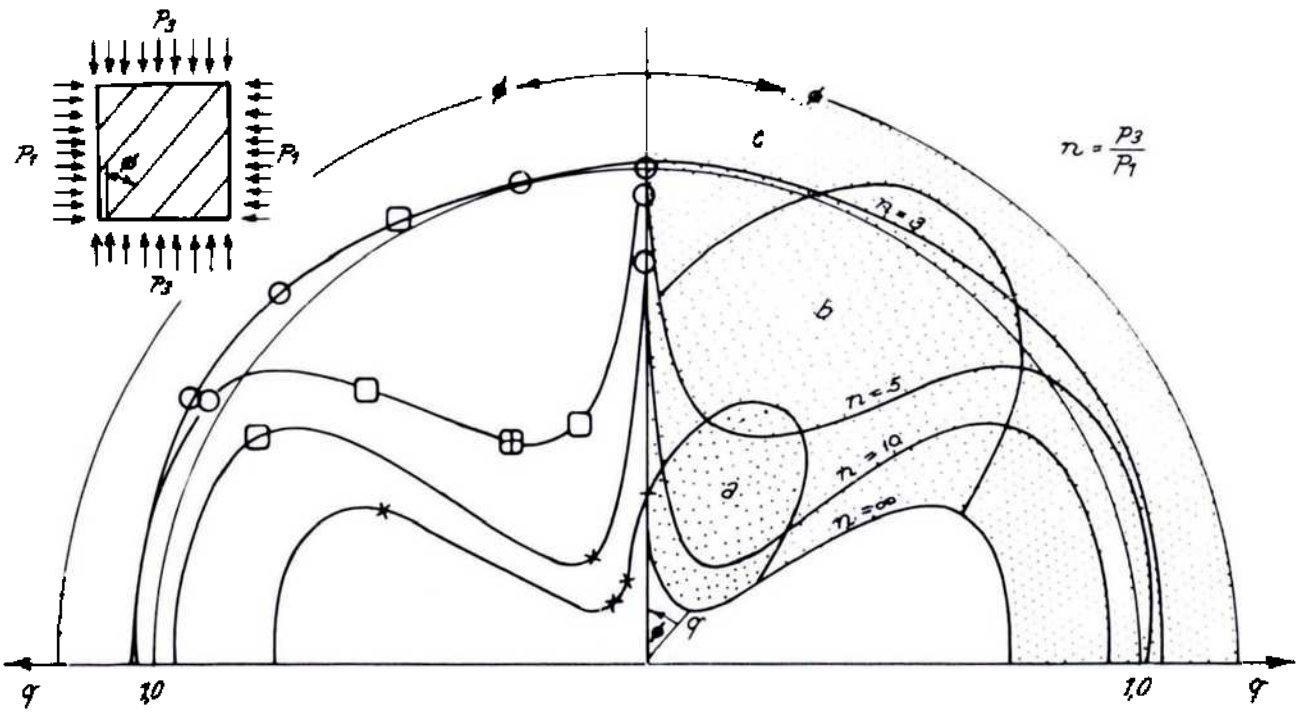

Fig. 10-145. Parameters which determine the gross strength of the anisotropic mass. Types of fracturing at $\chi_e = 1$ (left): + rupture involving joints; □ combined rupture; ○ rupture through the solid. Decisive strength parameters (right): *a* friction on joints, *b* bonding strength; *c* strength of the rock substance (after MÜLLER and PACHER, 1965).

of a polar diagram (Fig. 10-17) obtained from the theoretical relationships (Eqs. 10.34 and 10.35). In the case of discontinuous jointed system, the only change required is to introduce the different values of k (Eq. 10.34), replacing it by

$$k' = (1 - \chi_e)\tau_t + k \tag{10.68}$$

where k = cohesion of continuous joint (Eq. 10.34)

χ_e = degree of continuity of the joint such that $(1 - \chi_e)$ represents the the degree of rock bridging. For a continuous joint $\chi_e = 1$.

τ_t = shear strength of the solid rock.

The influence of the bridging (χ_e) is to raise the envelope up (Fig. 10-146). The influence of the two joints at the points where the locii of the equilibrium conditions meet (intersection of the two locii) signifies the concurrence of joint slippage. There is also the occurrence of "fresh fracturing" and the net effect is to disturb this region with the equilibrium curve taking a curvature (shown dotted in Fig. 10-147).

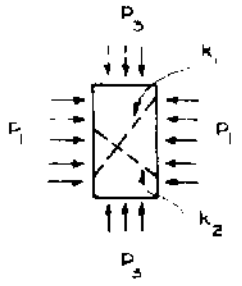

test case	joint k_1		joint k_2	
	χ	ϕ	χ	ϕ
——— I	1·0	40	} 10	40
····· II	1·0	25		
– – – – III	0·5	40		

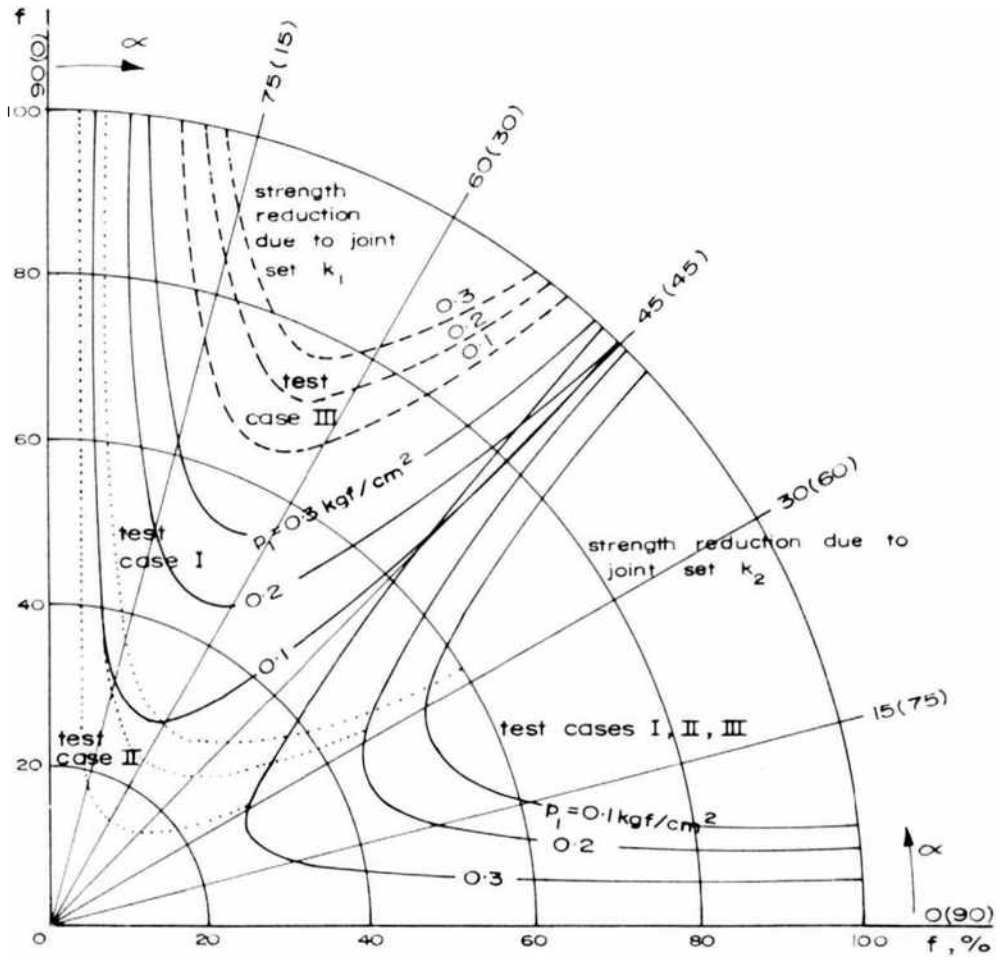

Fig. 10-146. Strength reduction as a function of Φ, α and χ

$$f = \frac{p_{3s}}{p_{3c}} \times 100$$

where p_{3s} is the strength of the system at p_1 lateral pressure; p_{3c} is the strength of the element at p_1 lateral pressure (after JOHN, 1969).

JOHN (1969) recognised three modes of failure:

1. Sliding along joints in which case the limiting stress ratio, n, depends solely upon the orientation and frictional properties of the joint.

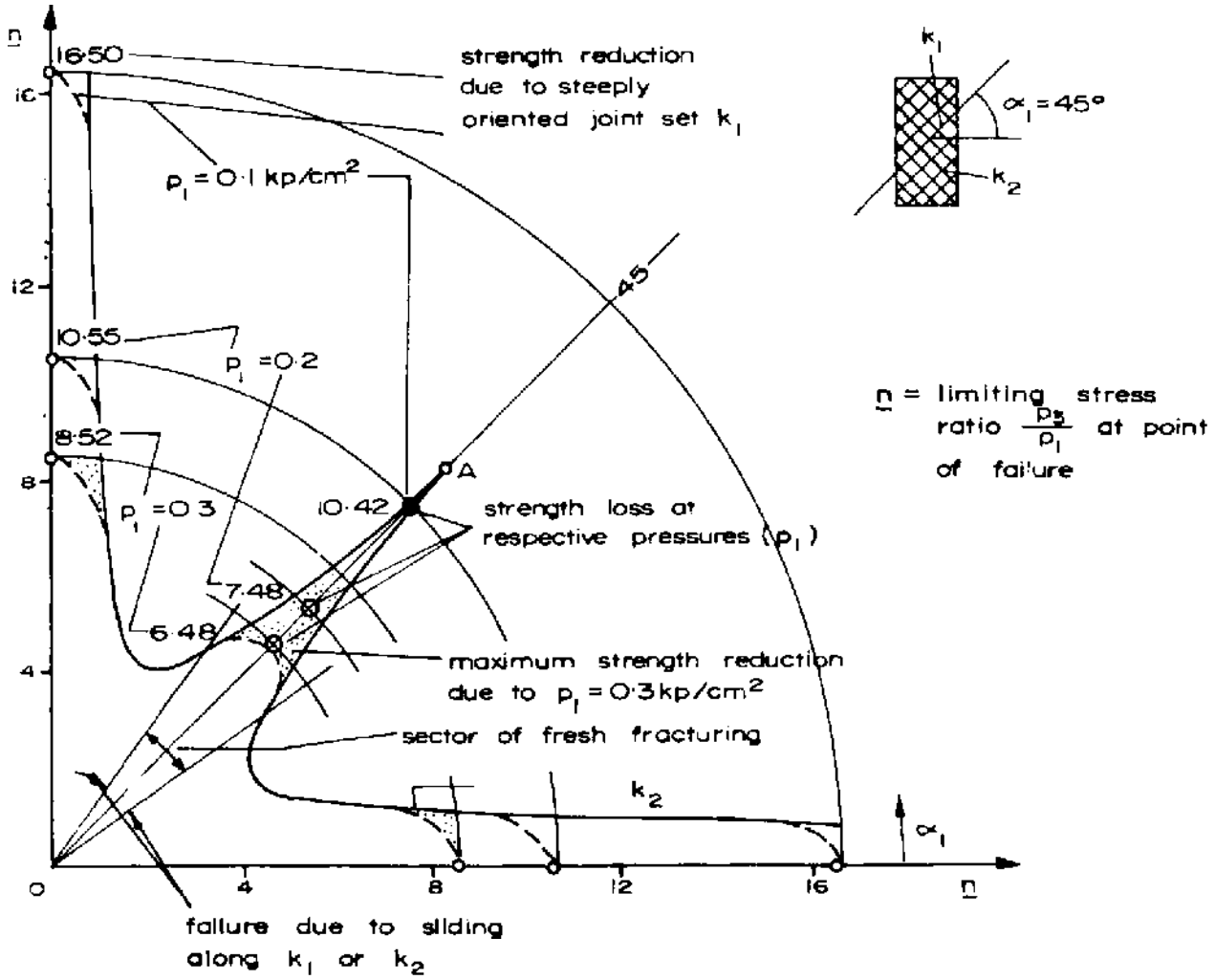

Fig. 10-147. Strength reduction caused by fresh fracturing in a system containing fully traversing joint sets k_1 and k_2 (after JOHN, 1969).

2. Shear through the rock material in which case the limiting stress ratio, n, depends upon the shear strength of an element and the confining pressure.
3. Shear partially through the rock material and partially through the joint which is a combination of the above two modes.

LADANYI and ARCHAMBAULT (1972) have found a similar fracture behaviour termed by them as slippage along a shear plane, shear zone including fracturing and shearing along a number of planes and kink bands depending upon the orientation of the joint plane with the principal stress direction and horizontal stress. More recent tests at the University of Karlsruhe by MÜLLER, FECKER and LAMA in a servo-controlled biaxial machine found that at higher values of n, large scale dilation occurs while at low values, failure occurs along a limited or a single shear plane.

10.8.2. Triaxial Conditions

PRICE (1958) tested Pennant sandstone by compressing it in two directions. Effect of confining pressure on rise in strength of specimens compressed parallel to the bedding planes is more pronounced than when compressed perpendicular to the bedding plane.

DONATH (1963) reported the effect of confinement on the ultimate strength of anisotropic rock —Martinsburg slate (Fig. 10-148). The effect is pronounced both at low and high confining pressures. The specimens compressed perpendicular to cleavage sustained the greatest differential stress and those compressed at an angle of 30 to cleavage showed the lowest strength. At high confining pressures, strength parallel to foliation is nearly equal to that of 90 orientation.

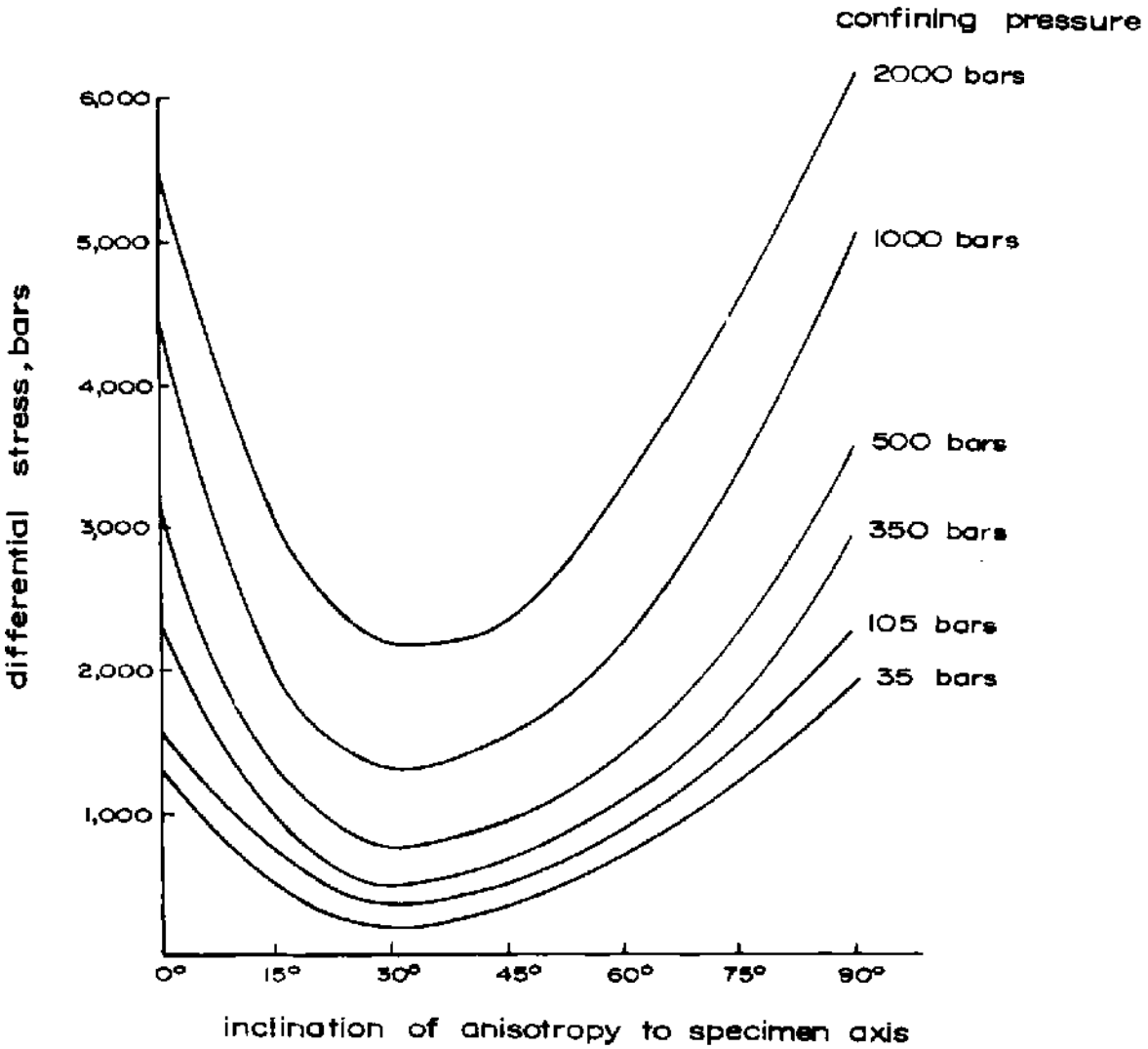

Fig. 10-148. Ultimate strength versus inclination of cleavage. Martinsburg slate (after DONATH, 1963).

The curves of differential stress vs. anisotropy are shifted upwards with increased confining pressure, the amount of shift being proportional to the increase in pressure. The effect of orientation on increase in differential stress is given in Fig. 10-149.

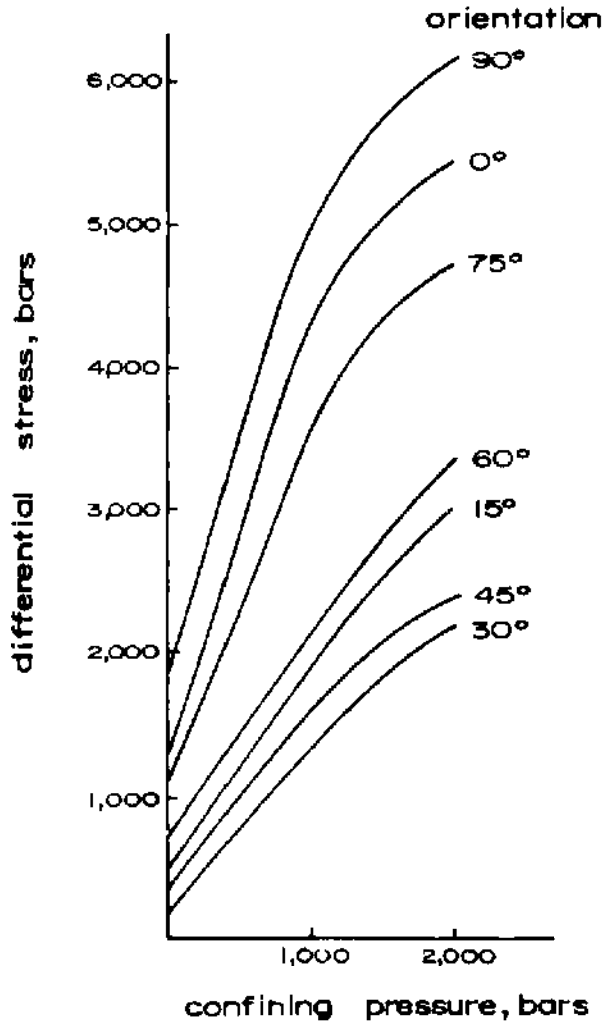

Fig. 10-149. Ultimate strength versus confining pressure, Martinsburg slate (after DONATH, 1963).

LANE and HECK (1964) tested specimens of Pikes Peak granite using 5.4 cm (2 1/8 in) diameter specimens (NX size) and of length 2 to $2^1/_2$ times the diameter. The specimens were tested after saturating with water for 3 days and then air drying just before testing. The rock consists of large crystals of orthoclase and microcline feldspar with an abundance of quartz crystals and lesser amounts of biotite and hornblende. The rock has little lineation or fabric structure and joints tend to be planar with varying degrees of roughness.

The procedure adopted by them is as follows: Specimens with pre-established failure plane at a joint, bedding, or other defects, are subjected to triaxial tests. After the specimens start failing under a first confining pressure (σ_{3-1}) the pressure is varied to the next higher stage and again the specimen is loaded until failure starts again. The confining pressure is raised once again to the next higher stage (σ_{3-3}) and the core loaded again to failure. MOHR's envelopes are constructed as shown in Fig. 10-150. Using a stage in this figure as an example, MOHR circle is drawn on the diameter A-B so that the coordinates of point A represent stress conditions on the minor principal plane (σ_3 and τ_3) and likewise the coordinates of the point B represent conditions on the major principal plane (σ_1 and τ_1), both τ_3 and τ_1 being zero on the principal plane. The line AC is then drawn parallel to the joint planes to intersect the circle at point C the coordinates of which give the stresses (σ and τ) on the joint plane. The MOHR's envelope is drawn as the average of the results similarly obtained for each MOHR circle (points 1 4) with its inclination considered as the joint friction angle.

They found that the inclination of MOHR's envelope is different for different joints (Fig. 10-151). The highest envelope represents tests on intact cores, the lowest from tests on open joints. Similar results were obtained from tests on quartz monzonite.

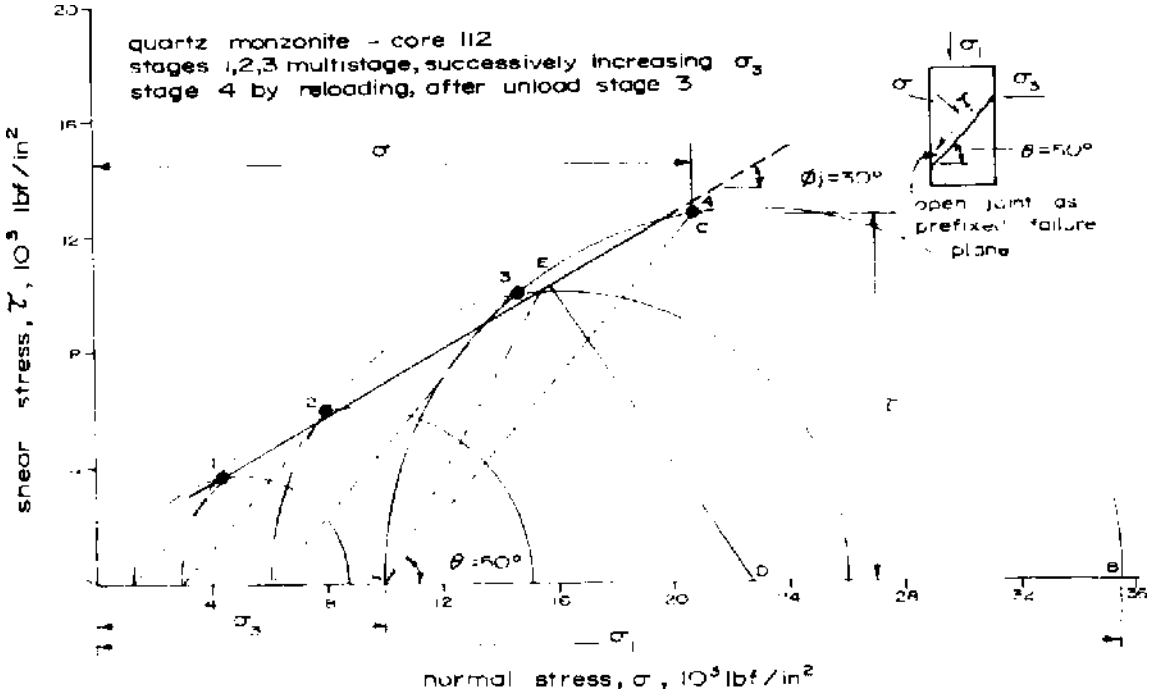

Fig. 10-150. Typical MOHR's circles (after LANE and HECK, 1964).

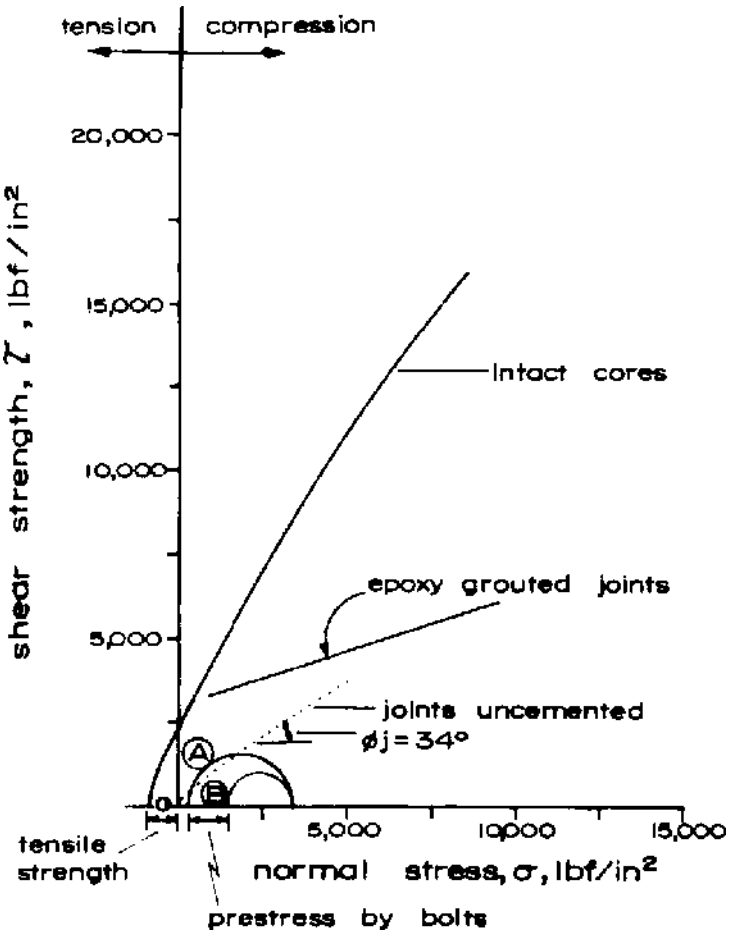

Fig. 10-151. Norad granite-Coarse grained (after LANE and HECK, 1964).

EVANS and POMEROY (1966) reported that strength of coal is dependent upon the direction of loading at small confining pressures (Fig. 10-152) but at higher confining pressures [above 13.8 MPa (2000 lbf/in^2)] the strength is independent of orientation.

Triaxial compression tests were conducted by YOUASH (1966) on a shale, a gneiss, and two sandstones under 0.1, 10.3, 20.7 and 31.0 MPa (15, 1500, 3000 and 4500 lbf/in^2) confining pressures. Cores 5.4 cm by 10.8 cm (2 1/8 in by 4$^1/_4$ in) were prepared with the layers dipping at 0 , 15 , 30 , 45 , 60 , 75 and 90 to the short cylinder axis. Plots of stress difference versus inclination of layering are concave upward with the maximum stress difference for 0 and 90 cores and the minimum for 45 and 60 core orientation (Figs. 10.153 to 10-156).

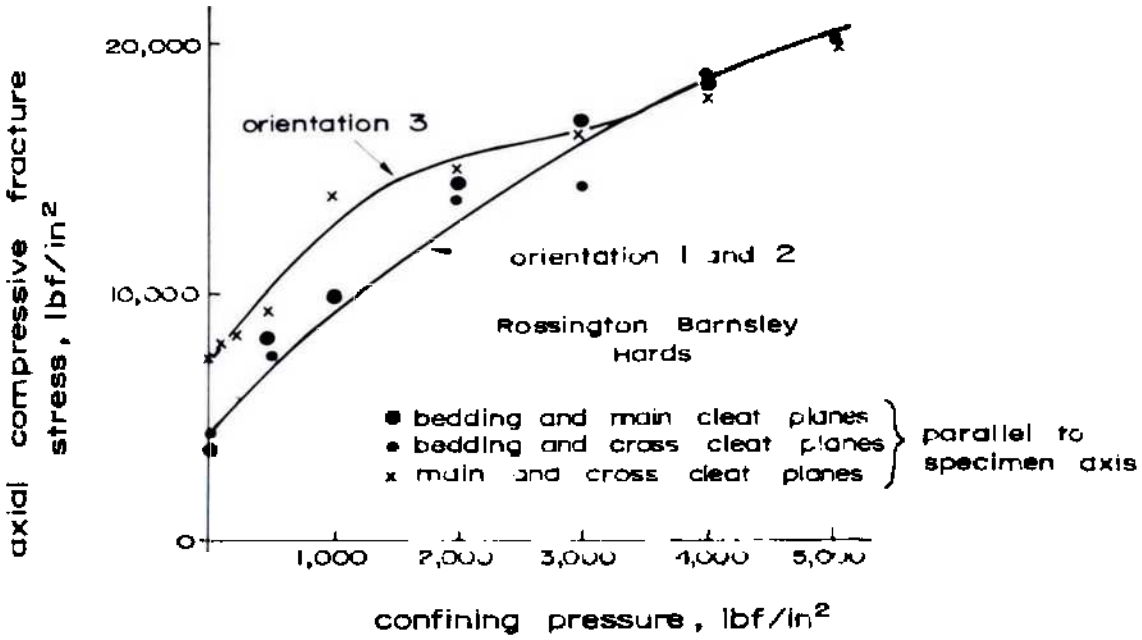

Fig. 10-152. Variation of axial compressive fracture stress with confining pressure for different specimen orientations (after EVANS and POMEROY, 1966).

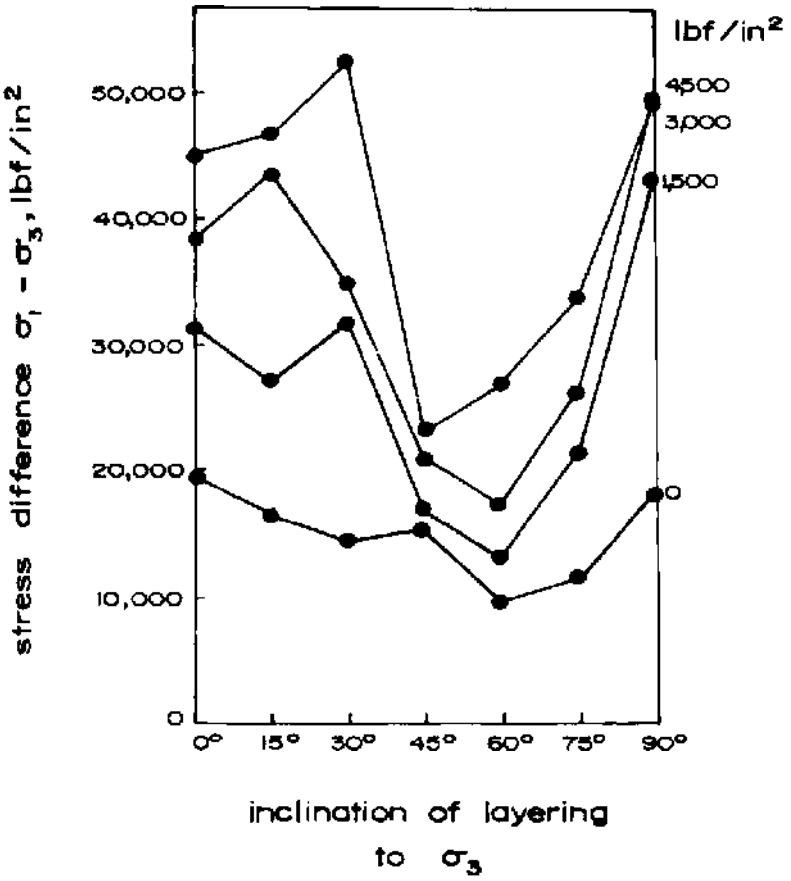

Fig. 10-153. Stress difference versus inclination of layering to minimum principal stress σ_3 for sandstone of Lyons Formation (after YOUASH, 1966).

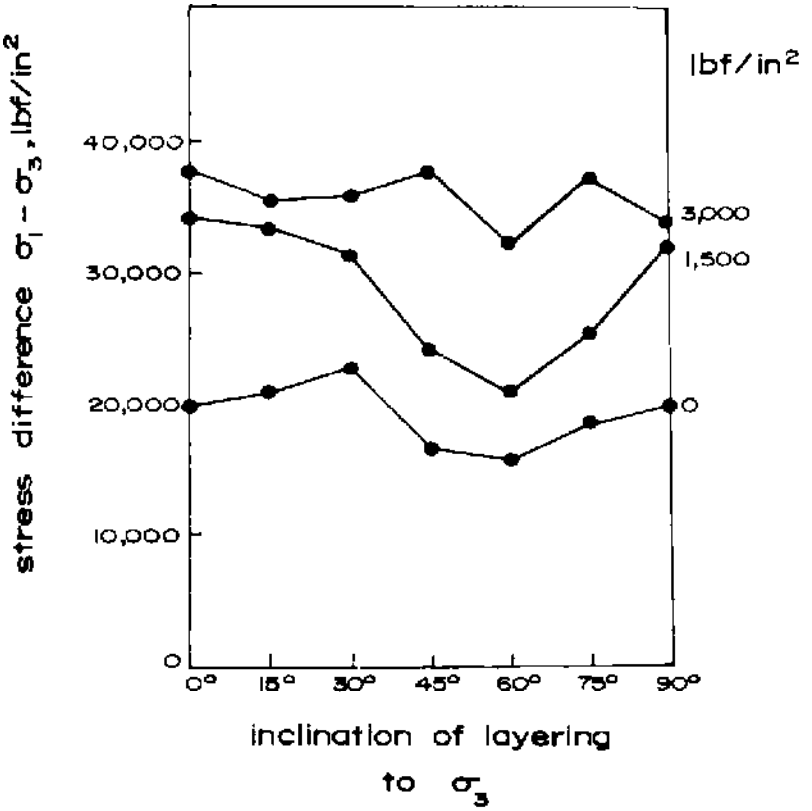

Fig. 10-154. Stress difference versus inclination of layering to minimum principal stress σ_3 for shale of Green River Formation (after YOUASH, 1966).

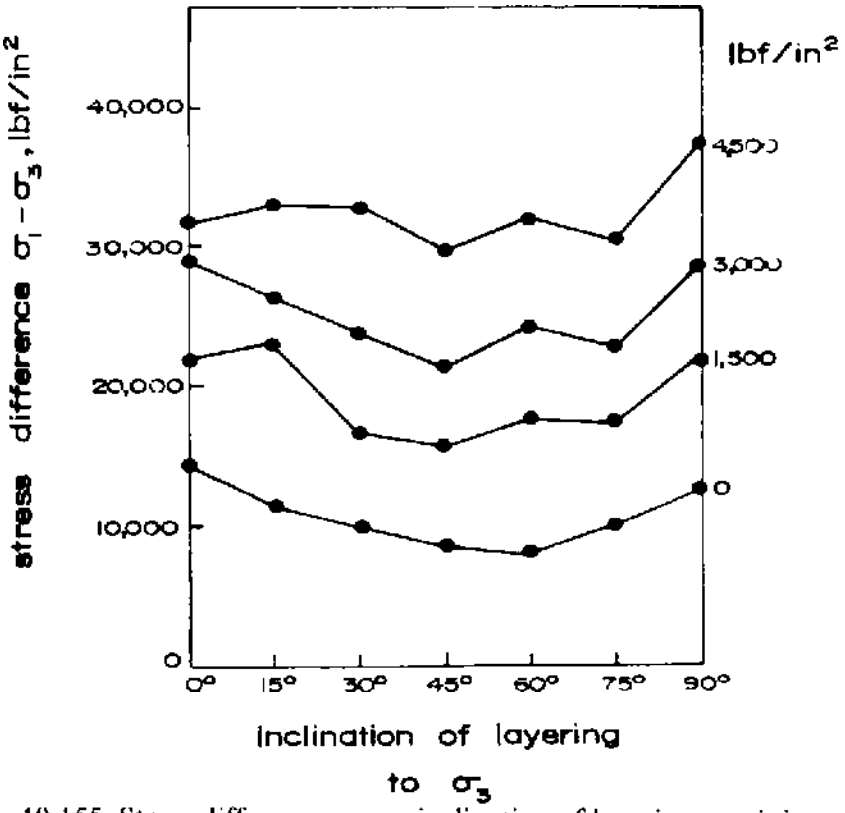

Fig. 10-155. Stress difference versus inclination of layering to minimum principal stress σ_3 for sandstone of Sunnyside Member (after YOUASH, 1966).

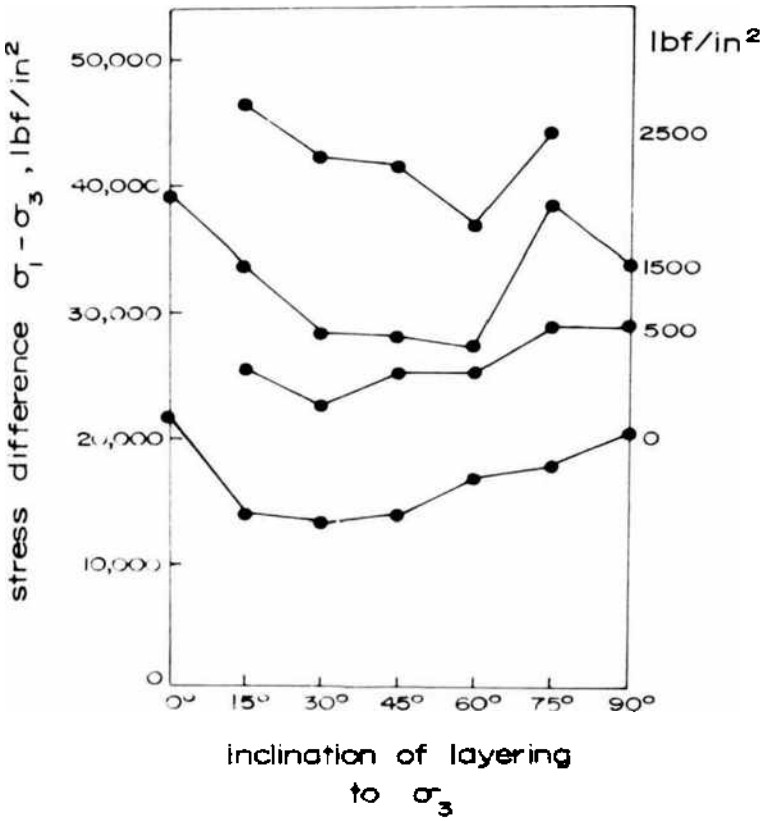

Fig. 10-156. Stress difference versus inclination of layering to minimum principal stress σ_3 for gneiss of Idaho Springs Formation (after YOUASH, 1966).

EINSTEIN et al (1969) investigated the influence of multiple joints on the strength of specimens using gypsum plaster as a model material. The test specimens were of size 10.16 cm × 10.16 cm × 20.32 cm (4 in × 4 in × 8 in) prepared with different sets of parallel, perpendicular and orthogonal joints (Fig. 10-157). He found that for a given normal stress, the shear stress sustained by the model with orthogonal joints was the lowest followed by the horizontal joints and vertical joints and in all the cases, the shear envelopes are lower than the unjointed rock though the failure occurs through the intact material and not by sliding along the joint surfaces (Fig. 10-158). At higher values of the normal stress, the shear stress envelopes converge but still lie below the unjointed model. Also, for each joint configuration, there is a systematic strength decrease with decreasing joint spacing.

The confining stress at which the transition from brittle behaviour (straight line portion of the stress—displacement curve with a sharp drop in stress beyond the peak) to ductile behaviour takes place (more curved stress – displacement relationship and continued plastic yielding at peak stress) is largest for the intact material, smaller for the vertically jointed material, still smaller for the horizontally jointed material and smallest for the orthogonally

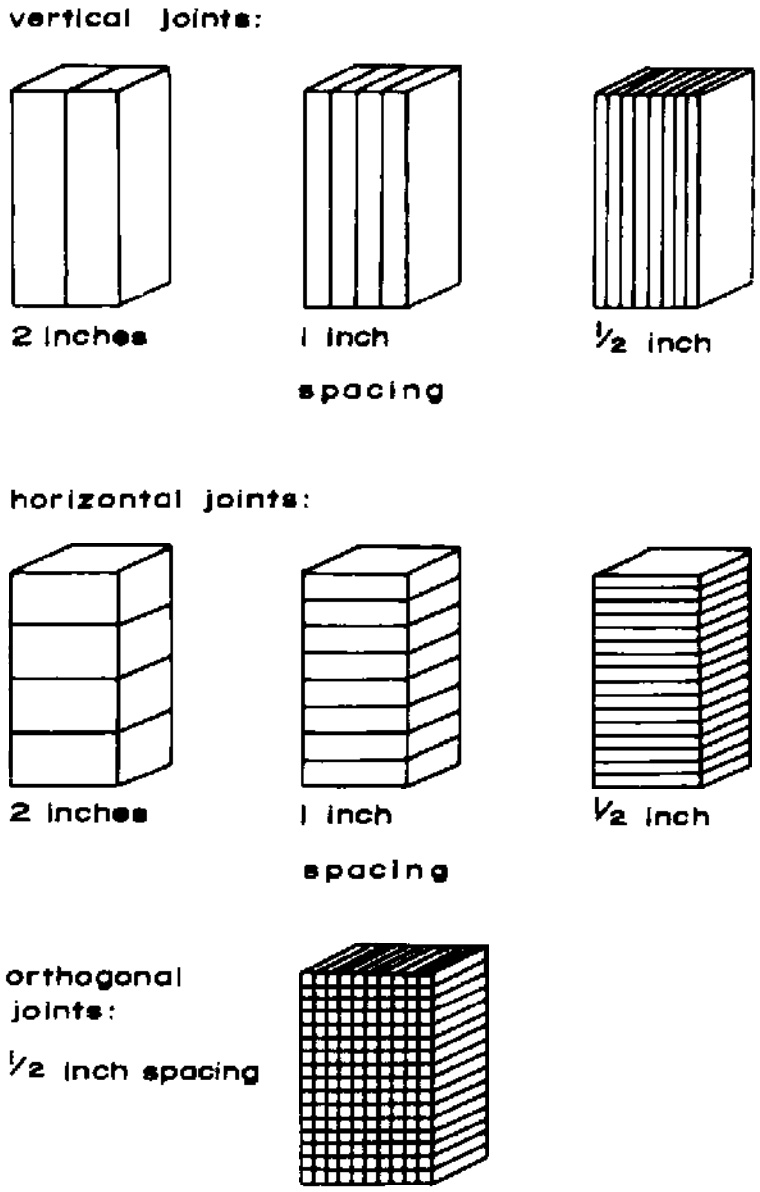

Fig. 10-157. Joint configurations (after EINSTEIN et al. 1969).

jointed material (Fig. 10-159). This transition stress systematically increases with increasing joint spacing for the vertically and horizontally jointed specimens (Fig. 10-160).

BROWN and TROLLOPE (1970) conducted tests in a triaxial cell for the strength of specimens prepared out of an assembly of 2.54 cm (1 in) cubes of plaster with varying degrees of joint orientation and under different confining pressures. They found that at lower confining pressures, the strength of the jointed specimens was lower than those of corresponding unjointed specimens. The lowest values obtained were for the specimens having joint inclination 30°/120°

with the major principal stress. The strength values for the various specimens were represented by them in the form of a power law as follows:

$$\frac{\tau - \tau_0}{\sigma_c} = Z\left(\frac{\sigma_n}{\sigma_c}\right)^{\xi}$$

and

$$Z = Z'\,\sigma_c^{(\xi - 1)} \qquad (10.69)$$

where ξ, Z and Z' are constants and their values are dependent upon the inclination of the joints with respect to the greatest principal stress (Table 19),

τ_0 and σ_c are the shear strength and uniaxial compressive strength of the material, and

τ is the shear strength of the jointed mass.

TABLE 19 Values of shear strength parameters

(after BROWN and TROLLOPE, 1970)

Specimen type	τ_0, lbf/in^2	Z'	Z	ξ
Unjointed	450	39	0.71	0.50
0 /90		66	0.94	0.47
15 /75		6.3	0.85	0.75
30 /60		0.84	0.84	1.00
45 /45		2.54	0.83	0.86

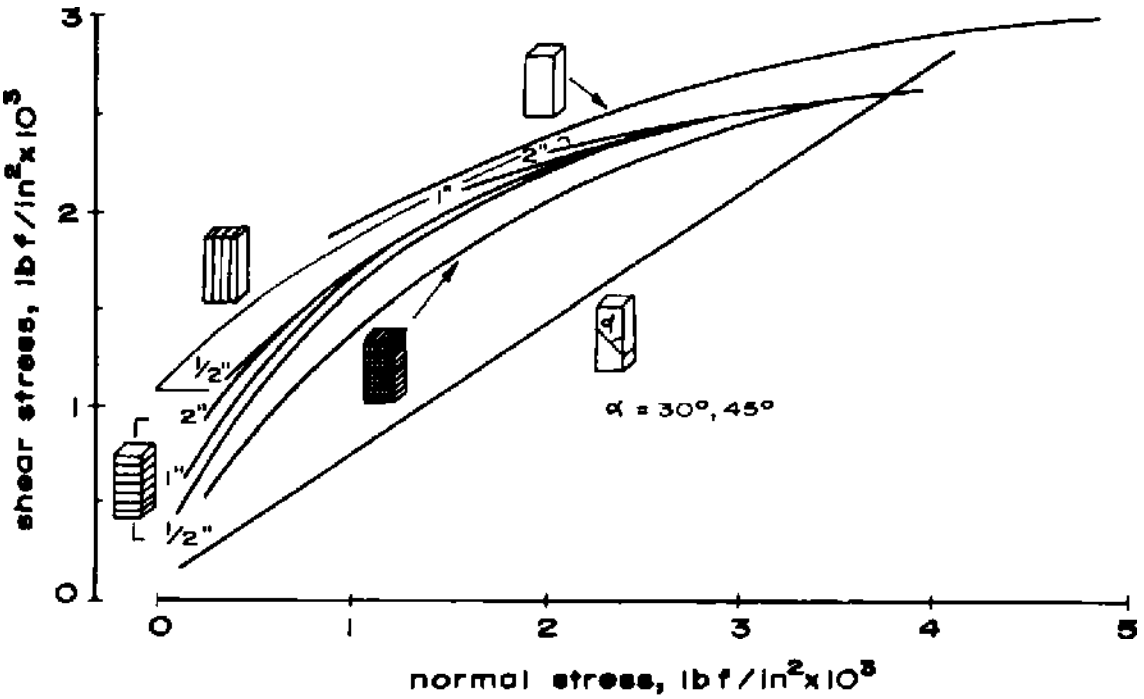

Fig. 10-158. MOHR envelopes for intact and jointed gypsum models (after EINSTEIN et al, 1969).

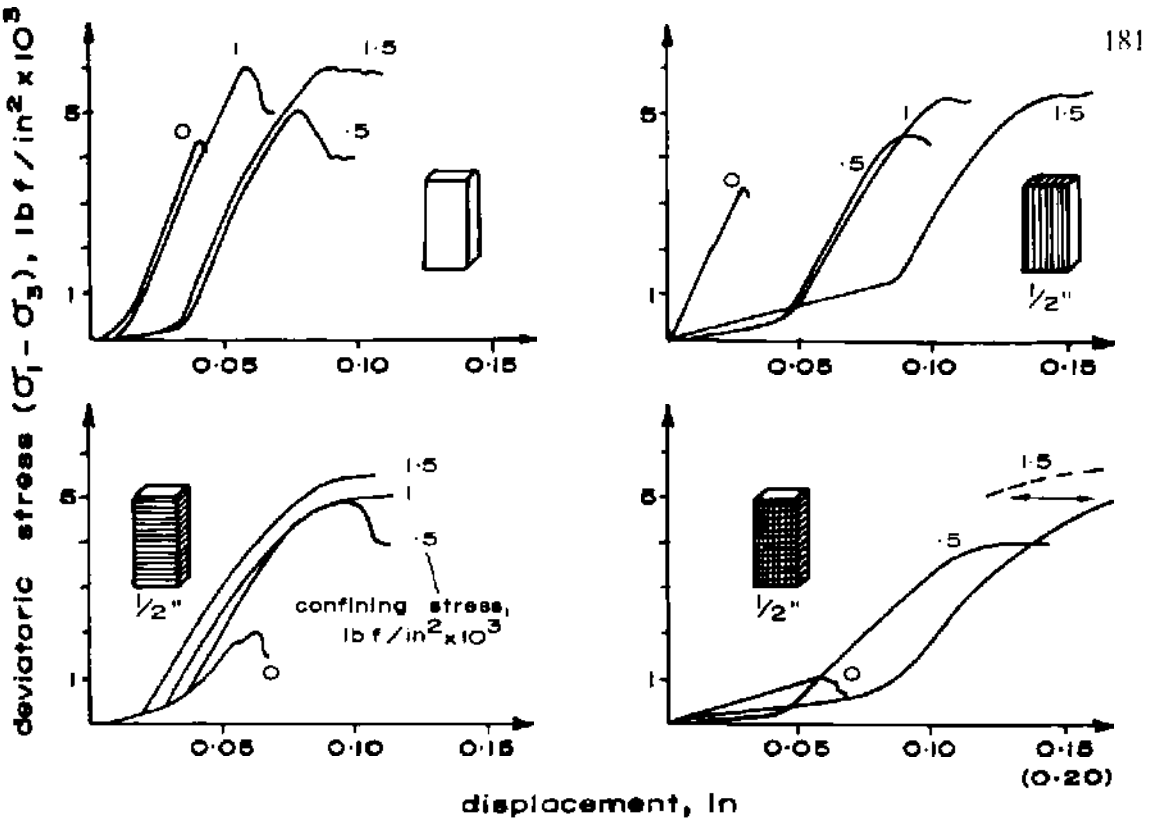

Fig. 10-159. Stress-displacement curves for different joint configurations and confining stresses (after EINSTEIN et al. 1969).

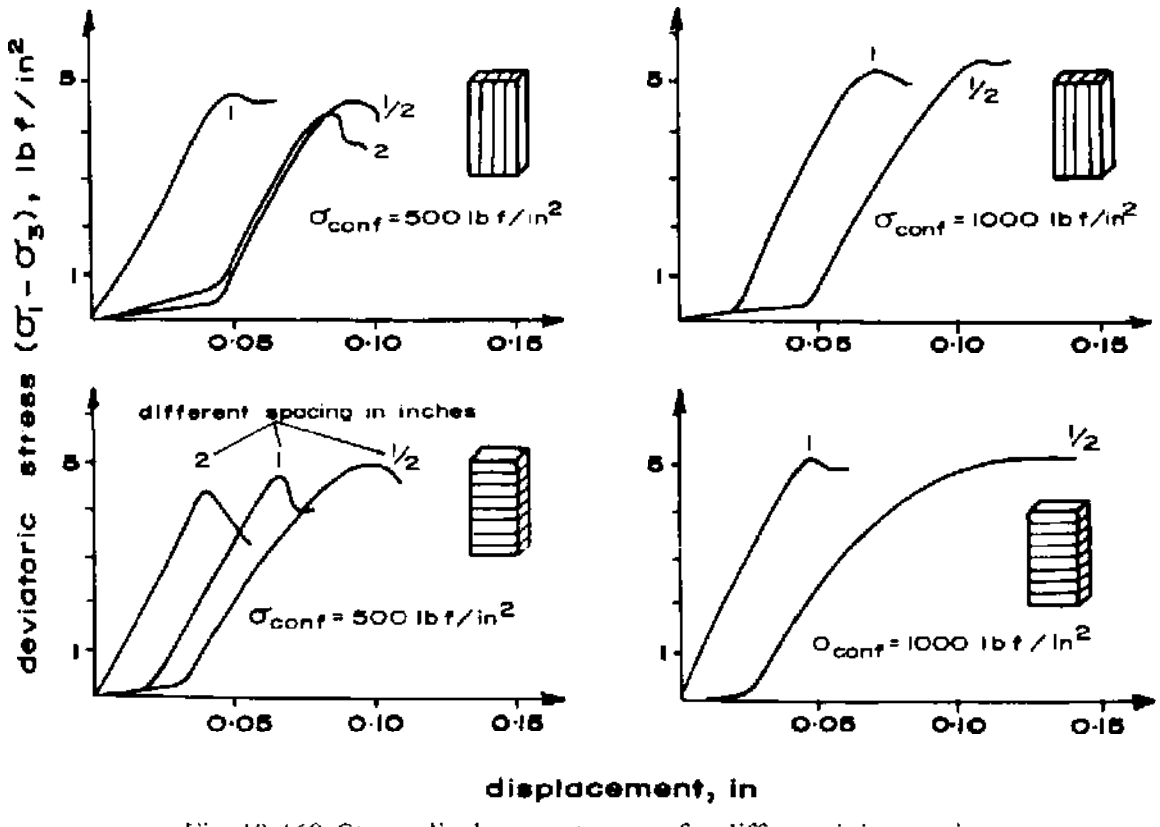

Fig. 10-160. Stress-displacement curves for different joint spacings and confining stresses (after EINSTEIN et al. 1969).

Under similar conditions, the influence of non-continuous joints using parallelopipedal and hexagonal blocks (Fig. 10-161) was investigated by BROWN (1970). He found that the MOHR-COULOMB's concept with certain modifications (making use of the curved envelope—Eq. 10.69) and the increased strength due to bridging can be used to describe the strength of specimens with discontinuous joints. The strength of the jointed models tested by him was represented by the relationship

$$\tau = c\chi_e k_j + (1-\chi_e)\tau_0 + c\chi_e \sigma_n \tan\phi_\mu + (1-\chi_e) Z_0' \sigma \xi_n \qquad (10.70)$$

where the strength of the unjointed specimen is given by

$$\tau = \tau_0 + Z_0' \sigma \xi_n$$

where τ = shear strength of the jointed rock at failure
c = mobilisation factor = 1
k_j = cohesion of joint
χ_e = degree of jointing
τ_0 = cohesion intercept in power law (Eq. 10.69) i.e. shear strength of the material
σ_n = normal stress
ϕ_μ = angle of joint friction
Z_0' = multiplier in strength power law (Eq. 10.69) and
ξ_n = normal stress index (Eq. 10.69).

The results calculated from the Eq. 10.70 and those obtained experimentally are shown in Table 20.

TABLE 20
Comparison of predicted (Eq. 10.70) and measured shear stress at failure of jointed specimens
(after BROWN, 1970)

Specimen	Confining pressure, lbf/in² (MPa)		Shear stress on failure at peak axial stress, lbf/in² (MPa)			
			Calculated		Measured from MOHR's circle plot	
Degree of jointing $\chi = 1/2$	200	(1.38)	860	(5.93)	610	(4.21)
	500	(3.52)	1,310	(9.0)	1,200	(8.27)
	1,000	(7.03)	1,810	(12.5)	1,810	(12.5)
$\chi = 1/3$	200	(1.38)	1,320	(9.1)	1,300	(8.96)
	500	(3.52)	1,610	(11.18)	1,620	(11.17)
	1,000	(7.03)	2,110	(14.6)	2,380	(16.41)
	2,000	(14.07)	2,760	(19.0)	3,220	(22.2)

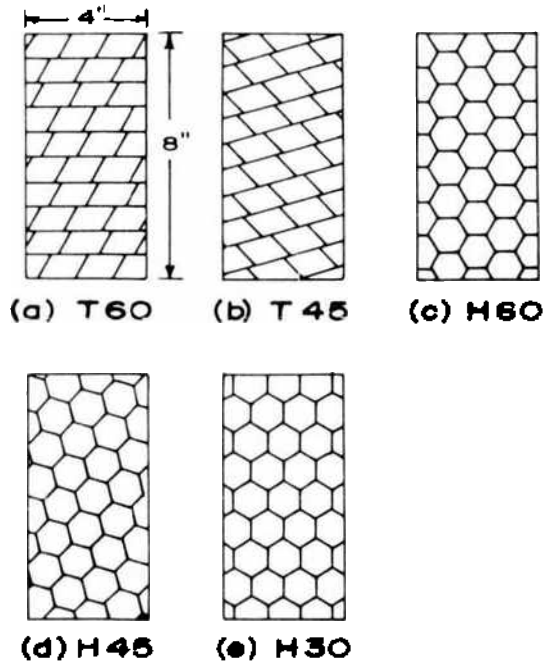

Fig. 10-161. Block-jointed specimen geometry (after BROWN, 1970).

BROWN (1970) pointed out two other types of failure in addition to those recognised by JOHN (1969). He found that besides the three types of failure described in the previous section, at low confining pressures, axial cleavage fractures occur splitting the elements constituting the test body. At low pressures he also observed collapse of the specimens due to block movement and opening of the joints. This type of failure was termed by him dilational failure.

MCGILL and RANEY (1970) conducted 89 tests on cores (3.2 cm (1.25 in) long and 1.2 cm (0.48 in) in diameter) of laminated dolomitic limestone from the Manlius Formation at confining pressures of 0.1, 20, 30, 40, 50, 60 and 80 MPa (14.5, 2901, 4351, 5801, 7252, 8702 and 11,603 lbf/in^2) (1,200, 300, 400, 500, 600 and 800 bars), and with the angle between laminae and maximum principal stress varying from 0 to 90°. In Fig. 10-162, plots of compressive strength versus laminae orientation at different confining pressures are given.

POMEROY, HOBBS and MAHMOUD (1971) studied the effect of weakness-plane orientations on the fracture of Barnsley Hards by triaxial compression. Barnsley Hards is a fairly homogeneous, dull bituminous coal with a volatile content of 36% (dry, ash-free). The bedding planes are well marked and there are two discernible cleat planes, the three families of weaknesses lying in mutually perpendicular directions. The cleats in the dominant direction are known as the main cleats and the less well-defined system as the cross-cleats. Cylinders were cut from the coal at different angles relative to the bedding planes but always with the cross-cleat plane parallel to the axis of the cylinder (the direction of

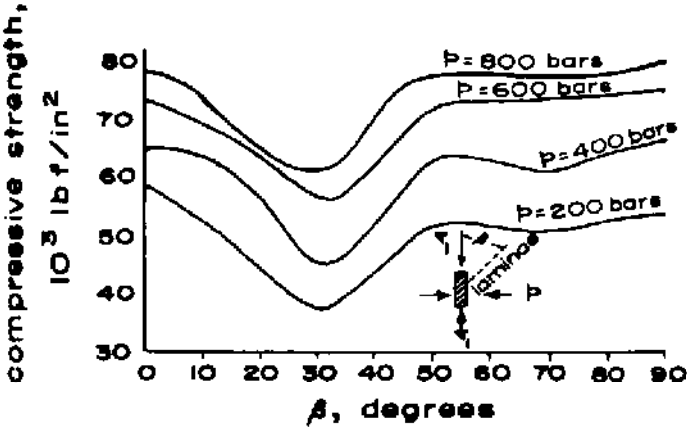

Fig. 10-162. Plots of compressive strength versus laminae orientation at different confining pressures (after McGILL and RANEY, 1970).

axial compression). As both the bedding plane and cross-cleat plane directions are defined by this method of specimen preparation, it follows that the orientation of the main cleat plane is uniquely defined as well.

The weakness-plane orientations are defined by (α, β, γ) where α, β and γ are the orientations to the specimen axis of the bedding planes, the main and the cross-cleat planes respectively, so that in the present experiments $\gamma = 0$ and $\alpha = 90 - \beta$. Cylinders (2.54 cm (1 in) in diameter; 5 cm (2 in) in length) were cut at angles to the bedding plane that differed by 15° intervals.

Graphs of fracture stress against confining pressure and weakness-plane orientations are given in Figs. 10-163 and 10-164.

For all orientations there is an increase in fracture stress with increase in confining pressure, the rate of increase being much the same for all orientations. The strongest orientations are consistently those of (90, 0, 0) and (75, 15, 0), that is the cylinders with the bedding plane perpendicular—or nearly perpendicular—to the applied axial load. The weakest orientation (30, 60, 0) can also be seen to be the same (Fig. 10-164) for each confining pressure.

The equation $\sigma_1 = A\sigma_3^b + \sigma_c$ was fitted to the results for each orientation. A and b are constants, σ_c the uniaxial compressive strength and σ_1 the fracture strength at a confining pressure σ_3. A plot of $(\sigma_1 - \sigma_c)$ against σ_3 on log-log scales gave the values of A and b listed in Table 21.

The ratios of the values of fracture strength for the orientation (90, 0, 0)/(30, 60, 0) and (90, 0, 0)/(0, 90, 0) are given in Table 22. These show that the effect of the bedding planes is greater than that of the cleat planes, the difference being particularly marked for uniaxial loading but persisting fairly constantly throughout the range of confining pressures used. The strength anisotropy is thus less marked when the specimens are subjected to triaxial loading, but differences do exist, even at the highest confining pressures used.

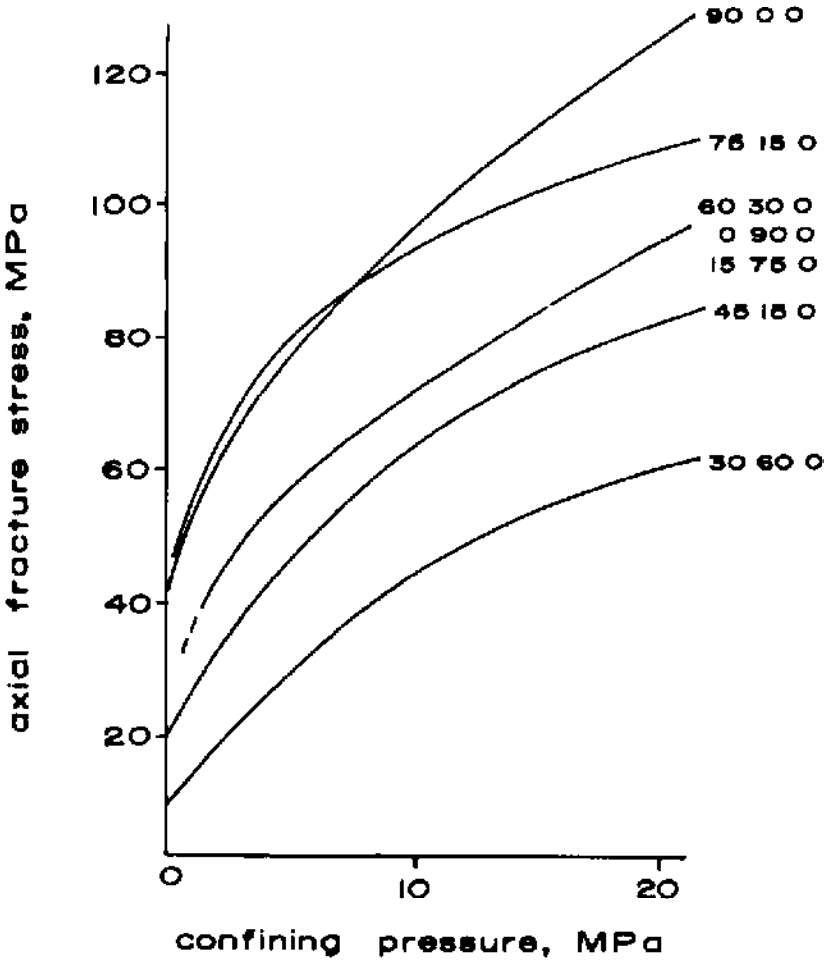

Fig. 10-163. Relationships between fracture stress and confining pressure for different weakness-plane orientations (after POMEROY et al, 1971).

TABLE 21

Values of A and b to satisfy $\sigma_1 = A\,\sigma_3{}^b + \sigma_c$

(after POMEROY et al, 1971)

Weakness-plane orientation	A	b
0, 90, 0	18.4	0.5
15, 75, 0	8.3	0.9
30, 60, 0	6.5	0.4
45, 45, 0	8.0	0.6
60, 30, 0	12.6	0.6
75, 15, 0	16.8	0.6
90, 0, 0	10.0	1.0

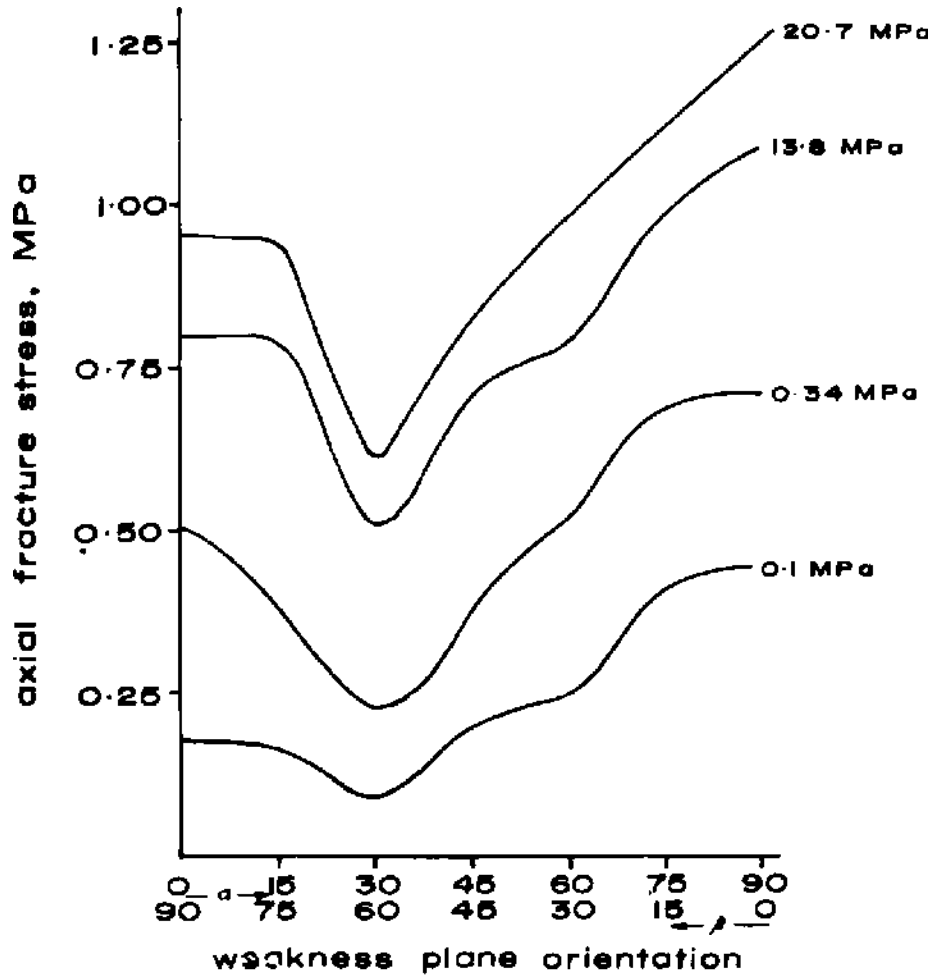

Fig. 10-164. Relationships between fracture stress and weakness-plane orientation for different confining pressures (after POMEROY et al. 1971).

TABLE 22

Fracture strength ratios

(after POMEROY et al. 1971)

Confining pressure MPa (lbf/in^2)	Fracture strength ratio	
	(90, 0, 0)/(30, 60, 0)	(90, 0, 0)/(0, 90, 0)
0.1 (14.5)	5.2	2.5
3.5 (507.6)	3.1	1.4
13.8 (2001.5)	2.1	1.4
20.7 (3002.2)	2.1	1.3

MOTOYAMA and HIRSCHFELD (1971) conducted tests on models using orthogonal and 45 oriented blocks with different joint densities. The model material had a strength of about 980 lbf/in^2 (7 MPa). The elements were accurately prepared (variation in dimensions for the mean value ± 0.15 to 0.6%). Their results are given in Figs. 10-165 and 10-166. Their conclusions are very similar to those drawn by other investigators that the strength of the jointed rock masses may be much more influenced by the joint system within the rock mass at low confining pressures than at high confining pressures. Confining pressure has greater influence on the strength of a model with two sets of joints than with one set of joints. Joint orientation is more important in triaxial conditions than the joint

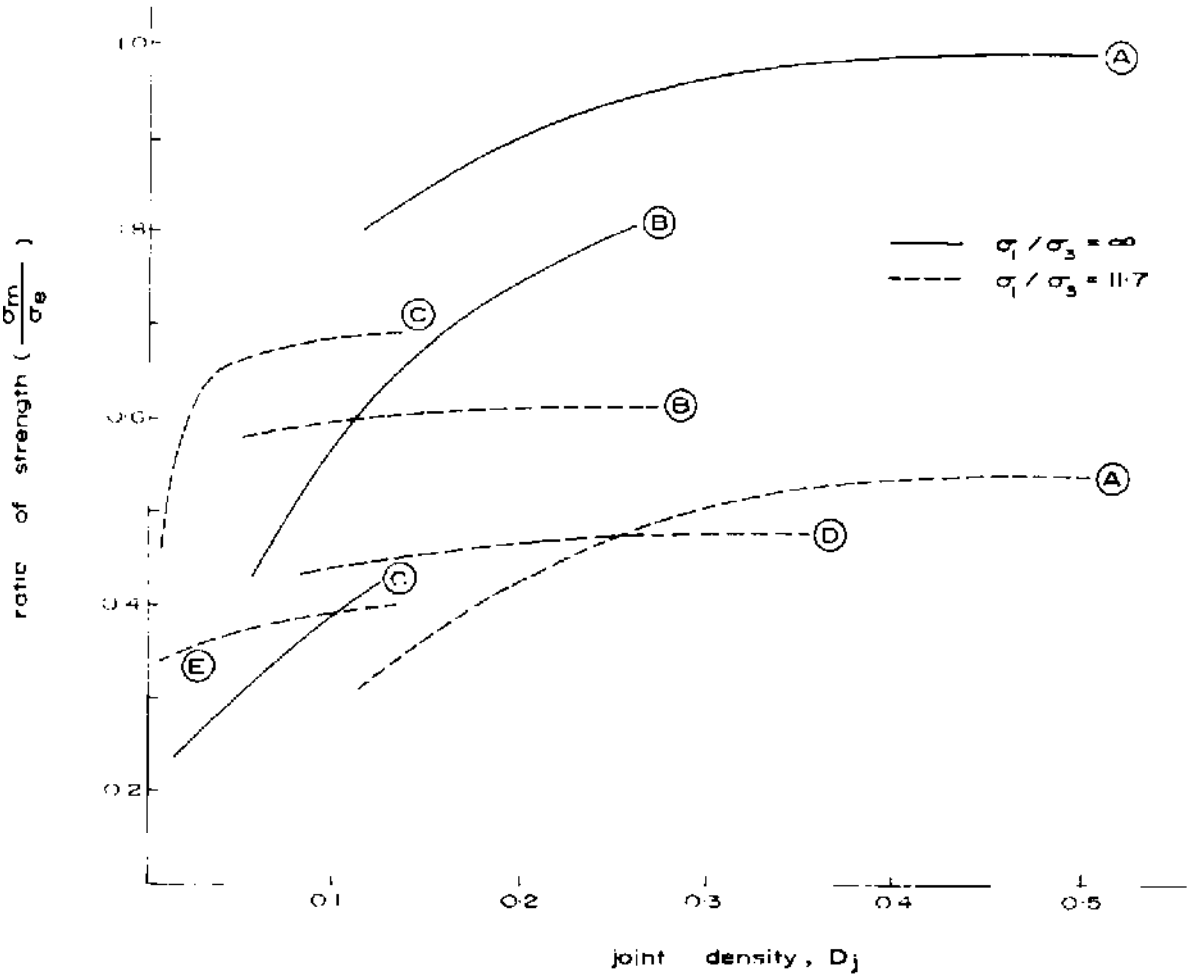

Fig. 10-165. Effect of joint configuration on the strength of jointed models
(A) vertical joints
(B) horizontal joints
(C) multiple orthogonal joints
(D) multiple inclined joints (45°)
(E) orthogonal inclined joints.

Note: Joint density $D_j = \dfrac{\text{volume of element}}{\text{volume of model}}$

(after MOTOYAMA and HIRSCHFELD, 1971).

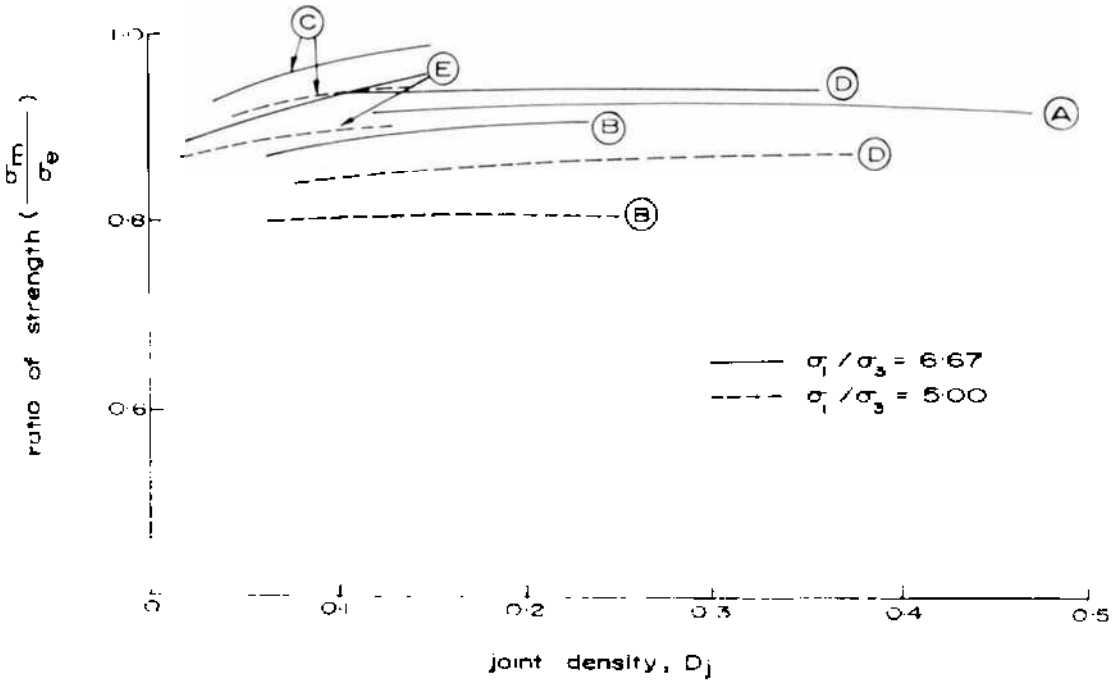

Fig. 10-166. Effect of joint configuration on the strength of jointed models.
(A) vertical joints
(B) horizontal joints
(C) multiple orthogonal joints
(D) multiple inclined joints (45)
(E) orthogonal inclined joints.
Note: Joint density $D_j = \frac{\text{volume of element}}{\text{volume of model}}$
(after MOTOYAMA and HIRSCHFELD, 1971).

density. Their influence tends to be less than 20 % at lateral pressures approaching the uniaxial compressive strength of the material. Even at confining pressures almost twice the uniaxial strength, the jointed model has lower strength than material.

Deformation modulus depends very strongly on joint configuration. It decreases in the order for intact, vertical joint, horizontal joint, orthogonal joint, multiple inclined joint and orthogonal inclined joint at all confining pressures. Increase in joint spacing increases the modulus value and so also confining pressure up to a certain limit.

10.9. Summary and Conclusions

The mechanical behaviour of a rock mass in situ is very complex and in no case can be predicted from tests in the laboratory on smaller intact specimens. The behaviour of a large mass is dependent upon the mechanical behaviour of the rock substance, the presence and absence of joints, the operating stress field and its orientation with respect to the joints and the joint density.

The sliding characteristics of a single joint can be predicted quite satisfactorily by using the Eq. 10.18 developed by LADANYI and ARCHAMBAULT (1969) and the relationship gives quite satisfactory results even with a multiple jointed system. MOHR theory could be successfully applied for practical problems in a multi-jointed system but has limitations at certain critical values of joint orientation where the zones of unstability due to the joint sets intersect or overlap. In this zone, the values obtained by this theory shall be more optimistic.

The frictional properties of a joint are dependent upon the material property as well as on joint roughness, normal stress, displacement history, presence or absence of water and gouge thickness. Angles of friction for some rocks are given in Table 23 (see also Table 30, Volume III).

The phenomenon of stick-slip is dependent upon the normal stress, surface geometry, strain rate and the stiffness of the loading system. The amplitude increases with increased normal stress and decreased loading system stiffness. This could well be the cause of irregular movement of rock mass.

TABLE 23

Approximate friction angles for some rocks (laboratory results)

(after HOEK, 1970)

Rock type	Intact rock (degrees)	Joint (degrees)	Residual (degrees)
Andesite	45	31–35	28–30
Basalt	48–50	47	*
Chalk	*	35–41	*
Diorite	53–55	*	*
Granite	50–64	*	31–35
Graywacke	45–50	*	*
Limestone	30–60	*	33–37
Monzonite	48–65	*	28–32
Porphyry	*	40	30–34
Quartzite	64	44	26–34
Sandstone	45–50	27–38	25–34
Schist	26–70	*	*
Shale	45–64	37	27–32
Siltstone	50	43	*
Slate	45–60	*	24–34

* Data not available

The uniaxial compressive strength, shear strength and strength under biaxial and triaxial stresses are dependent upon a number of factors such as the joint density, frictional properties, joint continuity, joint orientation and the material property. For the determination of the properties of a rock mass in situ, the sample to be tested must have at least 150 200 discontinuities.

The presence of joints decreases both the strength as well as the deformation modulus of the rock mass and the decrease in strength is more rapid for stronger rock material than for weaker rock material. The compressive strength of a jointed rock system may be only 25% of the rock material and the deformation modulus only 5% of the intact rock modulus.

The influence of constraining the jointed rock mass is to increase its strength and deformation modulus very rapidly. The influence is more marked for a multiple jointed system than for a single joint or a single joint set.

References to Chapter 10

1. AKAI, K., YAMAMOTO, K. and ARIOKA, M.: Experimental research on the structural anisotropy of crystalline schists. Rock Mech. in Japan, Vol. 1, 1970, pp. 32–34.
2. BAMFORD, W.E. Anisotropy, and the natural variability of rock properties. Proc. Symp. Rock Mech., Univ. Sydney, 1969, pp. 1–10.
3. BARLA, G. and GOFFI, L.: Direct tensile testing of anisotropic rocks. 3rd Cong. Int. Soc. Rock Mech., Denver, Colorado, Vol. II-A, 1974, pp. 93–98.
4. BARRON, K.: Brittle fracture initiation in and ultimate failure of rocks. Part III Anisotropic rocks: Experimental results. Int. J. Rock Mech. Min. Sci., Vol. 8, No. 6, Nov., 1971, pp. 565–575.
5. BARTON, N.R.: A model study of the behaviour of steep excavated rock slopes. Ph. D. Thesis, Univ. London, London, 1971a, 520 p.
6. BARTON, N.R.: A relationship between joint roughness and joint shear strength. Proc. Symp. Rock Fracture, Nancy, 1971b, Paper I–8.
7. BARTON, N.R.: Review of a new shear strength criterion for rock joints. Eng. Geol., Vol. 7, No. 4, April, 1973a, pp. 287–332.
8. BARTON, N.R.: A review of the shear strength of discontinuities in rock masses with particular reference to slope stability. Norweg. Geotech. Inst., Oslo, Int. Rep. 54204, Aug., 1973b, 164 p.
9. BERENBAUM, R. and BRODIE, I.: The tensile strength of coal. J. Inst. Fuel, Vol. 32, 1959, pp. 320–327.
10. BJERRUM, L.: Problems of soil mechanics and construction on soft clays. State of the Art Report to Session IV, 8th Int. Conf. Soil Mech. Found. Eng., Moscow, 1973.
11. BOCK, H.: Field studies on jointing in hardly tectonically stressed sedimentary rocks. Proc. Symp. Rock Fracture, Nancy, 1971, Paper I-12.
12. BORETTI-ONYSZKIEWICZ, W.: Joints in the flysch sandstones on the ground of strength examinations. Proc. 1st Cong. Int. Soc. Rock Mech., Lisbon, 1966, Vol. 1, pp. 153–157.
13. BORROSO, M.: Cement grouts and their influence on the shear strength of fissured rock masses. Proc. 2nd Cong. Int. Soc. Rock Mech., Belgrade, 1970, Vol. 3, pp. 189–195.
14. BOWDEN, F.P. and TABOR, D.: The area of contact between stationary and between moving surfaces. Proc. Roy. Soc. London, Series A, Vol. 169, 1939, pp. 391–413.
15. BOWDEN, F.P. and TABOR, D.: Friction and Lubrication. London, Methuen, 1967.
16. BRACE, W.F. and BYERLEE, J.D.: Recent experimental studies of brittle fracture of rocks. Proc. 8th Symp. Rock Mech., Minneapolis, Minn., 1966a, pp. 58–81.
17. BRACE, W.F. and BYERLEE, J.D.: Stick-slip as a mechanism for earthquakes. Science, Vol. 153, 1966b, pp. 990–992.
18. BRACE, W.F. and MARTIN, R.J.: A test of the law of effective stress for crystalline rocks of low porosity. Int. J. Rock Mech. Min. Sci., Vol. 5, No. 5, Sept., 1968, pp. 415–426.
19. BRIDGMAN, P.W.: Shearing phenomena at high pressure of possible importance for geology. J. Geol., Vol. 44, 1936, pp. 653–669.
20. BROMWELL, L.G.: The friction of quartz in high vacuum. Sc. D. Thesis, M.I.T., Cambridge, 1966.

21. BROWN, E.T.: Strength of models of rock with intermittent joints. J. Soil Mech. Found. Div., Am. Soc. Civ. Eng., Vol. 96, No. SM 6, Nov., 1970, pp. 1935–1949.

22. BROWN, E.T. and TROLLOPE, D.H.: Strength of a model of jointed rock. J. Soil Mech. Found. Div., Am. Soc. Civ. Eng., Vol. 96, No. SM2, March, 1970, pp. 685–704.

23. BYERLEE, J.D.: The frictional characteristics of Westerly granite. Ph. D. Thesis, M.I.T., Cambridge, 1966.

24. BYERLEE, J.D.: Theory of friction based on brittle fracture. J. Appl. Phys., Vol. 38, No. 7, June, 1967a. pp. 2928–2934.

25. BYERLEE, J.D.: Frictional characteristics of granite under high confining pressure. J. Geophys. Res., Vol. 72, No. 14, July 15, 1967b, pp. 3639–3648.

26. BYERLEE, J.D.: Brittle-ductile transition in rocks. J. Geophys. Res., Vol. 73, No. 14, July 15, 1968a, pp. 4741–4750.

27. BYERLEE, J.D.: Deformational characteristics of rock powders, Trans. Am. Geophys. Un., Vol. 49, 1968b, p. 314.

28. BYERLEE, J.D.: The fracture strength and frictional strength of Weber sandstone. Int. J. Rock Mech. Min. Sci. & Geomech. Abstr., Vol. 12, No. 1, Jan., 1975, pp. 1–4.

29. BYERLEE, J.D. and BRACE, W.F.: Stickslip, stable sliding, and earthquakes— Effect of rock type, pressure, strain rate, and stiffness. J. Geophys. Res., Vol. 73, No. 18, Sept. 15, 1968, pp. 6031–6037.

30. BYERLEE, J. and SUMMERS, R.: A note on the effect of fault gouge thickness on fault stability. Int. J. Rock Mech. Min. Sci. & Geomech. Abstr., Vol. 13, 1976, pp. 35–36.

31. CHAPPELL, B.A.: Friction characteristic of graphite coated bedding joints in shale. Int. J. Rock Mech. Min. Sci. & Geomech. Abstr., Vol. 12, No. 2, Feb., 1975, pp. 33–39.

32. CHRISTENSEN, R.J., SWANSON, S.R. and BROWN, W.S.: Torsional shear measurements of the frictional properties of Westerly granite, 3rd Cong. Int. Soc. Rock Mech., Denver, Colorado, Vol. II-A, 1974, pp. 221–225.

33. CLOOS, H.: Experiment zur inneren Tektonik. Centralbl. Mineral. Geol. u. Pal., 1928, pp. 609–621.

34. CORTHOUTS, L.T.: Sliding resistance of brittle surfaces. S.M. Thesis, M.I.T., Cambridge, 1966, 72 p.

35. COULSON, J.H.: The effects of surface roughness on the shear strength of joints in rock. Ph. D. Thesis, Univ. Illinois, Urbana, 1970.

36. CVETKOVIĆ, M.: Dimensions influence of tested samples on its uniaxial strength-polar strength (in French), 3rd Cong. Int. Soc. Rock Mech., Denver, Colorado, Vol. II-A, 1974, pp. 126–131.

37. DAYRE, M.: Yield laws of a slaty shale with a lineation in the slaty cleavage plane. Proc. 2nd Cong. Int. Soc. Rock Mech., Belgrade, 1970, Vol. 2, pp. 261–266.

38. DEMIRIS, C.A.: The influence of unevenness of loading surfaces on the strength of rock cubes, 3rd Cong. Int. Soc. Rock Mech., Denver, Colorado, Vol. II-A, 1974, pp. 132–137.

39. DIETERICH, J.H.: Time dependence in stick-slip sliding. Trans. Am. Geophys. Union, Vol. 51, No. 4, April, 1970, p. 423.

40. DIETERICH, J.H.: Time dependent friction in rocks. U.S. Geological Survey, Menlo Park, Calif. (Personal communication), 1972.

41. DONATH, F.A.: Strength variation and deformational behaviour in anisotropic rock. Proc. Int. Conf. State of Stress in the Earth's Crust, Santa Monica, California, 1963, pp. 280–297.

42. DONATH, F.A., FRUTH, L.S. and OLSSON, W.A.: Experimental study of frictional properties of faults. Proc. 14th Symp. Rock Mech., Univ. Park, Penn., June, 1972, pp. 189–222.

43. DRENNON, C.B. and HANDY, R.L.: Stick-slip of lightly loaded limestone. Int. J. Rock Mech. Min. Sci., Vol. 9, No. 5, Sept., 1972, pp. 603–615.

44. DUBE, A.K. and SINGH, B.: Determination of tensile strength of rocks by disc test method. J. Mines, Metals and Fuels, Vol. 17, No. 9, Sept., 1969, pp. 305–307.

45. DUNCAN, N.: Engineering Geology and Rock Mechanics. Vol. 2, London, Leonard Hill, 1969, 270 p.

46. DUNCAN, N. and SHEERMAN-CHASE, A.: Rock mechanics in the planning, design, and construction of civil engineering works. Civ. Eng. Public Works Rev., Vol. 60, No. 713, Dec., 1965, pp. 1751–1753, 1755–56 and Vol. 61, Nos. 714–716, Jan.-March, 1966, pp. 57–59, 213–215, 217, 327–330, 433, 613, 615, 617, 751–753.

47. DURAND, E. and COMES, G.: L'essai de torsion et la résistance au cisaillement des roches, 3rd Cong. Int. Soc. Rock Mech., Denver, Colorado, Vol. II-A, 1974, pp. 226–232.

48. EINSTEIN, H.H., BRUHN, R.W. and HIRSCHFELD, R.C.: Mechanics of jointed rock. Experimental and theoretical studies. M.I.T., Cambridge, Dept. Civil Engng., Rep., Aug., 1970. 115 p.

49. EINSTEIN, H.H., NELSON, R.A., BRUHN, R.W. and HIRSCHFELD, R.C.: Model studies of jointed-rock behaviour. Proc. 11th Symp. Rock Mech., Berkeley, California, 1969, pp. 83–103.

50. ENGELDER, J.T.: Quartz fault gouge, its generation and effect on the frictional properties of sandstone, Ph. D. Thesis, Texas A & M University, 1973.

51. EVANS, I. and POMEROY, C.D.: The strength of cubes of coal in uniaxial compression. Proc. Conf. Mech. Prop. Non-metallic Brittle Materials, London, 1958, pp. 5–28.

52. EVANS, I. and POMEROY, C.D.: The Strength, Fracture and Workability of Coal. London, Pergamon Press, 1966, 277 p.

53. FAIRHURST, C.: On the validity of the 'Brazilian' test for brittle materials. Int. J. Rock Mech. Min. Sci., Vol. 1, No. 4, Oct., 1964, pp. 535–546.

54. FECKER, E.: Geologische Kartierung des Gebietes nordwestlich von Neustadt/ Weinstrasse sowie Bau und Anwendung eines Profilographen. Diplom-Thesis, Univ. Karlsruhe, Karlsruhe, 1970.

55. FECKER, E. and RENGERS, N.: Measurement of large scale roughnesses of rock planes by means of profilograph and geological compass. Proc. Symp. Rock Fracture, Nancy, 1971, Paper 1-18.

56. GOLDSTEIN, M., GOOSEV, B., PYROGOVSKY, N., TULINOV, R. and TUROVSKAYA, A.: Investigation of mechanical properties of cracked rock. Proc. 1st Cong. Int. Soc. Rock Mech., Lisbon, 1966, Vol. 1, pp. 521–524.

57. GONANO, L.P.: Stress gradient and size effect phenomena in brittle materials. Ph. D. Thesis, James Cook Univ. of North Queensland, Townsville, 1974, 364 p.

58. GOODMAN, R.E.: The deformability of joints. Proc. Symp. Determination of the In Situ Modulus of Deformation of Rock, Denver, Colo., 1969. A.S.T.M. Spec. Tech. Pub. 477, 1970, pp. 174–196.

59. GOODMAN, R.E., HEUZE, F.E. and OHNISHI, Y.: Research on strength, deformability—water pressure relationship for faults in direct shear. Rep. ARPA Contract H0210020, Univ. Calif., Berkeley, 1972.

60. HANDIN, J.: Friction in rocks. Lecture delivered at Inst. Soil Mech. & Rock Mech., Univ. Karlsruhe, Karlsruhe, Oct., 1972a.

61. HANDIN, J. Mechanical properties of rocks affecting earthquakes. Centre for Tectonophysics, Texas A & M Univ., Contract No. 14-08-0001-12723, 1972b.

62. HANDIN, J. and STEARNS, D.W.: Sliding friction of rock. Trans. Am. Geophys. Union, Vol. 45, No. 1, March, 1964, p. 103.

63. HARDY, W.B. and HARDY, J.K.: Note on static friction and on the lubricating properties of certain chemical substances. Phil. Mag., 6th Series, Vol. 38, No. 233, July, 1919, pp. 32–48.

64. HAYASHI, M.: Strength and dilatancy of brittle jointed mass—The extreme value stochastics and anisotropic failure mechanism. Proc. 1st Cong. Int. Soc. Rock Mech., Lisbon, 1966, Vol. 1, pp. 295–302.

65. HOBBS, D.W.: The tensile strength of rocks. Int. J. Rock Mech. Min. Sci., Vol. 1, No. 3, May, 1964, pp. 385–396.

66. HOBBS, D.W.: A study of the behaviour of a broken rock under triaxial compression, and its application to mine roadways. Int. J. Rock Mech. Min. Sci., Vol. 3, No. 1, March, 1966, pp. 11–43.

67. HOBBS, D.W.: The behaviour of broken rock under triaxial compression. Int. J. Rock Mech. Min. Sci., Vol. 7, No. 2, March, 1970, pp. 125–148.

68. HOEK, E.: Fracture of anisotropic rock. J.S. African Inst. Min. Metall., Vol. 64, No. 10, May, 1964, pp. 501–518.

69. HOEK, E.: Estimating the stability of excavated slopes in opencast mines. Mining Ind. Trans. Inst. Min. Met., Section A, Vol. 79 (767), 1970, pp. 109–132.

70. HOEK, E. and BRAY, J. Rock Slope Engineering. London, Inst. Min. Metall., 1974, 309 p.

71. HOEK, E. and PENTZ, D.L.: Review of the role of rock mechanics research in the design of opencast mines. Proc. 9th Comm. Min. Metall. Cong., London, 1969, pp. 389–404.

72. HOLM, R.: Electric contacts. Uppasala, Almquist and Wiksells, 1946.

73. HORINO, F.G.: Effects of planes of weakness on uniaxial compressive strength of model mine pillars. U.S.B.M., R.I. 7155, 1968, 24 p.

74. HORINO, F.G. and ELLICKSON, M.L.: A method for estimating strength of rock containing planes of weakness. U.S.B.M. R.I. 7449, 1970, 29 p.

75. HORN, H.M. and DEERE, D.U.: Frictional characteristics of minerals. Geotechnique, Vol. 12, 1962, pp. 319–335.

76. HOSKINS, E.R., JAEGER, J.C. and ROSENGREN, K.J. A medium-scale direct friction experiment. Int. J. Rock Mech. Min. Sci., Vol. 5, No. 2, March, 1968, pp. 143–154.

77. JAEGER, J.C.: The frictional properties of joints in rock. Geofis. Pura e Appl., Vol. 43, 1959, pp. 148–158.

78. JAEGER, J.C.: Friction of rocks and stability of rock slopes. Geotechnique, Vol. 21, No. 2, June, 1971, pp. 97–134.

79. JAEGER, J.C. and COOK, N.G.W.: Fundamentals of Rock Mechanics. London, Methuen, 1969a, 513 p.

80. JAEGER, J.C. and COOK, N.G.W.: Friction in granular materials. Proc. Int. Conf. Struct., Solid Mech. and Eng. Design in Civil Eng. Mater., Southampton, 1969b. pp. 257 – 266.

81. JAEGER, J.C. and ROSENGREN, K.J.: Friction and sliding of joints. Proc. Aust. Inst. Min. Metall., No. 229, March, 1969, pp. 93–104.

82. JIMENEZ SALAS, J.A. and URIEL, S.: Some recent rock mechanics testing in Spain. Trans. 8th Cong. Large Dams, Edinburgh, 1964, Vol. 1., pp. 995–1002.

83. JOHN, K.W.: An approach to rock mechanics. J. Soil Mech. Found. Div., Am. Soc. Civ. Eng., Vol. 88, No. SM4, Aug., 1962, pp. 1–30.

84. JOHN, K.W.: Festigkeit und Verformbarkeit von druckfesten, regelmässig gefügten Diskontinuen. Inst. Soil Mech. & Rock Mech., Univ. Karlsruhe, Karlsruhe, Heft 37, 1969.

85. KAWAMOTO, T.: Macroscopic shear failure of jointed and layered brittle media. Proc. 2nd Cong. Int. Soc. Rock Mech., Belgrade, 1970, Vol. 2, pp. 215–221.

86. KRAGELSKII, I.V.: Friction and Wear. Translated from Russian. London, Butterworths, 1965, 346 p.

87. KRSMANOVIC, D.: Initial and residual shear strength of hard rocks. Geotechnique, Vol. 17, 1967, pp. 145–160.

88. KRSMANOVIC, D. and LANGOF, Z.: Large scale laboratory tests of the shear strength of rocky material. Rock Mech. Eng. Geol., Supplementum No. 1, 1964, pp. 20–30.

89. KUTTER, H.K.: Rotary shear testing of rock joints, 3rd Cong. Int. Soc. Rock Mech., Denver, Colorado, Vol. II-A, 1974, pp. 254–262.

90. KUZNECOV, G.N.: Graphical method to determine the strength of a nonhomogeneous jointed rock mass. Rock Mech., Vol. 2, 1970, pp. 75–92.

91. LADANYI, B. and ARCHAMBAULT, G.: Simulation of shear behaviour of a jointed rock mass. Proc. 11th Symp. Rock Mech., Berkeley, California, 1969, pp. 105–125.

92. LADANYI, B. and ARCHAMBAULT, G.: Evaluation of shear strength of a jointed rock mass. In French. Proc. 24th Int. Geological Cong., Montreal, 1972, pp. 249–260.

93. LAJTAI, E.Z.: The influence of interlocking rock discontinuities on compressive strength (model experiments). Rock Mech. Eng. Geol., Vol. 5, 1967, pp. 217–228.

94. LAJTAI, E.Z.: Shear strength of weakness planes in rock. Int. J. Rock Mech. Min. Sci., Vol. 6, No. 5, Sept., 1969a, pp. 499–515.

95. LAJTAI, E.Z.: Strength of discontinuous rocks in direct shear. Geotechnique, Vol. 19, 1969b, pp. 218–233.

96. LAJTAI, E.Z.: Unconfined shear strength of discontinuous rocks. Proc. 2nd Cong. Int. Soc. Rock Mech., Belgrade, Vol. 2, 1970, pp. 267–272.

97. LAMA, R.D.: Mechanical behaviour of jointed rock mass. Inst. Soil Mech. & Rock Mech., Univ. Karlsruhe, Karlsruhe, Rep. K-126, 1972.

98. LAMA, R.D.: The uniaxial compressive strength of jointed rock. Prof. L. Müller Festschrift, Inst. Soil Mech. & Rock Mech., Univ. Karlsruhe, Karlsruhe, 1974a, pp. 67–77.

99. LAMA, R.D.: Untersuchung des Rheologischen Verhaltens von geklüftetem Fels. SFD77, Jahresbericht, 1973. Inst. Soil Mech. & Rock Mech., Univ. Karlsruhe, Karlsruhe, 1974b.

100. LAMA, R.D.: The concept of creep of jointed rocks and the status of research project A-6. SFB77, Jahresbericht, 1974, Inst. Soil Mech. & Rock Mech., Univ. Karlsruhe, Karlsruhe, 1975a.

101. LAMA, R.D.: Institute of Soil Mechanics and Rock Mechanics, Univ. Karlsruhe, SFB Project A-7, 1975b (unpublished).

102. LAMA, R.D. and GONANO, L.P.: Size effect considerations in the assessment of mechanical properties of rock masses. Proc. 2nd Symp. Rock Mech., Dhanbad, 1976.

103. LAMBE, T.W. and WHITMAN, R.V.: Soil mechanics. New York, Wiley, 1969, 553 p.

104. LANE, K.S. and HECK, W.J.: Triaxial testing for strength of rock joints. Proc. 6th Symp. Rock Mech., Rolla, Missouri, 1964, pp. 98–108.

105. LINK, H.: Zur Beurteilung und Bestimmung der Gleitsicherheit von Gewicht- und Pfeilerstaumauern. Die Wasserwirtschaft, No. 1, 1967, pp. 35–46.

106. LITWINISZYN, J.: On certain linear and non linear strata theoretical models. Proc. 4th Int. Conf. Strata Control and Rock Mech., New York, 1964.

107. LOCHER, H.G.: Some results of direct shear tests on rock discontinuities. Proc. Int. Symp. Rock Mech., Madrid, 1968, pp. 171–173.

108. LOGAN, J.M., IWASAKI, T., FRIEDMAN, M. and KLING, S.A.: Experimental investigation of sliding friction in multilithologic specimens. Geol. Soc. Am. Eng. Geol. Case History No. 9, 1973, pp. 55–67.

109. LUNDBORG, N.: A statistical theory of the polyaxial compressive strength of materials. Int. J. Rock Mech. Min. Sci., Vol. 9, 1972, pp. 617–624.

110. MATHEWS, K.E.: Excavation design in hard and fractured rock at the Mount Isa mine, Australia. M.Sc. Thesis, Univ. Queensland, Brisbane, 1970.

111. MAURER, W.C.: Shear failure of rock under axial and hydrostatic pressure. Proc. 1st Cong. Int. Soc. Rock Mech., Lisbon, 1966, Vol. 1, pp. 337–341.

112. MCGILL, G.E. and RANEY, J.A.: Experimental study of faulting in an anisotropic, inhomogeneous dolomitic limestone. Geol. Soc. Am. Bull., Vol. 81, No. 10, Oct., 1970, pp. 2949–2958.

113. MENTER, J.W.: A study of boundary lubricant films by electron diffraction. Proc. Symp. Physics of Lubrication, Manchester, 1950. Brit. J. Appl. Phys., Supplement 1, 1951, pp. 52–53.

114. MOGI, K.: Pressure dependence of rock strength and transition from brittle fracture to ductiele flow. Bull. Earthquake Res. Inst., Tokyo Univ., Vol. 44, 1966, pp. 215–232.

115. MOGI, K.: Fracture and flow of rocks. Tectonophysics, Vol. 13, 1972, pp. 541–568.

116. MORGENSTERN, N.R.: The influence of groundwater on stability. Proc. 1st Int. Conf. Stability in Open Pit Mining, Vancouver, Canada, 1970, pp. 65–81.

117. MOTOYAMA, H. and HIRSCHFELD, R.C.: The effect of joint configurations on the strength and deformability of model rocks. Federal Railroad Administration, Department of Transportation, Washington, D.C., Report No. FRA-RT-73-25, 1971, 183 p.

118. MÜLLER, L.: Der Felsbau. Bd. 1. Stuttgart, Ferdinand Enke, 1963, 623 p.

119. MÜLLER, L.: The progressive failure in jointed media. Proc. 1st Cong. Int. Soc. Rock Mech., Lisbon, 1966, Vol. 1, pp. 679–686.

120. MÜLLER, L. and HOFMANN, H.: Selection, compilation and assessment of geological data for the slope problem. Proc. Symp. Planning Open Pit Mines, Johannesburg, 1970, pp. 153–170.

121. MÜLLER, L. and PACHER, F.: Modellversuche zur Klärung der Bruchgefahr geklüfteter Medien. Rock Mech. Eng. Geol., Supplementum No. 2, 1965, pp. 7–24

122. MURRELL, S.A.F.: The effect of triaxial stress systems on the strength of rocks at atmospheric temperatures. Geophys. J. Roy. Astr. Soc., Vol. 10, 1965, pp. 231–281.

123. NEWLAND, P.L. and ALLELY, B.H.: Volume changes in drained triaxial tests on granular materials. Geotechnique, Vol. 7, No. 1, March, 1957, pp. 17–34.

124. OBERT, L., BRADY, B.T. and SCHMECHEL, F.W.: The effect of normal stiffness on the shear resistance of rock. Rock Mech., Vol. 8, No. 2, 1976, pp. 57–72.

125. PATTON, F.D.: Multiple modes of shear failure in rock and related materials. Ph. D. Thesis, Univ. Illinois, Urbana, 1966a, 282 p.

126. PATTON, F.D.: Multiple modes of shear failure in rock. Proc. 1st Cong. Int. Soc. Rock Mech., Lisbon, 1966b, Vol. 1, pp. 509–513.

127. POMEROY, C.D., HOBBS, D.W. and MAHMOUD, A.: The effect of weakness-plane orientation on the fracture of Barnsley Hards by triaxial compression. Int. J. Rock Mech. Min. Sci., Vol. 8, No. 3, May, 1971, pp. 227–238.

128. PRICE, N.J.: A study of rock properties in conditions of triaxial stress. Proc. Conf. Mech. Prop. Non-metallic Brittle Materials, London, 1958, pp. 106–122.

129. RABINOWICZ, E.: Friction and Wear of Materials. New York, Wiley, 1965.

130. RAE, D.: The measurement of the coefficient of friction of some rocks during continuous rubbing. J. Sci. Inst., Vol. 40, No. 9, Sept., 1963, pp. 438–440.

131. RALEIGH, C.B. and PATERSON, M.S.: Experimental deformation of serpentinite and its tectonic implications. J. Geophys. Res., Vol. 70, No. 16, Aug., 15, 1965, pp. 3965–3985.

132. RENGERS, N.: Influence of surface roughness on the friction properties of rock planes. Proc. 2nd Cong. Int. Soc. Rock Mech., Belgrade, 1970, Vol. 1, pp. 229–234.

133. RENGERS, N.: Unebenheit und Reibungswiderstand von Gesteinstrennflächen. Inst. Soil Mech. & Rock Mech., Univ. Karlsruhe, Karlsruhe, Heft 47, 1971.

134. RIEDEL, W.: Zur Mechanik geologischer Brucherscheinungen. Centralbl. Mineral. Geol. u. Pal., 1929, pp. 354–368.

135. RIPLEY, C.F. and LEE, K.L.: Sliding friction tests on sedimentary rock specimens. Trans. 7th Cong. Large Dams, Rome, 1961, Vol. 4, pp. 657–671.

136. ROCHA, M.: Mechanical behaviour of rock foundations in concrete dams. Trans. 8th Cong. Large Dams, Edinburgh, 1964, pp. 785–832.

137. ROSENGREN, K.J.: Rock mechanics of the Black Star Open Cut, Mount Isa. Ph. D. Thesis, Australian National University, Canberra, 1968.

138. ROWE, P.W., BARDEN, L. and LEE, I.K.: Energy components during the triaxial cell and direct shear tests. Geotechnique, Vol. 14, No. 3, Sept., 1964, pp. 247–261.

139. RUIZ, M.D. and DE CAMARGO, F.P.: A large-scale field shear test on rock. Proc. 1st Cong. Int. Soc. Rock Mech., Lisbon, 1966, Vol. 1, pp. 257–261.

140. RUIZ, M.D., DE CAMARGO, F.P., MIDEA, N.F. and NIEBLE, C.M.: Some considerations regarding the shear strength of rock masses. Proc. Int. Symp. Rock Mech., Madrid, 1968, pp. 159–169.

141. SCHNEIDER, H.J.: SFB-77, Jahresbericht, 1972. Inst. Soil Mech. & Rock Mech., Univ. Karlsruhe, Karlsruhe.

142. SCHOLZ, C.H. and ENGELDER, J.T.: The role of asperity indentation and ploughing in rock friction, Parts I & II, Int. J. Rock Mech. Min. Sci. & Geomech. Abstr., Vol. 13, 1976, pp. 149–154, 155–163.

143. SCHOLZ, C., MOLNAR, P. and JOHNSON, T.: Detailed studies of frictional sliding of granite and implications for the earthquake mechanism. J. Geophys. Res., Vol. 77, No. 32, Nov. 10, 1972, pp. 6392–6406.

144. SERAFIM, J.L. and GUERREIRO, M.: Shear strength of rock masses at 3 Spanish dam sites. Proc. Int. Symp. Rock Mech., Madrid, 1968, pp. 147–157.

145. SKEMPTON, A.W.: Long term stability of clay slopes. Geotechnique, Vol. 14, No. 2, 1964, pp. 77–101.

146. SKEMPTON, A.W. and HUTCHINSON, J.: Stability of natural slopes and embankment foundations. Proc. 7th Int. Conf. Soil Mech. Found. Eng., Mexico, 1969, State of the Art volume, pp. 291–340.

147. TERZAGHI, K. and PECK, R.B.: Soil mechanics in engineering practice. 2nd edition. New York, Wiley, 1967, 729 p.

148. TROLLOPE, D.H.: The mechanics of discontinua or elastic mechanics in rock problems. In Rock Mechanics in Engineering Practice (Editors K.G. Stagg and O.C. Zienkiewicz), London, Wiley, 1968, pp. 275–320.

149. TSCHEBOTARIOFF, G.P. and WELCH, J.D.: Lateral earth pressures and friction between soil minerals. Proc. 2nd Int. Conf. Soil Mech. Found. Eng., 1948, Vol. 7, pp. 135–138.

150. TULINOV, R. and MOLOKOV, L.: Role of joint filling material in shear strength of rocks. Proc. Symp. Rock Fracture, Nancy, 1971, Paper II-24.

151. UFF, J.F. and NASH, J.K.T.L.: Anisotropy of shale due to folding. Proc. Geotechnical Conf. Shear Strength Properties of Natural Soils and Rocks, Oslo, 1967, Vol. 1, pp. 301–303.

152. U.S. Bureau of Reclamation. Bond strength between concrete and rock from Monticello dam site, Solano project, California. Concrete Lab. Rep. No. C-761, 1954.

153. WAGNER, G.: Kleintektonische Untersuchungen im Gebiet des Nördlinger Rieses. Geol. Jb., Vol. 81, 1964, pp. 519–600.

154. WALKER, P.E.: The shearing behaviour of a block jointed rock model. Ph. D. Thess, Queens Univ., Belfast, 1971.

155. WALSH, J.B.: Stiffness in faulting and in friction experiments. J. Geophys. Res., Vol. 76, No. 35, Dec., 10, 1971, pp. 8597–98.

156. WAWERSIK, W.R. and BROWN, W.S.: Creep fracture of rock. Report, Mech. Eng. Dept., Univ. Utah, Salt Lake City, July, 1973, 81 p.

157. WEIBULL, W.: A statistical theory of the strength of materials. Ingvetensk. Akad. Handl., Vol. 151, 1939, pp. 5–44.

158. WILLARD, R.J. and MCWILLIAMS, J.R.: Microstructural techniques in the study of physical properties of rock. Int. J. Rock Mech. Min. Sci., Vol. 6, No. 1, Jan., 1969, pp. 1–12.

159. WOHNLICH, H.M.: Kleintektonische Bruch- und Fliessdeformationen in Faltenjura. Ph. D. Thesis, Univ. Basel, Basel, Switzerland, 1968.

160. YEVDOKIMOV, P.D. and SAPEGIN, D.D.: Stability, shear sliding resistance and deformation of rock foundations. Clearinghouse Federal Sci. and Tech. Inf., Springfield, Va., 1967, 145 p.

161. YOUASH, Y.Y.: Experimental deformation of layered rocks. Proc. 1st Cong. Int. Soc. Rock Mech., Lisbon, 1966, Vol. 1, pp. 787–795.

Uncited References to Chapter 10

1. ADLER, L.: Failure in geologic material containing planes of weakness. Trans. A.I.M.E., Vol. 226, 1963, pp. 88–94.
2. AMMARI, I.S.Y.: Correlation of joint roughness with geology. M.Sc. Thesis, Univ. London, London, 1972.
3. ARCHARD, J.F.: Elastic deformation and the laws of friction. Proc. Roy. Soc. London, Series A, Vol. 243, No. 1233, 1958, pp. 190–205.
4. BIENIAWSKI, Z.T.: Mechanics of jointed rock masses. Rep. S. African, C.S.I.R., No. MEG 998, March, 1971, 42 p.
5. BIENIAWSKI, Z.T., DENKHAUS, H.G. and VOGLER, U.W.: Failure of fractured rock. Int. J. Rock Mech. Min. Sci., Vol. 6, No. 3, May, 1969, pp. 323–341.
6. BJURSTROM, S.: Estimating the stability and deformation behaviour of a rock mass. In Swedish. Proc. Conf. Rock Mech., Stockholm, Feb., 1971, pp. 47–61.
7. BRAY, J.W.: Limiting equilibrium of fractured and jointed rocks. Proc. 1st Cong. Int. Soc. Rock Mech., Lisbon, 1966, Vol. 1, pp. 531–535.
8. BRAY, J.W.: A study of jointed and fractured rock. Part I – Fracture patterns and their failure characteristics. Part II – Theory of limiting equilibrium. Rock Mech. Eng. Geol., Vol. 5, Nos. 2–3 and 4, 1967, pp. 117–136 and 197–216.
9. BRAYBOOKE, J.C.: The strength effect and measurement of discontinuity in rock masses. M. Sc. Thesis, Univ. London, London, 1966, 211 p.
10. BREKKE, T.L. and SELMER-OLSEN, R.: Stability problems in underground constructions caused by montmorillonite carrying joints and faults. Eng. Geol., Vol. 1, 1965, pp. 3–19.
11. BROWN, E.T.: Modes of failure in jointed rock masses. Proc. 2nd Cong. Int. Soc. Rock Mech., Belgrade, 1970, Vol. 2, pp. 293–298.
12. BROWN, E.T.: Strength-size effects in rock material. Proc. Symp. Rock Fracture, Nancy, 1971, Paper II-11.
13. BROWN, E.T. and HUDSON, J.A.: Discussion on "The operational strength of fissured clays by K.Y. Lo". Geotechnique, Vol. 20, No. 3, Sept., 1970, pp. 334–336.
14. BYERLEE, J.D.: The mechanics of stick-slip. Tectonophysics, Vol. 9, 1970, pp. 475–486.
15. BYERLEE, J.D.: Static and kinetic friction of granite at high normal stress. Int. J. Rock Mech. Min. Sci., Vol. 7, No. 6, Nov., 1970, pp. 577–582.
16. BYERLEE, J.D. and SUMMERS, R.: Stability sliding preceding stick-slip on fault surfaces in granite at high pressure, Pure & Appl. Geophys., Vol. 113, 1975, pp. 63–68.
17. CHAPPELL, B.A.: The mechanics of blocky material. Ph. D. Thesis, Australian National Univ., Canberra, 1972.
18. CHAPPELL, B.A.: Deformational response of blocky models. Int. J. Rock Mech. Min. Sci. & Geomech. Abstr., Vol. 11, No. 1, Jan., 1974, pp. 13–19.
19. CHAPPELL, B.A.: Component characteristics of jointed rock masses. Int. J. Rock Mech. Min. Sci. & Geomech. Abstr., Vol. 12, No. 4, April, 1975, pp. 87–92.
20. CHENEVERT, M.E. and GATLIN, C.: Mechanical anisotropies of laminated sedimentary rocks. Soc. Pet. Eng. J., Vol. 5, No. 1, March, 1965, pp. 67–77.
21. CUNDALL, P.A.: A computer model for simulating progressive, large-scale movements in blocky rock systems. Proc. Symp. Rock Fracture, Nancy, 1971, Paper II-8.

22. DEERE, D.U. and COULSON, J.H.: The effects of water and cement grout on the shear strength of natural and artificial joints in Grand Coulee granite. Rep., Dept. Civil Eng., Univ. Illinois, Urbana, 1970, 175 p.

23. DIETERICH, J.H.: Time-dependent friction in rocks. J. Geophys. Res., Vol. 77, No. 20, July 10, 1972, pp. 3690–3697.

24. DIETERICH, J.H.: Time-dependent friction as a possible mechanism for aftershocks. J. Geophys. Res., Vol. 77, No. 20, July 10, 1972, pp. 3771–3781.

25. DVORAK, A.: Influence of separation planes on the shear strength of rock masses. Proc. Geotechnical Conf. Shear Strength Properties of Natural Soils and Rocks, Oslo, 1967, Vol. 1, pp. 271–274.

26. EDWARDS, C.M. and HALLING, J.: Analysis of plastic interaction of surface asperities and its relevance to value of coefficient of friction. J. Mech. Eng. Sci., Vol. 10, No. 2, April, 1968, pp. 101–110.

27. ENGELDER, J.T.: Coefficient of friction for sandstone sliding on quartz gouge, 3rd Cong. Int. Soc. Rock Mech., Denver, Colorado, Vol. II-A, 1974, pp. 499–504.

28. ENGELDER, J.T., LOGAN, J.M. and HANDIN, J.: The sliding characteristics of sandstone on quartz fault gouge, Pure & Appl. Geophys., Vol. 113, 1975, pp. 69–86.

29. ERGUN, I.: Model studies of underground openings in jointed and fractured rock. Min. Res. Rep. No. 13, Royal School of Mines, London, Feb., 1967.

30. ERGUN, I.: Stability of underground openings in jointed media. Ph. D. Thesis, Univ. London, London, 1970.

31. ERGUN, I.: Stress distribution in jointed media. Proc. 2nd Cong. Int. Soc. Rock Mech., Belgrade, 1970, Vol. 1, pp. 497–507.

32. FAIRHURST, C.: Estimation of the mechanical properties of rock masses. Rep. Univ. Minnesota, Minneapolis, 1972.

33. FIGUEROA, A.: Point-contact friction: A possible index value for the residual shear strength of rocks. M. Sc. Thesis, Univ. London, London, 1971.

34. FRANKLIN, J., MANAILOGLOU, J. and SHERWOOD, D.: Field determination of direct shear strength, 3rd Cong. Int. Soc. Rock Mech., Denver, Colorado, Vol. II-A, 1974, pp. 233–240.

35. GOODMAN, R.E. and OHNISHI, Y.: Undrained shear testing of jointed rock. Rock Mech., Vol. 5, 1973, pp. 129–149.

36. GOODMAN, R.E., TAYLOR, R.L. and BREKKE, T.L.: A model for the mechanics of jointed rock. J. Soil Mech. Found Div., Am. Soc. Civ. Eng., Vol. 94, No. SM 3, May, 1968, pp. 637–659.

37. HANSAGI, I.: Numerical determination of mechanical properties of rock and of rock masses. Int. J. Rock Mech. Min. Sci., Vol. 2, No. 2, July, 1965, pp. 219–223.

38. HAYASHI, M.: On a mechanism of stress propagation in a cracked rock foundation — A proposed mechanical model for discontinuous media. Presented at the Rock Mech. Committee of the Civil Eng. Soc., Nov., 1962. Abstract-Int. J. Rock Mech. Min. Sci., Vol. 1, No. 2, March, 1964, p. 310.

39. HAYASHI, M.: Strength characteristics of discontinuous jointy masses. In Japanese. Tech. Rep. No. 65052, Res. Inst. Elec. Power Industry, Tokyo, 1965.

40. HAYASHI, M. and FUJIWARA, G.: A mechanism of anisotropic dilatancy and shear failure of laminated jointed rock mass. Tech. Rep. C. E. 7006, Central Res. Inst. Elect. Power Industry, Tokyo, 1968.

41. HAYASHI, M. and HIBINO, S.: Progressive relaxation of rock masses during excavation for underground cavity. Proc. Int. Symp. Rock Mech., Madrid, 1968, pp. 343–349.

42. HELFRICH, H.K.: Strength of rock and rock masses. Proc. 10th Cong. Int. Bur. Rock Mech., Leipzig, 1968, pp. 87–93.

43. HERMAN, L.R. and TAYLOR, M.A.: Characterisation of the structural behaviour of rock masses, Vols. I & II, USBM, OFR-67 (1)-75 & OFR-67 (2)-75, 1975.

44. HOWARD, T.R., BREKKE, T.L. and HOUSTON, W.N.: Laboratory testing of fault gouge material, Bull. Assoc. Engng Geol., Vol. XII, No. 4, 1975, pp. 303–315.

45. IIDA, R. and KOBAYASHI, S.: A mechanical consideration on the stress distributions and the characteristics of deformation in rock masses. Proc. 2nd Cong. Int. Soc. Rock Mech., Belgrade, 1970, Vol. 1, pp. 361–371.

46. JAEGER, J.C.: Shear fracture of anisotropic rocks. Geol. Mag., Vol. 97, 1960, pp. 65–72.

47. JOHN, K.W.: Civil engineering approach to evaluate strength and deformability of regularly jointed rock. Proc. 11th Symp. Rock Mech., Berkeley, California, 1969, pp. 69–80.

48. JOHN, K.W.: Engineering analyses of three-dimensional stability problems utilising the reference hemisphere. Proc. 2nd Cong. Int. Soc. Rock Mech., Belgrade, 1970, Vol. 3, pp. 385–391.

49. KANDAOÛROV, I.I., MOULLER, P.A. and OUVAROV, L.A.: Stress state and settlements of jointed rock masses. Proc. 2nd Cong. Int. Soc. Rock Mech., Belgrade, 1970, Vol. 1, pp. 341–349.

50. KANDAOUROV, I.T., OUVAROV, L.A. and KARPOV, N.M.: Constraintes dans les modèles des massifs rocheux fissures sans poussée horizontale, 3rd Cong. Int. Soc. Rock Mech., Denver, Colorado, Vol. II-A, 1974, pp. 156–160.

51. KENNEY, T.C.: Residual strength of fine-grained minerals and mineral mixtures. Norweg. Geotech. Inst., Oslo, Pub. No. 68, 1966.

52. KO, K.C. and HAAS, C.J.: The effective modulus of rock as a composite material. Int. J. Rock Mech. Min. Sci., Vol. 9, 1972, pp. 531–541.

53. KOBAYASHI, S.: Fracture criteria for anisotropic rocks. Kyoto Univ. Fac. Eng. Mem., Vol. 32, Part 3, 1970, pp. 307–333.

54. KOBAYASHI, Y., IIZUKA, A. and KUMAGAI, K.: Shear strength of rocks in situ along weak planes. Case of schist, mudstone and granite. Q. Rep. Railway Tech. Res. Inst., Japan. Vol. 7, No. 1, March, 1966, pp. 7–8.

55. KOLICKO, A.V.: Tensile strength of a jointed rock. (In Foundations of Hydraulic Structures) In Russian. Proc. Hydroproject Inst., Moscow, Vol. 33, 1974, pp. 93–104.

56. KRSMANOVIC, D.: Contribution to a study of the failure problem in rock mass. Proc. Geotechnical Conf. Shear Strength Properties of Natural Soils and Rocks, Oslo, 1967, Vol. I, pp. 275–282.

57. KRSMANOVIC, D. and MILIC, S.: Model experiments on pressure distribution in some cases of a discontinuum. Rock Mech. Eng. Geol., Suppl. I, 1964, pp. 72–87.

58. KRSMANOVIC, D., LANGOF, Z. and TUFO, M.: Some aspects of rupture of rocky mass. Rock Mech. Eng. Geol., Suppl. II, 1965, pp. 143–155.

59. KRSMANOVIC, D., TUFO, M. and LANGOF, Z.: Shear strength of rock masses and possibilities of its reproduction on models. Proc. 1st Cong. Int. Soc. Rock Mech., Lisbon, 1966, Vol. I, pp. 537–542.

60. KRUSE, G.H.: Deformability of rock structures. California State water project. Proc. Symp. Determination of the In Situ Modulus of Deformation of Rock, Denver, Colo., 1969. A.S.T.M. Spec. Tech. Publ. 477, 1970, pp. 58–88.

61. KUJUNDZIC, B. and STOJAKOVIC, M.: A contribution to the experimental investigation of changes of mechanical characteristics of rock massives as a function of depth. Trans. 8th Cong. Large Dams, Edinburgh, 1964, pp. 1051–1068.

62. KUTTER, H.K. and FIGUEROA, A.: Ermittlung eines einfachen Kennwortes zur Bestimmung der Reissfestigkeit von Gesteinstrennflächen. Rock Mech., Suppl. 2, 1973, pp. 53–70.

63. KVAPIL, R. and LAUFFER, K.: Supplement to the problem of stress distribution in samples under triaxial strain. In German. Bergakademie, Vol. 12, No. 11, 1960, pp. 587–594.

64. LAJTAI, E.Z.: The evolution of brittle fracture in rock. Dept. Geology, Univ. New Brunswick, Fredericton, 1972.

65. LAJTAI, E.Z.: Failure along planes of weakness. Can. Geotechnical J., Vol. 112, 1975, pp. 118–125.

66. LAMA, R.D.: The mechanics of jointed rocks. Proc. Symp. Rock Mech., Dhanbad, 1972 (Inst. Engrs., Calcutta, India, 1973, pp. 60–85).

67. LEONOV, M.P.: The relationship between jointing and deformability in ledge-ron base of the Krasnoyork hydro-electric power station. Hydrotechnical Construction, No. 4, April, 1974, pp. 311–314.

68. MARTIN, G.R. and MILLER, P.J.: Jointed strength characterisation of weathered rock, 3rd Cong. Int. Soc. Rock Mech., Denver, Colorado, Vol. II-A, 1974, pp. 263–270.

69. MASURE, P.: Behaviour of rock with two dimensional continuous anisotropy. In French. Proc. 2nd Cong. Int. Soc. Rock Mech., Belgrade, 1970, pp. 197–207.

70. MELLO-MENDES, F.: About the anisotropy of uniaxial compressive strength in schistose rocks. Proc. Symp. Rock Fracture, Nancy, 1971, Paper II-13.

71. MENCL, V.: Factor of strength of rock material in the strength of rock mass. Proc. 1st Cong. Int. Soc. Rock Mech., Lisbon, 1966, Vol. 1, pp. 289–290.

72. METCALF, J.R.: Angle of repose and internal friction. Int. J. Rock Mech. Min. Sci., Vol. 3, No. 2, May, 1966, pp. 155–161.

73. MOGILEVSKAYA, S.E.: Effect of geological factors on the shearing resistance along joints in rock, 3rd Cong. Int. Soc. Rock Mech., Denver, Colorado, Vol. II-A, 1974, pp. 263–270.

74. MORLAND, L.W.: Continuum model of regularly jointed mediums. J. Geophys. Res., Vol. 79, No. 2, Jan. 10, 1974, pp. 357–362.

75. MORLAND, L.W.: Elastic anisotropy of regularly jointed media, Rock Mech., Vol. 8, 1976, pp. 35–48.

76. MONJOIE, A.: Mechanical properties of the Silurian schists in Tihange (Belgium). Proc. 2nd Cong. Int. Soc. Rock Mech., Belgrade, 1970, Vol. 1, pp. 213–220.

77. MÜLLER, L., CESARE, T., FECKER, E. and MÜLLER, K.: Kriterien zur Erkennung von Bruchgefahr geklüfteter Medien—Ein Versuch. Rock Mech., Suppl. 2, 1973, pp. 71–92.

78. MÜLLER, L. and MALINA, H.: Distribution of shear stresses in a progressive failure surface. In German. Rock Mech. Eng. Geol., Vol. 6, 1968, pp. 216–224.

79. MÜLLER, L.: The mechanical properties of geological bodies. In German. Festschrift Kahler, Sonderheft 28, Klagenfurt, 1971, pp. 177–191.

80. MURRELL, S.A.F.: A criterion for brittle fracture of rocks and concrete under triaxial stress, and the effect of pore pressure on the criterion. Proc. 5th Symp. Rock Mech., Minneapolis, Minn., 1962, pp. 563–577.

81. NASCIMENTO, U. and TEIXEIRA, H.: Mechanisms of internal friction in soils and rocks. Proc. Symp. Rock Fracture, Nancy, 1971, Paper II-3.

82. NELSON, R.A. and HIRSCHFELD, R.C.: Modelling a jointed rock mass. M.I.T., Cambridge, Rept. R68–70, 1968, 218 p.

83. NIKITIN, A.A., SAPEGIN, D.D. and UVAROV, L.A.: Shear resistance of rock along joint planes under static and impulse loads, 3rd Cong. Int. Soc. Rock Mech., Denver, Colorado, Vol. II-A, 1974, pp. 302–310.

84. OLSSON, W.A.: Effect of temperature, pressure and displacement rate on the frictional characteristics of a limestone. Int. J. Rock Mech. Min. Sci. & Geomech. Abstr., Vol. 11, No. 7, July, 1974, pp. 267–278.

85. PAULDING, B.W.: Coefficient of friction of natural rock surfaces. J. Soil Mech. Found. Div., Am. Soc. Civ. Eng., Vol. 96, 1970, pp. 385–394, Vol. 97, SM 4, April, 1971, pp. 685–686.

86. PERAMI, R.: Mechanical behaviour under uniaxial stresses of rocks first micro-fissured by heating. Proc. Symp. Rock Fracture, Nancy, 1971, Paper II-14.

87. PINTO, J.L.: Deformability of schistous rocks. Proc. 2nd Cong. Int. Soc. Rock Mech., Belgrade, 1970, Vol. 1, pp. 491–496.

88. PIROGOV, I.A.: The study of tectonic ruptures and jointing of rocks and evaluation them as foundations of high concrete dams. Proc. Symp. Rock Fracture, Nancy, 1971, Paper I-16.

89. PITEAU, D.R.: Characterising and extrapolating rock joint properties in engineering practice. Proc. 20th Colloquium on Geomechanics, Salzburg, Austria, Sept., 1971, Paper 1.

90. PITEAU, D.R. and RUSSELL, L.: Cumulative sums technique—A new approach to analysing joints in rock. Proc. 13th Symp. Rock Mech., Urbana, Illinois, 1971, pp. 1–29.

91. ROCHA, M.: Some problems on failure of rock masses. Rock Mech. Eng. Geol., Suppl. 1, 1964, p. 1.

92. ROCHA, M.: Structural model techniques—Some recent developments. Lab. Nac. de Enge. Civil, Lisbon, No. 264, 1965, 49 p.

93. ROSENBLAD, J.L.: Geomechanical model study of the failure modes of jointed rock masses. U.S. Corps Engrs. Dept. Army, Missouri River, Omaha, Tech. Rept. MRD 1–71, 1971, 374 p.

94. RUPPENEIT, K.V. and TARASSOVA, I.V.: Influence of the cleavage of a rock mass upon the deformation modulus. Proc. 2nd Cong. Int. Soc. Rock Mech., Belgrade, 1970, Vol. 1, pp. 295–300.

95. SCHRADER, P.: Bruchbildung in Modellsubstanzen durch Deformierungen mit monokliner Symmetrie. Ph. D. Thesis, Ruhr Univ., Bochum, 1970.

96. SCHWARTZ, A.E.: Failure of rock in the triaxial shear test. Proc. 6th Symp. Rock Mech., Rolla, Missouri, 1964, pp. 109–151.

97. SHESHENYA, N.L.: Basic factors governing the extension of point shear strength measurements on the whole jointed rock mass. Proc. Symp. Rock Fracture, Nancy, 1971, Paper II-29.

98. SINGH, B.: Continuum characterisation of jointed rock masses. Parts I and II. Int. J. Rock Mech. Min. Sci., Vol. 10, 1973, pp. 311–335, 337–349.

99. SKINNER, A.E.: A note on the influence of interparticle friction on the shearing strength of a random assembly of spherical particles. Geotechnique, Vol. 19, 1969, pp. 150–157.

100. SOWERS, G.F., WILLIAMS, R.C. and WALLACE, T.S.: Compressibility of broken rock and the settlement of rockfills. Proc. 6th Int. Conf. Soil Mech. Found. Eng., Montreal, 1965.

101. SUDAKOV, V.B. et al.: Shear characteristics of horizontal expansion joints in the Toktogul hydro-electric station dam. Sov. Min. Sci., Vol. 10, 1974, pp. 401–403.

102. SWANSON, S.R. and BROWN, W.S.: The mechanical response of prefractured rock in compression. Rept., Mech. Eng. Dept., Univ. Utah, Salt Lake City, 1971.

103. TSYTOVICH, H.A., UKHOV, S.E. and KORNILOV, A.M.: Deformation of fissured rock. Proc. 3rd Budapest Conf. Soil Mech. Found. Eng., Budapest, Oct., 1968, pp. 227–241.

104. WANG, C.Y. and MORRISON, H.F.: Electrical resistivity of granite on frictional sliding: application to earthquake prediction. Geophys. Res. Letter, Vol. 2, No. 12, 1975, pp. 525–528.

105. WITHERS, J.H.: Sliding resistance along discontinuity in rock masses. Ph. D. Thesis, Univ. Illinois, Urbana, 1964.

106. WITTKE, W.: Influence of the shear strength of the joints on the design of prestressed anchors to stabilise a rock slope. Proc. Geotechnical Conf. Shear Strength Properties of Natural Soils and Rocks, Oslo, 1967, Vol. 1, pp. 311–318.

107. WU, T.H., DOUGLAS, A.G. and GOUGHNOUR, R.D.: Friction and cohesion of saturated clays. J. Soil Mech. Found. Div., Am. Soc. Civ. Eng., Vol. 88, SM 3, June, 1962, pp. 1–32.

CHAPTER 11

Classification of Rock

11.1. Introduction

With the developments in rock testing techniques and the influence of the individual parameters on the mechanical response of a rock, there has been a need to consolidate the data acquired together to give some simple numerical indices reliable enough for a practical rock engineer to determine the stability of his excavations and design a support system. Any amount of data obtained from testing has no meaning as long as it is not correlated with each other to give a meaningful picture of the rock mass as a whole and related to the type of excavation which is to be placed in it. These facts have been recognised for quite some time and attempts have been made by geologists and engineers to synthesise their experience in certain numerical values. Attempts have been made to classify rocks according to a combination of field and laboratory studies with the laboratory tests being limited to certain simple index tests. It is here that the geologists and engineers try to speak a language understandable to each other. There had been a wide gap between the practising rock engineer, the research scientist and the geologist and this gap has been slowly decreasing. In the last 15 years a number of classification systems have been put forward and improved upon. Because of the large number of parameters involved and the inherent variability in the rock properties a general classification which permits to arrive at a final decision whether a slope or an excavation is stable or requires to be bolted or lined is still very difficult. The long term stability of an unsupported opening, the design of a support system or the corrective measures to be adopted for an existing slope is still a difficult question. Till now no classification system has been put forward to take into account the time-effect. The design of underground caverns is still largely based upon precedent and the construction of large chambers under conditions not previously encountered is heavily based on extended previous experience coupled with observations during construction to confirm the suitability of the design. In spite of the highly developed

numerical techniques, experience overweighs several times the calculated results, the basic reasons behind this being that

1. the input data to the analysis are very meagre and are not very reliable when extended to large dimensions
2. the relative influence of the various values obtained from tests when considered altogether is not sufficiently known
3. the structural variations in the rock cannot be sufficiently accurately determined from surface observations or drilling and exploratory work with the techniques available presently and
4. the influence of time on these parameters has still not been sufficiently investigated.

In spite of these difficulties, much has been gained and more can be gained if both the geological considerations of the area and the mechanical response of the rock mass are considered simultaneously both in space and time.

This chapter contains a general appreciation of the origin of rocks and the defects in rocks from the point of view of rock mechanics. Emphasis is laid on the genetics of defect-structure in rocks such as folds, faults, joints and rock weathering. Joints, joint surveying and errors in joint surveys are discussed. The classification of intact rock and rock mass is discussed in detail. The classification of in situ rock from the point of view of tunnels and underground excavations is described and its use in determining the pressure on the support explained.

This chapter should be read in conjunction with other chapters especially Chapter 6 (Volume II), Chapter 8 (Volume III) and Chapter 10.

11.2. Minerals and Rocks

A rock is a mineral or an aggregate of minerals. A mineral is a natural inorganic substance of a definite structure and chemical composition. The most important elements that constitute about 99% of crust of the earth extending to upper 16 km (10 miles) are given in Table 24a. These elements and others (about 60 or so) which form the remaining 1%, occur in almost 1500 combinations called minerals. From the point of view of rocks, only 20 or 30 of these combinations are important (Table 24b).

A mineral usually occurs in crystals of characteristic shape representing its atomic structure. In a mass made up of many crystals crowded together, the crystal shape may not be evident, though an examination of individual grain will show consistency in the atomic structure. Certain minerals, however, may not develop any definite crystal shape due to very rapid cooling giving amorphous structure (e.g. glasses).

TABLE 24a

Important elements constituting earth's crust

(after CLARKE, 1924)

Element	Percent
Oxygen	49.78
Silicon	26.08
Aluminium	7.34
Iron	4.11
Calcium	3.19
Sodium	2.33
Potassium	2.28
Magnesium	2.24
Hydrogen	0.95
Titanium	0.35
Chlorine	0.21
Carbon	0.19
Phosphorous	0.11
Sulphur	0.11
Total	99.29

Some of the most important constituents of rock forming minerals are silicates, oxides, carbonates, sulphates, chlorides, phosphates, sulphides and native elements. Silicates are the most important and occur as metasilicates (H_2SiO_3-pyroxenes, amphiboles, leucites, etc.), orthosilicates (H_2SiO_4-mica, olivine, anorthite, nepheline, garnet, etc.) or products of $H_4SiO_3O_8$ (such as orthoclase and albite). The silicates of base elements such as Al, Fe, Mg, Ca, Na, K occur as anhydrous or hydrous depending upon the weathering processes to which these have been subjected. The chief anhydrous silicates in igneous rocks consist of feldspars, feldspathoids, pyroxenes, amphibolites, mica and olivine which on weathering give rise to hydrated products such as kaolinite, chlorite, serpentine, etc. The metamorphic rock silicates usually are sillimanite, kyanite, andalucite, scalprolite, epidote, etc.

Oxides are the next most important constituents of which quartz (SiO_2) dominates and exists in various forms such as chalcedony, cristobolite, tridymate as anhydrous and opal as hydrous. Another group of oxides is that of iron such as magnetite and hematite as anhydrous and limonite as hydrous.

TABLE 24b

Chemical composition of igneous and sedimentary rocks

(after GILLULY, WATERS and WOODFORD, 1959)

CONSTITUENT	IGNEOUS ROCKS	SEDIMENTARY ROCKS
SiO_2	59.14 %	57.95 %
TiO_2	1.05	0.57
Al_2O_3	15.34	13.39
Fe_2O_3	3.08	3.47
FeO	3.80	2.08
MgO	3.49	2.65
CaO	5.08	5.89
Na_2O	3.84	1.13
K_2O	3.13	2.86
H_2O	1.15	3.23
P_2O_5	0.30	0.13
CO_2	0.10	5.38
SO_3	...	0.54
BaO	0.06	...
C	...	0.66
Total	99.56	99.93

Note: The compositions in the table above are based on 5,159 analyses of igneous rocks compiled by F. W. Clarke, and on selected analyses of sedimentary rocks compiled by C.K. Leith and W.F. Mead. The sedimentary rocks have been weighted in the properties of 82 per cent shale, 12 per cent sandstone and 6 per cent limestone. The compositions are reported as *oxides*, which is the conventional system for reporting data on the composition of rocks and minerals.

Carbonates occur chiefly in sedimentary rocks in the form of calcite, dolomite and siderite and as weathering products in igneous rocks. Gypsum and anhydrite are sulphates and pyrite and pyrrhotite are sulphides. Table 25 gives a summary of the properties of these basic mineral constituents.

From the engineering point of view, the products of weathering of the silicates are important. Under the action of water and carbon dioxide, feldspars alter into clay minerals or white mica. The presence of clay at the site of a rock structure always places the engineer or the geologist on alert because of its very complex behaviour and marked influence on the stability. The clay minerals are essentially hydrous aluminium silicates or occasionally hydrous magnesium or iron silicates occurring in the form of flakes and can be divided

TABLE 25

Properties of important rock-forming minerals

(after GILLULY, WATERS and WOODFORD, 1959)

Common Carbonates, Sulfates, Chlorides, and Oxides

MINERAL	FORM	CLEAVAGE	HARD-NESS	SP. GR.	OTHER PROPERTIES
CALCITE. Calcium carbonate, $CaCO_3$.	"Dog-tooth" or flat crystals showing excellent cleavages; granular, showing cleavages; also masses too fine grained to show cleavages distinctly.	*Three highly perfect cleavages at oblique angles*, yielding rhomb-shaped fragments.	3	2.72	Commonly colorless, white, or yellow but may be any color owing to impurities. Transparent to opaque, transparent varieties showing *strong, double refraction* (e.g., 1 dot seen through calcite appears as 2). Vitreous to dull luster. *Effervesces readily in cold dilute hydrochloric acid.*
DOLOMITE. Calcium magnesium carbonate, $CaMg(CO_3)_2$.	*Rhomb-faced crystals showing good cleavage;* also in fine-grained masses.	*Three perfect cleavages* at oblique angles, as in calcite.	3.5–4	2.9	Variable in color, but commonly white. Transparent to translucent. Vitreous to pearly luster. *Powder will effervesce slowly in cold dilute hydrochloric acid, but coarse crystals will not.*
GYPSUM. Hydrous calcium sulfate, $CaSO_4 \cdot 2H_2O$.	Tabular crystals, and cleavable, granular, fibrous, or earthy masses.	*One perfect cleavage, yielding thin, flexible folia;* 2 other much less perfect cleavages.	2	2.2 2.4	Colorless or white, but may be other colors when impure. Transparent to opaque. Luster vitreous to pearly or silky. Cleavage flakes flexible but *not elastic* like those of mica.
HALITE. (Rock salt.) Sodium chloride, NaCl.	Cubic crystals in granular masses.	Excellent cubic cleavage (3 cleavages mutually at right angles).	2 2.5	2.1	*Colorless to white*, but of other colors when impure. The color may be unevenly distributed through the crystal. Transparent to translucent. Vitreous luster. *Salty taste.*
OPAL. Hydrous silica, with 3% to 12% water, $SiO_2 nH_2O$. Does not have a definite geometric internal structure, hence is a mineraloid, not a true mineral.	*Amorphous.* Commonly in veins or irregular masses showing a banded structure. May be earthy.	*None; conchoidal fracture.*	5.0 6.5	2.1 2.3	*Color highly variable, often in wavy or banded patterns.* Translucent or opaque. *Somewhat waxy luster.*

TABLE 25 (Cont)

Common Carbonates, Sulfates, Chlorides, and Oxides—Continued

MINERAL	FORM	CLEAVAGE	HARD-NESS	SP. GR.	OTHER PROPERTIES
CHALCEDONY. (Cryptocrystalline quartz.) Silicon dioxide, SiO_2.	Crystals too fine to be visible; sometimes conspicuously banded, or in masses.	None: *conchoidal fracture.*	6–6.5	2.6	Color commonly white or light gray, but may be any color owing to impurities. Distinguished from opal by *dull* or *clouded luster.*
QUARTZ. (Rock crystal.) Silicon dioxide, SiO_2.	*Six-sided prismatic crystals,* terminated by 6-sided triangular faces; also massive.	None or very poor; *conchoidal fracture.*	7	2.65	Commonly *colorless* or white, but may be yellow, pink, amethyst, smoky-translucent brown, or even black. *Transparent* to opaque. *Vitreous* to *greasy luster.*
MAGNETITE. A combination of ferric and ferrous oxides, Fe_3O_4.	Well-formed, 8-faced crystals, more commonly in compact aggregates, disseminated grains or loose grains in sand.	None; conchoidal or uneven fractures; may show a rough parting resembling cleavage.	5.5–6.5	5.0–5.2	*Black.* Opaque. Metallic to submetallic luster. *Black streak. Strongly attracted by a magnet.* Magnetite is an important iron ore.
HEMATITE. Ferric iron oxide, Fe_2O_3.	Highly varied, compact, granular, fibrous, or earthy, micaceous; rarely in well-formed crystals.	None, but fibrous or micaceous specimens may show parting resembling cleavage; splintery to uneven fracture.	5–6.5	4.9–5.3	Steel-gray, reddish-brown, red, or iron-black in color. Metallic to earthy luster. *Characteristic brownish-red streak.* Hematite is the most important iron ore.
"LIMONITE." Microscopic study shows that the material called limonite is not a single mineral. Most "limonite" is a very finely crystalline variety of the mineral **GOETHITE** containing absorbed water. Hydrous ferric oxide with minor amounts of other elements, roughly $Fe_2O_3 \cdot H_2O$.	Compact or earthy masses; may show radially fibrous structure.	None; conchoidal or earthy fracture.	1–5.5	3.4–4.0	*Yellow,* brown, or black in color. Dull earthy luster, which distinguishes it from hematite. *Characteristic yellow-brown streak.* A common iron ore.
ICE. Hydrogen oxide, H_2O.	Irregular grains; lacelike flakes with hexagonal symmetry; massive.	None; conchoidal fracture.	1.5	0.9	Colorless, white or blue. Vitreous luster. *Melts at 0° C.*, so is liquid at room temperature. *Low specific gravity.*

TABLE 25 (Cont)

Common Rock-Forming Silicates

POTASSIUM FELDSPAR. (Orthoclase, microcline, and sanidine.) Potassium aluminum silicate, $KAlSi_3O_8$.	Boxlike crystals; massive, with excellent cleavage.	One perfect and 1 good cleavage, making an angle of 90°.	6	2.5 - 2.6	Commonly *white, gray, pink*, or pale yellow; rarely colorless. Commonly opaque but may be transparent in volcanic rocks. Vitreous. Pearly luster on better cleavage. *Distinguished from plagioclase by absence of striations.*
PLAGIOCLASE FELDSPAR. (Soda-lime feldspars.) A solid solution group of sodium calcium aluminium silicates, $NaAlSi_3O_8$ to $CaAl_2Si_2O_8$.	In well-formed crystals and in cleavable or granular masses.	*Two good cleavages nearly at right angles* (86°). May be poor in some volcanic rocks.	6 6.5	2.6 2.7	Commonly *white* or *gray*, but may be other colors. Some gray varieties show a play of colors called *opalescence*. Transparent in some volcanic rocks. Vitreous to pearly luster. Distinguished from orthoclase by the presence on the *better cleavage surface of fine parallel lines or striations.*
MUSCOVITE. (White mica; isinglass.) A complex potassium aluminum silicate, $KAl_3Si_3O_{10}(OH)_2$ approximately, but varying.	Thin, scalelike crystals and scaly, foliated aggregates.	*Perfect in one direction, yielding very thin, transparent, flexible scales.*	2 3	2.8 - 3.1	*Colorless*, but may be gray, green, or light brown in thick pieces. *Transparent* to *translucent*. Pearly to vitreous luster.
BIOTITE. (Black mica.) A complex silicate of potassium, iron, aluminium, and magnesium, variable in composition but approximately $K(Mg,Fe)_3AlSi_3O_{10}(OH)_2$.	Thin, scalelike crystals, commonly 6 sided, and in scaly, foliated masses.	*Perfect in one direction, yielding thin, flexible scales.*	2.5 3	2.7 3.2	Black to dark brown. Translucent to opaque. Pearly to vitreous luster. White to greenish streak.

TABLE 25 (Cont)

Common Rock-Forming Silicates — Continued

MINERAL	FORM	CLEAVAGE	HARD-NESS	SP. GR.	OTHER PROPERTIES
PYROXENE. A solid-solution group of silicates. Chiefly silicates of calcium, magnesium, and iron, with varying amounts of other elements. The commonest varieties are *augite* and *hypersthene*.	Commonly in short, 8-sided, prismatic crystals; *the angle between alternate faces* nearly 90°. Also as compact masses and disseminated grains.	*Two cleavages at nearly 90°.* Cleavage not always well developed; in some specimens, conchoidal or uneven fracture.	5–6	3.2–3.6	Commonly greenish to black in color. Vitreous to dull luster. Gray-green streak. Distinguished from amphibole by the *right-angle cleavage, 8-sided crystals*, and by the fact that most crystals are short and stout, rather than long, thin prisms, as in amphibole.
AMPHIBOLE. A group of complex, solid-solution silicates, chiefly of calcium, magnesium, iron, and aluminium. Similar to pyroxene in composition, but containing a little hydroxyl (OH^-) ion. The commonest of the many varieties of amphibole is *hornblende*.	*Long, prismatic, 6-sided crystals*; also in fibrous or irregular masses of interlocking crystals and in disseminated grains.	*Two good cleavages meeting at angles of 56° and 124°.*	5–6	2.9–3.2	Color black to light green; or even colorless. Opaque. *Highly vitreous luster on cleavage surfaces.* Distinguished from pyroxene by the *difference in cleavage angle* and in crystal form. Amphibole also has much better cleavage and higher luster than pyroxene.
OLIVINE. Magnesium iron silicate, $(Fe,Mg)_2SiO_4$.	Commonly in small, *glassy grains* and granular aggregates.	So poor that it is rarely seen; *conchoidal fracture.*	6.5–7	3.2–3.6	*Various shades of green*, also yellowish; opalescent and brownish when slightly altered. *Transparent* to translucent. *Vitreous luster.* Resembles quartz in small fragments but has *characteristic greenish color*, unless altered.
GARNET. A group of solid solution silicates having variable proportions of different metallic elements. The most common variety contains calcium, iron, and aluminum, but garnets may contain many other elements.	Commonly in well-formed *equidimensional crystals* but also massive and granular.	None; *conchoidal or uneven fracture.*	6.5–7.5	3.4–4.3	Commonly *red, brown*, or *yellow*, but may be other colors. Translucent to opaque. *Resinous to vitreous luster.*
SILLIMANITE. (Fibrolite.) Aluminum silicate, Al_2SiO_5.	*In long slender crystals, or fibrous.*	Parallel to length, but rarely noticeable.	6–7	3.2	Gray, white, greenish-gray, or colorless *Slender prismatic crystals or in a felted mass of fibers.* Streak white or colorless.

TABLE 25 (Cont)

Common Rock-Forming Silicates—Continued

KYANITE. (Disthene.) Aluminum silicate, Al_2SiO_5.	Long, *bladelike crystals.*	One perfect, and one poor cleavage, both parallel to length of crystals; and a crude parting across the crystals.	4–7	3.5–3.7	Colorless, white, or a *distinctive pale blue color.* Can be scratched by knife parallel to cleavage, but is harder than steel across cleavage.
STAUROLITE. Iron-aluminum silicate, $Fe(OH)_2(Al_2SiO_5)_2$.	*Stubby prismatic crystals,* and in *cross-shaped twins.*	Poor and inconspicuous.	7–7.5	3.7	Red-brown or yellowish-brown to brownish black. Generally in well-shaped crystals larger than the minerals of the matrix enclosing them.
EPIDOTE. A complex group of calcium, iron, aluminum silicates, $Ca_2(Al,Fe)_3(SiO_4)_3(OH)$.	*Short, 6-sided crystals* or radiate crystal groups and in granular or compact masses.	One good cleavage; in some specimens, a second poorer cleavage at an angle of 115° with the first.	6–7	3.4	Characteristic *yellowish-green (pistachio green)* color. Vitreous luster.
CHLORITE. A complex group of hydrous magnesium aluminum silicates containing iron and other elements in small amounts.	Commonly in *foliated* or *scaly masses*, may occur in tabular, 6-sided crystals resembling mica.	*One perfect cleavage,* yielding thin, flexible, but inelastic, scales.	1–2.5	2.6–3.0	*Grass-green* to *blackish-green* color. Translucent to opaque. Greenish streak. Vitreous luster. *Very easily disintegrated.*
SERPENTINE. A complex group of hydrous magnesium silicates, roughly $H_4Mg_3Si_2O_9$.	Foliated or fibrous, usually massive.	Commonly only one cleavage, but may be in prisms. Fracture usually conchoidal or splintery.	2.5–4	2.5–2.65	*Feels smooth, sometimes greasy.* Color *leek-green* to *blackish-green* but varying to brownish-red, yellow, etc. *Luster resinous* to *greasy.* Translucent to opaque. Streak white.
TALC. Hydrous magnesium silicate, $Mg_3(OH)_2Si_4O_{10}$.	In tiny *foliated scales* and soft compact masses.	*One perfect cleavage,* forming thin scales and shreds.	1	2.8	White or silvery white to apple green. *Very soft,* with a *greasy feel.* Pearly luster on cleavage surfaces.

TABLE 25 (Cont)

Common Rock-Forming Silicates Continued

MINERAL	FORM	CLEAVAGE	HARDNESS	SP. GR.	OTHER PROPERTIES
KAOLINITE. Hydrous aluminum silicate, $H_4Al_2Si_2O_9$. Representative of the 3 or 4 similar minerals common in clays.	Commonly in soft, compact, *earthy masses.*	Crystals always so small that cleavage is invisible without microscope.	1–2	2.2–2.6	White color, but may be stained by impurities. *Greasy feel. Adheres to the tongue,* and *becomes plastic when moistened.* "*Claylike*" odor when breathed upon.
Important Ore Minerals					
GALENA. Lead sulfide, PbS.	Cubic crystals common, but mostly in coarse to fine granular masses.	*Perfect cubic cleavage* (three cleavages mutually at right angles).	2.5	7.3–7.6	*Silvery-gray color.* Metallic luster. Silvery-gray to grayish-black streak. Chief ore of lead.
SPHALERITE. Zinc sulfide (nearly always containing a little iron), ZnS.	Crystals common, but chiefly in fine to coarse-granular masses.	*Six highly perfect cleavages at 60° to one another.*	3.5–4	3.9–4.2	Color ranges from white to black but is commonly *yellowish-brown. Translucent* to opaque. *Resinous* to *adamantine luster.* Streak white, pale yellow or brown. Most important ore of zinc.
PYRITE. ("Fool's gold.") Iron sulfide, FeS_2.	*Well-formed crystals,* commonly cubic, with striated faces; also granular masses.	None; uneven fracture.	6–6.5	4.9–5.2	Pale *brassy-yellow color;* may tarnish brown. Opaque. Metallic luster. Greenish-black or brownish-black streak. Brittle. Not a source of iron, but used in the manufacture of sulfuric acid. Commonly associated with ores of several different metals.
CHALCOPYRITE. Copper iron sulfide, $CuFeS_2$.	Compact or disseminated masses, rarely in wedge-shaped crystals.	None; uneven fracture.	3.5–4	4.1–4.3	Brassy to *golden-yellow. Tarnishes* to blue, purple, and reddish iridescent films. Greenish-black streak. Distinguished from pyrite by deeper yellow color and softness. A common copper ore.
CHALCOCITE. (Copper glance.) Cuprous sulfide, Cu_2S.	Massive, rarely in crystals of roughly hexagonal shape. May be tarnished and stained to blue and green.	Indistinct, rarely observed.	2.5–3	5.5–5.8	Blackish-gray to steel gray, commonly *tarnished to green or blue.* Dark gray streak. *Very heavy.* Metallic luster. An important ore of copper.

TABLE 25 (Cont)

Important Ore Minerals — Continued

COPPER. (Native copper.) An element, Cu.	*Twisted and distorted leaves and wirelike forms; flattened or rounded grains.*	None.	2.5–3	8.8–8.9	*Characteristic copper color*, but commonly *stained green*. *Highly ductile* and malleable. Excellent conductor of heat and electricity. *Very heavy*.
GOLD. An element, Au.	Massive or in thin plates; also in flattened grains or scales; distinct crystals very rare.	None.	2.5–3	15.6–19.3	*Characteristic gold-yellow color and streak*. *Rarely in crystals*. *Extremely heavy*. Very malleable and ductile.
SILVER. An element, Ag.	In flattened grains and scales; rarely in wirelike forms, or in irregular needlelike crystals.	None.	2.5–3	10–11	*Color and streak are silvery-white*, but may be tarnished gray or black. *Highly ductile and malleable*. *Very heavy*. Mirrorlike metallic luster on untarnished surfaces.
CASSITERITE. Tin dioxide, SnO_2.	Well-formed, 4-sided prismatic crystals terminated by pyramids; 2 crystals may be intergrown to form knee-shaped twins; also as rounded pebbles in stream gravels.	None; curved to irregular fracture.	6–7	7	*Brown* to *black*. *Adamantine* luster. White to pale-yellow streak. Chief ore of tin.
URANINITE. (Pitchblende.) Uranium oxide, UO_2 to U_3O_8.	Regular 8-sided or cubic crystals; massive.	None; fracture uneven to conchoidal.	5–6	6.5–10	Color black to brownish-black. Luster submetallic, pitchlike, or dull. Chief mineral source of uranium, radium, etc.
CARNOTITE. Potassium uranyl vanadate, $K_2(UO_2)_2(VO_4)_2 \cdot 8H_2O$.	Earthy powder.	Not apparent.	Very soft	4.1 approx.	*Brilliant canary-yellow color*. An ore of vanadium and uranium.

into kaolinites (single tetrahedral silica sheet and single octahedral alumina sheet, a combination repeating itself), montmorillonites (alumina octahedral sheet between two silica tetrahedral sheets), and illites (similar to montmorillonite except that it occurs as an aggregate of smaller particles).

Kaolinites are subject to minimal expansion on contact with water and have a larger angle of internal friction than other clay minerals. Sometimes the clay minerals occur in round and flattened tubes such as halloysite which when wet acts like a pile of rollers and starts to flow.

Montmorillonite sheets being loosely bound, water molecules enter in between these sheets causing swelling, lowering internal friction giving high plasticity and high cracking on drying. As a result heavy damage may occur to structures placed on these either due to expansion and contraction or due to creep and flow.

When mica occurs in some rocks, these have to be given proper attention since easy cleavage of rocks containing this mineral may result to rapid deterioration after it is exposed to weathering (e.g. mica schist).

Certain hydrous silicates such as serpentine, chlorite, talc, illite require attention. Serpentine may be competent or soft and greasy having a low friction angle and even when competent can rapidly deteriorate into soft incompetent material under atmospheric action. Chlorites are not so hazardous as serpentine, but when present in joints may greatly decrease the frictional values and cause instability. Talc is very soft and is a very poor foundation material.

Among the oxides quartz is the most durable and reliable constituent of rocks and an increased percentage of this is an indication of greater stability of the structure placed in it.

11.3. Geological Classification of Rocks

From an engineering view point 'rock' means a compact semihard to hard mass of a variety of minerals, but the geological classification of rocks is based upon their origin and rocks are divided into three major groups: igneous, sedimentary and metamorphic. Igneous rocks are formed by the solidification of molten magma. Sedimentary rocks are derived from the weathering and denudation of igneous or other old rocks which may be either left in place or transported and deposited somewhere else and later consolidated and cemented together under depositional loads and percolating mineral waters. Metamorphic rocks are formed from pre-existing igneous and sedimentary rocks under the action of heat and pressure. These two factors act individually or together in combination with time.

Igneous Rocks

Igneous rocks are classified either depending upon the silica content or the mineralogical composition or the texture. On the basis of the silica content igneous rocks are subdivided into the following groups:
Acid igneous-silica content > 66%
Intermediate igneous-silica content 52 66%
Basic igneous-silica content 45–52%
Ultrabasic igneous-silica content < 45%

Using mineralogical composition as a classifying method, acid igneous rocks contain quartz in excess of 10%; intermediate igneous rocks contain less than 10%; in basic igneous rocks, quartz is either absent or is present only as an accessory mineral and in ultrabasic rocks quartz is completely absent. The presence of ferromagnesian minerals imparts colour to the igneous rocks and they tend to be darker as they pass from acid igneous to ultrabasic. Alkali feldspars (e.g. orthoclase, microcline and albite-rich plagioclase) are dominant in the intermediate igneous rocks while in basic rocks talc-alkali-feldspars (plagioclases) are the important constituents.

Some igneous rocks have a massive structure i.e. their minerals are not arranged in parallel or distinct layers while others may show definite flow structure. Depending upon the rate of cooling, their texture may be glassy (rapid cooling —e.g. outer surface of lava flows), fine grained or felsitic (rather rapid cooling but not so quickly to prevent crystallisation), granular (coarse grained crystals of more or less the same size) or porphyritic (large crystals embedded in a fine grained ground mass. Table 26 gives the classification of igneous rocks depending upon the composition and environments effecting texture. Table 27 gives the minerals associated with common igneous rocks.

During volcanic activity, with the ejection of lava, some air bubbles may be trapped giving vesicular texture and which may later be even filled with some other minerals. Volcanic ashes and tuffs so ejected may get solidified giving volcanic breccia embedded in a matrix of rapidly cooled lava giving pyroclastic texture.

Igneous rocks on solidification develop tensile joints as their mechanical constraints change depending upon their depth and existing stress field.

Sedimentary Rocks

There are four groups of sedimentary rocks, namely 1. Breccias and mechanical sediments not limestones 2. Limestones 3. Organic remains and 4. Evaporites. Many times sedimentary rocks are grouped depending upon the sedimentation environments such as:

TABLE 26

Classification of igneous rocks

(after GILLULY, WATERS & WOODFORD, 1959)

Textures	Predominant Minerals: Feldspar and Quartz	Feldspar Predominates (no quartz)	Ferro-magnesian Minerals and Feldspar (no quartz)	Ferro-magnesian Minerals (no quartz or feldspar)
Pyroclastic	**Volcanic tuff** (fragments up to 4 mm. in diameter) **Volcanic Breccia** (fragments more than 4 mm. in diameter)			Rocks of the texture and composition represented by this part of the table are rare or unknown.
Glassy	**Obsidian** (if massive glass) **Pumice** (if a glass froth)		**Basalt Glass**	
Aphanitic (generally porphyritic-aphanitic)	**Rhyolite** and **Dacite**	**Andesite**	**Basalt**	
Granular	**Granite** potassium feldspar predominates) and **Granodiorite** (plagioclase feldspar predominates)	**Diorite**	**Gabbro** **Dolerite** or **Diabase** (if fine grained)	**Peridotite** (with both olivine and pyroxene) **Pyroxenite** (with (pyroxene only) **Serpentine** (with altered olivine and pyroxene)

INCREASING GRAIN SIZE ↓

DECREASING SILICA CONTENT →

(a) *Continental environments*: i.e. essentially land areas, such as:
- (i) Fluviatile-deposits laid down by rivers;
- (ii) Lacustrine-deposits of fresh-water lakes;
- (iii) Salt lake-deposits formed by the shrinking and evaporation of salt-water lakes;
- (iv) Glacial-morainic debris, i.e. material deposited by glaciers
  and
  Fluvio-glacial deposits which are formed of material washed out of glaciers, and although originating as a result of ice action are later transported and deposited by water;
- (v) Aeolian-deposits transported and deposited by wind

(b) *Intermediate environments*, such as:
- (i) Deltaic-deposits formed in deltas;

TABLE 27

Minerals associated with igneous rocks

(after DUNCAN, 1969)

Granite the essential minerals are quartz and feldspar. Commonly, mica is present either as muscovite or biotite. Hornblende and tourmaline may be present.

The same mineralogical composition applies to the other acid, alkali-feldspar dominant rocks, namely: Quartz porphyry, microgranite, rhyolite, obsidian and pitchstone.

Granodiorite the essential minerals are quartz and plagioclase feldspar. Orthoclase feldspar, hornblende and biotite, are common.

The same mineralogical composition applies to the other acid, calc-alkali felspar dominant rocks namely: Microgranodiorite and dacite.

Syenite the chief constituent is orthoclase feldspar, usually forming well over half of the rock. Plagioclase present in smaller amount. Hornblende, biotite and sometimes augite may be present.

The same composition applies to the other intermediate, alkali-feldspar dominant rocks, namely: Microsyenite and trachyte.

Diorite the essential minerals are plagioclase feldspar and hornblende. Some biotite, orthoclase feldspar and quartz are present frequently.

The same composition applies to the other intermediate, calc-alkali-feldspar dominant rocks, namely: Microdiorite and andesite.

Gabbro essential minerals are plagioclase feldspar and augite. Hornblende and olivine may be present. Alkali gabbros may contain orthoclase feldspar.

The same composition applies to the other basic rocks, namely: *Dolerite* and *basalt*.

Dunite olivine is the main constituent.

Peridotite olivine is the main constituent, possibly with augite, hornblende and biotite.

Picrite contains some feldspar with olivine, augite and hornblende.

(ii) Estuarine-deposits formed in estuaries of rivers;
(iii) Shore deposits-formed along coast lines

(c) *Marine environments*: i.e. essentially deep water areas:
(i) Continental shelf-deposits;
(ii) Shallow water-deposits of the Continental shelf;
(iii) Deep water-deposits formed in depths of water less than 6,000 ft (1830 m);
(iv) Abyssal-deposits formed in depths of water greater than 6,000 ft (1830 m).

Because of the very mode of their formation the shape and size of grains of mechanically formed sediments depend upon the original shape of the material supplied by the older rocks (e.g. quartz-angular, feldspars-bounded by cleavage

planes and irregular mica flakes), method and amount of transport (air-highest rounding, ice-least rounding, water-medium rounding). The various grain sizes found in sedimentary rocks are given in Table 28.

TABLE 28

Fragment and grain sizes and corresponding sedimentary rock

(after KRYNINE and JUDD, 1957)

Material	Unified classification grading	Wentworth grading	Rock
Boulders	12 in	250 mm	Boulderstone
Cobbles	3–12 in	64–256 mm	Cobblestone
Gravel	$^1/_4$–3 in	4–64 mm	Conglomerate
Granules		2–4 mm	Conglomerate
Sand	0.003–$^1/_4$ in	1/16–2 mm	Sandstone
Silt	Less than 0.003 in	1/256–1/16 mm	Siltstone
Clay	Less than 0.003 in	Less than 1/256 mm	Claystone

Depending upon the grain size, texture and structure, the rocks are divided into clastic (composed of fragments of pre-existing rocks and minerals), fine crystalline (mostly with organic admixtures), amorphous and biofragmental (Table 29).

Because of the very mode of formation of the sedimentary rocks, they are bedded or stratified and separation planes are associated with the mode of deposition such as regular beddings and laminae, current bedding, cross bedding, graded bedding, slump bedding, current ripple marks and sun cracks (Fig. 11-1).

The mechanically placed sediments may be unconsolidated or consolidated and cemented. Consolidation takes place with increasing depth, gradual sinking, dewatering followed by cementation and even welding of individual grains and recrystallisation at greater depths and temperature or in the presence of certain solutions.

The most common cements found in sedimentary rocks are siliceous (SiO_2), calcareous ($CaCO_3$), ferrogenous and argillaceous (clay). Siliceous cement is most resistant to weathering and water action while clay is the least durable bonding material. Calcareous cement generally makes a durable rock but may be leached by acidic waters or those containing carbon dioxide. Ferrogenous cemented rocks are also liable to rapid weathering.

TABLE 29

Classification of sedimentary rocks

(after GILLULY, WATERS & WOODFORD, 1959)

Clastic Sedimentary Rocks

Consolidated Rock	Chief Mineral or Rock Components	Original Unconsolidated Debris	Diameter of Fragments
Conglomerate	Quartz, and rock fragments	Gravel (rounded pebbles)	More than 2 mm.
Breccia	Rock fragments	Rubble (angular fragments)	
Sandstone	...	Sand	2 to $\frac{1}{16}$ mm.
Quartz Sandstone	Quartz	Quartz-rich sand	
Arkose	Quartz and feldspar	Feldspar-rich sand	
Graywacke	Quartz, feldspar, clay, rock fragments, volcanic debris	"Dirty sand," with clay and rock fragments	
Shale	Clay minerals, quartz	Mud, clay and silt	Less than $\frac{1}{16}$ mm.
Clastic Limestone	Calcite	Broken and rounded shells and calcite grains	Variable

Organic and Chemical Sedimentary Rocks

Consolidated Rock	Chief Mineral or Rock Components	Original Nature of Material	Chemical Composition of Dominant Material
Limestone	Calcite	Shells; chemical and organic precipitates	$CaCO_3$
Dolomite	Dolomite	Limestone, or unconsolidated calcareous ooze, altered by solutions	$CaMg(CO_3)_2$
Peat and Coal	Organic materials	Plant fragments	C, plus compounds of C, H, O
Chert	Opal, chalcedony	Siliceous shells and chemical precipitates	SiO_2 and SiO_2nH_2O
Evaporites, or Salt Deposits	Halite, gypsum, anhydrite	Evaporation residues from the ocean or saline lakes	Varied, chiefly NaCl and $CaSO_4 2H_2O$

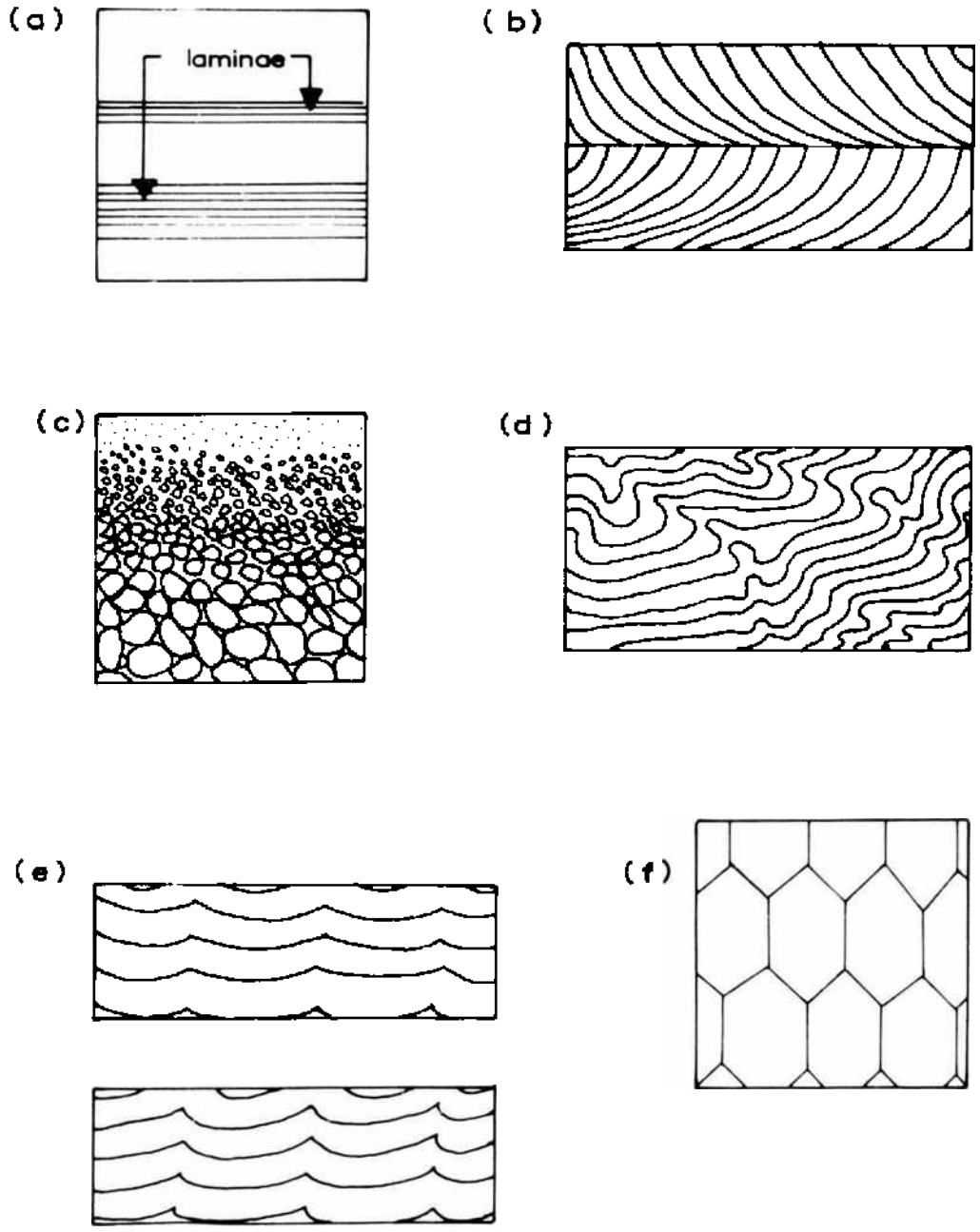

Fig. 11-1. Depositional features of sedimentary rocks
(a) Regular bedding
(b) Current bedding
(c) Graded bedding
(d) Slump bedding
(e) top-Wave ripple marks
bottom-Current ripple marks
(f) Sun cracks
(after DUNCAN, 1969).

Sedimentary rocks may at a later stage be subjected to tectonic stresses resulting in folding and faulting with more than one set of joints introduced in them.

From the engineering point of view, quartzite, siliceous and calcareous sandstones, arkose, and graywacke are competent rocks. Conglomerates, unless well cemented, may weather severely when exposed. Shales, claystones, mudstones and siltstones are of most concern to a rock mechanics engineer. Their strength and durability vary within wide limits. Sitlstones in general disintegrate very quickly on contact with water while shales may be quite hard and durable. All these when subjected to alternate dry and wet cycles revert to original clays.

Limestones and dolomites are in general competent materials for structures except when they contain clays. Cavernous limestones occurring under a reservoir or a dam may cause excessive leakage. Limestone is liable to decompose under heat and is not suitable as an aggregate in air strips for jet planes. Chalk is a weak variety of limestone and is not suitable for heavy structures. This is also true of marl.

Chalk with saturation moisture of about 20% often does not exhibit swelling on absorbing water. Non-calcareous rocks containing moisture behave as competent, but rocks containing argillaceous materials tend to be incompetent and require proper attention.

Almost all sedimentary rocks have a preferred fabric orientation and hence their properties are direction sensitive.

Metamorphic Rocks

There are two groups of metamorphic rocks: 1. Contact metamorphic, produced by local heating of country rock adjacent to igneous intrusions. 2. Regionally metamorphic rocks extending to over great distances and metamorphosed under the action of pressure and temperature. Metamorphic rocks are classified mostly on the basis of their mineralogy and texture. Table 30 gives the principal metamorphic rocks.

The texture produced in these rocks is the result of heat and pressure acting simultaneously. Hornfelsic texture is produced due to heat in the vicinity of igneous rocks and alters shales into hornfels. Under the influence of directed stresses, rocks develop slaty cleavage. Cleavage is also associated with changes in rock fabric and strong folding. Under the influence of both heat and pressure, the fluids in pores may migrate and crystallise on the fracture surfaces with their long axes aligned parallel to the cleavage giving a silky appearance or phyllite texture. Extensive folding and continued directed

TABLE 30

Classification of metamorphic rocks

(after GILLULY, WATERS & WOODFORD, 1959)

Name	Texture	Commonly Derived from	Chief Minerals
	Unfoliated or Faintly Foliated		
Hornfels	Hornfelsic	Any fine-grained rock	Highly variable
Quartzite	Granoblastic, fine grained	Sandstone	Quartz
Marble	Granoblastic	Limestone, dolomite	Calcite, magnesium and calcium silicates
Tactite	Granoblastic, but coarse and variable	Limestone or dolomite plus magmatic emanations	Varied; chiefly silicates of iron, calcium, and magnesium, such as garnet, epidote, pyroxene, amphibole
Amphibolite	Granoblastic	Basalt, gabbro, tuff	Hornblende and plagioclase, minor garnet and quartz
Granulite	Granoblastic	Shale, graywacke, or igneous rocks	Feldspar, pyroxene, garnet, kyanite, and other silicates
	Foliated		
Slate (and **Phyllite**)	Slaty	Shale, tuff	Mica, quartz
Chlorite schist	Schistose to slaty	Basalt, andesite, tuff	Chlorite, plagioclase, epidote
Mica schist	Schistose	Shale, tuff, rhyolite	Muscovite, quartz, biotite
Amphibole schist	Schistose	Basalt, andesite, gabbro, tuff	Amphibole, plagioclase
Gneiss	Gneissose	Granite, shale, diorite, mica schist, rhyolite, etc.	Feldspar, quartz, mica, amphibole, garnet, etc.
Migmatite	Coarsely banded, highly variable	Mixtures of igneous and metamorphic rocks	Feldspar, amphibole, quartz, biotite

stresses as in mountain building regions may further convert the texture into schistose and gneissose. Recrystallisation occurring under hydrostatic pressures and heat gives rise to granulites (granulite, quartzite and marble).

11.4. Defects in Rocks

All features, starting from ultra microscopic to macroscopic, that influence the strength and deformation properties of the rocks can be called defects. The influence of these defects is to decrease the load carrying capacity of rocks and cause concentration of stresses in certain directions around an excavation.

Defects in rocks can be grouped into the following categories: 1. Fabric defects and 2. Structural defects.

11.4.1. Fabric Defects

The component parts of a material may be arranged in some irregular or regular order relative to each other which defines what is known as rock fabric.

Fabric therefore refers to the spacial data about the grains constituting the rock mass, their orientation, mutual relationship to each other or packing. The measure of the fabric is therefore the orientation of the grain (inclination of a fixed direction, axis or plane within the grain) to a fixed direction outside it. The *c*-axis of quartz grains is a typical example of the use of the crystallographic plane with the geographic North as the exterior reference axis. Another way of describing the orientation of the grains is to refer apparent long axes of the grains with reference to the bedding planes or the geographic North. Obviously, therefore, there are two ways of analysing the orientation fabric, the crystallographic or petrographic fabric referring to internal crystallographic structure and the other relating to the morphology of the grain. As such 4 different types of fabric structure may be recognised (Fig. 11-2).

Preferred morphological orientation of grains in a rock is the result of several factors such as their mode of origin and initial shape (arrangement of pebbles and cobbles in a stream deposit, JOHANSSON, 1965) and their strain history. This is a result of the kinematic processes which the rock has undergone. The crystallographic fabric is the result of the stress field at the time of crystallisation or recrystallisation of the mineral grains and develops under sustained conditions of stress and temperature or both. In general the fabric development of one kind is coupled with the fading of the other fabric but the traces of this may be retained indicating thereby whole deformation history of the rock recorded in its "inherited fabric" (TURNER and WEISS, 1963).

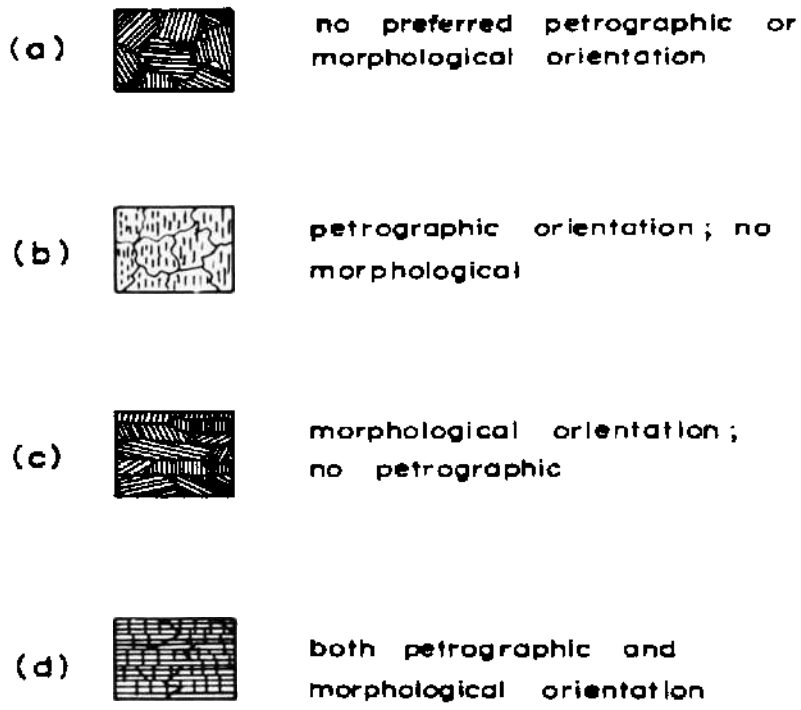

Fig. 11-2. Types of fabric structures in aggregates.

The usual method of determination of the fabric is to observe the thin sections under a microscope, though sometimes, examining hand specimens in the field using a magnifying glass and establishing the number of micas per unit area showing their basal sections (high lustre planes) could give an idea about morphological fabric. If the field of the hand specimen is taken as a unit area and the number of micas are determined on the three different faces of hand specimen, one could get a rough idea of the fabric. If the rock is layered, there shall be a preferred direction with a pronounced maximum number of micas. Same is true if other nonspherical grains are studied in a hand specimen.

In the study of crystallographic fabric, measurements are carried out on a single mineral entity such as quartz, mica, feldspar, calcite, hornblende which have easily recognisable crystallographic properties such as cleavage of mica, optical axes of quartz and hornblende, twinning planes of calcite, etc. The measure of the fabric orientation is the measurement of deviation from the reference direction leading to a range of measurements both of declination and bearing (Fig. 11-3). The degree of preferred orientation is estimated by the standard deviation (variance) and the variance ratio test (GRIFFITHS, 1967) gives a suitable method for testing significance of orientation. The smaller the variance, the higher the degree of orientation.

Crystallographic fabric studies have been found to be related to the stress field. TURNER et al (1956) found a close relationship between the imposed stress system and *c*-axis orientation of recrystallised calcite. Crystallographic

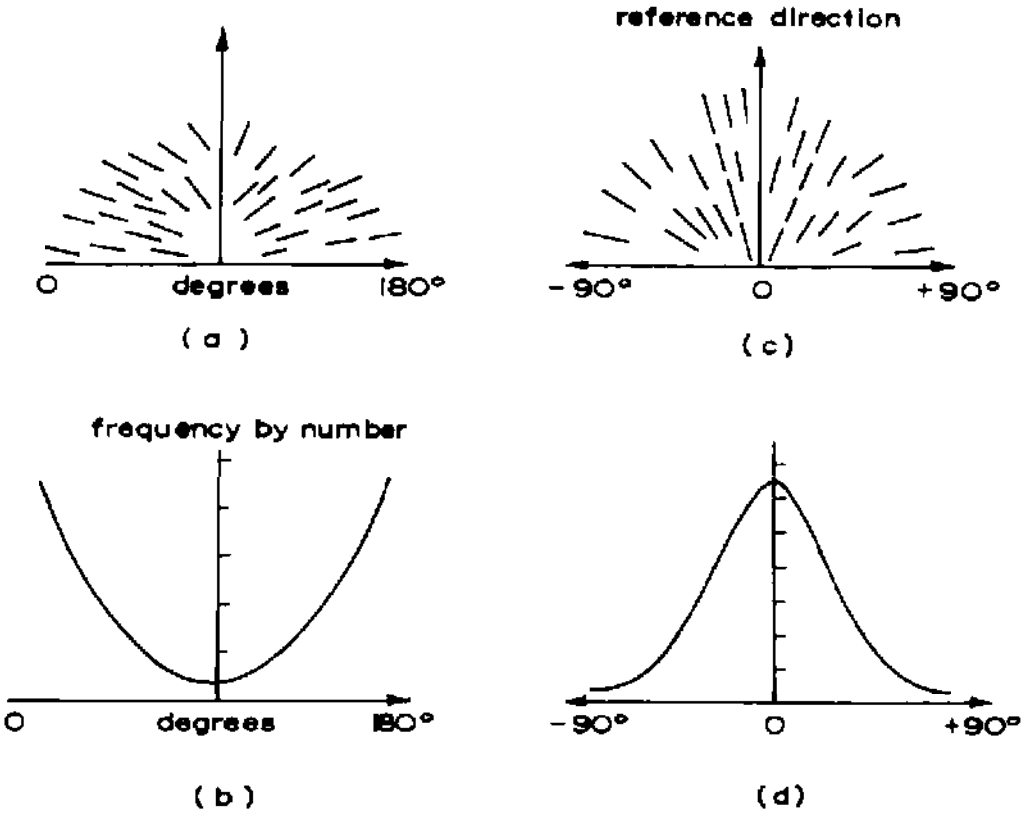

Fig. 11-3. Unimodality produced by rotation of reference directions
(a) Orientation of long 'a' axes; reference direction bedding
(b) U-shaped frequency distribution from (a)
(c) Orientation of long 'a' axes measured as deviations from bedding: reference direction rotated 90
(d) Unimodal frequency distribution from (c)
(after GRIFFITHS, 1967).

fabric that develops in an anisotropic mineral is dependent upon the stress field in such a way that the potential energy of the external forces and the potential energy of the system are minimised. The potential energy of an anisotropic mineral in an anisotropic field is a function of the orientation of the mineral relative to the stress field and will be minimum for certain orientations which this mineral will tend to take. Applying MACDONALD's (1957) thermodynamic predictions, BRACE (1960) showed that the $(10\bar{1}1]$ plane for calcite, $[10\bar{1}2]$ plane for high quartz, and the $[02\bar{2}1]$ plane for low quartz shall be oriented such that in a single component of stress these shall be perpendicular to the stress. In a triaxial nonhomogeneous stress field the orientation is dependent both on the stress difference and the confining pressure which indicates that theoretically similar fabric orientations are possible in rocks with same stress difference but different confining pressures. The equilibrium orientation of ice in different stress fields is given in Fig. 11-4. Work of GRIGGS, TURNER and HEARD (1960) showed that in the recrystallisation of calcite marble, grains have a strong preferred orientation parallel to the maximum

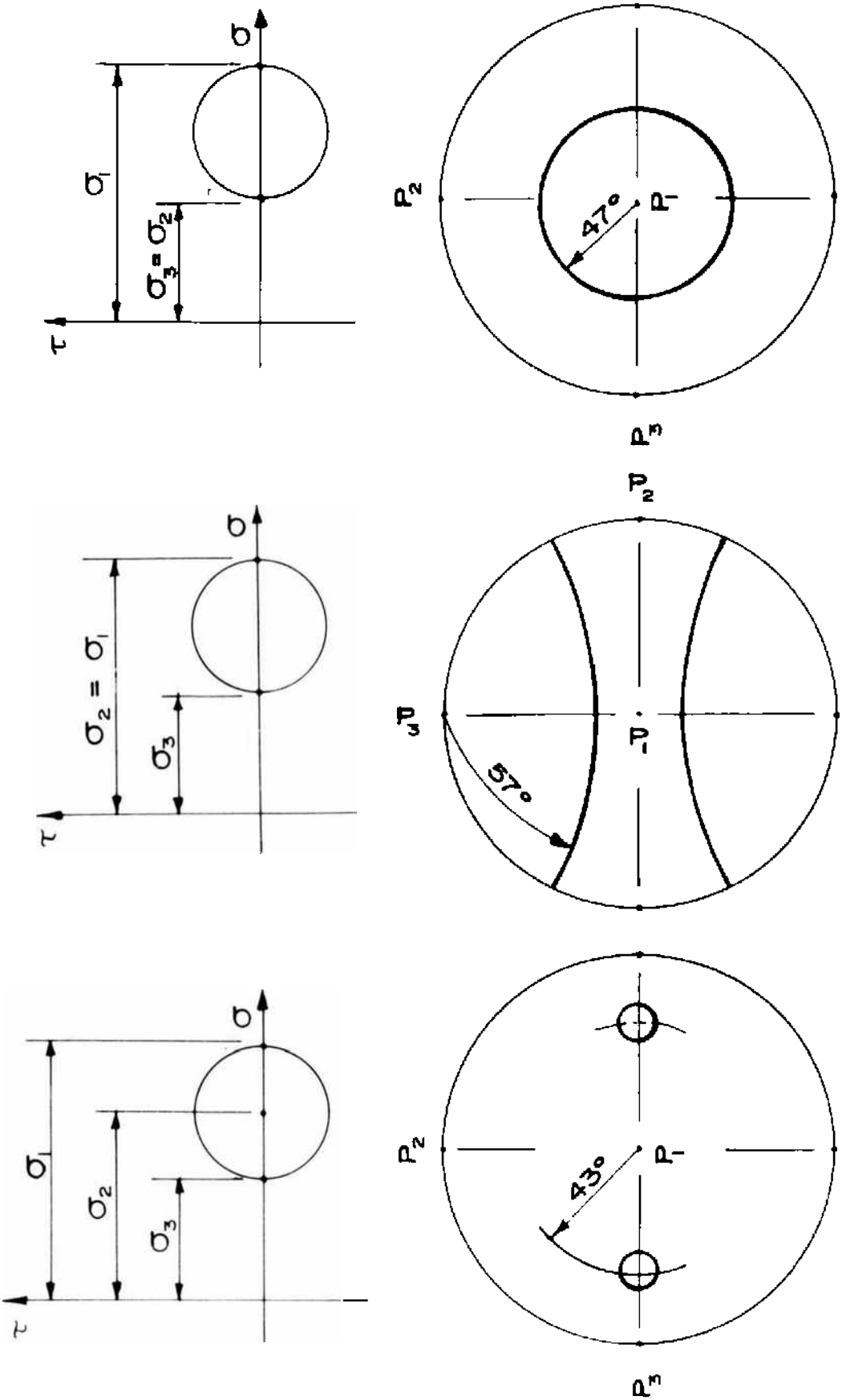

Fig. 11-4. Preferred orientation of ice in a general stress field. Heavy circles show upper hemisphere projections of c-axes (after BRACE 1960).

principal stress. This is also in accordance with the theoretical interpretations of KAMB (1959). In uniaxial compression tests, the *c*-axis of calcite is found to be perpendicular to the stress axis and in triaxial extension (with cylinders elongated in the direction of their axes and compressed radially) c-axis of the recrystallised grains is perpendicular to the axis of the cylinder and in the plane of greatest compression.

In practice, however, there has been little success in predicting stress from fabric studies. In some cases it has been possible to correlate the extreme stress history (only the last cycle) to the fabric orientation utilising the *c*-axis of quartz (PRICE, 1975), but the full objectives have not been realised. It has been often found that the orientation diagrams of different minerals in the same slide have different symmetries, for instance, mica planes are more or less parallel to main slip planes (*s*-plane) of schistosity showing monoclinic symmetry but the quartz grains shapes are inclined to this plane. The explanation very often put forward is that quartz is very mobile and that this different symmetry of quartz is due to later orientation of quartz. Similarly, in microfolds, it has been found that several kinds of deformations may have occurred in the same structure. The preferred orientation of minerals can assume the two basic patterns: maxima or girdles. There may be more than one maximum in a section but more than one girdle is quite common. There may be maxima enclosed in a girdle pattern (Fig. 11-5).

Some orientation patterns in terms of tectonic or growth structure are given in Fig. 11-6 (DE SITTER, 1964). The various features in Fig. 11-6 are explained below:

I. *A concentration of poles in one maximum(m).*
   (a) Presence of a single set of *s* planes, the pole of which coincides with *m*, commonly shown by (001) of mica either because of growth in a plane of least resistance or for mechanical reasons; common for (001) in mica and $(01\bar{1}2)$ of calcite (IA).
   (b) Presence of a single set of *s* planes within which *m* coincides with direction of slip. Very common in quartz (0001) (1B).
   (c) Presence of a '*b*' axis whose pole coincides with *m*, either for mechanical reasons or because of fabric growth of prismatic crystals in that direction; (001) in hornblende, for instance (IC).

II. *An arcuate girdle of concentration in a great circle.* The measured optical directions tend to fall within a plane surface.
   (a) The same case as in IA, but the single set of *s* planes has been folded; the fold axis is then the axis of the girdle (001) in mica and chlorite, $(01\bar{1}2)$ in calcite, (0001) in quartz (IIA).

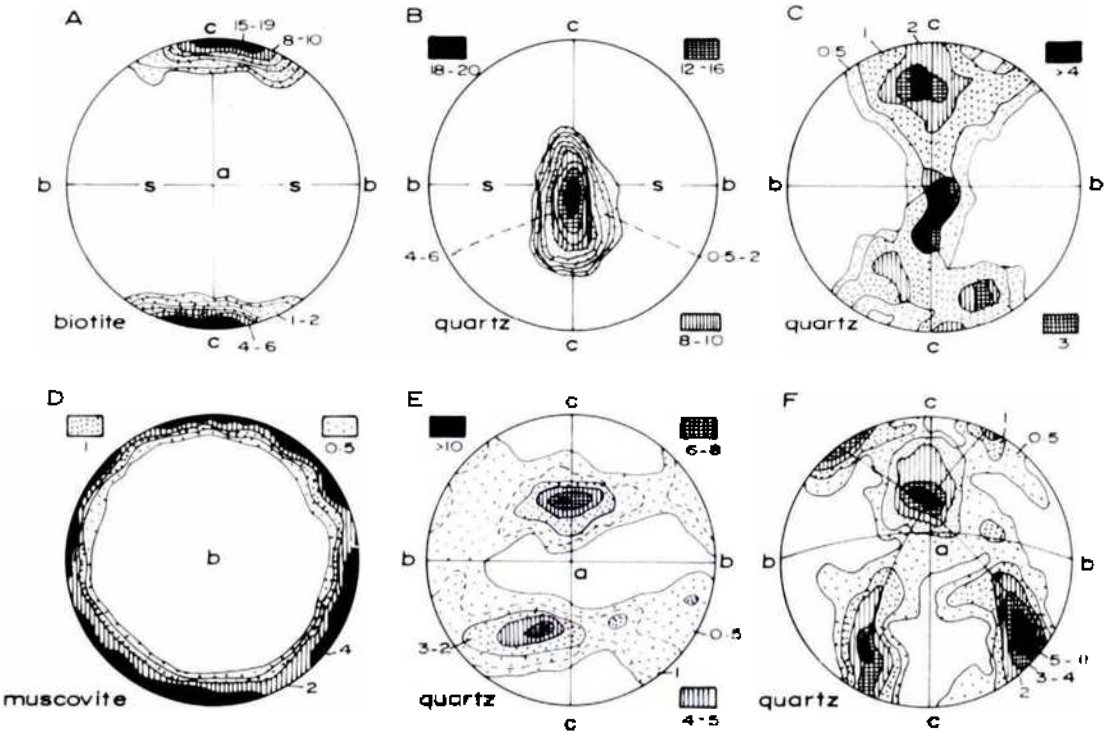

Fig. 11-5. Different patterns of preferred orientation
(A) Biotite axes maximum vertical to schistosity plane
Garnet schist from S. Valpurga d'Ultimo
(B) Quartz c-axes maximum parallel to 'a' axis in granite mylonite, Odenwald
(C) Girdle of quartz c-axes in 'ac' plane. Quartzite from the eastern Alps
(D) Girdle in 'ac' plane of muscovite cleavage. Mica schist from Schimborn
(E) Two small girdles of quartz optical axes. Granulite from Saxony
(F) Two crossing girdles of quartz optical axes. Granulite from Finland
(after NIGGLI, 1948).

(b) Intersection of several sets of *s* planes in a line coinciding with the axis of the girdle (*b* axis); (001) in mica and chlorite, $(01\bar{1}2)$ in calcite, (0001) in quartz (IIB).

(c) The same case as in IA or IB, but the faces or cleavage parallel to the axes of the prismatic minerals, and not the axes themselves.

(d) Growth of elongated crystals with their longest dimension (e.g., 001 in hornblende) oriented at random in a plane of minimum resistance to growth, which coincides with the plane of the girdle (IIC).

III. *A girdle which is not a great circle, but a small circle of the sphere of projection.* The measured optical lines thus tend to lie on the surface of a cone (III).

(a) The measured optical direction makes an angle with the crystal face oriented in *s*. This is essentially the same case as IA, except that some optical angles and not the crystal faces, are measured, as, for instance, the (0001) axis of calcite, which is oriented in the *s* plane according to its $(01\bar{1}2)$ faces. The diameter of the ring is then 52 .

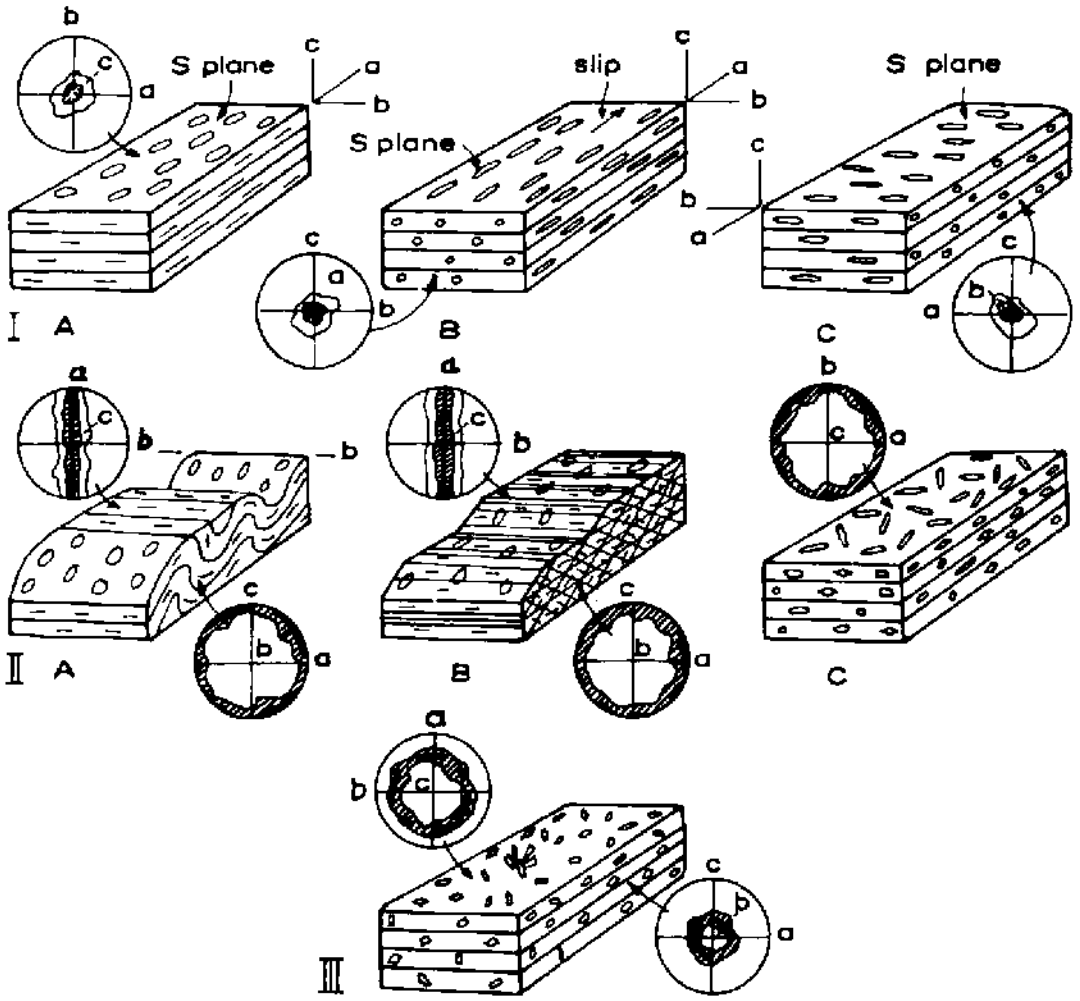

Fig. 11-6. Preferred orientation patterns of different structural features (after DE SITTER, 1964).

(b) The *b* axis is an axis of rotation, the pole of which coincides with the centre of the ring, Quartz diagrams very often show this arrangement.

A concise idea about the fabric types in the different types of rocks is given below.

In sedimentary rocks, if the detrital material is dimensionally anisotropic, then during transport it moves with the longer axis parallel to the current direction if in suspension and at right angles to the current direction if in traction (Fig. 11-7a) and this orientation can be maintained during deposition and subsequent compaction and cementation with some influence of the size of the substrata, its own (particle) shape and size and packing, etc. (CAILLEUX, 1938; HUTTA, 1956). Structural fabric of sedimentary rocks also gives an indication of the environments at the time of deposition (Fig. 11-7b). Beach and river deposits show pronounced preferred orientation and different degrees of imbrication of their particles (CAILLEUX, 1938). Glacial deposits are similarly

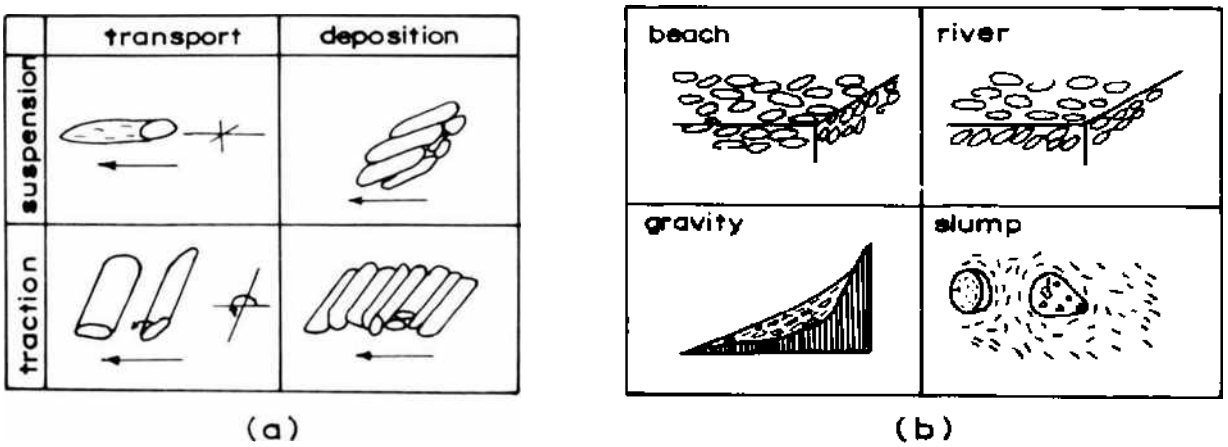

Fig. 11-7. Orientation of grains
(a) Influence of transport medium
(b) Influence of environment
(after GRIFFITHS, 1967).

influenced by the dominant directions of current (HOLMES, 1941) and so also the particles sliding in a gravitational field along a slope (MINER, 1934). Sediments with disturbed structures, sometimes called slump sediments, show patchy orientation patterns.

Crystallographic fabric and morphological fabric both are well developed in most of the metamorphosed rocks. The cleavage and schistosity in metamorphic rocks are classical examples of crystallographic and morphological fabrics. Slaty cleavage is a planar fabric that is a pervasive property of slate, and is formed perpendicular to the direction of maximum finite shortening of the rock being produced by the mechanical reorientation of the particles with some new growth of micaceous mineral. Schistosity in more highly metamorphosed rocks is produced by more or less recrystallisation of the components (TURNER, 1948; RAMSAY, 1967).

The amount of strain that the rock must undergo is important for the development of schistosity. Experimental studies of CLOOS (1947) indicate that about 30% is the deformation required for the development of slaty cleavage.

11.4.2. Structural Defects

Structural defects in rocks are of three types; folds, faults and joints. From the point of origin, these are the result of tectonic stresses to which rocks have been subjected during the course of their history. A general description of these is given below:

Folds

Folds can be defined as undulations in rocks and are features observed in layered rocks. The individual folds vary in dimensions from a few millimeters to many kilometers.

Folds have been classified in many ways. Descriptive or geometric classification is based upon the attitude of the limbs, axial surface and fold axis. Morphological classification is based upon the shape of folds and their relative number of anticlines and synclines, etc. Mechanic, kinematic and tectonic classifications are important from the rock mechanics point of view for they permit an insight into the tectonic regime, the forces involved and the mechanism of deformation.

The classification based upon external kinematics and tectonic forces recognises the subdivision of the folds and the associated structures depending upon the mechanism of formation. The following processes have been recognised (BADGLEY, 1965):

1. Folds related to vertical tectonics and gravity gliding
2. Folds resulting from differences in specific gravity
3. Folds resulting from differential subsidence
4. Folds due to pluton emplacement
5. Folds resulting from block uplift
6. Folds due to lateral compression
7. Folds due to regional coupling or simple shearing

Looking at the mechanics of their development, these processes may be grouped under two basic mechanisms, namely,

(i) flexure folding, (ii) shear folding (Fig. 11-8). In flexure folding or flexural slip folding (SANDER, 1930), the mechanism involves sliding of beds past each other. The higher competent strata slide upward towards anticlinal crest areas. The force causing this folding is considered to be lateral compression (or uplift) or coupling (Fig. 11-8b). In shear folding shearing or slipping occurs along closely spaced fractures (secondary *s*-surfaces) not parallel to the original bedding (primary *s*-surfaces) (Fig. 11-8a). The strain field at the two limbs of the fold changes both in value and direction as one moves away from the crest (Fig. 11-8b). At the interface of the adjacent beds displacement occurs.

The movements of different points during the development of a fold are given in Fig. 11-9. At the initial stages (in open folds) each point moves upward followed by a horizontal movement culminating in their final positions. In isoclinal folds the motion is predominantly vertical. Extensive thickness changes in folding take place. In isoclinal folds possibly large horizontal movements at the earlier stage of their development are followed by relief from the core to the surface crest of the fold.

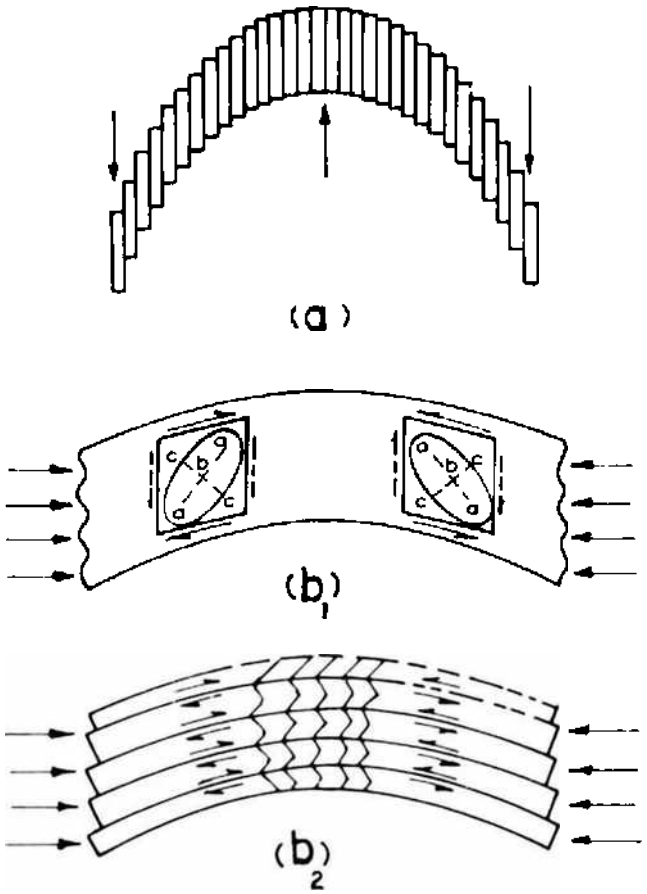

Fig. 11-8. Mechanism of folding
(a) Shear or slip folding
(b) Flexure folding (flexural slip) mechanism involving concentric shear motion (after BADGLEY, 1965).

The movement history at low displacement rates ranging in the order of 10^{-14} to 10^{-16} mm/s influences the 'inherent fabric' of rock producing a new 'deformational fabric' as described earlier and is also responsible for the development of certain oriented fractures.

As the folding strain under the influence of horizontal stress progresses further resulting in buckling of the beds (Fig. 11-10), multiple folds develop and the wave length of these is dependent upon the competency of the bed undergoing folding and the surrounding rocks. Both theoretical and experimental investigations have been conducted to interpret their wave lengths and shapes (BIOT, ODE and ROEVER, 1961; BIOT, 1964, 1965; CURRIE, PATNODE and TRUMP, 1962; RAMBERG, 1960, 1961, 1963). The wave length is directly proportional to the thickness of the competent layer (CURRIE, PATNODE and TRUMP, 1962).

A very important aspect of folding from an engineering point of view is the strains associated with it. For instance, during the buckling of beds the outer

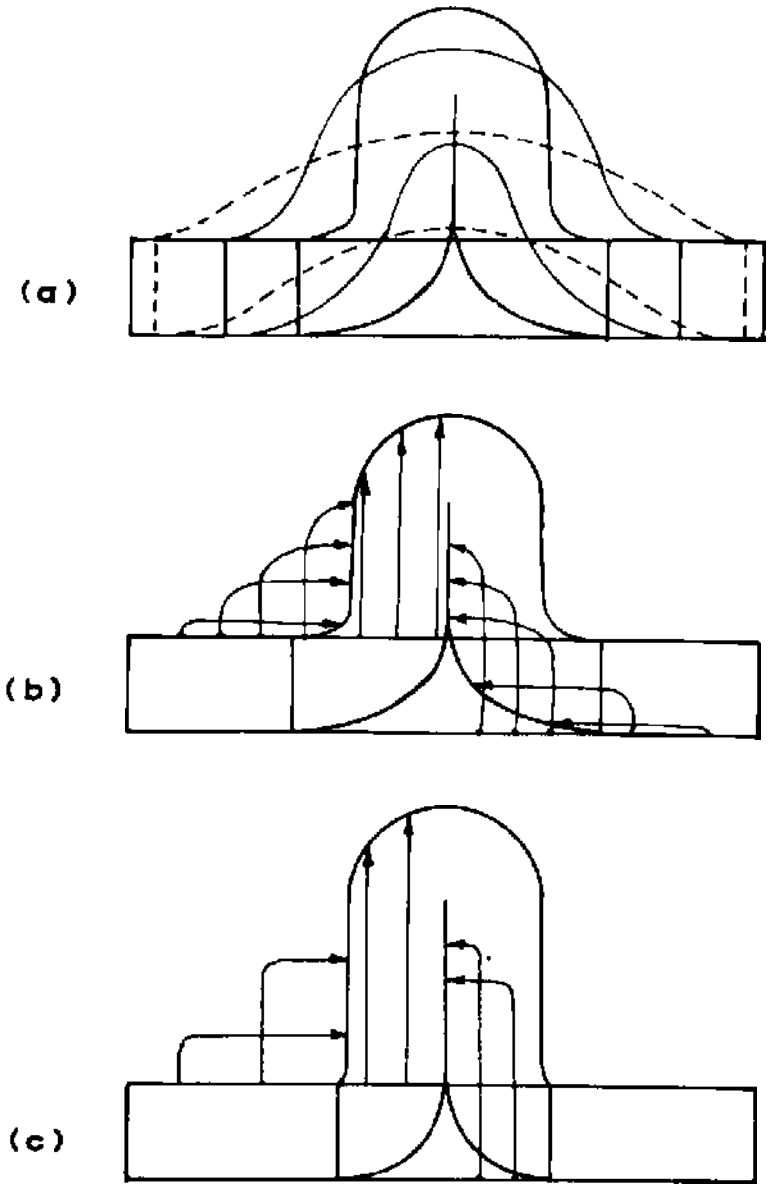

Fig. 11-9. (a) Stages in the evolution of a fold from an original horizontal sheet of rock to an eventual isoclinal position (heavy solid line).
(b) and (c) The arrows show the movements from various points on the original sheet to their final position (after BADGLEY, 1965).

layers slip over the inner layers (Fig. 11-11) giving homogeneously distributed strain or inhomogeneously distributed strain with more movement on the layer boundaries than in the centre of the layers (Fig. 11-11) giving slickenside and sigmoidal tension fissures (Fig. 11-12). These fractures are inclined at an angle, the inclination of which changes with respect to the bedding planes as one moves away from the crest (Fig. 11-12). The amount of slip is greatest at the limbs of the fold and is proportional to the layer thickness. These structures

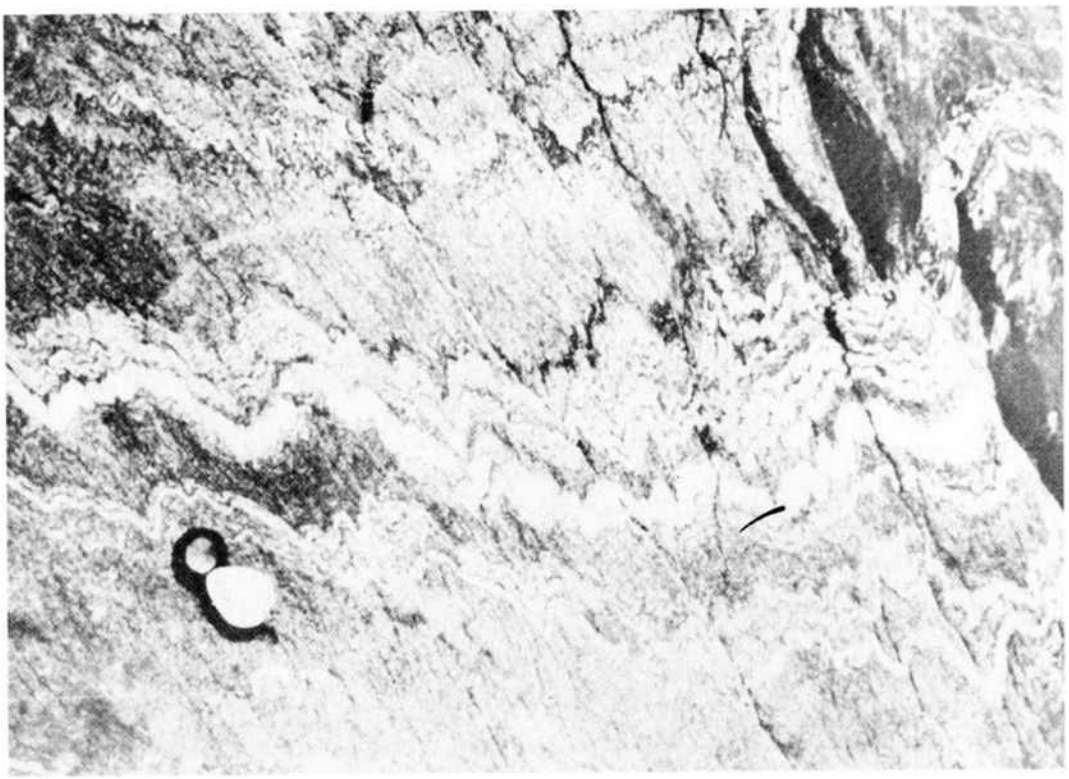

Fig. 11-10. Varying wavelengths of folds produced by buckling pegmatite sheets of variable thickness in a mica schist matrix.
Pennine Alps, Ticino, Switzerland
(after RAMSAY, 1967).

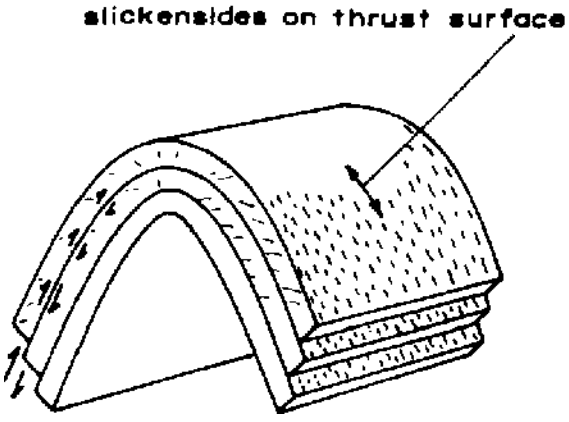

Fig. 11-11. Development of thrusts in a flexural-slip fold
(after RAMSAY, 1967).

are best developed in the fold limbs at the boundaries of the thickest and most competent beds and die away towards the hinge of the structure. Besides the development of tensional sigmoidal fissures, tensional joints may develop in layer progressively folded at the upper and lower boundaries of the beds and the depth to which they extend depends upon the position of the neutral surface

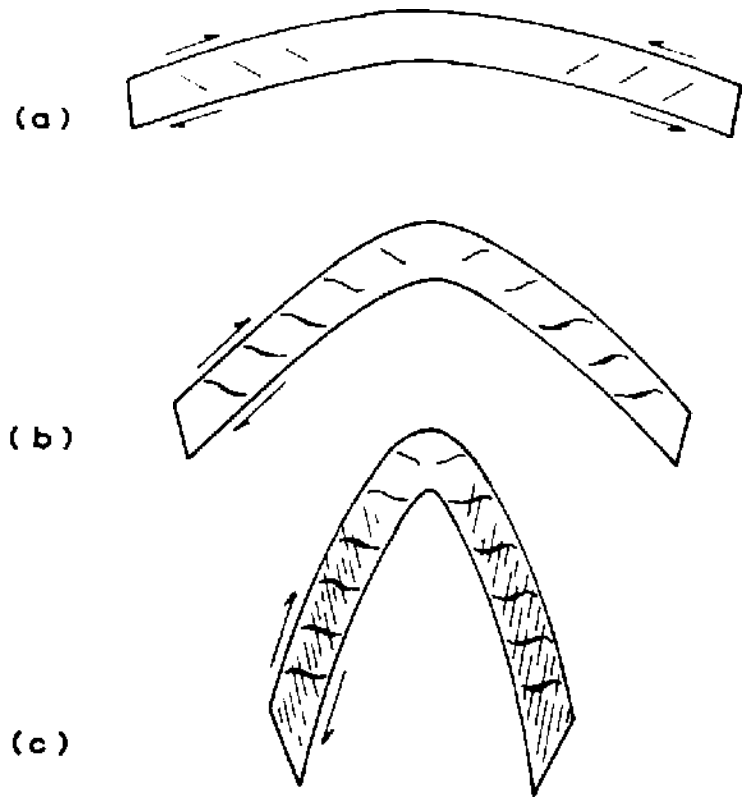

Fig. 11-12. Progressive development of sigmoidal tension fissures and slaty cleavage as a result of progressive fold development with internal deformation by flexural flow (after RAMSAY, 1967).

(Fig. 11-13). The amount of deformation (shortening) that the beds have undergone can be determined by measuring along the length of any lithological unit on the boundary of or inside the competent layer. Another method of determining the amount of deformation that the rocks have undergone is the study of deformed oolites and fossils (CLOOS, 1947; BREDDIN, 1956a, b, 1957) which change their shape under strain imposed upon them.

Faults

Faults are large discontinuities in geological formations along which intersected beds have moved past each other to produce certain displacements. From the genetic aspects, most faults are planes of shear fractures brought about by stresses and hence their direction and dip bear a definite relationship to the stresses that were in existence at the time of their formation. According to MOHR's criterion (Chapter V, Volume I), it has been pointed out that failure will occur at the point where the MOHR circle is a tangent to the MOHR envelope and that the inclination of this plane of failure with respect to the greatest principal stress for this condition is represented by the line joining the centre

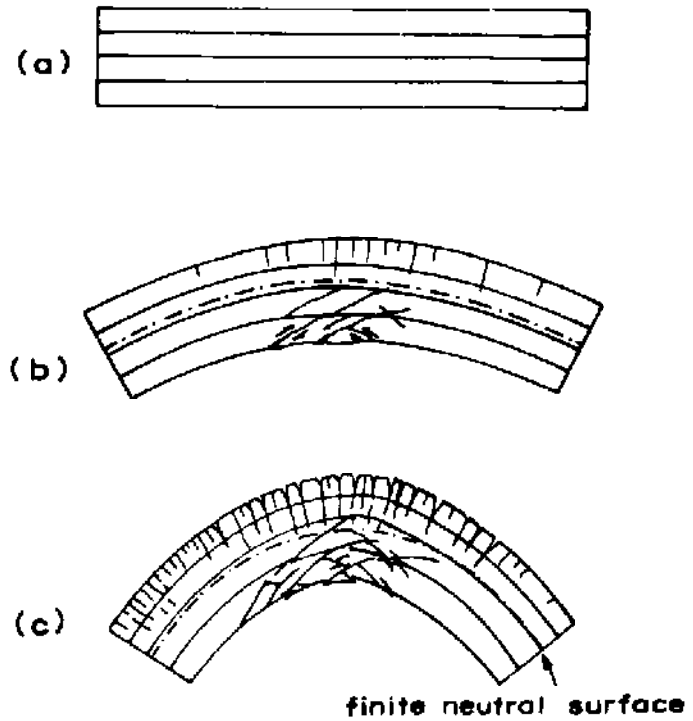

Fig. 11-13. Structures developed in a layer progressively folded and deformed by tangential longitudinal strain (after RAMSAY, 1967).

of the circle and the point of tangent on the MOHR envelope (Fig. 11-14). If it is uniaxial tension, then the failure plane is at right angles to the direction of this force. If it is a case of a triaxial stress field, the angle 2θ varies depending upon the nature of the stress field. The angle between the conjugate shear surfaces (2θ) increases as the lateral compression increases. If it is assumed that failure had occurred only under a compressive stress field, it is then possible to interpret the direction of maximum principal compressive stress and gain some idea about their ratios from the direction of the fault. Accordingly, therefore, the various types of faults would be then classified as follows:

(a) Normal faults; when greatest principal stress acts vertically and the least principal stress is horizontal.
(b) Wrench faults; when the greatest and least principal stresses act horizontally.
(c) Thrust faults; when greatest principal stress is horizontal and the least principal stress is vertical.

Besides this simple explanation which is associated with brittle fracture of hard rocks, faults occur as a result of large displacements produced under stresses in semibrittle and softer rocks. For example, in the case of a normal fault the cause of the greatest principal vertical stress and least principal horizontal stress directions may be radial (outward) stretching over the crest

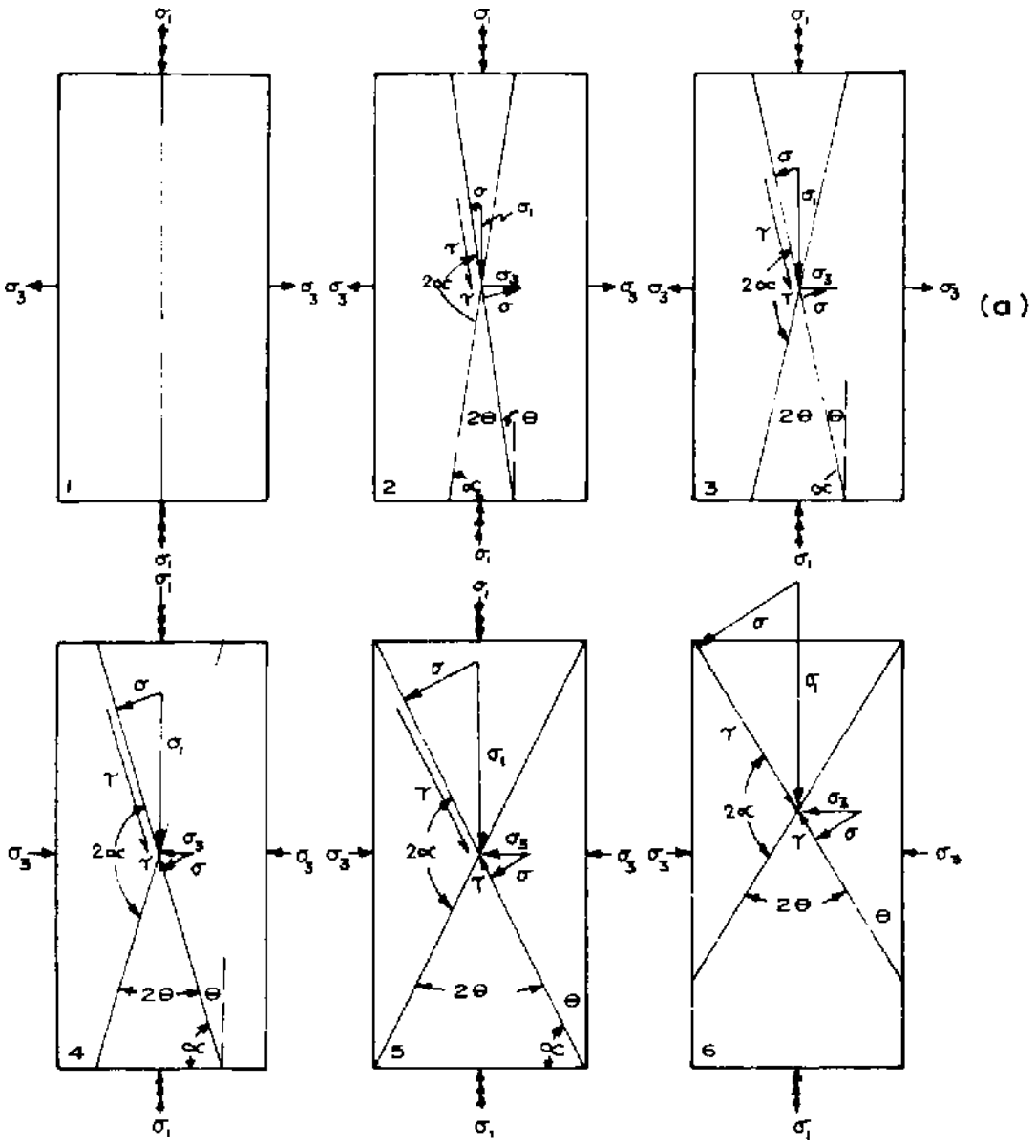

Fig. 11-14. (a) Resolution of forces acting on failure planes in rocks. The lateral force (σ_3) is tensional in the first three examples (1, 2, 3) but the confining pressure (σ_3) gradually increases from example 4 through to example 6. Note that the shear components (τ) of the external forces are additive in examples 2 and 3 but oppose each other in examples 4, 5, 6. The normal components (σ) oppose each other in examples 2 and 3 but are additive in examples 4, 5 and 6.

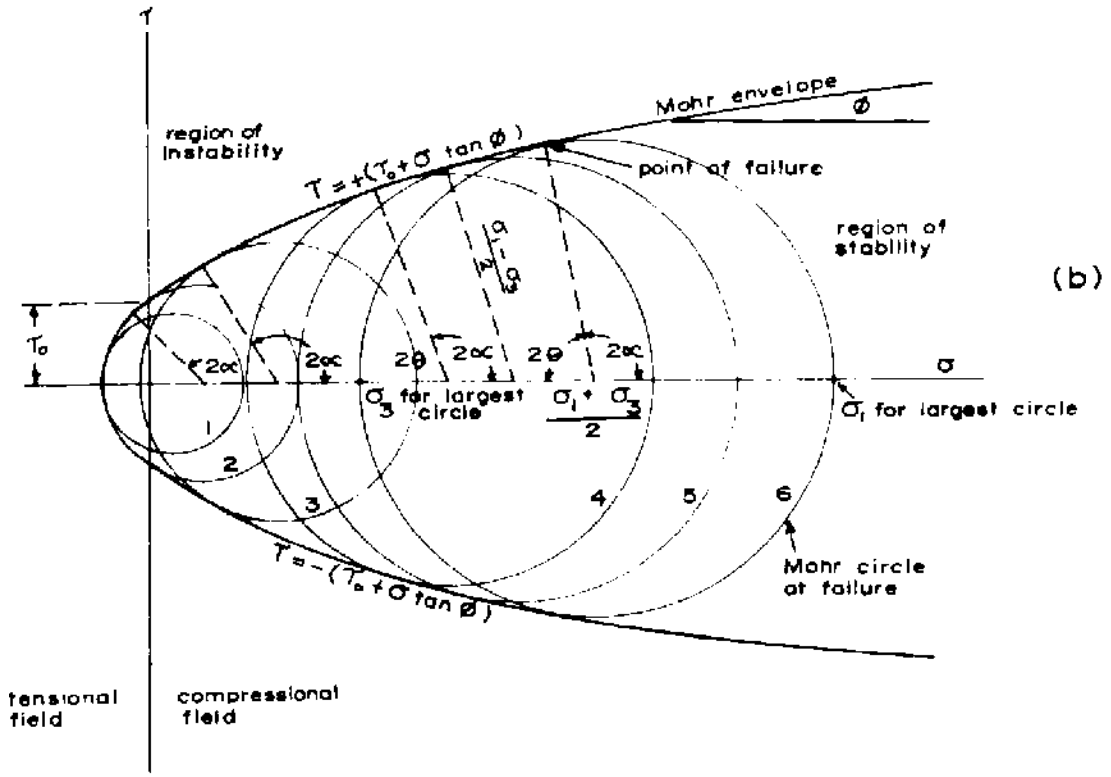

Fig. 11-14.
(b) In the corresponding MOHR circles (examples 1–6) note the gradual decrease in 2θ value as $\sigma_1 - \sigma_3$ decreases. The circle of failure becomes tangent to the MOHR envelope in the case of the smallest circle
(after BADGLEY, 1965).

of an anticline as result of folding. It may also be due to the expansion of the earth's crust which results in decreasing the net horizontal confining pressure. Such faults are formed on the limbs of an anticline and their intensity decreases as one moves towards the centre of the anticline. Such faults are also common at the edges of geosynclines giving features such as graben and horst structure (CLOOS, 1936) (Fig. 11-15).

Wrench faults and thrust faults are dominated by horizontal stresses. As a result of the continued action of the horizontal thrust the beds develop folds and as the development of the fold continues, the bending accompanying the development of an asymmetric fold (Fig. 11-16) weakens the steeper limbs shearing it apart with dragging against the fault.

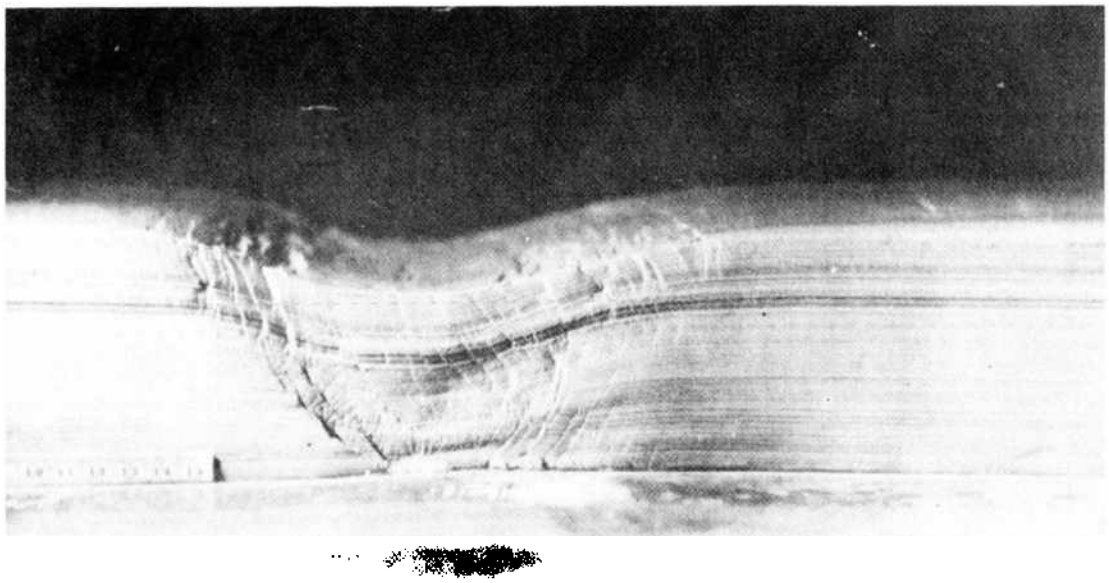

Fig. 11-15. Experimental graben produced in a cake of clay arched over a balloon (after CLOOS, 1936).

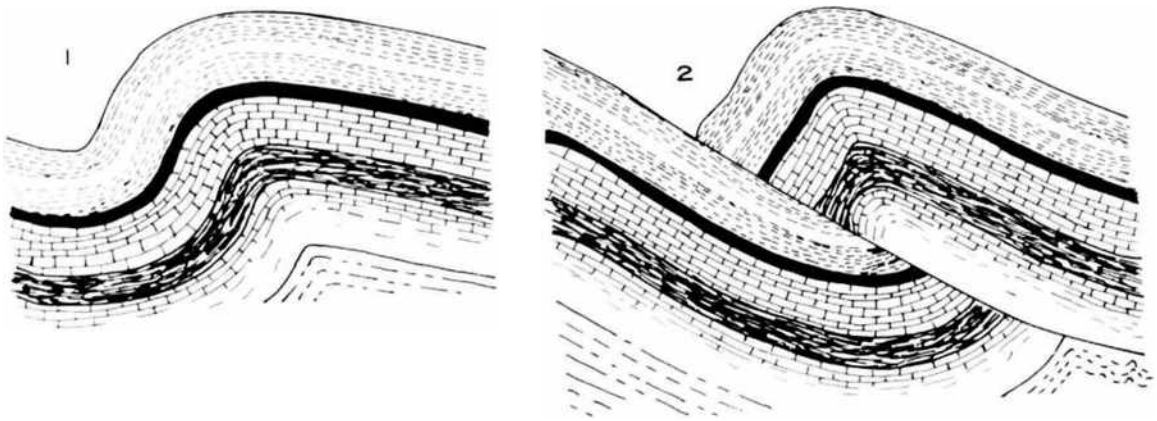

Fig. 11-16. Development of a break thrust. The strata are too competent to become overturned and stretched. The folding weakens the forelimb of the anticline by tension fracturing. Continued application causes a thrust to develop and utilises the already existing fractures (after WILLIS, 1893)

Joints

Joints are fractures in rocks along which there has been little or no displacement or a very slight movement normal to the joint surface.

There are two types of joints: systematic joints and nonsystematic joints (Fig. 11-17). Systematic joints occur in sets in which individual joints are

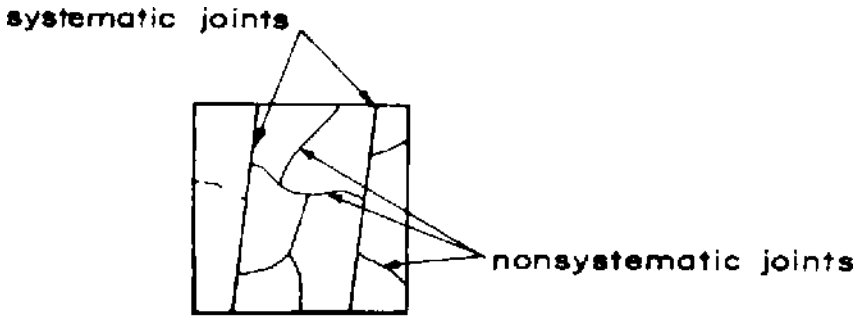

Fig. 11-17. Typical plan view of systematic and nonsystematic joints.

parallel or sub-parallel to each other. Nonsystematic joints do not have any definite pattern and frequently terminate at systematic joints.

Joints which cut through a number of beds or rock units and which can be followed several tens or hundreds of metres are termed master joints and those which are an order of magnitude smaller but are still large enough may be called major joints. Still smaller and relatively unimportant fractures may be called minor joints and those of only up to a few centimetres (like cleavage in coal) are called micro-joints. The joint set that is more developed (i.e. more frequent and larger) is called a primary set of joints and the other set is called a secondary set of joints.

Joints are secondary features of the rock tectonics and as such have a definite relationship with the regional structure. They are generally related to the predominant structural trend of the region such as fold axes and thrust faults, basin rims, monoclines, mountain uplifts or swell structures. Joints roughly parallel to the fold axis are formed due to tensile stress at high angle to the beddings (Fig. 11-18). These are called longitudinal joints. Cross joints are roughly perpendicular to fold axes and generally terminate against systematic joints. They have a more irregular surface than systematic joints (HODGSON, 1961). Diagonal joints generally occur in pairs more or less symmetrical to the longitudinal and cross joints with high angle to bedding and are the result of shear failures.

The genetics of joint formation under a general stress field is explained in Fig. 11-14. Obviously therefore, there may be tensional joints or shear joints. Shear joints are cut across the crystals and are commonly slickensided (Fig. 11-19) or a narrow cataclastic zone with offsetting on opposite sides of the fracture (Fig. 11-20). Tensional joints, on the other hand, have clean, granular breaks and may have plumose markings (Fig. 11-21).

From Fig. 11-14, it is clear that for $2\gamma = 180$, i.e. contained angle between the fractures to be zero (tensional joints) at least one of the principal stresses need to be zero or tensile. This means that tensional joints are near-surface features.

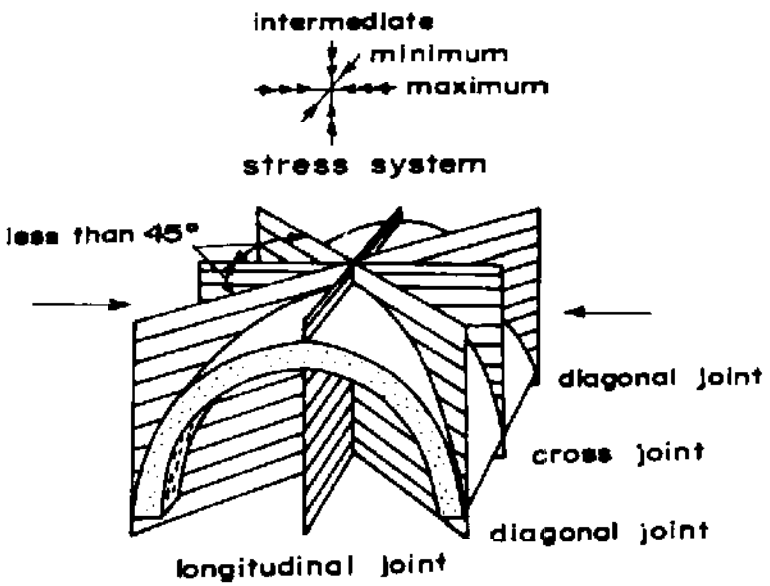

Fig. 11-18. Geometric orientation of longitudinal, cross and diagonal joints relative to fold axis and to principal stress axes (after WILLIS and WILLIS, 1934).

During the early stages of folding, the stress distribution in folded rock changes gradually, the compressive stress near the fold axis slowly changing from compressive to tensile and joints shall be first formed at the anticline ridge top while in deeper parts of the anticline limbs a higher stress difference will be required for failure. As joint development extends to deeper lying regions the critical stress circle will be larger and conjugate shear angle (contained angle between the joint sets $2\theta = 180 - 2\alpha$) will become larger and larger. The conjugate shear angle is therefore an indication of the depth of occurrence and the ratio of the maximum and minimum stresses that caused these joints.

If simple gravitational force is considered to cause jointing, it can be proved that jointing will occur only down to a certain depth and will cease as the realm of plastic deformation is reached or the stress difference to bring about necessary shear stress falls below the required value (PRICE, 1959).

There are different types of mechanism causing the development of forces that result in jointing. These may be gravitational forces due to the weight of the overlying strata, regional compression associated with thrusting, regional coupling, crustal shifting and nontectonic forces such as shrinkage due to cooling, dessication, etc.

In bedded formations only one set of shear is generally present. This occurs when the beds have been subjected to rotational stresses. Studies on joint development using clay as a model material conducted by CLOOS (1955) explain this very clearly. In Fig. 11-22 the surface of the clay was sprinkled with water to decrease surface tension and in the nonrotational experiment tension frac-

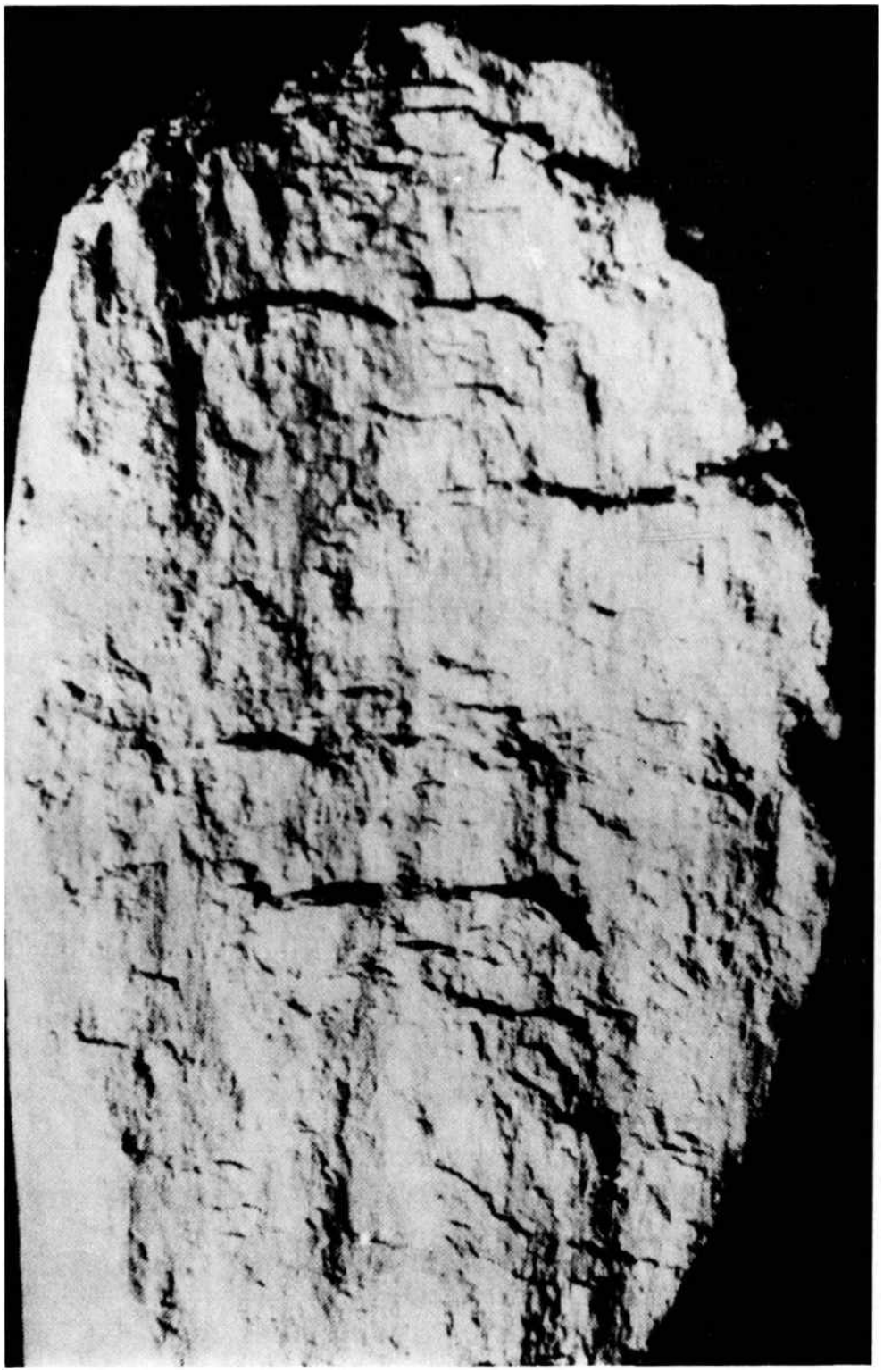

Fig. 11-19. Slickensides and small steps or ridges developed on shear surfaces (after PATERSON, 1958).

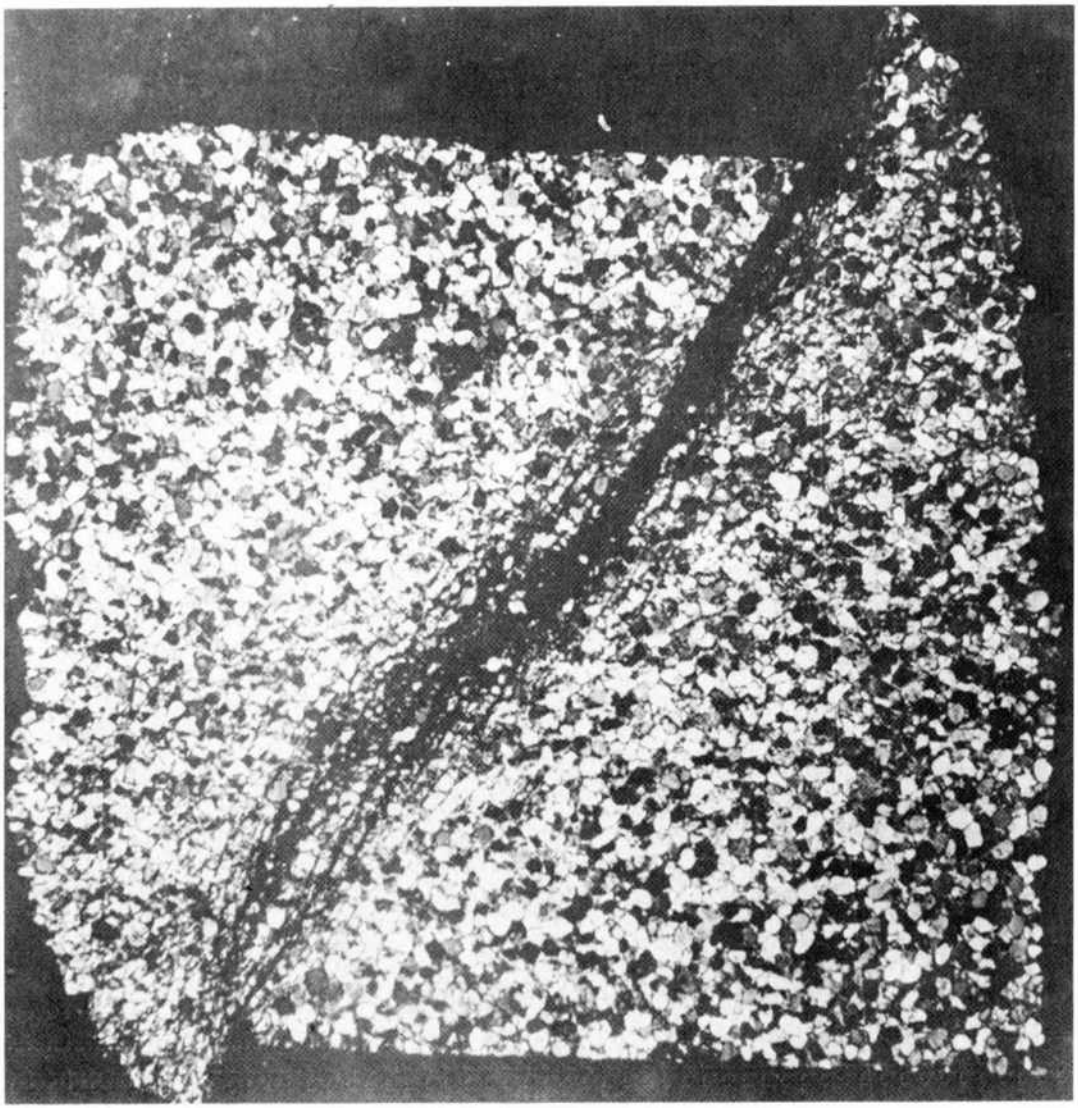

Fig. 11-20. Fault in St. Peter sandstone. Longitudinal compression (vertical). Confining pressure of 5000 bars, interstitial – water pressure of 1000 bars, temperature of 500° C, shortened 40 percent. Note the wide zone of mylonitised quartz. There is very little grain breakage away from the mylonitised zone (after GRIGGS and HANDIN, 1960).

tures were formed (Fig. 11-22a). When the clay surface was left dry the application of rotational stress produced conjugate shear fractures making 60° intersection angles initially (Fig. 11-22b). As deformation continued one of the two sets of fractures rotate to different angles, the conjugate shear angle 2θ to more than 90° and one of the fractures develop more than the other. The reason for the poor development of the second set until $2\theta = 90°$ is due to the space requirements of individual cleavage mullions (Fig. 11-22c) which

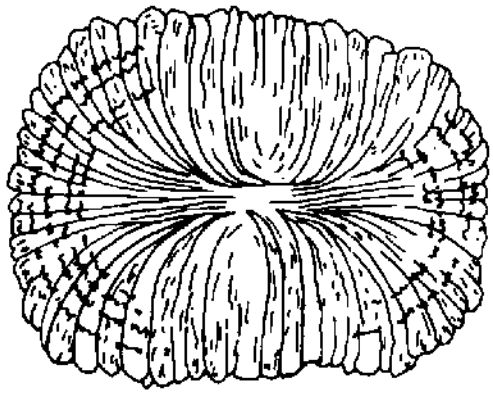

Fig. 11-21. Plumose structure on the faces of joints (after HODGSON, 1961).

will have to rotate against the normal component of regional stress. The second set of new fracture planes which is now parallel to bedding plane does not develop further because of the pre-existing bedding planes along which slip is concentrated.

Joints due to cooling and shrinkage are relief fractures and split the rock mass into columns. If rocks are perfectly homogeneous and if cooling (or drying) is also uniform, then cooling or drying centres shall be equally distributed in the rock (Fig. 11-23). The distances between the centres being equal, this results in equal tensional stresses with joints forming hexagonal shapes in plan. However, in practice, varied shapes occur due to nonconformity of cooling. However, some polygonal fractures could also be of tectonic origin (PRATT, 1958).

Cooling joints are more closely spaced near the margins of igneous bodies and become widely spaced as one moves into the interior and even may disappear at depth.

Some sheet structures and large foliations may be associated with unloading. JAHNS (1943) and CHAPMAN and RIOUX (1958) found sheet structure with the thickness of individual sheets increasing from almost 25 to 50 cm near the surface to several metres at depth and the sheet structure runs parallel to topography.

Concentric and radial jointing occurs in rocks overlying magmatic domes or surrounding the domes due to sagging of the roof into the magma reservoir or in the thrusting of the magmatic dome upward developing radial and tangential tensile stresses in the roof (Fig. 11-24).

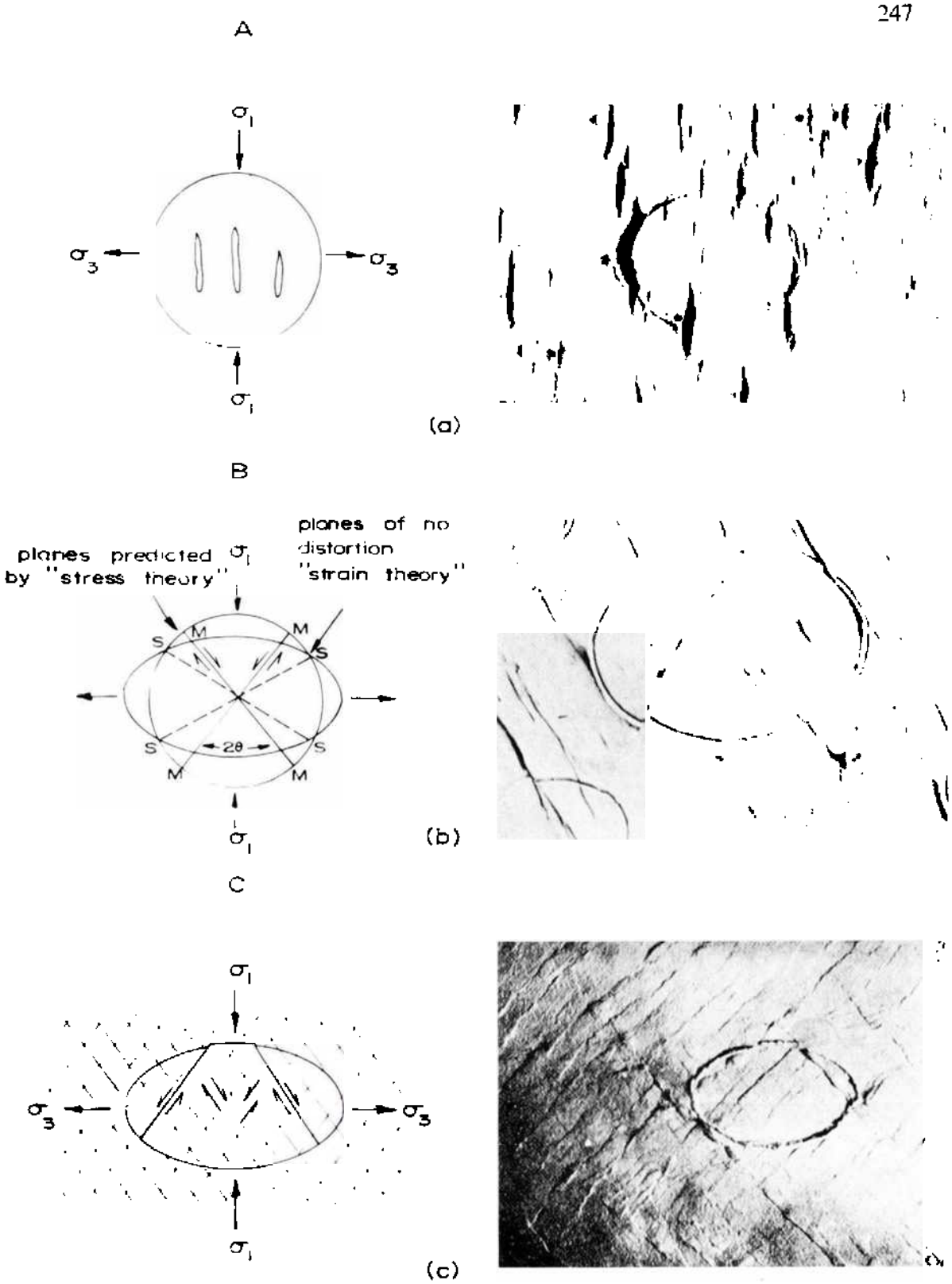

Fig. 11-22. Non-rotational deformation of wet clay. The surface of the clay was kept wet with water, in (a), to eliminate surface tension in the clay. It will be noted that the shear fractures have angular relations which are in agreement with the so-called 'stress theory of failure'
(after CLOOS, 1955).

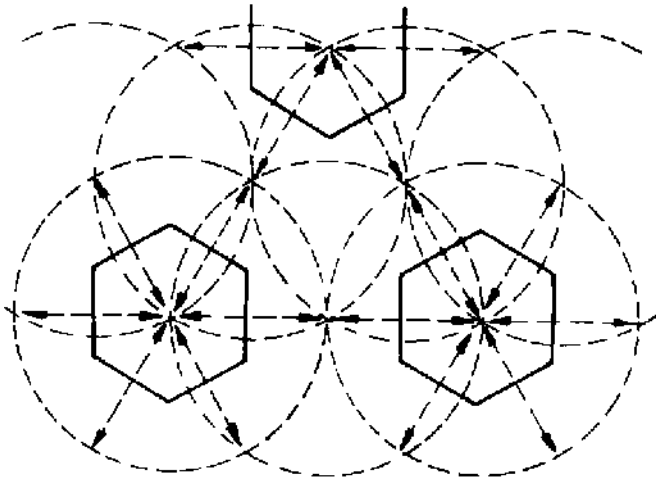

Fig. 11-23. Uniform cooling or drying in a homogeneous material occurs about centres which are equally distributed throughout a material in plan view (all centres are equidistant). Fractures develop at right angles to the tensional pull between centres, and individual fractures intersect to form symmetrical hexagons about each centre (after BADGLEY, 1965).

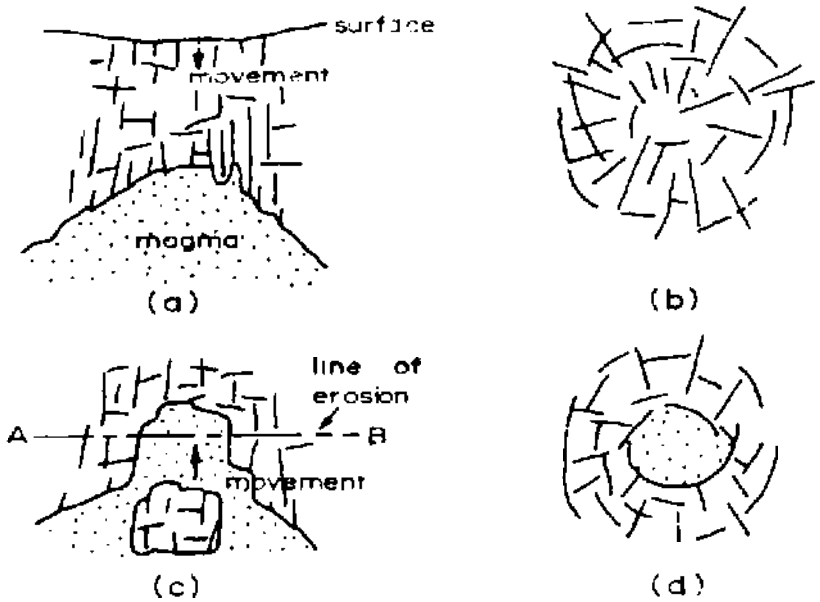

Fig. 11-24. Jointing in the country rock above and around a magmatic dome (a) and (b) Roof sags into magma reservoir giving radial and concentric joints (c) and (d) Radial and concentric joints developed due to tension in the roof as a result of uplift.

11.5. Joint Survey and Joint Analysis

In the analysis of any rock structure, a sample of joints at various positions in the rock mass made accessible by drilling, outcrops, trenches, shafts, tunnels, etc. is surveyed to assess the various properties of interest. The sample should be sufficiently large so that the information obtained is sufficiently accurate. Depending upon the size of the region involved, the number of observations may run to several thousands (9000 in de Beer's mine, South Africa, ROBERTSON, 1970; 24000 in C.S.A. mine, Cobar, N.S.W., Australia, BARTON, 1975a, b).

While conducting field survey, it is always advisable to divide the exposures into different zones of equal area (say 3 m × 3 m [10′ × 10′]). The joints that intersect this face of limited size are recorded. Sometimes line sampling technique is adopted in which all the joints which intersect a given line are recorded. Sampling a line of given length yields a smaller sample and hence is more economical to implement where extensive surfaces are available for sampling.

The various aspects that have to be considered in a joint survey are as follows:
(a) Joint frequency
(b) Joint length and joint continuity
(c) Joint roughness and
(d) Joint thickness.

(a) *Joint Frequency*

Joint frequency or degree of jointing is a term used to indicate the number of intersections of one particular joint set encountered in a linear transverse at right angle to the joint plane. From the point of view of definition, a straight line (tape) of length l is stretched out on the surface on which the joint frequency is to be measured (Fig. 11-25) and the number of joints (n) intersecting the line are counted starting from the first joint to the last joint on the line. The inclination of these joints (θ) with respect to the stretched line is measured using geological compass and the frequency (J_n) is given by

$$J_n = \frac{n \cos \theta}{l} \tag{11.1}$$

The equation 11.1 holds good only if the survey line is placed at right angle to the joint plane. In other cases the value so obtained will have to be corrected to account for the dip direction. Placing a survey line at an angle to the joint plane results in a greater number of joints which are normal to the line to be sampled and those parallel to the line are completely missed. In a general case

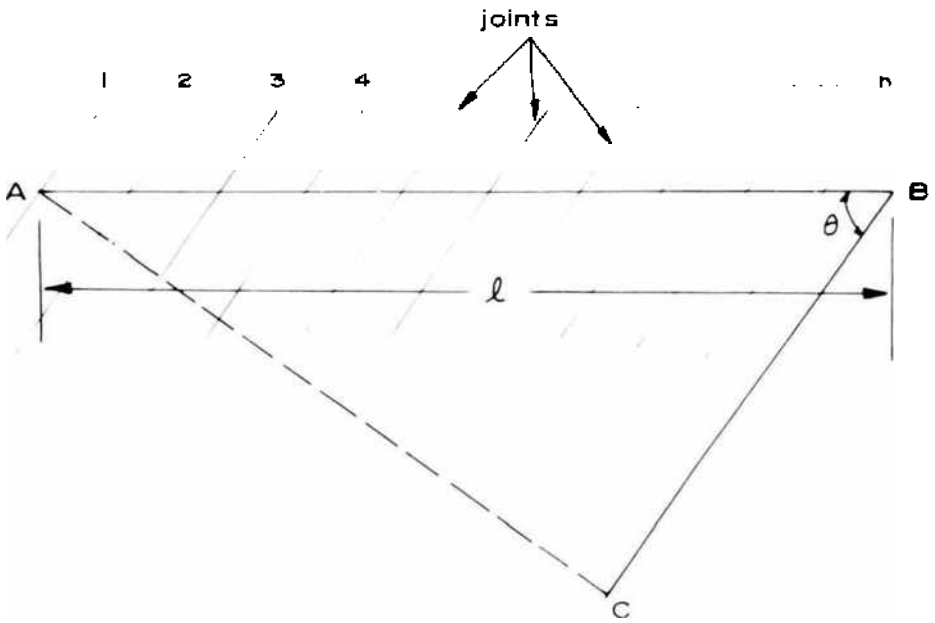

Fig. 11-25. Joint survey.

if a line has a dip of δl and a dip direction of θl (Fig. 11-26) and is used to survey different sets of joints and if the joint spacing of any joint set is J_s, then

$$J_s = \frac{l \cdot \cos \delta j \cdot \cos \theta j}{n} \tag{11.2}$$

The frequency is given by $$J_n = \frac{1}{J_s} \tag{11.3}$$

In practice, however, the θj and δj are not fixed numbers but have a certain distribution and a suitable method is to use the mid of the class interval selected in correlating the spacing or the frequency. For example, if the frequency calculated of any class interval from the above line is given by $J_n(\delta j, \theta j)$ for the class interval defined by the midpoints δj and θj, then the corrected frequency of this class $J_{n'}(\delta j, \theta j)$ can be given by (ROBERTSON, 1970)

$$J_{n'} = \frac{J_n(\delta j, \theta j)}{\cos(\theta l - \theta j) \times \cos[(\delta l + \delta j) - 90]} \tag{11.4}$$

While comparing joint frequencies obtained using different lengths of survey lines, the frequency should be reduced to a standard length of say unity or hundred. Most research workers use unity as the reference length.

Measurements have shown that joint frequency is dependent upon rock type and stress intensity causing jointing. HARRIS, TAYLOR and WALPER (1960) found that for a given rock lithology, joint frequency is inversely related to

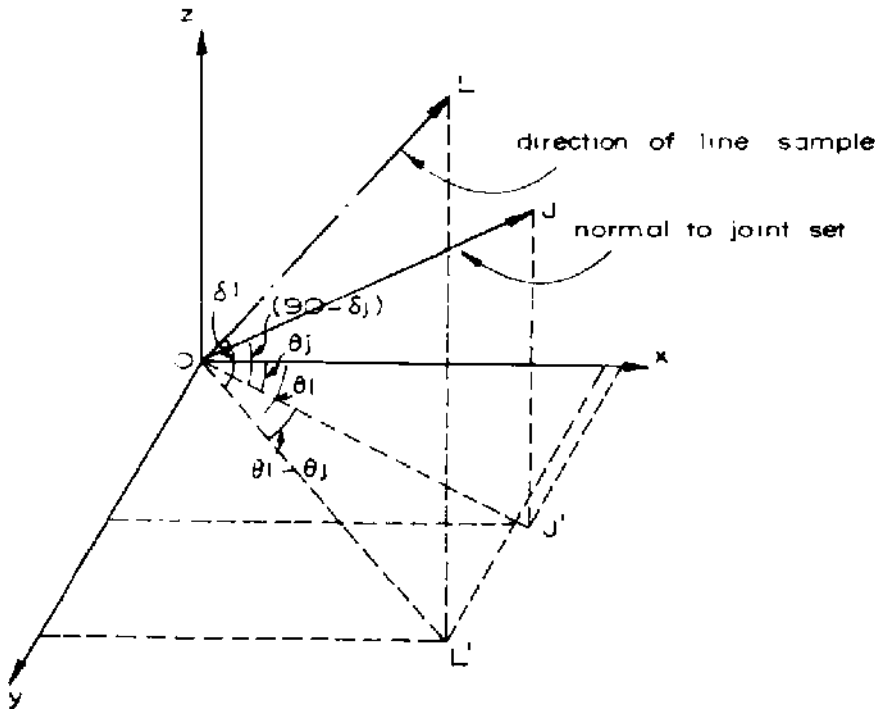

Fig. 11-26. Three dimensional representation of normal to joint set and sampling direction
(after ROBERTSON, 1970).

the bed thickness. For example, in two dolomite beds in the same locality, the one having joint frequency of 0.33 has a bed thickness of 3.0 m and the other having joint frequency of 1.0 has bed thickness of 0.33 m. A linear relationship between bed thickness and joint interval (inverse of joint frequency) has been reported by BOGDANOV (1947), NOVIKOVA (1947) and KIROLLOVA (1949) (Fig. 11-27). FOCARDI et al (1970), however, report a nonlinear relationship. The phenomenon has been explained by PRICE (1966) as a result of friction that exists between jointed bed under consideration and the adjacen' beds. The higher the friction between the beds the smaller the free gap between the development of required tensile stress and the 1st tensional joint and lower the unit tensile stress when distributed to the full thickness of the bed (Fig. 11-28). The higher the rock strength the lower is the frequency.

In case of shear joints, the frequency is dependent upon (stress field/rock strength) ratio. The higher this ratio the higher the frequency. In case of joints developed due to folding, the degree of tectonic deformation plays an important role. A comparative idea of the operating stresses could be obtained by comparing the joint frequency in different areas of similar bed thickness having same lithology and strength.

Joints are mapped in the field using the usual geological compass and determining their angle of dip, strike direction and other parameters. There are two methods of plotting the joints: 1. Equal area plot and 2. Rose diagram. The

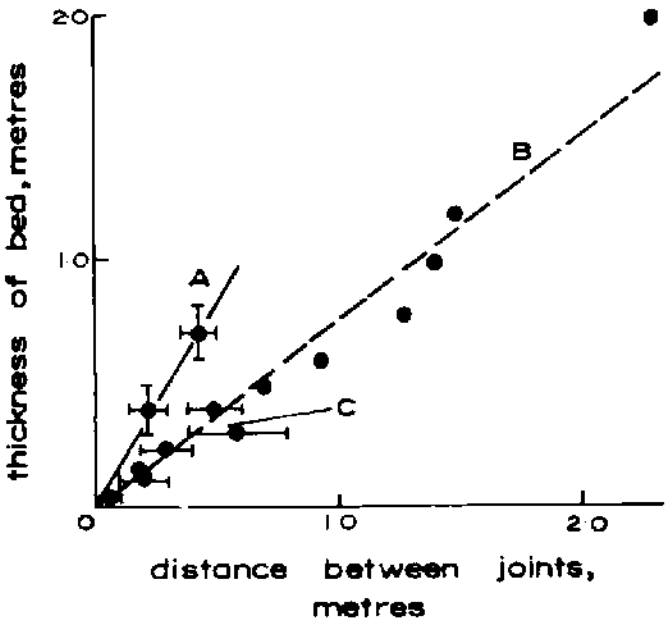

Fig. 11-27. Relationship between bed thickness and distance between joints (after PRICE, 1966).

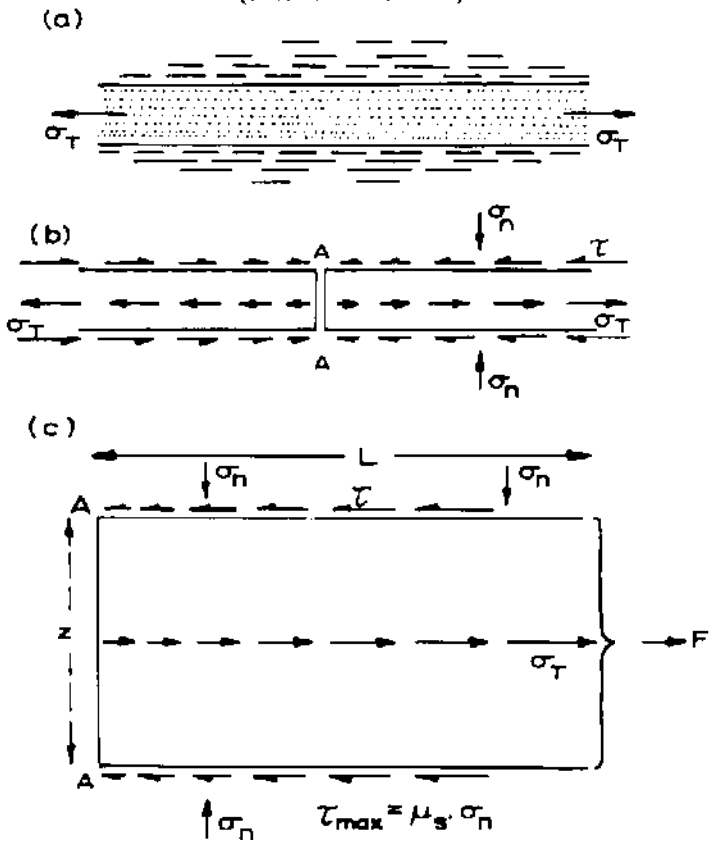

Fig. 11-28. (a) Uniform tensile stress σ_T acting in a single competent unit.
(b) Indicates the reduction in tensile stress due to the formation of a single joint coupled with the development of shear stresses along the bedding planes which prevent excessive opening of the joint.
(c) Details of stress intensity in section of competent bed length L and thickness Z (after PRICE, 1966).

method of representation of a plane on an equal area plot is given in Appendix V. The number of concentrations of poles to joints indicate the existence of the numbers of joint sets. For example, Fig. 11-29 indicates two concentrations of poles of joints with intersections plunging at a small angle from the horizontal.

The rose diagram, sometimes called star diagram or joint rose, is a useful representation when the directions of a large number of joints have been measured but the dip values are not known (e.g. in aerial photography). The distance from the centre (concentric circles) represents the number of measurements (20, 40, 60, 80, etc.) and radial lines represent the strikes measured from the North in the clockwise direction (Fig. 11-30). In this plot the total number of joints are counted in each 10 degree sector and plotted on a radial line bisecting the sector and lines are drawn connecting the points in the various sectors. Fig. 11-30, for example, represents rose diagram of two sets of joints with strikes nearly at right angles with one set having a higher frequency than the other. The method has a drawback that it does not give any information

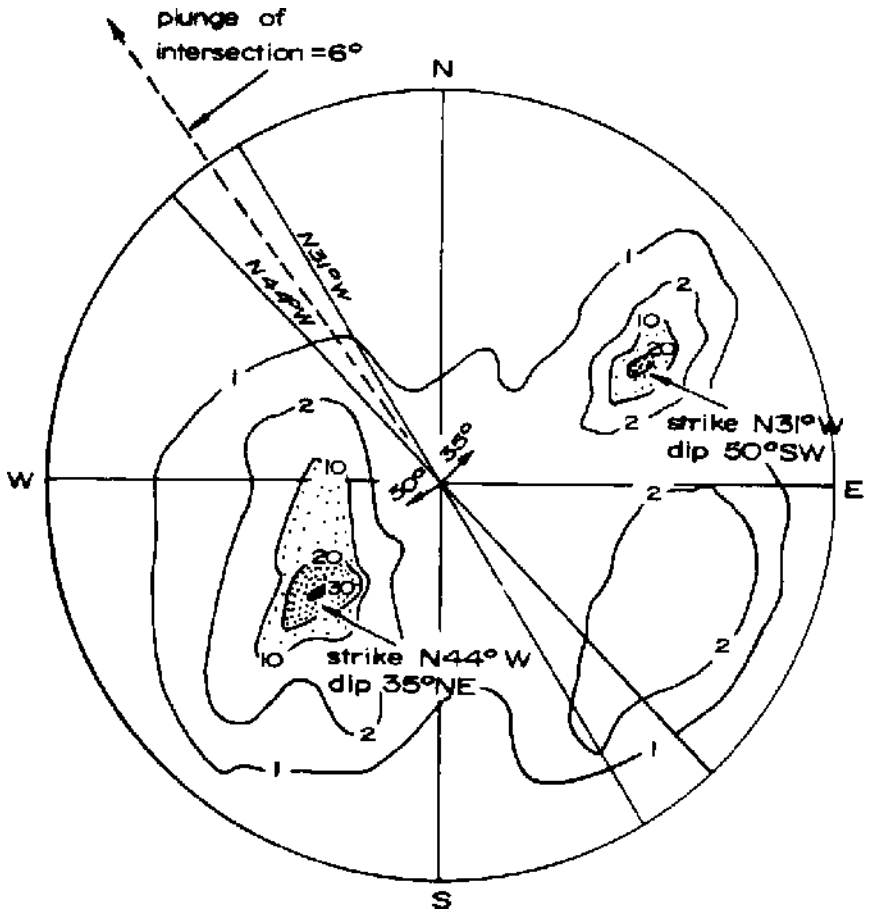

Fig. 11-29. Contoured equal-area plot of a joint system containing two joint sets. Lower hemisphere (after WAHLSTROM, 1973).

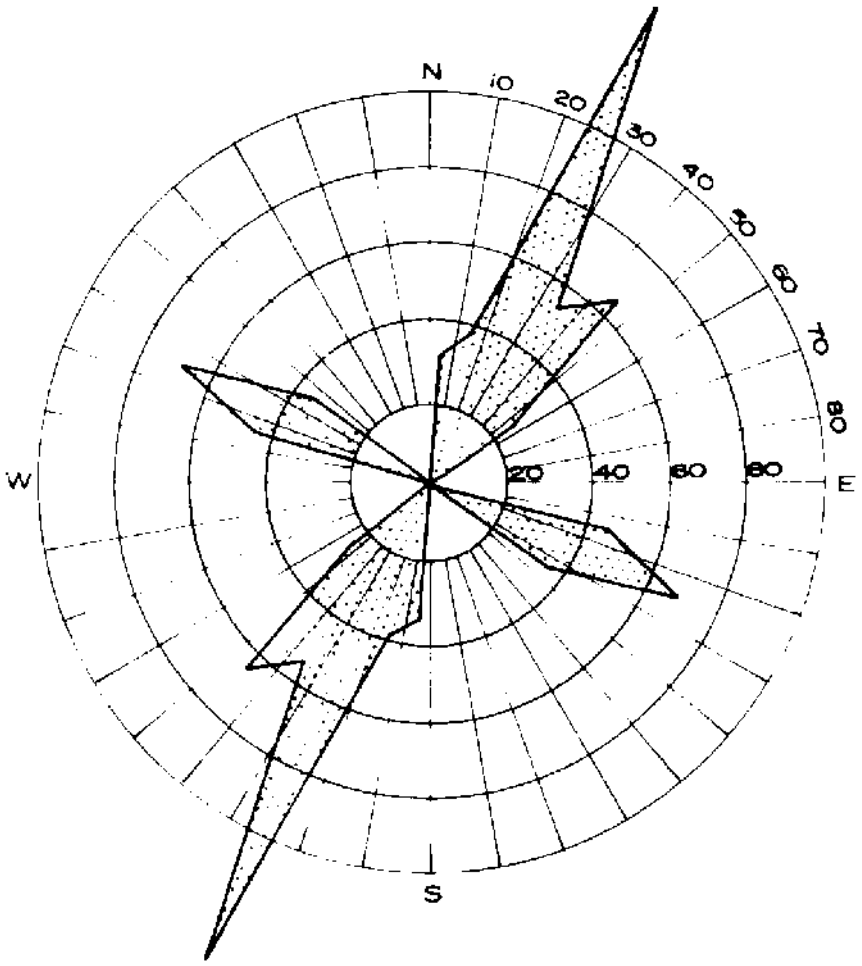

Fig. 11-30. Joint rose showing number of joints counted in each 10-degree sector. The plot shows two sets of joints with average strikes about N25 E and N65 W (after WAHLSTROM, 1973).

about the angle of dip of the joints and hence rarely used in engineering geological investigations. It is commonly used in coal mining in comparing the cleavage development in different coal seams.

Many times, when comparing the results of one set of observations at a place to another set at the same place or at two different places, difficulties arise in using the equal-area plots because of the different number of observations at two places. This can be overcome by calculating the density of jointing Δ defined by the relationship (DA SILVEIRA et al, 1966)

$$\Delta = \frac{200n}{N} \tag{11.5}$$

where n = number of joints covering 1% of the area of the hemisphere and

N = total number of observations

in which 200 is a scale factor chosen arbitrarily and found to be useful in practice. The unit density of jointing $\Delta = 1$ corresponds to the occurrence of 0.5% of the total number of joints.

The stereoplots have been adopted for computer print out for handling a large amount of data (ROSENGREN, 1968), but rectangular plots formed by a cylindrical equal spaced meridional projection (Fig. 11-31) (PINCUS, 1951,

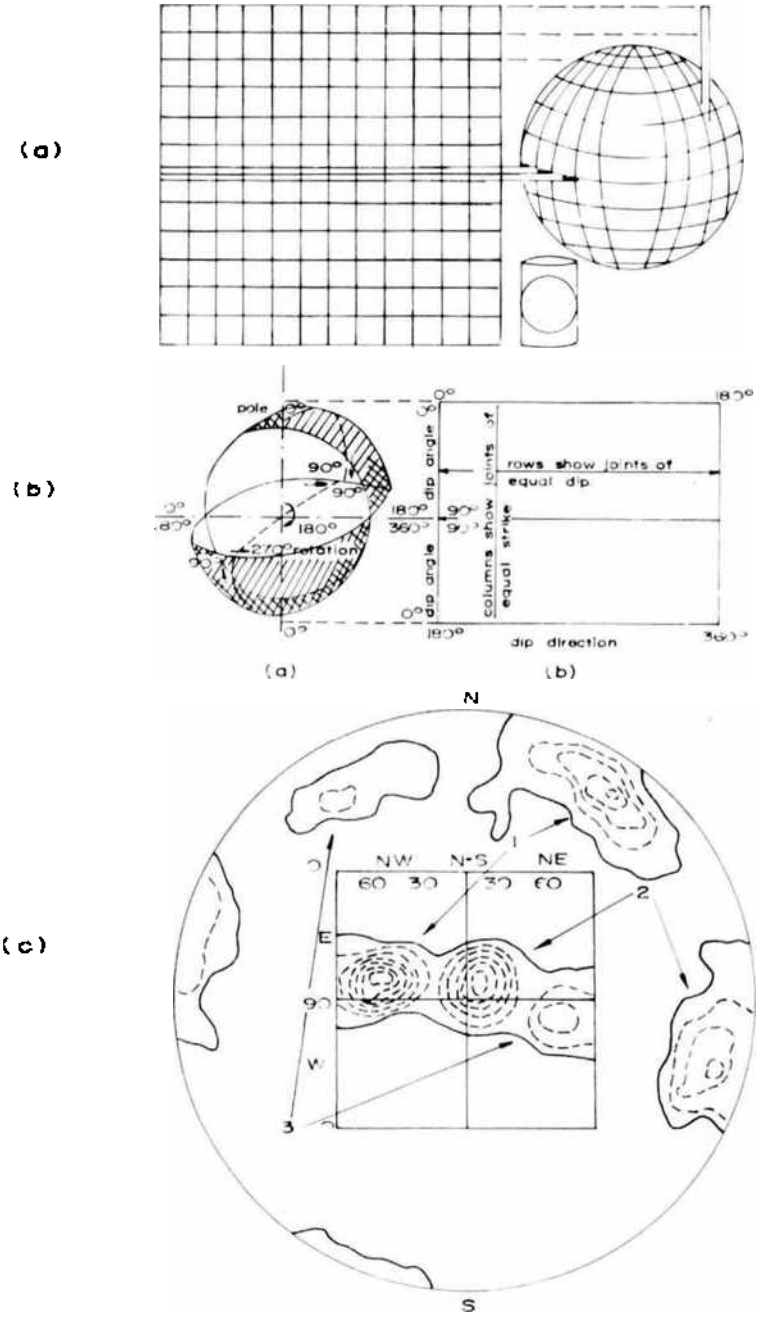

Fig. 11-31. (a) Cylindrical equal-spaced meridional projection
(b) The physical interpretation of the rectangle plot
(c) Comparison of the stereo and rectangle plots
(after PINCUS, 1951, 1953; ROBERTSON, 1970).

1953) are more useful for computer construction. This has the advantage of easy visual inspection but has the disadvantage that some of the properties of the geometric relationships between the joint planes which can be easily calculated in the equal area plot (SCHMIDT projections) are lost in this representation.

Determination of homogeneity of a rock mass with respect to the jointing can be done by establishing joint frequency, standard deviation, attitude of joints and coefficients of variation of distribution of joints calculated from observations made at different places in the rock mass. In case of homogeneous rock mass the coefficient of variation measures the regularity of the distribution and in heterogenous rock mass the deviation from homogeneity. Another method is to determine zones of rock mass where the number of joints of a given set exceeds a certain value fixed previously or with respect to the total number of joints of all sets. The change in the attitude of joint is another useful method of zoning of rock mass. This is particularly useful in rocks which have well developed planes of schistosity.

In same zone, many times, occur more than one set of joints and interpretation of it is not always easy, particularly when standard deviation is large. The personal judgement of the rock mechanics engineer should take into consideration the purpose of the joint study and the stress field attitude as well as the most likely direction of failure. When variations in dip and strike are greater than 30° then joints can definitely be treated as belonging to two different sets. In other cases petrographic examination of the joint fillings, if any, joint surfaces, if differ markedly, or the association of other structures could be an indication of dividing into more than one joint set. Another method of differentiation of joint group is by determining their length distribution as discussed later (joint length and joint continuity).

(b) *Joint Length and Joint Continuity (Degree of Separation)*

By treating that the exposed surface cuts the various joints and their trace "in the form of some cord" is visible as a joint, the length of all these visible cords is measured on a selected area of an exposure section. The average length of the trace is then given by:

$$L_1 = \frac{\text{total area of exposure}}{\text{total length of joint traces} \times \text{number of joints}}$$

Usually, the lengths of joints at different exposures are measured and plotted on a frequency diagram. The cumulative percent and length of joints have been found to have a linear relationship on log-probability scale (Fig. 11-32) as long as all the joint traces measured belong to the same group or if the average

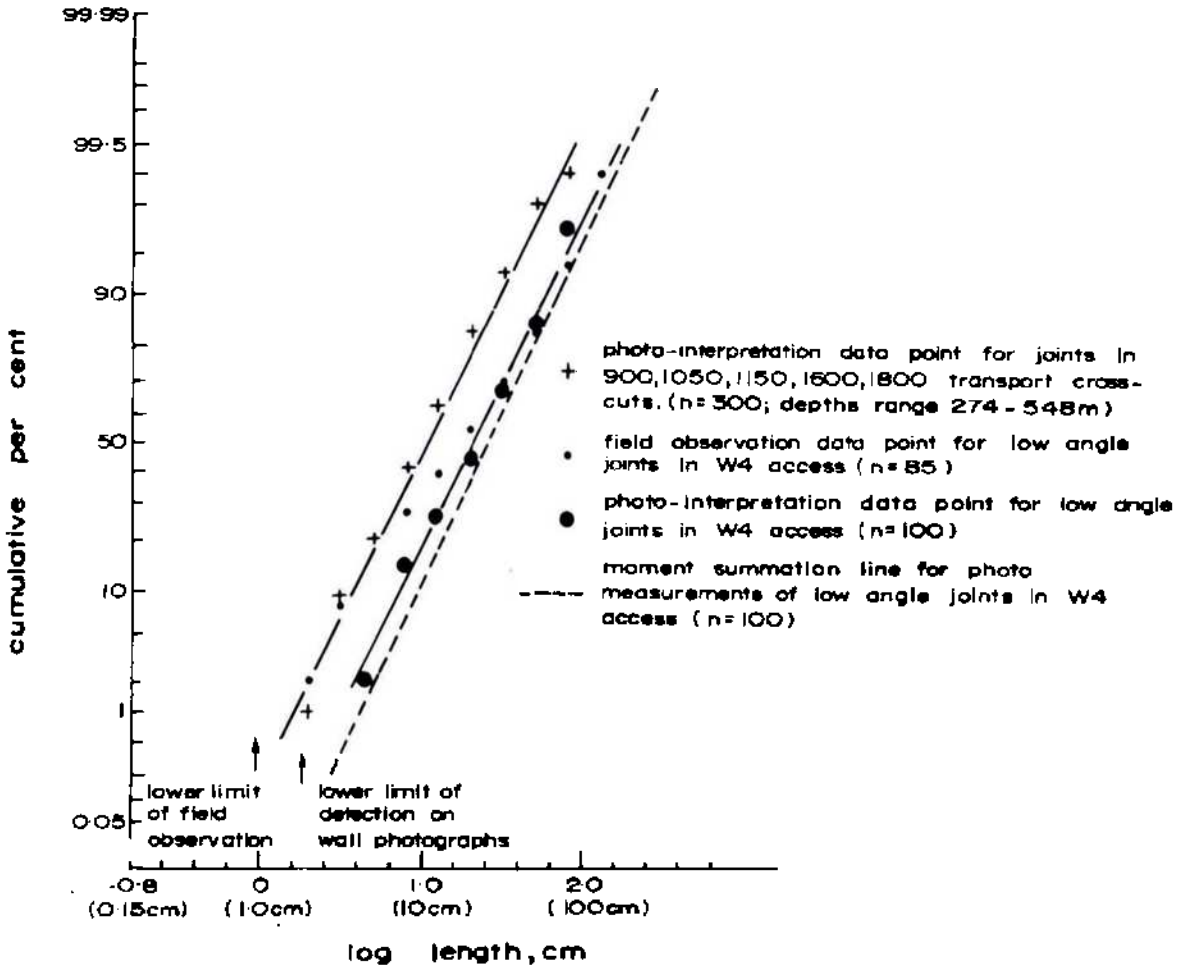

Fig. 11-32. Frequency distribution of "joint" trace length, C.S.A. mine (after BARTON, 1975a).

length of the two groups has the same distribution. In other cases the log normal curves will have two different inclinations (Fig. 11-33) indicating thereby two different distributions of the two different sites. In such a case they shall be required to be differentiated by replotting the values corresponding to the different sets which on the section show different inclinations to the horizontal or the vertical line. If observations are carried out on two planes at right angle to each other (e.g. side and roof of a tunnel), and if the mean lengths of the trace determined from these two sets of observations do not differ appreciably and on plotting them together on the log-log curve they follow a straight line, it can be assumed that the shape of the planar discontinuity is near to a circle or a square. If the mean values so determined are different, it is an indication that the shape of the discontinuity is not a circle but a rectangle or an ellipse or any other shape with the ratio between the major and minor axes far greater than unity.

Theoretical solutions to obtain the dimensions from a variety of shapes have been formulated (UNDERWOOD, 1969). If the joint plane is assumed circular

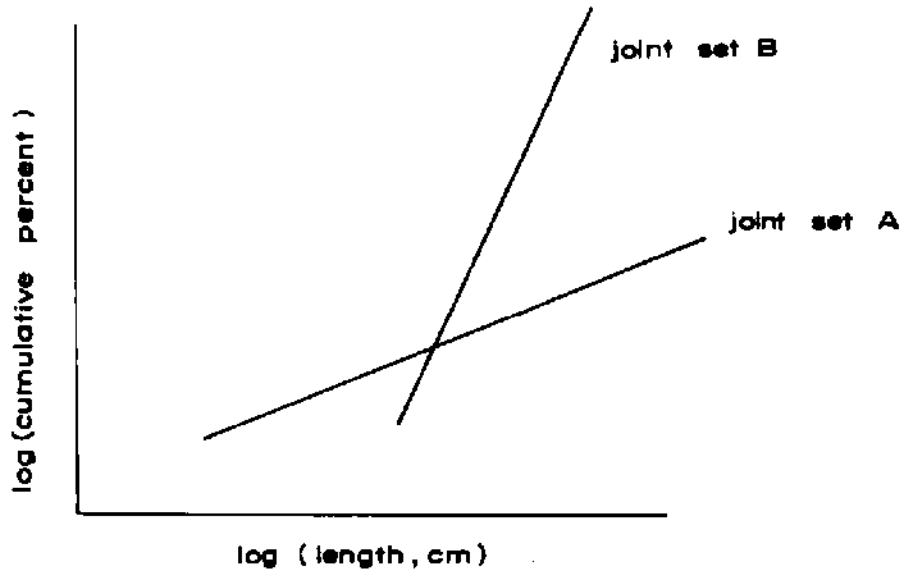

Fig. 11-33. Frequency distribution of two joint sets having two different mean lengths and standard deviations.

which forms the simplest case, the mean trace length L_t is not the mean joint length and a correction factor need to be applied using the relationship based upon the assumption that the trace determined is the cord of a set of approximately GAUSSIAN distributed circles

$$L_m = 1.25\, L_t \tag{11.6}$$

where L_m = mean length of the joint.

The area of planar continuity of circular shape is given by (ROBERTSON and STAMER, 1968; ROBERTSON, 1970)

$$A_c = \frac{16}{\pi^2} A' \tag{11.7}$$

where A' = joint area calculated from the visible mean trace length, or

$$A_c = \frac{4}{\pi} L_t^2 \tag{11.8}$$

The above correction factors are valid only on the assumption that the diameter of the joints are the same and hence are only an approximation.

The joints are not always continuous and their continuity is dependent upon the severity of the forces causing jointing and the amount of deformation that the rock has undergone. The area of the intact rock lying between the discontinuous joints is called the 'gap' or the 'bridge' and the effective joint area

as a function of the total area is called the joint continuity (PACHER, 1959; TERZAGHI, 1962).

From the data obtained on joint spacing J_s and joint length L_m, the joint continuity (χ_c) can be calculated. For circular joints

$$\chi_c = \left(\frac{J_s}{L_m}\right)^2 \tag{11.9}$$

For continuous joints $\chi_c = 1$ and for discontinuous $\chi_c < 1$. It is possible that different joint sets have different continuity values (Fig. 11-34).

The planar joint continuity surface χ_{ep} (Ebener Kluftflächenanteil — PACHER, 1959; MÜLLER, 1963) of a joint set is given by the product of mean joint continuity factor χ_c and joint frequency $J_{n'}$,

$$\chi_{ep} = \chi_c \times J_{n'} \tag{11.10}$$

and represents the joint continuity surface per unit area. In a given rock volume, intersected by three sets of joints K_1, K_2, K_3, the planar continuity factor of a given plane parallel to a given set is given by the average of the planar joint continuity surfaces of the other two sets of joints such as (Fig. 11-34)

$$\left(\frac{\chi_{ep_1} + \chi_{ep_2}}{2}\right) \text{ or } \left(\frac{\chi_{ep_2} + \chi_{ep_3}}{2}\right) \text{ or } \left(\frac{\chi_{ep_3} + \chi_{ep_1}}{2}\right)$$

for the planes parallel to the set K_3, K_1 and K_2.

The volumetric continuity factor representing the total area of the geological separations in a unit volume of rock is given by

$$\chi_{ev} = \left(\frac{\chi_{ep_1} + \chi_{ep_2} + \chi_{ep_3}}{3}\right) \tag{11.11}$$

The planar continuity factor of the different joint sets gives an idea of the strength of the rock mass and permeability in different directions. The volumetric joint continuity factor gives an idea of the dilation possibility, porosity and permeability of the rock mass as a whole. A much clearer picture of the rock mass influenced by the joints and their continuities emerges when their various values are represented for different joint sets against each other as in Table 31 which makes clear the use of above concepts in the form of an example.

Total planar continuity $\Sigma\chi_{ep} = 8.55\ m^2/m^3$

TABLE 31

Special quantification of the joint from the indices of individual joints

(after PACHER, 1959)

Joint set	Attitude: Strike direction	Attitude: Dip	Joint frequency $J_{n'}$, m^{-1}	Joint continuity χ_c	Planar joint continuity of the set χ_{ep}, m^2/m^3	Joint friction coefficient	Joint condition	Remarks
K_1	0	10	4.5	1.0	4.5	1.0	Filled with coal	–
K_2	35	80	4	1.0	4	0.84	Closed	Dominant joint set
K_3	120	80	0.2	< 0.25	0.05	—	—	–

Planar continuity factor

$$\frac{\chi_{ep_1} + \chi_{ep_2}}{2} = 1$$

$$\frac{\chi_{ep_2} + \chi_{ep_3}}{2} = 0.62$$

$$\frac{\chi_{ep_3} + \chi_{ep_1}}{2} = 0.62$$

$$\text{Volumetric continuity factor} = \left(\frac{\chi_{ep_1} + \chi_{ep_2} + \chi_{ep_3}}{3}\right)$$

$$= 0.72$$

$$\text{Average block size} = \frac{1}{J_{n'1}} \times \frac{1}{J_{n'2}} \times \frac{1}{J_{n'3}} = 0.27\ \text{m}^3$$

Ratio of joint frequencies $J_{n'1} : J_{n'2} : J_{n'3} = 4.5 : 4 : 0.2$

If the values of $J_{n'}$ in the three directions are equal then the rock mass can be described as blocky and if the two values are equal and the third greater, then the rock mass can be described as prismatic and if two values are small and the third value is high, it has a platy structure.

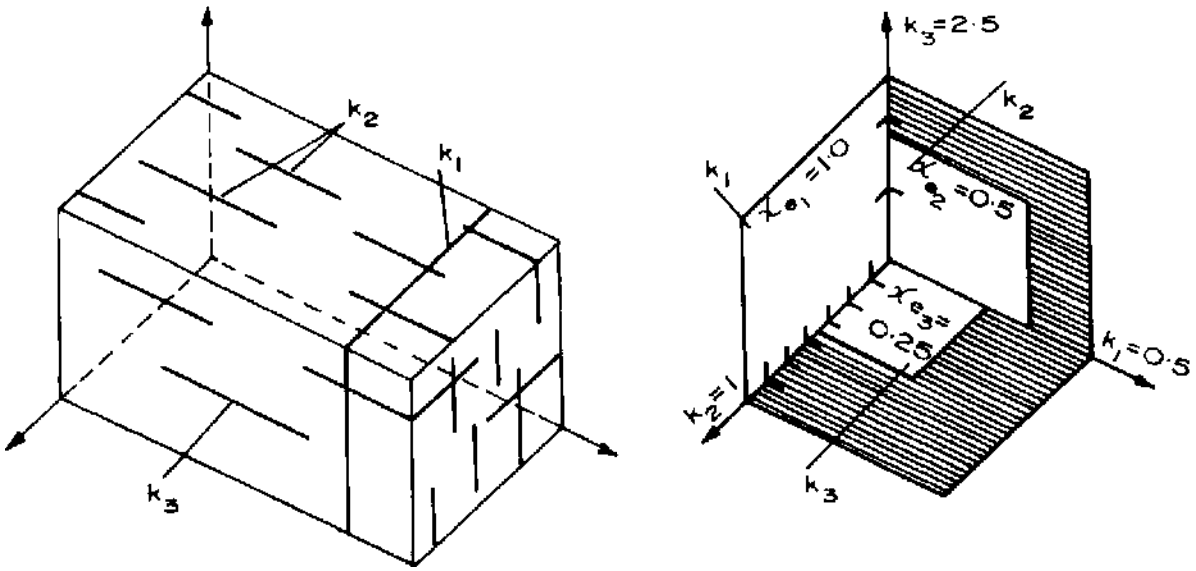

Fig. 11-34. Planar joint continuity, χ for the different joint sets (after PACHER, 1959).

It may be pointed out here that while considering joint continuity as a factor in determining the cohesion of a rock, its proportional effect should not be taken (as is usually done) until the stress field direction has been ascertained. TERZAGHI (1962), for example, considers that the effective cohesion c_{eff} can be given by

$$c_{eff} = c \cdot \frac{Ag}{A} \tag{11.12}$$

where c = cohesion of intact rock
Ag = total area of gap within the section and
A = total area of section through the rock

There are several reasons that can be put forward against this. Firstly the joint tips form points of high stress concentrations and secondly it has been found that joint propagation does not take place from tip to tip but may give a step like structure (Fig. 11-35). The direction of propagation of the joints depends upon the orientation of stress field and propagation takes place in such a way that it aligns itself in the direction of maximum compressive stress (MÜLLER, 1974 and 1975). The effect of this shall be to increase the c_{eff} value. Also the concept of joint continuity is valid only if joint propagation takes place from end to end. In other cases, its value will depend upon relative interval between the adjacent joint sets or some other point on the joint to which the propagating fracture meets depending upon the relative orientation of the stress field.

The volume of a unit block (V_{UB}) referred to as the smallest homogeneous rock unit produced as a result of various joint systems is given by

$$V_{UB} = \left(\frac{1}{J_{n'1}}\right) \times \left(\frac{1}{J_{n'2}}\right) \times \left(\frac{1}{J_{n'3}}\right) \tag{11.13}$$

where $J_{n'1}$, $J_{n'2}$ and $J_{n'3}$ are the frequencies of three orthogonal joint sets.

A number of joint spacing classifications have been proposed and the classification by DEERE (1963) has been widely accepted (Table 32). The thickness of beds in sedimentary rocks may be described in terms of the spacing between them and a classification is given in Table 33. Classification of joint spacing and block size suggested by I.S.R.M. (1975) is given in Tables 34 and 35 respectively. There is basically no difference in the various classifications proposed.

(c) and (d) Joint Roughness and Joint Thickness

Joint roughness influences both frictional resistance of joint as well as joint dilatation. The micro-asperities influence friction angle and macro-asperities influence dilatation. Total resistance to sliding (without separating the influence of dilatation) increases as joint roughness increases. A measure of joint roughness is the dilatation that the two surfaces will have on displacement along their length. Various techniques for measuring joint roughness are given in Chapter 10. From rock classification point, asperity height, thickness of filling, and nature of the filling material in the joints are important. Depending upon the thickness and the asperity height, either the joint filling material may control the behaviour of the joint completely or it may not. Clay fillings with other granular materials are particularly critical because of the danger of internal erosion. Clay filling may also result in liquifaction under dynamic loadings and will have to be properly studied.

When joints are very rough (macro-roughness or waviness) and roughness varies in different directions, this will result in keying action in one direction and relatively easier movement in the other direction. This is also influenced even in smooth joints in rocks with well defined fabric orientation. The platy form of grains aligned in any direction will favour slip in this direction and hinder in other directions. Studies conducted on phyllites have shown that friction angle for sliding parallel to lineation is 40° and across the lineation 42° (Fig. 11-36). Residual angles of friction decrease due to fracturing of the 'keys' and the broken material falling in between the surfaces acts as rollers except in very soft rocks where the difference in the value is negligible. When it is not possible to determine the roughness (Section 10.4.), the geologist can define the roughness into five categories. These categories of roughness which can

TABLE 32

Classification of joint spacing

(after DEERE, 1963)

Description	Spacing of joints
Very close	< 5 cm (< 2 in)
Close	5 to 30 cm (2 to 12 in)
Moderately close	30 cm to 1 m (1 to 3 ft)
Wide	1 to 3 m (3 to 10 ft)
Very wide	> 3 m (> 10 ft)

TABLE 33

Classification of bed thickness

(after DEERE, 1963)

Description	Thickness of bed
Very thin	< 5 cm (< 2 in)
Thin	5 to 30 cm (2 to 12 in)
Medium	30 cm to 1 m (1 to 3 ft)
Thick	1 to 3 m (3 to 10 ft)
Very thick	> 3 m (> 10 ft)

TABLE 34

Classification of joint spacing

(after I.S.R.M., 1975)

Classification	Joint spacing
Extremely close	< 3 cm
Very close	3 to 10 cm
Close	10 to 30 cm
Medium	30 to 100 cm
Wide	1 to 3 m
Very wide	3 to 10 m
Extemely wide	> 10 m

TABLE 35
Classification of block size
(after I.S.R.M., 1975)

Classification	Joint volume, m^{-3}
Massive	< 1.0
Large blocks	1 to 3
Medium size blocks	3 to 10
Small blocks	10 to 30
Very small blocks	> 30

Remark: - J.V. > 60 represents crushed rocks typical of clay free crushed zone.

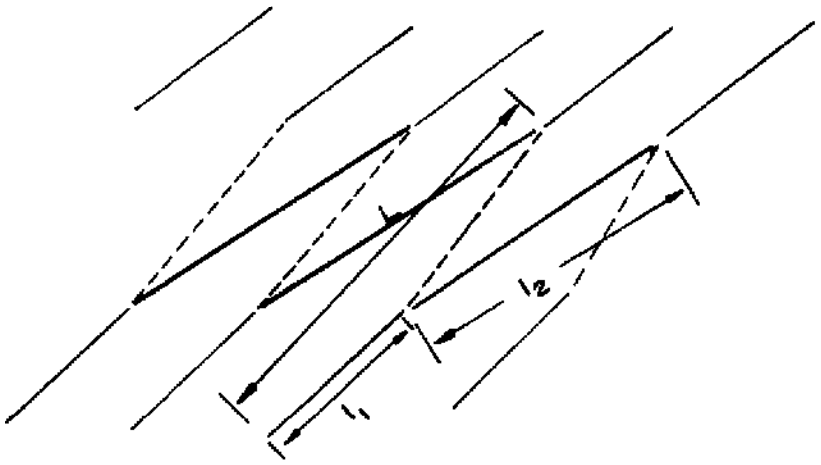

Fig. 11-35. Joint propagation in a certain hypothetical stress field

Calculated joint continuity $\chi = \frac{l_1}{L}$

Actual joint continuity $\chi = \frac{l_1}{l_1 + l_2}$

be classed easily in the field are given in Fig. 11-37. The waviness of joint can be determined by plotting the amplitude against the length measured by using a straight edge (1 m length) placed on the exposed joint roughness can be best described by stating the value in terms of the angle λ (Fig. 11-38).

Aperture

Aperture refers to such joints where the intervening space is filled with water or air or where the filling material has been washed away or the material has been dissolved by migrating waters or solutions or to an opening developed

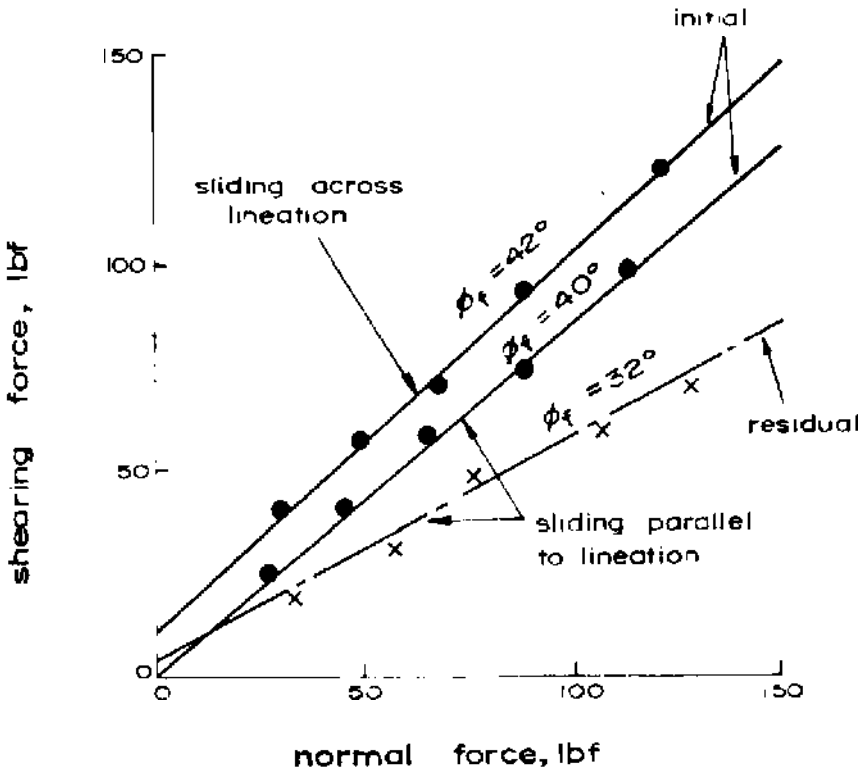

Fig. 11-36. Frictional behaviour of phyllite (after DUNCAN, 1969).

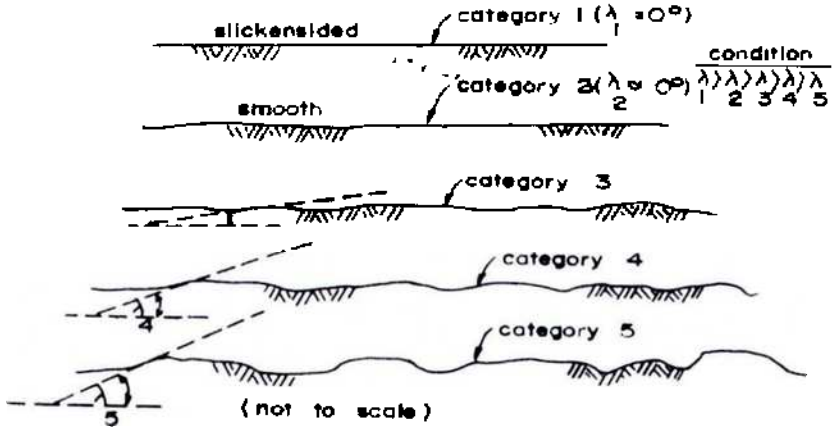

Fig. 11-37. Illustration of relative roughness of the five categories (after PITEAU, 1970).

due to shear movement along undulating joints. Knowledge of apertures is important to determine loosening and hydraulic conductivity.

Measurement of aperture can be made by a graduated rule or a feeler gauge. The surface of the exposure is cleaned properly to remove extraneous dirt filling the normally open joints. In bore holes, rubber packers may be pressed against the walls to obtain the impression and after withdrawing the packer, the width can be measured (FAIRHURST and ROEGIERS, 1972).

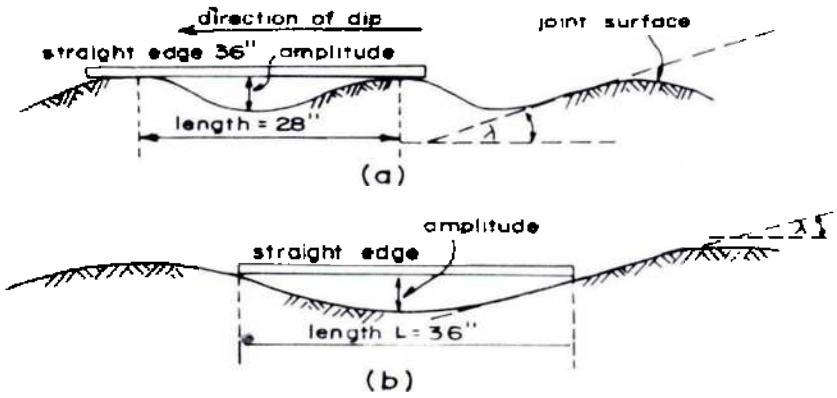

Fig. 11-38. Measurement of waviness of a joint plane (after PITEAU, 1970).

Hydraulic conductivity gives a much better idea of the joint aperture, if true length of the joint is known and if test can be conducted in a single joint. However, dead areas caused by asperity contacts will create difficulties in its estimation (SHARP and MAINI, 1972). When integral sampling technique (ROCHA, 1972) is adopted for weak rocks, the width of the aperture can be very easily measured from the core obtained. The apertures can be classified as given in Table 36.

TABLE 36

Classification of apertures

(after I.S.R.M., 1975)

Aperture width	Description	Remarks
< 0.1 mm	Very tight	
0.1 to 0.5 mm	Tight	Joints
0.5 to 2.5 mm	Moderately wide	
2.5 to 10 mm	Wide	
> 10 mm	Very wide	
1 to 10 cm	Large	Out washes discontinuities and joints displaced by tensile movements or major shears
10 to 100 cm	Very large	
> 1 m	Cavernous	

11.6. Errors in Joint Surveys

Some important points need to be considered when carrying out a joint survey. As long as plenty of irregular outcrops or excavations running at different angles to each other are available for examination, the joint survey data is likely to present a reasonably fair sample of the joints. However, if the outcrop is fairly unidirectional or if the joint survey is made only from holes drilled in one particular direction (say vertical), the joint survey is unlikely to provide even an approximate data of the area.

When joint survey is conducted from the drill records, the angle at which the joints intersect the bore hole is an important factor and appropriate correction has got to be applied as already indicated in the surveying of outcrop (Section 11.5.). If this correction is not applied and the results are compared with the results of the joint survey conducted on the outcrop, one is likely to get a polar diagram (Fig. 11-39) with an erroneous interpretation that the joints at depth are quite different than on the surface. Such diagrams can be redrawn by using a correction factor

$$N_{90} = \frac{N_\alpha}{\sin \alpha} \tag{11.14}$$

where N_{90} = number of joints intersected at 90° for a bore of length l
N_α = number of joints intersected at an angle α for the same bore length and
α = angle of inclination between joints and the borehole.

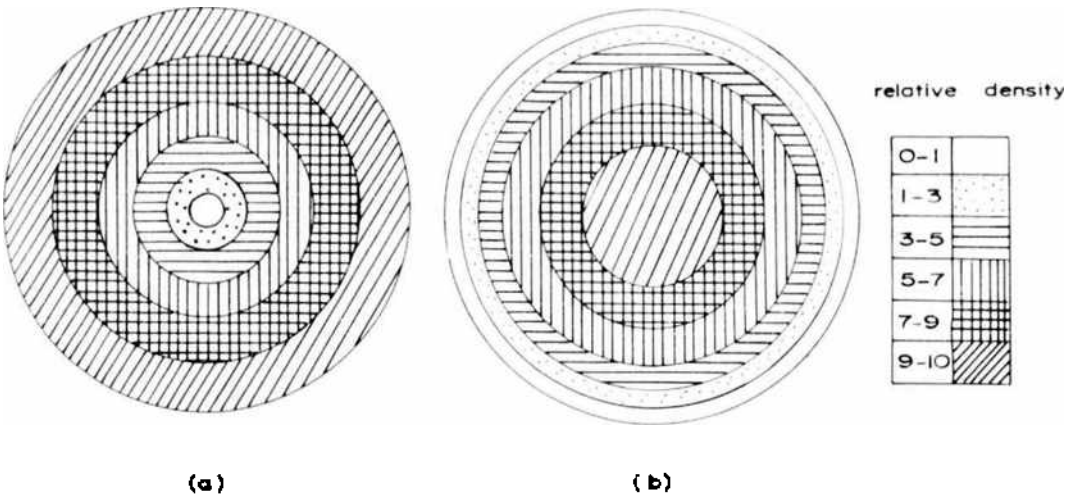

Fig. 11-39. Idealised contoured polar diagrams of random joints observed (a) on horizontal outcrop and (b) in a vertical drill hole. Figures indicate relative density of poles, i.e. number per unit area, on an arbitrary scale from 0 to 10 (after TERZAGHI, 1965).

However, when α is zero (i.e. the joints are parallel to the borehole), no correction can be applied and even a corrected version of the polar diagram will fail to indicate such joints or abundance of gently dipping joints which only one or more might have been intersected in the borehole of a limited length and could be an important joint set. As a result a borehole, depending upon its orientation, will give a blind zone, which is a great circle 90° from the axial point of the hole as defined in the section of the reference sphere (Fig. 11-40). The width of the blind zone (in terms of the angle) is dependent upon the length of the bore and the spacing of joints.

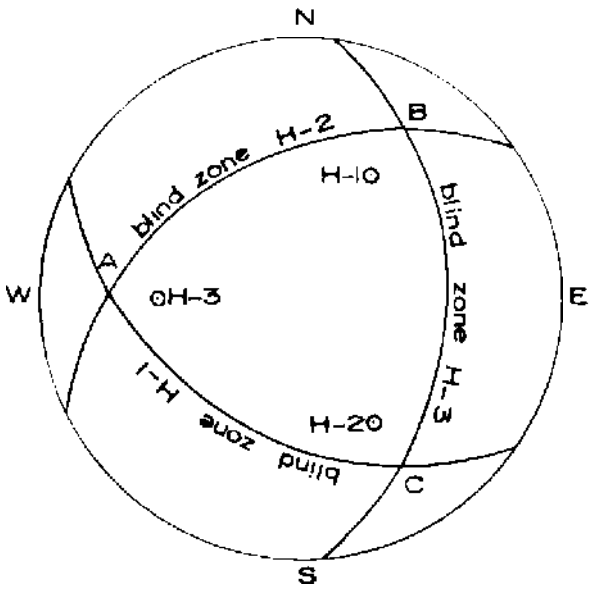

Fig. 11-40. Layout of a cluster of three drill holes permitting adequate observation of all joints, shown in equal-area projection (after TERZAGHI, 1965).

To avoid these errors in surveying it is important that at least one borehole should be available which intersects the joints at an angle not less than 30°. When a number of boreholes have been drilled at different angles, the corrected values of the poles (N_{90}) can be marked on the polar diagram and near the blind zone in any one diagram either the corrected count from one, or the average of the corrected counts from the others is substituted. Final interpretation should be based upon a collective diagram constructed from all the boreholes at the place where each number inscribed in this diagram is the sum of the numbers of poles divided by the number of boreholes. In the blind zone the sum of the poles from individual plots shall be divided by (n-1) where n is the number of holes or individual plots. Where two or more blind zones intersect (Points A, B and C in Fig. 11-40) the sum total of pole points in that common blind zone will need to be divided by the number (n-m) where m is the number of holes which have blind zones intersecting giving a common blind zone area.

11.7. Rock Weathering and Classification

Rock weathering is a process causing alteration of rock under the action of water, carbon dioxide and oxygen. The effect of weathering is not limited to surface but extends deeper depending upon the presence of channels permitting flow of water and communication with atmosphere. Weathering results in decreased competency of rock from the engineering standpoint and the depth to which weathering extends is important to determine in foundation work of structures. Weathered zone may exist even under unweathered younger sedimentary rocks particularly beneath major unconformities and their determination requires a careful study of the geologic history of the area.

The final product of weathering is an oxidised mineral residue or an aqueous pore solution containing the elements derived from the weathering process. The rate of weathering depends upon the freedom of movement of the weathering agents, the prevailing temperature and the mineralogical composition of the rock.

The minerals most susceptible to weathering are those which contain abundance of magnesium, calcium and iron. Magnesium and calcium are first oxidised into alkalis and are later removed by flushing or diffusion or may be converted to carbonates under the action of carbon dioxide. Iron after oxidation generally remains in the rock. Aluminium, silica and iron break down giving clay minerals and related fine grained micaceous minerals plus hydrated oxides of aluminium and iron. Under extreme conditions even silica may be leached leaving iron oxides and aluminium hydrates giving laterites. Feldspars break down to give clay minerals.

Some of the common minerals in igneous and metamorphic rocks or constituents of clastic sedimentary rocks are grouped into 3 groups depending upon their resistances to weathering (Table 37). It shall be clear that rocks rich in minerals having low weathering resistance decompose more easily than others.

The various weathering processes are concisely described below:
Mechanical weathering is the disintegration of rock due to the temperature changes (high and low temperatures), frost action, water cycles (wet and dry), expansion caused by trees and plant roots, etc. The influence extends to only a couple of metres.

Chemical dissolution under the influence of surface or underground water is a powerful weathering process. Removal of certain elements may take place by actual transport of water through rock cracks, joints or through pores along large distances or by diffusion and capillary transport through short distances in stagnant environments. Hydrothermal solutions may result in breakdown

of rocks (argillisation) producing clay mineral aggregates as a result of leaching of alkalis and alkaline earths. With imperfect leaching, chlorite and montmorillonite replace pre-existing silicate minerals which are most treacherous in any underground or surface excavations. Pyritisation provides a warning that rock has been subjected to hydrothermal solutions which might have caused other chemical breakdowns and replacement by clay minerals. Chloritisation is accompanied by argillic alteration and dolomitisation is an indication that there may be open spaces and loose aggregates and sand-size crystals that possess no cementing and could flow into the excavation. Some other processes such as silicification, sericitisation, sausuritisation, carbonisation do produce strengthening of the existing rock.

TABLE 37

Resistance to chemical weathering of common minerals of igneous and metamorphic rocks

(after WAHLSTROM, 1973)

1. Low resistance:	
olivine	staurolite
pyroxene	iron-rich garnet
hornblende	melilite
calcic plagioclase	epidote
biotite mica	feldspathoids
2. Intermediate resistance:	
intermediate plagioclase	sillimanite
sodic plagioclase	andalusite
orthoclase feldspar	kyanite
microcline feldspar	calcium aluminium garnet
muscovite mica	iron-poor garnet
	clinozoisite
3. High resistance:	
quartz	hematite
magnetite	tourmaline

In weathering (both mechanical and chemical) the availability of moisture is the most important single factor. An index "N" of the availability of water for weathering is given by WEINERT (1968) as a function of the total annual precipitation and the potential evaporation during the warmest month as follows:

$$N = \frac{12\,Ej}{Pa} \tag{11.15}$$

where Ej = potential evaporation in the warmest month and
Pa = annual precipitation.

TABLE 38

Description of a weathering profile for igneous and metamorphic rocks

(after PATTON and DEERE, 1970)

	Zone	Description	RQD (%)	Percent NX core recovery	Relative permeability	Relative strength
I. Residual soil	1A-A Horizon	top soil, roots, organic material – zone of leaching and eluviation – may be porous	–	0	medium to high	low to medium
	1B-B Horizon	– characteristically clay no relict structures – some enrichment of Fe, Al, Si. – may be cemented	—	0	low	commonly low, high if cemented
	1C-C Horizon	– relict rock structures retained. Silty grading to sandy material – < 10% core stones – often micaceous	0	generally 0–10	medium	low to medium (relict structures significant
II. Weathered rock	11A Transition	– highly variable, soil like to rock like – spheroidal weathering common – 10 to 95% core stones fines commonly fine to coarse sand	0 - 50	variable 10–90	high	medium to low
	11B Partly weathered rock	rock like, soft to hard rock - joints stained to altered – some alteration of feldspars and micas	50 75	generally > 90	medium to high	medium to high (intact rock masses)
III. Unweathered rock		no weathering of feldspars or micas - no iron stains along joints	> 75 generally > 90	generally 100	low to medium	high to very high (intact rock masses)

If the value of N is below 5, sufficient water is available for chemical decomposition of primary minerals into clay as a result of oxidation and hydration. If the value of N is greater than 5, weathering is basically mechanical without much change in mineralogy.

Weathering reduces the mechanical strength, increases deformability, porosity and permeability and develops a complex three-dimensional arrangement of unweathered, partially weathered and residual soil (PATTON and DEERE, 1970). Fig. 11-41 gives a typical weathering profile and Table 38 gives the relationship between the various weathered zones and the engineering parameters.

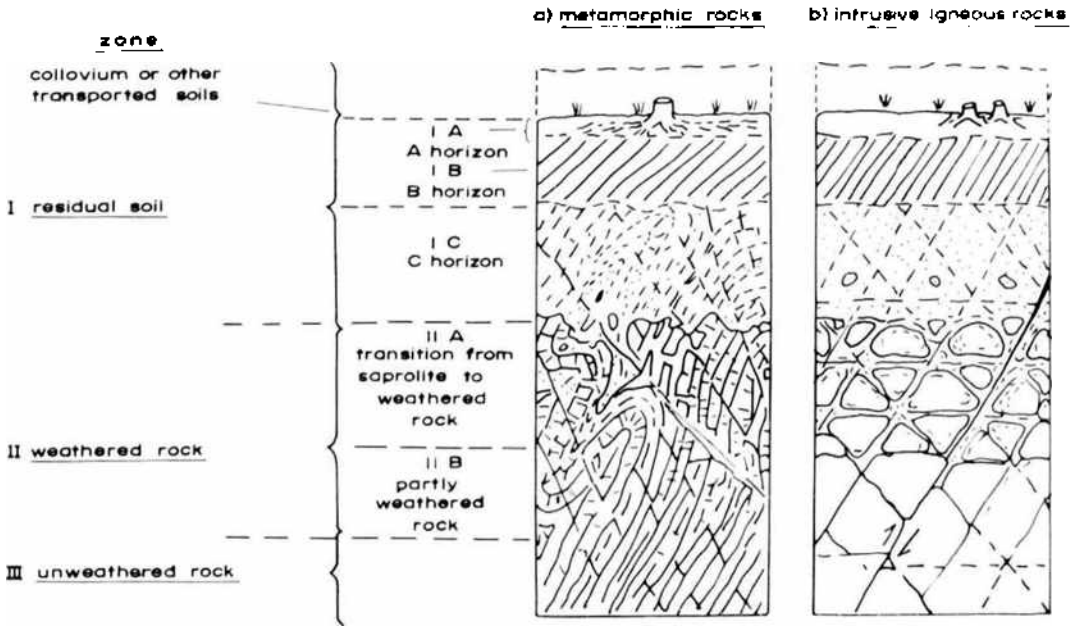

Fig. 11-41. Typical weathering profile for metamorphic and igneous rocks (after PATTON and DEERE, 1970).

The classification of rocks from the point of weathering recommended by the Geological Society of London (1970) and accepted by U.S. Task Committee for Foundations Design Manual (1972) is given in Table 39.

In most rocks the influence of life span of a structure will not alter the weathering state of the rock except in certain rocks containing ferro-magnesian minerals or weaker rocks such as clays, mudstones, shales, etc. which on coming in contact with water and cycles of wetting and drying crumble. An index-test of the weatherability of rock is the slake-durability test, swelling index or the void index (see Chapter 12., Section 12.7.). Weatherability is related to the ratio of the uniaxial compressive strength σ_c and swelling strain index ε_s called as the strength-swell ratio and is given in Table 40 (OLIVIER, 1973).

TABLE 39

Engineering classification of weathering

Classification	Description
Unweathered:	No visible signs of weathering. Rock fresh, crystals bright. Few discontinuities may show slight staining.
Slightly weathered rock:	Penetrative weathering developed on open discontinuity surfaces but only slight weathering of rock material. Discontinuities are discoloured and discolouration can extend into rock up to a few mm from discontinuity surface.
Moderately weathered rock:	Slight discolouration extends through the greater part of the rock mass. The rock material is not friable (except in the case of poorly cemented sedimentary rocks). Discontinuities are stained and/or contain a filling comprising altered materials.
Highly weathered rock:	Weathering extends throughout rock mass and the rock material is partly friable. Rock has no lustre. All material except quartz is discoloured. Rock can be excavated with geologist's pick.
Completely weathered rock:	Rock is totally discoloured and decomposed and in a friable condition with only fragments of the rock texture and structure preserved. The external appearance is that of a soil.
Residual soil:	Soil material with complete disintegration of texture, structure and mineralogy of the parent rock.

TABLE 40

Weatherability classification of sedimentary rock present in Orange-Fish tunnel

(after OLIVIER, 1973)

Weatherability discription	Strength-swell ratio, MPa $\sigma_c \varepsilon_s \times 10^n$
Excellent	> 8,0
Good	4,0–8,0
Fair	2,0–4,0
Poor	1,0–2,0
Very poor	< 1,0

11.8. Classification of Intact Rock

Classification of intact rock deals with the material removed from its environment and devoid of discontinuities. It includes any descriptive terminology relating the condition of its origin and certain visual observatations on its structure, composition, texture, grain size, porosity and sometimes some other index properties such as swelling strain index or slake durability. It is basically a geologist's classification and gives a fair idea to the engineer about the type of material that he has to deal with. The origin of the rock, for example igneous rock, is an indication to the engineer that it will have small directional anisotropy while metamorphic rock such as shale, chlorite, schist, have strong directional anisotropy. Similarly, limestone, gypsum and rock salt are associated with solution features such as caves, sink holes, etc. and lava flows with sheets and columnar joints and certain clays and shales are sensitive to moisture. It is therefore important that the rock engineer does not loose side of the immense wealth associated with the geological classification while considering the engineering classification of intact rock.

The index properties along with the compressive strength are the engineering classification of the rock substance and give an idea about the possible mechanical response of the rock. These form an important part of the overall classification of the rock as discussed later.

After an extensive study, HANDIN (1966) grouped the most commonly experienced rocks into seven lithological groups (Table 41) depending upon their general behaviour. The term lithology connoted in his classification system refers not only to the general rock type (e.g. sandstones, dolomites, shales) but also the minor variations in mineralogy, texture and cementing material. Tests conducted by RUIZ (1966) on 26 rock types from Brazil agree well with the lithological classification of HANDIN.

TABLE 41

Lithological classification of rock (after HANDIN, 1966)

Type	Rock material
1	Unfoliated igneous and metamorphic rocks, quartzite, highly silicacemented sandstone;
2	Slate and highly indurated shale;
3	Dolomite;
4	Moderately well cemented sandstone;
5	Limestone;
6	Schist, shale, mudstone, and poorly indurated siltstone;
7	Salt and gypsum.

The classification system that is of greater importance for an engineer is the one based upon numerical values. The purpose of it is to provide information on whether the strength of the intact material in itself is likely to be a source of trouble. COATES (1964), COATES and PARSONS (1966) have classified rock substance based upon compressive strength and deformation parameters determined in the laboratory. They divided the rock into weak (less than 5000 lbf/in^2 (35 MPa)), strong (between 5000 and 25000 lbf/in^2 (35 to 173 MPa)) and very strong (greater than 25000 lbf/in^2 (173 MPa)) categories. Further factors that they considered in the classification of rock substance are the prefailure deformation and failure characteristics. In the prefailure deformation the rocks may be classified as elastic if there is no creep at 50% of the compressive strength or viscous if the rocks creep at 50% of the compressive strength. (In such cases, it is desirable to give the creep rate.) In the failure characteristics if the failure is sudden the rocks are classified as brittle and if the failure is by flow, they are termed as plastic (25% of total strain before failure is permanent). This classification system is useful when classifying rocks for drilling, grinding and underground blasting purposes or for fragmentation on a smaller scale and in rocks which are massive in nature without joints. Some of the rocks classified by them are given in Table 42.

To include a wider range of materials met with in civil engineering, the strength classification has been extended by a number of authors (DEERE and MILLER, 1966; STAPLEDON, 1968; Geological Society of London, 1970; BROCH and FRANKLIN, 1972; JENNINGS et al, 1973; BIENIAWSKI, 1973). A general comparison of the various classes with numerical values of uniaxial compressive strength is given in Fig. 11-42. The classification scale of DEERE and MILLER (1960) has been more or less accepted now and this is represented in Table 43. This covers almost the complete range of the rocks met with in mining and civil engineering. The compressive strength is determined on specimens with the height/diameter ratio of at least 2. The division into class of highest strength is chosen at about 200 MPa which is almost the strength of very strong rocks such as quartzite, dolerite, gabbro, basalt, diabase, etc. The other classes are scaled down by a dividing factor of 2. The class B includes majority of coarse-grained igneous (granites, granodiorites) and stronger metamorphic rocks and some strong sandstones, limestones and dolomites. Class C includes most of shales, medium strength sandstones and limestones and metamorphic rocks having schistose structure such as chlorites, micaceous and talc schists. Class D includes coal and siltstones and many carbonaceous rocks while E includes low strength rocks such as mudstones, clay shales, rock salts, chalks and weathered rocks.

The deformation characteristics of the rock substance has also been considered in rock classification. It has been shown that stronger rocks in general have a high modulus. Instead of using the modulus value alone, the ratio of the

TABLE 42

Rock substance classification (after COATES and PARSONS, 1966)

Name	σ_c, kgf/cm^2	E, kgf/cm^2 $\times 10^5$	$\dot{\varepsilon}$, μ/hr	$\bar{\varepsilon}p$, %	Substance classification
Andesite	—	3.8	2.4	—	
	—	9.7	0.06	—	
Basalt	—	5.5	1.5	—	
Blastonite	1190	4.53	1.75	7.3	S, E, B
	((8))	((8))	((2))	((9))	
	(45.0)	(32.1)		(72)	
Chlorite	1120	6.09	1.42	4.7	S, E, B
	((10))	((10))	((4))	((6))	
	(8.0)	(8.81)	(6.60)	(40)	
Conglo-merate	2220	7.60	1.0	1.8	VS, E, B
	((32))	((32))	((3))	((2))	
	(22.5)	(15.7)	(40)		
Diabase	2180	9.48	0.9	0.7	VS, E, B
	((23))	((23))	((4))	((3))	
	(35.2)	(11.5)	(33)	(90)	
Flourite	1020	5.27	0.25	10.8	S, E, B
	((2))	((2))	((2))	((2))	
		—	—		
Granite 1	1720	6.58	0	1.0	S, E, B
	((7))	((8))	((2))	((2))	
	(17.4)	(10.7)			
Granite 2	2760	7.38	0.8	1.8	VS, E, B
	((5))	((5))	((4))	((10))	
	(4.0)	(4.8)	(91)	(108)	
Granite 3	1440	7.16	0.4	4.1	S, E, B
	((4))	((4))	((3))	((16))	
	(30.2)	(9.8)	(82.5)	82)	
Granite 4	3.8	1.1	—	—	
Granite 5	1400	5.4	1.4		S, E
Halite	156	1.84*	92.8	83.9	W, V, P
	((4))	((5))	((5))	((5))	
	(11.0)	(19.8)	(21.6)	(5.48)	
Hematite	1940	7.45	< 1	1.4	VS, E, B
	((9))	((9))	((3))	((3))	
	(6.57)	(11.3)		(8.0)	
Limestone 1	2780	5.89	3.6	1.5	VS, V, B
	((6))	((6))	((2))	((5))	
	(13.7)	(17.8)		(86)	

* Based on final unloading cycle.

TABLE 42 (continued)

Name	σ_c, kgf/cm^2	E, kgf/cm^2 $\times 10^5$	$\dot{\varepsilon}$, μ/hr	$\bar{\varepsilon}\rho$, %	Substance classification
Limestone 2	1340 ((7)) (37.2)	7.10 ((7)) (33.5)	0.7 ((7)) (117)	2.9 ((8)) (46)	S, E, B
Marble	883	6.4	13.1	18	S, V, B
Peridotite	1970 ((18)) (28.0)	5.52 ((18)) (7.7)	1.21 ((6)) (100)	0.7 ((8)) (67.4)	VS, E, B
Potash	127 ((7)) (20.7)	0.73* ((4)) (19.2)	20.0 ((7)) (56)	44.0 ((7)) (47)	W, V, P
Quartzite	2600 ((112)) (15.8)	8.14 ((112)) (2.5)	0 ((6)) -	2.9 ((10)) (42.5)	VS, E, B
Rhyolite	—	2.6	0.16	—	
Sandstone 1	920 ((5)) (3.8)	3.60 ((6)) (3.00)	1.75 ((2))	0.5 ((3)) (25)	S, E, B
Sandstone 2	850	1.0	115	31	S, V, P
Shale 1	1500 ((9)) (11.0)	3.52 ((9)) (27.2)	10.8 ((4)) (19.7)	7.4 ((9)) (35)	S, V, B
Shale 2	1100	1.8	4.9	—	S, V
Shale 3	600	1.3	100.4		S, V
Shale 4	600	1.3	45	—	S, V
Shale 5	600	1.3	180	—	S, V
Shale 6	20.2 ((2))	— — —	230 ((1)) —	30.5 ((2)) —	W, V, P
Siderite	2790 ((7)) (17.1)	9.05 ((8)) (3.97)	0 ((2)) -	0.40 ((3)) (64)	VS, E, B
Specularite-Magnetite	2360 ((11)) (20.1)	8.72 ((11)) (8.0)	0.77 ((10)) (133)	2.24 ((7)) (40)	VS, E, B

σ_c = uniaxial compressive strength, ((= number of specimens)), (= coefficient of variation); E = modulus of deformation; $\dot{\varepsilon}$ = strain rate, μ = microstrain; $\bar{\varepsilon}\rho$ = the ratio of irrecoverable strain to total strain; VS = very strong, S = strong, W = weak, E = elastic, V = viscous, B = brittle, P = plastic.

TABLE 43

Strength classification for rock substance

(after DEERE and MILLER, 1966)

Class	Description	Uniaxial compressive strength MPa
A	Very high strength	> 200
B	High strength	100 200
C	Medium strength	50 100
D	Low strength	25– 50
E	Very low strength	< 25

TABLE 44

Classification of intact rock based upon modulus ratio

(after DEERE and MILLER, 1966)

Class	Description	Modulus ratio
H	High modulus ratio	> 500
M	Medium modulus ratio	200- 500
L	Low modulus ratio	< 200

Note: Modulus ratio is defined as the ratio of the tangent modulus at 50 percent of the ultimate strength of the material to the uniaxial compressive strength.

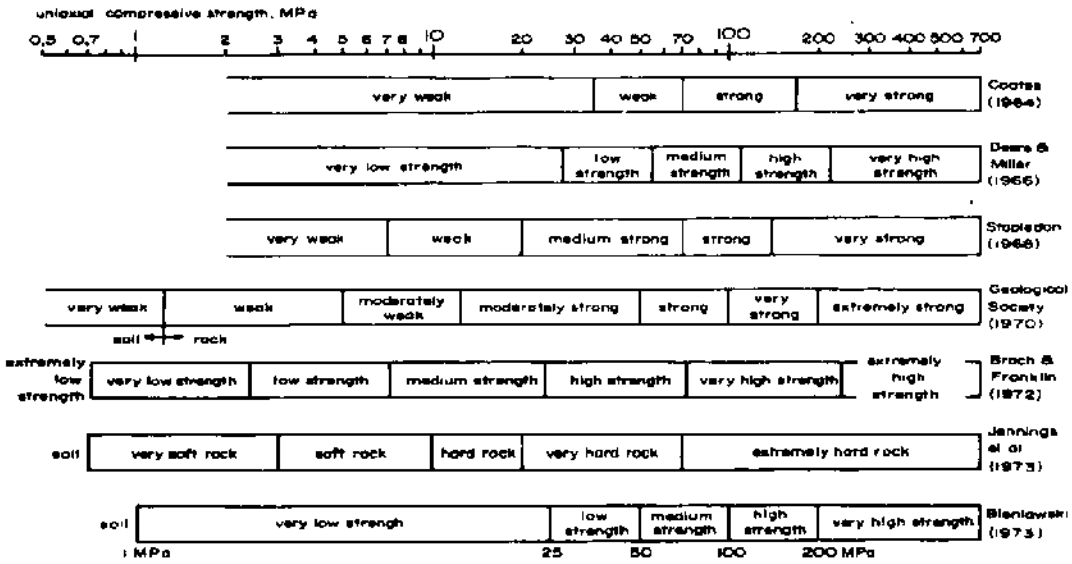

Fig. 11-42. Strength classifications for rock substance.

modulus and the uniaxial compressive strength called as "modulus ratio" has been used and the classification is given in Table 44.

Describing the rock together using both the classifications simultaneously gives a better idea of the rock type. Figs. 11-43 to 11-45 give visual classification plots of different rock types. The uniaxial compressive strength and modulus values are plotted on a log scale. The zones of high (> 500), medium (200 to 500) and low (< 200) modulus ratios are given by diagonal lines. Most of the igneous rocks have medium modulus ratios and so also is true of a majority of sedimentary and metamorphic rocks, though shales tend to have lower modulus and marbles higher modulus ratios.

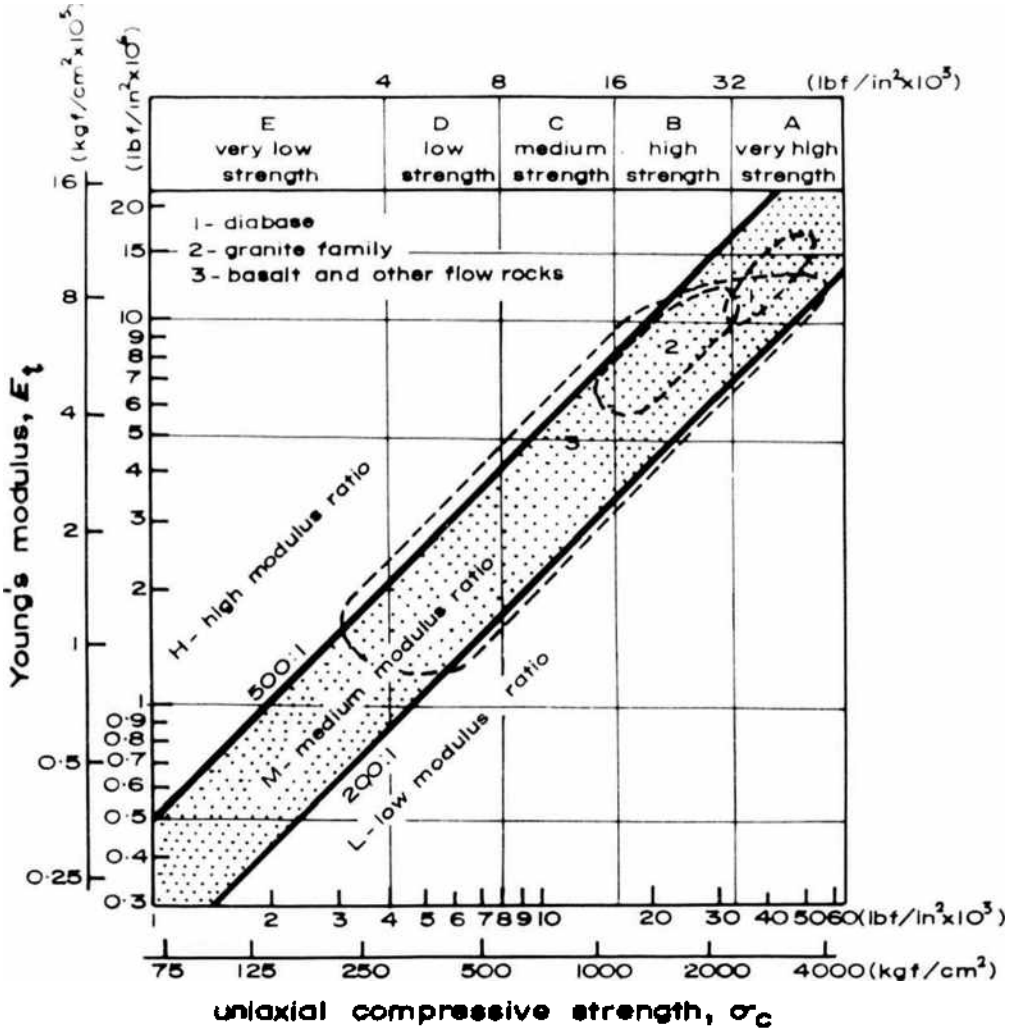

Fig. 11-43. Classification for intact rock substance – summary plot for igneous rocks (176 specimens, 75 % of points)
E_t = tangent modulus at 50 % ultimate strength
Class rock as AM, BH, BL, etc.
(after DEERE and MILLER, 1966).

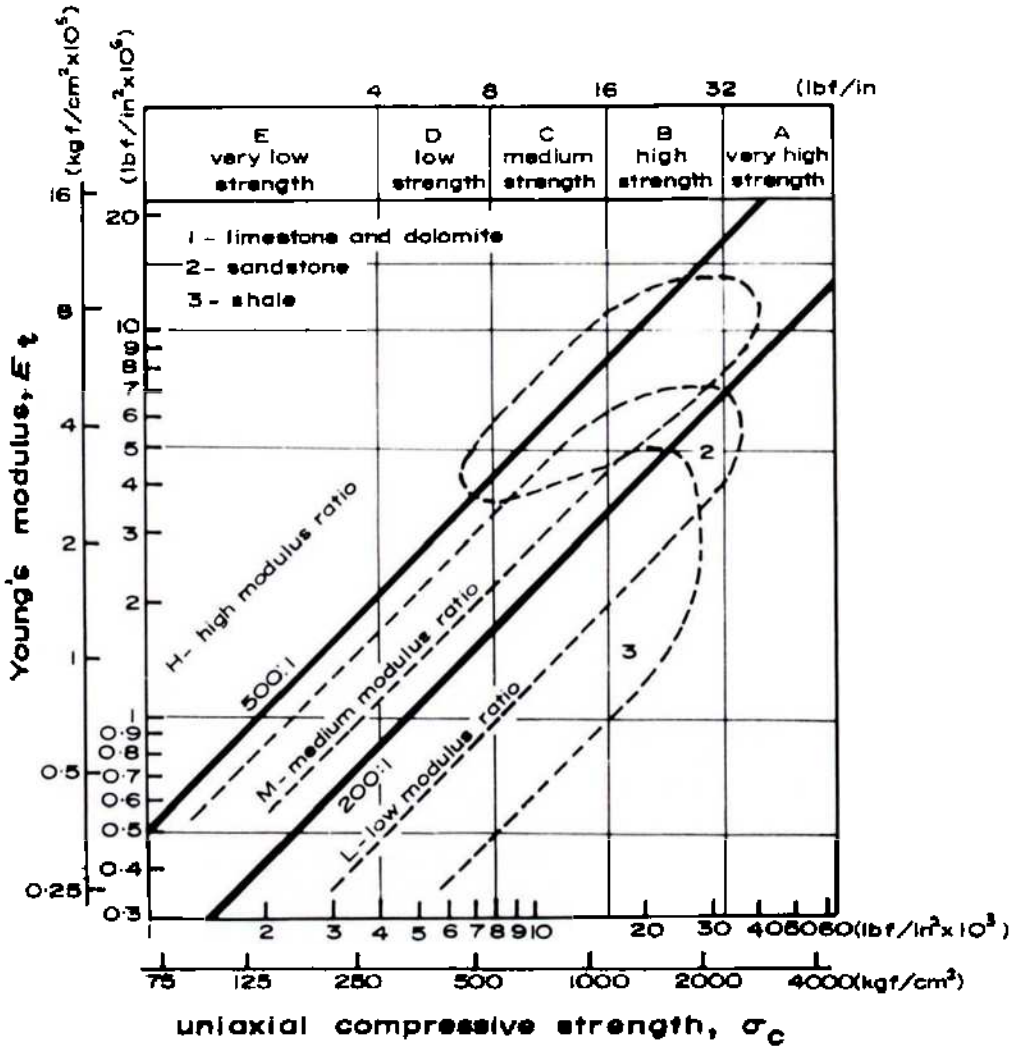

Fig. 11-44. Classification for intact rock substance summary plot for sedimentary rocks (193 specimens, 75% of points)
E_t tangent modulus at 50% ultimate strength
Class rock as AM, BH, BL, etc.
(after DEERE and MILLER, 1966).

Describing rocks using both these indices and designating them such *AM* (very high strength—medium modulus ratio), *CL* (medium strength—low modulus ratio), etc., the anisotropy of the rock substance due to mineralogy or other fabric features is taken into account. Rocks which have interlocking fabric and little or no anisotropy have a lower spread in the above diagrams. Rocks having well developed anisotropy (beddings in sandstones and shales in sedimentary rocks; lineations and foliations in schists) have elongated envelopes. The high modulus ratios of many of the schistose rocks with steep foliations with the horizontal (> 45° with machine platens) is not so much the result of inherently high modulus but rather the case of low strength because of premature failure. At lower angles of foliation (< 45° with machine platens) the closure of cracks which influences the modulus value greatly decreases without appreciably lowering the strength resulting in lower modulus ratios.

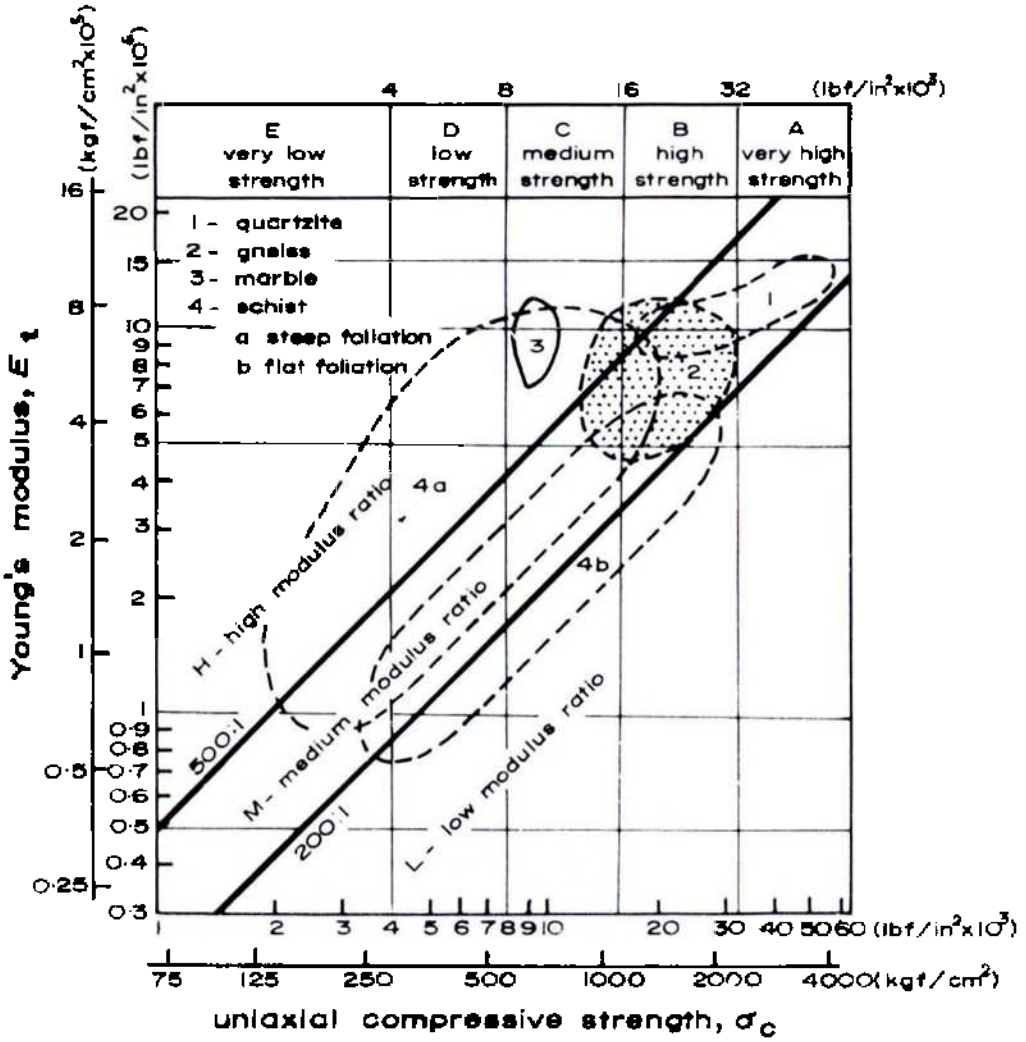

Fig. 11-45. Classification for rock substance summary plot for metamorphic rocks (167 specimens, 75 % of points)
E_t = tangent modulus at 50 % ultimate strength
Class rock as AM, BH, BL, etc.
(after DEERE and MILLER, 1966).

While determining compressive strength of rock, any of the methods described earlier (Chapter 2, Volume I) may be used. From the classification point of view, the point load test has been found to be sufficient. The point load strength index (Chapter 3, Volume I) calculated from the relationship $I_s = \frac{P}{D^2}$

where P is the failure load and D is the distance between the loading platens is related to the compressive strength σ_c by the relationship (BIENIAWSKI, 1975b)

$$\sigma_c = 24\, I_s \tag{11.16}$$

The modulus values can be determined by the techniques described in Chapter 6 (Volume II).

11.9. Classification of Rock In Situ

The first attempt to classify rock in situ was by TERZAGHI (1946) whose approach was descriptive and not defined by measurements. The first classification system based upon measurements taking into account the compressive strength of intact rock, joint spacing and in situ water has been due to the developments by the Salzburg School (JOHN, 1962; MÜLLER, 1963) on the lines set forth by STINI (1922, 1929 and 1951).

Salzburg School Classification

The classification system developed by the Salzburg School takes into consideration the following properties:

(a) Intact rock strength.
(b) Joints, their orientation, spacing, degree of jointing, extent, aperture and coefficients of friction.
(c) Presence or absence of water.
(d) Relative size of the tunnel and the open length* (in tunnelling only).

Figs. 11-46 and 11-47 represent the modified version as now commonly used. Fig. 11-46 represents the influence of the joint frequency and joint continuity (degree of separation) while Fig. 11-47 shows the influence of rock substance and joint spacing on overall strength of the rock mass. The combined effect of all the three factors (a, b, c) is shown in Fig. 11-48 in a very qualitative way. One point that is very clear from this representation is the influence of the joint fabric which becomes more significant as the strength of rock increases.

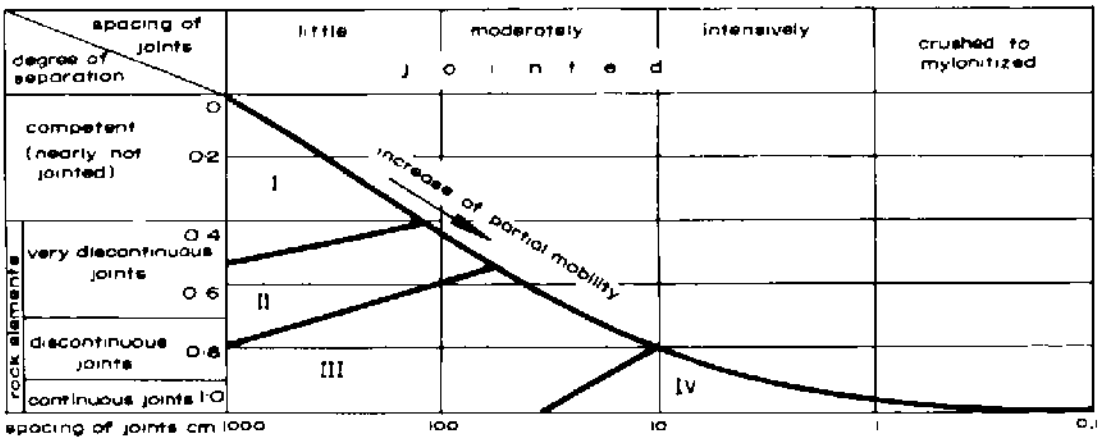

Fig. 11-46. Partial mobility of rock mass in relation to spacing of joints and degree of separation
I Quasimonolith; II Jointed rock; III Cracked rock; IV Shattered rock (after MÜLLER and HOFMANN, 1970).

*) Open length means unsupported length, i.e. distance between the face and the last support unit.

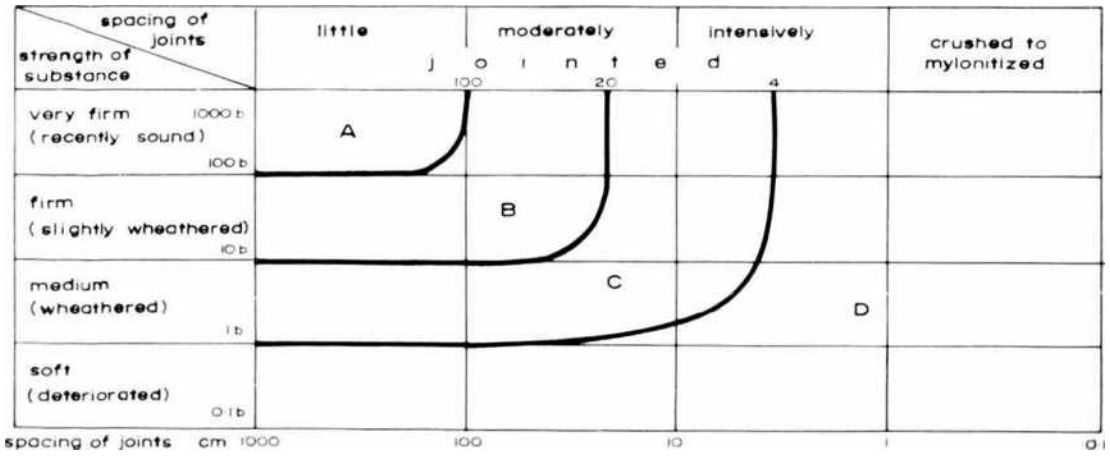

Fig. 11-47. Lines of equal mass strength depending on strength of rock material and spacing of joints
A. Strong rock; B. Medium rock; C. Weak rock; D. Very weak rock
(after MÜLLER and HOFMANN, 1970).

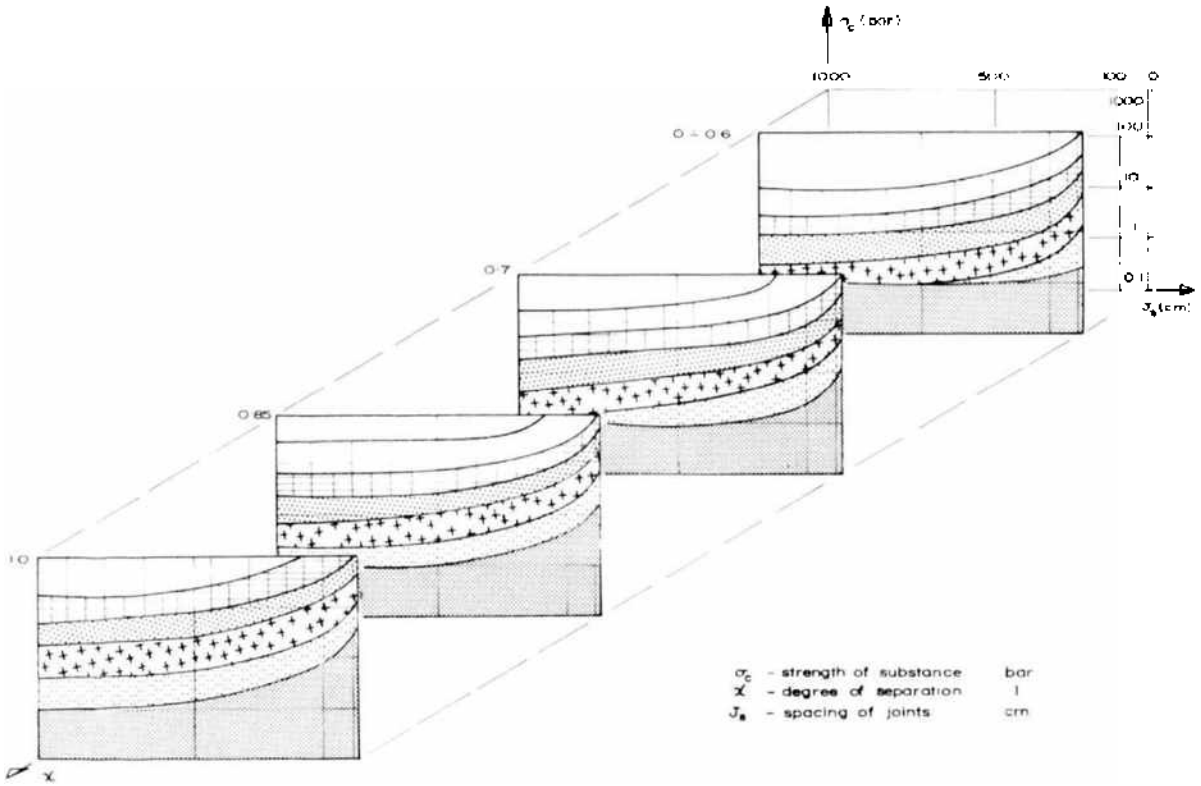

Fig. 11-48. Surfaces of equal strength of rock mass
(after MÜLLER and HOFMANN, 1970).

This classification system has been applied with success in tunnelling, in the determination of the stand-up time and the support calculations, but still it is very much subjective and that is the basic reason that it has not found world-wide acceptance in spite of its extensive and successful use in Central Europe.

Rock Quality Designation (*RQD*)

A method for quantitative description of rock mass and its classification was developed by DEERE (1963, 1968) and has been much applied in North America and other English-speaking countries. The classification index called rock quality designation (*RQD*) is based on analysis of recovered core taking into account the number of fractures and the amount of alteration or softening in the rock mass as observed in rock cores from a borehole. Instead of counting the fractures, the total length of the core pieces of size equal to and longer than 10 cm (4 in) which are hard and sound is measured. An example is given in Fig. 11-49 where the core recovery is calculated to be 83% but using the modified method for calculation of *RQD*, the core recovery is only 57% which gives the equivalent *RQD* for the rock mass.

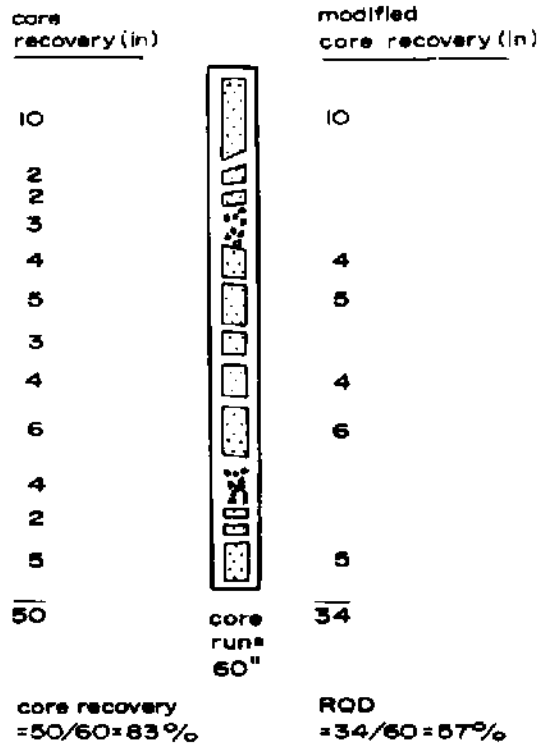

Fig. 11-49. Modified core recovery as an index of rock quality (after DEERE et al, 1966).

The end surfaces of fractured cores obtained can be grouped as follows (COON, 1968):

(1) Fresh, generally regular breaks which can be joined with only a hairline separation.
(2) Rounded surfaces which look like a blunted pencil.
(3) Smooth, apparently fresh surfaces which cannot be rejoined as in (1).
(4) Smooth to somewhat irregular surfaces containing weathering or alteration products, cementing agents and or slickensides.

The type (1) surface is formed during coring and such pieces should be joined together and core parts be considered as one piece. The type (2) might be a geological discontinuity or a break during coring and the rounded surface is invariably due to the rotation of the core barrel and core loss. The other two are definitely the discontinuities and may be neglected in the determination of *RQD*.

A good judgement is necessary in the case of sedimentary rocks and foliated metamorphic rocks to differentiate between fresh and existing fractures and the method is not as exact as in igneous and thick massive bedded deposits. In case of shales it is essential that cores are logged immediately upon removal from the core barrel before degradation due to cracking and slaking begins.

The *RQD* values determined by the above procedure are evaluated by classifying the rocks into categories given in Table 45. A good correlation has been found between *RQD* and fracture frequency, sonic velocity and electrical resistivity while in situ permeability bears no correlation with it (DEERE et al, 1966). Also, there is very little correlation between the frequency of fractures determined by *RQD* and borehole photography, the *RQD* giving higher values. Borehole photography records the orientation of major discontinuities only while *RQD* represents even minor discontinuities.

TABLE 45

Rock quality designation (*RQD*)

(after DEERE et al, 1966)

RQD, %	Rock quality
0 25	very poor
25- 50	poor
50 75	fair
75- 90	good
90–100	excellent

The selection of 10 cm (4 in) length of the core as the unit for reckoning or discarding the core in the determination of the *RQD* has no justification except experience. However, this value has been modified to obtain correlation between *RQD* and some other parameters such as velocity index[1]) (DEERE, MERRITT and COON, 1969) by increasing it to 12.5 cm (5 in) or taking a weighted average of the *RQD* determined by using different core lengths but much success has not been obtained particularly for lower values of *RQD*. A modified correlation by changing the boundaries of the velocity index and *RQD* is given

[1]) Velocity index is defined as the square of the ratio of in situ compressional wave velocity to intact compressional wave velocity.

in Table 46. Similarly, correlation between deformation modulus (static in situ tests by jacking, pressure chamber, cable testing), dynamic modulus, modulus ratio[2]), deformation ratio[3]) and *RQD* is poor because of quick drop in their value for lower *RQD* values (DEERE et al, 1969).

TABLE 46

Engineering classification of *RQD* and velocity index

(after MERRITT, 1968)

RQD	Velocity index	Engineering classification
0– 25	0–0.2	very poor
25 50	0.2 0.4	poor
50 75	0.4–0.6	fair
75– 90	0.6 0.8	good
90 100	0.8–1.0	very good

A correlation between *RQD* and joint volume J_v has been suggested by PALMSTROM (1975) as follows (Fig. 11-50):

$$RQD = 115 - 3.3\, J_v \text{ (approx.)}$$
$$[RQD = 100 \text{ for } J_v < 4.5]$$

This relationship can be used for estimating the *RQD* when core is not available. It may, however, be pointed out that J_v is more sensitive to joint frequency than *RQD*. PRIEST and HUDSON (1976) found good correlation (within 5%) between *RQD* and joint frequency per meter (λ) as follows:

$$RQD = 100\, e^{-0.1\lambda} [0.1\, \lambda + 1] \qquad (11.17)$$

The *RQD* is a measure of joint spacing and other discontinuities and hence compatible with Salzburg School classification and could be a good guide as to the stability of the rock mass in slopes, but has very limited application for underground structures. It does not take into account the rock strength parameters, frictional values, and a host of other factors important in the construction and support of underground excavations though a correlation between *RQD* and support requirements and rate of tunnel construction has been reported (DEERE, MERRITT and COON, 1969).

---

[2]) Modulus ratio is the ratio between the in situ modulus and intact modulus.

[3]) Deformation ratio is the ratio between elastic deformation and total deformation determined from the load-deformation curve.

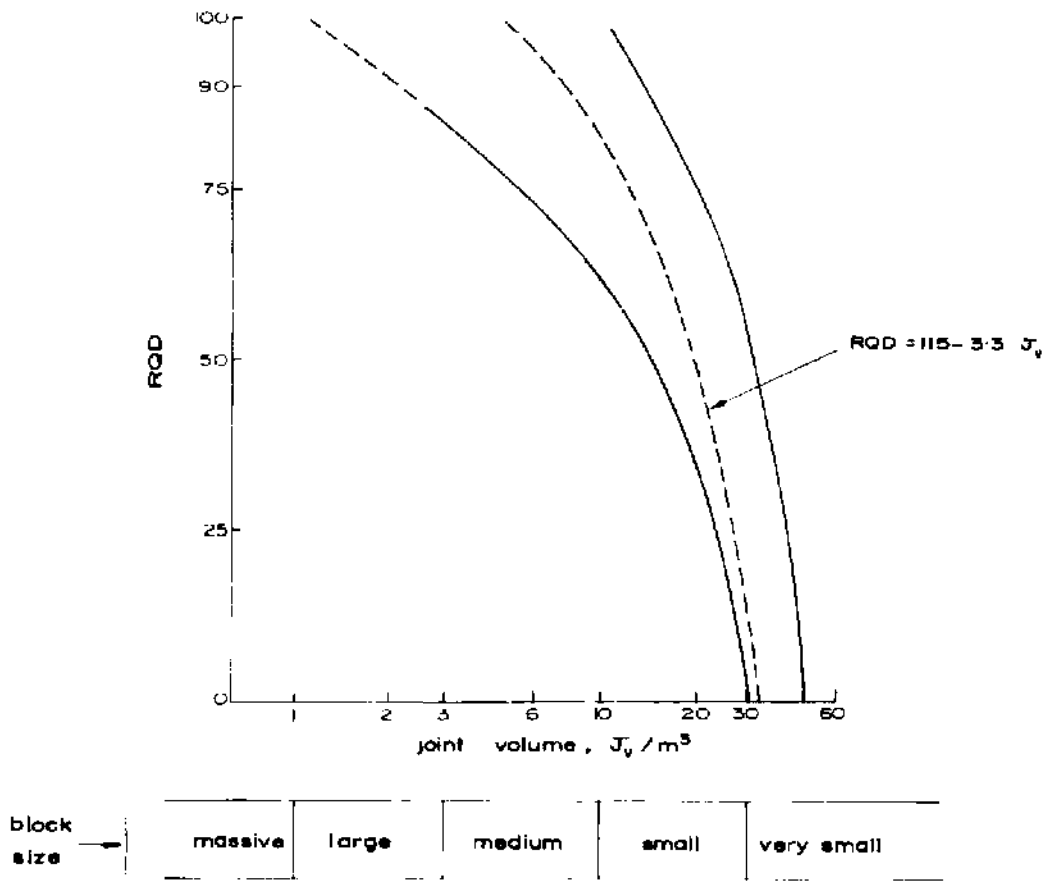

Fig. 11-50. Approximate relationship between RQD and joint volume J_v (block size) (after PALMSTROM, 1975).

11.10. Rock Classification for Underground Excavations

Any comprehensive rock mass classification for underground excavations should be objective and provide easy to determine indices which can be put together to give some common values reliable enough to divide the rock mass into groups of similar engineering behaviour from the point of view of the excavation techniques and support requirements. This is only possible if the classification system incorporates all the variables that enter to influence the structure placed in a rock mass. Three comprehensive classification systems developed independently which are based very heavily on the earlier concepts such as the Salzburg School classification and RQD are given here in detail.

11.10.1. South African Geomechanics Classification

According to this classification system (BIENIAWSKI, 1973 and 1975a) rock mass is divided into a number of regions having similar structural characteristics.

TABLE 47

Geomechanics classification of jointed rock masses

(after BIENIAWSKI, 1975a)

A. Classification parameters and their ratings

1	Strength of intact rock material	Point-load strength index	> 8 MPa	4–8 MPa	2–4 MPa	1–2 MPa	Use of uniaxial compressive test preferred		
		Uniaxial compressive strength	> 200 MPa	100–200 MPa	50–100 MPa	25–50 MPa	10–25 MPa	3–10 MPa	1–3 MPa
	Rating		15	12	7	4	2	1	0
2	Drill core quality *RQD*		90%–100%	75%–90%	50%–75%	25%–50%	< 25%		
	Rating		20	17	13	8	3		
3	Spacing of joints		> 3 m	1–3 m	0.3–1 m	50–300 mm	< 50 mm		
	Rating		30	25	20	10	5		
4	Condition of joints		Very rough surfaces Not continuous No separation Hard joint wall rock	Slightly rough surfaces Separation < 1 mm Hard joint wall rock	Slightly rough surfaces Separation < 1 mm Soft joint wall rock	Slickensided surfaces or Gouge < 5 mm thick or Joints open 1–5 mm Continuous joints	Soft gouge > 5 mm thick or Joints open > 5 mm Continuous joints		
	Rating		25	20	12	6	0		
5	Ground water	Inflow per 10 m tunnel length	none		< 25 litres/min	25–125 litres/min	> 125 litres/min		
		or							
		Ratio: joint water pressure / major principal stress	0		0.0–0.2	0.2–0.5	> 0.5		
		or							
		General conditions	Completely dry		Moist only (interstitial water)	Water under moderate pressure	Severe water problems		
	Rating		10		7	4	0		

TABLE 47 (continued)

B. Adjustment for joint orientations

Strike and dip orientations of joints		Very favourable	Favourable	Fair	Unfavourable	Very unfavourable
Ratings	Tunnels	0	−2	−5	−10	−12
	Foundations	0	−2	−7	−15	−25
	Slopes	0	−5	−25	−50	−60

C. Rock mass classes and their ratings

Class No.	I	II	III	IV	V
Description	Very good rock	Good rock	Fair rock	Poor rock	Very poor rock
Rating	100 − 90	90 − 70	70 − 50	50 − 25	< 25

D. Meaning of rock mass classes

Class No.	I	II	III	IV	V
Average stand-up time	10 years for 5 m span	6 months for 4 m span	1 week for 3 m span	5 hours for 1.5 m span	10 minutes for 0.5 m span
Cohesion of the rock mass	> 300 kPa	200–300 kPa	150–200 kPa	100–150 kPa	< 100 kPa
Friction angle of the rock mass	> 45°	40° − 45°	35° − 40°	30° − 35°	< 30°
Caveability of ore	Very poor	Will not cave readily Large fragments	Fair	Will cave readily Good fragmentation	Very good

e.g. the same rock type, the same joint spacing, etc. The following parameters of the regions are established:

1. Uniaxial compressive strength
2. *RQD*
3. Weathering and alteration character
4. Spacing of joints
5. Joint separation, continuity and filling
6. Ground water
7. Dip and strike of joints.

The rock mass has been classified into 5 classes and the relative indices of the various parameters for these classes are given in Table 47. Since all the parameters are not of equal importance, each parameter is assigned a rating, a weighted numerical value, and a sum total of all the values of the various parameters of the rock define the rock quality such as very good, good, etc.

It shall be clear from Table 47 that though ratings of other parameters are unaltered for tunnels, foundations and slopes, the rating of orientation of joints is of relatively smaller importance in tunnels, but of far higher importance in slopes and foundations (Table 47B). Similarly on longwall faces, the cleavage orientation to guard against fall of coal on the working front and the caveability of roof will be dependent upon orientation of cleavage and joints in the roof with respect to the line of faces and here the rating shall be different and shall be more or less in line with that used for tunnels.

The classification system, however, does not take into account the size of the opening with respect to the joint spacing or other parameters, but has been found to work for openings up to 12 m with success. Its application to support design is given in Table 48. The ratings obtained bear a non-linear relationship with the modulus reduction factor $\left(\frac{E_{\text{rock mass}}}{E_{\text{rock substance}}}\right)$ (Fig. 11-51) and is very much similar to that obtained for *RQD*.

BIENIAWSKI (1973) has used these classes to determine the stand up time in line with the concept put forward by LAUFFER (1958). The ratings determined tend to give lower stand up time than found by actual experience in a few cases where actual failures have been reported, hence, the values are on the conservative side.

TABLE 48

Guide for selection of primary support in horseshoe-shaped tunnels
Width: 5 to 12 m; Vertical stress below 30 MPa; Construction by drilling and blasting

(after BIENIAWSKI, 1975a)

Rock mass class	Excavation	Primary support		
		Rockbolts* (length for tunnel of 10 m width)	Shotcrete	Steel sets
I	Full face 3 m advance	Generally no support required except for occasional spot bolting		
II	Full face 1.0–1.5 m advance	Locally bolts in crown 2–3 m long, spaced 2–2.5 m with occasional wire mesh. Complete 20 m from face.	50 mm in crown as basis for waterproof	None
III	Top heading and bench 1.5–3 m advances in top heading	Systematic bolts 3–4 m long, spaced 1.5–2 m in crown and walls with wire mesh in crown. Complete 10 m from face.	50–100 mm in crown and 30 mm in sides	None
IV	Top heading and bench 1.0–1.5 m advance in top heading	Systematic bolts 4–5 m long, spaced 1–1.5 m in crown and walls with wire mesh. Complete 10 m from face	100–150 mm in crown and 100 mm in sides. Support to be installed as excavation proceeds	Occasional light ribs spaced 1.5 m where required
V	Multiple drifts 0.5–1 m advance in top heading	Systematic bolts 5–6 m long, spaced 1–1.5 m in crown and walls with wire mesh. Bolt invert. Complete 5 m from face	150–200 mm in crown, 150 mm in sides and 50 mm on face. Apply shotcrete as soon as possible after blasting	Heavy ribs spaced 0.75 m with steel lagging. Close invert

* 20 mm diameter, fully resin bonded, length $\frac{1}{2}$ tunnel width

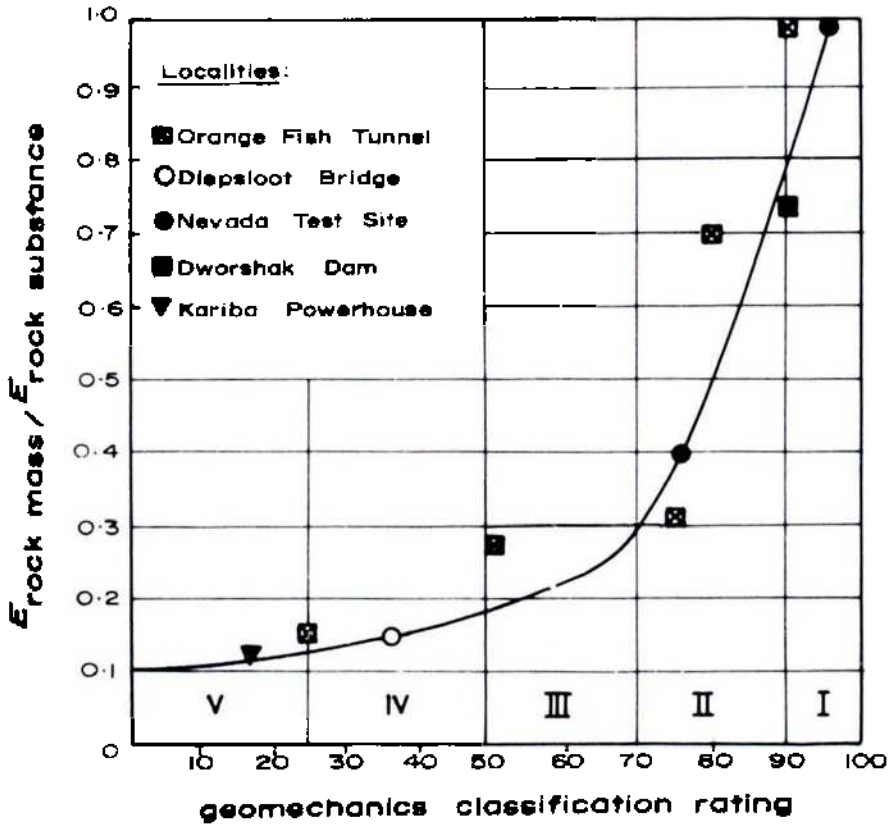

Fig. 11-51. Correlation between geomechanics classification rating and modulus reduction factor
(after BIENIAWSKI, 1975a).

11.10.2. Rock Structure Rating (*RSR*)

The concept of rock structure rating (*RSR*) has been developed by WICKHAM and TIEDEMANN (1972 and 1974) for use in rapid tunnelling and is based upon case history data of 53 tunnel projects with a total length of 200 miles (320 km) in U.S.A. mid-west with diameters ranging from 8 to 36 ft (2.4 to 10.8 m) and practical and empirical applications relating to tunnel construction. The *RSR* concept considers basically the following parameters:
Parameter A – Rock type, folding and discontinuities
Parameter B – Joint pattern (spacing) and orientation
Parameter C – Water inflow and joint openings.

The maximum value assigned to the parameter *A* is 30 which refers to an igneous rock with *RQD* of 75 to 90% or has been appraised by visual inspection as being good. The other values are given in Table 49. Slightly faulted or folded rock refers to the *RQD* of about 50–75; moderately faulted or folded has *RQD* equal to about 25–50 and intensely faulted or folded has *RQD* about less than 25.

TABLE 49

Rock structure rating, parameter *A* (rock type, folding and discontinuities)

(after WICKHAM and TIEDEMANN, 1974)

Basic rock type	Geological structure			
	Massive	Slightly folded or faulted	Moderately folded or faulted	Intensely folded or faulted
Type I	30	22	15	9
Type II	27	20	13	8
Type III	24	18	12	7
Type IV	19	15	10	6

The parameter *B* relates the influence of joint pattern, spacing, strike and dip with respect to the excavation's long axis and direction of drive. The maximum value of this parameter is 45 which corresponds to the excavation axis at right angle to the dip with the drive direction against dip in a massive rock with dip of joints between 50 and 90°. The joint spacings here are divided into 6 classes and the dip into 3 classes. The respective ratings are given in Table 50.

The parameter *C* takes into consideration the overall quality of rock structure indicated by the numerical sum of the parameters *A* and *B*, the water inflow and the conditions of joint surfaces such as tight or cemented, slightly weathered or severely weathered or open. The maximum value of this parameter is 25 for a tight or cemented joint under no water conditions. The flow rate in gallons/minute per 1000 ft of excavation length is divided into 4 classes and the sum of the parameters *A* and *B* into two classes. The various ratings are given in Table 51.

The final *RSR* value for any geological condition is then the sum total of the parameters ($A + B + C$). The value shall range from 25 to 100 which reflect the quality of rock irrespective of the size of the excavation or the method of excavation. The values hold good mostly for excavations driven with blasting. These values can be improved by multiplying by a factor when an excavation is driven by a machine. The multiplication factor can be determined from Fig. 11-52.

WICKHAM and TIEDEMANN (1974) have found good correlation between rock loads on steel ribs used as support in tunnels and *RSR* values. A *RSR* value of 19 meant an extremely heavy support and an *RSR* of 80 or more meant almost no support requirements. It may be mentioned that the relationship is not linear. The system has been successfully employed to evaluate support

TABLE 50

Rock structure rating, Parameter 'B', joint pattern, direction of drive

(after WICKHAM and TIEDEMANN, 1974)

	Average joint spacing	Strike ⊥ to axis					Strike // to axis		
		Direction of drive					Direction of drive		
		Both	With dip		Against dip		Both		
		Dip of prominent joints					Dip of prominent joints		
		Flat	Dipping	Vertical	Dipping	Vertical	Flat	Dipping	Vertical
1	Very closely jointed (< 2 in)	9	11	13	10	12	9	9	7
2	Closely jointed (2 to 6 in)	13	16	19	15	17	14	14	11
3	Moderately jointed (6 in to 1 ft)	23	24	28	19	22	23	23	19
4	Moderate to blocky (1 to 2 ft)	30	32	36	25	28	30	28	24
5	Blocky to massive (2 to 4 ft)	36	38	40	33	35	36	34	28
6	Massive (> 4 ft)	40	43	45	37	40	40	38	34

Notes: Flat 0–20 ; Dipping 20 –50 ; Vertical 50 –90

TABLE 51

Rock structure rating, parameter *C*, ground water, joint condition

(after WICKHAM and TIEDEMANN, 1974)

Anticipated water inflow gallons/min/1000'	Sum of parameters *A* + *B*					
	13–44			45–75		
	Joint condition					
	good*	fair	poor	good	fair	poor
None	22	18	12	25	22	18
Slight (< 200 gpm)	19	15	9	23	19	14
Moderate (200 to 1000 gpm)	15	11	7	21	16	12
Heavy (> 1000 gpm)	10	8	6	18	14	10

*good – tight or cemented
fair – slightly weathered
poor – severely weathered or open

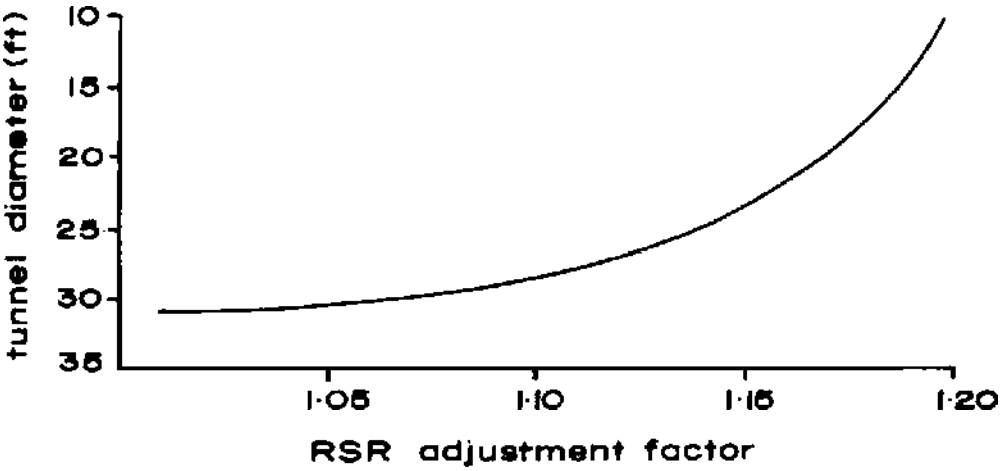

Fig. 11-52. *RSR* adjustment for tunnel boring machine operation (after WICKHAM, TIEDEMANN and SKINNER, 1972).

requirements of steel ribs, shotcrete and roof bolts both in tunnelling and mining projects and in determining rock loads on support system. The correlation between the *RSR* values and actual ground support is obtained by the use of a "rib-ratio" (*RR*) which gives a relationship between steel rib support used in tunnel and theoretical rib support determined from a common datum condition. Rib ratio (*RR*) is determined using TERZAGHI empirical formula (TERZAGHI, 1946) for maximum roof load for loose, cohesionless sand below water table. For a tunnel with a semicircular arch

$$P_1 = [1.38(B+H)] \times B \times \gamma_t \qquad (11.18a)$$

For a circular tunnel or where height = width = diameter

$$P_1 = 2.76\, B^2 \gamma_1 \tag{11.18b}$$

where P_1 = vertical load on rib, lb/linear foot
B = tunnel width or diameter (for circular tunnel), ft
H = height of the tunnel, ft
γ_1 = unit weight of sand (120 lb/ft^3)

Theoretical spacing S_d in feet is then given by

$$S_d = \frac{P_r}{P_1} \tag{11.19}$$

where P_r = chart value of allowable load in lb per foot of tunnel width (Table 52).

Rib ratio is expressed as the ratio of the spacing for datum condition and actual rib spacing used for tunnel and is given by

$$RR = \frac{S_d}{S_a} \times 100$$

where S_a = actual spacing (ft) of ribs used in sample tunnel.

The RSR and RR were found to have a relationship

$$(RR + 80)\,(RSR + 30) = 8800 \tag{11.20}$$

and is derived from the average curve obtained from the different case studies (Fig. 11-53) and some typical values of RR for different RSR values are given in Table 53. The unit rock load Wr in kips/ft^2 is given by (assuming weight of wet sand = 120 lb/ft^3)

$$Wr = \frac{D}{302}\left[\left(\frac{8800}{RSR + 30}\right) - 80\right] \tag{11.21}$$

where D = diameter of tunnel, ft.

For a general case

$$Wr = \left[\left(\frac{8800}{RSR + 30}\right) - 80\right] \times \frac{P_r}{S_d} \times 10^{-5}$$

Thus, for example, if the RSR value is 40 and the tunnel diameter is 20 ft, then the anticipated rock load (Eq. 11.21) that shall have to be supported will be 3 kips.

TABLE 52

Continuous ribs. Capacity in lb/ft of tunnel width Minimum fibre stress – 24000 lb/in²

(after PROCTOR and WHITE, 1946)

Beam		Width of tunnel to outside design concrete line															
		14'–0"	16'–0"	18'–0"	20'–0"	22'–0"	24'–0"	26'–0"	28'–0"	30'–0"	32'–0"	34'–0"	36'–0"	38'–0"	40'–0"	42'–0"	44'–0"
Nominal Depth, Flange Width and Type	Wt. per foot	40"	42"	44"	46"	48"	50"	52"	54"	56"	58"	60"	62"	64"	66"	68"	70"
		Maximum Blocking Point Spacing															
4" I	7.7	2750	2470														
4" × 4" H	13.0	4780	4310	3910	3570												
5" I	10.0	4030	3620	3280	2990												
5" × 5" Stanchion	16.0	6920	6220	5630	5130												
5" × 5" H	18.9	7860	7060	6390	5820												
6" I	12.5	5590	5030	4540	4130	3790											
6" I	17.25	7100	6380	5770	5260	4830	4450										
6" × 4" Light beam	12.0	5510	4940	4460	4060	3730											
6" × 4" Light beam	16.0	7540	6760	6110	5510	5100	4710										
6" × 6" Stanchion	15.5	7450	6670	6030	5490	5030	4650										
6" × 6" H	20.0	9550	8560	7740	7050	6460	5960	5530	5140								
6" × 6" H	25.0	11800	10570	9570	8710	7980	7360	6830	6350	5930							
7" I	15.3			5990	5450	4990	4610										
8" I	18.4			7640	6950	6370	5880										
8" I	23.0			9100	8290	7600	7010	6500	6040	5640	5280	4960	4670				
8" × 4" Light beam	15.0			6320	5750	5270	4860										
8" × 8" H	34.3			14950	13610	12460	11500	10670	9920	9250	8670	8150	7680	7270	6880	6530	6210
8" × 5¼" W.F.	17.0			7310	6680	6120	5650	5240									
8" × 5¼" W.F.	20.0			8730	7950	7250	6710	6230	5780	5400							
8" × 6½" W.F.	24.0			10600	9650	8830	8150	7560	7020	6560	6150	5770	5440	5150	4880		
8" × 6½" W.F.	28.0			12450	11260	10310	9520	8830	8200	7650	7170	6740	6360	6020	5700		
8" × 8" W.F.	31.0			13820	12590	11530	10640	9860	9160	8560	8020	7530	7100	6720	6360	6040	5750
8" × 8" W.F.	35.0			15640	14250	13110	12040	11160	10370	9690	9070	8530	8040	7600	7200	6830	6500
8" × 8" W.F.	40.0			17870	16270	14890	13750	12740	11840	11050	10360	9740	9180	8680	8220	7800	7420
8" × 8" W.F.	48.0				19640	17990	16600	15390	14290	13360	12510	11760	11090	10390	9840	9340	8890
8" × 8" W.F.	58.0					21700	20030	18560	17240	16110	15110	14210	13400	12660	12000	11390	10830
8" × 8" W.F.	67.0					25100	23190	21500	19970	18650	17470	16420	15480	14650	13880	13160	12540
10" I	25.4					9610	8860	8210	7630	7130	6680	6280	5920	5600	5340	3040	4800
10" I	35.0					12520	11540	10740	9940	9290	8700	8170	7710	7290	6900	6550	6230
10" × 5-3/4" W.F.	21.0					8220	7580	7020	6520	6090	5710	5370	5060	4790	4530	4310	4100
10" × 5-3/4" W.F.	25.0					9870	9120	8450	7860	7340	6880	6470	6100	5790	5490	5210	4960
10" × 8" W.F.	33.0					13130	12080	11210	10430	9740	9130	8580	8090	7650	7250	6890	6560
10" × 8" W.F.	39.0					15630	14420	13360	12410	11590	10870	10210	9640	9120	8640	8210	7810
10" × 8" W.F.	45.0					18100	16680	15450	14370	13420	12580	11830	11160	10550	10000	9500	9040
10" × 10" W.F.	49.0						18290	16970	15770	14730	13820	12990	12250	11580	10980	10430	9930
10" × 10" W.F.	54.0						20200	18750	17410	16270	15260	14340	13530	12790	12130	11520	10960
10" × 10" W.F.	66.0						24950	22900	21280	19870	18630	17520	16520	15620	14810	14070	13390
12" × 8" W.F.	45.0									14170	13280	12490	11790	11150	10570	10050	9560
12" × 10" W.F.	53.0									16870	15820	14880	14040	13280	12600	11960	11400
12" × 12" W.F.	65.0									20780	19500	18330	17290	16370	15530	14750	14050

Values shown are for stress of 24 Kips
For 27 Kips divide by 0.889

TABLE 53

RSR values and rib ratios

(after WICKHAM and TIEDEMANN, 1974)

RSR	27	30	35	40	45	50	55	60	65	70	77
RR	74	67	55	46	37	30	24	18	13	8	2

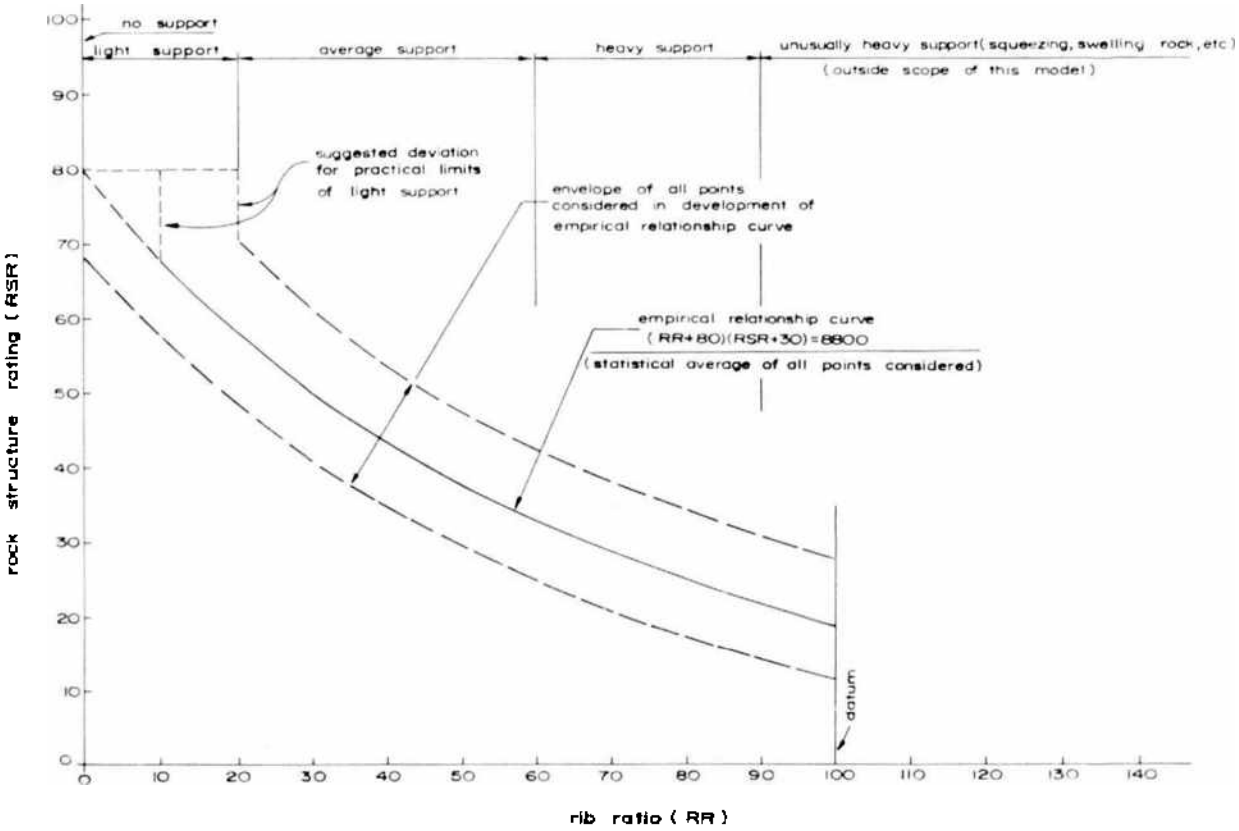

Fig. 11-53. Correlation of RSR and RR (after WICKHAM and TIEDEMANN, 1974).

It shall be pointed out that since most of the case history data pertain to steel rib support, the correlation primarily relates to steel support. However, when rock bolts and shotcrete are used, the following relationships have been suggested.

Rock bolting:

$$\text{Spacing, in ft, } S = \sqrt{\frac{Bs}{Wr}} \tag{11.22}$$

where Bs = allowable tensile load of the bolt, kips

Wr = rock load determined from RSR considerations, kips/ft^2

Shotcrete:

$$\text{Nominal thickness, in inches, } t = 1 + \frac{Wr}{1.25} \tag{11.23}$$

The rock bolt relationship, however, gives conservative figures.

It shall be borne in mind that all these calculations give results under normal conditions and do not take care of certain special conditions such as swelling ground or squeezing ground and take no cognisance of high ground stresses.

11.10.3. Rock Mass Quality

Rock mass quality (Q) has been developed by BARTON, LIEN and LUNDE (1974a, b) basically considering the tunnels and large underground chambers under a variety of rock conditions and support systems. The case records on which Q is based included 13 igneous, 24 metamorphic and 9 sedimentary rock types. A large number of case records (more than 80) included clay mineral joint fillings of different kinds including swelling clays while most of the joints were unfilled and unweathered or slightly weathered. The system takes into consideration six parameters to determine the rock mass quality, namely,

Rock quality designation RQD (after DEERE, 1968)
Joint set number J_n
Joint roughness number J_r
Joint alteration number J_a
Joint water reduction factor – J_w
Stress reduction factor – SRF

The rock mass quality Q is calculated from the relationship

$$Q = \left(\frac{RQD}{J_n}\right) \times \left(\frac{J_r}{J_a}\right) \times \left(\frac{J_w}{SRF}\right) \tag{11.24}$$

The first term in the above equation (RQD/J_n) refers to the overall structure of the rock mass and in a crude way represents the size of the block with extreme values of 200 and 0.5. The second term represents roughness and degree of alteration of joint wall and fillings and is a rough measure of interblock shear strength. The $\tan^{-1}(J_r/J_a)$ approximately gives the shear strength of the joints. The third term refers to two stress parameters and is a complicated empirical factor describing active stresses.

The numerical ratings of the various parameters are given in Tables 54 to 56.

TABLE 54

Descriptions and ratings for the parameters RQD, J_n and J_r

(after BARTON, LIEN and LUNDE, 1974a)

1.	**Rock quality designation**	(RQD)	
A.	Very poor	0 - 25	Note:
B.	Poor	25 - 50	(i) Where RQD is reported or measured as ≤ 10 (including 0) a nominal value of 10 is used to evaluate Q in Eq. (11.24)
C.	Fair	50 - 75	
D.	Good	75 - 90	
E.	Excellent	90 - 100	(ii) RQD intervals of 5, i.e. 100, 95, 90 etc. are sufficiently accurate
2.	**Joint set number**	(J_n)	
A.	Massive, no or few joints	0.5 - 1.0	
B.	One joint set	2	
C.	One joint set plus random	3	
D.	Two joint sets	4	
E.	Two joint sets plus random	6	
F.	Three joint sets	9	
G.	Three joint sets plus random	12	Note:
H.	Four or more joint sets, random, heavily jointed, "sugarcube", etc.	15	(i) For intersections use ($3.0 \times J_n$)
J.	Crushed rock, earthlike	20	(ii) For portals use ($2.0 \times J_n$)
3.	**Joint roughness number**	(J_r)	
	(a) Rock wall contact and (b) Rock wall contact before 10 cms shear		
A.	Discontinuous joints	4	Note:
B.	Rough or irregular, undulating	3	(i) Add 1.0 if the mean spacing of the relevant joint set is greater than 3 m
C.	Smooth, undulating	2	
D.	Slickensided, undulating	1.5	
E.	Rough or irregular, planar	1.5	
F.	Smooth, planar	1.0	(ii) $J_r = 0.5$ can be used for planar slickensided joints having lineations, provided the lineations are favourably orientated
G.	Slickensided, planar	0.5	
	(c) No rock wall contact when sheared		
H.	Zone containing clay minerals thick enough to prevent rock wall contact	1.0 (nominal)	
J.	Sandy, gravelly or crushed zone thick enough to prevent rock wall contact	1.0 (nominal)	

TABLE 55 ▶

Descriptions and ratings for the parameters J_a and J_w

(after BARTON, LIEN and LUNDE, 1974a)

4.	**Joint alteration number**	(J_a)	(Φ_r)	Note:
	(a) Rock wall contact		(approx.)	(i) Values of Φ_r
A.	Tightly healed, hard, non-softening, impermeable filling i.e. quartz or epidote	0.75	( )	are intended as an approximate guide to the mineralogical properties of the alteration products, if present
B.	Unaltered joint walls, surface staining only	1.0	(25 35)	
C.	Slightly altered joint walls. Non-softening mineral coatings, sandy particles, clay-free disintegrated rock etc.	2.0	(25 35)	
D.	Silty-, or sandy-clay coatings, small clay-fraction (non-softening)	3.0	(20 25)	
E.	Softening or low friction clay mineral coatings, i.e. kaolinite, mica. Also chlorite, talc, gypsum and graphite etc., and small quantities of swelling clays. (Discontinuous coatings, 1 2 mm or less in thickness)	4.0	(8 16)	
	(b) Rock wall contact before 10 cms shear			
F.	Sandy particles, clay-free disintegrated rock etc.	4.0	(25 30)	
G.	Strongly over-consolidated, non-softening clay mineral fillings (Continuous, < 5 mm in thickness)	6.0	(16 24)	
H.	Medium or low over-consolidation, softening, clay mineral fillings. (Continuous, < 5 mm in thickness)	8.0	(12 16)	
J.	Swelling clay fillings, i.e. montmorillonite (Continuous, < 5 mm in thickness). Value of J_a depends on percent of swelling clay-size particles, and acces to water etc.	8.0 12.0	(6 12)	
	(c) No rock wall contact when sheared			
K, L.	Zones or bands of disintegrated			
M.	or crushed rock and clay (see G, H, J for description of clay condition)	6.0, 8.0 or 8.0 12.0	(6 24)	
N.	Zones or bands of silty- or sandy clay, small clay fraction (non-softening)	5.0		
O, P.	Thick, continuous zones or	10.0, 13.0	(6 24)	
R.	bands of clay (see G, H, J for description of clay condition)	or 13.0-20.0		

TABLE 55 (continued)

5. **Joint water reduction factor**	(J_w)	Approx. water pressure (kg/cm^2)	
A. Dry excavations or minor inflow, i.e. < 5 l/min. locally	1.0	< 1	Note: (i) Factors C to F are crude estimates. Increase J_w if drainage measures are installed (ii) Special problems caused by ice formation are not considered
B. Medium inflow or pressure occasional outwash of joint fillings	0.66	1.0–2.5	
C. Large inflow or high pressure in competent rock with unfilled joints	0.5	2.5–10.0	
D. Large inflow or high pressure, considerable outwash of joint fillings	0.33	2.5–10.0	
E. Exceptionally high inflow or water pressure at blasting, decaying with time	0.2–0.1	> 10.0	
F. Exceptionally high inflow or water pressure continuing without noticeable decay	0.1–0.05	> 10.0	

TABLE 56

Descriptions and ratings for the parameter *SRF*

(after BARTON, LIEN and LUNDE, 1974a)

6. **Stress reduction factor**	(*SRF*)	
(a) Weakness zones intersecting excavation, which may cause loosening of rock mass when tunnel is excavated		Note: (i) Reduce these values of *SRF* by 25–50% if the relevant shear zones only influence but do not intersect the excavation
A. Multiple occurrences of weakness zones containing clay or chemically disintegrated rock, very loose surrounding rock (any depth)	10.0	
B. Single weakness zones containing clay, or chemically disintegrated rock (depth of excavation ≦ 50 m)	5.0	
C. Single weakness zones containing clay, or chemically disintegrated rock (depth of excavation > 50 m)	2.5	
D. Multiple shear zones in competent rock (clay free), loose surrounding rock (any depth)	7.5	

TABLE 56 (continued)

E.	Single shear zones in competent rock (clay free) (depth of excavation $\leqq$ 50 m)		5.0	
F.	Single shear zones in competent rock (clay free) (depth of excavation > 50 m)		2.5	
G.	Loose open joints, heavily jointed or "sugar cube" etc. (any depth)		5.0	
	(b) Competent rock, rock stress problems	σ_c/σ_1	σ_t/σ_1	
H.	Low stress, near surface	> 200	> 13	2.5
J.	Medium stress	200 10	13 0.66	1.0
K.	High stress, very tight structure (Usually favourable to stability, may be unfavourable to wall stability)	10 5	0.66 0.33	0.5 2.0
L.	Mild rock burst (massive rock)	5–2.5	0.33 0.16	5 10
M.	Heavy rock burst (massive rock)	< 2.5	< 0.16	10 20
	(c) Squeezing rock; plastic flow of incompetent rock under the influence of high rock pressures			
N.	Mild squeezing rock pressure			5 10
O.	Heavy squeezing rock pressure			10 20
	(d) Swelling rock: chemical swelling activity depending on presence of water			
P.	Mild swelling rock pressure			5 10
R.	Heavy swelling rock pressure			10 15

(ii) For strongly anisotropic stress field (if measured): when $5 \leqslant \sigma_1/\sigma_3 \leqq 10$, reduce σ_c and σ_t to 0.8 σ_c and 0.8 σ_t; when $\sigma_1/\sigma_3 > 10$, reduce σ_c and σ_t to 0.6 σ_c and 0.6 σ_t where: σ_c = unconfined compression strength, σ_t = tensile strength (point load), σ_1 and σ_3 = major and minor principal stresses

(iii) Few case records available where depth of crown below surface is less than span width. Suggest *SRF* increase from 2.5 to 5 for such cases (see *H*)

In the use of the tables for estimating rock mass quality Q, the following points should be kept in view:

1. When bore core is unavailable, *RQD* can be estimated from the number of joints per unit volume, in which the number of joints per metre for each joint set are added. A simple relation can be used to convert this number to *RQD* for the case of clay-free rock masses.

$$RQD = 115 - 3.3\, J_v \text{ (approx.)} \tag{11.25}$$

where J_v = total number of joints per m^3

($RQD = 100$ for $J_v < 4.5$)

2. The parameter J_n representing the number of joint sets will often be affected by foliation, schistosity, slatey cleavage or bedding, etc. If strongly developed these parallel "joints" should obviously be counted as a complete joint set. However, if there are few "joints" visible, or only occasional breaks in bore core due to these features, then it will be more appropriate to count them as "random joints" when evaluating J_n in Table 54.

3. The parameters J_r and J_a should be relevant to the weakest significant joint set or clay filled discontinuity in a given zone. However, if the joint set or discontinuity with the minimum value of (J_r/J_a) is favourably oriented for stability, then a second, less favourably oriented joint set or discontinuity may sometimes be of more significance, and its higher value of (J_r/J_a) should be used when evaluating Q.

4. When a rock mass contains clay, the factor *SRF* appropriate to loosening loads should be evaluated (Table 56; 6a). In such cases the strength of the intact rock is of little interest. However, when jointing is minimal and clay is completely absent, the strength of the intact rock may become the weakest link, and the stability will then depend on the ratio (rock stress/rock strength) (Table 56, 6b). A strongly anisotropic stress field is unfavourable to stability and is roughly accounted for as in Note (ii), Table 56.

5. In general the compressive and tensile strengths (σ_c and σ_t) of the intact rock should be evaluated in the direction that is unfavourable for stability. This is especially important in the case of strongly anisotropic rocks. In addition, the test specimens should be saturated if this condition is appropriate to present or future in situ conditions. A very conservative estimate of strength should be made for those rocks that deteriorate when exposed to moist or saturated conditions.

When the rock mass quality varies markedly from place to place it is desirable to map and classify these zones separately. The system does not take into account special features such as swelling and softening clay zones or large unstable wedges which require individual treatment.

Empirical relationships between rock mass quality Q and roof and wall support pressures have been determined and are given as follows:

For a medium with two sets of joints

$$Wr = \frac{2.0}{J_r} Q^{0.33} \tag{11.26}$$

For a medium with three sets of joints

$$Wr = \frac{2 J_n^{0.5} Q^{0.33}}{3 J_r} \tag{11.27}$$

where Wr = support pressure in roof or walls, kgf/cm^2.

The relationship (11.26) is represented in Fig. 11-54 with different values of J_r. The shaded portion is the estimate of the expected range in practice from case records.

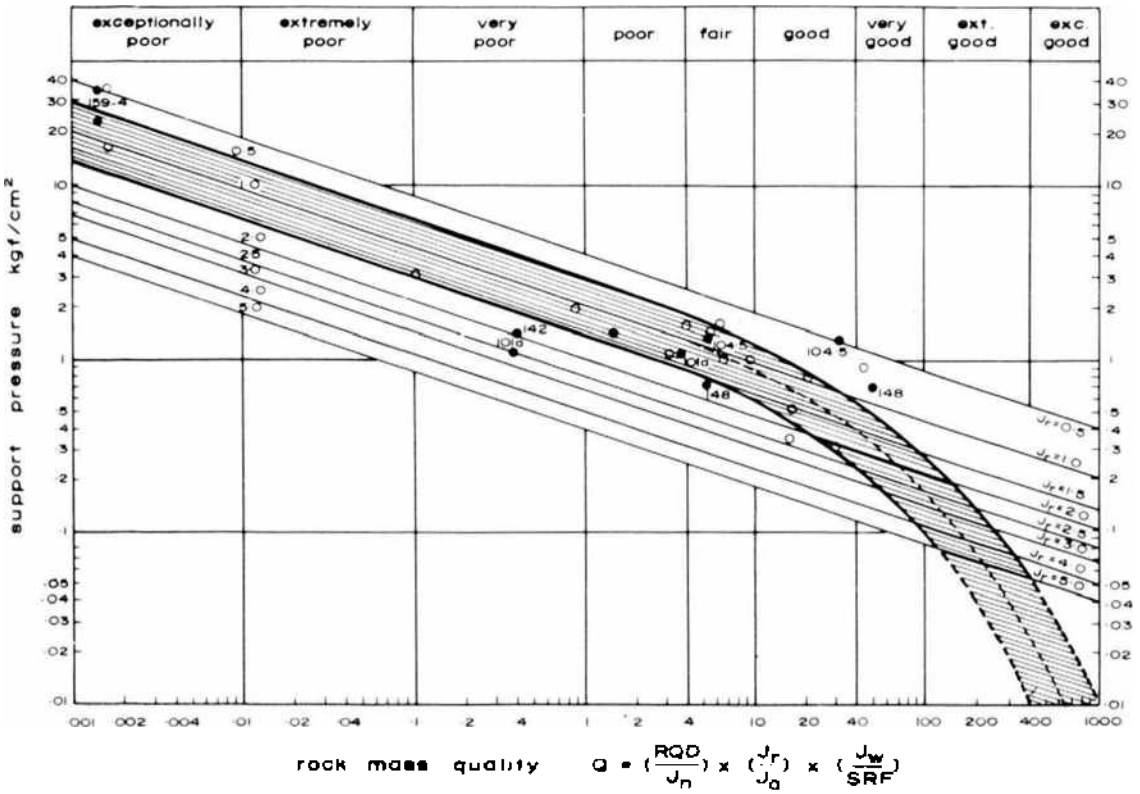

Fig. 11-54. Empirical method for estimating the support pressure. Plotted points refer to case records describing measured or designed roof support pressures (after BARTON, LIEN and LUNDE, 1974a).

While calculating rock pressure, the higher value of Q than obtained shall be used. The modified value may be 5 Q for the Q value > 10 (good rocks), 2.5 Q for $0.1 < Q < 10$ (intermediate rocks) and 1.0 Q for $Q < 0.1$ (poor rocks).

The rock mass quality system has been found to be very useful particularly for predicting the self supporting excavations and support requirements using shotcrete and bolting.

11.11. Summary

While classifying rock masses from an engineering point of view, the origin of the rocks and their geological history are very important aspects and should not be overlooked. An immense amount of information about the possible shape of structural defects, the influence of weathering and even possibly the nature of stress field can be obtained from the general geology of the region.

The surveying of joints from the bore holes and outcrops is an important aspect of any engineering geological study and precautions should be taken in their interpretation. It is not always true that the joint set having a larger frequency is also more dominant. It shall depend upon the type of structure—slope or a tunnel—and proper appreciation is essential.

The rock classification systems described are based upon empirical interpretation of the successful case histories and hence tend to perpetuate the conservatism and overdesigning of the support system. Their comparison with actual failure cases shall be the most important step forward. Nevertheless, these help in arriving at quick decisions.

The South African geomechanics classification is more universal than the other two and shall be preferred in the study of rock slopes. The *RSR* classification shall be better used with steel rib support in medium strength rocks while the Rock Mass Quality classification shall be more appropriate for hard highly jointed rocks. All classifications give conservative results for softer rocks.

References to Chapter 11

1. Badgley, P.C.: Structural and Tectonic Principles. New York, Harper & Row, 1965, 521 p.
2. Barton, C.M.: An analysis of rock structure and fabric in the C.S.A. mine, Cobar, N.S.W., C.S.I.R.O., Australia, Div. Appl. Geomech., Tech. Paper, 1975a.
3. Barton, C.M.: Geomechanics of high rise filled stopes: Rock fabric quantification in relation to engineering design at C.S.A. mine, Cobar, C.S.I.R.O., Australia, Div. Appl. Geomech., AMIRA Project Report 4, 1975b.
4. Barton, N., Lien, R. and Lunde, J.: Engineering classification of rock masses for the design of tunnel support. Rock Mech., Vol. 6, No. 4, Dec., 1974a, pp. 189–236.
5. Barton, N., Lien, R. and Lunde, J.: Analysis of rock mass quality and support practice in tunnelling, and a guide for estimating support requirements. Norwegian Geotech. Inst., Int. Rep. 54206, 1974b, 74 p.
6. Bieniawski, Z.T.: Engineering classification of jointed rock masses. Trans. S. African Instn. Civ. Engrs., Vol. 15, No. 12, Dec., 1973, pp. 335–344.
7. Bieniawski, Z.T.: Case studies: Prediction of rock mass behaviour by the geomechanics classification. Proc. 2nd Aust.-N.Z. Conf. Geomech., Brisbane, 1975a, pp. 36–41.
8. Bieniawski, Z.T.: The point-load test in geotechnical practice. Eng. Geol., Vol. 9, 1975b, pp. 1–11.
9. Biot, M.A.: Theory of viscous buckling of multilayered fluids undergoing finite strain. Phys. of Fluids, Vol. 7, 1964, pp. 855–859.
10. Biot, M.A.: Theory of viscous buckling and gravity instability of multilayers with large deformation. Geol. Soc. Am. Bull., Vol. 76, 1965, pp. 371–378.
11. Biot, M.A., Ode, H. and Roever, W.L.: Experimental verification of the folding of stratified viscoelastic media. Geol. Soc. Am. Bull., Vol. 72, 1961, pp. 1621–1630.
12. Bogdanov, A.A.: The intensity of cleavage as related to the thickness of the bed (In Russian). Sov. Geol., Vol. 16, 1947.
13. Brace, W.F.: Orientation of anisotropic minerals in a stress field: Discussion. Geol. Soc. Am. Mem. 79, 1960, pp. 9–20.
14. Breddin, H.: Die tektonische Deformation der Fossilien im Rheinischen Schiefergebirge. Deut. Geol. Ges. Z., Vol. 196, 1956a, pp. 227–305.
15. Breddin, H.: Die tektonische Gesteinsdeformation im Karbongürtel Westdeutschlands und Südlimburgs. Deut. Geol. Ges. Z., Vol. 107, 1956b, pp. 232–260.
16. Breddin, H.: Tektonische Fossil- und Gesteinsdeformation im Gebiet von St. Goarhausen. Decheniana, Vol. 110, 1957, pp. 289–350.
17. Broch, E. and Franklin, J.A.: The point-load strength test. Int. J. Rock Mech. Min. Sci., Vol. 9, 1972, pp. 669–697.
18. Cailleux, A.: La disposition individuelle des galets dans les formations détritiques. Rev. Geograph. Phys. Geol. Dynamique, Vol. 11, 1938, pp. 171–198.
19. Chapman, C.A. and Rioux, R.L.: Statistical study of topography, sheeting and jointing in granite, Acadia National Park, Maine. Am. J. Sci., Vol. 256, 1958, pp. 111–127.
20. Clarke, F.W.: The data of geochemistry. U.S. Geol. Survey Bull. 770, 1924.

21. CLOOS, E.: Boudinage. Trans. Am. Geophys. Union, Vol. 28, 1947, pp. 626–632.
22. CLOOS, E.: Experimental analysis of fracture patterns. Geol. Soc. Am. Bull., Vol. 66, 1955, pp. 241–256.
23. CLOOS, H.: Einführung in die Geologie. Berlin, Borntraeger, 1936, pp. 258–272.
24. COATES, D.F.: Classification of rocks for rock mechanics. Int. J. Rock Mech. Min. Sci., Vol. 1, No. 3, May, 1964, pp. 421–429.
25. COATES, D.F. and PARSONS, R.C.: Experimental criteria for classification of rock substances. Int. J. Rock Mech. Min. Sci., Vol. 3, No. 3, July, 1966, pp. 181–189.
26. COON, R.F.: Correlation of engineering behaviour with the classification of in situ rock. Ph. D. Thesis, Univ. Illinois, Urbana, 1968, 236 p.
27. CURRIE, J.B., PATNODE, H.W. and TRUMP, R.P.: Development of folds in sedimentary strata. Geol. Soc. Am. Bull., Vol. 73, No. 6, June, 1962, pp. 655–673.
28. DASILVEIRA, A.F., RODRIGUES, F.P., GROSSMANN, N.F. and MENDES, F. DE M.: Quantitative characterisation of the geometric parameters of jointing in rock masses. Proc. 1st Cong. Int. Soc. Rock Mech., Lisbon, 1966, Vol. 1, pp. 225–233.
29. DEERE, D.U.: Technical description of rock cores for engineering purposes. Rock Mech. Eng. Geol., Vol. 1, 1963, pp. 18–22.
30. DEERE, D.U.: Geological considerations. Chapter in Rock Mechanics in Engineering Practice (Editors K.G. Stagg and O.C. Zienkiewicz), London, Wiley, 1968, pp. 1–20.
31. DEERE, D.U., HENDRON, A.J., PATTON, F.D. and CORDING, E.J.: Design of surface and near-surface construction in rock. Proc. 8th Symp. Rock Mech., Minneapolis, Minn., 1966, pp. 237–302.
32. DEERE, D.U., MERRITT, A.H. and COON, R.F.: Engineering classification of in situ rock. U.S. Air Force Systems Command, Air Force Weapons Lab., Kirtland Air Force Base, New Mexico, Tech. Rep. AFWL-TR-67-144, Jan., 1969, 269 p.
33. DEERE, D.U. and MILLER, R.P.: Engineering classification and index properties for intact rock. U.S. Air Force Systems Command, Air Force Weapons Lab., Kirtland Air Force Base, New Mexico, Tech. Rep. AFWL-TR-65-116, 1966.
34. DE SITTER, L.U.: Structural Geology. New York, McGraw-Hill, 1964, 551 p.
35. DUNCAN, N.: Engineering geology and rock mechanics, Vols. I and II, London, Leonard Hill, 1969.
36. FAIRHURST, C. and ROEGIERS, J.C.: Estimation of rock permeability by hydraulic fracturing — A suggestion. Discussion in Proc. Symp. Percolation through Fissured Rock, Stuttgart, Germany, 1972, Paper D-2.
37. FOCARDI, P., GANDOLFI, S. and MIRTO, M.: Frequency of joints in turbidite sandstone 2nd Cong. Int. Soc. Rock Mech., Belgrade, Vol. I, 1970, Pap. I-16.
38. Geological Society of London: Engineering Group Working Party. The logging of rock cores for engineering purposes. Q.J. Eng. Geol., Vol. 3, No. 1, 1970, pp. 1–24.
39. GILLULY, J., WATERS, A.C. and WOODFORD, A.O.: Principles of Geology, W.H. Freeman & Co., San Francisco, 1959.
40. GRIFFITHS, J.C.: Scientific Method in Analysis of Sediments. New York, McGraw-Hill, 1967, 508 p.
41. GRIGGS, D. and HANDIN, J.: Observations on fracture and a hypothesis of earthquakes. Geol. Soc. Am. Mem. 79, 1960, pp. 347–364.
42. GRIGGS, D.T., TURNER, F.J. and HEARD, H.C.: Deformation of rocks at 500° to 800° C. Geol. Soc. Am. Mem. 79, 1960, pp. 39–104.
43. HANDIN, J.: Strength and ductility. Section in Handbook of Physical Constants (S.P. Clark, Editor), Geol. Soc. Am. Mem. 97, 1966, pp. 223–289.

44. HARRIS, J.F., TAYLOR, G.L. and WALPER, J.L.: Relation of deformational fractures in sedimentary rocks to regional and local structures. Bull. Am. Assoc. Pet. Geol., Vol. 44, 1960, pp. 1853–1960.

45. HODGSON, R.A.: Regional study of jointing in Comb Ridge-Navajo mountain area, Arizona and Utah. Bull. Am. Assoc. Pet. Geol., Vol. 45, No. 1, Jan., 1961, pp. 1–38.

46. HOLMES, C.D.: Till fabric. Geol. Soc. Am. Bull., Vol. 52, 1941, pp. 1299–1354.

47. HUTTA, J.J.: Relation of dimensional orientation of quartz grains to directional permeability in sandstones. M.S. Thesis, Dept. Mineralogy, Penn. State Univ., Univ. Park, Penn., 1956, 97 p.

48. I.S.R.M.: Description of rock masses, joints and discontinuities. 2nd draft, August, 1975.

49. JAHNS, R.A.: Sheet structure in granites; its origin and use as a measure of glacial erosion in New England. J. Geol., Vol. 51, 1943, pp. 71–98.

50. JENNINGS, J.E., BRINK, A.B.A. and WILLIAMS, A.A.B.: Revised guide to soil profiling. Trans. S. African Instn. Civil Engrs., Vol. 15, No. 1, Jan., 1973, pp. 3–12.

51. JOHANSSON, C.E.: Structural studies of sedimentary desposits. Geologiska Foreningens i Stockholm Forhandlingar, Vol. 87, 1965, pp. 3–61.

52. JOHN, K.W.: An approach to rock mechanics. J. Soil Mech. Found. Div., Am. Soc. Civ. Eng., Vol. 88, SM-4, Aug., 1962, pp. 1–30.

53. KAMB, W.B.: Theory of preferred crystal orientations developed by crystallisation under stress. J. Geol., Vol. 67, 1959, pp. 153–170.

54. KIROLLOVA, I.V.: Some problems of the mechanics of folding (In Russian). Trans. Geofian, Vol. 6, 1949.

55. KRYNINE, D.P. and JUDD, W.R.: Principles of Engineering Geology and Geotechnics. New York, McGraw-Hill, 1957, 730 p.

56. LAUFFER, H.: Gebirgsklassifizierung für den Stollenbau. Geol.- u. Bauwesen, Vol. 24, 1958, pp. 46–51.

57. MACDONALD, G.J.F.: Thermodynamics of solids under non-hydrostatic stress with geological applications. Am. J. Sci., Vol. 225, 1957, pp. 266–281.

58. MERRITT, A.H.: Engineering classification for in situ rock. Ph. D. Thesis, Univ. Illinois, Urbana, 1968.

59. MINER, N.A.: Talus slopes of the Gaspé Peninsula. Science, Vol. 79, 1934, pp. 229–230.

60. MÜLLER, K.E.H.: Zur Definition des Durchtrennungsgrades. Rock Mech., Supl. 3, 1974, pp. 17–29.

61. MÜLLER, K.E.H.: Zur Definition des Durchtrennungsgrades. SFB, Jahresbericht 1974, Inst. Boden- u. Felsmech., Univ. Karlsruhe, Karlsruhe, 1975.

62. MÜLLER, L.: Der Felsbau. Stuttgart, Ferdinand Enke-Verlag, 1963, 624 p.

63. MÜLLER, L. and HOFMANN, H.: Selection, compilation and assessment of geological data for the slope problem. Proc. Symp. Planning Open Pit Mines, Johannesburg, 1970, pp. 153–170.

64. NIGGLI, P.: Gestein- und Minerallagerstätten. Basel, Berkhauser Verlag, 1948.

65. NOVIKOVA, A.C.: The intensity of cleavage as related to the thickness of the bed. (In Russian). Sov. Geol., Vol. 16, 1947.

66. OLIVIER, H.G.: Note on the swelling properties and other related geomechanical parameters of Karoo strata as encountered in the Orange-Fish tunnel. Report, Oviston Laboratories, 1973, 7 p.

67. PACHER, F.: Kennziffern des Flächengefüges. Geol- u. Bauwesen, Vol. 24, 1959, pp. 224–227.

68. PALMSTROM, A.: Karakterisering av oppsreknigsgrad og fjellmassers kvalitet. Int. Rep., Ing. A. B. Berdal, Mariesvei 20, 1322 Hovik, Oslo, 1975, 26 p.

69. PATERSON, M.S.: Experimental deformation and faulting in Wombeyan marble. Geol. Soc. Am. Bull., Vol. 69, 1958, pp. 465–476.

70. PATTON, F.D. and DEERE, D.U.: Geological factors controlling slope stability in open pit mines. Proc. 1st Int. Conf. Stability in Open Pit Mining, Vancouver, Canada, 1970, pp. 23–47.

71. PINCUS, H.J.: Quantitative comparative analysis of fractures in gneisses and overlying sediment rocks of Northern New Jersey. Geol. Soc. Am. Bull., Vol. 62, 1951, pp. 81–130.

72. PINCUS, H.J.: The analysis of aggregates of orientation data in the earth sciences. J. Geol., Vol. 61, 1953, pp. 482–509.

73. PITEAU, D.R.: Geological factors significant to the stability of slope cut in rock. Proc. Symp. Planning Open Pit Mines, Johannesburg, 1970, pp. 33–53.

74. PRATT, W.E.: Large-scale polygonal jointing. Bull. Am. Assoc. Pet. Geol., Vol. 42, 1958, pp. 2249–2251.

75. PRICE, G.P.: Quartz c-axis fabric analysis by the photometric method. Ph. D. Thesis, Univ. Sydney, Sydney, 1975.

76. PRICE, N.J.: Mechanics of jointing in rocks. Geol. Mag., Vol. 96, No. 2, March-April, 1959, pp. 149–167.

77. PRICE, N.J.: Fault and joint development in brittle and semi-brittle rock. Oxford, Pergamon, 1966, 176 p.

78. PRIEST, S.D. and HUDSON, J.A.: Discontinuity spacings in rock, Int. J. Rock Mech. Min. Sci. & Geomech. Abstr., Vol. 13, 1976, pp. 135–148.

79. PROCTOR, R.V. and WHITE, T.L.: Rock Tunnelling with Steel Supports. Youngstown, Ohio, Commercial Shearing & Stamping Co., 1946, 278 p.

80. RAMBERG, H.: Relationships between length of arc and thickness of ptygmatically folded veins. Am. J. Sci., Vol. 258, 1960, pp. 36–46.

81. RAMBERG, H.: Contact strain and folding instability of a multi-layered body under compression. Geol. Rund., Vol. 51, 1961, pp. 405–439.

82. RAMBERG, H.: Fluid dynamics of viscous buckling applicable to folding of layered rocks. Bull. Am. Assoc. Pet. Geol., Vol. 47, 1963, pp. 484–515.

83. RAMSAY, J.G.: Folding and fracturing of rocks. New York, McGraw-Hill, 1967, 568 p.

84. ROBERTSON, A.M.: The interpretation of geological factors for use in slope theory. Proc. Symp. Planning Open Pit Mines, Johannesburg, 1970, pp. 55–71.

85. ROBERTSON, A.M. and STAMER, R.: The interpretation of joint survey data. Report on the stability of side slopes of the big holes of the de Beer's mine, Kimberley, South Africa, 1968.

86. ROCHA, M.: Discussion in Proc. Symp. Percolation through Fissured Rock, Stuttgart, Germany, 1972, pp. 11–15.

87. ROSENGREN, K.J.: Rock mechanics of the Black Star open cut, Mount Isa. Ph. D. Thesis, Aust. Nat. Univ., Canberra, 1968.

88. RUIZ, M.D.: Some technological characteristics of twenty-six Brazilian rock types. Proc. 1 st Cong. Int. Soc. Rock Mech., Lisbon, 1966, Vol. 1, pp. 115–119.

89. SANDER, B.: Gefügekunde der Gesteine. Berlin, Springer, 1930.

90. SHARP, J.C. and MAINI, Y.N.T.: Fundamental considerations on the hydraulic characteristics of joints in rock. Proc. Symp. Percolation through Fissured Rock, Stuttgart, Germany, 1972, Paper T 1-4.

91. STAPLEDON, D.H.: Discussion of paper "Classification of rock substances" by D.F. COATES. Int. J. Rock Mech. Min. Sci., Vol. 5, No. 4, July, 1968, pp. 371-373.

92. STINI, J.: Technische Geologie. Stuttgart, Enke Verlag, 1922.

93. STINI, J.: Technische Gesteinskunde. Wien, Springer Verlag, 1929.

94. STINI, J.: Tunnelbaugeologie. Wien, Springer Verlag, 1951.

95. TERZAGHI, K.: Rock defects and loads on tunnel supports. In Rock Tunnelling with Steel Supports by R.V. PROCTOR and T.L. WHITE. Youngstown, Ohio, Commercial Shearing and Stamping Co., 1946, pp. 15-199.

96. TERZAGHI, K.: Stability of steep slopes on hard unweathered rock. Geotechnique, Vol. 12, 1962, pp. 251-270.

97. TERZAGHI, R.D.: Sources of error in joint surveys. Geotechnique, Vol. 15, 1965, pp. 287-304.

98. TURNER, F.G.: Review of current hypotheses and tectonic significance of schistosity in metamorphic rocks. Trans. Am. Geophys. Union, Vol. 29, 1948, pp. 558–564.

99. TURNER, F.J., GRIGGS, D.T., CLARK, R.H. and DIXON, R.H.: Deformation of Yule marble. Part 7. Geol. Soc. Am. Bull., Vol. 67, 1956, pp. 1259-1294.

100. TURNER, F.J. and WEISS, L.E.: Structural Analysis of Metamorphic Tectonites. New York, McGraw-Hill, 1963, 545 p.

101. UNDERWOOD, E.E.: Quantitative Stereology. Reading, Massachusetts, Addison Wesley, 1969, 274 p.

102. U.S. Task Committee for Foundations Design Manual, Am. Soc. Civ. Eng. Subsurface investigation for design and construction of foundations of buildings: Part II. J. Soil Mech. Found. Div., Am. Soc. Civ. Eng., Vol. 98, SM6, June, 1972, pp. 557-578.

103. WAHLSTROM, E.E.: Tunnelling in rock. Amsterdam, Elsevier, 1973, 250 p.

104. WEINERT, H.H.: Engineering petrology for roads in South Africa. Eng. Geol., Vol. 2, 1968, pp. 363–395.

105. WICKHAM, G.E. and TIEDEMANN, H.R.: Research in ground support and its evaluation for coordination with system analysis in rapid excavation. U.S.B.M. Contract Report II-0210038, ARPA Program, 1972.

106. WICKHAM, G.E. and TIEDEMANN, H.R.: Ground support prediction model (RSR concept). U.S.B.M. Contract Report H-020075, ARPA Program, 1974.

107. WICKHAM, G.E., TIEDEMANN, H.R. and SKINNER, E.H.: Support determinations based on geologic predictions. Proc. North American Rapid Excavation Tunnelling Conf., Chicago, 1972, Vol. I, pp. 43–64.

108. WILLIS, B.: Mechanics of Appalachian structure. U.S. Geol. Survey, 13th Annual Report, Part II, 1893.

109. WILLIS, B. and WILLIS, R.: Geologic Structures. McGraw-Hill, 1934, 544 p.

Uncited References to Chapter 11

1. AISENSTEIN, B.: Some observations on deconsolidation of limey rocks on steep slopes. Proc. 6th Int. Conf. Soil Mech. Found. Eng., Montreal, 1965, Vol. 2, pp. 439–441.
2. ANON: Proposal for rock classification. Proc. 10th Cong. Int. Bur. Rock Mech., Leipzig, 1968, pp. 787–788.
3. AUFMUTH, R.E.: Site engineering indexing of rock. Field Testing and Instrumention of Rock, A.S.T.M., Spec. Tech. Pub. 554, 1970.
4. AUFMUTH, R.E.: A systematic determination of the engineering criteria for rock. Bull. Assoc. Eng. Geol., Vol. 11, No. 3, 1974, pp. 235–245.
5. BARTON, C.M.: Simplified procedures for the vector summation and statistical analysis of spherically distributed point clusters. C.S.I.R.O., Australia, Div. Appl. Geomech., Tech. Rep. No. 20, 1974.
6. BALTOSSER, R.W. and LAWRENCE, H.W.: Application of well logging techniques in metallic mineral mining. Geophysics, Vol. 35, No. 1, Feb., 1970, pp. 143–152.
7. BONIFACE, A.: Stereographic aid for oriented borehole core. Trans. S. African Instn. Civil Engrs., Vol. 16, No. 6, June, 1974, pp. 199–202.
8. BORETTI-ONYSZKIEWICZ, W.: Joints in the flysch sandstones on the ground of strength examinations. Proc. 1st Cong. Inst. Soc. Rock Mech., Lisbon, 1966, Vol. 1, pp. 153–157.
9. BROOKER, P.I.: Avoiding unnecessary drilling. Proc. Aust. Inst. Min. Metall., No. 253, March, 1975, pp. 21–23.
10. CECIL, O.S.: Correlation of rock bolts, shotcrete support and rock quality parameters in Scandinavian tunnels. Ph. D. Thesis, Univ. Illinois, Urbana, 1970.
11. CHAPMAN, R.W.: Criteria for the mode of emplacement of the alkaline stock at Mount Monadrak, Vermont. Geol. Soc. Am. Bull., Vol. 65, 1954, pp. 97–114.
12. CHATTERJI, G.C.: Thoughts on studies concerning microrelief. Proc. Ind. Soc. Eng. Geol., Oct., 1968.
13. CLAR, E.: Zur Darstellung der Klüftigkeit von Felsaufschlüssen. Geol.- u. Bauwesen. Vol. 7, No. 1, 1939.
14. CLOOS, H.: Experimente zur inneren Tektonik. Centralbl. Minerol. Geol. u. Pal., 1928, pp. 609–621.
15. CLOOS, H.: Zur experimentellen Tektonik I. Methodik und Beispiele. Die Naturwissenschaften, Vol. 18, No. 34, 1930, pp. 741–747.
16. CLOOS, H.: Hebung, Spaltung, Vulkanismus. Geol. Rund. Vol. 30, 1939.
17. COON, R.F. and MERRITT, A.H.: Predicting in situ modulus of deformation using rock quality indexes. Proc. Symp. Determination of the In-situ Modulus of Deformation of Rock, Denver, Colo., 1969, A.S.T.M. Spec. Tech. Publ. 477, 1970, pp. 154–173.
18. COTTISS, G.I., DOWELL, R.W. and FRANKLIN, J.A.: A rock classification system applied in civil engineering. Parts I and II. Civil Eng. Public Works Rev., June and July, 1971.
19. Cumming, J.D.: Diamond Drilling Handbook. Toronto, Smith & Sons, 1956.
20. DENISSOV, N.J., PAUSHKIN, G.A. and ZAYTZEV, A.S.: Applying the information received in the process of drilling for the estimation of the state of rocks. Proc. 1st Cong. Int. Soc. Rock Mech., Lisbon, 1966, Vol. 1, pp. 199–203.

21. DIETERICH, J.H.: Origin of cleavage in folded rocks. Am. J. Sci., Vol. 267, No. 2, Feb., 1969, pp. 155–165.

22. DIETERICH, J.H.: Computer experiments on mechanics of finite amplitude folds. Can. J. Earth Sci., Vol. 7, No. 2, April, 1970, pp. 467–476.

23. DIETERICH, J.H. and CARTER, N.L.: Stress-history of folding. Am. J. Sci., Vol. 267, No. 2, Feb., 1969, pp. 129–154.

24. DIXON, H.W.: Decomposition products of rock substances—Proposed engineering geological classification. Proc. Symp. Rock Mech., Univ. Sydney, 1969, pp. 39–44.

25. ERZHANOV, Z.S. and EGOROV, A.K.: The mathematical theory of the formation of folds in the earth's crust. Proc. 2nd Cong. Int. Soc. Rock Mech., Belgrade, 1970, Vol. 1, pp. 457–462.

26. EURENIUS, J. and FAGERSTROM, H.: Sampling and testing of soft rock with weak layers. Geotechnique, Vol. 19, No. 1, 1969, pp. 116–132.

27. FOOKES, P.G. and DENNESS, B.: Observational studies on fissure patterns in Cretaceous sediments of South East England. Geotechnique, Vol. 19, No. 4, 1969, pp. 453–477.

28. FOOKES, P.G. and HIGGINBOTTOM, I.E.: The classification and description of near-shore carbonate sediments for engineering purposes. Geotechnique, Vol. 25, No. 2, June, 1975, pp. 406–411.

29. FOOKES, P.G. and PARRISH, D.G.: Observations on small scale structural discontinuities in the London clay and their relationship to regional geology. Q.J. Eng. Geol., Vol. 1, No. 4, 1969, pp. 217–240.

30. FRANKLIN, J.A.: Observations and tests for engineering description and mapping of rocks. Proc. 2nd Cong. Int. Soc. Rock Mech., Belgrade, 1970, Vol. 1, pp. 11–16.

31. FRANKLIN, J.A., BROCK, E. and WALTON, G.: Logging the mechanical character of rock. Trans. Inst. Min. Metall., Section A, Vol. 80, 1971, pp. A1–A9.

32. FOURMAINTRAUX, D.: Quantification of discontinuities of rock and rock masses — Methods and applications. Rock Mech., Vol. 7, No. 2, June, 1975, pp. 83–100.

33. GAMBLE, J.C.: Durability—plasticity classification of shales and other argillaceous rocks. Ph. D. Thesis, Univ. Illinois, Urbana, 1971.

34. Geol. Soc. Am.: Application of geology to engineering practice. Berkey Volume, New York, Geol. Soc. Am., 1950, 327 p.

35. GOETZE, C.: Sheared iherzolites from the point of view of rock mechanics. Geology (G.S. Am.), Vol. 3, No. 4, April, 1975, pp. 172–173.

36. GRAMBERG, J.: Bruchbildung, Bewegungen und Spannungen um eine Abbaustrecke bei einseitigem Abbau. Gebirgsdruck und Grubenausbau, (Informationstagung), 13–14 Nov., 1969.

37. GRAMBERG, J.: The axial cleavage fracture. Eng. Geol., Vol. 1, 1965, pp. 31–72.

38. HAGERMAN, T.H.: Rock bodies and particular zones in rock. The geological structure as a factor in rock stability. Proc. 1st Cong. Int. Soc. Rock Mech., Lisbon, 1966, Vol. 1, pp. 159–162.

39. HAGERMAN, T.H.: Different types of rock masses from rock mechanics point of view. Rock Mech. Eng. Geol., Vol. 4, 1966, pp. 183–198.

40. HAMEL, J.V. and ADAMS, R.: Discussion on "Some field examples of toppling failure by DE FREITAS, M.H. and WATTERS, R.J." Geotechnique, Vol. 24, No. 4, Dec., 1974, pp. 691–693.

41. HANSAGI, I.: Mining way of defining the mechanical properties of rock and of the classification of rock. Proc. 1st Cong. Int. Soc. Rock Mech., Lisbon, 1966, Vol. 1,

pp. 179–183.

42. HANSAGI, I.: A method of determining the degree of fissuration of rock. Int. J. Rock Mech. Min. Sci. & Geomech. Abstr., Vol. 11, No. 10, Oct., 1974, pp. 379–388.
43. HENDRON, A.J., CORDING, E.J. and AIYER, A.K.: Analytical and graphical methods for the analysis of slopes in rock masses. U.S. Army Eng. Waterways Exp. Stn., Corps of Engrs, N.C.G. Tech. Rep., July, 1971, 162 p.
44. HOEPPENER, R.: Vorläufige Mitteilung über ein genetisches System tektonischer Gefügetypen. N. Jb. Geol. Peläont, 1959, pp. 363–367.
45. HOEPPENER, R.: Physical tectonic representation of offine deformation and of stress conditions by means of equal area spherical projection. Rock Mech., Vol. 2, No. 1, 1964, pp. 22–44.
46. HOEPPENER, R., KALTHOFF, E. and SCHRADER, P.: Fracturing of rocks during homogeneous deformations. In German. Geol. Rund., Vol. 59, 1969, pp. 179–193.
47. HOLLINGSWORTH, J.: A review of the work on overbreak in stopes at the C.S.A. mine, Cobar, N.S.W. Parts 1 and 2. C.S.I.R.O., Australia. Div. Appl. Geomech., Report No. 20, 1974.
48. HUBAUX, A.: Scheme for a quick description of rocks. J. Int. Assoc. Math. Geology, Vol. 3, 1971, pp. 317–322.
49. HUGHES, M.D.: Diamond drilling for rock mechanics investigations. Proc. Symp. Rock Mech., Univ. Sydney, 1969, pp. 135–139.
50. IIDA, R., OKAMOTO, R. and YASUE, T.: Geological rock classification of dam foundation, Rock Mechanics in Japan, Vol. 1, 1970, pp. 161–163.
51. ILIEV, I.G.: An attempt to estimate the degree of weathering of intrusive rocks from their physico-mechanical properties. Proc. 1st Cong. Int. Soc. Rock Mech., Lisbon, 1966. Vol. 1, pp. 109–114.
52. INGLES, O.G. and LAFEBER, D.: The investigation and development of crack and joint systems in granular masses. C.S.I.R.O., Australia, Div. Appl. Geomech., Res. Rep. No. 97, 1967.
53. INGLES, O.G. and LAFEBER, D.: The influence of volume defects on the strength and strength isotropy of stabilised clays. Eng. Geol., Vol. 1, No. 4, June, 1966, pp. 305–310.
54. JAARSVELD, A.P. VON.: Site exploration in tunnelling projects. Rep. S. African C.S.I.R., No. MEG 1008, 1971.
55. JEFFERS, J.P.: Core barrel designed for maximum core recovery and drilling performance. Proc. Diamond Drilling Symp., Adelaide, 1966.
56. JOHN, M.: Properties and classification of rocks with reference to tunnelling. C.S.I.R., South Africa, MEG 1020, 1971.
57. JOHN, M.: Tunnelling in rock. Rep. S. African C.S.I.R., No. MEG 1037, 1971.
58. JOVAN, S. and BOZINOVIC, D.: On a geotechnical classification of terrain. Proc. 1st Cong. Int. Soc. Rock Mech., Lisbon, 1966, Vol. 1, pp. 121–124.
59. KALTHOFF, E.: Bruchbildung in Modellsubstanzen bei Deformationen mit axialer und rhombischer Symmetrie. Ph. D. Thesis, Ruhr Univ., Bochum, 1970.
60. KIRKBY, M.J.: Landslides and weathering rates. Proc. Conf. Stability and Conservation, Naples, Geol. Appl. Idrogol, Vol. 8, 1973, pp. 171–183.
61. KREBS, E.: Optical surveying with the borehole periscope. Min. Mag., Vol. 116, No. 6, June, 1967, pp. 390–399.
62. LAKSHMANAN, J. and ALLARD, P.: Seismic logging: a means to investigate rock fissuration. Proc. Symp. Rock Fracture, Nancy, 1971, Paper I-20.

63. LANE, K.S.: Stability of reservoir slopes. Proc. 8th Symp. Rock Mech., Minneapolis, Minn., 1966, pp. 321–336.

64. LOMBARDI, G.: The influence of rock characteristics on the stability of rock cavities. Tunnels and Tunnelling, Vol. 2, 1970, pp. 19 to 22 and 104–109.

65. MAHTAB, M.A., BOLSTAD, D.D., ALLDREDGE, J.R. and SHANLEY, R.J.: Analysis of fracture orientations for input to structural models of discontinuous rock. U.S.B.M., R.I. 7669, 1972, 76 p.

66. MATULA, M.: Engineering geologic investigations of rock heterogeneity. Proc. 11th Symp. Rock Mech., Berkeley, California, 1969, pp. 25–42.

67. MCMAHAN, B.K.: Indices related to the mechanical properties of jointed rock. Proc. 9th Symp. Rock Mech., Colorado School of Mines, 1967, pp. 117–128.

68. MOGILEVSKAYA, S.E.: Morphology of joint surfaces in rock and its importance for engineering geological examination of dam foundations. 2nd Int. Cong. Int. Assoc. Engng Geol., Sao Paulo, Vol. II, 1974, pap. V 1–17.1.

69. MILLER, R.P.: Engineering classification and index properties for intact rock. Ph. D. Thesis, Univ. Illinois, Urbana, 1965.

70. MÜLLER, L.: Untersuchungen über statische Kluftmessungen. Geol.- u. Bauwesen, Vol. 1, No. 3, 1933, pp. 26–82.

71. MÜLLER, L.: Der Kluftkörper, Geol.- u. Bauwesen, Vol. 18, No. 1, 1950.

72. MÜLLER, L.: Baugeologie der Festgesteine, Felsbaumechanik. Grundbau Taschenbuch, Band I, 1970.

73. MÜLLER, L.: Geomechanische Auswirkungen von Abtragungsvorgängen. Geol. Rund., Band 59, No. 1, 1969, pp. 163–178.

74. MÜLLER, L.: Gestein und Gebirgseigenschaften in Abhängigkeit von betrachtetem Größenbereich: Deut. Geol. Ges. Z., Vol. 119, 1967, pp. 65–70.

75. MÜLLER, L.: The presentation of geologic planes in structural drawings. Geol.- u. Bauwesen, Vol. 20, No. 1, 1963.

76. OBERTI, G. and FUMAGALLI, E.: Investigations of tunnel and penstock linings in anisotropic media. Proc. 6th Int. Conf. Soil Mech. Found. Eng., Montreal, 1965, Vol. 2, pp. 405–409.

77. ORR, C.N.: The geological description of in situ rock mass as input data for engineering design. Rep. S. African C.S.I.R., No. MEG/344, ME 1274, 1974, 133 p.

78. OVERBEY, W.K., KOMAR, C.A. and PASINI, J.: Predicting probable roof fall areas in advance of mining by geological analysis. U.S.B.M. Tech. Prog. Rep. (TRP) 70, 1973, 17 p.

79. PITEAU, D.R.: Classification and extrapolating rock joint properties in engineering practice. Rock Mech., Suppl. No. 2, 1973, pp. 5–31.

80. PROCTOR, R.J.: Mapping geological conditions in tunnels. Bull. Assoc. Eng. Geol., Vol. 8, 1971, pp. 1–43.

81. RANKILOR, P.P.: A suggested system of logging rock cores for engineering purposes. Bull. Assoc. Eng. Geol., Vol. 11, No. 3, pp. 247–258.

82. RICHARDS, L.R.: Classification and weathering of near-surface jointed rock. M. Sc. Thesis, Univ. London, London, 1972, 165 p.

83. ROBERTSON, A.M.: The interpretation of geological factors for use in slope theory. Proc. Symp. Planning Open Pit Mines, Johannesburg, 1970, pp. 55–71.

84. ROSENGREN, K.J.: Diamond drilling for structural purposes at Mount Isa. Proc. Symp. Aust. Diamond Drilling Assoc., Surfers Paradise, 1969.

85. ROTH, E.: Gefügeanalytische Untersuchungen im Marlsburgpluton. Ph. D. Thesis, Univ. Karlsruhe, Karlsruhe, 1969.

86. SAVICH, A.I. and KERESELIDZE, S.B.: Establishment of parameters for the zone to be stripped in the foundation of arch dam. Hydrotechnical Construction, Vol. 6, June, 1974, pp. 512–518.

87. SHANLEY, R.J. and MAHTAB, M.A. FRACTAN: A computer code for analysis of clusters defined on the unit hemisphere. U.S.B.M.I.C. 8671, 1975, 49 p.

88. SCOTT, S.H., LEE, F.T., CARROLL, R.D. and ROBINSON, C.S.: The relationship of geophysical measurements to engineering and construction parameters in the Straight Creek Tunnel pilot bore, Colorado. Int. J. Rock Mech. Min. Sci., Vol. 5, No. 1, Jan., 1968, pp. 1–30.

89. SHEA, H.J.: Proposal for a particle size grade scale based on 10. Geology (G.S. Am.), Vol. 1, No. 1, 1973, pp. 3–8.

90. HILLS, E.S.: Elements of Structural Geology. 2nd edition. Chapman & Hall, 1972, 500 p.

91. SHORT, N.M.: Borehole TV camera gives geologists inside story. Min. Eng., Vol. 15, No. 1, Jan., 1963, pp. 41–47.

92. SLY, D.G.: A new cutter liner system for soft sediments cores. Eng. Geol., Vol. 1, No. 4, 1966, pp. 343–344.

93. SPEARS, D.A. and TAYLOR, R.K.: The influence of wheathering on the composition and engineering properties of in situ coal measure rocks. Int. J. Rock Mech. Min. Sci., Vol. 9, 1972, pp. 729–756.

94. SPENCER, E.W.: Introduction of the Structure of the Earth. New York, McGraw-Hill, 1969, 597 p.

95. STONE, R.O. and DUYUNDJI, J.: A study of microrelief – its mapping, classification and quantification by means of a Fourier analysis. Eng. Geol., Vol. 1, No. 2, Dec., 1965.

96. TAYLOR, L.C.: Geometric analysis of geological separation for slope stability investigations. Bull. Assoc. Eng. Geol., Vol. 7, Nos. 1 and 2, 1970, pp. 67–85.

97. VOIGHT, B.: On the functional classification of rocks for engineering purposes. Proc. Int. Symp. Rock Mech., Madrid, 1968, pp. 131–135.

98. VON THUN, J.L. and TARBOX, G.S.: Deformation moduli determined by joint-shear index and shear catalog. Proc. Symp. Rock Fracture, Nancy, 1971, Paper II-23.

99. WALSH, J.D. and HOLLINGSWORTH, J.: Sampling and preparation of natural soils for quantitative three-dimensional fabric analysis. C.S.I.R.O., Australia, Div. Appl. Geomech., Tech. Rep. No. 7, 1968.

100. WATKINS, M.D.: Terminology for describing the spacing of discontinuities of rock masses. Q. J. Eng. Geol., Vol. 3, 1970, pp. 193–195.

101. WENTWORTH, C.K.: A scale of grade and class terms for clastic sediments. J. Geol., Vol. 30, 1922.

102. YOUNG, J.D.: Diamond drilling core orientation. B.H.P. Tech. Bull., No. 24.

103. ZEMANEK, J., CALDWELL, R.L. and GLENN, E.L.: The borehole televiewer. A new logging concept for fracture location and other types of borehole inspection. J. Pet. Tech., Vol. 21, 1969, pp. 762–774.

104. ZEMANEK, J., GLENN, E., NORTON, L.J. and CALDWELL, R.L.: Formation evaluation by inspection with borehole televiewer. Geophysics, Vol. 35, No. 2, April, 1970, pp. 254–269.

CHAPTER 12

Miscellaneous Properties of Rock

12.1. Introduction

This chapter deals with the general physical properties such as grain density, bulk density, porosity, water content, void index, permeability, swelling and slake-durability index properties and grain size. A special emphasis has been laid on the determination of permeability of rock masses in situ and conductivity of joints and the various factors that influence these parameters.

12.2. Density

Density is defined as mass per unit volume. If the weight (force), and not the mass, of a unit volume is measured, a unit weight is obtained. The density is related to its unit weight as follows:

$$\text{Density} = \frac{\text{unit weight}}{\text{acceleration due to gravity}} \tag{12.1}$$

In practical work it has been common practice to use weight units as force units: in other words, the unit of force has been that force which, when applied to unit mass, produces an acceleration g (acceleration due to gravity), rather than unit acceleration. This has several disadvantages. To obviate these, density is used which is independent of g.

The mass of a unit volume of rock in its natural state is different from the mass of the same volume of rock containing only of its solid phase. Because of this, two terms "bulk density" or simply "density" and "grain density" are in common use.

12.2.1. Grain Density

Grain density ρ_g is the mass of a unit volume of the grains (i.e. solid phase or mineral skeleton) of a rock.

$$\rho_g = \frac{m_g}{V_g} \tag{12.2}$$

where m_g = mass of grains and
V_g = volume of grains.

The grain density of a rock is wholly dependent on the grain densities of the minerals forming it, and is calculated by the formula

$$\rho_g = \sum_{i=1}^{i=n} \rho_i V_i \tag{12.3}$$

where n = number of minerals forming the rock
ρ_i = grain density of each mineral and
V_i = volume of each mineral.

The grain density is commonly determined by either of the two methods: Pycnometric method and Buoyancy method. In both cases, the rock is powdered in an agate or jasper mortar and sieved through a 0.22 mm (0.01 in) mesh sieve (BELIKOV et al, 1967).

Pycnometric method

A pycnometer with a capacity of 20 to 100 cm^3 (usually 50 cm^3) (1 to 6 in^3 (usually 3 in^3)) is selected and after proper cleaning and drying its mass determined while empty. Then after filling to the mark with distilled water, its mass is determined. The difference in masses between the filled and the empty pycnometer gives its capacity. After pouring a sample (15 to 20 g) (250 to 300 grains) of powdered rock into the pycnometer with the aid of a funnel, it is dried in an oven at a temperature of 105 °C (221 °F) for a period of 24 hours (to a constant mass) and then cooled in a desiccator. Its total mass is determined from which the mass of the sample is calculated. The pycnometer is then filled to one-third with distilled water and heated on sand bath for 30 to 60 minutes to remove air from the rock sample. After heating, the pycnometer is cooled to room temperature, distilled water is filled up to the mark, and the mass of the filled pycnometer is determined. The grain density of the rock is calculated from the following equation:

$$\rho_g = \frac{m_g \rho_w}{m_1 + m_g - m_2} \tag{12.4}$$

where ρ_g = grain density
m_g = mass of the grains in the sample
ρ_w = density of water
m_1 = mass of the pycnometer when filled with water and
m_2 = mass of the pycnometer with the sample, filled to the mark with water.

If the rock contains water-soluble minerals, inert chemicals, e.g., carbon tetrachloride, naphtha, toluene, etc. are used. Vacuum saturation may be used instead of heating in an apparatus capable of a vacuum less than 800 Pa (17 lbf/ft^2).

At least 3 tests are performed and this method gives an accuracy of ± 20 kg/m^3 (1 lb/ft^3).

Buoyancy method

This method is more accurate than the previous method but is also more laborious. A pycnometer of about 50 cm^3 (3 in^3) is used. After determining its mass, it is filled to one-third of its capacity with the powdered sample. The mass of the pycnometer with the powder is determined in air and the mass of the sample is calculated.

Then the pycnometer with the sample is half filled with liquid (usually carbon tetrachloride; density = 1600 kg/m^3 (99.9 lb/ft^3)) and deaerated in a vacuum chamber until no more air bubbles are released from the sample. The pycnometer is then removed from the vacuum chamber, filled with liquid to its neck, stoppered and left to stand for 24 hours until the suspended particles have settled and the liquid has acquired the room temperature. It is then filled to the top with the liquid and its mass determined in the same liquid after suspending it in a beaker containing the liquid from the balance beam. It is essential that no air bubbles adhere to the immersed pycnometer or to the dipped section of the wire.

The pycnometer is then emptied and washed with the same liquid; then filled with another portion of liquid and its mass determined while suspending it into the liquid-filled beaker. Care should be taken to see that the liquid level in the beaker is the same as before.

The grain density of the rock is calculated from the following relationship:

$$\rho_g = \frac{m_g \rho_l}{m_g - m_{g_l}} \tag{12.5}$$

where m_g = mass of grains in air
ρ_l = density of the liquid and
m_{g_l} = mass of grains in liquid.

This method is recommended for rocks having a porosity less than 3%. The accuracy is ± 1 kg/m^3 (0.05 lb/ft^3). The accuracy increases with increase in the density of the liquid used. Any liquid can be used keeping in view that it has a good wetting property. Carbon tetrachloride which has a density of 1600 kg/m^3 (99.9 lb/ft^3) is a common weighing medium because of its high density and good wetting property. It is however important that the weighing liquid should have low volumetric expansion with temperature otherwise an accurate temperature control of the surroundings shall be needed.

When working with rocks of lower densities, the accuracy can be enhanced by reducing the density determined from Equation 12.5 to the density of water at 4°C and by applying the correction to the buoyancy in air. The following relationship can be applied:

$$\rho_g^4 = \frac{m_g \rho_1 (\rho_w^4 - \lambda)}{m_g - m_{g_1}} + \lambda \tag{12.6}$$

where ρ_g^4 = density reduced to the density of water at 4°C
ρ_w^4 = density of water at 4°C and
λ = density of air at a given temperature.

The values of the correction factor $(\rho_w^4 - \lambda)$ at various temperatures are given in Table 57.

TABLE 57
VALUES OF $(\rho_w^4 - \lambda)$ AT VARIOUS TEMPERATURES
(after BELIKOV et al, 1967)

Temperature °C	$\rho_w^4 - \lambda$	Temperature °C	$\rho_w^4 - \lambda$	Temperature °C	$\rho_w^4 - \lambda$	Temperature °C	$\rho_w^4 - \lambda$
10	0.99853	18	0.99742	26	0.99561	34	0.99319
11	0.99843	19	0.99723	27	0.99534	35	0.99266
12	0.99832	20	0.99703	28	0.99506	36	0.99250
13	0.99820	21	0.99682	29	0.99477	37	0.99214
14	0.99807	22	0.99660	30	0.99447	38	0.99177
15	0.99793	23	0.99636	31	0.99415	39	0.99141
16	0.99777	24	0.99612	32	0.99384	40	0.99104
17	0.99760	25	0.99587	33	0.99352		

Since the volume of the sample taken is small, it is important that the sample represents all the mineral constituents that are present in the rock. It is recommended that a sufficiently large sample of rock be crushed and ground

so that the whole of it passes through the 0.22 mm (0.01 in) sieve and then a required quantity of the same be taken by using the well known methods of coning and quartering and other sampling techniques used for powder materials.

It is also advisable to determine the density of the liquid used unless it is of high purity and an accurate value has been provided by the supplier. The density of the liquid can be determined, first, by determining the mass of an inert solid in air, m_a, then in water, m_w, and finally in the liquid of interest, m_l. The density of the liquid is calculated from the following equation:

$$\rho_l = \frac{m_a - m_l}{m_a - m_w} \tag{12.7}$$

12.2.2. Bulk Density

The bulk density (many times simply called "density") is defined as the mass of a unit volume of a rock. It depends upon the mineralogical composition, porosity and amount of water present in the pores. If bulk volume of the specimen is V_b (i.e. pore volume V_p + grain volume V_g) and bulk specimen mass is m_b (mass of grains m_g + mass of water in the pores m_w), then

$$\text{bulk density or density of rock } \rho = \frac{m_b}{V_b}$$

$$= \frac{m_g + m_w}{V_p + V_g} \tag{12.8}$$

If the rock is completely dry, then dry density of rock ρ_d is obtained.

$$\rho_d = \frac{m_g}{V_b} = \frac{m_g}{V_p + V_g} \tag{12.9}$$

If the rock is saturated with water, then saturated density of rock ρ_s is calculated from the equation

$$\rho_s = \frac{m_g + V_p \times \text{density of water}}{V_b} \tag{12.10}$$

Usually, the dry density of rock is determined and quoted as one of the rock parameters unless otherwise specified.

The bulk density can be determined by either of the two methods:
1. Method of measurements
2. Buoyancy method.

Method of measurements

When rocks can be cut into regular-shaped (cylindrical or prismatic) specimens, the volume of the specimen can be found by measuring its dimensions. For cylindrical specimens, the diameters are measured both at the two ends and at the middle twice at right angles to each other, and the heights are measured at 4 points (ends of two diameters right angle to each other drawn on flat ends). The average values so obtained can be used for calculating the volume. Similarly, for prismatic specimens, the measurements are done both at the ends and at the centre. An accurate value of the volume of a cubic specimen can be obtained by measuring the lengths of the 12 edges of the cube and finding the mean value. The measurements are made with an accuracy of 0.05 mm (0.002 in).

After drying the specimen to constant mass at a temperature of 105 C (221 F) (usually 24 hours) and allowing it to cool in a desiccator for 30 minutes, the mass of the specimen is determined.

The differences in values obtained should not exceed 20 kg/m^3 (1 lb/ft^3) but in some cases large variations may be noticed when the specimens contain large pores or caverns, joints, ore impregnations and other inclusions of heavy minerals. By choosing appropriate size specimens, errors can be reduced.

Buoyancy method

After cleaning the adhering particles from the surface of a specimen with a brush, it is dried to a constant mass. The mass of the specimen is then determined in air and then saturated with water or naphtha (if the rock contains water-soluble minerals) in a vacuum of less than 800 Pa (17 lbf/ft^2) for a period of at least one hour, with periodic agitation to remove trapped air. After saturation, the specimen is surface dried with a moist cloth and its mass determined first in air, and then hydrostatically in a beaker filled with the saturating fluid.

The dry density of rock is calculated from the following relationship:

$$\rho_d = \frac{m_a \times \rho_l}{m_{sa} - m_{sl}} \tag{12.11}$$

where ρ_d = dry density of rock
m_a = mass of the dry specimen in air
ρ_l = density of liquid
m_{sa} = mass of the saturated-surface-dry specimen in air and
m_{sl} = mass of the saturated specimen when immersed in the liquid.

Densities of some important rocks and minerals are given in Table 58. Rocks containing heavy minerals posess high densities. Igneous an metamorphic

TABLE 58

DENSITIES OF ROCKS AND MINERALS, kg/m³

(after CLARK, 1966; DALY, MANGER and CLARK, 1966)

	Range of density	Mean density
Holocrystalline Igneous Rocks		
Granite	2516–2809	2667
Granodiorite	2668–2785	2716
Syenite	2630–2899	2757
Quartz diorite	2680–2960	2806
Diorite	2721–2960	2839
Norite	2720–3020	2984
Gabbro	2850–3120	2976
Diabase	2804–3110	2965
Peridotite	3152–3276	3234
Dunite	3204–3314	3277
Pyroxenite	3100–3318	3231
Anorthosite	2640–2920	2734
Natural Glasses		
Rhyolite obsidian	2330–2413	2370
Trachyte obsidian	2435–2467	2450
Pitchstone	2321–2370	2338
Andesite glass	2400–2573	2474
Leucite tephrite glass	2520–2580	2550
Basalt glass	2704–2851	2772
Crystalline Rocks		
Tonalite		2765
Olivine dolerite		2889
Dolerite	2800–2925	2863
Eclogite		3415
Sedimentary Rocks		
Sandstone	2170–2700	
Limestone	2370–2750	
Dolomite	2750–2800	
Chalk	2230	
Marble	2750	
Shale	2060–2660	
Sand	1920–1930	
Metamorphic Rocks		
Gneiss	2590–3060	2703
Schist	2700–3030	2790
Slate	2720–2840	2810
Amphibolite	2790–3140	2990
Granulite	2630–3100	2830
Eclogite	3338–3452	3392

TABLE 58 (continued)

	Range of density	Mean density
Monomineralic Aggregates		
Hortonolite dunite		3760
Pyroxenite	3250–3310	3280
Diopside		3240
Hornblendite	3120–3220	3170
Serpentine	2440 2650	2550
Talc		2790
Chlorite		2790
Hematite		4100
Magnetite		4600
Soapstone		2840
Grossularite		3490
Garnet		3930
Anhydrite	2820 2930	2887
Rocksalt	2100–2180	2140
Polyhalite		2760

rocks (excepting glasses) have high densities. For example, the density of certain types of gabbro exceeds 3000 kg/m^3. Granites have densities of 2600 to 2800 kg/m^3 while certain very porous sandstones may have densities quite small even falling down to 2100. The density of natural glasses is lower than that of the corresponding rocks because of the air trapped in them.

The density of rocks depends upon porosity, joints and other open spaces present. For the same rock type, the density increases as the depth increases due to decreased frequency of open cracks or closure of the cracks, etc. under pressure of overlying rocks. Weathering of rocks near their outcrops decreases the density firstly due to fracturing, secondly due to increase in volume of certain minerals as they come in contact with water (montmorillonites, anhydrites) and thirdly due to decomposition under the influence of atmospheric action (alteration of feldspars into clay minerals under the action of water and carbon dioxide).

Since most of the common rock-forming minerals have densities in the range 2650 to 2800 kg/m^3 (166 to 175 lb/ft^3), it could be argued that the presence of pore space in a rock would affect to a large extent the density of the rock. Since the presence of pores affects the mechanical properties of rocks, there is a possibility that relationships exist between density and mechanical properties of rocks.

JUDD and HUBER (1961) described a statistical approach for correlating physical properties of rocks. They concluded that there is a direct slightly curvilinear relationship between density and modulus of rigidity and YOUNG's modulus.

D'ANDREA, FISCHER and FOGELSON (1965) determined nine rock properties for rocks coming from 49 locations. Plots of specific gravity (density of rock/density of water) versus other properties are given in Fig. 12-1. These plots indicate trends but additional data are required for definition.

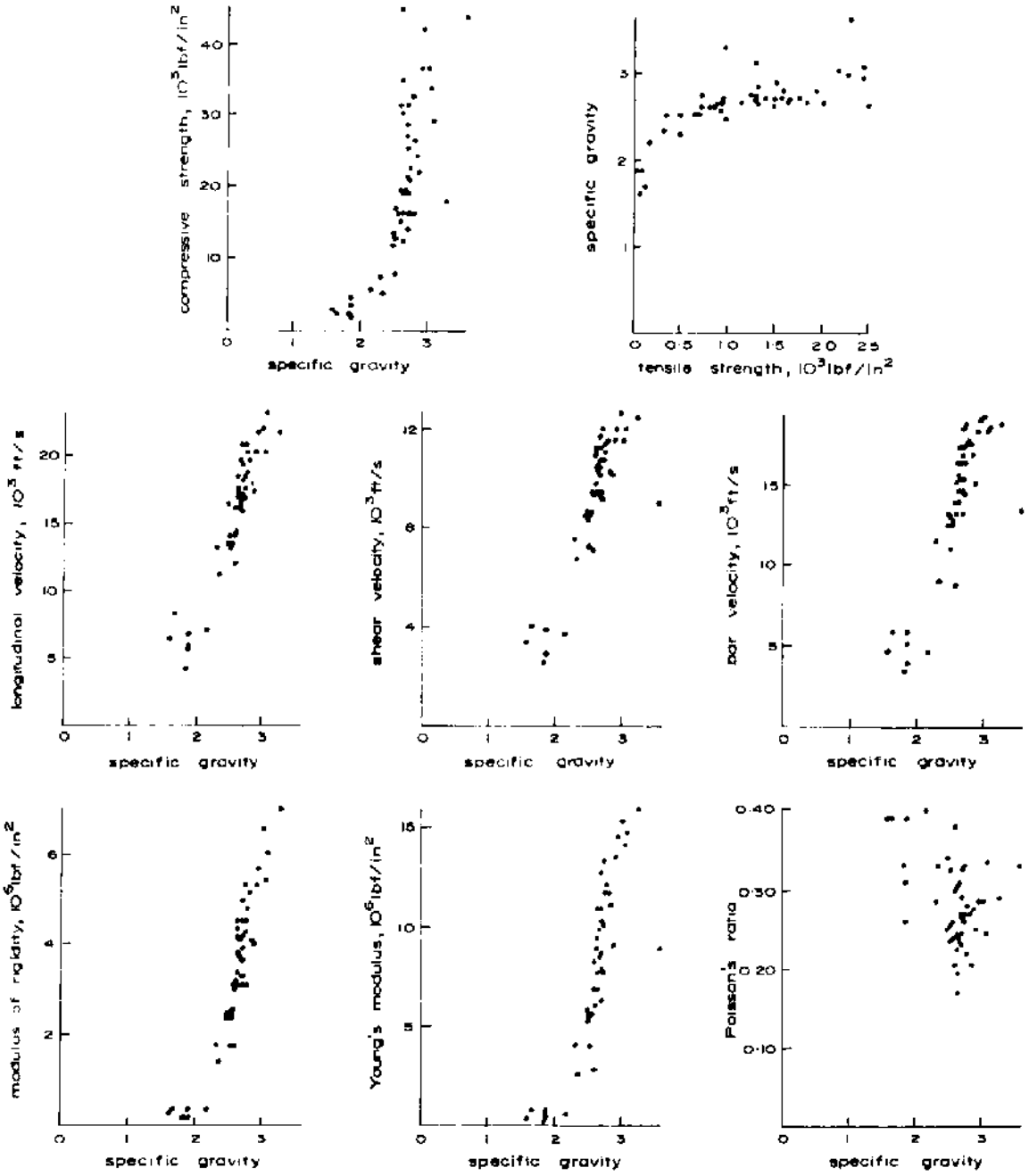

Fig. 12-1. Plots of specific gravity versus other properties (after D'ANDREA, FISCHER and FOGELSON, 1965).

SMORODINOV et al (1970) determined the following relationship (Fig. 12-2) between density, ρ and compressive strength, σ_c for the group of carbonate rocks after analysing experimental data on 110 tests of samples (density range 1.55 to 2.86 g/cm^3):

$$\sigma_c = 0.88\, e^{2.85\rho} \tag{12.12}$$

This equation has a correlation coefficient of 0.91 ± 0.017.

Another empirical equation was deduced for the group of carbonate rocks with density less than 2.65 g/cm^3:

$$\sigma_c = 0.95\, e^{2.85\rho} \tag{12.13}$$

The correlation coefficient for this equation is 0.95 ± 0.012.

The effect of density on wave velocity is shown in Fig. 12-3. (The effect of porosity is also shown in this figure which will be referred to later). The trend is very similar to the one given in Fig. 12-1. The velocity increases exponentially with increasing density.

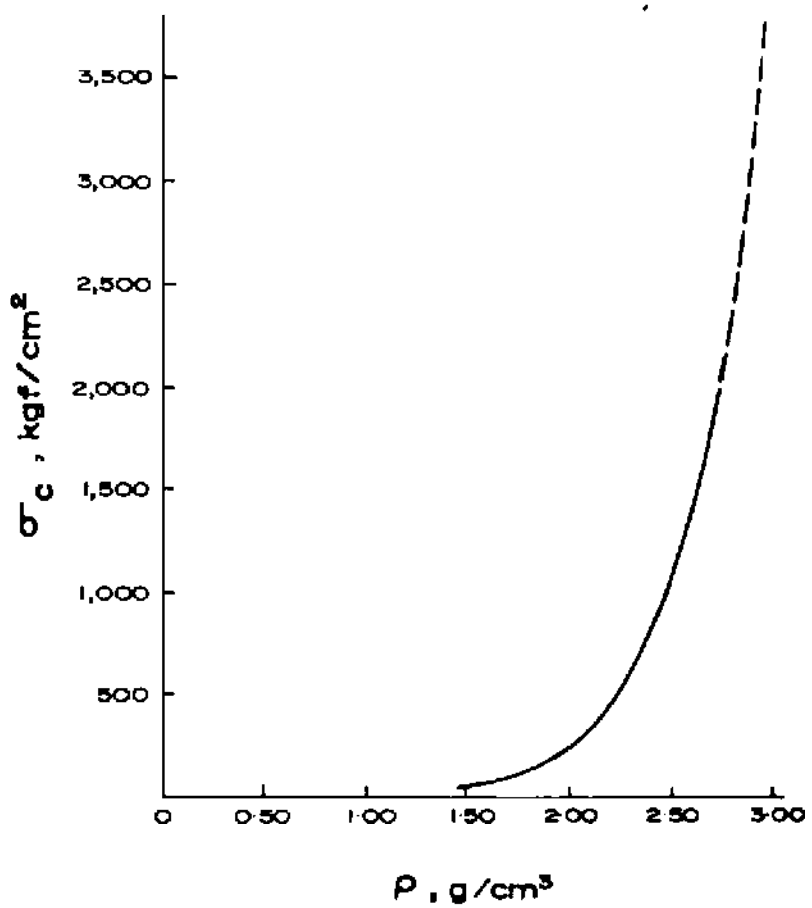

Fig. 12-2. Density, ρ versus compressive strength, σ_c for the group of carbonate rocks (after SMORODINOV et al, 1970).

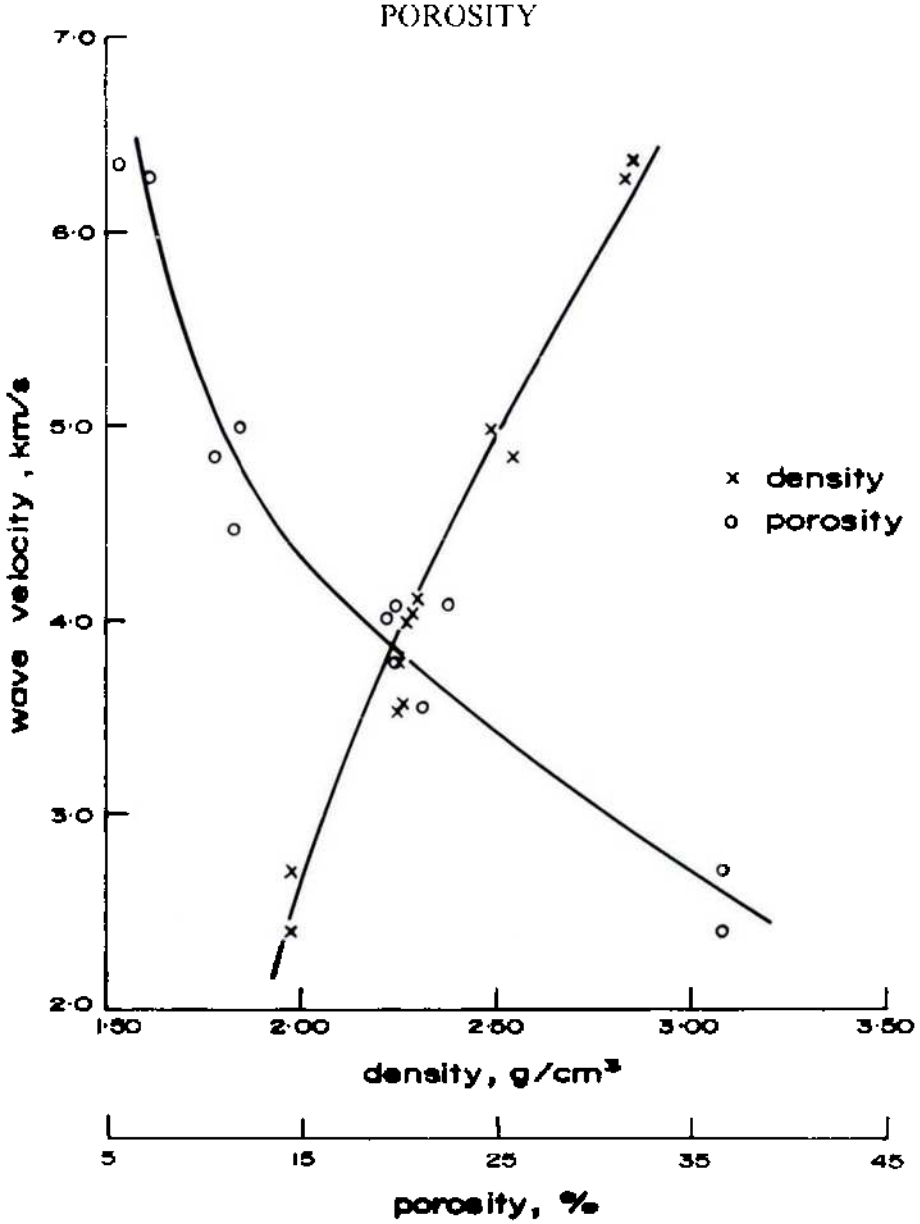

Fig. 12-3. Effect of density and porosity on wave velocity (after RAMANA and VENKATANARAYANA, 1971).

12.3. Porosity

The porosity of a rock is defined as the ratio of the volume of internal open spaces (also referred to as pores, interstices or voids) to the bulk volume of the rock.

$$\text{Porosity, } n = \frac{\text{Pore volume, } V_p}{\text{Bulk volume, } V_b}$$

$$= \frac{V_p}{\text{Volume of grains, } V_g + \text{Pore volume, } V_p} \qquad (12.14)$$

The porosity can also be expressed in terms of grain density, ρ_g and dry density of rock, ρ_d as follows:

$$n = \frac{\rho_g - \rho_d}{\rho_g} \tag{12.15}$$

The porosity of a rock depends upon its mode of formation and the following factors in general influence the porosity of rocks:

1. Size distribution of grains
2. Shape of grains
3. Solidity of grains
4. Orientation of grains
5. Degree of compaction
6. Amount of non-granular material (colloids or cement) in pores or coating the grains.

During subsequent periods, the rocks may have deformed developing cracks, fissures and joints or even certain minerals might have been dissolved away or chemically changed giving a decrease or an increase in porosity.

There are open pores (pores inter-connected with each other and linked to the external surface) and closed pores (pores that are locked up in the rock having no connection with the external surface or open pores) in a rock. Obviously, therefore, porosity is expressed as either total or apparent porosity. When all the pores are taken into account, then porosity value obtained is called total porosity. When open pores only (i.e. closed pores excluded) are considered, then porosity obtained is called apparent porosity.

12.3.1. Total Porosity

If the porosity is determined from equation (12.15), then ρ_g and ρ_d are to be determined. The methods described above for the determination of grain density and bulk density can be used. Since the sample is powdered for the determination of grain density, the porosity calculated is total porosity.

12.3.2. Apparent Porosity

If two of the three volumes, namely, pore volume, grain volume and bulk volume are determined, the porosity can be calculated. In this section, methods which do not require powdering of the sample are given. However, the pore volume measured is of interconnected pores. Hence the value calculated is the apparent porosity.

(a) Pore volume

The pore volume can be determined by two methods, namely, (*i*) Gravimetric method and (*ii*) Volumetric method.

(*i*) *Gravimetric method:* The pore volume of a rock specimen may be determined from the difference between the masses of saturated-surface-dry and oven-dry specimen. The specimen is oven-dried to determine the mass of grains, m_g. It is then saturated with water under vacuum, surface-dried with a moist cloth and its mass, $m_{w.sat}$ determined. The pore volume, V_p is calculated as

$$V_p = \frac{m_{w.sat} - m_g}{\rho_w} \tag{12.16}$$

where ρ_w = density of water.

The volume obtained by this method is only that of the open pores connected to the surface.

(*ii*) *Volumetric method:* Two porosimeters are given below.

WASHBURN-BUNTING *porosimeter:* This porosimeter makes use of a modified TOEPLER pump (used in high-vacuum techniques) in order to produce the barometric vacuum and remove air from a dried specimen.

The porosimeter consists of two containers A and B (Fig. 12-4) attached to each other through a ground joint lubricated with grease. The bottom part A has a volume of 50 cm^3 (3 in^3) and is attached from the bottom to a 500 cm^3 (30 in^3) levelling bulb containing mercury resting on a movable support (not shown in figure). The stem of the container B is graduated in 0.05 cm^3 (0.0025 in^3) divisions from zero at the stopcock to 3.5 cm^3 (0.2 in^3) near the bottom. The procedure requires the following steps:

1. Fill levelling bulb with mercury and adjust height until meniscus is in bottom part of A.
2. Place specimen in A with a short piece of piano wire looped over it to prevent the specimen from floating upwards when the mercury is introduced.
3. Attach B to A and fasten securely with rubber bands between lugs.
4. Elevate the bulb until the meniscus stands above the level of the stopcock.
5. Close stopcock. The only air in the chamber is now that which occupied the pores of the specimen at atmospheric pressure.
6. Lower the bulb until the meniscus stands as in 1, and hold in that position for two or three minutes to permit the reduced pressure in the chamber to draw air out of the specimen.
7. Elevate bulb until the menisci in bottle and graduated stem are on a common level. The air in the graduated stem is then at atmospheric pressure. Read the graduated stem at the meniscus level.

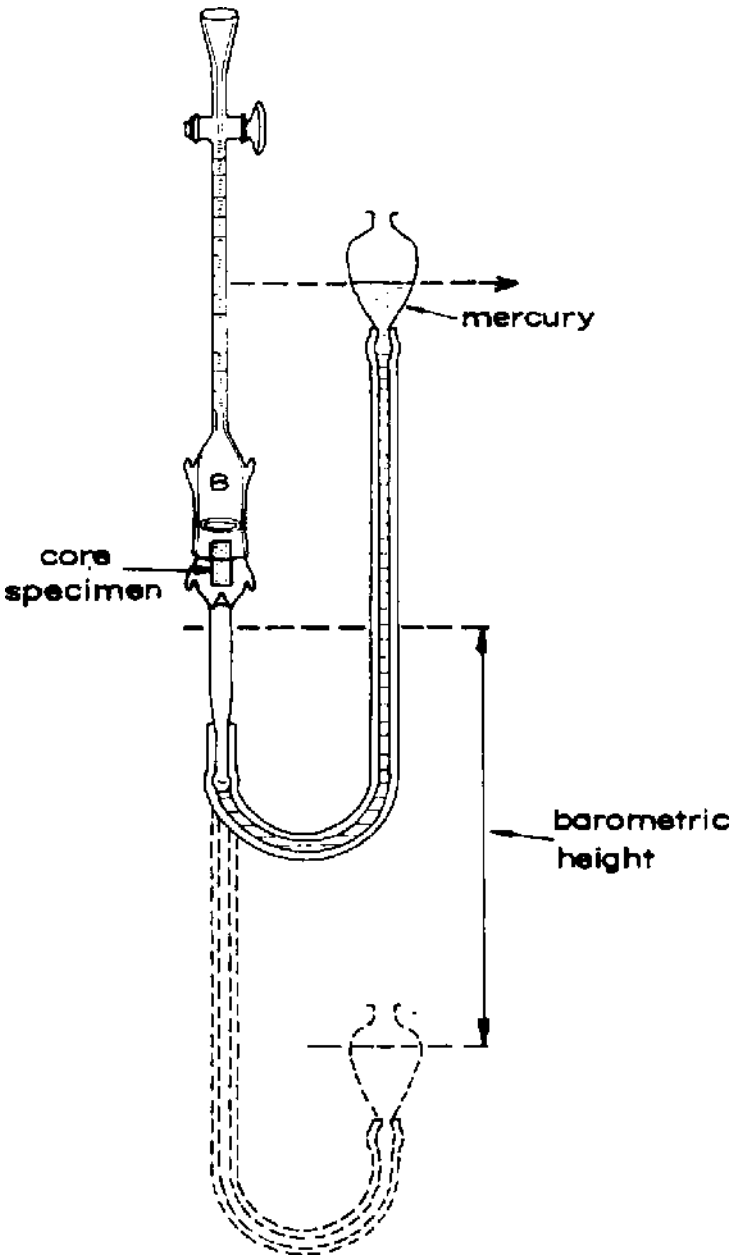

Fig. 12-4. Washburn-Bunting porosimeter
(after PIRSON, 1958).

8. Open stopcock and repeat 4, 5, 6 and 7 so as to make sure that all air has been removed from specimen. Read the stem again and add this reading to the one obtained in 7.
9. Remove specimen from A and substitute there for a solid piece of glass approximating in size and shape that of the specimen. Repeat operations 1 to 7 and record the volume of air found as the instrumental correction to be substracted from the reading obtained with the specimen to give the pore volume of the specimen. This instrumental correction is made necessary because of air adsorbed on the glass surfaces.

The volume determined needs correction for any temperature change during the test and the value may be reduced to the normal temperature and pressure if the prevailing conditions were different. The pore volume obtained is only of pores open to the surface.

RITTER *and* DRAKE *mercury porosimeter:* This porosimeter can be used for the determination of the apparent porosity of solid samples as well as the determination of the pore size distribution in them. The size of the sample handled is usually very small and therefore it gives only the micro- or semi-micro porosities.

The apparatus is designed to measure small changes in the volume of a mass of mercury in which the porous material under study is immersed when the mercury is subjected to varying external pressures. The volume changes are measured electrically in a glass dilatometer placed in a thermostated high-pressure bomb subjected to fluid pressures up to 69 MPa (10,000 lbf/in^2).

The dilatometer is of the usual one-piece type. Samples varying from 1 to 20 g are normally charged, and the capillary tubing has a cross-sectional area of about 0.04 cm^3/cm. Larger or smaller capillary tubing may be used for very porous or slightly porous material.

The dilatometer is provided with a device for observing the height of mercury in the capillary when enclosed in an opaque metal bomb. A metal wire is strung taut along the inside of the capillary tubing and made one arm of a resistance bridge. The length of the exposed wire is then equal to the length of capillary not filled with mercury. Since the mercury column will act as a conductor of effectively zero resistance, shorting out more or less of the wire as the mercury is raised or lowered, the resistance of the wire-mercury conductor is a measure of the mercury height. If the tubing is of uniform diameter and the wire of uniform resistance, then the change in resistance of the wire-mercury conductor will be a direct measure of the change in volume of the mercury.

Fig. 12-5 is a diagram of the dilatometer (RITTER and DRAKE, 1945). The wire is looped over a bridge fused across the junction of capillary to bulb, and passes up through the capillary and out through side holes in the tubing. The ends are separately anchored between cushioned nuts threaded on an insulating screw. Another nut provided with locknut is threaded on the inner end of the screw, so that when this nut is tightened the screw is backed out of the tube and the wire thereby stretched taut. The smooth glass bridge allows the tension to equalise over both branches and obviates separate tightening. RITTER and DRAKE (1945) used No. 32 platinum wire. Platinum is used because it is the only common metal with an air-stable surface not attacked by mercury, and this size is a compromise between sturdiness and flexibility.

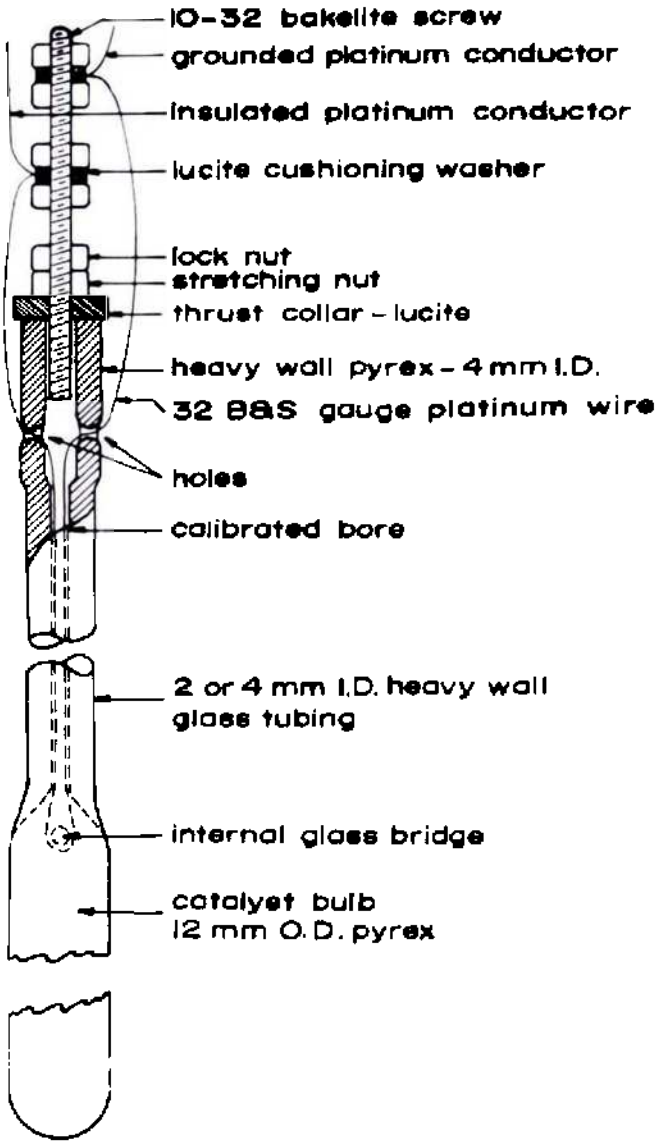

Fig. 12-5. Mercury dilatometer
(after RITTER and DRAKE, 1945).

The dilatometer is calibrated directly in cubic centimeters per ohm by taking coordinated readings of resistance and weight of mercury buretted from a stopcock sealed temporarily to the bottom of the dilatometer, while the latter is held at 0 °C in an ice bath. For convenience, only those dilatometers exhibiting a constant cm^3/ohm conversion factor are retained for use. Dilatometer, for example, had an average conversion factor of 0.608 cm^3/ohm with an average deviation over its useful length of 0.002 cm^3/ohm.

The dilatometer is filled with sample through its open bottom, sealed off, and placed in the filling pistol as shown in Fig. 12-6. The pistol is evacuated at about 0.13 Pa (10^{-3} mm of mercury) for 30 minutes, during which time

the mercury is poured back and forth several times between the reservoir and the barrel of the pistol. Finally, the pistol is up-ended with the dilatometer head down, isolated from the vacuum line, and the vacuum broken by removing the stopcock plug. Atmospheric pressure forces mercury through the dilatometer head and fills the entire vessel with mercury.

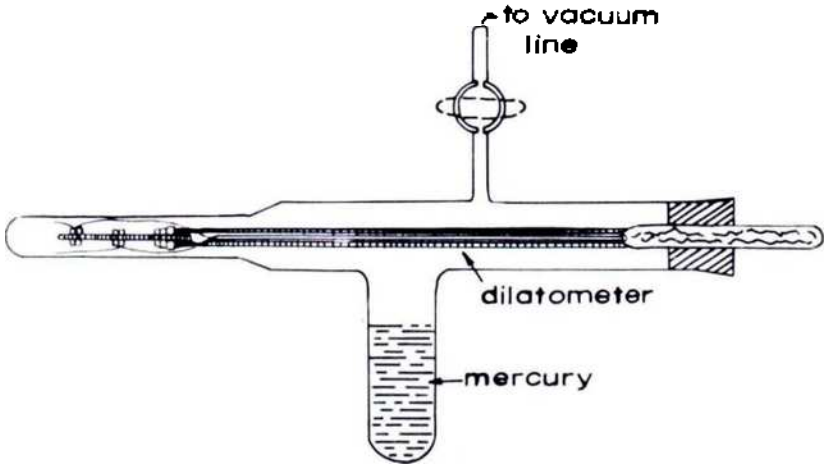

Fig. 12-6. Filling pistol for dilatometer (after RITTER and DRAKE, 1945).

In operation, the filled dilatometer is placed in a high-pressure bomb with one end of the resistance wire grounded and the other brought through an insulated lead in the bomb head. Pressures up to 13.79 MPa (2000 lbf/in^2) are supplied from a full cylinder of nitrogen and read on a dial gauge ($\neq$ 70 kPa or 10 lbf/in^2) calibrated against a dead weight gauge. Pressures from 13.79 to 68.95 MPa* (2000 to 10,000 lbf/in^2) are generated by forcing oil into the bomb with a hand-operated fuel-injection pump and read directly on the dead weight gauge. The initial 13.79 MPa (2000 lbf/in^2) of gas pressure provides a cushion at the top of the bomb which prevents oil from the pump from spilling over into the top of the dilatometer at the higher pressures and consequent fouling of the capillary tube.

Pressuring is stopped from time to time and coordinated readings of pressure and resistance are made. With some materials there is a measurable rate of penetration and time is allowed for the resistance to rise to its equilibrium value. When the pressure is rapidly applied there is a noticeable rise in temperature and time is allowed for the system to cool and the resistance to fall to its equilibrium value. Corrections to the observed gauge pressure are made by adding atmospheric pressure plus the average mercury height in the dilatometer.

*) Presently equipment for porosity determination using mercury up to 60 000 lbf/in^2 (414 MPa) is commercially available (Carlo-Erba, Italy).

The compressibility of mercury and the change of resistance with pressure of platinum are both negligible in this pressure range.

The method is a handy tool in the determination of the pore size distribution of the rock specimens if the porosity is determined at different confining pressures. WASHBURN and BUNTING (1922) pointed out that surface tension opposes the entrance into a small pore of any liquid having an angle of contact greater than 90 . This can be overcome by the application of external pressure. The pressure required to force a liquid into a pore of given size is given by

$$p \cdot r = -2\sigma \cos \theta \tag{12.17}$$

where p = pressure
r = pore radius
σ = surface tension and
θ = contact angle.

Eq. 12.17 assumes circular cross-section of the pores. If the pores have any other cross-section, the constant will have another value instead of 2. The effect will be to change the radii calculated by a certain constant factor.

This Eq. 12.17 shows that a non-wetting fluid will not enter pores at all and that when pressure is raised to any finite value, the fluid will penetrate and fill all the pores having radii greater than that calculated from the Eq. 12.17. As the pressure is increased the amount of liquid absorbed increases at a rate proportional to the differential pore volume due to pores of size corresponding to the instantaneous pressure. Thus a given pore size distribution gives rise to a unique pressuring curve. Table 59 gives the pore radius with pressure for several values of contact angle.

If the total volume of all pores having radii between r and $r+dr$ is

$$dV = D(r)dr \tag{12.18}$$

where $D(r)$ is the distribution function for pore size, from Eq. 12.17, assuming constant σ and θ,

$$pdr + rdp = 0 \tag{12.19}$$

Eliminating r and dr from Eqs. (12.17), (12.18) and (12.19) gives

$$dV = D(r)\frac{2\sigma \cos \theta}{p^2} dp$$

$$= -D(r)\frac{r}{p} dp \tag{12.20}$$

TABLE 59

Variation of pore radius with pressure for several values of contact angle

(after RITTER and DRAKE, 1945)

Pressure lbf/in^2	Pore radius for contact angles of 140 Å	112 Å	180 Å
25	42,680	20,840	55,680
100	10,670	5,210	13,920
200	5,330	2,600	6,960
300	3,560	1,740	4,640
400	2,670	1,300	3,480
500	2,135	1,040	2,780
700	1,520	744	1,990
1,000	1,067	521	1,392
1,500	712	347	928
2,000	533	260	696
3,000	356	174	464
4,000	267	130	348
5,000	214	104	278
6,000	178	87	232
7,000	152	74	199
8,000	133	65	174
9,000	119	58	155
10,000	107	52	139

The volume measured by the dilatometer is the volume of all pores having radii greater than r, i.e., the total pore volume, V_0, decreased by the volume, V, or pores smaller than r. Thus the pressuring curves plot $V_0 - V$ as a function of p. The slope of the pressuring curve, $\frac{d(V_0 - V)}{dp} = -\frac{dV}{dp}$, is then an experimentally determinable quantity and Eq. 12.20 may now be rewritten in the form

$$D(r) = \frac{p}{r}\frac{d(V_0 - V)}{dp} \tag{12.21}$$

in which all the terms on the right are known or determinable.

Values of the derivative in Eq. 12.20 required to evaluate $D(r)$ are readily obtained by graphical differentiation. For a number of values of p, the pressuring curve is differentiated to obtain $d(V_0-V)/dp$, r is calculated from Eq. 12.17, and $D(r)$ is calculated from Eq. 12.20. Plotting $D(r)$ against r gives the distribution curve. Pressuring curves and distribution curves for two porous materials are given in Figs. 12-7 and 12-8. By differentiating and applying Eq. 12.20, Fig. 12-8 is obtained which gives the pore distribution function of these materials.

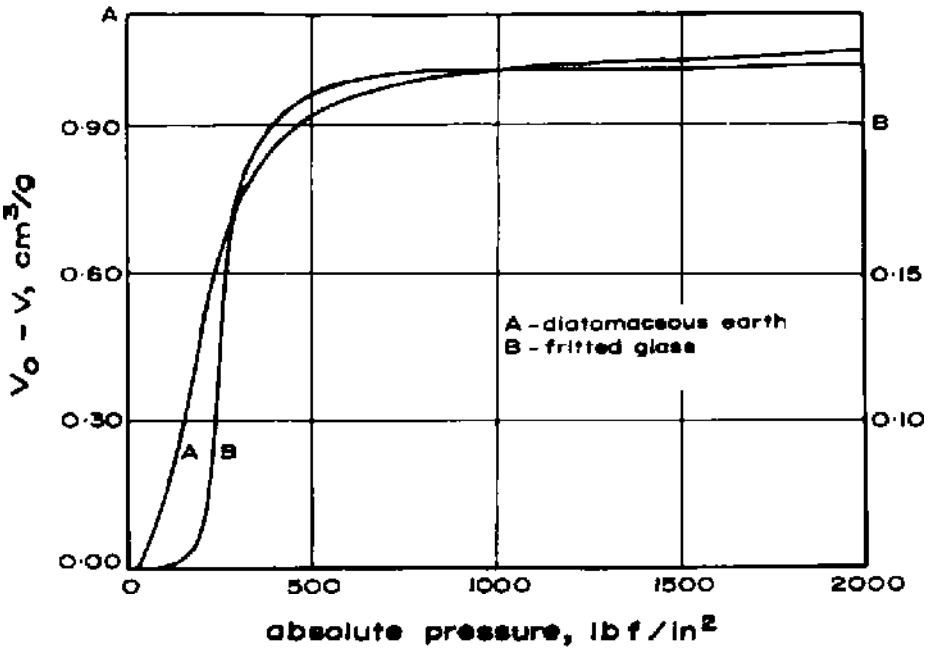

Fig. 12-7. Pressuring curves for diatomaceous earth and fritted glass (after RITTER and DRAKE, 1945).

It may be pointed out that both in the gravimetric as well as volumetric methods, the porosity measured depends upon the method of measurement. The variations may be attributed mainly to two factors which influence the results oppositely. Certain liquids may be adsorbed by the surface of the rock giving decrease in volume or increase in weight giving values higher than true densities. Alternatively, slow or incomplete penetration of the pores by the fluid or incomplete release of contained gas will lead to low apparent density. In this case a density drift may be observed with time. When mercury is used as a displacement fluid, then depending upon its angle of contact with the rock, the smallest pore that can be penetrated may be of the order of 50 Å[1] (Table 59) at high pressures of the order of 68.95 MPa (10,000 lbf/in^2). At such high pressures the correction due to the compressibility of the materials becomes essential to apply. The error due to compressibility in certain rocks such as coal, may be very high.

[1] Å = Angstrom = 10^{-8} cm

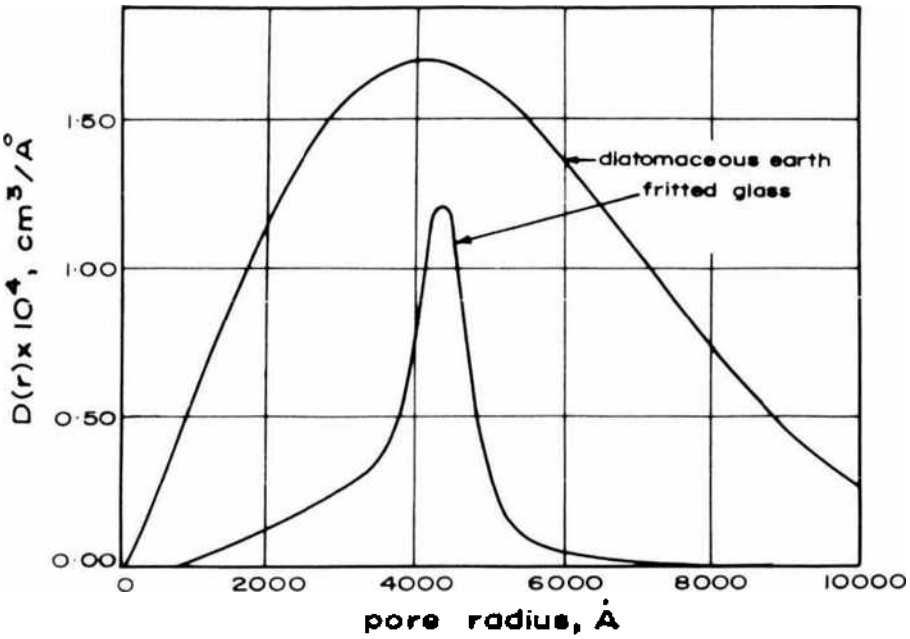

Fig. 12-8. Distribution functions for diatomaceous earth and fritted glass (after RITTER and DRAKE, 1945).

Certain other fluids because of their lower molecular volume than mercury (such as helium) can penetrate more easily and measurements at high pressures can be avoided. FRANKLIN (1949) studied this problem in connection with coal. Helium molecule owing to its extremely small size (molecular diameter 2 Å) can penetrate into pores narrower than 3 Å and because of its small VAN DER WAAL's field results in negligible adsorption on solids at room temperatures. As such measurements using helium as a displacement fluid have been now almost regarded as true densities. However, mercury displacement method gives an easy way of determining the pore size distribution. For more accurate purposes, it is suggested that measurements may be made by both methods. Studies on coal (VAN KREVELEN, 1961) have shown that it contains two pore systems, a macro-pore system which is accessible to mercury under pressure and a micro-pore system which even at very high pressures cannot be permeated by mercury, but both these systems are completely accessible to helium.

Some recent studies using ion thinning of polished surfaces of rocks and surface electron microscopy (SPRUNT and BRACE, 1974) have revealed that cavities present in rocks are of different shapes. Some are long and crack-like, some are slot-like with rounded and blunted ends, some are circular or triangular and some are simply irregular. The frequency distribution of length of cavities observed in Westerly granite is given in Fig. 12-9. If the ratio of minimum to maximum cross-section of an opening called as the aspect ratio,

α, be plotted against the number of cavities (total observations = 80 in this case), the distribution is shown in Fig. 12-10. The low aspect ratio cavities ($\alpha \leq 10^{-1}$) in unstressed samples have blunt, circular or square terminations. The long narrow, sharp ended cracks typical of brittle fracture were rarely observed in the rocks (granites, diabase, gabbro) examined by them. The number of these low aspect ratio cavities sharing a common point of intersection varied from 2 to 6 depending upon the rock. The high aspect ratio cavities ($\alpha > 10^{-1}$) appear scattered or are joined by low aspect ratio cavities and are found concentrated in certain mineral grains while the other mineral grains may be free of these (microcline in Westerly granite or plagioclase in San Marcos gabbro).

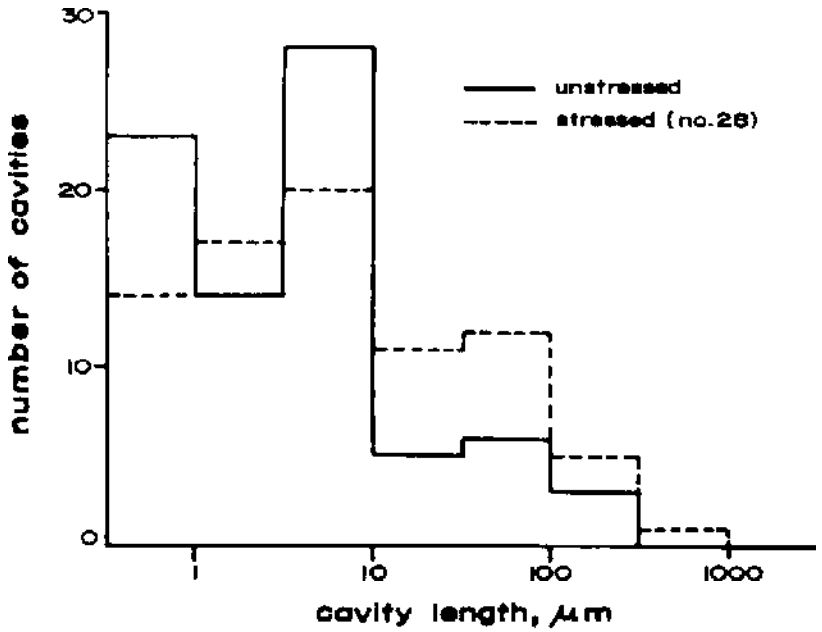

Fig. 12-9. Frequency distribution of cavity length in stressed and unstressed Westerly granite. The samples contained 80 randomly selected cavities. (after SPRUNT and BRACE, 1974).

In mechanically stressed rocks, the low aspect ratio cavities tend to increase and there seems to be a strong preferred orientation and the bridges formed between them tend to break under mechanical and thermal stresses. The length of the low aspect ratio cavities is about 1/10th the grain size. Some closely placed low aspect ratio cavities have length equal to the grain size.

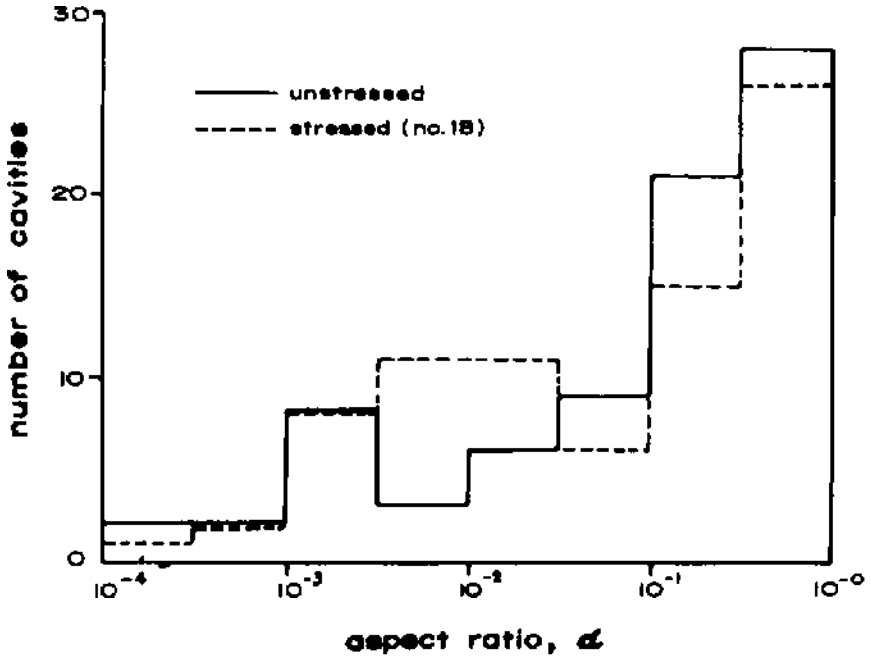

Fig. 12-10. Frequency distribution of cavity aspect ratio in unstressed and stressed Westerly granite. In each a random sample of 80 cavities was compared. (after SPRUNT and BRACE, 1974).

(b) Grain volume

Grain volume can be determined by two methods, namely, Pulverisation method and BOYLE's law method. Pulverisation method has already been described under "Grain Density". Porosity calculated from bulk volume and grain volume using the pulverisation method is termed total porosity, since the pore volume obtained includes that of 'closed' pores.

BOYLE's *law method:* The pressure-volume relationship for a vessel or bomb filled with gas only is first obtained, and repeated when the vessel is filled with specimen plus gas. The difference in compressibility is due to the volume of incompressible grains, V_g, and this volume can be calculated from the results. Various instruments have been developed using this principle and some of them are described in detail below.

(i) U.S. Bureau of Mines apparatus: Fig. 12-11 shows the assembly of the apparatus as used by the U.S. Bureau of Mines (TALIAFERRO et al, 1937; RALL and TALIAFERRO, 1949; RALL et al, 1954) and includes both a spring gauge and a dead-weight gauge for measuring the pressure. The pressure bomb consists of a steel cylinder of 1.75 in (4.45 cm) outside diameter, 3.25 in (8.26 cm) long; the inside dimensions are 1 in by 1.875 in (2.54 cm by 4.76 cm). The cap or cover of the bomb is ground to fit, and is held tightly in place with a clamp.

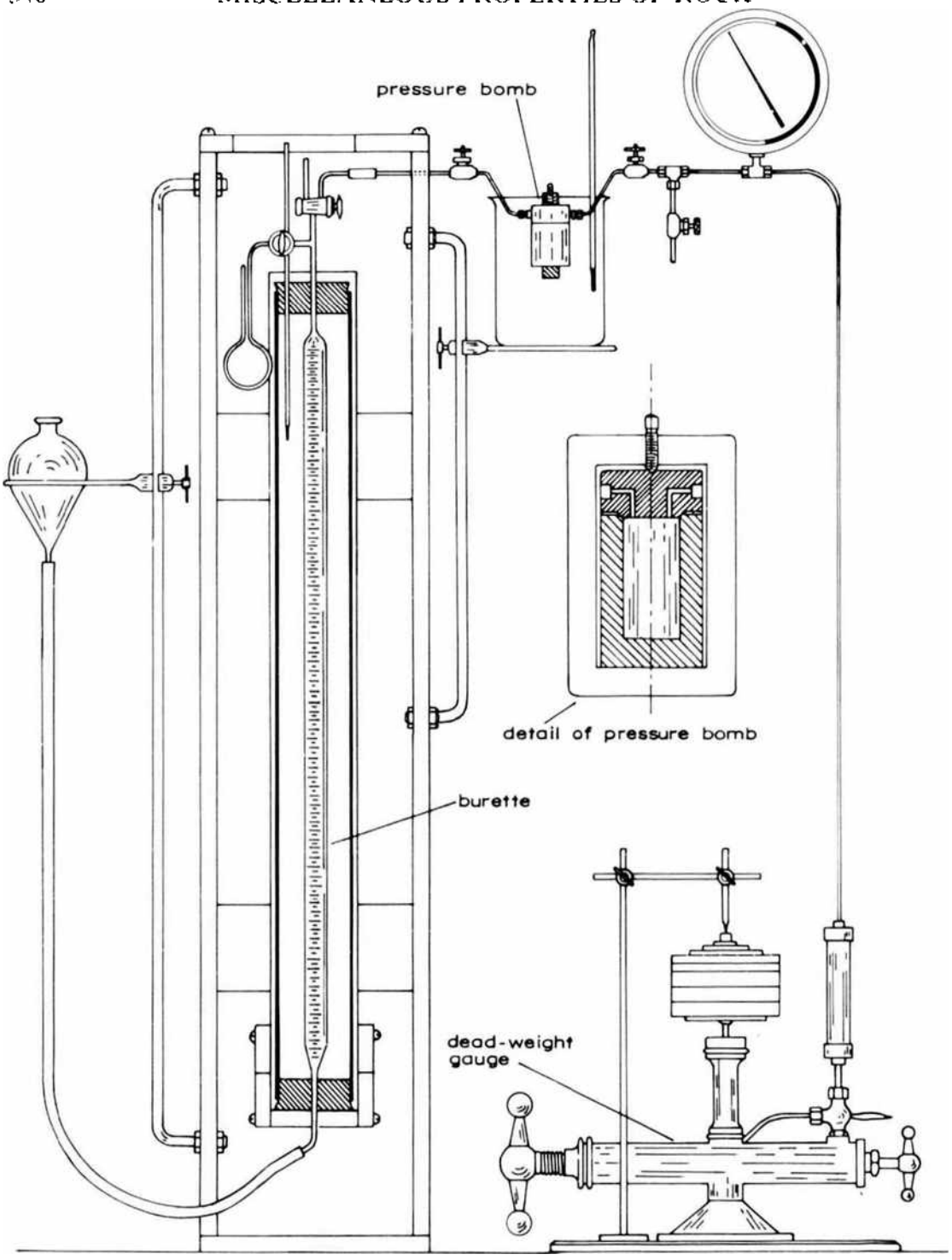

Fig. 12-11. U.S. Bureau of Mines apparatus for porosity determinations (after RALL et al, 1954).

The actual volume of the bomb need not be greatly in excess of the volume of the specimen under examination, and a number of steel discs of the diameter of the bomb are inserted into the bomb to make its volume conform to the volume of the specimen under examination.

Different gases and pressures may be used in the determination; however, it was found convenient for laboratory purposes to use air at pressures of 75 to 100 lbf/in^2 (517 to 690 kPa). After the compressed gas in the bomb has come to the temperature of the bath and the pressure determined accurately, it is released into the water-jacketed burette—where its volume is measured at the temperature of the bath surrounding the burette and at atmospheric pressure.

The data required for the determination of the volume of the bomb (V_1), along with the actual observations and calculations for such a determination using compressed air, are as follows:

Pressure in the bomb (p_1) = 100.0 lbf/in^2, gauge
Temperature of the air in the bomb (T_1) = 66.5 F
Barometric pressure (p_2) = 14.375 lbf/in^2
Volume of air after expansion (burette measurement) (V_b) = 92.02 cm^3
Temperature of air in burette (T_2) = 73.9 F
The burette volume measured at 73.9 F is converted to a volume at 66.5 F.

$$92.02 \times \frac{526.5}{533.9} = 90.74 \text{ cm}^3$$

The absolute pressure of the air in the bomb is 100.0 + 14.375 = 114.375 lbf/in^2. Air does not follow exactly the pressure-volume relationship expressed by BOYLE's law for an ideal gas ($p_1 V_1 = p_2 V_2$) and with a decrease in pressure is more expansible than an ideal gas. Accordingly, a correction factor is applied to the equation of BOYLE's law to give:

$$\left(1 + \frac{n}{100}\right) p_1 V_1 = p_2 V_2$$

$$\text{or} \quad V_2 = \frac{\left(1 + \frac{n}{100}\right) p_1}{p_2} V_1$$

where n = the percent deviation.

For the pressure and temperature of the air in this particular determination, the value of n is 0.23, and the value of the term:

$$\left(1 + \frac{n}{100}\right) \frac{p_1}{p_2} \text{ becomes } 1.0023 \times \frac{114.375}{14.375} = 7.9748$$

The value 7.9748 may be considered as the number of atmospheres of compressed air contained in the bomb before expansion. After expansion, one atmosphere of air remains in the bomb; and, therefore, the volume measured by the burette is equivalent to only 6.9748 atmospheres of air. In other words, after the air in the bomb has expanded into the burette, the air in the bomb

is at atmospheric pressure, and the total volume of air after expansion (V_2) is equal to the volume measured in the burette plus the volume remaining in the bomb.

The simplified equation for determining the volume of the bomb (V_1) then becomes:

$$V_1 = \frac{V_b}{6.9748}, \text{ or } V_1 = \frac{90.74}{6.9748} = 13.009 \text{ cm}^3$$

which is the volume of the empty bomb.

The same laboratory procedure and calculations as described above are followed when the specimen is placed in the bomb. For the specimen referred to in this discussion, the volume of space in the bomb occupied by compressed air with the specimen contained in it was 4.918 cm^3. Therefore, the volume of the grains in the specimen is the difference between 13.009 and 4.918, or 8.091 cm^3.

(ii) KOBE porosimeter: This porosimeter (Fig. 12-12) has been recommended by the International Society for Rock Mechanics (1972) and has the following features:

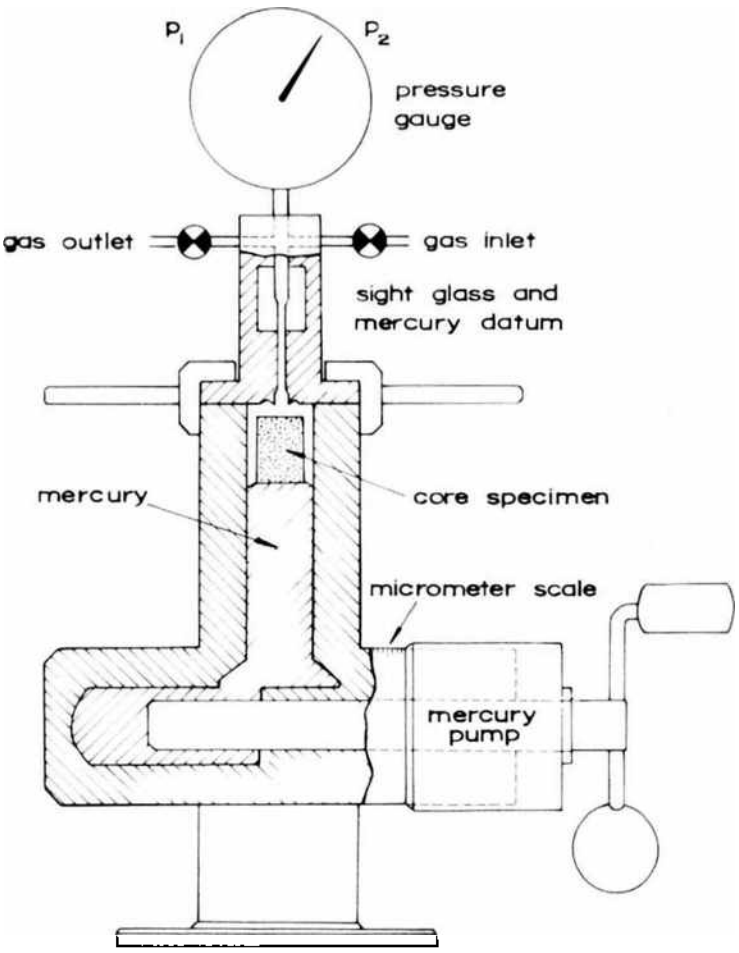

Fig. 12-12. Schematic diagram of a KOBE porosimeter (after I.S.R.M., 1972).

It consists of a mercury screw-piston pump with micrometer graduated to measure the volume of displaced mercury to an accuracy of 0.01 cm^3 (0.0005 in^3). Conveniently one turn of the screw pump changes the volume of the specimen chamber by 1 cm^3 (0.05 in^3). The specimen chamber has a removable cap to allow easy insertion of the specimen. The mercury datum level register consists of either a sight glass inscribed with a reference line, or an electric indicator-contact. It is provided with a gas inlet and outlet, each with a shutoff valve, and a source of inert gas such as helium. Air may be used with some loss of accuracy, but must be adequately dry. A precision pressure gauge with a range from one atmosphere to about three or four atmospheres is provided and is connected to measure the gas pressure in the specimen chamber.

The procedure for the determination of the porosity of the specimens with this apparatus is as follows:

(a) The mercury pump reading at the start of each compression or displacement cycle is termed the 'start point'. Inlet and outlet valves are closed at the start of a compression cycle so that the initial pressure p_1 is atmospheric. The start point and also the pressure p_2 at the end of a compression cycle are usually selected as standard for the apparatus, to ensure that the specimen still floats on mercury at the end of the cycle, hence avoiding imbibition that might occur if specimens became deeply immersed.

(b) To flush the specimen chamber with gas, the inlet valve is closed, the outlet opened and the pump advanced until mercury reaches the datum. The outlet is then half shut, the inlet opened and the pump retracted to beyond the start point. First the inlet and then the outlet valve is closed.

(c) To determine the compression factor C_f for the cell, the specimen chamber is first flushed with gas, the outlet valve opened and the pump advanced to the start point. The outlet valve is shut with the specimen chamber at atmospheric pressure p_1. The pump is advanced and micrometer reading C_0 taken when the pressure reaches p_2. The chamber is again flushed with gas, and with the outlet valve open the pump is advanced to a new start point 10 cm^3 (0.5 in^3) beyond the original one. The outlet is closed with the chamber at atmospheric pressure p_1 and the pump is advanced, and the micrometer reading C_1 is taken when the pressure again reaches p_2.

The compression factor is computed from the formula:

$$C_f = 10/(10-(C_0-C_1)) \tag{12.22}$$

This factor is dependent on ambient pressure and should be periodically checked.

(d) Each test comprises a displacement stroke followed by a compression

stroke with the specimen chamber empty (a blank run), then a displacement stroke followed by a compression stroke with the specimen in the chamber. The procedure is as follows:

(e) With the inlet valve shut and the outlet open, the pump is advanced until the mercury reaches the datum. The micrometer reading R_1 is recorded.

(f) The chamber is flushed with gas, the pump advanced to the start point and the valves closed with the chamber at atmospheric pressure p_1. The pump is advanced and a micrometer reading R_2 recorded when the pressure reaches p_2.

(g) The specimen is inserted in the chamber. The chamber is flushed with gas and step (e) repeated, recording the displacement stroke micrometer reading R_3 at which mercury reaches the datum.

(h) Step (f) is repeated, recording the compression stroke micrometer reading R_4 when the pressure again reaches p_2.

The calculations are as follows:

Grain volume is calculated from the relationship:

$$V_g = C_f (R_4 - R_2) \tag{12.23}$$

With this test, bulk volume V_b can also be determined and is given by:

$$V_b = R_3 - R_1 \tag{12.24}$$

RAMANA and VENKATANARAYANA (1971, 1974) have developed a porosimeter for rocks of porosity in excess of 3%. The porosimeter is simple to operate and gives approximate values since the error for low porosity rocks is high and secondly the use of atmospheric pressure limits to the large diameter pores being taken into account.

(c) Bulk volume

Although the bulk volume may be computed from measurements (by vernier or micrometer) of the dimensions of a regularly shaped prism or cylinder, the usual procedure utilises the observation of the volume of liquid displaced by the specimen. This procedure is particularly desirable, as the bulk volume of irregularly-shaped specimens can be determined as rapidly as that of regularly-shaped specimens.

The liquid displaced by a specimen can be observed either volumetrically or gravimetrically. In either procedure it is necessary to prevent liquid penetration

into the pore space of the rock. This can be accomplished (1) by coating the rock with paraffin or a similar substance, (2) by saturating the rock with the liquid into which it is to be immersed, or (3) by using mercury, which by virtue of its surface tension and wetting characteristics does not tend to enter the small pore spaces of most intergranular materials at or near atmospheric pressure.

Gravimetric determination of bulk volume can be accomplished by observing the loss in mass of the specimen when immersed in a liquid or by observing the change in mass of a pycnometer when filled with mercury and when filled with mercury and the specimen. The details are summarised in the examples.

Example 1. Coated specimen immersed in water.
Mass of dry specimen in air = A
Mass of dry specimen coated with paraffin = B
Mass of coated specimen immersed in water at 40 °F = C
Mass of paraffin = $B - A$

$$\text{Volume of paraffin} = \frac{B-A}{\text{density of paraffin}}$$

Mass of water displaced = $B - C$

$$\text{Volume of water displaced} = \frac{B-C}{\text{density of water}}$$

$$\text{Volume of water displaced} - \text{Volume of paraffin} = \left(\frac{B-C}{\text{density of water}}\right) - \left(\frac{B-A}{\text{density of paraffin}}\right)$$

= Bulk volume of specimen

Example 2. Water-saturated specimen immersed in water.
Mass of dry specimen in air = A
Mass of saturated surface-dry specimen in air = B
Mass of saturated specimen in water at 40 °F = C
Mass of water displaced = $B - C$

$$\text{Volume of water displaced} = \frac{B-C}{\text{density of water}}$$

= Bulk volume of specimen

This method is not suitable to friable, swelling or slaking rocks.

Example 3. Dry specimen immersed in mercury pycnometer.
Mass of dry specimen in air = A
Mass of pycnometer filled with mercury at 20 °C = B
Mass of pycnometer filled with mercury and specimen at 20 °C = C
Mass of specimen + Mass of pycnometer filled with mercury = $A + B$

Mass of mercury displaced $= A + B - C$

$$\text{Volume of mercury displaced} = \frac{A + B - C}{\text{density of mercury}}$$

$$= \text{Bulk volume of specimen}$$

Determination of bulk volume volumetrically utilises a variety of specially constructed pycnometers or volumeters. In the case of an electric pycnometer the specimen is immersed in the core cylinder, which causes a rise in the level of the connecting U tube. The change in the level is sensed by the micrometer screw. The resulting change in level is read directly in volume from the micrometer scale. Either dry or saturated specimens may be used in the device.

The RUSSEL volumeter shown in Fig. 12-13 also provides for direct reading of the bulk volume. A saturated specimen is placed in the specimen bottle after a zero reading is established with fluid in the volumeter. The resulting increase in volume is the bulk volume. Only saturated or coated specimens may be used in the device.

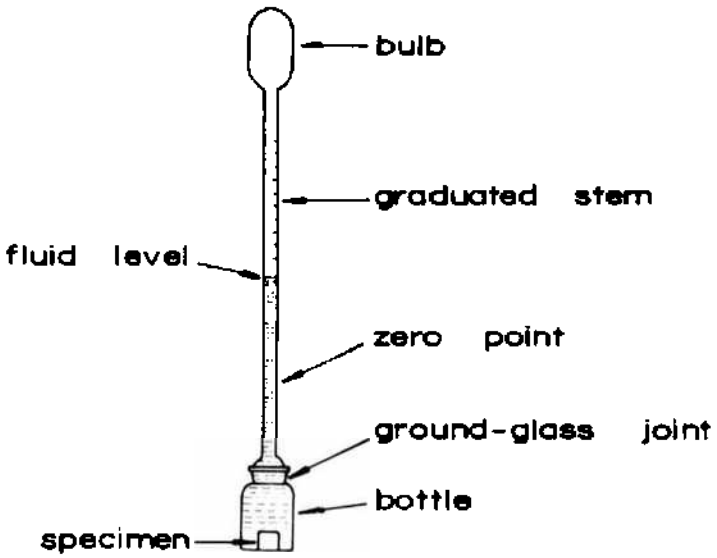

Fig. 12-13. RUSSELL volumeter (after AMYX et al, 1960).

12.3.3. Effect of Porosity on Mechanical Properties of Rocks

All strength properties of rocks fall with increase in porosity (PRICE, 1960; KOWALSKI, 1966; SMORODINOV et al, 1970; RZHEVSKY and NOVIK, 1971; DUBE and SINGH, 1972). The reasons are:

1. Stress concentration caused on the boundary of the pores reduces the strength.

2. Decrease in the bearing area of the rock causes decrease in strength.
3. The pores may be filled with water or some other liquid which may help in crack propagation by reacting at the points of stress concentration or by reducing its surface energy.

SCHILLER (1958) gave the following relationship between compressive strength and porosity:

$$\sigma_{cn} = \sigma_{co}\left(1 - a\sqrt{\frac{n}{n_{cr}}}\right) \tag{12.25}$$

where σ_{cn} = compressive strength at porosity n
σ_{co} = inherent strength of the material (zero porosity)
n = porosity of the material
n_{cr} = critical porosity when $\sigma_c = 0$
a = constant, the value of which depends upon the shape of the pores.

PRICE (1960) studied the effect of porosity on the strength of coal measure rocks. After correcting the strength values to 55% quartz content and air-dry condition, he found that compressive strength decreases linearly with increase in porosity (Fig. 12-14). For every one percent increase in porosity, the strength decreased by 4%.

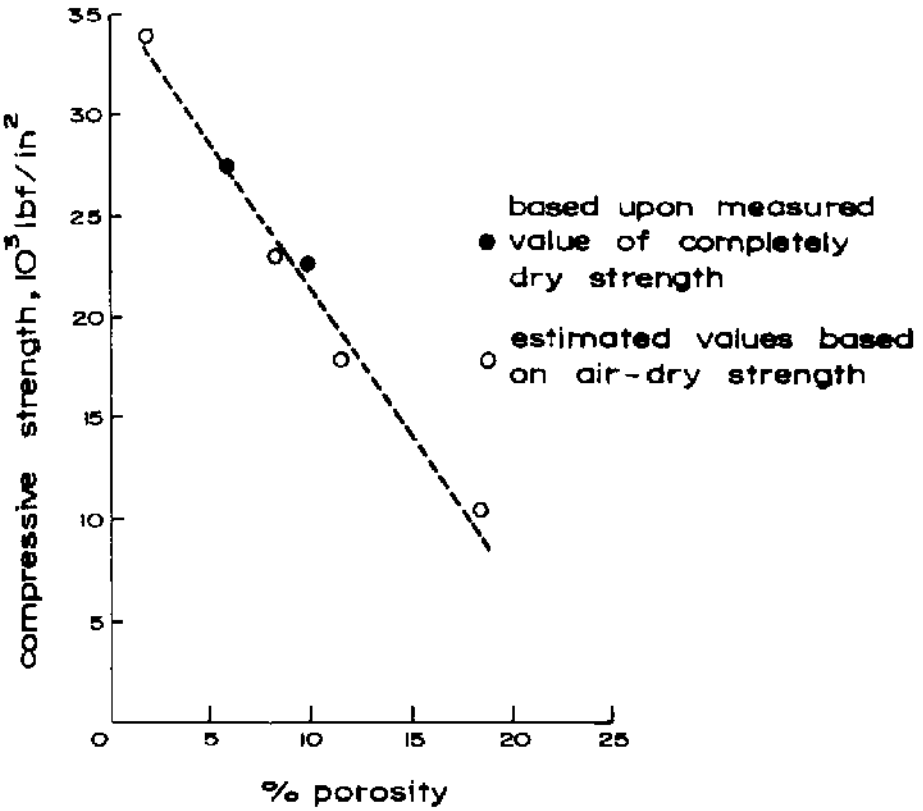

Fig. 12-14. Porosity versus compressive strength of coal measure rocks (after PRICE, 1960).

KOWALSKI (1966) reported the dependence of compressive strength σ_c on porosity n as follows:

$$\sigma_c = d\left(\frac{n}{1-n}\right)^c \tag{12.26}$$

where d and c are constants. The values of these constants depend (among others) on the kind of rock, its water saturation and on the direction of load in comparison with the direction of bedding or other structural elements. For limestones and marbles, he gave the values of d and c when the rocks were compressed perpendicular to bedding and parallel to bedding in air-dry condition and with water saturation (Table 60).

TABLE 60

The values of constants *d* and *c*

(after KOWALSKI, 1966)

Test Condition	*d*	*c*
Air-dry, compression ⊥ to bedding	261.1	0.358
Air-dry, compression ∥ to bedding	177.2	0.260
Water-saturation, compression ⊥ to bedding	127.5	0.444
Water-saturation, compression ∥ to bedding	111.1	0.041

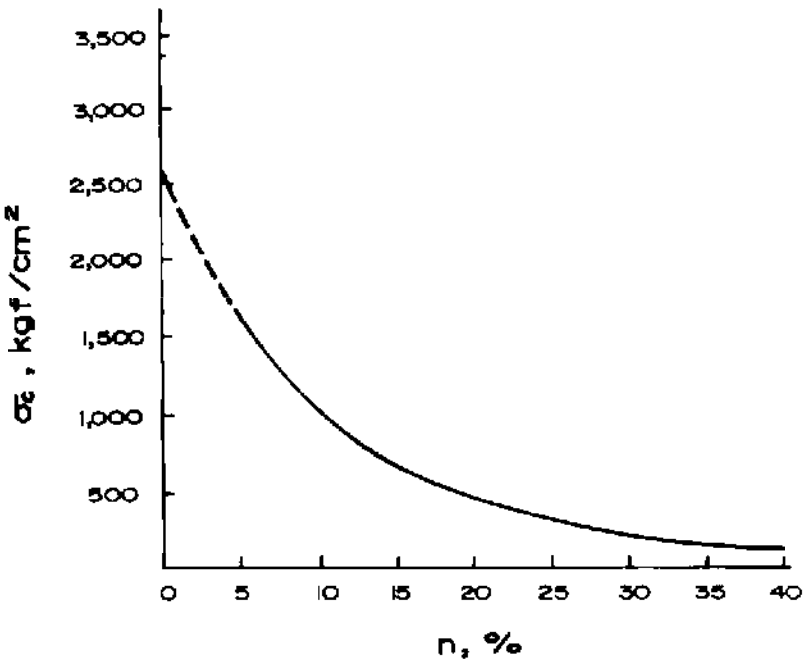

Fig. 12-15. Porosity, n versus compressive strength, σ_c for carbonate rocks (after SMORODINOV et al, 1970).

SMORODINOV et al (1970) reported the relationships between compressive strength and porosity of various rocks. For a group of carbonate rocks, the relationship is given in Fig. 12-15. The equation for the curve is

$$\sigma_c = 2590\, e^{-0.09\, n} \tag{12.27}$$

where n = porosity.

The correlation equation for the relationship between compressive strength and porosity of quartz rocks is the following:

$$\sigma_c = 3500\, e^{-0.108\, n} \tag{12.28}$$

The plot of this relationship is shown in Fig. 12-16.

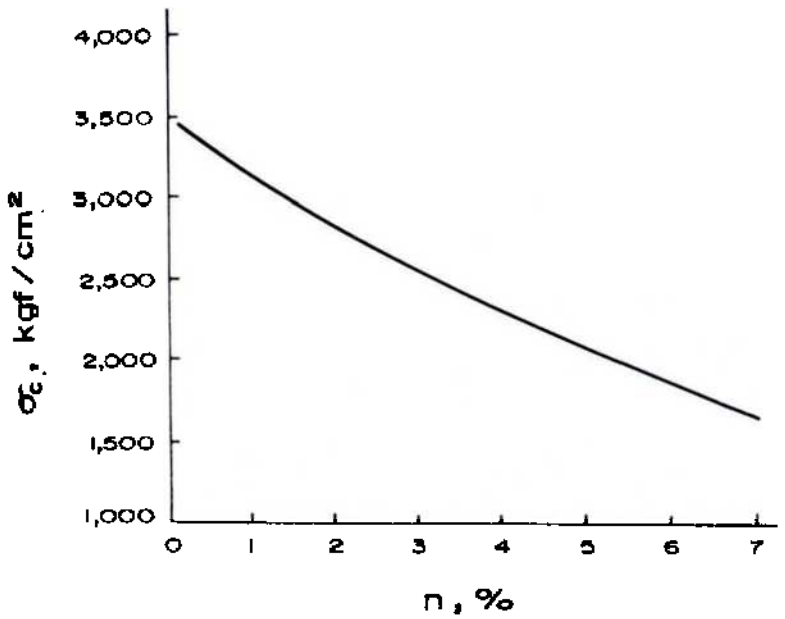

Fig. 12-16. Porosity, n versus compressive strength, σ_c for quartz rocks (after SMORODINOV et al, 1970).

RZHEVSKY and NOVIK (1971) reported the relationship (Fig. 12-17) of the nature

$$\sigma_{cn} = \sigma_{co}(1\text{-}An)^2 \tag{12.29}$$

In particular, for the limestones of the Korobcheyev deposit

$$\sigma_c = 1220\,(1\text{-}2.7n)^2 \tag{12.30}$$

The experimental data available show that the parameter A for rocks may vary within the limits of 1.5 and 4.

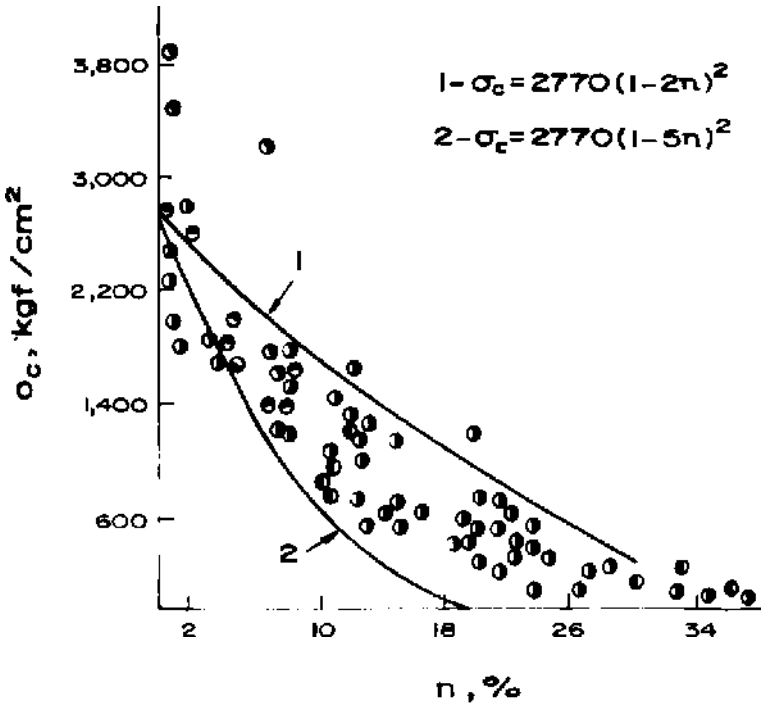

Fig. 12-17. Porosity, n versus compressive strength, σ_c for carbonates
1 and 2 – limiting curves
(after RZHEVSKY and NOVIK, 1971).

DUBE and SINGH (1972) reported the effect of porosity on tensile strength (Brazilian test) of dry and saturated sandstone (Fig. 12-18). In both cases, tensile strength decreased as the porosity of sandstone increased.

RAMANA and VENKATANARAYANA (1971) reported the effect of porosity on wave velocity (Fig. 12-3). The wave velocity decreases exponentially with increasing porosity.

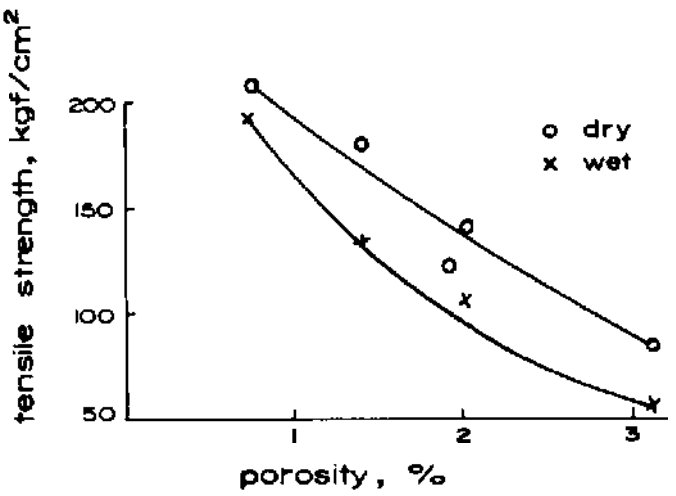

Fig. 12-18. Effect of porosity on tensile strength of sandstone
(after DUBE and SINGH, 1972).

For similar rocks, density and porosity are related. In the case of Palaeozoic sandstones of Arkansas, BRANNER (1937) showed that the densities of 82 samples varied between 2.1 and 2.7 g/cm^3, and the porosities between 0 and 22.5%. The distribution of his plotted points is found to be substantially linear and the empirical relationship between the two is

$$n = 104 - 40\,\rho \tag{12.31}$$

where n = porosity, %
ρ = density, g/cm^3.

DAVIS (1954) also found a linear relationship in testing 370 samples from other localities, which indicates the equation:

$$n = 106 - 40\,\rho \tag{12.32}$$

Some other authors have obtained slightly different relationships though the nature of the relationship still remains linear.

Analysis of data compiled by DALY et al (1966) on sedimentary rocks (sandstone, limestone, dolomite, chalk, marble, shale, claystone, slate, sand, clay, gravel, alluvium and soils) gave the following equation with a correlation coefficient of -0.9648.

$$n = 146.14 - 53.92\,\rho \tag{12.33}$$

When only sandstone was considered, the correlation coefficient improved slightly to -0.9674 with the following relationship

$$n = 157.93 - 59.39\,\rho \tag{12.34}$$

Analysis of data reported by RAMANA and VENKATANARAYANA (1971) gave the following equation with a correlation coefficient of -0.9468.

$$n = 96.49 - 32.29\,\rho \tag{12.35}$$

12.4. Water Content

The water content of a rock is the quantity of water in the rock pores expressed as a percentage of the mass of a perfectly dry rock specimen.

In order to determine the natural water content, the sample is paraffinised immediately after separation from the place of sampling.

The natural water content is calculated as the difference in the masses of the original and the dried samples, referred to the dry mass and expressed in percent.

The determinations are made as follows: The paraffin is peeled off and two small portions of rock are taken from the centre of the sample. The masses of the portions are determined immediately after extraction. The samples are then dried to constant mass at 105 C (221 F) and masses determined again.

The calculations are made using the relationship

$$w = \frac{m_s - m}{m} \times 100 \tag{12.36}$$

where w = water content, %
m_s = mass of the moist rock and
m = dry mass.

Saturation moisture can be calculated by drying, placing the specimen in a vacuum chamber and then introducing water into the vacuum chamber in which the specimen is placed. The time period for which a specimen is allowed to remain in water is very critical. Certain rocks may get saturated in a couple of hours while others may need 5 or more days. Under such conditions, it is preferable to apply water under pressure 15 MPa (2200 lbf/in^2) (150 atmospheres) for 24 hours and then determine the mass of the moist rock. The complete saturation moisture content can be calculated using the Eq. 12.36 as above.

A definite relationship exists between the saturation moisture content and bulk density of the rock. For crystalline rocks, it is more or less linear.

12.5. Void Index

Void index is defined as the mass of water contained in a rock sample after a one hour period of immersion, as a percentage of its initial desiccator-dry-mass (I.S.R.M., 1972). It is nothing but a measure of porosity of the rock and is extensively used as the primary characteristic of rock material in engineering. Void index should only be determined for rocks that do not appreciably disintegrate when immersed in water.

The method suggested by International Society for Rock Mechanics (1972) is given below:

The test requires the following apparatus:

(a) A sample container of non-corrodible material, water tight and of sufficient capacity to contain the sample packed in dehydrated silica gel.

(b) A quantity of dehydrated silica gel.

(c) A balance of adequate capacity, accurate to 0.5 g (0.001 lb).

The test procedure is as follows: A representative sample is selected comprising at least ten rock lumps, each having a mass of at least 50 g (0.1 lb), to give a total sample mass of at least 500 g (1 lb). The sample in an air-dry condition is packed into the container, each lump separated from the next and surrounded by crystals of dehydrated silica gel. The container is left to stand for a period of 24 hours. The container is emptied, the sample removed, brushed clean of loose rock and silica gel crystals and its mass A measured to 0.5 g (0.001 lb). The sample is replaced in the container and water is added until the sample is fully immersed. The container is agitated to remove bubbles of air and is left to stand for a period of one hour. The sample is removed and surface-dried using a moist cloth, care being taken to remove only surface water and to ensure that no fragments are lost. The mass B of surface-dried sample is measured to 0.5 g (0.001 lb).

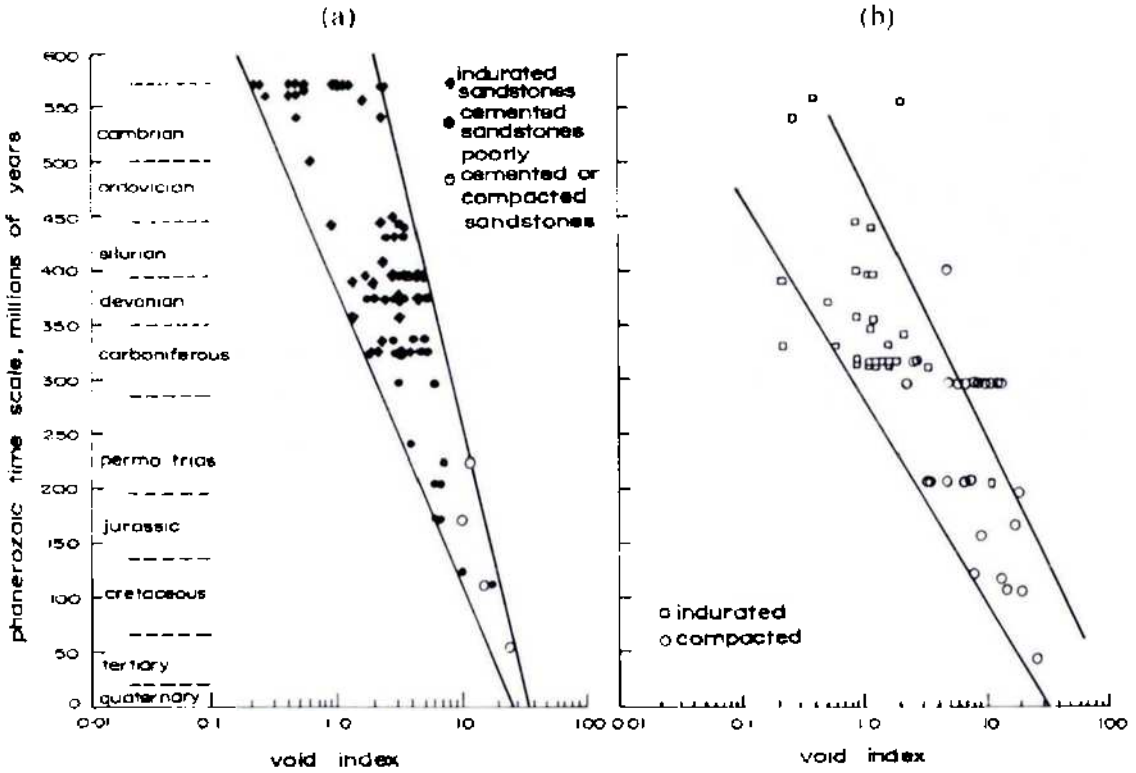

Fig. 12-19. (a) Void index versus age of sandstones
(b) Void index versus age of shales, marls, mudstones, etc.
(after DUNCAN et al, 1968).

The void index, I_v, is calculated from the relationship

$$I_v = \frac{B-A}{A} \times 100\% \tag{12.37}$$

The results of the void index test should be reported to the nearest 1% and the report should specify that the void index has been determined as the water content after desiccator drying followed by a one-hour period of immersion.

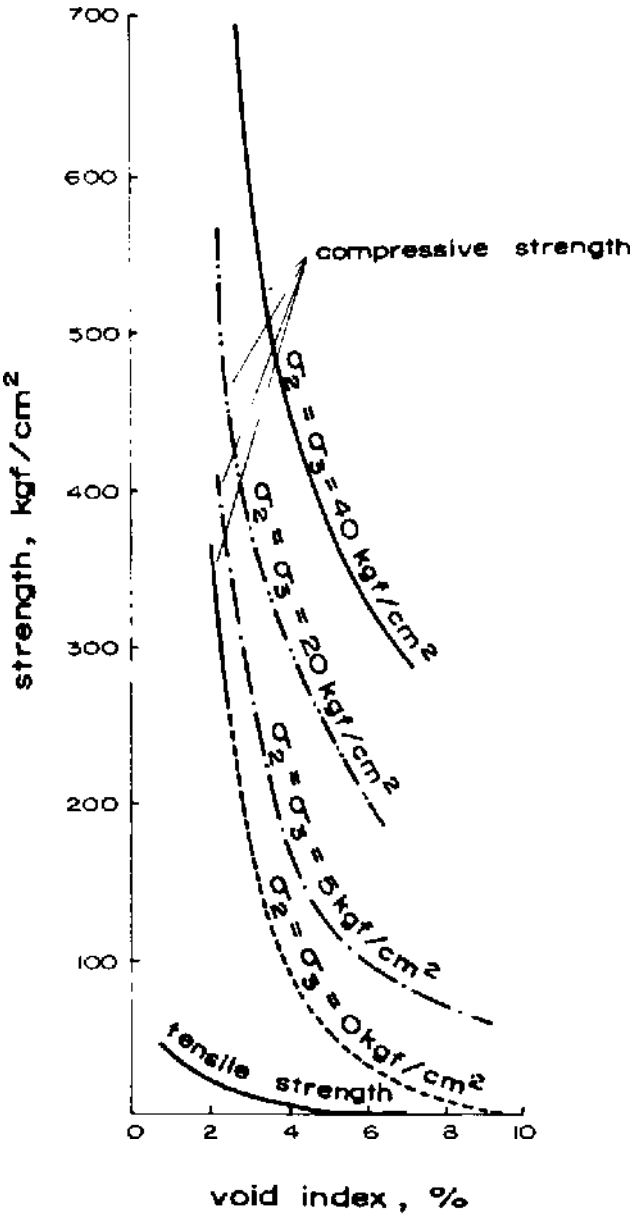

Fig. 12-20. Void index versus compressive and tensile strengths of granite (after SERAFIM and LOPES, 1962).

Void index is also sometimes called the index of alteration and depends upon the type and age of rock material. For sandstones, shales, marls, mudstones, etc., the relationships between void index and age of rock are given in Fig. 12-19 (DUNCAN et al, 1968). There seems to be a remarkable correlation between them.

SERAFIM and LOPES (1962) correlated the void index values of granite with the compressive strength measured in uniaxial and triaxial tests. There is also correlation between void index and tensile strength. Fig. 12-20 gives the results.

There is also a straight-line correlation between the laboratory-determined seismic velocity and the void index. Results of DUNCAN et al (1968) are given in Fig. 12-21.

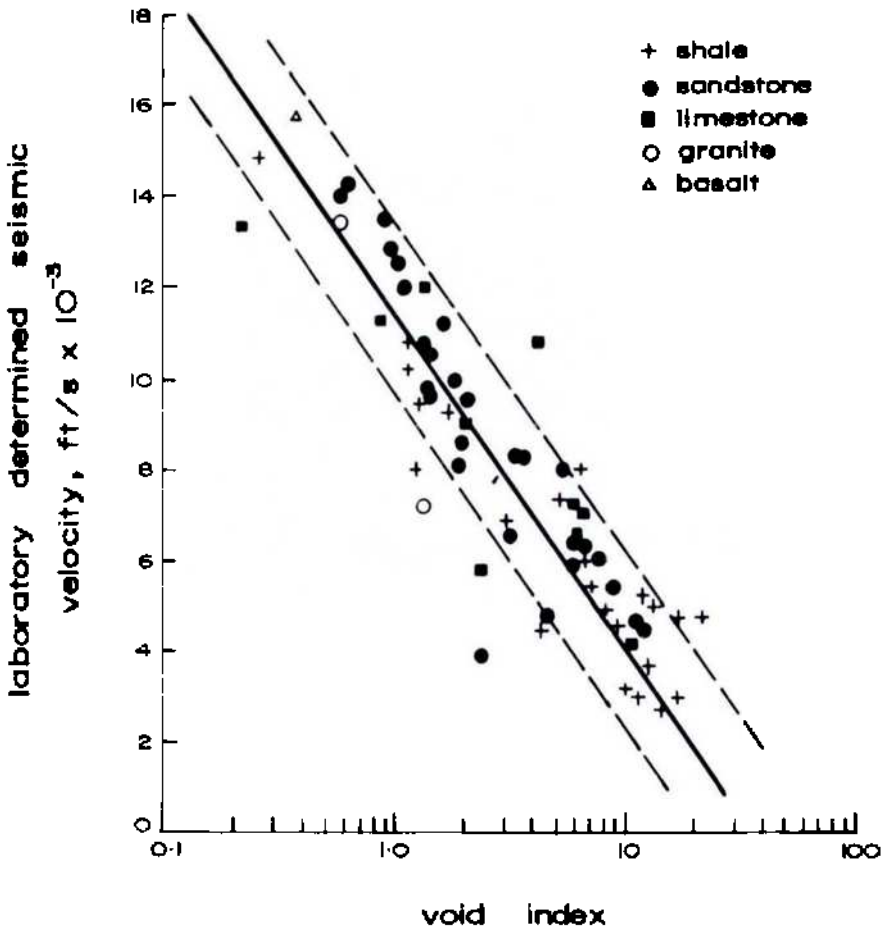

Fig. 12-21. Laboratory determined seismic velocity versus void index (after DUNCAN et al, 1968).

12.6. Permeability

Rocks are permeable to the passage of fluids by virtue of their porosities. Certain rocks (e.g. volcanic glasses) may, however, be porous without being permeable, as in the case of sealed pores. Permeability, therefore, is an expression of the freedom of fluid motion within or through a porous body. The porosity of a rock influences the permeability, but there may not be any quantitative relationship between them, for two rocks (e.g. clay and gravel) may have equal porosities but different permeabilities. However, for sandstones, carbonates and limestones, straight-line relationships (Fig. 12-22) were reported between permeability and porosity (RZHEVSKY and NOVIK, 1971). For oil sands, permeability and grain diameter bear a parabolic relationship (NUTTING, 1930).

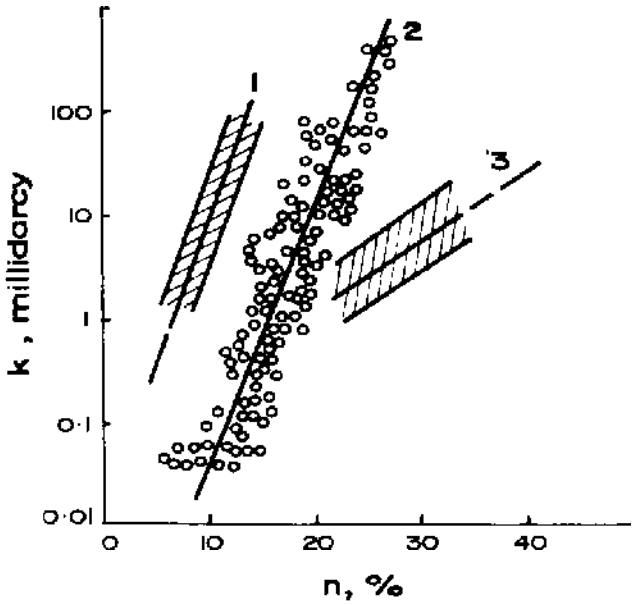

Fig. 12-22. Correlation graph showing dependence of the coefficient of permeability, k on porosity, n of rocks: 1–sandstones; 2–carbonate deposits; 3–Devonian chalky limestone (the zones of scatter of points are hatched) (after RZHEVSKY and NOVIK, 1971).

The following three units are commonly used for permeability:

Darcy: Through a rock of 1 darcy, a fluid of 1 centipoise viscosity (water has 1 centipoise viscosity at 68 °F (20 °C)) moves at the rate of 1 cm per second under a pressure gradient of 1 atmosphere per cm (1034 cm of water at the same temperature). This unit is used by petroleum engineers.

Velocity of flow: Through a rock of unit permeability, water of 1 centipoise viscosity moves 1 cm per second at 100% gradient. Note that this rate of flow

is the same as stated in defining the darcy, though in this case the gradient is 1 : 1 rather than 1034 : 1. The term 'Velocity of flow' is most commonly used in civil engineering, engineering geology and soil mechanics.

Meinzer unit: Through a rock of 1 Meinzer unit, 1 gallon per day of water at 60 °F moves through each square foot of cross-section at a 100% gradient. This unit is used by hydrologists and civil engineers in the United States.

TABLE 61

Coefficients of permeability (to water) of various rock materials and rock masses

(after SERAFIM, 1968)

Rock material	k (cm/s) (lab. determination)
Sandstone (Cretaceous flysch)	10^{-8} to 10^{-10}
Siltstone (Cretaceous flysch)	10^{-8} to 10^{-9}
Granite	5×10^{-11} to 2×10^{-10}
Slate	7×10^{-11} to 1.6×10^{-10}
Breccia	4.6×10^{-10}
Calcite	7×10^{-10} to 9.3×10^{-8}
Limestone	7×10^{-10} to 1.2×10^{-7}
Dolomite	4.6×10^{-9} to 1.2×10^{-8}
Sandstone	1.6×10^{-7} to 1.2×10^{-5}
Hard mudstone	6×10^{-7} to 2×10^{-6}
Black schists (fissured)	10^{-4} to 3×10^{-4}
Fine-grained sandstone	2×10^{-7}
Oolitic rock	1.3×10^{-6}
Bradfort sandstone	2.2×10^{-5} to 6×10^{-7}
Glenrose sandstone	1.5×10^{-3} to 1.3×10^{-4}
Altered granite	0.6 to 1.5×10^{-5}
Rock mass	**(in situ determinations)**
Arterite migmatites	3.3×10^{-3}
Chloritized arterites and shales	0.7×10^{-2}
Gneiss	1.2×10^{-3} to 1.9×10^{-3}
Pegmatoid granite	0.6×10^{-3}
Lignite layer	1.7×10^{-2} to 23.9×10^{-2}
Sandstone	10^{-2}
Mudstone	10^{-4}
Oocene limestone	10^{-2} to 10^{-4}

A rock having a permeability of 1 darcy, has permeability of 18.2 Meinzer units and 9.7×10^{-4} cm/s.

Certain authors use Lugeon as the measure of the in situ permeability of rock. This is derived after the name of the French engineer who devised the pump-in test using a single bore hole to determine the groutability of rock. A rock mass is considered to accept grout if it has permeability of 1 Lugeon which represents flow of 1 litre of water per minute through a bore hole of 1 metre length at a pressure of 10 kgf/cm^2 (0.98 MPa).

The range of variation of permeabilities of rocks is very large. MUSKAT (1949) reported permeabilities of commercial oil- or gas-bearing sandstones from 5 to 5000 millidarcys (1 millidarcy = 0.001 darcy). Permeabilities to water of various rock materials and rock masses compiled by SERAFIM (1968) are given in Table 61. Permeability determined in situ may be 1,000 to 10,000 times higher than that obtained from tests in the laboratory. The method used for determination of permeability will depend upon the rock type. Some of the most commonly used methods are given below.

12.6.1. Laboratory Tests for Determination of Permeability of Rock Specimens

Permeability is measured by a variety of methods. In all these methods, some fluid is passed under pressure through a rock specimen held fast in a metal ring by a rubber gasket. The pressure is measured at the entrance to and the exit from the specimen; the run length is recorded and the quantity of seeping fluid is determined (its viscosity is known). The permeability is calculated using the following relationship:

$$k = \eta \frac{q}{A} \frac{l}{(p_i - p_0)} \tag{12.38}$$

where k = permeability, darcy
η = viscosity of the fluid at the temperature of the experiment, centipoise
q = quantity of the fluid seeping through the specimen in one second, cm^3/s
l = length of the specimen, cm
A = cross-sectional area of the specimen perpendicular to direction of flow, cm^2
p_i = absolute pressure at the point of entrance to the specimen, atmosphere and
p_0 = absolute pressure at the point of exit from the specimen, atmosphere.

Specimen preparation

The preparation of the specimen for permeability test is a very important phase of the test. Depending upon the test procedure adopted, the sample is cut to required dimensions using a flushing liquid (usually water). Before cutting of the sample, the sample should be saturated with the fluid to prevent mudding of the forces due to capillary effects. Failure to saturate the sample results in blocking of the pores with the mud and causes serious reduction of permeability. In case it is not possible to cut the sample, the specimen may be moulded as is the usual practice in soil mechanics. The samples containing oil should be treated to remove all traces of oil as far as possible. This is best done by fitting the sample in a 10 to 15 cm (4 to 6 in) long tube and inserting the tube into the Soxlet extraction apparatus using carbon tetrachloride or benzol as a solvent with the sample end downwards. It may be pointed out that depending upon the sample size and its porosity, a considerable time is usually required to free it from contained oil.

Determination of air permeability

Cylindrical specimens, 2 cm (1 in) in diameter and 2 to 3 cm (1 in) long, are usually used for permeability measurements. To calculate permeability of a cylinder, the dimensions of length and cross-section may be measured directly by calipering or by measuring the length and computing the cross-sectional area by dividing the bulk volume by the length. These measurements are taken before the specimen is used for its permeability measurement. If the specimen is to be mounted in plastic or pitch, it must be measured before mounting. However, if a mounted core is cut or sectioned to clean its ends, the length must be remeasured after cutting.

The clean specimen is placed in an appropriate holder in the permeameter so that any bypassing of air around the sides of the specimen or the mounting is eliminated (Fig. 12-23). Dry clean air is passed through the core and the rate of flow of the air determined from the pressure difference across a calibrated orifice or other suitable flow-rate measuring device. The differential pressure across the specimen may be adjusted to give appropriate or convenient rates of flow. The inlet air pressure and the air flow rates are recorded. From these measurements and the specimen dimensions, the dry-air permeability may be calculated from the equation (12.39) using appropriate viscosity value for the air at the temperature of the test.

If q is the rate of flow of outlet air, referred to mean pressure in the system i.e. $\left(\frac{p_i+p_0}{2}\right)$, the air permeability is given by

$$k = \frac{2q_0p_0l\eta}{(p_i^2-p_0^2)A} \tag{12.39}$$

where k = permeability, darcy
η = viscosity of air, centipoise
q_0 = rate of flow of air in the system at the outlet, cm^3/s
l = length of the specimen, cm
A = cross-sectional area of the specimen perpendicular to direction of flow, cm^2
p_i = absolute air pressure at the point of inlet to the specimen, atmosphere and
p_0 = absolute air pressure at the point of outlet from the specimen, atmosphere.

For convenience in applying the proper values of viscosity at various temperatures, Table 62 gives viscosity of air at various temperatures.

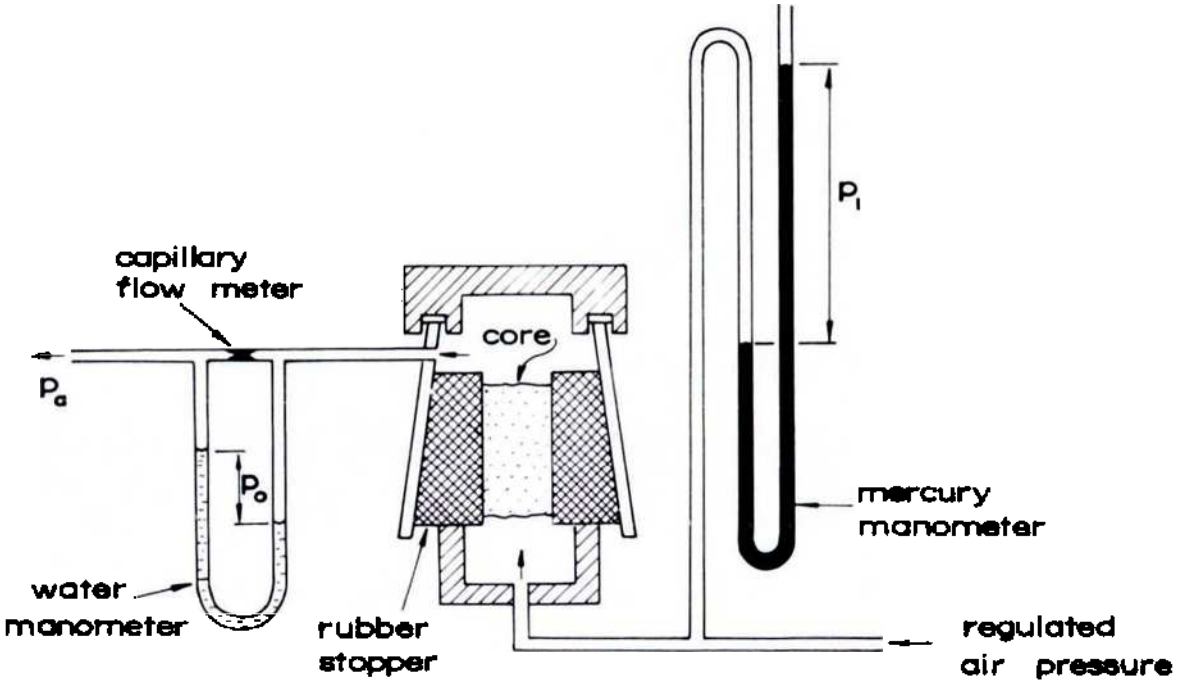

Fig. 12-23. Schematic diagram of permeability – measuring apparatus (after PIRSON, 1958).

TABLE 62

Viscosity of air

Temp., C	Viscosity, centipoise
0	0.01709
10	0.01759
20	0.01808
30	0.01856
40	0.01904
50	0.01951

When permeability is required in a radial direction (permeability is a highly directional property), cylindrical cores with a central hole are used with the end faces sealed and the cylindrical walls open. Computation of radial permeability is then obtained from the following equation:

$$k = \frac{\eta q_0 ln\left(\frac{r_0}{r_i}\right)}{\pi l\,(p_i^2 - p_0^2)} \tag{12.40}$$

where k = permeability, darcy
η = viscosity of air, centipoise
q_0 = rate of flow of outlet air, cm^3/s
r_0 = outer radius of specimen, cm
r_i = inside radius of hole, cm
l = axial length of core, cm
p_i = absolute pressure at the inlet, atmosphere and
p_0 = absolute pressure at the outlet, atmosphere.

Determination of liquid permeability

Liquid permeability determinations are infrequently made in petroleum industry to determine the oil flow characteristics of the rocks essential in well design. Due to the time required to fully saturate the specimen and establish steady state flow, and the difficulty of finding a liquid which is completely inert with respect to the rock, the method requires careful planning. Water permeability determinations are commonly made by civil engineers, engineering geologists and hydrologists as a routine test in all minor and major works.

Basically, the two permeability tests i.e. longitudinal and radial, are used. Cylindrical specimens of diameter 60 mm (2.5 in) and length varying up to 150 mm (6.0 in) are used. Pressure gradients up to 1 in 1000 are used in the laboratory, whereas gradients of only 1 in 10 are usual in situ to obtain measurable rate of percolation.

Longitudinal percolation test: Some laboratories use the apparatus derived from conventional soil-testing equipment (Fig. 12-24), where the rock specimen is encapsulated in an epoxy resin, with the object of preventing leakage along the external cylindrical face of the specimen. Under practical conditions this is not always possible, and in addition it is difficult to remove the epoxy coating when the specimen is required for further tests.

The apparatus shown in Fig. 12-25 was developed by the Paris Laboratory where the specimen is protected with a plastic coating and immersed into water under pressure. The radial component of the water pressure being

greater to the pressure in the specimen itself, no water can seep along the cylindrical face. This apparatus is much simpler and it requires less time for preparation.

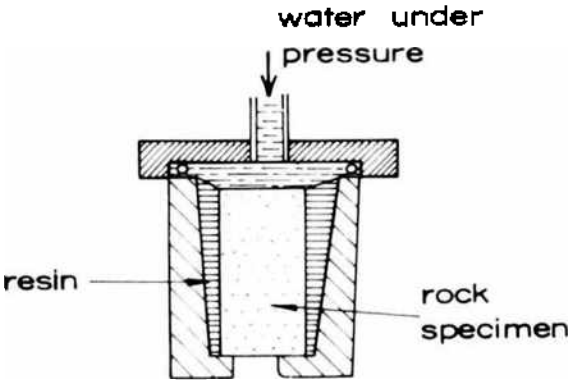

Fig. 12-24. Longitudinal percolation test (after JAEGER, 1972).

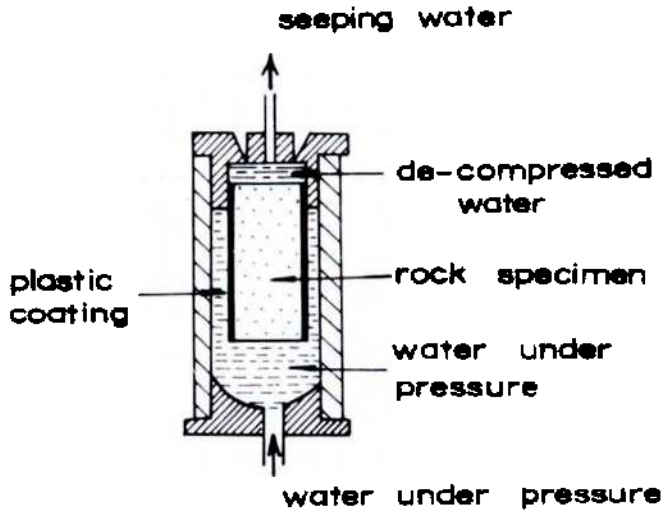

Fig. 12-25. Longitudinal percolation test developed by Paris Laboratory (after JAEGER, 1972).

The longitudinal percolation test cannot be applied to very impervious rocks, the permeability limit being about 10^{-8} cm/s.

Radial percolation tests: Cylindrical specimens, 60 mm (2.5 in) diameter and 150 mm (6.0 in) long with a central hole of 12 mm (0.5 in) diameter drilled from one end to a depth of 125 mm (5.0 in) are used. The open end is closed by a tube 25 mm (1.0 in) long (Fig. 12-26).

The specimen can either be introduced into a cell containing water under pressure, the central cavity remaining connected to atmospheric pressure, or

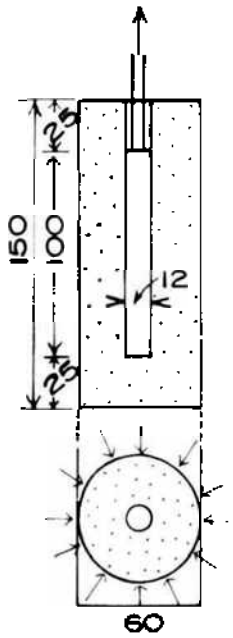

Fig. 12-26. Standard rockspecimen prepared for radial percolation tests (dimensions in mm) (Paris Laboratory) (after JAEGER, 1972).

water can be injected under pressure inside the specimen. The water will percolate across the rock and the flow being radial over almost the whole height of the specimen, this test is called 'radial percolation test'. When water pressure is applied to the exterior side of the cylinder, the flow is convergent and when water is under pressure inside the specimen, the flow is divergent.

If p is the percolation pressure and l is the length of inside hole (disregarding the ends), the flow rate q across a coaxial cylinder of radius r is:

$$q = k 2\pi r l \, (dp/dr) \tag{12.41}$$

taking the viscosity of water as 1 centipoise.
Rewriting equation (12.41)

$$\frac{dr}{r} = k \frac{2\pi l}{q} dp$$

After integration over the whole length of the path taken by the water (between r_i and r_0) this equation becomes

$$ln \frac{r_0}{r_i} = k \frac{2\pi l}{q} p$$

$$k = \frac{q}{2\pi l p} ln \frac{r_0}{r_i} \tag{12.42}$$

When pressure is applied to the exterior side of the specimen, all the internal stresses are compressive. When pressure is applied inside the specimen, all the internal stresses are tensile. By testing under both conditions of flow, it is possible to compare the permeability obtained for the same specimen under tensile stress field with that under compressive stress field.

Radial percolation under variable stress: In the simple radial percolation tests described above, the stress on the specimen cannot be varied independently of the applied pressure. Fig. 12-27 explains the method where the stress on the cylindrical specimen is different from the test pressure. The specimen which is the same as used for the simple radial percolation test is surrounded by a thin layer of a very permeable powdery material which is kept in place by a plastic sleeve. The specimen so prepared is enclosed in a cell in which the pressure p_1 is maintained.

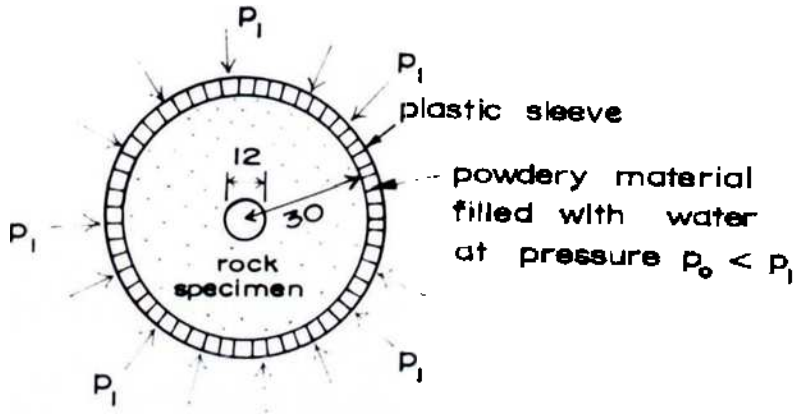

Fig. 12-27. Radial percolation test under a pressure $p_1 > p_0$ (p_0 = water pressure, dimensions in mm)
(after JAEGER, 1972).

If water penetration is at a pressure $p_0 < p_1$, the water will percolate through the specimen under that pressure. The powdery material in this case will now transmit the pressure $p_1 - p_0$ to the specimen.

A series of tests can be carried out either by maintaining p_1 constant and varying p_0 or by maintaining p_0 constant and varying p_1. These tests have shown that the permeability coefficient decreases more rapidly under an increasing stress p_1 than under an increasing water pressure p_0. This method produces similar stress conditions to those existing, for example, in the rock abutment under a dam where p_1 and p_0 are independent.

This test is very informative, but is time consuming. JAEGER (1972) suggested that the ordinary radial percolation tests (convergent as well as divergent) should be considered as standard and results be summarised as follows:

A diagram showing the frequencies of the value k_0, obtained for a pressure $p_0 = 0$ (point of intersection of the curve $k = k(p)$ with the ordinate $p = 0$ on the diagrams) for a number of tests should be drawn illustrating the homogeneity of the specimens tested.

The parameter

$$s = \frac{k_{-1}}{k_{50}} \tag{12.43}$$

where k_{-1} = permeability for divergent flow under a pressure of -1 kgf/cm^2 and
k_{50} = permeability for converging flow under a pressure of 50 kgf/cm^2

should be calculated which gives the influence of convergent and divergent flows and an indication of the stress field on the permeability. This result should be reported along with the permeability test of rock at different confining pressures.

Results: HABIB and VOUILLE (1966) tested, among other rocks, limestone and hard sandstone containing spherically shaped voids and observed no change in permeability with pressure in the longitudinal flow tests. With a microfractured quartz containing parallel fractures as well as a stratified hard schist, permeability decreased with pressure.

Many other investigators (FATT and DAVIS, 1952; FATT, 1953; MCLATCHIE, HEMSTOCK and YOUNG, 1958; WYBLE, 1958; GRAY, 1962) also reported the influence of confining pressure on permeability. MCLATCHIE, HEMSTOCK and YOUNG (1958) reported an inverse correlation between true permeability and amount of permeability reduction under moderate confining pressure and a direct correlation between clay content and permeability reduction. WYBLE (1958) and GRAY (1962) also investigated the direction heterogeneity in permeability values. WYBLE (1958) found that the reduction in permeability in certain samples of sandstones was greater in vertical direction than in horizontal direction while the results of GRAY (1962) show greater reduction in horizontal direction than in vertical direction.

Fig. 12-28 indicates variations of the coefficient of permeability of four rocks as measured by radial flow across rock cores with a central hole (LONDE and SABARLY, 1966). It is seen that permeability for these rocks is not sensitive to pressure at the pressures investigated. It is, however, important to note that at higher pressures, there may occur cracking of the specimens and this critical pressure will then raise the permeability. Decrease in permeability is an indication of the closure of the cracks and pore space compressibility which is further a function of amount and type of the cement binding the grains, and also decrease in tortuosity (MORLIER, 1971).

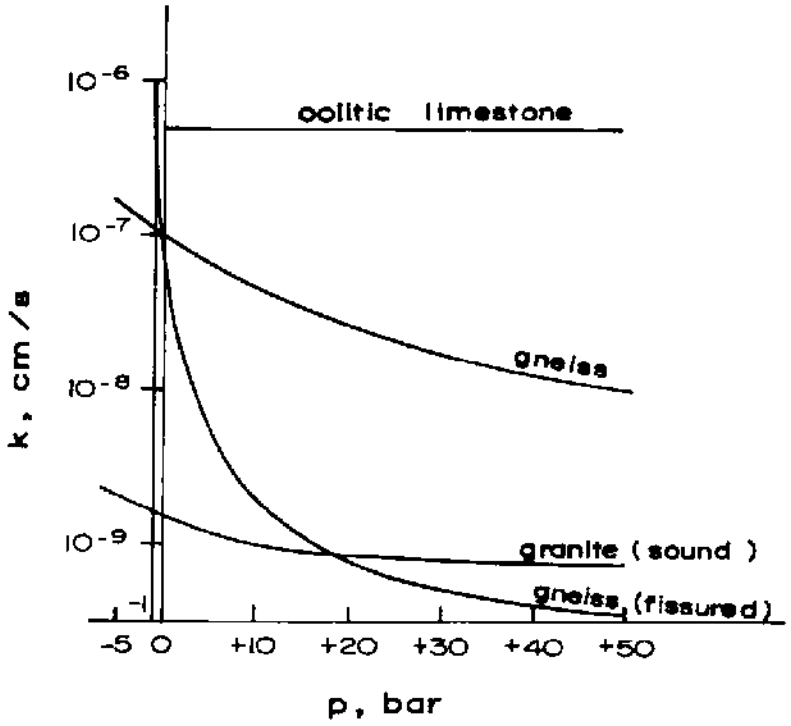

Fig. 12-28. Results of radial percolation test (after LONDE and SABARLY, 1966).

The decrease in the permeability is also dependent upon the shape and orientation of the pores and cracks with respect to the major stress direction. When rock contains spherical connected openings, the permeability obtained from cores drilled in different directions are independent both of the pressure and the direction.

Rocks show permeability hysteresis (Figs. 12-29 and 12-30) which has been reported by many investigators (KNUTSON and BOHOR, 1962; JAEGER, 1972; SARIDA, LETIRANT and BARON, 1974). This seems to be an indication of the internal changes namely grain rupture and pore collapse that take place in the specimen. If the pores are spherical, there is much less likelihood of these changes taking place when the specimen is subjected to a hydrostatic pressure in a bomb. An idea of the shape and orientation of the pores can be obtained by determining the change in directional permeability if oriented cores are subjected to different hydrostatic pressures and their permeabilities determined afterwards.

Change in stress field from $+ve$ to $-ve$ results in opening out of the cracks at right angles and hence a sudden increase in permeability (Fig. 12-30).

The influence of temperature on the permeability has been studied by AFINOGENOV (1969) on certain rocks and found a decrease in permeability with rise in temperature. The decrease in value is rather small and he associates it with the decreasing modulus of elasticity of the rocks with rise in temperature.

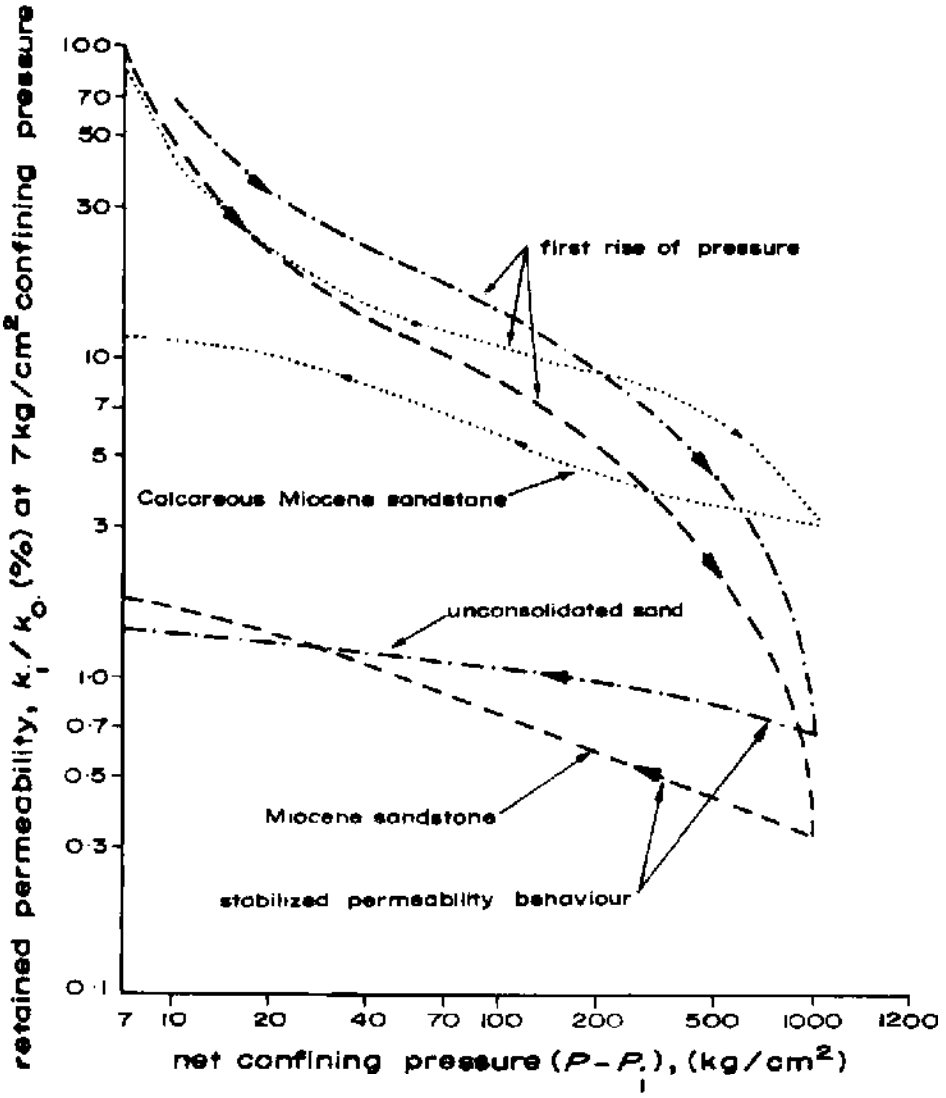

Fig. 12-29. Permeability of sandstones versus net confining pressure (after KNUTSON and BOHOR, 1962).

In certain rocks such as Precambrian cherts, the permeabilities may be of the order of 10^{-2} to 10^{-7} millidarcy (SANYAL, KVENVOLDEN and MARSDEN, 1971). The measurement of such low values requires high upstream pressures. SANYAL et al (1972) have developed a liquid permeameter where the high pressure is developed by a pump based upon the thermal expansion of the liquid to increase pressures up to 60 MPa (10,000 lbf/in^2) and maintained. The pressure is measured using a low displacement diaphram-type transducer. Permeability is measured indirectly from the decline of pressure over a period of time.

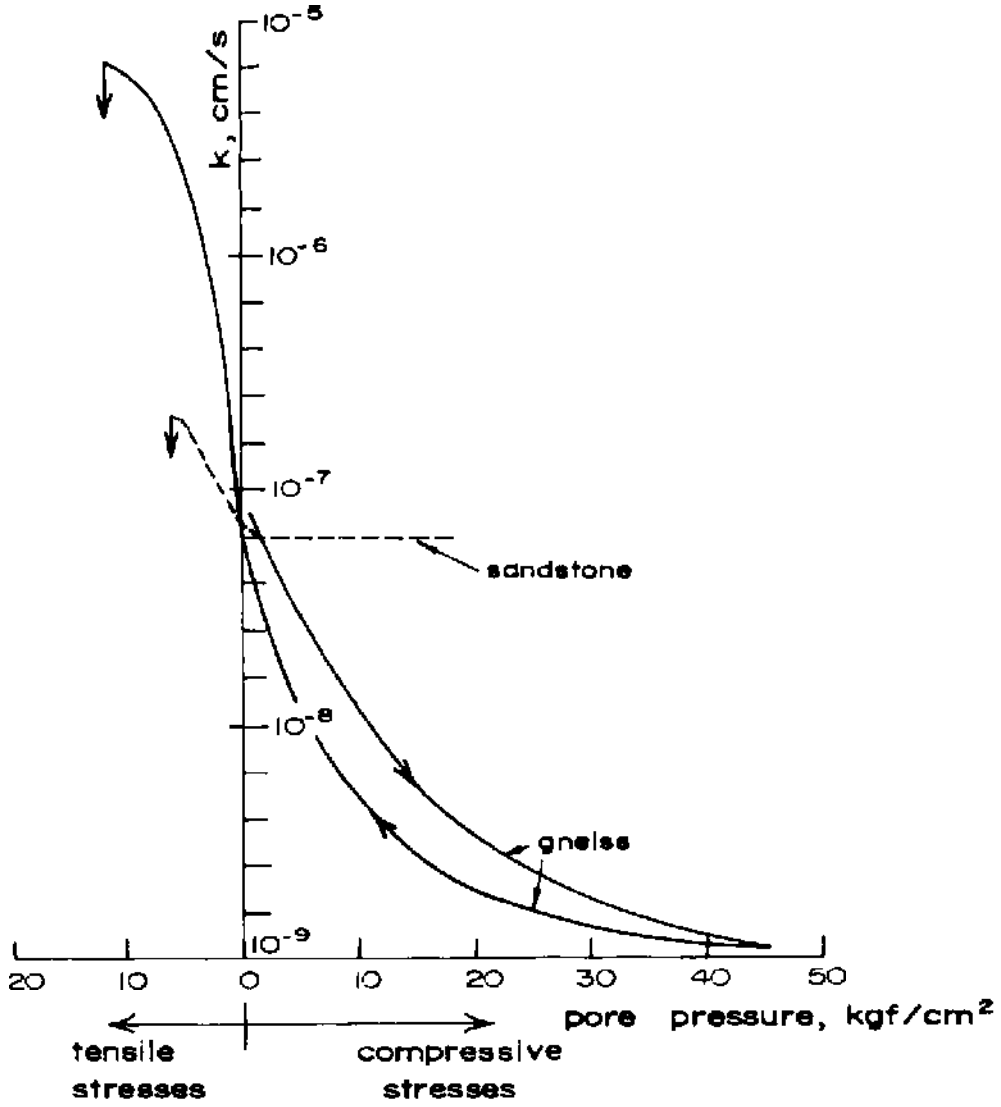

Fig. 12-30. Radial percolation tests. Results for fissured rock (gneiss) and rock with spherical voids (sandstone) (after JAEGER, 1972).

12.6.2. Permeability of Rock Masses In Situ

Laboratory tests on cores do not indicate hydraulic properties of large fractures, joints, etc. found in rock mass unless the specimens are large enough that they represent fairly well the structure of that rock mass and are subjected to the same stress field in which they lie in situ. If the structural units are large, the required size of the specimen may be formidably large. An alternative method of measuring the permeability of a large number of small samples obtained from the rock mass in different orientations may well provide an

acceptably repeatable value of the permeability, but the average may not necessarily represent the field permeability as can be readily shown with reference to a hypothetical structure (Fig. 12-31) with vertical and horizontal joints. A sample with a width of $\frac{W}{2}$ and length exceeding L can never provide a continuous flow path and the measured conductivity[1] will be zero.

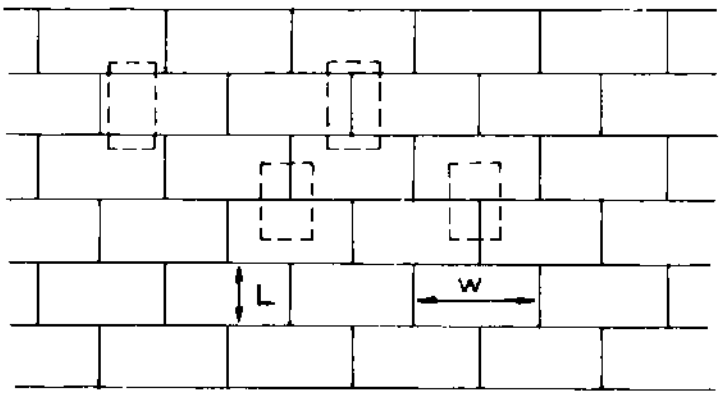

Fig. 12-31. A hypothetical structure showing that any sample of the size shown in the dotted outlines cannot truly represent the whole material. However placed, the sample will have a zero longitudinal conductivity.

In the in situ measurements for permeability, two situations may occur. Firstly, the ground is fully saturated and secondly the ground is unsaturated and saturation condition must be imposed artificially as part of the measuring technique. The two cases are discussed as under.

Saturated ground

When the ground is fully saturated, pumping tests are made to determine the permeability of strata located below the water table. The most commonly used method is the THIEM's (1906) method and is described below.

(a) THIEM's *method:* Fig. 12-32(a) is a vertical section through a stratum located between two relatively impervious strata. A bore hole is drilled to the bottom of the layer, and water is pumped from the bore hole at a constant rate until the water level in the bore hole becomes almost stationary. Once this state has been established, the permeability k is calculated from the following equation:

$$k = \frac{Q}{2\pi H (h_2 - h_1)} \ln \frac{r_2}{r_1} \tag{12.44}$$

[1] A differentiation is usually made between permeability of a porous medium and the capacity to permit fluid flow of an opening usually referred to as conductivity.

where k = permeability of the layer, cm/s
Q = quantity of water pumped, cm^3/s
H = thickness of the bed, cm
h_1 and h_2 = piezometric levels in the adjacent holes, cm and
r_1 and r_2 = distance to the adjacent holes from the pump hole, cm.

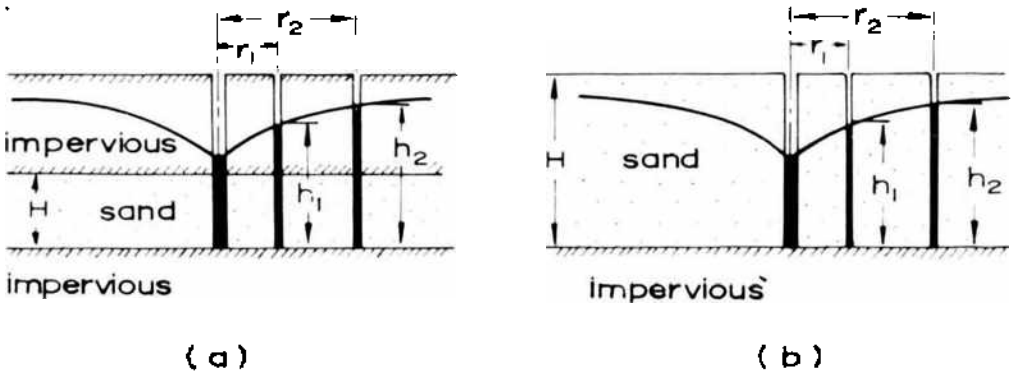

Fig. 12-32. Diagram illustrating flow of water toward bore hole during pumping test (a) if piezometric level lies above pervious layer; (b) if free water surface lies within pervious layer (after TERZAGHI and PECK, 1948).

If the free-water surface is located below the top of the stratum the permeability of which is to be measured, as shown in Fig. 12-32(b), the permeability is calculated from the following equation:

$$k = \frac{Q}{\pi (h_2^2 - h_1^2)} \ln \frac{r_2}{r_1} \tag{12.45}$$

A pumping test requires the drilling of one test bore, commonly 10 or 12 in (25 or 30 cm) in diameter, and at least 8 observation bores located on two straight lines through the centre of the test bore. One of these lines is located approximately in the direction of the ground-water flow, and the other line at right angles to it. In this way anisotropy in permeability in different directions can be determined.

(b) KIRKHAM's *method:* THIEM's method is useful only when pumping rates are high so that a certain level difference due to draw-down can be easily and accurately measured which many times require large diameter holes. In cases where the holes are drilled only for permeability studies and are to be abandoned later, it is very expensive to drill deep holes of large diameter. KIRKHAM's (1945) method is useful under such conditions. In this method a short length of perforated tube with a closely fitted rivet is driven into the ground. When the tube has reached the required depth, the rivet is hammered down using an internal plunger to the exact measured desired depth (Fig. 12-33).

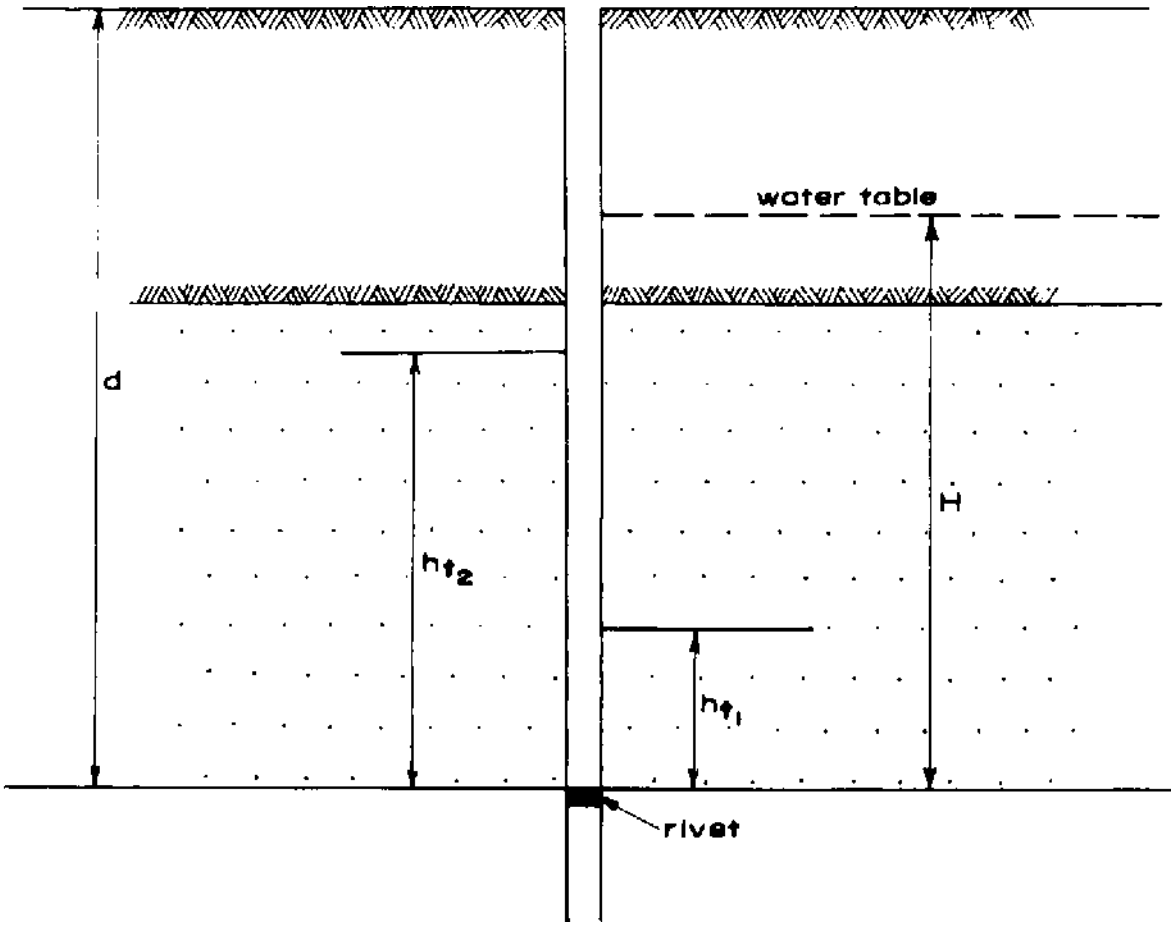

Fig. 12-33. KIRKHAM's method of determination of permeability.

The tube is left in position for some time to allow the water level rise to an equilibrium level. The level is then suddenly depressed using a high capacity bore hole pump. The level is noted and water level is recorded with time. The permeability k can be calculated from the relationship

$$k = \frac{\pi r^2}{At} ln \left[\frac{H - h_{t_1}}{H - h_{t_2}} \right] \tag{12.46}$$

where r = radius of the tube
H = height of the water table from the rivet
h_{t_1} = height of water in the tube from the rivet at the time t_1
h_{t_2} = height of water in the tube from the rivet at the time t_2
t = time interval between the two readings $(t_2 - t_1)$, and
A = proportionality constant.

The values of A as determined by SMILES and YOUNGS (1965) are given in Table 63.

TABLE 63

Piezometer shape factor A (expressed as the ratio A/r for various cylindrical cavities of length l and radius r at depths d from surface)

(after SMILES and YOUNGS, 1965)

	A/r values					
	For $l/r =$					
d/r	0	0.5	1.0	2.0	4.0	8.0
20	5.6	8.7	10.6	13.8	18.6	26.9
16	5.6	8.8	10.7	13.9	19.0	27.4
12	5.6	8.9	10.8	14.0	19.4	28.3
8	5.7	9.0	11.0	14.3	19.8	29.1
4	5.8	9.3	11.5	15.0	21.0	30.8

A more simplified relationship is given by BARRON et al (1970) for the water head above the ground water as follows:

$$k = 2.3\, r \log_{10}\left[\frac{H_1}{4H_2 t}\right] \tag{12.47}$$

where H_1 = water head over ground water level at the time t_1, cm
H_2 = water head over ground water at the time t_2, cm
t = time $(t_2 - t_1)$, s and
r = radius of the bore hole, cm.

Unsaturated ground

In unsaturated ground, water is required to be pumped into the ground. The tests are based on measuring the amount of water accepted by the ground through the open bottom of a pipe or through an uncased section of the hole. Two methods have been developed by the U.S. Bureau of Reclamation (1960, 1963) and are described below.

1. *Open-end tests:* Figs. 12-34(A) and (B) show tests made through the open end of a pipe casing which has been sunk to the desired depth and which has been carefully cleaned out just to the bottom of the casing. When the hole extends below the ground-water table, it is recommended that the hole be kept filled with water during cleaning and especially during withdrawal of tools to avoid squeezing of soil into the bottom of the pipe. After the hole is cleaned to the proper depth, the test is begun by adding clear water through a metering system to maintain gravity flow at a constant head. In tests above the water

table (Fig. 12-34(B)) a stable, constant level is rarely obtained and a surging of the level within a few tenths of a foot (~ 10 cm) at a constant rate of flow for about 5 minutes is considered satisfactory.

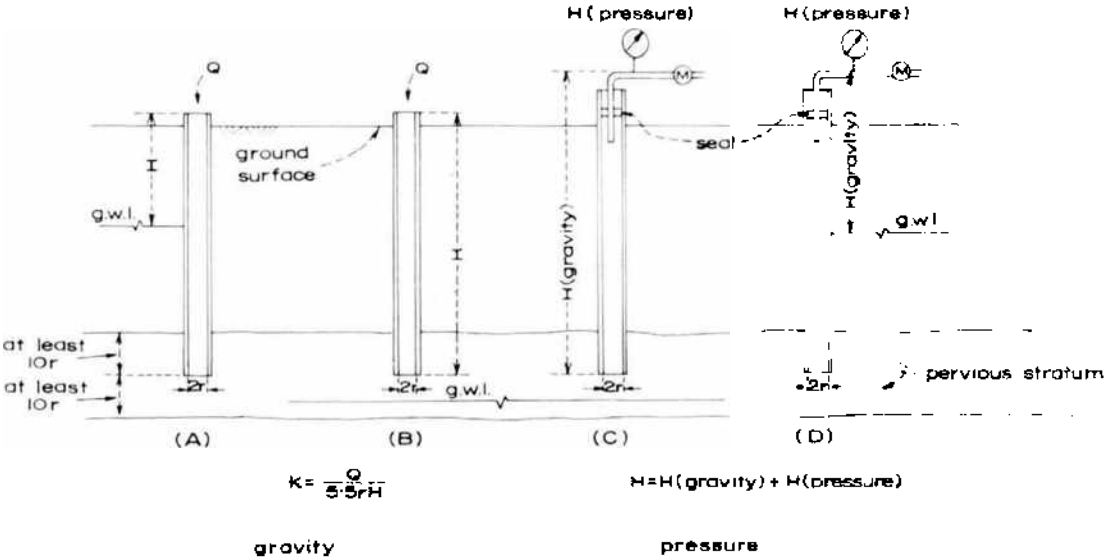

Fig. 12-34. An open-end pipe test for soil permeability (after U.S. Bureau of Reclamation, 1960 and 1963).

If it is desired to apply pressure to the water entering the hole, the pressure, in units of head, is added to the gravity head as shown in Figs. 12-34(C) and (D). Measurements of constant head, constant rate of flow into the hole, size of casing pipe, and elevations of top and bottom of casing are recorded. The permeability is obtained from the following empirical relation determined by electric analogy experiments:

$$k = \frac{Q}{5.5\,rH} \tag{12.48}$$

where k = permeability, Meinzer
Q = constant rate of flow into the hole, gallons/day
r = internal radius of casing, ft. and
H = differential head of water, ft.

The value of H for gravity tests made below water table is the difference in feet between the level of water in the casing and the ground-water level. For tests above water table, H is the depth of water in the hole. For pressure tests the applied pressure is added to the gravity head to obtain H.

2. *Packer tests:* Fig. 12-35 shows a permeability test made in a portion of a bore hole below the casing. This test can be made both above and below the

water table provided the hole remains open. It is commonly used for pressure testing of bed rock, but it can be used in unconsolidated materials where a top packer is placed just inside the casing.

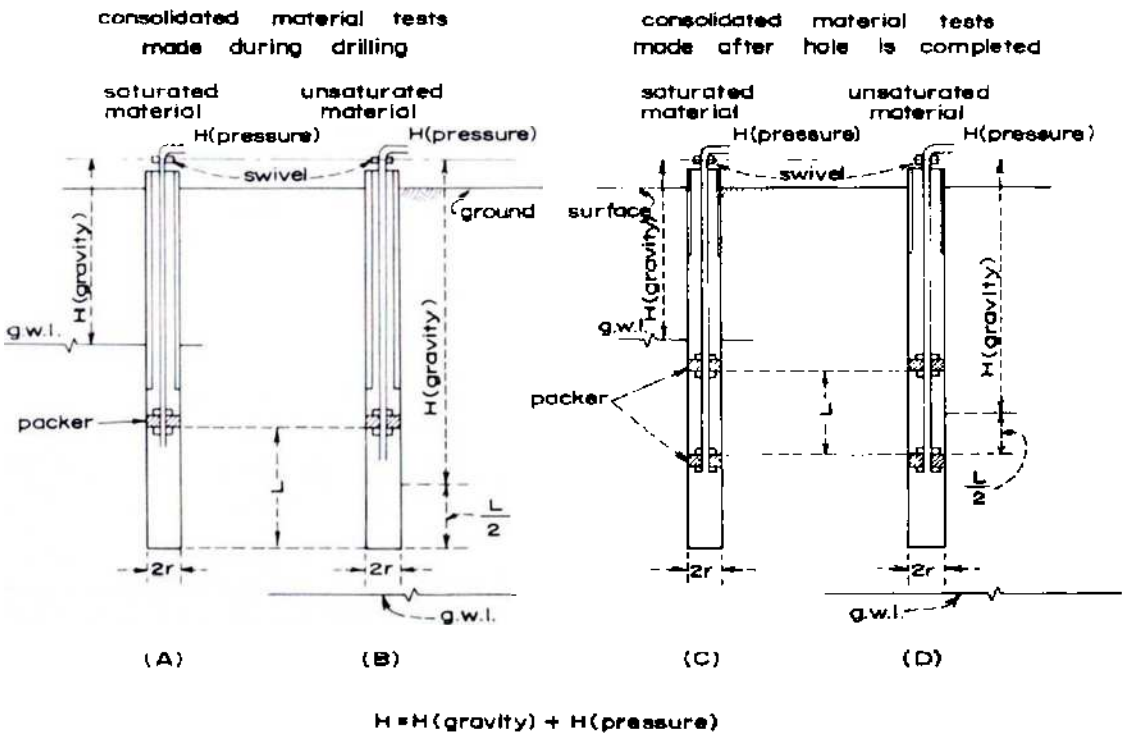

Fig. 12-35. The packer test for soil permeability (after U.S. Bureau of Reclamation, 1960 and 1963).

The formulas for this test are:

$$k = \frac{Q}{2\pi LH} \ln \frac{L}{r};\ L \geqq 10r \tag{12.49}$$

$$k = \frac{Q}{2\pi LH} \sin h^{-1} \frac{L}{2r};\ 10r > L \geqq r \tag{12.50}$$

where k = permeability
Q = constant rate of flow into the hole
L = length of the portion of the hole tested
H = differential head of water and
r = radius of hole tested.

These formulas have best validity when the thickness of the stratum tested is at least 5 L, and they are considered to be more accurate for tests below groundwater table than above it.

Where the test length is below the water table, H is the distance in feet from the water table to the swivel plus applied pressure in units of feet of water. Where the test length is above the water table, H is the distance in feet from the centre of the length tested to the swivel plus the applied pressure in units of feet of water. For gravity tests (no applied pressure) measurements for H are made to the water level inside the casing (usually the level of the ground).

The usual procedure is to drill the hole, remove the core barrel or other tool, seat the packer, make the test, remove the packer, drill the hole deeper, set the packer again to test the newly drilled section, and repeat the test (see Fig. 12-35(A)). If the hole stands without casing, a common procedure is to drill it to final depth, fill with water, surge it, and bail it out. Then set two packers on pipe or drill stem as shown in Figs. 12-35(C) and (D). The length of packer when expanded should be five times the diameter of the hole. The bottom of the pipe holding the packer must be plugged and its perforated portion must be between the packers. In testing between two packers, it is desirable to start from the bottom of the hole and work upward.

Leakage through the packers introduces a serious error. This can be detected if 3 packers are used and the permeability of each chamber is measured individually and then together. If the sum total when measured together exceeds the total when measured separately, it is an indication of packer leakage.

Another simple way of determining leakage past the packers is to use packers with an electric transducer system (MAINI, 1971; MAINI, NOORISHAD and SHARP, 1972). The transducer is connected to a continuous recording device. The flow is commenced in the test section (Fig. 12-36) and packers are gradually inflated to avoid air bubbles. As the packers take on a seal, the test cavity pressure builds up to a steady value while the flow rate decreases as the leakage stops.

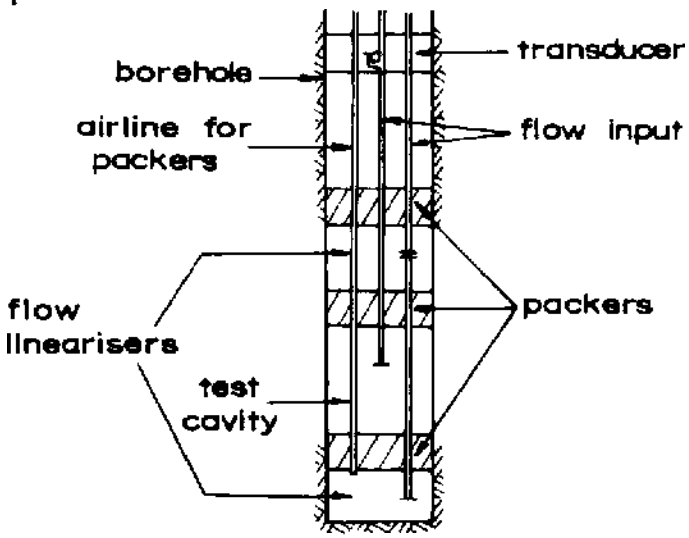

Fig. 12-36. Packer leakage detection system (after MAINI, NOORISHAD and SHARP, 1972).

Remarks: Pumping tests are time consuming and costly and generally are limited to a few on a project. Hence, it is difficult if not impossible to (a) determine permeability of more than one part of a complex rock mass, (b) indicate uniformity of any part of the mass or (c) establish averages which can be used with confidence.

Packer tests are common and can be made in holes of usual diamond-drilling size, the packers can be set to test any interval of open hole, and can be reset repeatedly.

Generally, water pressure, at the section under test, can be between 1.1 and 2.5 times the hydrostatic head without danger of opening fractures. Where permeability is high, it is an advantage to test at a low pressure difference to limit pipe friction and the likelihood of turbulence. Where it is low, a higher pressure difference provides a measurable inflow with less time.

Conductivity of joints

Packer test can be employed for determining conductivity of individual joints. This test is also called LUGEON test. One Lugeon unit corresponds to a flow of 1 litre per minute per metre length of the bore hole at a pressure of 10 kgf/cm^2. The test for a joint conductivity is shown in Fig. 12-37. The quantity of water q that would filtrate per unit of time from A to B along the joint $a\,a'$, considered of uniform opening e, is given by:

$$q = \frac{\pi e^2}{12\eta} \cdot \frac{p_1 - p_2}{ln\dfrac{d}{r_0}} \tag{12.51}$$

where the symbols have the meaning indicated in the Fig. 12-37, r_0 is the radius of the bore hole, and η is the viscosity of water and p_1 and p_2 are the pressures at the joint level.

The flow is usually measured for various pressures. The standard pressure of measurement is 10 kgf/cm^2. It may, however, be pointed out that deformation of the rock mass takes place under the application of pressure. If the pressure exceeds the internal stress of the rock mass, the joints may open and the results obtained will be grossly misleading. LONDE and SABARLY (1966) have shown that if the pressure of 10 kgf/cm^2 extends over a circular area of 2 m in radius it will deform a rock of a modulus of elasticity of 200,000 kgf/cm^2 by about 0.3 mm. This may result in conductivity even 100 Lugeon units in a rock mass that had the joints completely closed before the test started.

The conductivity is very sensitive to changes in aperture and it has been reported that flows show proportionality to the 3rd power of the joint aperture

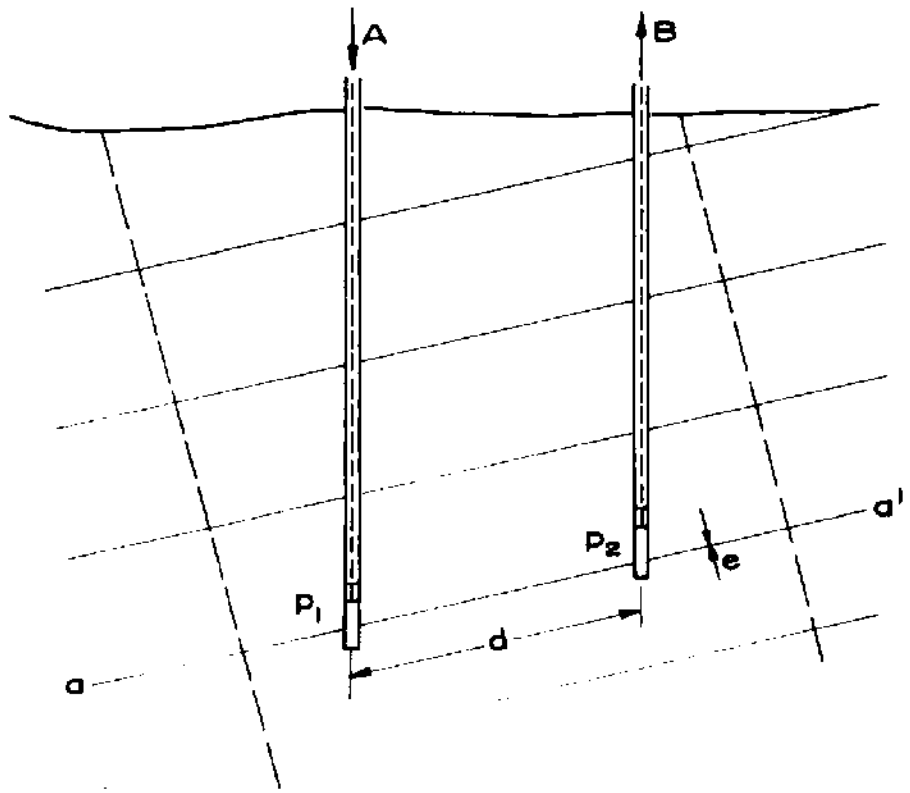

Fig. 12-37. Conductivity test in a joint (after SERAFIM and DEL CAMPO, 1965).

(SNOW, 1972). This may permit a rough estimate of the joint opening also under a given stress system and even an idea about the stress field if tests are conducted at different pressures.

The determination of joint parameters is not easy. Attempts have been made to measure joint openings and define these in terms of their width, fillings, etc. by bore hole camera surveys (BANKS, 1972) but it is very difficult to assign an average value.

There are certain other objections to the test. It is very difficult in practice to incorporate in the test section only a single joint except in special cases such as determination of the conductivity of a fault. The relationship (12.51) does not take into account the influence of natural flow and also assumes that the flow is laminar. In cases of joints with wider openings, the flow is bound to be turbulent which shall mean higher pressure losses. LOUIS and MAINI (1970) have made a theoretical analysis of the various factors.

It may be unnecessary to determine the conductivity of each joint to calculate the conductivity of a set of joints. The conductivity of each set of joints can be determined if the orientation and position of a joint system has been correctly studied.

If a rock body contains 3 joint sets (k_1, k_2 and k_3), the optimum hole direction for testing set k_1 is parallel to the other two sets k_2 and k_3.

It is preferable to carry out the test at various pressures and plot the flow rate against pressure or gradient. The usual curve obtained is given in Fig. 12-38. The various effects (1. Laminar flow, 2. Turbulence effect, 3. Turbulence offset by fissure expansion, 4. Predominance of fissure expansion) can be easily detected from the curve. In very deformable rocks, the effects 2 and 3 may be absent. Such a curve also gives an idea of the maximum pressure to be applied in further tests and the deformability of the joints.

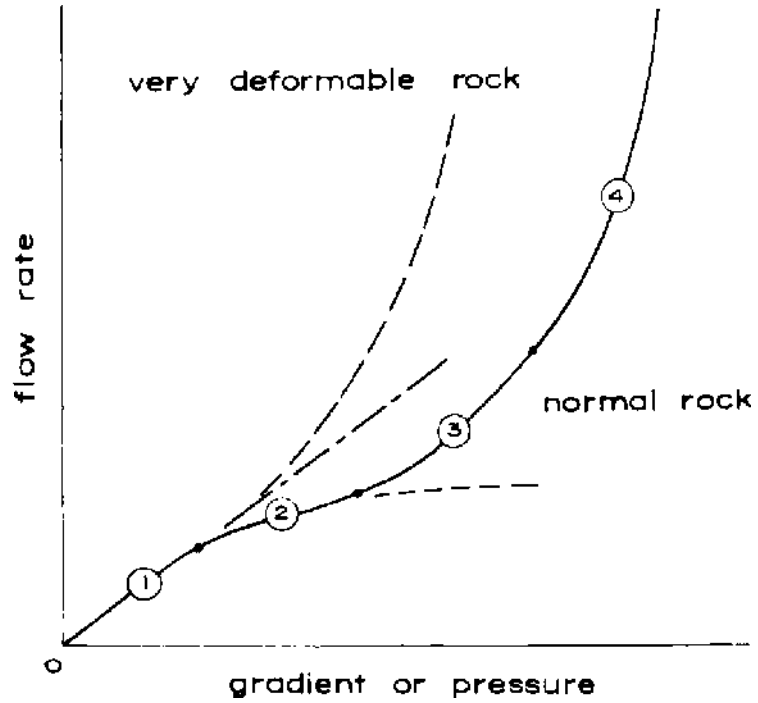

Fig. 12-38. Typical results of field water test.
1. Laminar flow; 2. Turbulence effect; 3. Turbulence offset by fissure expansion; 4. Predominance of fissure expansion effects.
(after LOUIS and MAINI, 1970).

When the flow is turbulent, the laminar coefficient of conductivity k is related to the turbulent coefficient of conductivity k' through the relationship

$$k' = A \sqrt{k} \tag{12.52}$$

where A = constant of each joint. BANKS (1972) found that the value of A could be taken as $\sqrt{1}$ cm/s.

The changes in conductivity of joints with normal stress and shear displacement are very much likely and their influence is determined by the nature of

the joint surfaces (roughness). In general, increase in normal stress will decrease the conductivity due to decrease in joint openings and increase in displacement will increase conductivity but only to a certain extent (SHARP and MAINI, 1972).

Fig. 12-39 gives the results of tests conducted by OHNISHI and GOODMAN (1974) on rough joints of granite using a thick-walled cylinder in the laboratory applying divergent flow at 50 lbf/in^2 (0.35 MPa) inside pressure and one atmospheric outside pressure as a function of effective normal stress, joint closure and flow rate. A logarithmic plot of flow rate versus joint aperture gives a straight line. Between 70 lbf/in^2 (0.5 MPa) and 300 lbf/in^2 (2.14 MPa), joint aperture varied approximately with effective normal stress $\sigma^{-0.53}$ and flow rate varied approximately with $\sigma^{-1.4}$. These exponents increase for higher effective normal stresses.

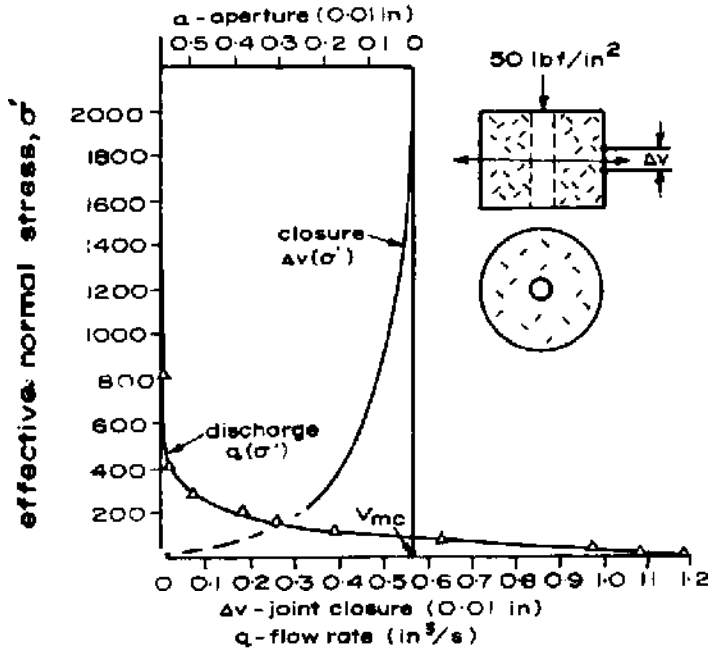

Fig. 12-39. Radial permeability test on rough joint in granite; joint compression and discharge under changing normal stress (after OHNISHI and GOODMAN, 1974).

In a fractured or jointed rock, the permeability is mainly controlled by the fractures or joints and pores play an insignificant role. MORDECAI and MORRIS (1974) conducted air permeability tests on a number of coal measure rocks subjected to triaxial stresses and found that the spread of the permeability after fracture between the rocks is much smaller than before fracture indicating thereby that the induced fractures control conductivity.

However, it is not always essential that fractured rocks will have greater conductivity than porous rocks. The relative influences may be different. MICHEL (1972) showed that for a porous rock, such as Lias claystone, the ground water flow was greater than the so-called fissured limestones and sandstones.

The permeability of the joints or rocks should theoretically be independent of the type of fluid used if the viscosity of the fluid has been taken into consideration. DI BIAGIO and MYRVOLL (1972), however, reported that the results were erratic in their tests at two underground power stations in Norway.

Certain new methods are being developed using tracer technique. One of the methods is the dilution test wherein the region of the bore hole under investigation is isolated using packers and a certain quantity of salt solution is introduced. The concentration of the salt solution changes as the natural water flow through the region washes away some of the solution. The rate of dilution is governed by the hydraulic gradient, conductivity of the joint and size of the bore hole (HALEVY et al, 1966; MAINI, 1968, 1971). The rate of dilution is a function of the seepage velocity and if the dilution rate is measured with time, it is possible to calculate or have a check on the permeability measured by other methods. By measuring concentration at different sites, it is possible to calculate the flow velocity in different directions.

In another technique, radioactive tracers such as Chromium-51, Iodine-131, are pumped in with the water in one bore hole and the time is noted for their arrival at different locations. This gives a fairly accurate idea of the seepage velocities in different directions (WURZEL and WARD, 1965). However, it may not be possible sometimes to measure the time of tracer arrival due to disappearance of the tracer. This can be overcome if large diameter bore hole is used (WURZEL, 1972). It may be pointed out that when radioactive tracers are used, their half-life decay time is an important consideration.

12.7. Swelling and Slake-Durability Index Properties

A number of rocks particularly those containing clays are prone to swelling, cracking and disintegration when exposed to short term weathering processes of wetting and drying. Besides, supports placed in excavations made in such rocks experience cycles of increased and decreased pressures depending upon the wetting and drying cycles. Special tests are required to estimate this aspect of mechanical behaviour. These tests are called index tests and can be used for classifying and comparing one rock with another. The swelling strain index should not, for example, be taken as the actual swelling strain that the rock would develop in situ, even if the test is carried out under similar loading and water content conditions. However it definitely gives an approximate idea of

its behaviour. These tests basically simulate natural wetting and drying processes.

These tests are commonly required for classification or characterisation of the softer rock materials. They may also be used, however, for characterisation of harder rocks where the rock condition, its advanced state of weathering for example, indicates that they are appropriate.

Rocks that disintegrate during the tests may be further characterised using soil classification tests such as determination of the liquid and plastic limits, the grain size distribution, or the content and type of clay minerals present.

The methods as suggested by the International Society for Rock Mechanics (I.S.R.M.) Committee on Laboratory Tests (1972) are given as under:

1. Swelling pressure index under conditions of zero volume change.
2. Swelling strain index for a radially confined specimen with axial pressure.
3. Swelling strain developed in an unconfined specimen.
4. Slake-durability index.

Where possible, undisturbed rock specimens should be tested, as rock fabric has an important influence on the properties to be measured. Where this is not possible, for example the sample is too weak or damaged, the swelling tests may be carried out on remoulded specimens. Remoulding should be according to standard procedures for soil compaction, and the procedure followed should be reported along with the results.

12.7.1. Swelling Pressure Index under Conditions of Zero Volume Change

This test is intended to measure the pressure necessary to constrain an undistributed rock specimen at constant volume when it is immersed in water. Usually, the apparatus may be adapted from that used for soil consolidation testing, and consists essentially of the following (Fig. 12-40):

(a) A metal ring for rigid radial restraint of the specimen, polished and lubricated to reduce side friction and of depth at least sufficient to accommodate the specimen.
(b) Porous plates to allow water access at top and bottom of the specimen, the top plate of such a diameter as to slide freely in the ring. Filter papers may be inserted between specimen and plates.
(c) A cell to contain the specimen assembly, capable of being filled with water to a level above the top porous plate. The principal features of the cell and specimen assembly are illustrated in Fig. 12-40.

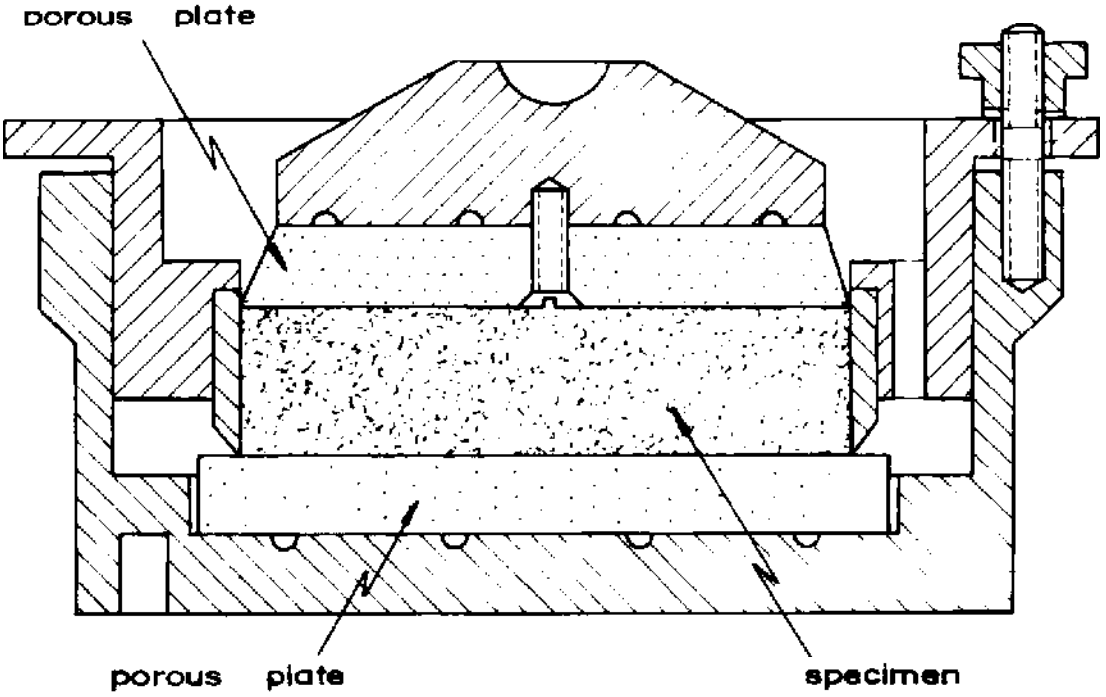

Fig. 12-40. Cell and specimen assembly for confined swelling tests (after I.S.R.M., 1972).

(d) A micrometer dial gauge or other device reading to 0.0025 mm (0.0001 in), mounted to measure the swelling displacement at the central axis of the specimen.
(e) A load measuring device capable of measuring to an accuracy of 1%, the force required to resist swelling.
(f) A loading device such as screw jack, capable of continuous adjustment to maintain the specimen at constant volume as swelling pressure develops. The force should be applied through rigid members to ensure that the porous plates remain flat.

The method of preparation of test specimens is as follows:

For testing at natural initial water content, sample preparation should be such as to retain water content to within 1% of its in situ value. Duplicate specimens should be prepared from the same sample, one being used for water content determination and the other for swell testing.

For testing at an artificially controlled initial water content the sample may be brought to equilibrium weight in a constant humidity environment. Duplicate specimens should then be prepared from the same sample, one being used for water content determination and the other for swell testing.

The specimen should conform closely to the geometry of a right cylinder. It should have a diameter not less than 2.5 times its thickness. The thickness

should exceed 15 mm or ten times the maximum grain diameter, whichever is greater. The specimen should be a close fit in the ring.

The inclination of bedding or foliation with respect to the specimen axis should be recorded.

The procedure for conducting the test is as follows:

The apparatus is assembled and a small axial force is applied to the specimen.

The cell is then flooded with water to cover the top porous plate, and the swelling force is recorded as a function of time elapsed.

The applied force is regularly adjusted to maintain zero specimen swell throughout the test with an accuracy of ± 0.01 mm (0.004 in).

Swelling force should continue to be recorded until it reaches a constant level or passes a peak.

The swelling pressure index is given by:

$$\text{Swelling pressure index} = \frac{F}{A} \tag{12.53}$$

where F = maximum axial swelling force recorded during the test and
A = cross-sectional area of the specimen.

The results should be reported for at least three specimens per sample. The following information should be included in the report for each specimen:

1. The swelling pressure index
2. The initial water content of the specimen: whether this corresponds to the natural water content, and if so the method of storage prior to testing.
3. The diameter and thickness of the specimen, together with the inclination of bedding or foliation with respect to the specimen axis.

12.7.2. Swelling Strain Index for a Radially Confined Specimen with Axial Pressure

This test is intended to measure the axial swelling strain developed against a constant axial pressure, when a radially confined, undisturbed rock specimen is immersed in water.

The apparatus is essentially the same as that described under 12.7.1. The metal ring should be of depth at least sufficient to accommodate the specimen when fully swollen. A loading device such as dead weight, or weight and lever system, capable of applying a sustained pressure of 5 kPa (70 lbf/in^2) to the specimen

is required. This pressure is maintained within 1% throughout the swelling of the specimen.

The method of preparation of test specimens is the same as described under 12.7.1. and that the specimen should have a diameter not less than ten times its thickness.

The procedure for conducting the test is as follows:

The initial thickness and diameter of the specimen are recorded to within 0.1%.

The apparatus is assembled and the specimen loaded axially to an axial pressure of 3 kPa (40 lbf/in^2).

The cell is then flooded with water to cover the top porous plate, and the swelling displacement recorded as a function of time elapsed.

Swelling displacement should be continuously recorded until it reaches a constant level or passes a peak.

The swelling strain index is given by:

$$\text{Swelling strain index} = \frac{d}{L} \times 100\% \tag{12.54}$$

where d = maximum swelling displacement recorded during the test and
L = initial thickness of the specimen.

Reporting of results is the same as given under 12.7.1.

12.7.3. Swelling Strain Developed in an Unconfined Specimen

This test is intended to measure the swelling strain developed when an unconfined, undisturbed rock specimen is immersed in water. The test should only be applied to specimens that do not change their geometry appreciably on slaking; less durable rocks are better tested using a confined swelling test.

The apparatus consists essentially of the following:

(a) A cell to contain the specimen assembly, capable of being filled with water to a level above the top of the specimen.

The principal features of the cell and specimen assembly are illustrated in Fig. 12-41.

(b) A micrometer dial gauge or other device reading to 0.0025 mm (0.0001 in) mounted to measure the swelling displacement on the central axis of the

specimen. Additional gauges may be employed to simultaneously measure swelling displacements in directions orthogonal to the test.

(c) Bearing plates of glass or other hard materials which may be cemented to the specimen with water-stable adhesive. These plates should be small compared with the area of specimen exposed to water, and are positioned at points of gauging and of support to prevent indentation of the specimen.

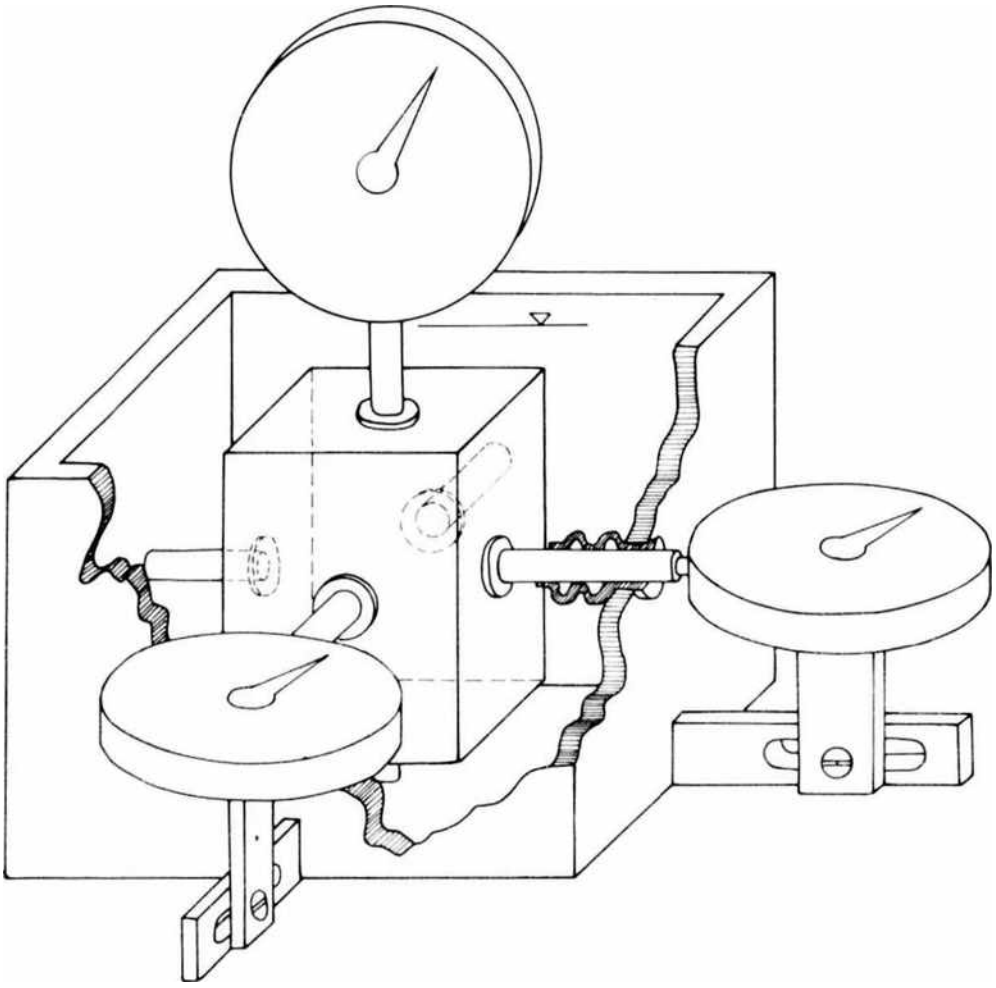

Fig. 12-41. Cell and specimen assembly; unconfined swelling tests (after I.S.R.M., 1972).

The preparation of test specimens is as follows:

For testing at natural initial water content, preparation should be such as to retain water content to within 1 % of its in situ value. Duplicate specimens should be prepared from the same sample, one being used for water content determination and the other for swell testing.

For testing at an artificially controlled initial water content the sample may be first prepared into specimens, then brought to equilibrium weight in a constant humidity environment. Duplicate specimens should be prepared from the sample, one being used for water content determination and the other for swell testing.

The specimen may take the form of a right cylinder or a rectangular prism. The minimum specimen dimension should exceed 15 mm or ten times the maximum grain diameter, whichever is greater.

The specimen should preferably be machined so that an axis is perpendicular to any bedding or foliation. The inclination of the directions of swell measurement with respect to this bedding or foliation should be recorded.

The procedure for conducting the test is as follows:

Gauge points are marked to coincide with the axis or axes of the specimen. The initial specimen dimensions are measured between these gauge points to an accuracy better than 0.1%.

Bearing plates are then positioned at each gauge point and the apparatus assembled. The specimen should be supported only at gauge points on the specimen axes.

The cell is then flooded with water to cover the specimen, and the swelling displacement or displacements recorded as a function of time elapsed.

Swelling displacement should continue to be recorded until it reaches a constant level or passes a peak.

The swelling strain for each direction of measurement is calculated as follows:

$$\text{Unconfined swelling strain in direction } X = \frac{d}{L} \times 100\% \tag{12.55}$$

where X = direction relative to the bedding or foliation
d = maximum swelling displacement recorded in direction X during the test and
L = initial distance between gauge points in direction X.

The results should be reported for at least three specimens per sample. The following information should be included in the report for each specimen:

1. Unconfined swelling strains and their directions with respect to bedding or foliation.
2. The initial water content of the specimen; whether this corresponds to the natural water content, and if so the method of storage prior to testing.
3. The shape and initial dimensions of the specimen.
4. A description of any visible deterioration during slaking.

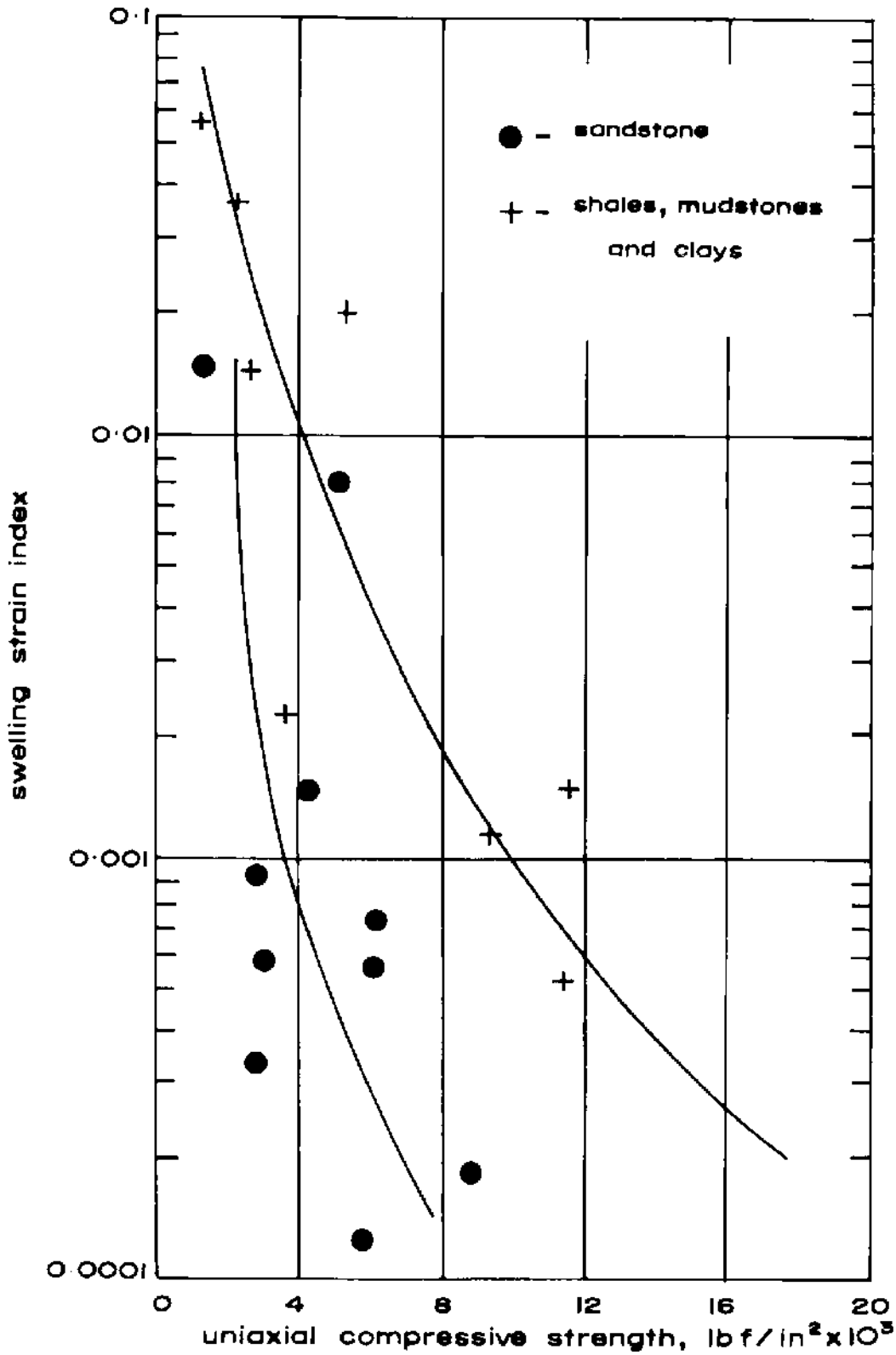

Fig. 12-42. Relationship between uniaxial compressive strength and swelling strain index (after DUNCAN, 1969).

In the swelling index tests, peak values are usually obtained within 5–10 minutes, but for certain rocks, collapse may take much longer time even up to a year or so. As such tests should be carried out for longer periods if any rock is suspected of weakness or if it contains certain clayey constituents in the form of pockets and when the porosity of rock is small and pore size is also small.

Swelling also depends upon the degree of cementation. If the cementation bond is strong, swelling is small and the time required to achieve peak will be large. If the bond is weak, considerable swelling occurs and the peak is arrived quickly.

The swelling characteristic of a rock is the function of its moisture content, grain size, nature of the bond between the grains and the chemical properties of the grain material. The size of the pores governs the capillary suction pressures developed and perhaps also the osmotic suction and gravitational suction. The extent of cementation governs the ability of the individual grains to reorient themselves under the influence of stresses developed. If the bond is strong, expansion will be negligible. A weak bond will show swelling and therefore swelling could be regarded as a measure of the bond strength and strength of the rock. Tests conducted on sandstones, clays, mudstones and

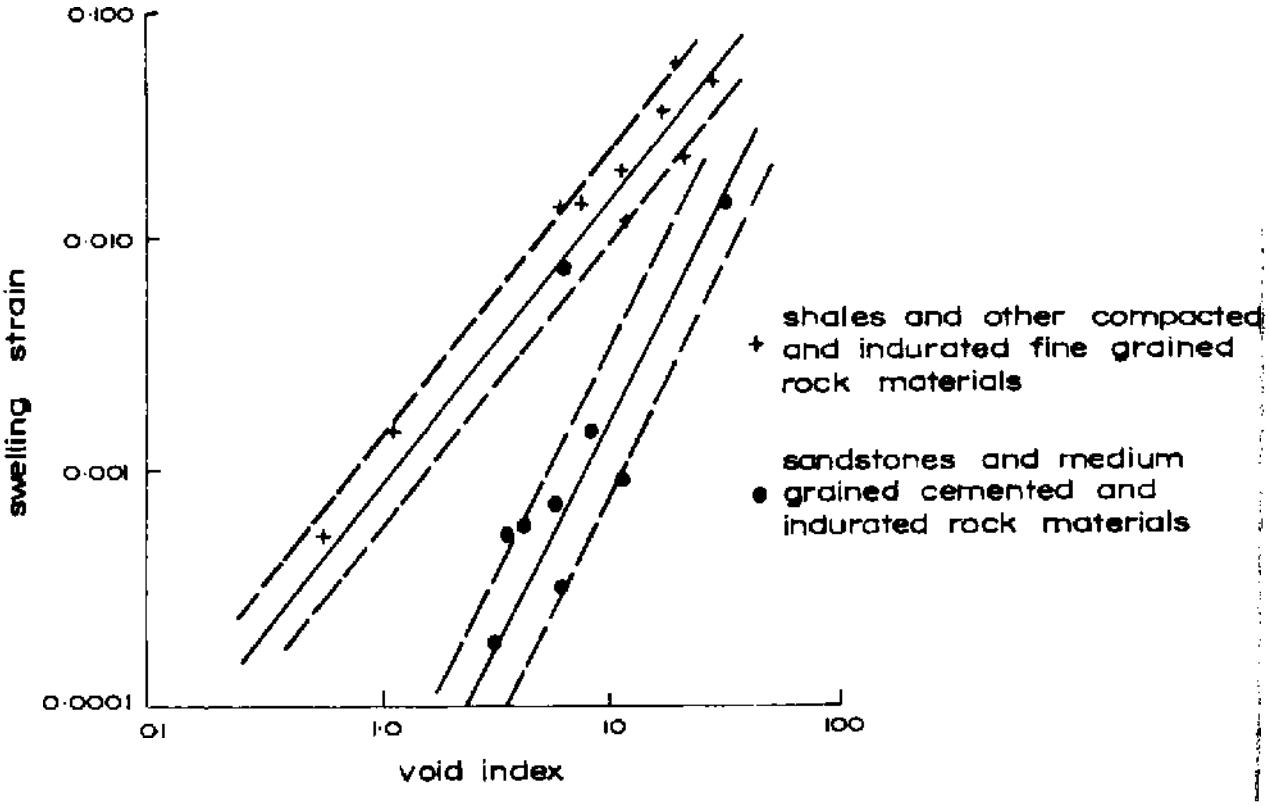

Fig. 12-43. Swelling strain versus void index (after DUNCAN et al, 1968).

shales show some form of relationship between the compressive strength and swelling strain index (Fig. 12-42). Sandstones with uniaxial compressive strength greater than 6000 lbf/in^2 (40 MPa) (400 kgf/cm^2) rarely show any significant swelling. Swelling pressure index under zero volume change is dependent upon the swelling strain and YOUNG's modulus of the rock.

DUNCAN et al (1968) tested 61 different rock types including sandstones, mudstones, limestones and granites. Swelling was mostly observable in the case of clays, shales, marls and sandstones (11 out of 13 cases), almost 40% of granites showed swelling (5 out of 12 cases) and about 50% of sandstones (11 out of 23 cases) while none of the limestones (zero out of 13 cases) showed swelling. The void index of the limestones investigated was in the range of 0.2 to 4.3%. The non-dilatational effect in limestones seem to be due to the solubility of calcite.

The relationship between swelling strain and void index for various rocks is given in Fig. 12-43. It is predominantly linear. Similarly linear relationship exists between bulk density and swelling strain index.

12.7.4. Slake-Durability Index

This test is intended to assess the resistance offered by a rock sample to weakening and disintegration when subjected to two standard cycles of drying and wetting.

The apparatus consists essentially of the following:

(a) A test drum comprising a 2 mm standard mesh[1] cylinder of unobstructed length 100 mm and diameter 140 mm, with solid fixed base capable of withstanding a temperature of 105 °C. It has a solid removable lid and is sufficiently strong to retain its shape during use. Neither the exterior of the mesh nor the interior of the drum should be obstructed, for example by reinforcing members.

(b) A trough, to contain the test drum supported with axis horizontal in a manner allowing free rotation, capable of being filled with a slaking fluid such as water to a level 20 mm below the drum axis. The drum is mounted to allow 40 mm unobstructed clearance between the trough and the base of the mesh. The principal features of the trough and drum assembly are illustrated in Fig. 12-44.

(c) A motor drive capable of rotating the drum at a speed of 20 rpm, the speed to be held constant to within 5 per cent for a period of 10 minutes.

---

[1] International Standards Organisation. R 565. Woven Wire Cloth and Perforated Plates in Test Sieves, 1967.

(d) An oven capable of maintaining a temperature of 105 C to within 3 C for a period of at least 12 hours.

(e) A balance capable of weighing the drum plus sample to an accuracy of 0.5 g.

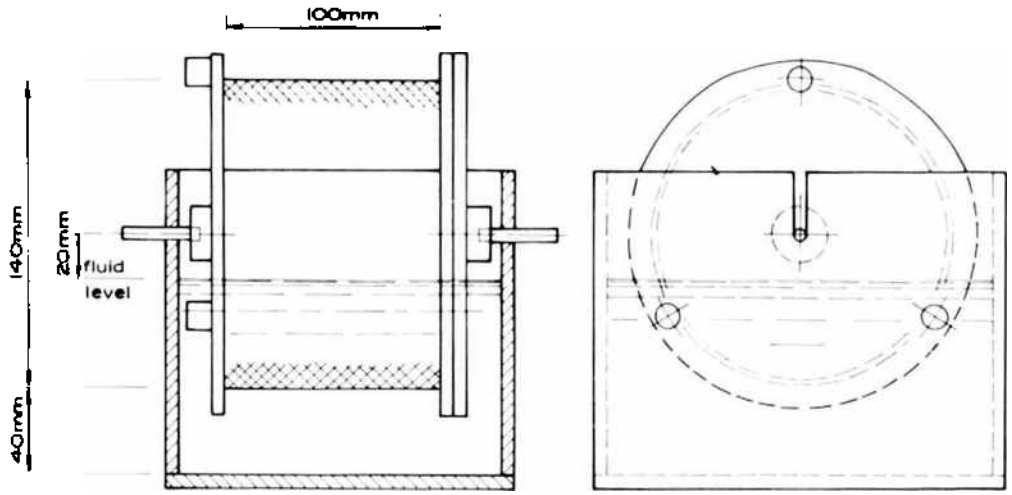

Fig. 12-44. Critical dimensions of slake-durability test equipment (after I.S.R.M., 1972; also FRANKLIN and CHANDRA, 1972).

The procedure for conducting the test is as follows:

(a) A representative sample is selected comprising ten rock lumps, each weighing 40–60 g, to give a total sample weight of 450–550 g. Lumps should be roughly spherical in shape, and corners should be rounded during preparation.

(b) The sample is placed in a clean drum and is dried to constant weight at a temperature of 105 C, usually requiring from 2 to 6 hours in the oven. The weight A of the drum plus sample is recorded. The sample is then immediately tested.

(c) The lid is replaced, the drum mounted in the trough and coupled to the motor.

(d) The trough is filled with slaking fluid, usually tap water at 20 C, to a level 20 mm below the drum axis, and the drum rotated at 20 rpm for a period of 10 min.

(e) The drum is removed from the trough, the lid removed from the drum, and the drum plus retained portion of the sample dried to constant weight at 105 C. The weight B of the drum plus retained portion of the sample is recorded.

(f) Steps (c) (e) are repeated and the weight C of the drum plus retained portion of the sample is recorded.

(g) The drum is brushed clean and its weight D is recorded.

The calculation for slake durability index (second cycle) is done as follows:

$$\text{Slake durability index, } I_{d_2} = \frac{C-D}{A-D} \times 100\% \qquad (12.56)$$

The following information should be included in the report for each sample tested:

1. The slake durability index (second cycle) to the nearest 0.1 per cent.
2. The nature and temperature of the slaking fluid: usually tap water at 20 °C, but for example distilled water, natural ground water, sea water, a dilute acid or a dispersing agent may be specified.
3. The appearance of fragments retained in the drum.
4. The appearance of material passing through the drum.

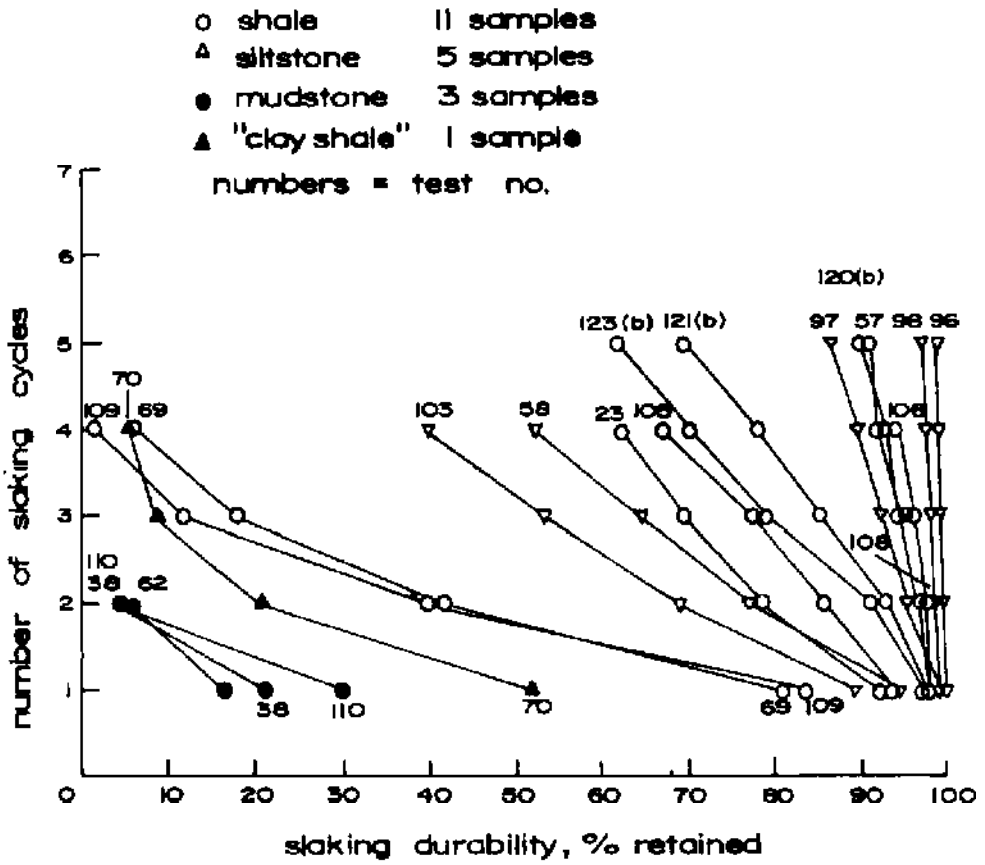

Fig. 12-45. Influence of the number of slaking cycles on slake-durability (after GAMBLE, 1971).

The second cycle slake durability index, calculated as above, with tap water at 20°C, is proposed for use in rock classification. However, samples with second cycle indexes from 0 to 10 per cent should be further characterised by their first cycle slake durability indexes as follows:

$$\text{Slake durability index } I_{d_1} = \frac{B-D}{A-D} \times 100\% \qquad (12.57)$$

Indexes taken after three or more cycles of slaking and drying may be useful when evaluating rocks of higher durability (Fig. 12-45).

Rocks giving low slake-durability results should be subjected to soils classification tests, such as determination of ATTERBERG limits or sedimentation-size analysis. A classification combining slake durability index and plasticity index (Fig. 12-46) is suggested in cases where a greater depth of characterisation, particularly of argillaceous rocks, is required.

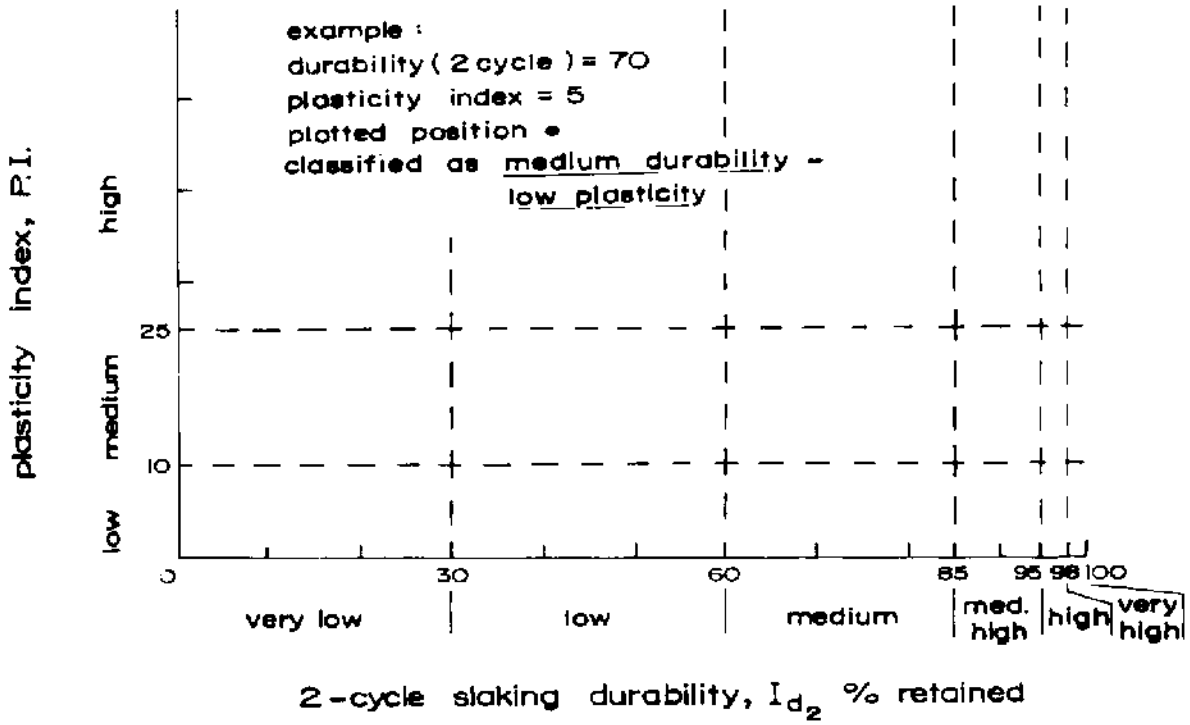

Fig. 12-46. A suggested durability-plasticity classification (after GAMBLE, 1971).

12.8. Grain Size

The size of grains in a heterogeneous aggregate such as rock, may be expressed in different ways, and the form chosen will depend upon the state of aggregation of the rock and the method and purpose of the determination. The method of size analysis may be:

1. Visual
2. Mechanical
3. Both visual and mechanical.

Visual analysis is most common for rocks. Mechanical methods such as sieving are commonly used for soils and can be found in several books on Soil Mechanics and Mineral Processing and shall not be discussed here. Visual analysis is done with the aid of a microscope, a camera or both. Simple inspection with a microscope equipped with a micrometer eyepiece gives an idea about the maximum and minimum size of the grains, the degree of rounding and a large number of micrometer measurements gives an approximation of the average grain diameter. By photographing the surface (or the slide) of the rock, and projecting the negative on to a ruled screen with a total magnification of about 20,000 diameters, the average diameter of the individual grains can be easily read with a millimetre scale and size-frequency distribution can be made.

The averaging of the grain size is not an easy solution. The accuracy depends upon the shape of the grains and it is important to choose an expression which rightly conveys the grain size. When the shape is spherical or nearly spherical, the mean diameter can be taken as the average diameter of the grain. When the grains are prismatic and elongated, the best value for the average diameter of a grain is the harmonic mean which is given by:

$$d_{av} = \frac{3\,lbt}{lb + lt + bt} \tag{12.58}$$

where d_{av} = average diameter
l = length
b = breadth and
t = thickness.

Certain other average values are also sometimes referred, such as, arithmetical mean, length mean, average volume, surface mean, weight mean (Table 64). The arithmetical mean is the one most commonly employed, but it does not have much significance for heterogeneous materials and a small proportion of large grains has small significance on its value. The length mean represents the surface observed and the total surface or volume of the particle has no significance upon it. The average volume can be considered as that diameter

TABLE 64

Log and computation sheet for particle size determination with the microscope

(after TICKELL, 1947)

Material Diatomite
Source – Bradley, Calif.

Particle size distribution

1 micrometer scale division = 12.5 microns

Scale Division Range	d	Count	Freq. n	nd	Products nd^2	nd^3	nd^4
0.5 – 1.0	.75				—	—	—
1.0 – 1.5	1.25	///	3	4	5	6	7
1.5 – 2.0	1.75	////	4	7	12	21	37
2.0 – 2.5	2.25	//// ////	10	22	51	114	257
2.5 – 3.0	2.75	//// //// ////	15	41	114	312	860
3.0 – 3.5	3.25	//// //// //// //// //// //// //// //// //// ///	48	156	507	1,645	5,340
3.5 – 4.0	3.75	//// //// //// //// //// //// //// //// //// //// //	52	195	732	2,640	10,140
4.0 – 4.5	4.25	//// //// //// //// //// //// //// //// //// //// /	51	216	923	3,915	16,630
4.5 – 5.0	4.75	//// //// //// //// //// //// //// ///	38	180	859	4,070	19,350
5.0 – 5.5	5.25	//// //// //// /	16	84	441	2,315	12,150
5.5 – 6.0	5.75	//// //// //// /	16	92	529	3,045	17,500
6.0 – 7.0	6.5	//// //// ///	13	84	550	3,570	23,200
7.0 – 8.0	7.5	//// ////	10	75	562	4,219	31,600
8.0 – 9.0	8.5	///	3	25	217	1,840	15,700
9.0 – 10.0	9.5	///	3	28	271	2,570	24,400
10.0 – 11.0	10.5		—			—	-
		Totals	282	1,212	5,773	30,582	177,172

Arithmetical Mean $= \frac{\Sigma nd}{\Sigma n} = \frac{1212}{282} = 4.3$ div. $= 53.8$ microns.

Length Mean $= \frac{\Sigma nd^2}{\Sigma nd} = \frac{5773}{1212} = 4.8$ div. $= 59.5$ microns.

Average Volume $= \left|\frac{\Sigma nd^3}{\Sigma n}\right|^{\frac{1}{3}} = \left|\frac{30,582}{282}\right|^{\frac{1}{3}} = 4.8$ div. $= 59.5$ microns.

Surface Mean $= \frac{\Sigma nd^3}{\Sigma nd^2} = \frac{30,582}{5,773} = 5.3$ div. $= 66.3$ microns.

Weight Mean $= \frac{\Sigma nd^4}{\Sigma nd^3} = \frac{177,172}{30,582} = 5.8$ div. $= 72.5$ microns.

whose corresponding volume divided into the total volume equals the total number of grains. It gives results larger than the arithmetical or length mean, but the large grains of a mixture, where small grains greatly predominate, do not affect the average. The surface mean is based upon the total surface of the particle and is thought to give the best value for non-metallic minerals. The weight mean is based upon the volume of the particle and gives the highest value than other means. It is of importance in the study of pulverised coal and ore-dressing problems.

The measurement of the thickness of the particle poses a difficult problem. The method requires the preparation of the rock surface and photographing it in reflected light and then repolishing by taking away slices of a given thickness accurately measured. The average values of l, b, t (for different particles) can then be accurately calculated. In general, however, b and t may be taken as equal and the formula $d_{av} = \sqrt{l \times b}$ may be used.

For randomly distributed grains, for example igneous rocks, it may suffice to make only sections for cores drilled in any one direction and measuring the diameter always in one direction with respect to the microscopic field.

For sedimentary rocks where the difference between the values in the two directions is large (elongated grains) it is required to make thin sections both in the horizontal and vertical directions of the bedding planes and calculating the average values as above.

The particle size record is usually done in some form as shown in Table 64. The results are then plotted in the form of a histogram or in the form of a distribution curve with y-axis representing the cumulative frequency (%) the x-axis representing the size giving the socalled cumulative frequency distribution curve (Fig. 12-47). The curves are plotted on a semi-logarithmic scale. This has the advantage of saving space and requires less computation while it can be easily read out.

Many times it is more useful to plot the frequency (%)—grain diameter giving the so-called frequency distribution curves of the mathematical statistics. Numerical data cannot be taken from the curves but they facilitate the visualisation of the type of sample represented and reveal its characteristics. Some types of curves and their characteristic interpretations are given in Fig. 12-48. The high peak of the frequency curve is called the mode. It represents the size of grains that is most abundant. The relative height of the mode and the way in which the frequencies are grouped on each side of it are characteristic of the material.

Lack of symmetry about the mode is called skewness and a close bunching of frequencies at the mode (high narrow peak) is called kurtosis. A frequency distribution curve can be characterised by these two. In a normal curve,

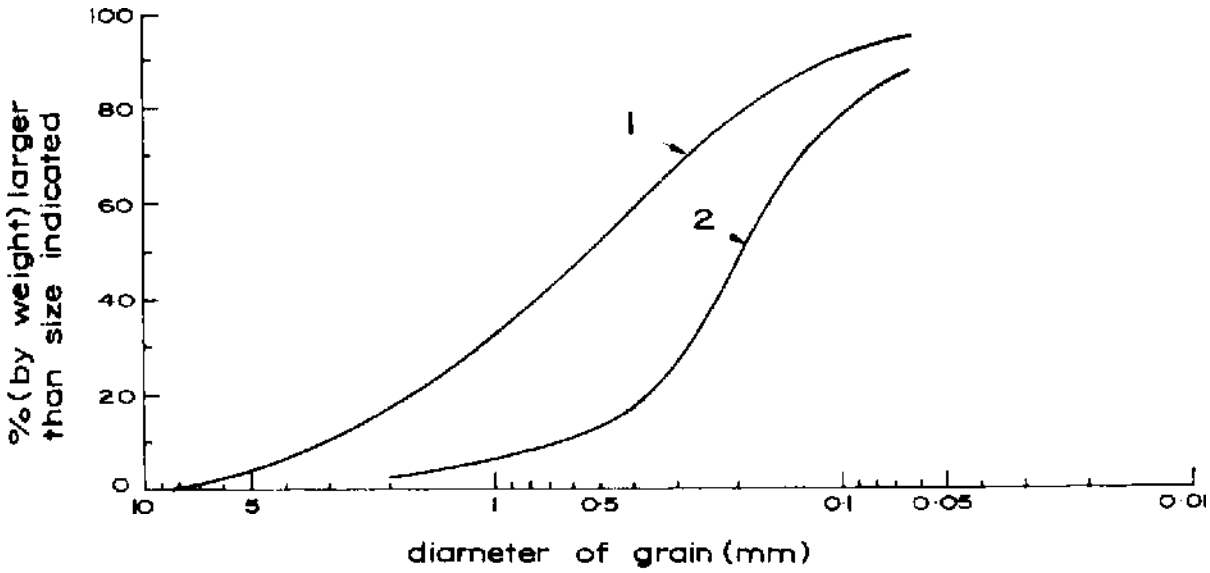

Fig. 12-47. Cumulative % frequency curves, semi-log ruling (after TICKELL, 1947).

skewness = 0 and kurtosis = 0.263. A kurtosis greater than 0.263 signifies a steep curve. These are calculated as follows:

$$\text{Skewness} = P_{50} - \frac{1}{2}(P_{10} + P_{90}) \tag{12.59}$$

$$\text{Kurtosis} = \frac{P_{25} - P_{75}}{2(P_{10} - P_{90})} \tag{12.60}$$

where P_{50} = the 50 percentile; or the size of grain where 50% are larger and 50% smaller
P_{10} = the 10 percentile; or the size of grain where 10% are larger and 90% smaller
P_{90} = the 90 percentile
P_{25} = the 25 percentile and
P_{75} = the 75 percentile.

Thus, for example, in Fig. 12-47, for sample 1, the values are:

$P_{50} = 0.52$
$P_{10} = 3.10$
$P_{90} = 0.10$
$P_{25} = 1.40$
$P_{75} = 0.22$

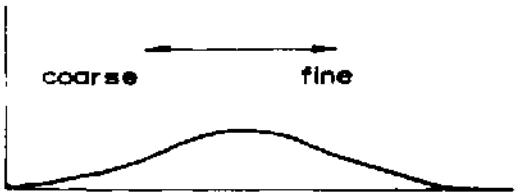

normal curve

represents a purely random distribution

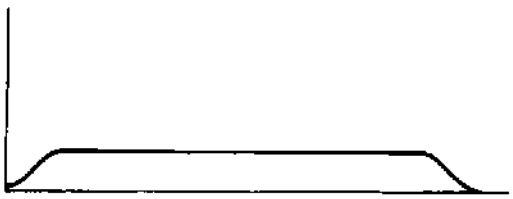

flat symmetrical curve

represents a nearly perfect assortment

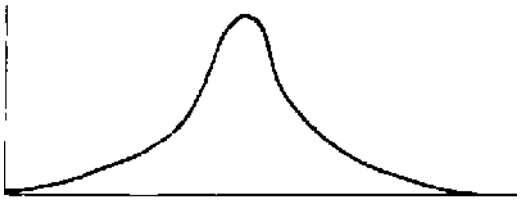

steep symmetrical curve

represents an abundance of medium grades, with equal distributions of the coarse and fine grades

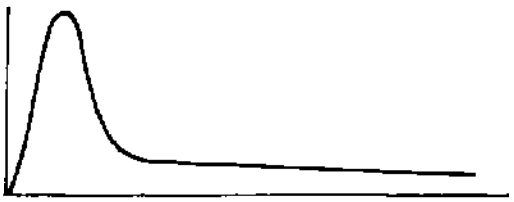

steep asymmetrical curve

represents an even assortment of fine and medium grades, contained in the interstices of a preponderance of coarse material

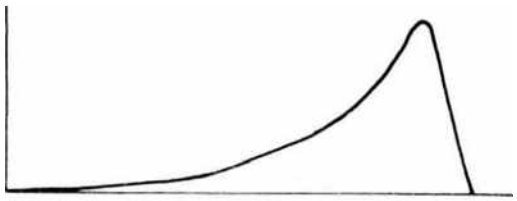

steep asymmetrical curve

represents a preponderance of fine material, but no extremely fine grains

Fig. 12-48. Types of frequency curves (after TICKELL, 1947).

$$\text{Therefore skewness} = 0.52 - \frac{1}{2}(3.10 + 0.10)$$

$$= -1.03$$

$$\text{Kurtosis} = \frac{1.4 - 0.22}{2(3.1 - 0.10)} = 0.197$$

Negative skewness indicates that more of the material is fine-grained than coarse-grained and positive skewness indicates that more of the material is coarse-grained than fine-grained.

In the last few years, photographic techniques have been highly developed and are coupled with automatic computing system. These usually go under the name of "image analysers" and are being used in medicine, biology and metallurgy on increasing scale (FISHER and NAZARETH, 1968). Its use in rock microscopy to date has been extremely small. The system works on counting the contrast spots on the slide or photograph of the object and programmed to evaluate the number or counts, area of the dark spots (particles), projected length or longest chord, total or mean perimeter, mean linear intercept and form factor etc. The scanning equipment can be connected to the microscope or used with an epidiascope or 16 or 35 mm cine film record, the only condition being that there should be a good contrast available between the background and the grains under study. Certain techniques like etching, fluorescent dye, use of certain filters for coloured particles etc. may be used to enhance contrast.

References to Chapter 12

1. AFINOGENOV, YU. A.: How the liquid permeability of rocks is affected by pressure and temperature. Sov. Min. Sci., No. 6, 1969, pp. 638–645.
2. AMYX, J.W., BASS, D.M. and WHITING, R.L.: Petroleum Reservoir Engineering. New York, McGraw-Hill, 1960, 610 p.
3. BANKS, D.C.: In situ measurements of permeability in basalt. Proc. Symp. Percolation through Fissured Rock, Stuttgart, Germany, 1972, Paper T1-A.
4. BARRON, K., HEDLEY, D.G.F. and COATES, D.F.: Field instrumentation for rock slopes. Proc. 1st Int. Conf. Stability in Open Pit Mining, Vancouver, Canada, 1970, pp. 143–168.
5. BELIKOV, B.P., ZALESSKII, B.V., ROZANOV, YU. A., SANINA, E.A. and TIMCHENKO, I.P.: Methods of studying the physicomechanical properties of rocks. In Physical and Mechanical Properties of Rocks by B. V. Zalesski (Editor). Translated from Russian. Jerusalem, Israel Program for Scientific Translations, 1967, pp. 1–58.
6. BRANNER, G.C.: Sandstone porosities in Palaeozoic region in Arkansas. Bull. Am. Assoc. Petr. Geol., Vol. 31, 1937, pp. 67–79.
7. CLARK, S.P.: Thermal conductivity. In Handbook of Physical Constants by S.P. Clark (Editor). Geol. Soc. Am. Mem. 97, 1966, pp. 459–482.
8. DALY, R.A., MANGER, G.E. and CLARK, S.P.: Density of rocks. In Handbook of Physical Constants by S.P. CLARK (Editor). Geol. Soc. Am. Mem. 97, 1966, pp. 19–26.
9. D'ANDREA, D.V., FISCHER, R.L. and FOGELSON, D.E.: Prediction of compressive strength from other rock properties. U.S.B.M., R.I. 6702, 1965, 23 p.
10. DAVIS, D.H.: Estimating porosity of sedimentary rocks from bulk density. J. Geol., Vol. 62, 1954, pp. 102–107.
11. DI BIAGIO, E. and MYRVOLL, F.: In situ tests for predicting the air and water permeability of rock masses adjacent to underground openings. Proc. Symp. Percolation through Fissured Rock, Stuttgart, Germany, 1972, Paper T1-B.
12. DUBE, A.K. and SINGH, B.: Effect of humidity on tensile strength of sandstone. J. Mines, Metals and Fuels, Vol. 20, No. 1, Jan., 1972, pp. 8–10.
13. DUNCAN, N.: Engineering geology and rock mechanics, Vol. 1. London, Leonard Hill, 1969, 252 p.
14. DUNCAN, N., DUNNE, M.H. and PETTY, S.: Swelling characteristics of rock. Water Power, Vol. 20, 1968, pp. 185–192.
15. FATT, I.: The effect of overburden pressure on relative permeability. J. Pet. Tech., Vol. 5, No. 10, Oct., 1953, pp. 15–16.
16. FATT, I. and DAVIS, D.H.: Reduction in permeability with overburden pressure. Trans. A.I.M.E., Vol. 195, 1952, p. 329.
17. FISHER, C. and NAZARETH, L.J.: Classified treatments for the application of the quantimet to stereological problems. The Microscope, Vol. 16, 1968, pp. 95–104.
18. FRANKLIN, J.A. and CHANDRA, R.: The slake-durability test. Int. J. Rock Mech. Min. Sci., Vol. 9, 1972, pp. 325–341.
19. FRANKLIN, R.E.: A study of the fine structure of carbonaceous solids by measurements of true and apparent densities. Trans. Faraday Soc., Vol. 45, 1949, pp. 274–286.
20. GAMBLE, J.C.: Durability-plasticity classification of shales and other argillaceous rocks. Ph. D. Thesis, Univ. Illinois, Urbana, Illinois, 1971.

21. GRAY, D.H.: The effect of stress on the directional properties of reservoir rocks. M.S. Thesis, Univ. Calif., Berkeley, Calif., 1962.

22. HABIB, P. and VOUILLE, G.: Sur la disparition de l'echelle aux hautes pressions. C.R. Acad. Sci. Paris, Vol. 262B, 1966, pp. 715–717.

23. HALEVY, E., MOSER, H., ZELLHOFER, O. and ZUBER, A.: Borehole dilution techniques: A critical review. Proc. Symp. Isotopes in Hydrology, Vienna, 1966, pp. 531–563.

24. I.S.R.M. Committee on Laboratory Tests: Suggested methods for determining water content, porosity, density, absorption and related properties and swelling and slake-durability index properties. Document No. 2, Nov., 1972, 36 p.

25. JAEGER, C.: Rock Mechanics and Engineering. Cambridge, University Press, 1972, 417 p.

26. JUDD, W.R. and HUBER, C.: Correlation of rock properties by statistical methods. Proc. Int. Symp. Min. Res., Rolla, Missouri, 1961, Vol. 2, pp. 621–648.

27. KIRKHAM, D.: Proposed method for field measurement of permeability of soil below the water table. Soil Sci. Soc. Am. Proc., Vol. 10, 1945, pp. 58–68.

28. KNUTSON, C.F. and BOHOR, B.F.: Reservoir rock behaviour under moderate confining pressure. Proc. 5th Symp. Rock Mech., Minneapolis, Minn., 1962, pp. 627–658.

29. KOWALSKI, W.C.: The interdependence between the strength and voids ratio of limestones and marls in connection with their water saturating and anisotropy. Proc. 1st Cong. Int. Soc. Rock. Mech., Lisbon, 1966, Vol. 1, pp. 143–144.

30. LONDE, P. and SABARLY, F.: Permeability distribution in arch dam foundations as a function of the stress field. Proc. 1st Cong. Int. Soc. Rock Mech., Lisbon, 1966, Vol. 2, pp. 517–521.

31. LOUIS, C. and MAINI, Y.N.T.: Determination of in situ hydraulic parameters in jointed rock. Proc. 2nd Cong. Int. Soc. Rock Mech., Belgrade, 1970, Vol. 1, pp. 235–245.

32. MAINI, Y.N.T.: In situ hydraulic parameters in jointed rock — Their measurement and interpretation. Ph. D. Thesis, Univ. London, London, 1971, 325 p.

33. MAINI, Y.N.T.: The use of radioisotopes in rock mechanics. D.I.C. Thesis, Univ. London, London, 1968, 25 p.

34. MAINI, Y.N.T., NOORISHAD, J. and SHARP, J.: Theoretical and field considerations on the determination of in situ hydraulic parameters in fractured rock. Proc. Symp. Percolation through Fissured Rock, Stuttgart, Germany, 1972, Paper T1-E.

35. MCLATCHIE, A.S., HEMSTOCK, R.A. and YOUNG, J.W.: The effective compressibility of reservoir rock and its effects on permeability. J. Pet. Tech., Vol. 10, 1958, pp. 49–51.

36. MICHEL, G.: Knowledge of the groundwater conductivity of Mesozoic rock of East-Westphalia from experience in well sinkings. Proc. Symp. Percolation through Fissured Rock, Stuttgart, Germany, 1972, Paper T3-F.

37. MORDECAI, M. and MORRIS, L.H.: The effects of stress on the flow of gas through coal measure strata. Min. Engr., No. 164, July, 1974, pp. 435–443.

38. MORLIER, P.: Evolution of petrophysical parameters of cracked rock with pressure. Proc. Symp. Rock Fracture, Nancy, 1971, Paper II-15.

39. MUSKAT, M.: Physical Principles of Oil Production. New York, McGraw-Hill, 1949, 922 p.

40. NUTTING, P.G.: Physical analysis of oil sands. Bull. Am. Assoc. Pet. Geol., Vol. 14, 1930, pp. 1337–1349.

41. OHNISHI, Y. and GOODMAN, R.E.: Results of laboratory tests on water pressure and flow in joints. Proc. 3rd Cong. Int. Soc. Rock Mech., Denver, 1974, Vol. II, Part A, pp. 660–666.

42. PIRSON, S.J.: Oil Reservoir Engineering. 2nd edition, New York, McGraw-Hill, 1958, 735 p.

43. PRICE, N.J.: The compressive strength of coal measure rocks. Coll. Eng., Vol. 37, 1960, pp. 283–292.

44. RALL, C.G., HAMONTRE, H.C. and TALIAFERRO, D.B.: Determination of porosity by a Bureau of Mines method: A list of porosities of oil sands. U.S.B.M., R.I. 5025, 1954, 24 p.

45. RALL, C.G. and TALIAFERRO, D.B.: A Bureau of Mines method for determining porosity: A list of porosities of oil sands. U.S.B.M., R.I. 4548, 1949, 28 p.

46. RAMANA, Y.V. and VENKATANARAYANA, B.: An air porosimeter for the porosity of rocks. Int. J. Rock Mech. Min. Sci., Vol. 8, No. 1, Jan., 1971, pp. 2953.

47. RAMANA, Y.V. and VENKATANARAYANA, B.: Calibration of air porosimeter – Nature of the curve. Int. J. Rock Mech. Min. Sci. and Geomech. Abstr., Vol. 11, No. 7, July, 1974, pp. 279–280.

48. RITTER, H.L. and DRAKE, L.C.: Pore-size distribution in porous materials. Ind. Eng. Chem. Anal. Ed., Vol. 17, No. 12, Dec., 1945, pp. 782–786.

49. RZHEVSKY, V. and NOVIK, G.: The Physics of Rocks. Moscow, MIR Publishers, 1971, 320 p.

50. SANYAL, S.K., KVENVOLDEN, K.A. and MARSDEN, S.S. Jr.: Permeabilities of Precambrian Onverwacht cherts and other low permeability rocks. Nature, Vol. 232, No. 5309, July 30, 1971, pp. 325–327.

51. SANYAL, S.K., PIRNIE, R.M. III, CHEN, G.O. and MARSDEN, S.S. Jr.: A novel liquid permeameter for measuring very low permeability. Soc. Pet. Eng. J., Vol. 12, No. 3, June, 1972, pp. 206–210.

52. SARDA, J.P., LETIRANT, P. and BARON, G.: Influence of external stresses and fluid pressure on the flow in fissured rocks. Proc. 3rd Cong. Int. Soc. Rock Mech., Denver, 1974, Vol. II, Part A, pp. 667–673.

53. SCHILLER, K.K.: Porosity and strength of brittle solids (with particular reference to gypsum). Proc. Conf. Mech. Prop. Non-metallic Brittle Materials, London, 1958, pp. 35–45.

54. SERAFIM, J.L.: Influence of interstitial water on the behaviour of rock masses. In Rock Mechanics in Engineering Practice by K.G. STAGG and O.C. ZIENKIEWICZ (Editors). London, Wiley, 1968, pp. 55–97.

55. SERAFIM, J.L. and DEL CAMPO, A.: Interstitial pressures on rock foundations of dams. J. Soil Mech. Found. Div., Am. Soc. Civ. Eng., Vol. 91, No. SM5, Sept., 1965, pp. 65–85.

56. SERAFIM, J.L. and LOPES, J.J.B.: In situ shear tests and triaxial tests of foundation rocks of concrete dams. Lab. Nacional de Engenharia Civil., Tech. Paper No. 190, 1962, 7 p.

57. SHARP, J.C. and MAINI, Y.N.T.: Fundmental considerations on the hydraulic characteristics of joints in rock. Proc. Symp. Percolation through Fissured Rock, Stuttgart, Germany, 1972, Paper T1-F.

58. SMILES, D.E. and YOUNGS, E.G.: Hydraulic conductivity determinations by several field methods in a sand tank. Soil Sci., Vol. 99, 1965, pp. 83–87.

59. SMORODINOV, M.I., MOTOVILOV, E.A. and VOLKOV, V.A.: Determinations of correlation relationships between strength and some physical characteristics of rocks. Proc. 2nd Cong. Int. Soc. Rock. Mech., Belgrade, 1970. Vol. 2, pp. 35–37.

60. SNOW, D.T.: Fundamentals and in situ determination of permeability (General Report of Theme 1). Proc. Symp. Percolation through Fissured Rock, Stuttgart, Germany, 1972, Paper G1.

61. SPRUNT, E.S. and BRACE, W.F.: Direct observation of microcavities in crystalline rocks. Int. J. Rock Mech. Min. Sci. and Geomech. Abstr., Vol. 11, No. 4, April, 1974, pp. 139–150.

62. TALIAFERRO, D.B., JOHNSON, T.W. and DEWEES, E.J.: A method of determining porosity: A list of porosities of oil sands. U.S.B.M., R.I. 3352, 1937, 24 p.

63. TERZAGHI, K. and PECK, R.B.: Soil Mechanics in Engineering Practice. New York, Wiley, 1948, 566 p.

64. THIEM, G.: Hydrologische Methoden. Leipzig, Gebhart, 1906, 56 p.

65. TICKELL, F.G.: The Examination of Fragmental Rocks. Stanford, University Press, 1947, 154 p.

66. U.S. Bureau of Reclamation: Design of small dams. 1960.

67. U.S. Bureau of Reclamation: Earth manual. Denver, 1963, 783 p.

68. VAN KREVELEN, D.W. Coal: Typology, Chemistry, Physics and Constitution. Amsterdam, Elsevier, 1961, 514 p.

69. WASHBURN, E.W. and BUNTING, E.N.: The determination of the porosity of highly vitrified bodies. J. Am. Cer. Soc., Vol. 5, 1922, pp. 527–537.

70. WURZEL, P.: Radioisotopes in underground water investigations in Rhodesia. Trans. Geol. Soc. S. Africa, Vol. 75, 1972, pp. 5–10.

71. WURZEL, P. and WARD, P.R.B.: A simplified method of groundwater direction measurement in single borehole. J. Hydrology, Vol. 3, 1965, pp. 97–105.

72. WYBLE, D.O.: Effect of applied pressure on the conductivity, porosity and permeability of sandstones. Trans. AIME, Vol. 213, 1958, pp. 430–432.

Uncited References to Chapter 12

1. AFINOGENOV, YU. A. and KASYANOV, M.V.: Influence of heteroaxial compression of rock specimens on their porosity and permeability. Sov. Min. Sci., Vol. 9, No. 3, May-June, 1973, pp. 326–328.
2. ALEKSEYEV, A.D., BREKHUNETS, A.G. and ZHURAVLEV, V.I.: Use of NMR to study the hydrodynamic properties of rocks. Sov. Min. Sci., No. 2, March-April, 1970, pp. 136–138.
3. ARNOLD, M.: Laboratory determination of the coefficient of electroosmotic permeability of a soil. Geotechnique, Vol. 23, No. 4, Dec., 1973, pp. 581–588.
4. BERNAIX, J.: New laboratory methods of studying the mechanical properties of rocks. Int. J. Rock Mech. Min. Sci., Vol. 6, No. 1, Jan., 1969, pp. 43–90.
5. BISHOP, A.W. and AL-DHAHIR, Z.A.: Some comparisons between laboratory tests, in situ tests and full scale performance, with special reference to permeability and coefficient of consolidation. Proc. Conf. In-situ Invest. Soils and Rocks, London, 1969, pp. 251–264.
6. BOLTWER, H.: Planning and interpreting soil permeability measurements. J. Irrigation, Drainage Div., Am. Soc. Civ. Eng., Vol. 95, IR 3, Sept., 1969, pp. 391–402.
7. BRADLEY, J.S., DUSCHATKO, R.W. and HINCH, H.H.: Pocket permeameter: Hand-held device for rapid measurement of permeability. Bull. Am. Assoc. Pet. Geol., Vol. 56, No. 3, March, 1972, pp. 568–571.
8. DICK, R.C.: Insitu measurement of rock permeability: Influence of calibration errors on test results, Bull. Assoc. Engng Geol., Vol. XII, No. 3, 1975, pp. 193–211.
9. CALDWELL, J.A.: Fluid flow in rock masses. In Stability of Rock Slopes. S. African Instn. Civ. Engrs., Johannesburg, 1973, Chapter 7, pp. 7.1–7.85.
10. CHERNYSHEV, S.N.: Estimation of the permeability of the jointy rocks in massif. Proc. Symp. Percolation through Fissured Rock, Stuttgart, Germany, 1972, Paper T1-G.
11. COLONNA, J., BRISSAUD, F. and MILLET, J.L.: Evolution of capillarity and relative permeability hysteresis—Laboratory test shows the effects of alternate displacements of water and gas on hydrodynamic characteristics of rock. Soc. Pet. Eng. J., Vol. 12, No. 1, 1972, pp. 28–38.
12. CROOK, J.M. and HOWELL, F.T.: Three new simple tests for measuring and estimating the permeability of the permo-triassic sandstones of northwest England. Geotechnique, Vol. 20, No. 4, 1970, pp. 446–451.
13. CROOK, J.M., HOWELL, F.T., WOODHEAD, F.A. and WORTHINGTON, P.F.: Permeation properties of Bunter sandstones from the Cheshire and Fylde basins. Geotechnique, Vol. 23, No. 2, June, 1973, pp. 262–265.
14. GIBSON, R.E.: An extension of the theory of constant head in situ permeability test. Geotechnique, Vol. 20, No. 2, June, 1970, pp. 193–197.
15. GODSE, V.B. and SINGH, M.: Groundwater movement studies in radioactive waste storage site, Trombay. Bhaba Atomic Res. Centre, Bombay, India, Report No. BARC-478, 1970, 14 p.
16. GRIFFITHS, J.C.: Scientific Method in Analysis of Sediments. New York, McGraw-Hill, 1967, 508 pp.

17. HARPER, T.R.: Some observations of the influence of geological environment upon groundwater. Proc. Symp. Percolation through Fissured Rock, Stuttgart, Germany, 1972, Paper T4-D.
18. HARPER, T.R.: A technique of field permeability testing employing a single packer suspended by wire line. Proc. 3rd Cong. Int. Soc. Rock Mech., Denver, 1974, Vol. 2, Part B, pp. 705–712.
19. HOLLABAUGH, G.R. and SLOTBOOM, R.A.: A vertical permeability study—Contribution of cross-flow and method for averaging vertical permeabilities. Soc. Pet. Eng. J., Vol. 12, No. 3, 1972, pp. 199–205.
20. HOWELL, F.T., PAYNE, C.J. and THOMPSON, P.J.: A permeameter for investigating the passage of water through unfissured samples of Permo-Triassic sandstone. Civil Eng. Public Works Rev., Vol. 67, No. 788, March, 1972, pp. 261–262.
21. HOWELL, F.T. and WOODHEAD, F.A.: A null method for the estimation of the permeability of irregular specimens of permeable strata. Geotechnique, Vol. 22, No. 2, June, 1972, pp. 352–356.
22. HUBERT, M.K.: The Theory of Groundwater Motion and Related Papers. New York, Hafner Publ. Co., 1969, 311 p.
23. HUPPLER, J.D.: Water flood relative permeabilities in composite cores. J. Pet. Tech., May, 1969, pp. 539–540.
24. I.A.E.A.: Guidebook on Nuclear Techniques in Hydrology. Vienna, Int. Atomic Energy Agency, 1969, 214 p.
25. JOUANNA, P.: Laboratory tests on the permeability of micaschist samples under applied stresses. Proc. Symp. Percolation through Fissured Rock, Stuttgart, Germany, 1972, Paper T2-F.
26. KLEMENTEV, I.: Lever-type apparatus for electrically measuring volume change. Geotechnique, Vol. 24, No. 4, Dec., 1974, pp. 670–671.
27. KLOCK, G.O., BOERSMA, L. and DE BACKER, L.W.: Pore size distributions as measured by mercury intrusion and their use in predicting permeability. Soil Sci. Soc. Am. Proc., Vol. 33, No. 1, 1969, pp. 12–15.
28. KOWALSKI, W.C.: The interdependence between strength, softening, swelling and shrinkage of Cretaceous marl. Proc. Int. Cong. Int. Assoc. Eng. Geol., Paris, 1970, pp. 457–464.
29. LANCASTER-JONES, P.F.F.: The interpretation of Leugeon water-test, Q. J. Engng. Geol., Vol. 9, 1975, pp. 151–154.
30. LONDE, P.: Rock mechanics and dam foundation design. Int. Commission on Large Dams, Committee on International Relations, 1973.
31. MUNDI, E.K. and WALLACE, J.R.: On the permeability of some fractured crystalline rocks. Bull. Assoc. Eng. Geol., Vol. 10, No. 4, 1973, pp. 299–312.
32. MUSKAT, M.: The flow of homogeneous fluids through porous media. New York, McGraw-Hill, 1937.
33. MURAYAMA, S. and YAGI, N.: Swelling of mudstone due to sucking of water. Rock Mech. in Japan, Vol. 1, 1970, pp. 65–67.
34. NINI, H.: Engineering geological classification and measurement of the broken bed rock in Finland. 2nd Int. Cong. Int. Assoc. Engng. Geol., Sao Paulo, Vol. 1, 1974, pap. IV-6.1.
35. OWENS, W.W. and ARCHER, D.L.: The effect of rock wettability on oil water relative permeability relationships. J. Pet. Tech., Vol. 23, July, 1971, pp. 873–878.

36. PASCAL, H.: Concerning several methods of the in situ determination of permeability in porous media. In French. Rev. Inst. Franc. Petr., Vol. 24, No. 3, 1969, pp. 275–289.

37. PRYOR, W.A.: Reservoir inhomogeneities of some recent sand bodies – Measurement of permeability, porosity and texture. Soc. Petr. Eng. J., Vol. 12, No. 3, 1972, pp. 229–245.

38. RIEKE, H.H. III and CHILINGARIAN, G.V.: Compaction of Argillaceous Sediments. Amsterdam, Elsevier, 1974, 424 p.

39. RAYMOND, G.P. and AZZOUZ, M.M.: Permeability determination for predicting rates of consolidation. Proc. Conf. In-situ Invest. Soils and Rocks, London, 1969, pp. 285–293.

40. REMY, J.P.: The measurement of small permeabilities in the laboratory. Geotechnique, Vol. 23, No. 3, Sept., 1973, pp. 454–458.

41. SCHNEIDER, F.N. and OWENS, W.W.: Sandstone and carbonate two and three phase relative permeability characteristics. Soc. Petr. Eng. J., Vol. 10, No. 1, 1970, pp. 75–84.

42. SNOW, D.T.: Rock fracture spacings, openings & porosities. J. Soil Mech. & Found. Div. ASCE, SM-1, Jan. 1968, pp. 73–91.

43. SOMERTON, W.H., MASONHEIMER, R. and SINGHAL, A.: Study of pore and matrix anisotropy of porous rocks, 2nd Cong. Int. Soc. of Rock Mech., Belgrade, Vol. 1, 1970, Pap. 1–21.

44. SOMERTON, W.H., SOYLEMZOGEN, I.M. and DUDLEY, R.C.: Effect of stress on the permeability of coal. U.S.B.M. Openfile Report 45–74, 56 p.

45. WARDLAW, N.C.: Pore geometry of carbonate rocks as revealed by pore casts and capillary pressure, Am. Assoc. Petrol. Geol., Vol. 60, 1976, pp. 245–257.

46. WARREN, N.: Theoretical calculation of compressibility of porous media. J. Geophys. Res., Vol. 78, No. 2, Jan. 10, 1973, pp. 352–362.

47. WEINBRANDT, R.M. & FATT, I.: Scanning electron microscope study of the pore structure of sandstone, 11th Symp. Rock Mech., Berkeley, 1968, pp. 629–641.

APPENDIX V

Stereographic Projections

Principle of Stereographic Projections

The strike of any structural plane is measured in terms of 360° compass-rose setting the 0° due North and graduating clockwise. The dip is measured with respect to the horizontal plane and its azimuth is given with respect to the North-South line. Thus, for example, the location of a plane in space can be truely defined by stating that its direction of strike say 300° and dip 50° South-West (Fig. 1a). If a sphere is drawn around the point *O* lying in this plane, such that the point *O* (Fig. 1b) lies at the centre of this sphere, the plane shall cut the sphere boundaries along a great circle. Thus the great circle is defined as the intersection of a sphere by any plane passing through the centre of the sphere. The spherical projection of the lower half of this great circle on a two dimensional horizontal plane (equatorial plane) passing through *O* is called the stereographic projection of this plane (Fig. 2a). It can be obtained by joining all points of the great circle to the zenith *P* of the sphere cutting the equatorial plane (Fig. 2b).

The stereogram is an arc of a circle. If a series of planes is projected striking N-S, and dipping E (or W), at various angles we get a net of meridional (great circle) curves. Similarly, the projections of the small circles[1] can also be obtained giving circular arcs. If N and S are taken as centres and a series of small circles is drawn with increasing radius, we shall get their projections in a similar way as a series of arcs. These stereograms of the great and small circles together give a stereographic net called the 'WULFF net' (Fig. 3) which represents the stereograms for every 10° increase in the dip angle.

(1) A small circle is the intersection of a sphere by any plane not passing through the centre of the sphere.

APPENDIX

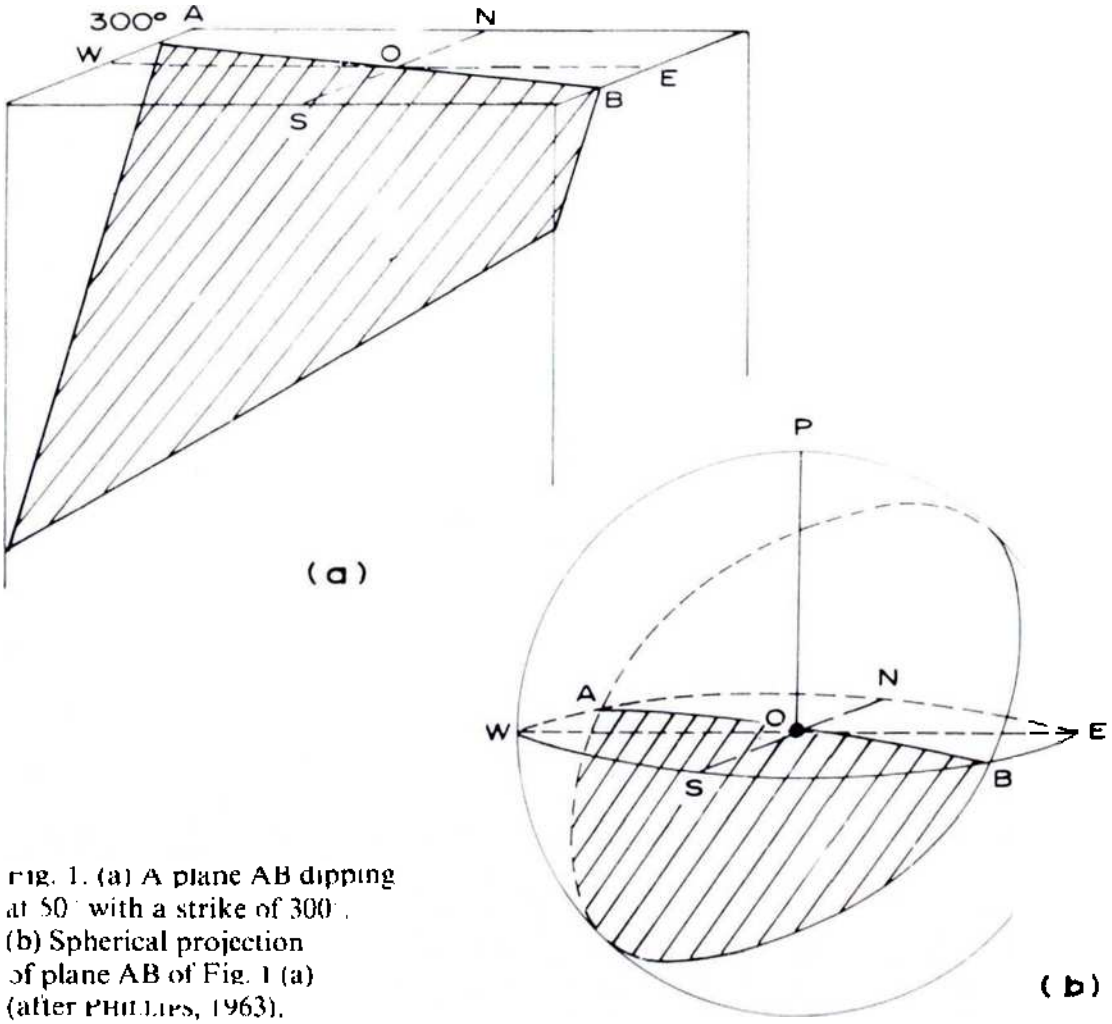

Fig. 1. (a) A plane AB dipping at 50° with a strike of 300°. (b) Spherical projection of plane AB of Fig. 1 (a) (after PHILLIPS, 1963).

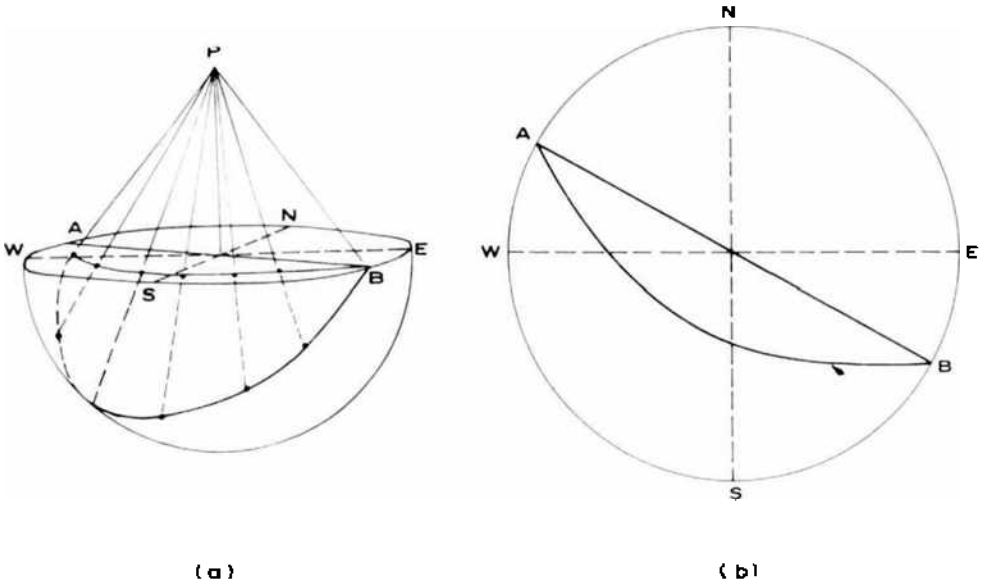

Fig. 2. (a) Stereographic projection of the plane AB (Fig. 1). (b) Completed stereogram of the plane AB (after PHILLIPS, 1963).

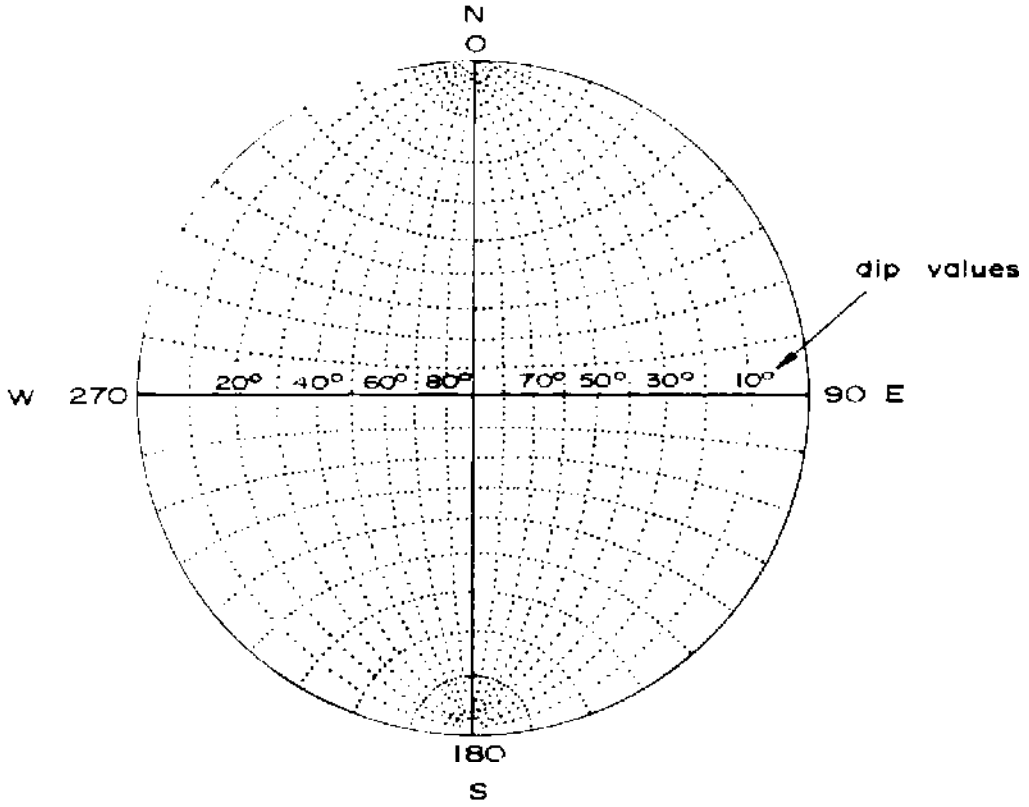

Fig. 3. A 'WULFF' stereographic net.

Tracing the Stereographic Projection of a Joint Plane

It is not essential to go through the complicated drawing for tracing the stereographic projection of any plane or a joint, but the WULFF net can be easily used for the purpose. A sheet of tracing paper on which the stereogram is required to be drawn, is placed over such a net. The N-S and E-W lines on this paper are drawn and the strike direction marked. A circle of diameter equal to that of the WULFF net is also drawn over it. The tracing paper is then so rotated that the strike direction corresponds with the N-S line of the WULFF net with the centres of two circles always coinciding with each other. The stereogram is then traced out running along the line of corresponding dip.

The true dip is measured from the outermost circle (primitive) which represents a plane with angle of dip = 0 (flat) and the N-S line represents a plane with an angle of dip = 90 . Thus for the plane with strike of 300° and dip of 50° , the distance *e-f* (Fig. 4) represents the true dip which is measured by dropping a right angle from the centre of the stereographic net to the projection of the plane and measuring this point of intersection from the primitive.

To determine apparent dip in any other direction, what is required is to draw the azimuth line in the direction its value is required to be determined and

measure out the distance from the outermost circle on rotation. For example, the apparent dip of this plane in the W-direction is only *a-b* and is equal to 16°.

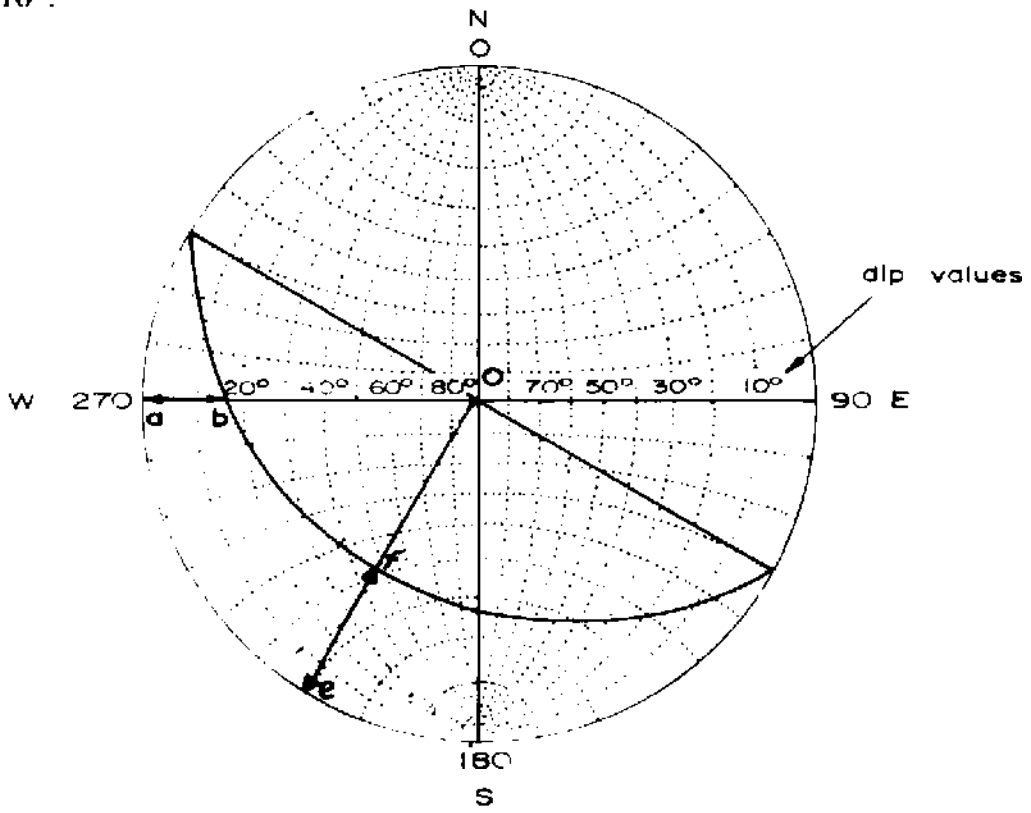

Fig. 4. Stereogram for determination of true and apparent dip (after PHILLIPS, 1963).

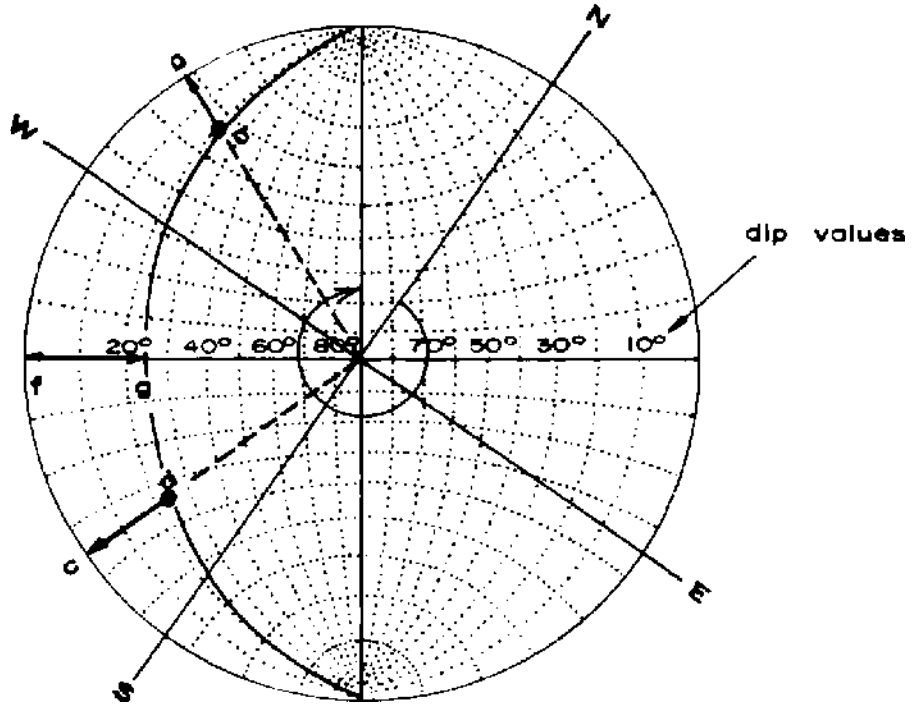

Fig. 5. Stereographic determination of true dip from two apparent dips (after PHILLIPS, 1963)

Similarly, if the apparent dip values of any joint plane are known in any two directions, these points can be marked out on the WULFF net (Fig. 5) (*ab* and *cd*). The net may then be rotated over another net so that the 2 points lie on one of the great circles marked on the underlying net and running from North to South. This then gives the projection of the joint plane and the azimuth measured from the North in the clockwise direction gives the strike direction. If a fault plane is represented, then the hade of the fault is given by measuring from the centre of the net (*og* in Fig. 5).

Intersection of Two Joints

When more than one joint plane is present in a rock mass, the determination of the line of intersection of these becomes very important. This problem is of fundamental basis in the analysis of the slope stability in jointed rocks (JOHN, 1968; MARKLAND, 1972 and HOEK and BRAY, 1974).

The projections of the two joint planes are plotted as usual independently (Fig. 6). The point of intersection (*p*) of the two stereograms gives the projection of the line of intersection of the two planes. The distance *pq* represents the plunge. Thus, when one joint plane with a strike of N 110° E and dip of 20° S and another with a strike of N 75° E and dip of at 60° S are plotted, they intersect along a line bearing 247° and plunge of 14° (Fig. 6a).

If the two joint sets are dipping in the exactly opposite directions as in Fig. 6b, the bearing of the line of intersection is given by the equator *pg* and this line of intersection has zero plunge.

Preferred Orientation of Discontinuities

In actual practice, one is hardly concerned with an individual structural discontinuity. A large number of scattered observations are taken and have to be presented and these invariably do not group into one, two or three sets of discontinuities. It is invariably required to determining the most probable orientation of the various discontinuities present in the field observations.

Here it becomes usually impossible to draw each of the various discontinuities measured as it would make the diagram extremely crowded. A more simple way of representing the individual plane of discontinuity is to represent it by a single point called the pole to the plane. The pole to the plane is the point at which the surface of the sphere is pierced by the radial line placed normal to the plane (Fig. 7). Thus the pole to the plane *bCOD* in Fig. 7 is represented by *P*. The distance from the centre *O* represents the dip of the plane $OP = ab$.

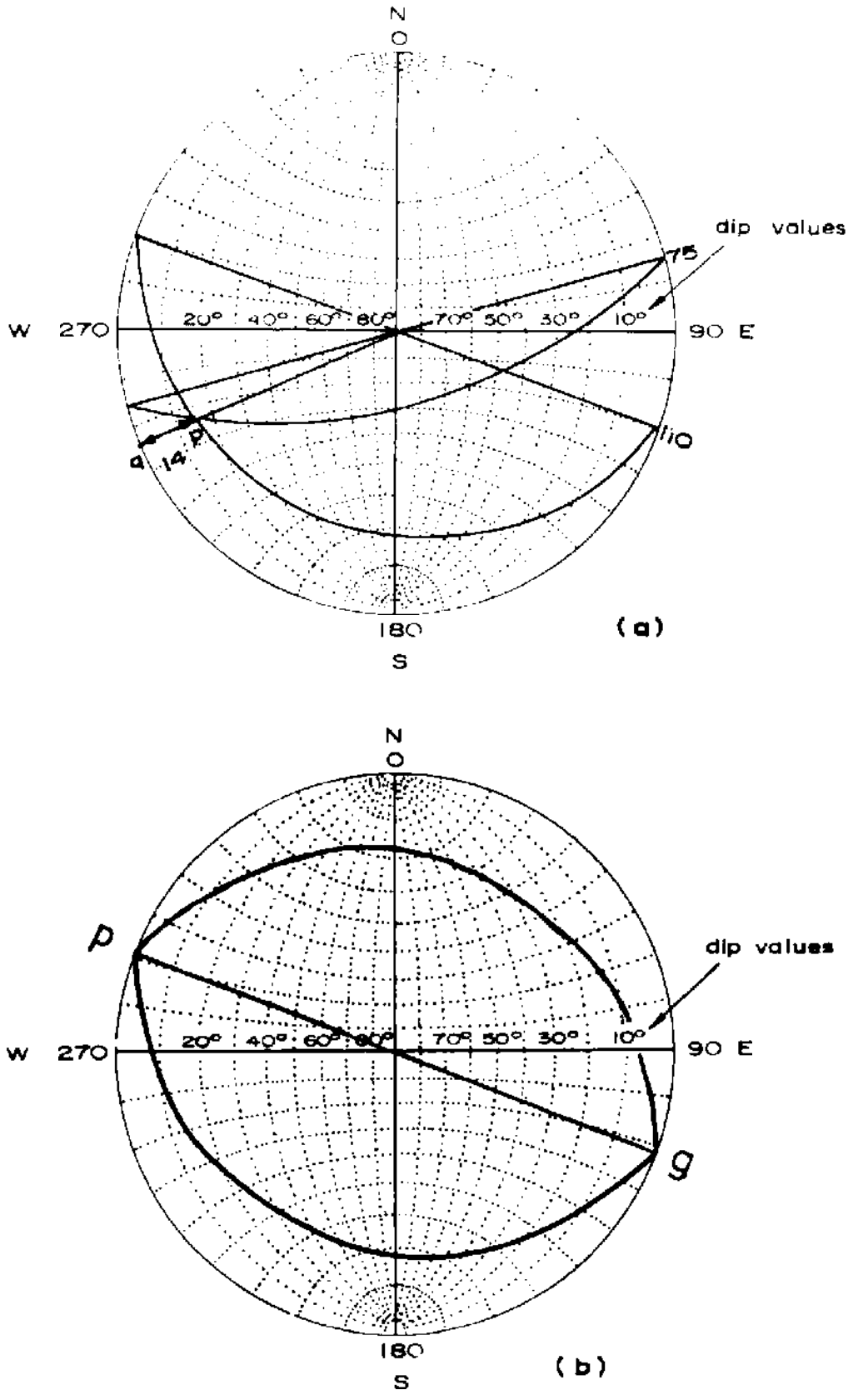

Fig. 6. Intersection of two planes.

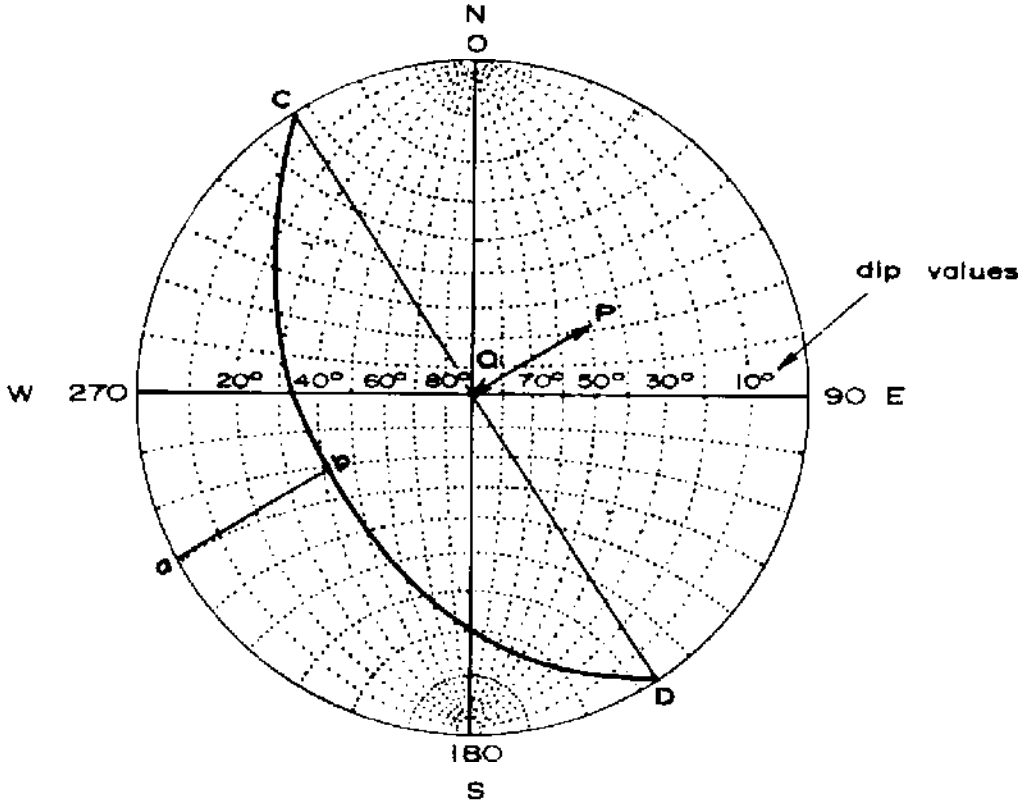

Fig. 7. Pole 'P' of a plane *hCOD*.

In practice, the poles are not plotted on the WULFF net because of the disadvantage associated with it that it is an unequal area-net. Usually the LAMBERT equal area projection called as the SCHMIDT net (Fig. 8) or the polar equal area net (Fig. 9) is used. In this case a family of small circles is centred about the extremity of the axis normal to the plane of projection and the great circles pass through this axis.

In any tectonic study of an area, the poles of the planes observed are plotted on an equal area net (Fig. 10). This plot shows a clear concentration of the poles near the primitive in the N-E and S-W quadrants, but a more clear and numerical picture is obtained by using a contouring technique commonly used in structural geology (MÜLLER, 1933, 1963; BILLINGS, 1942).

The equal area projection of the poles is placed over a squared paper (Fig. 11) and scanned by moving a thin transparent plastic scale with a 1 cm diameter hole cut at the ends in such a way that the centre of the scale coincides with the centre of the polar diagram. The number of poles falling in the circular hole are counted and marked with a certain number say 5. The circular hole may be either centred on the crosslines (Fig. 11) or at the junctions of the major and minor circles. For centres lying on the primitive, the same figure is written at both the ends (e.g. number 2 at the North and South). After the diagram has been scanned, contours are drawn and the area shaded showing the different density of the pole concentrations (Fig. 12).

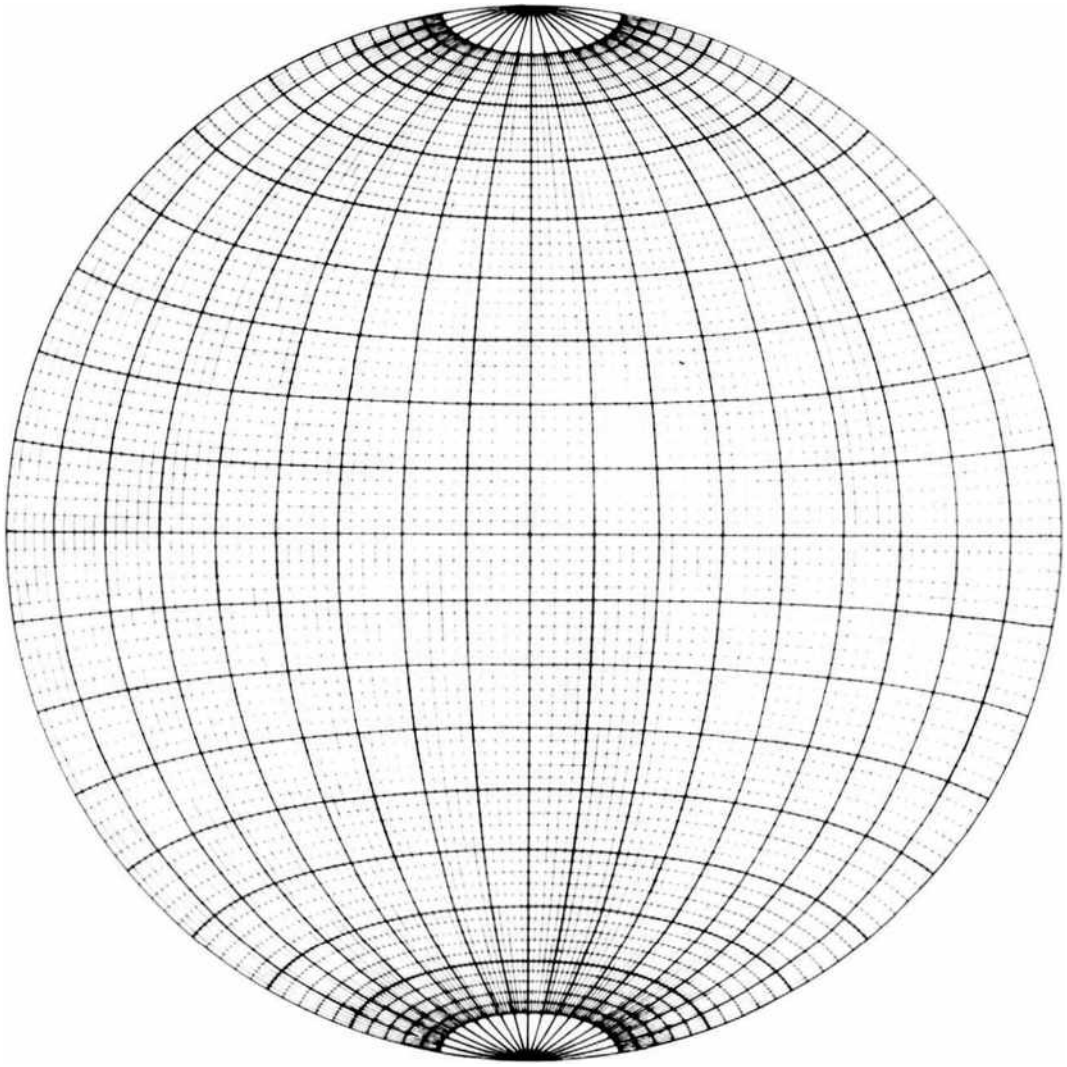

Fig. 8. SCHMIDT net.

Fig. 12 shows that the area has two major sets of complimentary joint systems making an angle of about 110° almost symmetrically about the N-S line and a minor joint system running E-W almost bisecting the angle formed between the two joints N-S.

The positioning of these poles near the primitive also shows that the joints are statistically more or less vertical though there might be some local variations in individual joints.

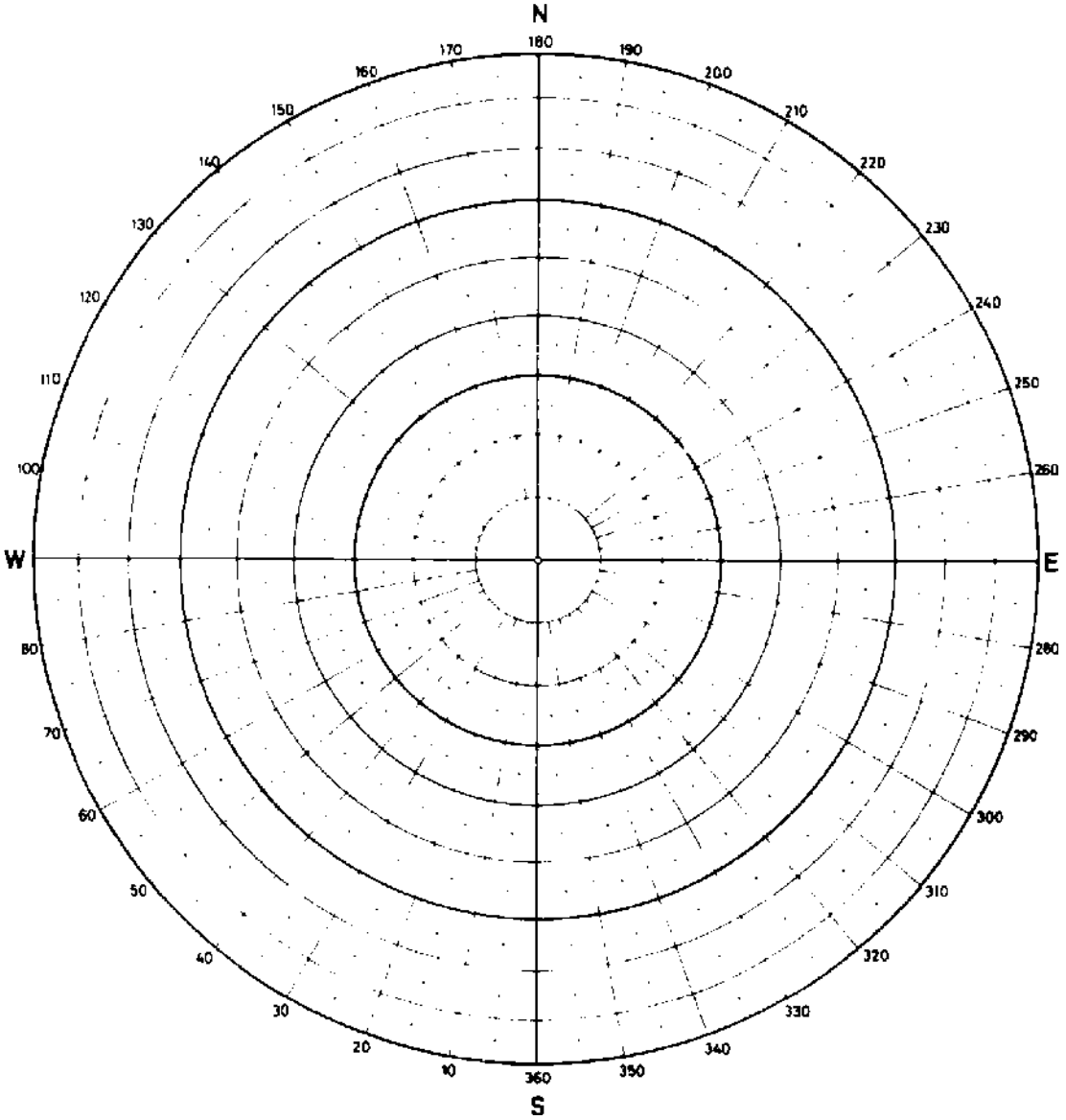

Fig. 9. Polar equal area net.

Accuracy of the Stereographic Projection Technique

The accuracy of the data obtained in the stereographic projection analysis depends upon the size of the net used. Usually, a 20 cm diameter net with every 2 degree graduations is commonly adopted for most of the field and laboratory analysis in the engineering geology and rock mechanics problems. Greater accuracy is reached using WULFF net when the angles of dip are small; and when dips are large the SCHMIDT net or the polar equal area net is advisable.

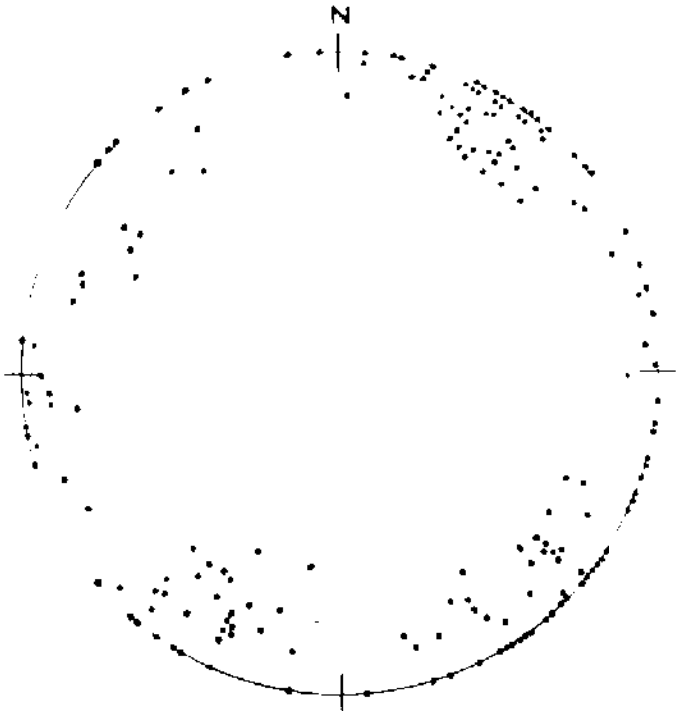

Fig. 10. Equal-area projection of the poles of joints (after PHILLIPS, 1963).

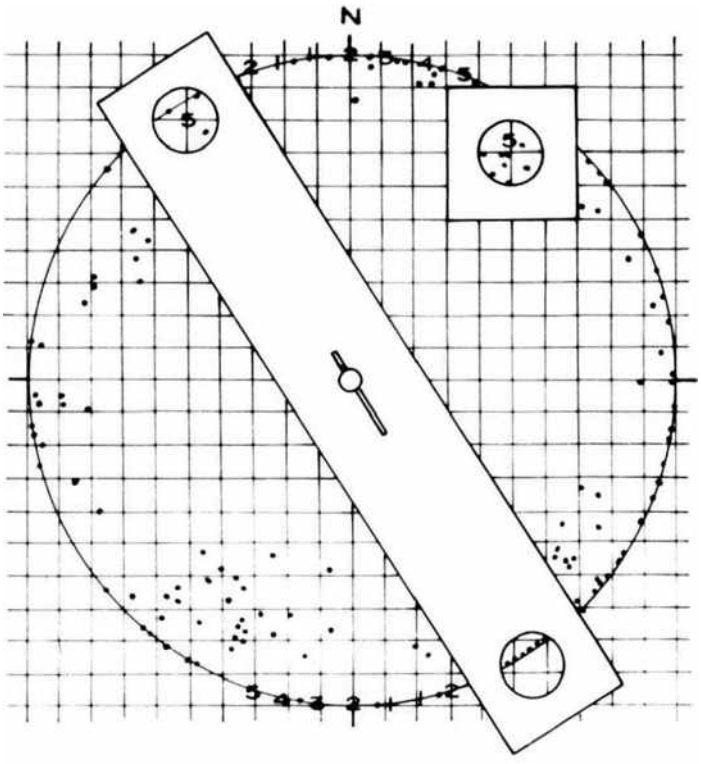

Fig. 11. Counting of the projection of Fig. 10 (after PHILLIPS, 1963).

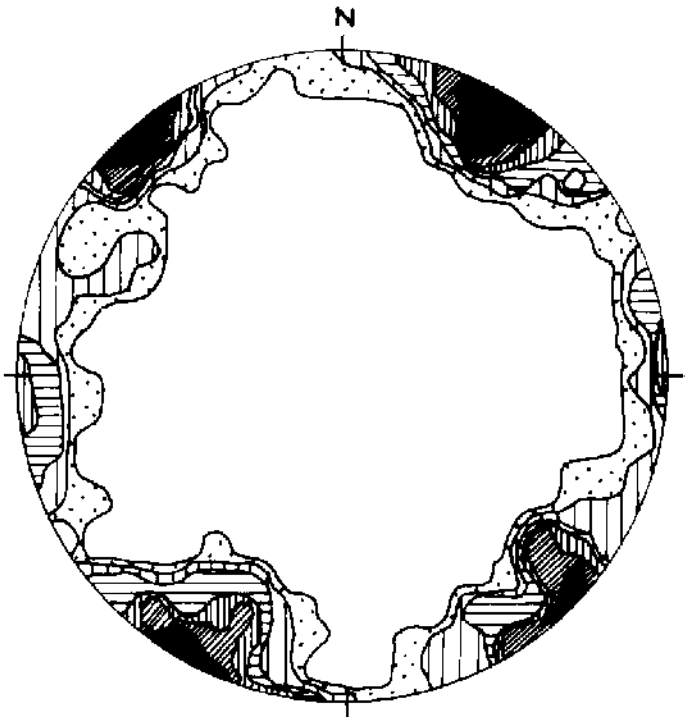

Fig. 12. The projection of Fig. 10 contoured and shaded (after PHILLIPS, 1963).

When two planes intersect at lower angles, the error in the graphical construction is enhanced and it is advisable that in such cases, a larger number of observations be made.

There are many other applications of the stereographic projections than outlined here. PHILLIPS (1963) has discussed the technique and its applications in a very lucid way. Some other standard works may be referred to for more details.

References to Appendix V

1. BILLINGS, M.P.: Structural Geology. Englewood Cliffs, N.J., Prentice-Hall, 1942.
2. HOEK, E. and BRAY, J.: Rock Slope Engineering. London, Inst. Min. Metall., 1974, 309 p.
3. JOHN, K.W.: Graphical stability analysis of slopes in jointed rock. J. Soil Mech. Found. Div., Am. Soc. Civ. Eng., Vol. 94, 1968, pp. 497 526. (Discussion and closure, Vol. 95, 1969, pp. 1541 1545).
4. MARKLAND, J.T.: A useful technique for estimating the stability of rock slopes when the rigid type sliding failure is expected. Imp. Coll. Rock Mech. Res. Rep. No. 19, May, 1972, 10 p.
5. MÜLLER, L.: Untersuchungen über statistische Kluftmessung. Geol.- u. Bauwesen, Jahrg. 5, 1933, pp. 185–255.
6. MÜLLER, L.: Der Felsbau. Bd. I. Stuttgart, Ferdinand Enke, 1963. 623 p.
7. PHILLIPS, F.C.: The Use of Stereographic Projection in Structural Geology. 2nd edition. London, Edward Arnold, 1963, 86 p.

APPENDIX VI

Definition of Some Rock Mechanics Terms

(extracted from the document on Terminology as prepared by the Commission on "Terminology, Symbols and Graphic Representation" of the International Society for Rock Mechanics
(Final Draft: July 1975)

ENGLISH
FRENCH
GERMAN

To facilitate search, the corresponding definitions of terms in English, French and German have been assigned a number as given in the Index below.

ENGLISH

INDEX

W

Y

APPENDIX

ENGLISH

INDEX

1 – coefficient of friction	A constant proportionality factor, μ relating normal stress and the corresponding critical shear stress at which sliding starts between two surfaces: $\tau = \mu \cdot \sigma$
2 – angle of internal friction, angle of shear resistance	The angle, ϕ between the axis of normal stress and the tangent to the Mohr envelope at a point representing a given failure-stress condition for solid material.
3 – angle of repose	The maximum angle with respect to the horizontal plane that the surface of a pile of a loose material will assume
4 – deviator of stress/strain	The stress/strain tensor obtained by subtracting the mean of the normal stress/strain components of a stress/strain tensor from each normal stress/strain component
5 – stress ellipsoid	The representation of the state of stress in the form of an ellipsoid whose semi-axes are proportional to the magnitudes of the principal stresses and lie in the principal directions. The coordinates of a point P on this ellipsoid are proportional to the magnitudes of the respective components of the stress across the plane normal to the direction OP, where O is the centre of the ellipsoid
6 strain ellipsoid	The representation of the strain in the form of an ellipsoid into which a sphere of unit radius deforms and whose axes are the principal axes of strain
7 – elastic strain energy	Potential energy stored in a strained solid and equal to the work done in deforming the solid from its unstrained state less any energy dissipated by inelastic deformation
8 – stress/strain field	The ensemble of stress/strain states defined at all points of an elastic solid
9 – rock mechanics	Theoretical and applied science of the mechanical behaviour of rock
10 – mathematical model	The representation of a physical system by mathematical expressions from which the behaviour of the system can be deduced with known accuracy

11 – **mohr circle of stress/strain**	A graphical representation of the components of stress/strain acting across the various planes at a given point, drawn with reference to axes of normal stress /strain and shear stress strain
12 - **Mohr envelope**	The envelope of a sequence of Mohr circles representing stress conditions at failure for a given material
13 – **strain/stress rate**	Rate of change of strain/stress with time
14 -- **rock mass**	Rock as it occurs in-situ, including its structural discontinuities
15 – **stability**	The condition of a structure or a mass of material when it is able to support the applied stress for a long time without suffering any significant deformation or movement that is not reversed by the release of stress
16 – **stress/strain tensor**	The second order tensor whose diagonal elements consist of the normal stress/strain components with respect to a given set of coordinate axes and whose off-diagonal elements consist of the corresponding shear stress/strain components
17 – **finite element**	One of the regular geometrical shapes into which a figure is subdivided for the purpose of numerical stress analysis
18 – **bending**	Process of deformation normal to the axis of an elongated structural member when a moment is applied normal to its long axis
19 – **uniaxial compression, unconfined compression**	Compression caused by the application of normal stress in a single direction
20 – **biaxial compression**	Compression caused by the application of normal stresses in three perpendicular directions
21 -- **triaxial compression**	Compression caused by the application of normal stresses in three perpendicular directions
22 – **uniaxial state of stress**	State of stress in which two of the three principal stresses are zero
23 – **biaxial state of stress**	State of stress in which one of the three principal stresses are zero

24 — triaxial state of stress	State of stress in which none of the three principal stresses are zero
25 — contraction	Linear strain associated with a decrease in length
26 — dilatation, volumetric strain	The quotient of the change in volume and the original volume of an element of material under stress
27 — deformation	A change in shape or size of a solid body
28 — distortion	A change in shape of a solid body
29 — displacement	A change in position of a material point
30 — extension	Linear strain associated with an increase in length
31 — plane stress/strain	A state of stress/strain in a solid body in which all stress/strain components normal to a certain plane are zero
32 — principal stress/strain	The stress/strain normal to one of three mutually perpendicular planes on which the shear stresses/strains at a point in a body are zero
33 — pure shear	A state of strain resulting from that stress condition most easily described by a Mohr circle centered at the origin
34 — simple shear	Shear strain in which displacements all lie in one direction and are proportional to the normal distances of the displaced points from a given reference plane. The dilatation is zero.
35 — linear (normal) strain	The change in length per unit of length in a given direction
36 — shear strain	The change in shape, expressed by the relative change of the right angles at the corner of what was in the undeformed state an infinitessimally small rectangle or cube
37 — residual strain	The strain in a solid associated with a state of residual stress
38 — permanent strain	The strain remaining in a solid with respect to its initial condition after the application and removal of stress greater than the yield stress. (Commonly also called "residual" strain)

39 — body force
A force such as gravity whose effect is distributed throughout a material body by direct action on each elementary part of the body independent of the others

40 — external force
A force that acts across external surface elements of a material body

41 — normal force
A force directed normal to the surface element across which it acts

42 — shear force
A force directed parallel to the surface element across which it acts

43 — surface force
Any force that acts across an internal or external surface element in a material body, not necessarily in a direction lying in the surface

44 — head
Pressure at a point in a liquid expressed in terms of the vertical distance of the point below the surface of the liquid

45 — overburden load
The load on a horizontal surface underground due to the column of material located vertically above it

46 — primary state of stress
The stress in a geological formation before it is disturbed by man-made works

47 — secondary state of stress
The resulting state of stress in the rock around man-made excavations or structures

48 — hydrostatic pressure
A state of stress in which all the principal stresses are equal (and there is no shear stress)

49 — residual stress
Stress remaining in a solid under zero external stress after some process that causes the dimensions of the various parts of the solid to be incompatible under zero stress, e.g. (i) deformation under the action of external stress when some parts of the body suffer permanent strain; (ii) heating or cooling of a body in which the thermal expansion coefficient is not uniform throughout the body

50 — compressive stress
Normal stress tending to shorten the body in the direction in which it acts

51 — shear stress
Stress directed parallel to the surface element across which it acts

52 — tensile stress — Normal stress tending to lengthen the body in the direction in which it acts

53 — attenuation — Reduction in the amplitude of a wave with the distance of propagation from its source

54 — damping — Reduction in the amplitude of vibration of a body or system due to dissipation of energy internally or by radiation

55 — rise time — The interval of time required for the leading edge of a pulse to rise from some specified small fraction to some specified larger fraction of the maximum value

56 — decay time — The interval of time required for a pulse to decay from its maximum value to some specified fraction of that value

57 — dispersion — The phenomenon of varying speed of transmission of waves, depending on their frequency

58 — natural frequency — The frequency at which a body or system vibrates when unconstrained by external forces

59 — microseism — Seismic pulses of short duration and low amplitude often occurring previous to failure of a material or structure

60 — seismic velocity — The velocity of seismic waves in geological formations

61 — longitudinal wave — A wave in which the displacement at each point of the medium is normal to the wave front

62 — transverse wave, shear wave — A wave in which the displacement at each point of the medium is parallel to the wave front

63 — shock wave — A wave of finite amplitude characterized by a shock front, a surface across which pressure, density and internal energy rise almost discontinuously, and which travels with a speed greater than the normal speed of sound

64 — surface wave — A wave confined to a thin layer at the surface of a body

65 — wavefront — (a) A continuous surface over which the phase of a wave that progresses in three dimensions is constant (b) A continuous line along which the phase of a surface wave is constant

66 – stress	Force acting across a given surface element, divided by the area of the element
67 – inelastic deformation	The portion of deformation under stress that is not annulled by removal of stress
68 – yield stress	The stress beyond which the induced deformation is not fully annulled after complete destressing
69 – rock	Any naturally formed aggregate of mineral matter occurring in large masses or fragments
70 – intact rock	Material of the rock mass, typically represented by whole drill core not affected by the gross structural discontinuities
71 – shear plane	A plane along which failure of material occurs by shearing
72 – cohesion	Shear resistance at zero normal stress. (An equivalent term in rock mechanics is intrinsic shear strength)
73 – constitutive equation	Force-deformation function for a particular material
74 – creep	Time dependent deformation
75 – dilatancy	Property of volume increase under loading
76 – ductility	Condition in which material can sustain permanent deformation without losing its ability to resist load
77 – elasticity	Property of material which returns to its original form or condition after the applied force is removed
78 – elastic limit	Point on stress/strain curve at which transition from elastic to inelastic behaviour takes place
79 – fatigue	Decrease of strength by repetitive loading
80 – fatigue limit	Point on stress/strain curve below which no fatigue can be obtained regardless of number of loading cycles
81 – hardness	Resistance of a material to indentation or scratching
82 – stiffness	Force-displacement ratio
83 – homogeneity	Having the same properties at all points

84 — heterogeneity	Having different properties at different points
85 — hysteresis	Incomplete in recovery of strain during unloading cycle due to energy consumption
86 — isotropy	Having same properties in all directions
87 — anisotropy	Having diferent properties in different directions
88 — modulus of elasticity, Young's modulus	The ratio of stress to corresponding strain below the proportional limit of a material
89 — modulus of deformation	The ratio of stress to corresponding strain during loading of a rock mass including elastic and inelastic behaviour
90 — secant modulus	Slope of the line connecting the origin and a given point on the stress/strain curve
91 — tangent modulus	Slope of the tangent to the stress/strain curve at a given stress value (generally taken at a stress equal to half the compressive strength)
92 — unloading modulus	Slope of the tangent to the unloading stress-strain curve at a given stress value
93 — bulk modulus, incompressibility	Ratio of hydrostatic pressure to the volumetric strain which it produces
94 — plasticity	Property of a material to continue to deform indefinitely while sustaining a constant stress
95 — viscoelasticity	Property of materials which strain under stress partly elastically and partly viscously, i.e. whose strain is partly dependent on time and magnitude of stress
96 — stress relaxation	Stress release due to creep
97 — retardation	Delay in deformation
98 — thixotropy	The property of liquefying on being shaken and of reforming on standing
99 — weathering	The process of disintegration and decomposition as a consequence of exposure to the atmosphere, to chemical action and to the action of frost, water and heat

100 — Poisson's ratio	The ratio of the shortening in the transverse direction to the elongation in the direction of an applied force in a body under tension below the porportional limit
101 — failure	Failure in rocks means exceeding of maximum strength of the rock or exceeding the stress or strain requirement of a specific design
102 — failure criterion	Theoretically or empirically derived stress or strain relationschip characterizing the occurrence of failure in the rock
103 — progressive failure	Formation and development of localized fractures which, after additional stress increase eventually form a continuous rupture surface and thus lead to failure after steady deterioration of the rock
104 — brittle fracture	Sudden failure with complete loss of cohesion across a plane
105 — fracture pattern	Spatial arrangement of a group of fracture surfaces
106 — disking	Breakage of a hard rock core into disks during diamond drilling caused by high field stresses
107 — plane of weakness	Surface or narrow zone with a (shear or tensile) strength lower than that of the surrounding material
108 — rock burst	Sudden explosive-like release of energy due to the failure of a brittle rock of high strength
109 — sliding	Relative displacement of two bodies along a surface, without loss of contact between the bodies
110 — spalling	(a) Longitudinal splitting in uniaxial compression (b) Breaking-off of plate-like pieces from a free rock surface
111 — buckling	Instability of a column or a plate under sufficient high load due to sudden deflection of the structure
112 — strength	Maximum stress which a material can resist without failing for any given type of loading
113 — size effect	Influence of specimen size on its strength or other mechanical parameters
114 — peak shear strength	Maximum shear strength along a failure surface

115 — residual shear strength Shear strength along a failure surface after a large displacement

116 — discontinuity surface Any surface across which some property for a rock mass is discontinuous. This includes fracture surfaces, weakness planes, and bedding planes but the term should not be restricted only to mechanical continuity

117 — joint A break of geological origin in the continuity of a body of rock occurring either single, or more frequently in a set or system, but not attended by a visible movement parallel to the surface of discontinuity

118 — fault A fracture or fracture zone along which there has been displacement of the two sides relative to one another parallel to the fracture. (This displacement may be a few centimeters or many kilometers)

119 — fracture The general term for any mechanical discontinuity in the rock; it therefore is the collective term for joints, faults, cracks, etc.

120 — fissure A gapped fracture

121 — rupture That stage in the development of a fracture where instability occurs. It is not recommended that the term rupture be used in rock mechanics as a synonym for fracture

122 — crack A small fracture, i.e. small with respect to the scale of the feature in which it occurs

123 — bedding Applies to rocks resulting from consolidation of sediments and exhibiting surfaces of separation (bedding planes) between layers of the same or different materials, e.g., shale, siltstone, sandstone, limestone, etc.

124 — thickness The perpendicular distance between bounding surfaces such as bedding or foliation planes of a rock

125 — dip The angle at which a stratum or other planar feature is inclined from the horizontal

126 — strike The direction or azimuth of a horizontal line in the plane of an inclined stratum, joint, fault, cleavage plane or other planar feature within a rock mas

127 – outcrop The exposure of the bedrock at the surface of the ground

128 – bedrock The more or less continuous body of rock which underlies the overburden soils

129 – overburden The loose soil, sand, silt or clay that overlies bedrock. In some usages it refers to all material overlying the point of interest (e.g., a tunnel crown), also the total cover of soil and rock overlying an underground excavation

130 – texture The arrangement in space of the components of a rock body and of the boundaries between these components

131 – fabric The orientation in space of the elements composing the rock substance

132 – structure One of the larger features of a rock mass, like bedding, foliation, jointing, cleavage or brecciation; also th. sum total of such features as contrasted with texture. Also, in a broader sense, it refers to the structural features of an area such as anticlines or synclines

133 – schistosity The variety of foliation that occurs in the coarser-grained metamorphic rocks and is generally the result of the parallel arrangement of platy and ellipsoidal mineral grains within the rock substance

134 – lineation The parallel orientation of structural features that are lines rather than planes; some examples are parallel orientation of the long dimensions of minerals; long axes of pebbles; striae on slickensides; and cleavage-bedding plane intersections

135 – foliation The somewhat laminated structure resulting from segregation of different minerals into layers parallel to the schistosity

136 – cleavage The tendency to cleave or split along definite parallel planes, which may be highly inclined to the bedding. It is a secondary structure and is ordinarily accompanied by at least some recrystallization of the rock

137 – hanging wall The mass of rock above a discontinuity surface

138 – footwall The mass of rock beneath a discontinuity surface

139 — subsidence

The downward displacement of the overburden (rock and/or soil) lying above an underground excavation or adjoining a surface excavation. Also the sinking of a part of the earth's crust

140 — karst

A geologic setting where cavities are developed in massive limestone beds by solution by flowing water. Caves and even underground river channels are produced into which surface runoff drains and often result in the land above being dry and relatively barren

141 — landslide

The perceptible downward sliding or movement of a mass of earth, rock or mixture of both

142 — filling

Generally the material occupying the space between fracture surfaces, in joints, faults, and other rock discontinuities. The filling material may be clay, gouge, various natural cementing agents or alteration products of the adjacent rock

143 — slickenside

The polished and striated surface that results from friction along a fault plane or other movement surfaces in a rock mass

144 — mylonite

A microscopic breccia with flow structure formed in fault zones

145 — joint/fault set

A group of more or less parallel joints/faults

146 — joint/fault system

Consists of two or more joint/fault sets or any group of joints/faults with a characteristic pattern, e.g., radiating, concentric, etc.

147 — joint pattern

A group of joints which form a characteristic geometrical relationship, and which can vary considerable from one location to another within the same geologic formation

148 — joint diagram

A diagram constructed by accurately plotting the strike and dip of joints to illustrate the geometrical relationship of the joints within a specified area of geologic investigation

149 — conjugate joints/faults

Two sets of joints/faults that formed under the same stress conditions (usually shear pairs)

150 – fault breccia — The assemblage of brocken rock fragments frequently found along faults. The fragments may vary in size from inches to feet

151 – fault gouge — A clay-like material occurring between the walls of a fault as a result of the movement along the fault surfaces

152 – fold — A bend in the strata or other planar structure within the rock mass

153 – permeability — The capacity of a rock to conduct liquid or gas. It is measured as the proportionality constant, k, between flow velocity, v, and hydraulic gradient, i; $v = k.i$

155 – hydraulic gradient — The change of pressure head per unit of distance at a given point and in a given direction

157 – moisture content — The percentage by weight of water contained in the pore space of a rock or soil with respect to the weight of the solid material

158 – degree of saturation — The extent or degree to which the voids in rock contain fluid (water, gas or oil). Usually expressed in percent related to total void or pore space

160 – percolation — Movement, under hydrostatic pressure, of water through the smaller interstices of rock or soil, excluding movement through large openings such as caves and solution channels

163 – porosity — The ratio of the aggregate volume of voids or interstices in a rock or soil to its total volume

FRENCH

INDEX

1 — coefficient de frottement

Rapport de la contrainte normale et de la contrainte tangentielle au contact de deux surfaces lorsqu'elles commencent (ou continuent) à glisser l'une sur l'autre.

2 — angle de frottement interne

Angle de l'axe des contraintes normales et de la tangente à la courbe intrinsèque en un point de cette courbe.

3 — angle de talus naturel

Angle maximal de la surface libre d'un talus de matériau meuble par rapport au plan horizontal.

4 — déviateur du tenseur des contraintes/déformations

Tenseur S obtenu en retranchant d'un tenseur σ de valeurs principales σ_1, σ_2, σ_3 un tenseur isotrope de valeurs principales égales à $1/3\ (\sigma_1 + \sigma_2 + \sigma_3)$. (Même définition applicable en déformation.)

5 — ellipsoide des contraintes

Représentation du tenseur des contraintes en un point d'un solide par un ellipsoide lieu de l'extrémité du vecteur contrainte et dont les axes coincident en direction et proportion avec les contraintes principales.

6 — ellipsoide des déformations

Représentation du tenseur des déformations en un point d'un solide par un ellipsoide résultant de la déformation d'une sphère centrée sur le point considéré.

7 — energie de déformation élastique

Energie potentielle contenue dans un solide déformé, égale au travail de déformation du solide à partir de l'état non déformé diminué de l'énergie dissipée par déformation non élastique.

8 — champ de contraintes/ /déformations

Ensemble des états de contrainte/déformation en tout point d'un solide.

9 — mécanique des roches

Science théorique et appliquée du comportement mécanique des roches.

10 — modèle mathématique

Représentation d'un phénomène par des expressions mathématiques d'où l'on peut déduire d'une façon plus ou moins approchée le comportement d'un système.

11 — cercle de Mohr des contraintes/déformations

Dans un plan rapporté aux axes σ (contrainte normale) τ (contrainte tangentielle) le cercle de Mohr est centré sur l'axe σ et passe par les points représentatifs des deux contraintes principales extrêmes σ_1 et σ_3. C'est le lieu de l'extrémité des vecteurs (σ, τ) représentatifs des contraintes agissant sur les facettes contenant le vecteur de la contrainte intermédiaire. (Même définition applicable en déformation.)

12 — courbe intrinsèque	Enveloppe de cercles de Mohr qui représentent l'état de contrainte à la rupture pour un matériau donné.
13 — vitesse de contrainte/ /déformation	Vitesse de variation d'une contrainte/déformation.
14 — massif rocheux	Roche comme elle se présente in situ y compris ses discontinuités structurales.
15 — stabilité	État d'une structure ou d'un massif qui reste apte à résister aux sollicitations qu'elle subit.
16 — tenseur des déformations/ /contraintes	Tenseur du deuxième ordre représentant respectivement l'ensemble des dilatations et des distorsions autour d'un point, ou l'ensemble des contraintes s'exerçant sur les différentes facettes autour d'un point.
17 — élément fini	Elément de la décomposition d'une structure en parties discrètes pour l'analyse numérique de son comportement.
18 — flexion	Réaction d'une structure allongée à un moment fléchissant.
19 — compression uniaxiale	Compression causée par l'application d'une contrainte normale selon une seule direction.
20 — compression biaxiale	Compression causée par l'application de contraintes normales selon deux directions perpendiculaires.
21 — compression triaxiale	Compression causée par l'application de contraintes normales selon trois directions perpendiculaires.
22 — état de contrainte uniaxial	État de contrainte dans lequel deux des trois contraintes principales sont nulles.
23 — état de contrainte biaxial	État de contrainte dans lequel une des trois contraintes principales est nulle.
24 — état de contrainte triaxial	État de contrainte dans lequel aucune des trois contraintes principales n'est nulle.
25 — contraction	Diminution relative de la distance entre deux points d'un solide.
26 — dilatation cubique	Variation relative du volume d'un élément de matière.

27 — déformation	Modification des distances mutuelles des différents points d'un corps.
28 — distorsion	Voir 36
29 — déplacement	Changement de position d'un point matériel.
30 — extension	Augmentation relative de la distance entre deux points d'un solide.
31 — contrainte/déformation plan	État de contrainte/déformation dans un corps solide tel que la contrainte/déformation normale à un certain plan soit nulle en tout point.
32 — contrainte/déformation principale	Contrainte/déformation normale à l'un des trois plans mutuellement perpendiculaires sur lequel les contraintes/déformations de cisaillement en un point d'un corps sont nulles.
33 — cisaillement pur	Déformation de cisaillement où les déplacements de tous les points sont parallèles et proportionnels à la distance à un plan de référence.
34 — cisaillement simple	État de contrainte dans lequel l'une des contraintes principales est nulle, les deux autres égales et de signe contraire.
35 — dilatation linéaire	Variation relative de la distance entre deux points d'un solide.
36 — distorsion	Variation de l'angle formé par deux segments issus d'un même point qui étaient perpendiculaires entre eux avant déformation.
37 — déformation residuelle	Déformation qui persiste au temps après disparition de la sollicitation.
38 — déformation permanente	Limite vers laquelle tend la déformation résiduelle au bout d'un temps infini.
39 — force de volume	Force dont l'intensité est proportionelle au volume de l'élément auquel elle s'applique. Exemple: la gravité.
40 — force extérieure	Force résultant du contact d'un solide avec le milieu extérieur.
41 — effort normal	Effort dirigé perpendiculairement à l'élément de surface sur lequel il agit.

42 – effort de cisaillement	Effort dirigé parallèlement à l'élément de surface sur lequel il agit.
43 – force de surface	Force dont l'intensité est proportionnelle à la superficie de l'élément auquel elle s'applique.
44 – charge hydraulique	Pression statique ou dynamique en un point d'un fluide.
45 – charge de couverture	Charge verticale ou poids des matériaux susjacents.
46 – état de contrainte naturel	État de contrainte dans un massif avant travaux.
47 – état de contrainte induit	État de contrainte dans un massif après travaux.
48 – pression hydrostatique	État de contrainte dans lequel toutes les contraintes principales sont égales.
49 – contrainte residuelle	État de contrainte existant dans un corps non soumis à des sollicitations. Cet état de contrainte résulte du passé rhéologique du matériau.
50 – contrainte de compression	Contrainte normale tendant à raccourcir un solide dans la direction suivant laquelle elle agit.
51 – contrainte de cisaillement	Contrainte parallèle à l'élément de surface sur lequel elle agit.
52 – contrainte de traction	Contrainte normale tendant à allonger un solide dans la direction suivant laquelle elle agit.
53 – attenuation	Réduction d'amplitude d'une onde en fonction de la distance à la source.
54 – amortissement	Réduction d'amplitude d'une onde en fonction du temps, due à la non élasticité du milieu.
55 – temps de montée	Intervalle de temps nécessaire pour que l'amplitude d'une onde en un point passe d'une valeur conventionnelle petite à une autre valeur conventionnelle proche de l'amplitude maximale.
56 – temps de descente	Intervalle de temps nécessaire pour que l'amplitude d'une onde en un point passe d'une valeur conventionnelle proche de l'amplitude maximale à une autre valeur conventionnelle petite.
57 – dispersion	Phénomène de variation de la vitesse de transmission des ondes en fonction de leur fréquence.

58 — fréquence propre	Fréquence à laquelle un corps ou un système oscille quand il n'est pas soumis à une sollicitation vibratoire.
59 — microbruit	Impulsion sismique de courte durée et de petite amplitude qui se produit souvent avant que la roche casse.
60 — célérité sismique	Célérité des ondes sismiques dans les formations géologiques.
61 — onde longitudinale	Onde telle que la direction du déplacement des particules en tout point du milieu soit normale au front d'onde.
62 — onde transversale, onde de cisaillement	Onde telle que la direction du déplacement des particules en tout point du milieu soit parallèle au front d'onde.
63 — onde de choc	Onde ayant une amplitude finite, caracterisée par une surface (ou volume de trés faible épaisseur) de part et d'autre de laquelle un phénomène physique subit une brusque variation.
64 — onde de surface	Onde se propageant dans une couche de très faible épaisseur à la surface d'un corps.
65 — front d'onde	Surface (ou ligne) continue sur laquelle la phase d'une onde de volume ou de surface est constante.
66 — vecteur contrainte	Force de contact s'exerçant sur une facette, rapportée à l'aire de cette facette.
67 — déformation non élastique	Voir 38
68 — seuil de plasticité	Valeur de la sollicitation à partir de laquelle apparaissent des déformations permanentes.
69 — roche	Tout agrégat de matière minérale formé naturellement et se présentant en grande masse ou en fragments.
70 — matrice rocheuse	Matériau situé entre les discontinuités (matériau des blocs). La matrice varie avec l'échelle et la maille des discontinuités considérées.
71 — surface de cisaillement	Surface de rupture d'une roche soumise à des efforts de cisaillement.
72 — cohésion	Résistance au cisaillement sous contrainte normale nulle.
73 — loi de comportement	Relation sollicitation-déformation d'un matériau donné.

74 — fluage

a) Sens usuel: Déformation retardée d'un solide sous l'action d'une force ou d'une contrainte constante. b) Sens strict: Déformation retardée non recouvrable au déchargement.

75 — dilatance

Propriété qu'ont certains corps d'augmenter de volume sous l'action d'un état de contrainte de cisaillement simple.

76 — ductilité

Aptitude d'un matériau à subir sans fractures de grandes déformations.

77 — elasticité

Propriété d'un corps qui reprend la forme et les dimensions qu'il avait avant une sollicitation, lorsqu'on supprime cette sollicitation.

78 — limite d'elastiticité

Valeur maximale de la sollicitation pour laquelle n'apparaissent pas de déformations permanentes.

79 — fatigue

Variation des propriétés mécaniques sous l'effet de charges répétées.

80 — limite de fatigue

Niveau de contrainte au-dessous duquel le phénomène de fatigue n'apparait pas quel que soit le nombre de cycles de chargement.

81 — dureté

Résistance d'un solide à la pénétration, c'est-à-dire à une déformation de sa surface.

82 — raideur

Propriété d'un solide caractérisant la grandeur de la déformation qu'il subit pour un accroissement de contrainte donné. Plus cette déformation est faible, plus le corps est raide.

83 — homogénéité

Qualité d'un corps qui possède les mêmes propriétés en tout point.

84 — hetérogénéité

Qualité d'un corps qui ne possède pas les mêmes propriétés en tout point.

85 — hystérésis

Apparition d'un retard dans l'évolution d'un phénomène physique par rapport à un autre. Exemple: hystérésis des cycles de charge.

86 — isotropie

Qualité d'un corps dont les propriétés physiques sont identiques dans toutes les directions.

87 — hétérotropie

Qualité d'un corps dont les propriétés sont différentes suivant les directions.

88 — module d'Young

C'est le module E qui, pour un solide isotrope ou non, élastique linéaire, soumis à une contrainte uniaxiale, apparaît dans la relation $\sigma_{ii} = E.\varepsilon_{ii}$ entre la contrainte principale non nulle et la dilatation linéaire dans la direction de cette contrainte.

89 — module de déformation

Rapport entre contrainte appliquée et déformation correspondante lors du chargement d'un massif rocheux.

90 — module d'élasticité secant

Pente de la droite reliant l'origine à un point donné de la courbe contrainte-déformation

91 — module d'élasticité tangent

Pente de la tangente à la courbe contrainte-déformation en un de ses points.

92 — module de déchargement

Pente de la tangente à la tranche de la courbe contrainte-déformation qui correspond au déchargement.

93 — coefficient de dilatation cubique

Rapport entre la pression hydrostatique et la dilatation cubique résultante

94 — plasticité

Aptitude d'un corps à subir des déformations permanentes.

95 — viscoélasticité

Propriété d'un corps dont les caractéristiques élastiques varient en fonction de la vitesse d'application des sollicitations

96 — relaxation

Libération de contrainte en fonction du temps dans un solide auquel on a imposé une déformation maintenue ensuite constante.

97 — retard

Voir 74

98 — thixotropie

Propriété d'un corps très visquex qui se liquéfie lorqu'on l'agite, puis retrouve sa viscosité initiale après un certain temps de repos.

99 — altération

Modification (généralement dégradation) des propriétés mécaniques d'une roche sous l'effect d'agents extérieurs: air, eau de percolation, choc thermique.

100 – coefficient de Poisson — Pour un solide isotrope linéaire soumis à une contrainte uniaxiale, le coefficient de Poisson est l'opposé du rapport de la dilatation linéaire, dans n'importe quelle direction perpendiculaire à la contrainte principale non nulle, à la dilatation linéaire dans la direction de cette contrainte.

101 – rupture — Dépassement de la résistance maximale de la roche.

102 – critère de rupture — Relation théorique ou empirique entre contrainte et déformation qui caractérise la rupture d'une roche.

103 – rupture progressive — Rupture d'un bloc rocheux résultant de la formation et du développement de surfaces de rupture localisées.

104 – rupture fragile — Rupture acompagnée d'une diminution brusque et importante de la résistance.

105 – structure de la fracturation — Disposition spatiale des systèmes de fractures.

106 – disquage — Séparation d'une carotte de roche dure en disques, provoquée par de fortes contraintes naturelles.

107 – surface de moindre résistance — Surface ou zone peu épaisse dont la résistance est inférieure à celle du matériau qui l'entoure.

108 – coup de terrain — Rupture par libération soudaine d'énergie élastique dans une roche fragile.

109 – glissement — Mouvement relatif de deux corps sans perte de contact.

110 – écaillage — (a) Séparation en éléments longitudinaux en compression simple.
(b) Formation d'éléments en plaquettes à la surface libre d'un massif.

111 – flambement — Déformation latérale instable des structures allongées lorsqu'elles sont comprimées perpendiculairement à leur plus petite dimension.

112 – résistance — Contrainte maximale qu'un matériau peut supporter sans se rompre. (La résistance dépend du critère de rupture.)

113 – effet d'échelle — Influence des dimensions de l'échantillon sur la résistance ou sur d'autres paramètres mécaniques.

114 — résistance maximale au cisaillement, résistance au pic	Résistance maximale au cisaillement d'une surface de rupture.
115 — résistance de cisaillement résiduelle	Résistance au cisaillement d'une surface de rupture après un grand déplacement
116 — surface de discontinuité	Surface ou zone mince à l'intérieur d'un milieu continu ou entre deux milieux continus différents, en général assimilable à un plan sur une certaine étendue.
117 — diaclase	Fracture sans rejet, transversale à la stratification ou à la schistosité.
118 — faille	Surface de discontinuité avec déplacement tangentiel des deux lèvres, appelé rejet, souvent souligné par des stries, avec ou sans interposition d'une zone broyée. (Une fracture, un joint de stratification, un ensemble de fissures peuvent jouer le role d'une faille.)
119 — fracture	Surface de non adhérence de grande étendue partageant le volume considéré en parties distinctes. Exemples: diaclase, joint de stratification ouvert au voisinage du sol.
120 — fissure	Surface de non adhérence, d'étendue limitée, ne traversant pas le volume considéré. Exemples: fissures de retrait à la surface du béton ou de l'argile.
121 — rupture	État instable auquel peut conduire l'extension de la fracturation
122 — petit fissure	Voir 120
123 — stratification	Disposition d'une roche sédimentaire en bancs parallèles, de composition identique ou différenciée, séparés par des joints de stratification.
124 — épaisseur de couche	Distance normale entre fractures de la même famille.
125 — pendage	Angle d'un plan de fracture ou d'un joint de stratification avec le plan horizontal.
126 — direction	Azimuth d'une horizontale d'un plan de fracture ou d'un joint de stratification.
127 — affleurement	Exposition d'une roche à la surface du terrain naturel.
128 — "bedrock"	Massif rocheux sousjacent au sol de couverture.

129 — couverture	Sol meuble situé au-dessus de la roche solide. Ce mot est aussi employé pour désigner tout le massif situé au-dessus du point considéré par exemple la couverture de sol et roche sus-jacente à une excavation souterraine.
130 — texture	Disposition et dimensions relatives des éléments composant une matrice rocheuse.
131 ——	(il n'y a pas de terme correspondant en français.)
132 — structure	Manière dont sont disposés les blocs ou couches constituant un massif rocheux.
133 — schistosité	Disposition de nombreuses roches métamorphiques en feuillets parallèles de même nature, qui favorise leur séparation suivant des joints très rapprochés.
134 — Lineation	Orientation des caractéristques structurales sous forme de lignes plutôt que plans parallèles.
135 — foliation	Orientation des caractéristiques structuraies sous forme de plans parallèles à la schistosité.
136 — clivage	Aptitude d'un cristal à se séparer facilement suivant certaines directions de plan du réseau cristallin. Désigne aussi l'opération de séparation en deux parties ou en feuillets minces d'un cristal et par extension la séparation d'un matériau schisteux, notamment des schistes ardoisiers.
137 — compartiment supérieur	Masse de rocher située au-dessus d'une surface de discontinuité.
138 — compartiment inférieur	Masse de rocher située au-dessous d'une surface de discontinuité.
139 — subsidence	Affaissement de surface dû soit à la réalisation de cavités souterraines, soit à des phénomènes hydrauliques ou géologiques.
140 — karst	Cavités qui se développent par dissolution dans des bancs de calcaire massif.
141 — glissement de terrain	Mouvement perceptible vers le bas d'une masse de terre ou de roche.
142 — remplissage	Matérieu meuble en général remplissant l'épaisseur d'une surface de séparation ou d'une fracture.

143 — surface lissée Surface des épontes d'une faille ou d'une autre fracture lissée par le cisaillement.

144 — mylonite Brèche de faille à structure fine et laminée.

145 — famille de fractures Groupe de fractures plus ou moins parallèles.

146 — système de fractures Ensemble de deux ou plusieurs familles de fractures.

147 — réseau de fractures Disposition géométrique caractéristique de fractures.

148 — diagramme de fractures Diagramme sur lequel ont été reportées, suivant une certaine convention, les mesures des paramètres caractérisant l'orientation de fractures existant dans une certaine zone du massif.

149 — fractures conjuguées Deux familles de fractures (failles) formées par la même sollicitation tectonique (généralement directions conjuguées de cisaillement).

150 — brèche de faille Conglomérat formé de fragments anguleux résultant du broyage des épontes d'une faille.

151 — argile de faille Matériau argileux souvent présent entre les épontes d'une faille et créé par le déplacement relatif de ces épontes.

152 — pli Courbure d'un élément du massif originellement plan (strate par exemple).

153 — perméabilité Aptitude d'une roche à se laisser traverser par des fluides.

155 — gradient hydraulique Variation de la charge hydraulique par unité de distance en un point donné et dans une direction donnée.

157 — teneur en eau Pourcentage en poids de l'eau contenue dans les vides d'une roche ou d'un sol, rapporté au poids du matériau solide.

158 — degré de saturation Degré de remplissage des vides d'une roche par un fluide, généralement exprimé en pourcentage par rapport au volume total des vides.

160 — percolation Écoulement d'eau interstitielle dans les vides d'un sol ou d'une roche.

163 — porosité Rapport entre le volume des vides d'une roche ou d'un sol et son volume total.

GERMAN

INDEX

1 — Reibungsbeiwert Ein konstanter Proportionalitätsfaktor μ, der das Verhältnis zwischen Normalspannung und der Schubspannung bestimmt, bei der der Gleitvorgang zwischen zwei Oberflächen beginnt: $\tau = \mu \cdot \sigma$

2 — Reibungswinkel Der Winkel ø zwischen der Normalspannungsachse und der Tangente an die Mohr'sche Hüllkurve an einem Punkt, der einen gegebenen Bruchspannungszustand für festes Material darstellt

3 — Schüttwinkel Der größtmögliche Winkel, bezogen auf die waagerechte Ebene, den die Oberfläche einer Schüttung von losem Material annehmen wird

4 — Spannungs/Dehnungs/deviator Der Spannungs/Dehnungs/tensor, der erhalten wird durch Subtraktion des Mittels der Normalspannungs/Dehnungs/komponenten eines Spannungs/Dehnungs/tensors von jeder Normalspannungs/Dehnungs/komponente

5 — Spannungsellipsoid Die Darstellung des Spannungszustandes in Form eines Ellipsoids, dessen Halbachsen proportional zu den Größen der Hauptspannungen sind und in den Hauptrichtungen liegen. Die Koordinaten eines Punktes P auf dieser Ellipsoid sind proportional zu den Größen der entsprechenden Spannungskomponenten, die auf derjenigen Ebene wirken, die senkrecht zur Richtung OP steht, wobei O der Mittelpunkt des Ellipsoids ist

6 — Verformungs/Dehnungs/ellipsoid Die Darstellung der Dehnung in Form eines Ellipsoids, zu dem eine Kugel mit Einheitsradius verformt wird und dessen Achsen die Hauptdeformationsachsen sind

7 — elastische Formänderungsenergie Potentielle Energie, die in einem verformten Festkörper gespeichert ist und die, unter Abzug der durch inelastische Verformung verbrauchten Energie, derjenigen Arbeit gleich ist, die zur Verformung des Festkörpers aus seinem unverformten Zustand benötigt wird

8 — Spannungs/Dehnungs/feld Die Summe der Spannungs/Dehnungs/zustände, die für sämtliche Punkte eines elastichen Körpers definiert sind

9 — Felsmechanik	Die theoretische und angewandte Wissenschaft des mechanischen Verhaltens von Fels
10 — mathematisches Modell	Die Darstellung eines physikalischen Systems durch mathematische Ausdrücke, aus denen das Verhalten des Systems mit einem bekannten Genauigkeitsgrad abgeleitet werden kann
11 — Mohrscher Spannungs/ /Dehnungs/kreis	Eine graphische Darstellung der Spannungs/Dehnungs/komponenten die an einem gegebenen Punkt auf den verschiedenen Ebenen wirken, wobei die Bezugsachsen Normal-bzw. Scher/spannung/dehnung sind
12 — Mohrsche Hüllkurve	Die Umhüllende einer Reihe von Mohrscher Kreise, die für ein gegebenes Material die Spannungs/Dehnungs/zustände im Augenblick des Bruches darstellen
13 — Verformungs/Belastungs/ /geschwindigkeit	Änderung der Dehnung/Spannung mit der Zeit
14 — Gebirge, Fels	Das in situ vorliegende Gestein einschließlich seiner Trennflächen
15 — Standsicherheit	Der Zustand eines Bauwerkes oder einer Materialmasse, bei dem dies (e) die über einen langen Zeitraum hinweg wirkenden Spannungen tragen kann, ohne bedeutsame Verformungen oder Verschiebungen zu erfahren, welche bei Entspannung nicht rückgängig gemacht werden
16 — Dehnungs/Spannungs/tensor	Der Tensor zweiter Ordnung, dessen diagonale Elemente aus den Normal-Dehnungs/Spannungs/ /komponenten hinsichtlich eines gegebenen Koordinatensystems und dessen nicht-diagonale Elemente aus den entsprechenden Scher-Dehnungs/ /Spannungs/komponenten bestehen
17 — Finites Element	Eine der regelmäßigen geometrischen Formen, in die eine Figur zum Zwecke der numerischen Spannungsanalyse aufgegliedert ist
18 — Biegung	Verformungsvorgang normal zur Längsachse eines langgestreckten Bauteils, wenn ein Moment senkrecht zu dessen Längsachse angreift

19	**einachsige Kompression, seitlich unbehinderte Kompression**	Zusammendrückung durch eine Normalspannung in einer einzigen Richtung
20	**zweiachsige Kompression**	Zusammendrückung durch Normalspannungen in zwei zueinander rechtwinkligen Richtungen
21	**dreiachsige Kompression**	Zusammendrückung durch Normalspannungen in drei zueinander rechtwinkligen Richtungen
22	**einachsiger Spannungszustand**	Spannungszustand, bei dem zwei der drei Hauptspannungen gleich null sind
23	**zweiachsiger Spannungszustand**	Spannungszustand, bei dem eine der drei Hauptspannungen gleich null ist
24	**dreiachsiger Spannungszustand**	Spannungszustand bei dem keine der drei Hauptspannungen gleich null ist
25	**– Kontraktion**	Lineare Dehnung, die mit einer Längenabnahme einhergeht
26	**– Dilatation, relative Volumenänderung**	Der Quotient aus Volumenänderung und ursprünglichem Volumen eines unter Spannung stehenden Materialteilchens
27	**– Verformung**	Eines Form oder Größenänderung eines Festkörpers
28	**– Verzerrung**	Eine Formänderung eines Festkörpers
29	**– Verschiebung**	Ein Ortswechsel eines Materialpunktes
30	**– Streckung**	Lineare Dehnung, die mit einer Längenzunahme einhergeht
31	**– ebener Spannungs/ /Dehnungs/zustand**	Ein Spannungs/Dehnungs/zustand in einem Festkörper, bei dem alle Spannungs/Dehnungs/ /komponenten, die senkrecht zu einer gewissen Ebene stehen, gleich null sind
32	**– Haupt/spannung/dehnung**	Die Spannung/Dehnung, die senkrecht zu einer der drei gegeneinander senkrecht stehenden Ebenen verläuft, auf welchen die Scher/spannungen/ /dehnungen an einem Punkt in einem Körper gleich null sind

33 — reine Scherung	Ein Dehnungszustand, der von jenem Spannungszustand herrührt, der durch einen Mohrschen Kreis beschrieben wird, der am Nullpunkt seinen Mittelpunkt hat
34 — einfache Scherung	Scherverformung, bei der die Verschiebungen alle in einer Richtung liegen und proportional zu den Normalabständen der verschobenen Punkte von einer gegebenen Bezugsebene sind. Die Volumenveränderung ist gleich null
35 — lineare (normale) Dehnung	Die Längenänderung pro Längeneinheit in einer gegebenen Richtung
36 — Scherdehnung, Scherverformung	Die Formänderung, die durch die relative Änderung der rechten Winkel am Eckpunkt derjenigen Form ausgedrückt wird, die im unverformten Zustand ein unendlich kleines Rechteck oder ein unendlich kleiner Kubus war
37 — Restdehnung	Die Dehnung in einem Festkörper, die mit Restspannungen einhergeht
38 — bleibende Dehnung	Die Dehnung, die in einem Festkörper im Vergleich zu seinem Anfangszustand verbleibt, nach dem eine Spannung, die die Fließgrenze überstiegen hat, angelegt und wieder beseitigt wurde (allgemein auch mit "Restdehnung" bezeichnet)
39 — Massenkraft	Eine Kraft, wie z.B. die Schwerkraft, deren Wirkung über Materialkörper verteilt ist, und zwar durch direkte Wirkung auf jedes Elementarteilchen des Körpers, unabhängig von den anderen
40 — äußere Kraft	Eine Kraft, die an äußeren Oberflächenteilchen eines Materialkörpers angreift
41 — Normalkraft	Eine Kraft, die in senkrechter Richtung auf einem Oberflächenteilchen angreift
42 — Scherkraft	Eine Kraft, die in paralleler Richtung an einem Oberflächenteilchen angreift
43 — Oberflächenkraft	Jede Kraft, die an einem inneren oder äußeren Oberberflächenteilchen eines Materialkörpers angreift, ohne unbedingt in einer in der Oberfläche gelegenen Richtung zu liegen

44 – Druckhöhe	Druck an einem Punkte in einer Flüssigkeit, der durch dem vertikalen Abstand zwischen dem Punkt und der Flüssigkeitsoberfläche ausgedrückt wird
45 – Überlagerungsdruck	Die Last, die auf einer unterirdischen horizontalen Fläche infolge der darüber lagernden Materialsäule ruht
46 – primärer Spannungszustand	Spannung in einer geologischen Formation, bevor diese durch künstliche Einwirkungen gestört wird
47 – sekundärer Spannungszustand	Der Spannungszustand im Gestein, der sich durch künstliche Ausbrüche und Bauten ergibt
48 – hydrostatischer Druck	Ein Spannungszustand, bei dem alle Hauptspannungen gleich sind (und keine Scherspannungen existieren)
49 – Restspannung	Diejenige Spannung, welche in einem Festkörper trotz äußerer Entspannung nach einem Vorgang verbleibt, der die Dimensionen der verschiedenen Materialteilchen bei Entlastung nicht mehr ineinanderpassen läßt. Z.B. (i) Verformung unter Einwirkung äußerer Spannungen, bei der einzelne Teile des Körpers bleibende Verformungen erfahren. (ii) Erhitzung oder Abkühlung eines Körpers, in dem der Wärmeausdehnungskoeffizient innerhalb des Körpers nicht gleichmäßig ist
50 – Druckspannung	Normalspannung, die den Körper in derjenigen Richtung zu verkürzen sucht, in welcher sie wirkt
51 – Scherspannung	Spannung, die in paralleler Richtung an einem Oberflächenteil angreift
52 – Zugspannung	Normalspannung, die den Körper in derjenigen Richtung zu verlängern sucht, in welcher sie wirkt
53 – Amplitudenabnahme	Verringerung der Amplitude einer Welle mit deren Entfernung von der Quelle
54 – Dämpfung	Verminderung der Schwingungsamplitude eines Körpers oder Systems infolge interner oder durch Ausstrahlung verursachter Energieverzehrung

55 — **Anstiegszeit**	Der Zeitraum, den die führende Front einer Welle benötigt, um von einem bestimmten spezifischen kleinen Bruchteil bis auf einen bestimmten größeren spezifischen Bruchteil des Höchstwertes der Amplitude anzusteigen
56 — **Ausschwingzeit**	Der Zeitraum, der erforderlich ist, damit bei einer Welle deren Amplitude von ihrem Höchstwert auf einen bestimmten spezifischen Bruchteil abfällt
57 — **Dispersion**	Das Phänomen wechselnder Wellengeschwindigkeit in Abhängigkeit derer Frequenz
58 — **natürliche Frequenz**	Die Frequenz, bei der ein Körper oder ein System schwingt, wenn er keinem Zwang durch äußere Kräfte unterliegt
59 — **Mikroseismik**	Seismische Störungen von kurzer Dauer und geringer Amplitude, die oft vor dem Bruch eines Materials oder eines Bauwerkes eintreten
60 — **seismische Geschwindigkeit**	Die Geschwindigkeit von Erdbebenwellen in geologischen Formationen
61 — **Longitudinalwelle**	Eine Welle, bei der die Verschiebung an jedem Punkte des Mediums senkrecht zur Wellenfront ist
62 — **Transversalwelle, Scherwelle**	Eine Welle, bei der die Verschiebung an jedem Punkt des Mediums parallel zur Wellenfront ist
63 — **Stoßwelle**	Eine Welle mit endlicher Amplitude, die durch eine Stoßfront gekennzeichnet ist, das ist eine Oberfläche, über die hinweg Druck, Dichte und innere Energie fast diskontinuierlich ansteigen, und die mit einer Geschwindigkeit wandert, die größer als die normale Schallgeschwindigkeit ist
64 — **Oberflächenwelle**	Eine Welle, die auf eine dünne Schicht an der Oberfläche eines Körpers beschränkt ist
65 — **Wellenfront**	(1) Eine durchgehende Oberfläche, entlang der die Phase einer in drei Dimensionen fortschreitenden Welle konstant ist (2) Eine durchgehende Linie, entlang welcher die Phase einer Oberflächenwelle konstant ist

66 – **Spannung**	Eine über eine gegebene Oberfläche, und zwar pro Flächeneinheit wirkende Kraft
67 – **inelastische Verformung**	Derjenige Anteil an der unter Spannung erfolgten Verformung, der durch die Beseitigung der Spannung nicht rückgängig gemacht wird
68 – **Fließgrenze**	Diejenige Spannung, bei deren Überschreiten die bewirkte Verformung auch nach völliger Entlastung nicht ganz rückgängig gemacht wird
69 – **Fels**	Jede natürlich gebildete Anhäufung von Mineralsubstanz, die in großen Massen oder Bruchstücken vorkommt
70 – **Festgestein**	Der Gesteinsmasse entstammendes Material, wofür ein ganzer Bohrkern der keine größeren Trennflächen aufzeigt, typisch wäre
71 – **Scherfläche**	Eine Ebene, entlang welcher im Material ein Scherbruch auftritt
72 – **Kohäsion**	Scherfestigkeit bei einer Normalspannung, die gleich Null ist (ein gleichwertiger Ausdruck in der Felsmechanik ist intrinsische Scherfestigkeit)
73 – **Stoffgleichung, Stoffgesetz**	Kraft-Verformungsbeziehung für ein bestimmtes Material
74 – **Kriechen**	Zeitabhängige Verformung
75 – **Dilatanz**	Eigenschaft der Volumenvergrößerung unter Scherbeanspruchung
76 – **Duktilität**	Derjenige Zustand, bei dem Material eine bleibende Verformung erfährt, ohne dabei seine Tragfähigkeit zu verlieren
77 – **Elastizität**	Eigenschaft eines Materials, das in seine ursprüngliche Form oder Zustand nach der Entlastung zurückkehrt
78 – **Elastizitätsgrenze**	Derjenige Punkt auf der Spannungs-Dehnungskurve, an dem der Übergang vom elastichen zum inelastischen Verhalten stattfindet

79 — Ermüdung	Abnahme der Festigkeit durch wiederholte Belastung
80 — Dauerfestigkeit	Diejenige Spannung, unterhalb der keine Ermüdung auftritt, und zwar unabhängig von der Anzahl der Belastungen
81 — Härte	Widerstand eines Materials gegen Einbeulung oder gegen Kratzen
82 — Steifigkeit	Verhältnis von Kraft zu Verschiebung
83 — Homogenität	Mit den gleichen Eigenschaften an allen Punkten ausgestattet
84 — Heterogenität	Mit verschiedenen Eigenschaften an verschiedenen Punkten ausgestattet
85 — Hysteresis	Unvollständige Aufhebung der Dehnung während der Entlastung infolge Energieverbrauchs
86 — Isotropie	Mit den gleichen Eigenschaften in sämtlichen Richtungen ausgestattet
87 — Anisotropie	Mit verschiedenen Eigenschaften in verschiedenen Richtungen ausgestattet
88 Elastizitätsmodul, Young Modul	Das Verhältnis von Spannung zur entsprechenden Dehnung unterhalb der Proportionalitätsgrenze eines Materials
89 — Verformungsmodul	Das Verhältnis Spannung zu entsprechender Dehnung (Formänderung) während der Belastung einer Gesteinsmasse, und zwar einschließlich des elastischen und des inelastischen Verhaltens
90 — Sekantenmodul	Neigung der Linie, die den Ursprung mit einem gegebenen Punkt auf der Spannungs-Dehnungskurve verbindet
91 — Tangentenmodul	Neigung der an die Spannungs-Dehnungkurve an einem gegebenen Spannungswert angelegten Tangente (im allgemeinen bei einer Spannung, die gleich der halben Druckfestigkeit ist)
92 — Entlastungsmodul	Neigung der Tangente an den Entlastungszweig der Spannungs-Dehnungskurve bei einem gegebenen Spannungswert

93 – Kompressionsmodul	Verhältnis von hydrostatischem Druck zu relativer Volumenänderung, welche er hervorruft
94 – Plastizität	Die Eigenschaft eines Materials, sich unbegrenzt unter einer konstanten Spannung zu verformen
95 – Viskoelastizität	Die Eigenschaft eines Materials, sich unter Spannung teils elastisch, teils viskos (d.h. dessen Dehnung ist teilweise von der Zeit und der Größe der Spannung abhängig) zu verformen
96 – Spannungsrelaxation	Entspannung infolge von Kriechen
97 – Retardation	Verzögerung der Verformung
98 – Thixotropie	Die Eigenschaft sich aufgrund von Erschütterungen zu verflüssigen und durch Stehen sich wieder zu verfestigen
99 – Verwitterung	Der Vorgang des Zerfallens und der Zersetzung infolge der Aussetzung an die Atmosphäre, durch chemische Einwirkung und die Einwirkung von Frost, Wasser und Hitze
100 - Poissonsche Querdehnungszahl	Verhältnis zwischen Kürzung in der Querrichtung eines Körpers zu dessen Verlängerung in der Längsrichtung bei Zugbeanspruchung und zwar unterhalb der Proportionalitätsgrenze
101 – Bruch	Bruch im Fels bedeutet das Überschreiten der maximalen Festigkeit des Felses oder das Überschreiten der für eine bestimmte konstruktive Maßnahme vorgeschriebenen Anforderung an die Spannung (Druckänderung) oder Verformung
102 – Bruchkriterium	Die theoretisch oder empirisch abgeleitete Spannungs-bsw. Dehnungsverhältnisse, die das Eintreten des Bruches im Fels kennzeichnen
103 – Progressiver Bruch	Bildung und Weiterentwicklung örtlicher Gesteinsrisse, die nach weiterer Spannungssteigerung schließlich eine durchlaufende Bruchfläche bilden und so durch laufende Entfestigung zum Bruch führen
104 – Sprödbruch	Plötzlicher Bruch mit völligem Kohäsionsverlust entlang einer Fläche

105 — Riβbild	Räumliche Anordnung einer Gruppe von Bruchflächen
106 — "disking" (Zerfall eines Bohrkerns in Scheiben)	Zerbrechen eines harten Gesteinskerns in Scheiben beim Kernbohren, hervorgerufen durch hohe in-situ-Spannungen
107 — Trennfläche	Fläche oder eng begrenzter Bereich mit einer Scher- oder Zugfestigkeit (Bruchfestigkeit), die niedriger ist als derjenigen des umgebenden Materials
108 — Gebirgsschlag	Plötzliche explosionsartige Energiefreigabe aufgrund von Bruchvorgängen eines spröden Gesteins hoher Bruchfestigkeit
109 — Gleitung	Relative Verschiebung zweier Gesteinskörper entlang einer Oberfläche ohne Verlust des Zusammenhanges zwischen den Gesteinskörpern
110 — Abplatzen	(1) Abspaltung von Gesteinsstücken in Längsrichtung bei einaxialem Druckversuch (2) Abbrechen plattenartiger Stücke von einer freien Gesteinsoberfläche
111 — Knickung	Instabilität einer Säule oder einer Platte unter genügend hoher Belastung infolge plötzlichen Nachgebens
112 — Festigkeit	Die maximale Spannung, die ein Material ertragen kann, ohne daβ es bei irgendeinem Beanspruchungszustand zu Bruch geht
113 — Maβstabseffekt	Der Einfluβ der Größe des Untersuchungsstückes auf seine Festigkeit oder auf sonstige mechanische Kenngrößen
114 — (maximale) Scherfestigkeit	Höchste Scherspannung entlang einer Bruchfläche
115 — Restscherfestigkeit, Gleitfestigkeit	Die Scherspannung entlang einer Bruchfläche nach einer groβen Gleitverschiebung

116 – **Diskontinuitätsfläche**	Jede Oberfläche, über die hinweg irgendeine Gesteinseigenschaft sich diskontinuierlich (unstetig) ändert. Das schließt Klüfte, Störungen und Schichtflächen ein, jedoch sollte der Ausdruck nicht nur auf die Diskontinuität mechanischer Eigenschaften beschränkt werden
117 – **Kluft**	Ein geologisch bedingtes Unterbrechen des Zusammenhanges eines Gesteinskörpers, wobei dieser Bruch einzeln vorkommen kann oder, was häufiger ist, in Scharen oder in einem Bruchsystem; parallel zur Bruchfläche sind keine sichtbaren Relativbewegungen eingetreten
118 – **Störung**	Ein Bruch oder eine Bruchzone, entlang welcher es eine Gleitverschiebung der beiden gegenüberliegenden und zum Bruch parallel verlaufenden Seiten gegeben hat. Diese Gleitverschiebung kann wenige Zentimeter oder viele Kilometer betragen)
119 **Ruptur**	Der algemeine Ausdruck für jegliche mechanische Diskontinuität im Gestein; deshalb stellt es den Sammelbegriff für Klüfte, Störungen, Risse usw. dar
120 **Spalte**	Eine klaffende Ruptur
121 **Bruch (im engeren Sinne)**	Dasjenige Stadium in der Entwicklung eines Bruches, wo Instabilität eintritt.
122 – **Riß**	Eine kleine Ruptur, d.h. klein im Hinblick auf seine vergleichbare Umgebung
123 – **Schichtung**	Tritt in Gesteinen auf, die durch Verfestigung von Sedimenten entstanden sind und Trennflächen (Schichtflächen) zwischen den Ablagerungsschichten gleichen oder verschiedenen Materials aufweisen, z.B. Tonstein, Schluffstein, Sandstein, Kalkstein usw.
124 – **Mächtigkeit**	Der senkrechte Abstand zwischen Grenzflächen wie z.B. Schichtflächen eines Gesteins
125 – **Fallen**	Der Winkel, unter dem eine Schicht oder irgendein anderes Planargefüge zur Waagerechten geneigt ist
126 – **Streichen**	Richtung bzw. Azimut einer horizontalen Linie in der Fläche einer geneigten Schicht, Kluft, Störung oder eines sonstigen Planargefüges im Fels

127 — **Ausbiß**	Der Aufschluß des festen anstehenden Gesteines an der Erdoberfläche
128 — **anstehender Fels**	Der mehr oder weniger kontinuierliche Fels, der unter den auflagernden Böden gelegen ist
129 — **Überlagerung, Deckgebirge**	Der lockere Boden, Sand, Schluff oder Ton, der dem festen anstehenden Gestein auflagert. Manchmal wird damit auch sämtliches Material gemeint, das zwischen einem bestimmten Ort (z.B. Tunnelfirste) und der Erdoberfläche gelagert ist, also die gesamte Boden- und Felsüberdeckung über einem Felshohlraum
130 — **Struktur, Gefüge**	Die Raumanordnung (Raumerfüllung) der Bestandteile eines Gesteinskörpers sowie der Begrenzungsflächen zwischen diesen Bestandteilen
131 — **Gefüge**	Die Orientierung im Raum, die die Gesteinssubstanz zusammensetzenden Bestandteile
132 — **Textur**	Eine der allgemeineren Erscheinungsformen eines Gebirgskörpers, wie Schichtung, Kristallisationsschieferung, Klüftung, Schieferung und Brekzienbildung; auch die Gesamterfassung derartiger Phänomene in Gegenüberstellung zur Struktur.
133 — **Schieferung (bei metamorphen Gesteinen)**	Eine besondere Art der Schieferung, die in grobkörnigen metamorphen Gesteinen vorkommt und die im allgemeinen das Ergebnis der parallelen Anordnung plattiger und elliptisch ausgebildeter Mineralkörner innerhalb der Gesteinssubstanz darstellt
134 — **Lineamentierung**	Die parallele Ausrichtung von Gefügeelementen eines Gesteins, die eher Linien als Ebenen sind. Einige Beispiele sind parallele Ausrichtung der langen Achsen von Mineralen oder Kieseln; Gleitstreifen auf Rutschflächen und Schnitte von Schicht- und Schieferungsflächen
135 — **Schiefrigkeit (im rein beschreibenden Sinne)**	Die lamellenartige, geplättete Struktur, die sich aus der Absonderung verschiedener Minerale schichtparallel zur Schieferung ergibt

136 — Transversalschieferung — Die Neigung Schieferung auszubilden oder entlang bestimmter paralleler Ebenen Abspaltung zu zeigen, die eine starke Neigung zur Schichtablagerung aufweisen können. Es handelt sich dabei um eine Sekundärstruktur und wird gewöhnlich von Rekristallisierung des Gesteins begleitet

137 — Hangendes — Die Gesteinsmasse über einer Unstetigkeitsfläche

138 — Liegendes — Die Gesteinsmasse unter einer Unstetigkeitsfläche

139 — Erdsenkung, Bodensenkung — Die abwärts gerichtete Verlagerung des Deckgebirges, das über einem Untertageabbau liegt oder das an einem Übertageabbau angrenzt. Ebenso auch das Absinken eines Teiles der Erdrinde

140 — Karst — Ein Gebiet, in dem durch den Lösungsvorgang fließenden Wassers in massiven Kalksteinschichten Höhlen gebildt werden. Höhlen und sogar unterirdische Flußbette entwickeln sich, in die Oberflächenwasser abfließt und so oft zur Austrocknung und Verödung des darüberliegenden Landes führt

141 — Erdrutsch — Das Abrutschen oder die wahrnehmbare Abwärtsbewegung einer Boden- oder Felsmasse oder einer Mischung von beiden

142 — Füllung, Kluftfüllung — Im allgemeinen dasjenige Material, welches den Raum zwischen Kluftflächen, Störungsflächen und sonstigen Diskontinuitäten ausfüllt. Das Füllmaterial kann dargestellt werden von Ton, Zerreibsel, verschiedenen natürlichen Zemeten oder Verwitterungsprodukten vom angrenzenden Gestein

143 — "slickenside" (kleine Gesteinsrutschflächen) — Die polierte und mit Gleitstreifen versehene Oberfläche, die sich aus der Reibung entlang einer Störungsfläche oder sonstiger Bewegungsflächen in einer Gesteinsmasse ergibt

144 — Mylonit — Eine mikroskopische Brekzie mit Fluidaltextur, die sich in Störungszonen bildet

145 — Kluft/Trennflächen/schar — Eine Gruppe mehr oder weniger paralleler Klüfte/ /Trennflächen

146 – Kluft/Trennflächen/system	Besteht aus zwei oder mehreren Kluft/ /Trennflächen/scharen oder irgendeiner Gruppe von Klüften mit charakteristischem Anlageplan, z.B. konzentrische Anordnung
147 – Luft-Anlageplan	Eine Gruppe von Klüften, die eine bestimmte charakteristische geometrische Figur bilden, die sich jedoch innerhalb der gleichen geologischen Formation von einem Orte zum anderen beträchtlich verändern kann
148 – Kluftdiagramm	Ein Diagramm, in dem das Streichen und Fallen von Klüften genau eingetragen wird, um innerhalb eines eindeutig abgegrenzten geologischen Gebietes die geometrische Beziehung der Klüfte klar herauszustellen
149 – konjugierte Klüfte/ /Trennflächen	Zwei Kluft/Trennflächen/scharen, die sich unter den gleichen Spannungsbedingungen gebildet haben (für gewöhnlich Scherflächenpaare)
150 – Störungsbrekzie	Gesamtheit zerbrochener Gesteinsbruchstücke, die häufig in Störungszonen angetroffen werden. Die Bruchstücke können cm- bis m-Größe haben
151 – Zerreibsel in Störungszonen	Ein tonartiges Material, das in Störungszonen als Ergebnis der Bewegung entlang von Störungsflächen anzusehen ist
152 – Falte	Eine Umbiegung der Schichten oder sonstigen planparalleler Strukturen innerhalb des Gesteins
153 – Durchlässigkeit	Die Fähigkeit eines Gesteins Flüssigkeit oder Gase weiterzuleiten. Sie wird gemessen als Proportionalitätskonstante k zwischen Durchflußgeswindigkeit v und hydraulischem Gradienten i $v = ki$
155 – hydraulischer Gradient	Die Änderung der Druckhöhe pro Einheit der Entfernung an einem gegebenen Punkt und in einer gegebenen Richtung
157 – Wassergehalt	Der Gewichtsprozentsatz an Wasser, bezogen auf das Gewicht der Feststoffsubstanz, der im Porenraum eines Festgesteines oder Bodens enthalten ist
158 – Sättigungsgrad	Maß für den Grad, bis zu dem in dem Porenraum des Gesteins Flüssigkeit (Wasser, Gas oder Öl) enthalten ist; für gewöhnlich ausgedrückt in Prozent, bezogen

	auf den Gesamthohlraum oder auf den Gesamtporenraum
160 – Durchströmung	Die unter hydrostatischem Druck erfolgende Bewegung des Wassers durch die kleineren Zwischenräume von Festgestein oder Boden, nicht jedoch die Bewegung von Wasser durch weite Öffnungen wie Höhlen und Lösungskanäle
163 – Porosität	Das Verhältnis des Gesamtvolumens an Poren- oder Zwischenräumen in einem Festgestein oder Boden zum Gesamtvolumen

APPENDIX VII

Imperial, Metric and SI Units

TABLE 1
SI Units and Symbols

Base Units

Quantity	Unit	SI Symbol	Formula
length	metre	m	...
mass	kilogram	kg	...
time	second	s	...
electric current	ampere	A	...
thermodynamic temperature	kelvin	K	...
amount of substance	mole	mol	...
luminous intensity	candela	cd	...

Supplementary Units

plane angle	radian	rad	...
solid angle	steradian	sr	...

Derived Units

acceleration	metre per second squared	...	m/s^2
activity (of a radioactive source)	disintegration per second	...	(disintegration)/s
angular acceleration	radian per second squared	...	rad/s^2
angular velocity	radian per second	...	rad/s
area	square metre	...	m^2
density	kilogram per cubic metre	...	kg/m^3
electric capacitance	farad	F	$A \cdot s/V$
electrical conductance	siemens	S	A/V
electric field strength	volt per metre	...	V/m
electric inductance	henry	H	$V \cdot s/A$
electric potential difference	volt	V	W/A
electric resistance	ohm	Ω	V/A
electromotive force	volt	V	W/A
energy	joule	J	$N \cdot m$
entropy	joule per kelvin	...	J/K
force	newton	N	$kg \cdot m/s^2$
frequency	hertz	Hz	(cycle)/s
illuminance	lux	lx	lm/m^2
luminance	candela per square metre	...	cd/m^2
luminous flux	lumen	lm	$cd \cdot sr$
magnetic field strength	ampere per metre	...	A/m
magnetic flux	weber	Wb	$V \cdot s$
magnetic flux density	tesla	T	Wb/m^2
magnetomotive force	ampere	A	...
power	watt	W	J/s
pressure	pascal	Pa	N/m^2
quantity of electricity	coulomb	C	$A \cdot s$
quantity of heat	joule	J	$N \cdot m$
radiant intensity	watt per steradian	...	W/sr
specific heat	joule per kilogram-kelvin	...	$J/kg \cdot K$
stress	pascal	Pa	N/m^2
thermal conductivity	watt per metre-kelvin	...	$W/m \cdot K$
velocity	metre per second	...	m/s
viscosity, dynamic	pascal-second	...	$Pa \cdot s$
viscosity, kinematic	square metre per second	...	m^2/s
voltage	volt	V	W/A
volume	cubic metre	...	m^3
wavenumber	reciprocal metre	...	(wave)/m
work	joule	J	$N \cdot m$

TABLE 2
Prefixes used in SI Units

Multiplication Factors	Prefix	SI Symbol
1 000 000 000 000 = 10^{12}	tera	T
1 000 000 000 = 10^{9}	giga	G
1 000 000 = 10^{6}	mega	M
1 000 = 10^{3}	kilo	k
100 = 10^{2}	hecto	h
10 = 10^{1}	deka	da
0.1 = 10^{-1}	deci	d
0.01 = 10^{-2}	centi	c
0.001 = 10^{-3}	milli	m
0.000 001 = 10^{-6}	micro	μ
0.000 000 001 = 10^{-9}	nano	n
0.000 000 000 001 = 10^{-12}	pico	p
0.000 000 000 000 001 = 10^{-15}	femto	f
0.000 000 000 000 000 001 = 10^{-18}	atto	a

TABLE 3
Inch-Millimetre Equivalents

(Note: All values in this table are exact, based on the relationship 1 in = 25.4 mm. By manipulation of the decimal point, any decimal value or a multiple of an inch may be converted into its exact equivalent in millimetres)

in.	0	1	2	3	4	5	6	7	8	9
						mm				
0		25.4	50.8	76.2	101.6	127.0	152.4	177.8	203.2	228.6
10	254.0	279.4	304.8	330.2	355.6	381.0	406.4	431.8	457.2	482.6
20	508.0	533.4	558.8	584.2	609.6	635.0	660.4	685.8	711.2	736.6
30	762.0	787.4	812.8	838.2	863.6	889.0	914.4	939.8	965.2	990.6
40	1016.0	1041.4	1066.8	1092.2	1117.6	1143.0	1168.4	1193.8	1219.2	1244.6
50	1270.0	1295.4	1320.8	1346.2	1371.6	1397.0	1422.4	1447.8	1473.2	1498.6
60	1524.0	1549.4	1574.8	1600.2	1625.6	1651.0	1676.4	1701.8	1727.2	1752.6
70	1778.0	1803.4	1828.8	1854.2	1879.6	1905.0	1930.4	1955.8	1981.2	2006.6
80	2032.0	2057.4	2082.8	2108.2	2133.6	2159.0	2184.4	2209.8	2235.2	2260.6
90	2286.0	2311.4	2336.8	2362.2	2387.6	2413.0	2438.4	2463.8	2489.2	2514.6
100	2540.0	...	...	...	...	...	...	...	...	...

TABLE 4

Pressure and Stress Equivalents; Pounds-Force per Square Inch and Thousand Pounds-Force per Square Inch to Kilopascals (Kilonewtons per Square Metre) and Megapascals (Meganewtons per Square Metre)

(Note: This table may be used to obtain SI equivalents of values expressed in psi or ksi. SI values are usually expressed in kPa (kN/m^2) when original value is in psi, and in MPa (MN/m^2) when original value is in ksi.

This table may be extended to values below 1 or above 100 psi (ksi) by manipulation of the decimal point and addition.)

	0	1	2	3	4	5	6	7	8	9
psi ksi	kPa (kN/m^2) MPa (MN/m^2)									
0	0.0000	6.8948	13.7895	20.6843	27.5790	34.4738	41.3685	48.2633	55.1581	62.0528
10	68.9476	75.8423	82.7371	89.6318	96.5266	103.4214	110.3161	117.2109	124.1056	131.0004
20	137.8951	144.7899	151.6847	158.5794	165.4742	172.3689	179.2637	186.1584	193.0532	199.9480
30	206.8427	213.7375	220.6322	227.5270	234.4217	241.3165	248.2113	255.1060	262.0008	268.8955
40	275.7903	282.6850	289.5798	296.4746	303.3693	310.2641	317.1588	324.0536	330.9483	337.8431
50	344.7379	351.6326	358.5274	365.4221	372.3169	379.2116	386.1064	393.0012	399.8959	406.7907
60	413.6854	420.5802	427.4749	434.3697	441.2645	448.1592	455.0540	461.9487	468.8435	475.7382
70	482.6330	489.5278	496.4225	503.3173	510.2120	517.1068	524.0015	530.8963	537.7911	544.6858
80	551.5806	558.4753	565.3701	572.2648	579.1596	586.0544	592.9491	599.8439	606.7386	613.6334
90	620.5281	627.4229	634.3177	641.2124	648.1072	655.0019	661.8967	668.7914	675.6862	682.5810
100	689.4757									

TABLE 5

Pressure and Stress Equivalents; Metric Engineering to SI Units

(Note: This table may be used for obtaining SI equivalents of quantities expressed in kgf/cm^2 by multiplying the given values by 10^{-2}.

This table may be extended to values below 1 or above 100 kgf/cm^2 by manipulation of the decimal point and addition.)

	0	1	2	3	4	5	6	7	8	9
kgf/mm^2	MPa (MN/m^2)									
0		9.8066	19.6133	29.4200	39.2266	49.0332	58.8399	68.6466	78.4532	88.2598
10	98.0665	107.8731	117.6798	127.4864	137.2931	147.0998	156.9064	166.7130	176.5197	186.3264
20	196.1330	205.9396	215.7463	225.5530	235.3596	245.1662	254.9729	264.7796	274.5862	284.3928
30	294.1995	304.0062	313.8128	323.6194	333.4261	343.2328	353.0394	362.8460	372.6527	382.4594
40	392.2660	402.0726	411.8793	421.6860	431.4926	441.2992	451.1059	460.9126	470.7192	480.5258
50	490.3325	500.1392	509.9458	519.7524	529.5591	539.3658	549.1724	558.9790	568.7857	578.5924
60	588.3990	598.2056	608.0123	617.8190	627.6256	637.4322	647.2389	657.0456	666.8522	676.6588
70	686.4655	696.2722	706.0788	715.8854	725.6921	735.4988	745.3054	755.1120	764.9187	774.7254
80	784.5320	794.3386	804.1453	813.9520	823.7586	833.5652	843.3719	853.1786	862.9852	872.7918
90	882.5985	892.4052	902.2118	912.0184	921.8251	931.6318	941.4384	951.2450	961.0517	970.8584
100	980.6650									

TABLE 6
Selected Convertion Factors

To convert from	to	multiply by
atmosphere (760 mm Hg)	pascal (Pa)	$1.013\,25 \times 10^{5}$
board foot	metre^3 (m^3)	$2.359\,737 \times 10^{-3}$
Btu (International Table)	joule (J)	$1.055\,056 \times 10^{3}$
Btu (International Table)/hour	watt (W)	$2.930\,711 \times 10^{-1}$
Btu (International Table) · in./s · ft^2 · °F (k, thermal conductivity)	watt/metre-kelvin (W/m · K)	$5.192\,204 \times 10^{2}$
calorie (International Table)	joule (J)	4.186 800*
centipoise	pascal-second (Pa · s)	$1.000\,000^* \times 10^{-3}$
centistokes	metre^2/second (m^2/s)	$1.000\,000^* \times 10^{-6}$
circular mil	metre^2 (m^2)	$5.067\,075 \times 10^{-10}$
degree Fahrenheit	degree Celsius	$t_C = (t_F - 32)/1.8$
foot	metre (m)	$3.048\,000^* \times 10^{-1}$
foot^2	metre^2 (m^2)	$9.290\,304^* \times 10^{-2}$
foot^3	metre^3 (m^3)	$2.831\,685 \times 10^{-2}$
foot-pound-force	joule (J)	1.355 818
foot-pound-force/minute	watt (W)	$2.259\,697 \times 10^{-2}$
foot/second^2	metre/second^2 (m/s^2)	$3.048\,000^* \times 10^{-1}$
gallon (U.S. liquid)	metre^3 (m^3)	$3.785\,412 \times 10^{-3}$
horsepower (electric)	watt (W)	$7.460\,000^* \times 10^{2}$
inch	metre (m)	$2.540\,000^* \times 10^{-2}$
inch^2	metre^2 (m^2)	$6.451\,600^* \times 10^{-4}$
inch^3	metre^3 (m^3)	$1.638\,706 \times 10^{-5}$
inch of mercury (60 °F)	pascal (Pa)	$3.376\,85 \times 10^{3}$
inch of water (60 °F)	pascal (Pa)	$2.488\,4 \times 10^{2}$
kilogram-force/centimetre^2	pascal (Pa)	$9.806\,650^* \times 10^{4}$
kip (1000 lbf)	newton (N)	$4.448\,222 \times 10^{3}$
kip/inch^2 (ksi)	pascal (Pa)	$6.894\,757 \times 10^{6}$
ounce (U.S. fluid)	metre^3 (m^3)	$2.957\,353 \times 10^{-5}$
ounce-force (avoirdupois)	newton (N)	$2.780\,139 \times 10^{-1}$
ounce-mass (avoirdupois)	kilogram (kg)	$2.834\,952 \times 10^{-2}$
ounce-mass/ft^2	kilogram/metre^2 (kg/m^2)	0.305 152
ounce-mass/yard^2	kilogram/metre^2 (kg/m^2)	$3.390\,575 \times 10^{-2}$
ounce (avoirdupois)/gallon (U.S. liquid)	kilogram/metre^3 (kg/m^3)	7.489 152
pint (U.S. liquid)	metre^3 (m^3)	$4.731\,765 \times 10^{-4}$
pound-force (lbf avoirdupois)	newton (N)	4.448 222
pound-mass (lbm avoirdupois)	kilogram (kg)	$4.535\,924 \times 10^{-1}$
pound-force/inch^2 (psi)	pascal (Pa)	$6.894\,757 \times 10^{3}$
pound-mass/inch^3	kilogram/metre^3 (kg/m^3)	$2.767\,990 \times 10^{4}$
pound-mass/foot^3	kilogram/metre^3 (kg/m^3)	$1.601\,846 \times 10$
quart (U.S. liquid)	metre^3 (m^3)	$9.463\,529 \times 10^{-4}$
ton (short, 2000 lbm)	kilogram (kg)	$9.071\,847 \times 10^{2}$
torr (mm Hg)	pascal (Pa)	$1.333\,22 \times 10^{2}$
watt-hour	joule (J)	$3.600\,000^* \times 10^{3}$
yard	metre (m)	$9.144\,000^* \times 10^{-1}$
yard^2	metre^2 (m^2)	$8.361\,274 \times 10^{-1}$
yard^3	metre^3 (m^3)	$7.645\,549 \times 10^{-1}$

* Exact

ABOUT THE AUTHORS

R. D. Lama was born in India on April 1, 1940 and received the Degree of Bachelor of Science (with merit) from the Punjab University in 1957 and the Degree of Bachelor of Science in Mining Engineering in 1961 from the Banaras Hindu University standing First Class First throughout. He worked for one year in the Research Department of the Bengal Coal Co. and then left for higher studies to Poland on a Government of India Scholarship. During the period 1962–66 he worked in the Academy of Mining and Metallurgy, Cracow, Poland and obtained the Degree of Doctor of Technical Science in 1966 with a thesis on rock bursts and mechanical behaviour of coal seams in-situ.

In 1967 he joined Banaras Hindu University as a Reader in Coal Mining where he had been engaged in the teaching of Rock Mechanics, and Ground Movement to the post-graduate and under-graduate students. In 1971, he worked for six months with the Institute of Underground Mining, Akademia Gorniczo-Hutnicza, Cracow, on the problems associated with the prediction of cracking and crack density around tunnels. From December 1971 to December 1974, he worked with Professor L. Müller Salzburg under the programme SFB-77 of the German Science Foundation in the Institute of Soil Mechanics and Rock Mechanics, University of Karlsruhe, West Germany, on certain aspects of jointed rock masses including development of servo-controlled testing facility for studies on jointed rock systems. In January 1975, he joined the Division of Applied Geomechanics, CSIRO, Australia, first as a Senior Research Scientist and since July 1976 as Principal Research Scientist where he is working on various problems of underground coal mine designs, excavations placed in jointed rocks, outbursts of gas and coal etc.

Dr. Lama was awarded Banaras Hindu University Gold Medal, Nand Lal Gold Medal of the Banaras Hindu University and Roberton Medal of the Mining, Geological and Metallurgical Institute of India for his outstanding academic record. He is a member of the International Society for Rock Mechanics, Canadian Institute of Mining and Metallurgy, Association of the Mining Engineers and Technicians Poland, the Australian Geomechanics Society and Fellow of the Institution of Engineers (India).
Dr. Lama has published more than 50 papers in various journals in the field of rock mechanics and its applications to mining.

V. S. Vutukuri was born in India on September 22, 1937. In 1960 he received the Degree of Bachelor of Science in Mining Engineering from Banaras Hindu University. He received the Degree of Master of Science in Mining Engineering from University of Wisconsin in 1965. Between 1960 and 1964 he held the post of Lecturer in Mining Engineering at Banaras Hindu University. He then went to University of Wisconsin on study leave for postgraduate studies on a Wisconsin Alumni Research Foundation Fellowship. After completing the requirements for M. S. Degree, he joined the staff of White Pine Copper Company and was engaged with them for 6 months, in rock mechanics and rock breaking research. In 1966, he returned to Banaras Hindu University. He was promoted to Reader in 1966. In 1970 he emigrated to Australia and joined the University of New South Wales, Broken Hill Division as Lecturer in Mining Engineering. In 1978 he has been promoted to Senior Lecturer. In 1975, while on sabbatical leave, he was Research Associate in the Department of Mining Engineering of University of Newcastle upon Tyne for 5 months, Visiting Research Associate in the Department of Mineral Engineering of Pennsylvania State University for 2 months and Visiting Professor in the College of Engineering, Guindy, Madras for 6 months. His special interests are in rock mechanics and rock fragmentation.

He is a Member of the Mining, Geological and Metallurgical Institute of India, a Member of the American Institute of Mining, Metallurgical and Petroleum Engineers, a Member of the International Society for Rock Mechanics and an Associate Member of the Australasian Institute of Mining and Metallurgy.

Mr. Vutukuri has more than 30 publications to his credit.

Author Index

Subject Index

Author Index for Volumes I-IV

Subject Index for Volumes I-IV

HANDBOOK
ON
MECHANICAL PROPERTIES OF ROCKS

CONTENTS

Volume I

HANDBOOK
ON
MECHANICAL PROPERTIES OF ROCKS

CONTENTS

Volume II

HANDBOOK
ON
MECHANICAL PROPERTIES OF ROCKS

CONTENTS

Volume III

Series on Rock and Soil Mechanics
Vol. 1 (1971/74) No. 2

The Science of Rock Mechanics

PART 1
STRENGTH PROPERTIES OF ROCKS

By Prof. Dr. **W. Dreyer**, Technical University Clausthal, Germany

1972, reprinted 1973, 500 pages, 200 references, 86 tables, 137 figures,
price: US $ 30.00 hard cover

International Standard Book Number: 0-87849-002-7.
Library of Congress Catalog Card Number: 78-149276.

The present volume is the first – in itself complete – part of the monography "The Science of Rock Mechanics". It comprises primarily the relationship between state of stress, strength of rocks and their determining textural data. As the description of the mechanical behavior of rocks under compressive load is extremely incomplete without adequate consideration of the petrographic parameters such as mineral composition, mineral interlocking, granulation, grain density and porosity, the author has treated the mineral content of all investigated rock samples quantitatively and formulated them mathematically.

The operation of caverns in salt deposits for the purpose of storage requires intimate knowledge of stability and convergence behavior of an underground system. The solution to this highly complex rock mechanics problem is discussed in a special chapter.

"Originality in its true and good sense of the word is the great advantage of this book. Here, a professor has not written a seventh book out of six others, but a researcher has presented his field of interest and especially the results of his own studies, extending over almost two decades, among them many to be published for the first time."

TRANS TECH PUBLICATIONS

Trans Tech House **CH-4711 Aedermannsdorf** **Switzerland**

Series on Rock and Soil Mechanics
Vol. 2 (1974/77) No. 3

PROCEEDINGS FIRST CONFERENCE ON ACOUSTIC EMISSION/MICROSEISMIC ACTIVITY IN GEOLOGIC STRUCTURES AND MATERIALS

By **H. Reginald Hardy, jr., and Frederick W. Leighton**

1977, 490 pages, 235 figures, 480 references, US Dollar 40.00 (sFr. 100.00)

The rationale for organizing this conference developed from the feelings of the conference co-chairmen that the time had come to bring together the ideas and experiences of various workers involved in the application of acoustic emission/microseismic activity in the geomechanics area. It was clear that there were a considerable number of persons, throughout the world, who were actively engaged in basic and applied research in this area including, amongst others, those involved in such widely varying interests as the following:

- **Rock Burst Mechanics**
- **Underground Gas Storage Reservoir Stability**
- **Stability of Earth Filled Dams**
- **Earthquake Mechanics**
- **Hydrofracturing Research**
- **Slope Stability Monitoring**
- **Fundamental Behavior of Geologic Materials**
- **Strata Control in Coal and Hardrock Mines**
- **Comminution**

The proceedings include an introductory section presenting an historical review of the subject, the full text of all papers presented at the conference, general concluding remarks, a master bibliography, and a list of the conference participants and their affiliations. The proceedings represent the most comprehensive review of the subject published to date. In all a total of 25 papers are included. These deal with a wide range of laboratory, field and analytical aspects of acoustic emission/microseismic activity in the areas of **mining, petroleum,** and **civil engineering,** and in **geology** and **geophysics.**

TRANS TECH PUBLICATIONS

Trans Tech House **CH-4711 Aedermannsdorf** **Switzerland**

Series on Rock and Soil Mechanics
Vol. 2 (1974/77) No. 5

SOIL MECHANICS FOR OFF-ROAD VEHICLE ENGINEERING

By **Leslie L. Karafiath**, Grumman Aerospace Corporation, Bethpage, New York, and **Edward A. Nowatzki**, University of Arizona, Tuscon, Arizona

1978, 520 pages, 204 figs, US Dollar 54.00 (sFr. 135.00)

The ability to move vehicles over natural terrain is of paramount importance to a wide variety of disciplines, for example, automotive, military, mechanical, aerospace, construction and agricultural engineering. Workers in these disciplines would have to evaluate an enormous quantity of soil mechanics publications to extract the information that is useful for them. Recognizing this difficulty, the authors attempt to assess the value of published soil mechanics and other retlated literature from the viewpoint of off-road locomotion and to present a balanced discussion of the most important ideas.

Because the field of off-road vehicle engineering is expanding so rapidly, this book is not the final word on the topic. It is, however, the first to bring together in one place the results of efforts in a wide variety of disciplines and to present the latest technically sound concepts on the subject. In short, it provides a rational basis for the analysis of off-road locomotion problems and, as such, is a "must" for workers in the field of vehicle mobility. Because of this departure from some of the more conventional methods of soil-structure analysis it is also recommended for workers in the field of soil mechanics.

TRANS TECH PUBLICATIONS

Trans Tech House **CH-4711 Aedermannsdorf** **Switzerland**

Series on Rock & Soil Mechanics
Vol. 2 (1974-77) No. 4

THE PRESSUREMETER AND FOUNDATION ENGINEERING

by **F. BAGUELIN, J. F. JÉZÉQUEL, D. H. SHIELDS,** France and Canada

January 1978, 624 pages, 314 figs, US Dollar 52.00 (or sFr. 130.00) cloth

PREFACE

The design and construction of foundations require a thorough knowledge of the behaviour of soils and rocks in the field. Since even elaborate laboratory tests on large subsurface samples can at best only approximate the field conditions, in-situ tests are often preferable. The pressuremeter is probably the most versatile in-situ testing device available at present for investigating static and cyclic strength and deformation properties of soils and rocks.

Based on the authors' comparisons between the results of standardized pressuremeter tests and both static and standard penetration tests under different site conditions, the merits and limitations of the various methods of field investigations can readily be assessed. At the same time the extensive experience gained by these reliable, practical and semi-empirical methods of using pressuremeter data becomes available to other types of field investigations to their mutual benefit. These approaches require mature engineering judgment and sound experience based on performance observations on structures during and after construction. In this way pressuremeter tests can lead to safe and economical solutions to many geotechnical problems, as shown in this warmly recommended book.

G. G. MEYERHOF

TRANS TECH PUBLICATIONS

Trans Tech House CH-4711 Aedermannsdorf Switzerland

Series on Rock and Soil Mechanics
Vol. 1 (1971/74) No. 3

FOUNDATION INSTRUMENTATION

By **Dr. Thomas H. Hanna**, Professor of Civil and Structural Engineering, University of Sheffield, England

1973. 372 pages, 251 figures, 520 references, price: US $ 35.00 hard cover

Contents

"The book represents a fine help and a welcome treasury of methods and devices for every civil and structural engineer concerned with the design and construction of civil engineering works, since the ground always affects the stability and performance of these structures. It can be recommended warmly to students and civil engineers in the field of design, construction and research."

Applied Mechanics Reviews

"This most interesting book includes a very large number of references and a list of instrument suppliers. It will probably become one of the most widely used tools for soil and foundation engineers who understand the need for performance evaluation."

Canadian Geotechnical Journal

"The book can obviously be recommended to all people dealing with foundations, earth and rockfill dams, tunnels, and soil mechanics in general."

Water Power

TRANS TECH PUBLICATIONS

Trans Tech House **CH-4711 Aedermannsdorf** **Switzerland**